AREVA

CoC 1004

STANDARDIZED NUHOMS®

Amendment 10 Application

NON- PROPRIETARY

UFSAR Appendix T – 61BTH Part 2 of 2

VOLUME 2 OF 4

TRANSNUCLEAR INC.

APPENDIX T

NUHOMS® 61BTH DSC

TABLE OF CONTENTS

Page

T.1 General Discussion T.1-1
T.1.1 Introduction T.1-3
T.1.2 General Description of the NUHOMS®-61BTH System T.1-4
T.1.2.1 NUHOMS®-61BTH System Characteristics T.1-4
T.1.2.2 Operational Features T.1-7
T.1.2.3 Cask Contents T.1-8
T.1.3 Identification of Agents and Contractors T.1-9
T.1.4 Generic Cask Arrays T.1-10
T.1.5 Supplemental Data T.1-11
T.1.6 References T.1-12
T.2 Principal Design Criteria T.2-1
T.2.1 Spent Fuel To Be Stored T.2-2
T.2.1.1 General Operating Functions T.2-4
T.2.2 Design Criteria for Environmental Conditions and Natural Phenomena T.2-5
T.2.2.1 Tornado Wind and Tornado Missiles T.2-5
T.2.2.2 Water Level (Flood) Design T.2-5
T.2.2.3 Seismic Design T.2-5
T.2.2.4 Snow and Ice Loading T.2-6
T.2.2.5 Combined Load Criteria T.2-6
T.2.3 Safety Protection Systems T.2-9
T.2.3.1 General T.2-9
T.2.3.2 Protection By Multiple Confinement Barriers and Systems T.2-9
T.2.3.3 Protection By Equipment and Instrumentation Selection T.2-9
T.2.3.4 Nuclear Criticality Safety T.2-9
T.2.3.5 Radiological Protection T.2-10
T.2.3.6 Fire and Explosion Protection T.2-10
T.2.4 Decommissioning Considerations T.2-11
T.2.5 Summary of NUHOMS®-61BTH System Design Criteria T.2-12
T.2.5.1 61BTH DSC Design Criteria T.2-12
T.2.5.2 HSM-H Models 80, 102, 152, 202 and HSM-H Design Criteria T.2-12
T.2.5.3 OS197/OS197H/OS197FC-B TCs Design Criteria T.2-13
T.2.6 References T.2-14
T.3 Structural Evaluation T.3.1-1
T.3.1 Structural Design T.3.1-1
T.3.1.1 Discussion T.3.1-1
T.3.1.2 Design Criteria T.3.1-3
T.3.2 Weights T.3.2-1
T.3.3 Mechanical Properties of Materials T.3.3-1
T.3.3.1 Material Properties T.3.3-1

T.3.3.2 Materials Durability T.3.3-1
T.3.4 General Standards for Casks T.3.4-1
T.3.4.1 Chemical and Galvanic Reactions T.3.4-1
T.3.4.2 Positive Closure T.3.4-7
T.3.4.3 Lifting Devices T.3.4-7
T.3.4.4 Heat and Cold T.3.4-7
T.3.5 Fuel Rods T.3.5-1
T.3.5.1 Material Properties of High Burnup Fuel T.3.5-1
T.3.5.2 Side Drop Analysis T.3.5-4
T.3.5.3 End Drop Analysis T.3.5-6
T.3.6 Structural Analysis (Normal and Off-Normal Operations) T.3.6-1
T.3.6.1 Normal Operation Structural Analysis T.3.6-1
T.3.6.2 Off-Normal Load Structural Analysis T.3.6-19
T.3.6.3 Damaged Fuel Cladding Structural Evaluation T.3.6-22
T.3.7 Structural Analysis (Accidents) T.3.7-1
T.3.7.1 Tornado Winds/Tornado Missile T.3.7-2
T.3.7.2 Earthquake T.3.7-2
T.3.7.3 Flood T.3.7-4
T.3.7.4 Accidental Cask Drop T.3.7-4
T.3.7.5 Loss of Neutron Shield T.3.7-17
T.3.7.6 Lightning T.3.7-17
T.3.7.7 Blockage of Air Inlet and Outlet Openings T.3.7-17
T.3.7.8 DSC Leakage T.3.7-17
T.3.7.9 Accident Pressurization of DSC T.3.7-17
T.3.7.10 Reduced HSM Air Inlet and outlet Shielding T.3.7-18
T.3.7.11 Fire and Explosion T.3.7-18
T.3.7.12 Load Combinations T.3.7-18
T.3.8 References T.3.8-1
T.4 Thermal Evaluation T.4-1
T.4.1 Discussion T.4-1
T.4.2 Summary of Thermal Properties of Materials T.4-4
T.4.3 Specifications for Neutron Absorber Thermal Conductivity T.4-12
T.4.4 Thermal Analysis of HSM and HSM-H with 61BTH DSC T.4-13
T.4.4.1 Ambient Temperature Specification T.4-13
T.4.4.2 Thermal Analysis of HSM-H with 61BTH DSC T.4-13
T.4.4.3 HSM-H Air flow Analysis (Stack Effect Calculations) T.4-14
T.4.4.4 Description of the Thermal Model of HSM-H with 61BTH DSC T.4-15
T.4.4.5 Description of the HSM-H Blocked Vent Model T.4-17
T.4.4.6 Description of Cases Evaluated for the HSM-H T.4-17
T.4.4.7 HSM-H Thermal Model Results T.4-17
T.4.4.8 Evaluation of HSM-H Performance T.4-18
T.4.5 Thermal Analysis of Transfer Casks with 61BTH DSC T.4-19
T.4.5.1 Thermal Model of 61BTH DSC in the OS197FC-B T.4-19
T.4.5.2 Analysis Cases for OS197FC-B TC with 61BTH DSC T.4-21
T.4.5.3 OS197FC-B TC Thermal Model Results T.4-22

T.4.5.4 Evaluation of OS197FC-B TC Performance T.4-26
T.4.6 NUHOMS®-61BTH DSC Thermal Analysis T.4-27
T.4.6.1 Heat Load Zoning Configurations T.4-27
T.4.6.2 NUHOMS® 61BTH DSC Thermal Analysis Model T.4-28
T.4.6.3 Mesh Sensitivity Study T.4-28
T.4.6.4 Axial Heat Flux Profile T.4-28
T.4.6.5 Heat Generation for the DSC Basket Model T.4-29
T.4.6.6 DSC Thermal Evaluation for Normal Conditions of Storage and Transfer T.4-29
T.4.6.7 DSC Thermal Evaluation for Off-Normal Conditions T.4-33
T.4.6.8 DSC Thermal Evaluation for Accident Conditions T.4-35
T.4.7 Thermal Evaluation for Loading/Unloading Conditions T.4-38
T.4.7.1 Maximum Fuel Cladding Temperatures during Vacuum Drying T.4-38
T.4.7.2 Evaluation of Thermal Cycling of Fuel Cladding during Vacuum Drying, Helium Backfilling and Transfer Operations T.4-39
T.4.7.3 Reflooding Evaluation T.4-39
T.4.8 Determination of Effective Thermal Properties of the Fuel, Basket and Air Within the HSM-H Closed Cavity T.4-41
T.4.8.1 Determination of Bounding Effective Fuel Thermal Conductivity T.4-41
T.4.8.2 Calculation of Fuel Effective Specific Heat and Density T.4-43
T.4.8.3 61BTH DSC Basket Effective Thermal Properties T.4-44
T.4.8.4 Effective Air Conductivity in the HSM-H Closed Cavity T.4-45
T.4.8.5 Effective Thermal Conductivity within Neutron Shield T.4-45
T.4.9 References T.4-46
T.5 Shielding Evaluation T.5-1
T.5.1 Discussion and Results T.5-5
T.5.2 Source Specification T.5-6
T.5.2.1 Gamma Source Term for MCNP Models T.5-8
T.5.2.2 Neutron Source Term for MCNP Models T.5-9
T.5.2.3 Axial Peaking T.5-10
T.5.2.4 ANISN Evaluation of Bounding Source Terms T.5-11
T.5.2.5 Reconstituted Fuel T.5-13
T.5.3 Material Densities T.5-15
T.5.4 Shielding Evaluation T.5-16
T.5.4.1 Computer Program T.5-16
T.5.4.2 Spatial Source Distribution T.5-16
T.5.4.3 Cross Section Data T.5-17
T.5.4.4 Flux-to-Dose-Rate Conversion T.5-17
T.5.4.5 Methodology T.5-17
T.5.4.6 Assumptions T.5-18
T.5.4.7 Normal Condition Models T.5-19
T.5.4.8 Accident Condition Models T.5-22
T.5.4.9 OS197FC-B TC Models During Fuel Loading Operations T.5-22

T.5.5 Appendix T.5-24
T.5.5.1 Sample SAS2H/ORIGEN-S Input File T.5-24
T.5.5.2 Sample HSM-H MCNP5 Model T.5-27
T.5.5.3 Sample HSM Model 102 MCNP 5 Model T.5-47
T.5.5.4 Sample OS197FC-B TC MCNP4C2 Model T.5-74
T.5.5.5 Sample ANISN Model (TC –Group 23) T.5-91
T.5.6 References T.5-96
T.6 Criticality Evaluation T.6-1
T.6.1 Discussion and Results T.6-2
T.6.2 Package Fuel Loading T.6-3
T.6.3 Model Specification T.6-4
T.6.3.1 Description of Calculational Model T.6-4
T.6.3.2 Package Regional Densities T.6-6
T.6.4 Criticality Calculation T.6-7
T.6.4.1 Calculational Method T.6-8
T.6.4.2 Fuel Loading Optimization T.6-11
T.6.4.3 Criticality Results T.6-20
T.6.5 Critical Benchmark Experiments T.6-21
T.6.5.1 Benchmark Experiments and Applicability T.6-21
T.6.5.2 Results of the Benchmark Calculations T.6-22
T.6.6 Appendix T.6-23
T.6.6.1 References T.6-23
T.6.6.2 Calculation of Water Area at the Corner Rail Locations T.6-24
T.6.6.3 Damaged Fuel Analysis T.6-24
T.6.6.4 CSAS25 Input Deck for Design Basis Intact Fuel Assembly Case T.6-26
T.6.6.5 CSAS25 Input Deck for Design Basis Damaged Fuel Assembly Cases T.6-38
T.7 Confinement T.7-1
T.7.1 Confinement Boundary T.7-2
T.7.1.1 Confinement Vessel T.7-2
T.7.1.2 Confinement Penetrations T.7-3
T.7.1.3 Seals and Welds T.7-3
T.7.1.4 Closure T.7-3
T.7.2 Requirements for Normal Conditions of Storage T.7-4
T.7.2.1 Release of Radioactive Material T.7-4
T.7.2.2 Pressurization of Confinement Vessel T.7-4
T.7.3 Confinement Requirements for Hypothetical Accident Conditions T.7-5
T.7.3.1 Fission Gas Products T.7-5
T.7.3.2 Release of Contents T.7-5
T.7.4 References T.7-6
T.8 Operating Systems T.8-1
T.8.1 Procedures for Loading the Cask T.8-2
T.8.1.1 Preparation of the Transfer Cask and DSC T.8-2
T.8.1.2 DSC Fuel Loading T.8-3

T.8.1.3 DSC Drying and Backfilling T.8-5
T.8.1.4 DSC Sealing Operations T.8-8
T.8.1.5 Transfer Cask Downending and Transport to ISFSI T.8-9
T.8.1.6 DSC Transfer to the HSM T.8-10
T.8.1.7 Monitoring Operations T.8-12
T.8.2 Procedures for Unloading the Cask T.8-16
T.8.2.1 DSC Retrieval from the HSM T.8-16
T.8.2.2 Removal of Fuel from the DSC T.8-16
T.8.3 Identification of Subjects for Safety Analysis T.8-24
T.8.4 Fuel Handling Systems T.8-24
T.8.5 Other Operating Systems T.8-24
T.8.6 Operation Support System T.8-24
T.8.7 Control Room and/or Control Areas T.8-24
T.8.8 Analytical Sampling T.8-24
T.8.9 References T.8-25
T.9 Acceptance Tests and Maintenance Program T.9-1
T.9.1 Acceptance Tests T.9-1
T.9.1.1 Visual Inspection T.9-1
T.9.1.2 Structural T.9-1
T.9.1.3 Leak Tests T.9-2
T.9.1.4 Components T.9-2
T.9.1.5 Shielding Integrity T.9-2
T.9.1.6 Thermal Acceptance T.9-2
T.9.1.7 Poison Acceptance T.9-3
T.9.2 Maintenance Program T.9-12
T.9.3 References T.9-13
T.10 Radiation Protection T.10-1
T.10.1 Occupational Exposure T.10-2
T.10.2 Off-Site Dose Calculations T.10-3
T.10.2.1 Activity Calculations T.10-6
T.10.2.2 Dose Rates T.10-7
T.10.3 References T.10-9
T.11 Accident Analyses T.11-1
T.11.1 Off-Normal Operations T.11-2
T.11.1.1 Off-Normal Transfer Loads T.11-2
T.11.1.2 Extreme Temperatures T.11-3
T.11.1.3 Off-Normal Releases of Radionuclides T.11-4
T.11.1.4 Radiological Impact from Off-Normal Operations T.11-4
T.11.2 Postulated Accidents T.11-5
T.11.2.1 Reduced HSM Air Inlet and Outlet Shielding T.11-5
T.11.2.2 Earthquake T.11-6
T.11.2.3 Extreme Wind and Tornado Missiles T.11-6
T.11.2.4 Flood T.11-7
T.11.2.5 Accidental TC Drop T.11-8

T.11.2.6 Lightning T.11-9
T.11.2.7 Blockage of Air Inlet and Outlet Openings T.11-9
T.11.2.8 DSC Leakage T.11-10
T.11.2.9 Accident Pressurization of DSC T.11-10
T.11.2.10 Fire and Explosion T.11-11
T.11.3 References T.11-12
T.12 Conditions for Cask Use - Operating Controls and Limits or Technical Specifications T.12-1
T.13 Quality Assurance T.13-1
T.14 Decommissioning T.14-1

LIST OF TABLES

		Page
Table T.1-1	Key Design Parameters of the NUHOMS®-61BTH System(1)	T.1-13
Table T.2-1	BWR Fuel Specification for the Fuel to be Stored in the NUHOMS®-61BTH DSC	T.2-15
Table T.2-2	BWR Fuel Assembly Design Characteristics(1) for the NUHOMS®-61BTH DSC	T.2-17
Table T.2-3	BWR Fuel Assembly Initial Lattice Average Enrichment v/s Minimum B10 Requirements for the NUHOMS®-61BTH DSC Poison Plates (Intact Fuel)	T.2-18
Table T.2-4	BWR Fuel Assembly Initial Lattice Average Enrichment v/s Minimum B10 Requirements for the NUHOMS®-61BTH DSC Poison Plates (Damaged Fuel)	T.2-19
Table T.2-5	BWR Fuel Qualification Table for Zone 1 Fuel with 0.22 kW per Assembly for the NUHOMS®-61BTH DSC	T.2-20
Table T.2-6	BWR Fuel Qualification Table for Zone 2 Fuel with 0.35 kW per Assembly for the NUHOMS®-61BTH DSC	T.2-21
Table T.2-7	BWR Fuel Qualification Table for Zone 3 Fuel with 0.393 kW per Assembly for the NUHOMS®-61BTH DSC	T.2-22
Table T.2-8	BWR Fuel Qualification Table for Zone 4 Fuel with 0.480 kW per Assembly for the NUHOMS®-61BTH DSC	T.2-23
Table T.2-9	BWR Fuel Qualification Table for Zone 5 Fuel with 0.54 kW per Assembly for the NUHOMS®-61BTH DSC	T.2-24
Table T.2-10	BWR Fuel Qualification Table for Zone 6 Fuel with 0.7 kW per Assembly for the NUHOMS®-61BTH DSC	T.2-25
Table T.2-11	Summary of 61BTH-DSC Load Combinations	T.2-27
Table T.2-12	Summary of Stress Criteria for Subsection NB Pressure Boundary Components	T.2-31
Table T.2-13	Summary of Stress Criteria for Subsection NG Components	T.2-32
Table T.2-14	Summary of NUHOMS®-61BTH DSC Design Loadings(1)(2)	T.2-33
Table T.3.1-1	Primary Stress Intensity Limits	T.3.1-6
Table T.3.1-2	ASME Code Alternatives for the NUHOMS®-61BTH DSC Confinement Boundary	T.3.1-7
Table T.3.1-3	ASME Code Alternatives for the NUHOMS®-61BTH DSC Basket	T.3.1-9
Table T.3.2-1	Summary of the NUHOMS®-61BTH System Component Weights(4)	T.3.2-2
Table T.3.5-1	Temperature Dependent Material Properties of Zircaloy-2 Material	T.3.5-10
Table T.3.5-2	Maximum Overhang Length of Fuel Assembly	T.3.5-11
Table T.3.5-3	Fuel Assembly Data for Side Drop	T.3.5-12
Table T.3.5-4	Finite Element Model for Side Drop	T.3.5-13
Table T.3.5-5	Summary of Stress Results for 75g Side Drop	T.3.5-14
Table T.3.5-6	Finite Element Model Data for End Drop	T.3.5-15
Table T.3.6-1	NUHOMS® Normal Operating Loading Identification	T.3.6-33
Table T.3.6-2	NUHOMS® Off-Normal Operating Loading Identification	T.3.6-34
Table T.3.6-3	Mechanical Properties of Materials	T.3.6-35
Table T.3.6-4	Maximum NUHOMS®-61BTH DSC Stresses for Normal and Off-Normal Loads (Type 1 DSC)	T.3.6-36

Table T.3.6-5 Maximum NUHOMS®-61BTH DSC Stresses for Normal and Off-Normal Loads (Type 2 DSC) T.3.6-37
Table T.3.6-6 Design Parameters of 61BTH BWR Fuel Assemblies T.3.6-38
Table T.3.6-7 Computed Maximum Fuel Rod Stresses and their Ratio to Yield Strength T.3.6-39
Table T.3.6-8 OS197FC-B TC Enveloping Thermal Stresses T.3.6-40
Table T.3.6-9 OS197/OS197H/OS197FC-B TC Combined Stresses For Normal Condition Loads(1)(2) T.3.6-41
Table T.3.7-1 Postulated Accident Loading Identification T.3.7-20
Table T.3.7-2 Maximum NUHOMS®-61BTH Type 1 DSC Stresses for Drop Accident Loads(2) T.3.7-21
Table T.3.7-3 Maximum NUHOMS®-61BTH Type 2 DSC Stresses for Drop Accident Loads(2) T.3.7-22
Table T.3.7-4 Fuel Assembly Weight Simulation Based on 1g Load T.3.7-23
Table T.3.7-5 Stress Summary of the Type 1 Basket Due to Side Drop Loads – 75g T.3.7-24
Table T.3.7-6 Stress Summary of the Type 2 Basket Due to Side Drop Loads – 75g T.3.7-25
Table T.3.7-7 Stress Summary of the Type 1 Basket due to 60g End Drop Load T.3.7-26
Table T.3.7-8 Stress Summary of the Type 2 Basket due to 60g End Drop Load T.3.7-27
Table T.3.7-9 Mechanical Properties of Materials T.3.7-28
Table T.3.7-10 Summary of Pressure Loads Used for Different Drop Orientations T.3.7-29
Table T.3.7-11 Summary of Basket Buckling Analysis T.3.7-30
Table T.3.7-12 NUHOMS®-61BTH Type 1 DSC Enveloping Load Combination Results for Normal and Off-Normal Loads T.3.7-31
Table T.3.7-13 NUHOMS®-61BTH Type 2 DSC Enveloping Load Combination Results for Normal and Off-Normal Loads T.3.7-32
Table T.3.7-14 NUHOMS®-61BTH Type 1 DSC Enveloping Load Combination Results for Accident Loads T.3.7-33
Table T.3.7-15 NUHOMS®-61BTH Type 2 DSC Enveloping Load Combination Results for Accident Loads T.3.7-34
Table T.3.7-16 NUHOMS®-61BTH Type 1 DSC Enveloping Load Combination Results for Accident Loads T.3.7-35
Table T.3.7-17 NUHOMS®-61BTH Type 2 DSC Enveloping Load Combination Results for Accident Loads T.3.7-36
Table T.3.7-18 DSC Enveloping Load Combination Table Notes T.3.7-37
Table T.4-1 Bulk Air Temperatures at Specified HSM-H Regions for the Various Cases(1) T.4-48
Table T.4-2 HSM-H Components Normal and Off-Normal Maximum Temperatures, 31.2 kW Heat Load T.4-49
Table T.4-3 HSM-H Components Maximum Temperatures (°F), 31.2 kW Decay Heat Load, 117°F Ambient, Blocked Vent Accident (Case 5) T.4-50
Table T.4-4 Summary of OS197/OS197H/OS197FC-B Load Cases for 61BTH Type 1 DSC T.4-51
Table T.4-5 Summary of OS197FC-B Load Cases for 61BTH Type 2 DSC T.4-52
Table T.4-6 Cask DSC Gap Hydraulic Characteristics as a Function of Circumferential Position T.4-53

Table T.4-7 OS197/OS197H/OS197FC-B TC Components and DSC Shell Steady State Temperatures for 61BTH Type 1 DSC under Normal and Off-Normal Conditions T.4-54
Table T.4-8 OS197/OS197H/OS197FC-B TC Components and DSC Shell Temperatures for 61BTH Type 2 DSC under Normal and Off-Normal Conditions @ 28 Hr T.4-55
Table T.4-9 OS197FC-B TC Components and DSC Shell Steady State Temperatures for 61BTH Type 2 DSC under Normal and Off-Normal Conditions and Air Circulation T.4-56
Table T.4-10 TC Components and DSC Shell Steady-State Temperatures for a Loss of Neutron Shield T.4-57
Table T.4-11 TC Components and DSC Shell Temperatures for Fire Accident Temperatures with 31.2 kW Decay Heat Load T.4-58
Table T.4-12 Fuel Cladding Normal Condition Maximum Temperatures T.4-59
Table T.4-13 61BTH Type 1 DSC Basket Assembly Maximum Normal Operating Component Temperatures T.4-60
Table T.4-14 61BTH Type 2 DSC Basket Assembly Maximum Normal Operating Component Temperatures T.4-61
Table T.4-15 Initial Helium Fill Gas Molar Quantities T.4-62
Table T.4-16 Maximum Normal Operating DSC Cavity Condition Pressures T.4-63
Table T.4-17 Fuel Cladding Off-Normal Condition Maximum Temperatures T.4-64
Table T.4-18 61BTH Type 1 DSC Basket Assembly Maximum Off-Normal Operating Component Temperatures T.4-65
Table T.4-19 61BTH Type 2 DSC Basket Assembly Maximum Off-Normal Operating Component Temperatures T.4-66
Table T.4-20 Maximum Off-Normal Operating Condition DSC Cavity Pressures T.4-67
Table T.4-21 Fuel Cladding Accident Condition Maximum Temperatures T.4-68
Table T.4-22 61BTH Type 1 DSC Basket Assembly Accident Maximum Component Temperatures T.4-69
Table T.4-23 61BTH Type 2 DSC Basket Assembly Accident Maximum Component Temperatures T.4-70
Table T.4-24 Maximum Accident Condition DSC Cavity Pressures T.4-71
Table T.4-25 Vacuum Drying Fuel Cladding Maximum Temperatures T.4-72
Table T.4-26 61BTH Type 1 DSC Basket Assembly Maximum Component Temperatures during Vacuum Drying T.4-73
Table T.4-27 61BTH Type 2 DSC Basket Assembly Maximum Component Temperatures during Vacuum Drying T.4-74
Table T.4-28 61BTH Type 1 DSC Shell Temperatures for Storage in HSM T.4-75
Table T.4-29 DSC Cavity Free Volumes T.4-76
Table T.4-30 Fuel Rod Helium Fill Gas Released per DSC T.4-77
Table T.4-31 Fission Gas Released per DSC T.4-78
Table T.5-1 Summary of NUHOMS®-61BTH DSC in HSM-H, Bounding Maximum and Average Dose Rates, HLZC #6(2) T.5-98
Table T.5-2 Summary of NUHOMS®-61BTH DSC in HSM Model 102, Bounding Maximum and Average Dose Rates T.5-99

Table T.5-3 Summary of NUHOMS®-61BTH DSC in HSM Model 80 Maximum and Average Dose Rates T.5-100
Table T.5-4 Summary of NUHOMS®-61BTH DSC, OS197FC-B TC Maximum Dose Rates During Transfer Operations T.5-101
Table T.5-5 Summary of NUHOMS®-61BTH DSC, OS197FC-B TC Maximum Dose Rates During Decontamination and Welding Operations T.5-102
Table T.5-6 BWR Fuel Assembly Material Mass T.5-103
Table T.5-7 Elemental Composition of LWR Fuel-Assembly Structural Materials T.5-104
Table T.5-8 Flux Scaling Factors By Fuel Assembly Region T.5-105
Table T.5-9 Gamma and Neutron Source Term for 0.22 kW Fuel in TC for HLZC 6 (31 GWd/MTU, 0.9 wt. % U-235 and 11.7-Year Cooled Fuel) T.5-106
Table T.5-10 Gamma and Neutron Source Term for 0.48 kW Fuel in TC for HLZC 6, HSM Model 80 and 102 for HLZC 1 (25 GWd/MTU, 1.0 wt. % U-235 and 3.2-Year Cooled Fuel) T.5-107
Table T.5-11 Gamma and Neutron Source Term for 0.54 kW Fuel in TC for HLZCs 6 and 7 (25 GWd/MTU, 0.9 wt. % U-235 and 3.0-Year Cooled Fuel) T.5-108
Table T.5-12 Gamma and Neutron Source Term for 0.7 kW Fuel in TC for HLZC 6 (62 GWd/MTU, 2.6 wt. % U-235 and 7.1-Year Cooled Fuel) T.5-109
Table T.5-13 Gamma and Neutron Source Term for 0.48 kW Fuel in TC for HLZC 7 (62 GWd/MTU, 2.6 wt. % U-235 and 14.0-Year Cooled Fuel) T.5-110
Table T.5-14 Gamma and Neutron Source Term for 0.22 kW Fuel in HSM-H for HLZC 6 (13 GWd/MTU, 1.8 wt. % U-235 and 3.0-Year Cooled Fuel) T.5-111
Table T.5-15 Gamma and Neutron Source Term for 0.48 kW Fuel in HSM-H for HLZC 6 (24 GWd/MTU, 1.3 wt. % U-235 and 3.0-Year Cooled Fuel) T.5-112
Table T.5-16 Gamma and Neutron Source Term for 0.54 kW Fuel in HSM-H for HLZC 6, HSM Model 80 and 102 for HLZC 2 (25 GWd/MTU, 0.9 wt. % U-235 and 3.0-Year Cooled Fuel) T.5-113
Table T.5-17 Gamma and Neutron Source Term for 0.7 kW Fuel in HSM-H for HLZC 6 (34 GWd/MTU, 2.0 wt. % U-235 and 3.1-Year Cooled Fuel) T.5-114
Table T.5-18 Gamma and Neutron Source Term for 0.393 kW Fuel in HSM Model 80 and Model 102 for HLZC 2 (62 GWd/MTU, 2.6 wt. % U-235 and 21.4-Year Cooled Fuel) T.5-115
Table T.5-19 Shielding Material Densities T.5-116
Table T.5-20 Material Densities Used in ANISN Models T.5-119
Table T.5-21 Neutron Source for ANISN Calculation T.5-120
Table T.5-22 ANISN Response Function for the OS197FC-B TC Due to Radial Zone 1 ..... T.5-121
Table T.5-23 ANISN Response Function for the OS197FC-B TC Due to Radial Zone 2 ..... T.5-122
Table T.5-24 ANISN Response Function for the OS197FC-B TC Due to Radial Zone 3 ..... T.5-123
Table T.5-25 ANISN Response Function for the OS197FC-B TC Due to Radial Zone 4 ..... T.5-124
Table T.5-26 Flux to Dose Rate Conversion Factors T.5-125
Table T.5-27 Surface Average Dose Rates (mrem/hr) on HSM Model 80 and 102 with 61BT DSC T.5-126

Table T.5-28 Maximum Surface Dose Rates (mrem/hr) on HSM Model 80 and 102 with 61BT DSC T.5-127
Table T.5-29 Total Dose Rates (mrem/hr) at the Center of Transfer Cask Side Surface for 0.70 kW/FA HLZC #6 ..... T.5-128
Table T.6-1 Minimum B10 Content as a Function of Enrichment T.6-65
Table T.6-2 Authorized Contents for NUHOMS®-61BTH System T.6-66
Table T.6-3 Parameters for BWR Assemblies for Shipment T.6-67
Table T.6-4 Summary of Criticality Analyses T.6-69
Table T.6-5 Material Property Data T.6-70
Table T.6-6 Most Reactive Fuel Type T.6-71
Table T.6-7 Most Reactive Configuration – Intact Fuel T.6-74
Table T.6-8 Criticality Analysis Results for Intact Fuel T.6-76
Table T.6-9 Most Reactive Configuration – Double Shear T.6-79
Table T.6-10 Most Reactive Configuration – Optimum Rod Pitch T.6-80
Table T.6-11 Most Reactive Configuration – Variations T.6-83
Table T.6-12 Criticality Analysis Results for Damaged Fuel (4 Assemblies) T.6-84
Table T.6-13 Criticality Analysis Results for Damaged Fuel (16 Assemblies) T.6-86
Table T.6-14 Criticality Results T.6-88
Table T.6-15 Benchmarking Results T.6-89
Table T.6-16 USL-1 Results T.6-92
Table T.6-17 USL Determination for Criticality Analysis T.6-93
Table T.9-1 Boron Content Borated Aluminum (90% B10 Credit) T.9-14
Table T.9-2 Specified Boron Carbide Areal Density Metal Matrix Composites (90% B10 Credit) T.9-15
Table T.9-3 Specified B10 Areal Density Boral® (75% B10 credit) T.9-16
Table T.10-1 Occupational Exposure Summary, 61BTH System T.10.10
Table T.10-2 Total Annual Exposure, 61BTH within HSM-H T.10.11
Table T.10-3 Total Annual Exposure, 61BTH within HSM Model 102 ..... T.10.12
Table T.10-4 Total Annual Exposure, 61BTH within HSM Model 80 ..... T.10.13
Table T.10-5 HSM-H Gamma-Ray Spectrum Calculation Results T.10.14
Table T.10-6 HSM-H Neutron Spectrum Calculation Results T.10.14
Table T.10-7 HSM Model 102 Gamma-Ray Spectrum Calculation Results T.10.15
Table T.10-8 HSM Model 102 Neutron Spectrum Calculation Results T.10.16
Table T.10-9 Summary of ISFSI Surface Activities, 61BTH DSC within HSM-H T.10.17
Table T.10-10 Summary of ISFSI Surface Activities, 61BTH DSC within HSM Model 102 ..... T.10.18
Table T.10-11 MCNP Front Detector Dose Rates for 2x10 Array, 61BTH DSC within HSM-H T.10.19
Table T.10-12 MCNP Back Detector Dose Rates for the Two 1x10 Arrays, 61BTH DSC within HSM-H T.10.20
Table T.10-13 MCNP Side Detector Dose Rates, 61BTH DSC within HSM-H T.10.21
Table T.10-14 MCNP Front Detector Dose Rates for the 2x10 Array, 61BTH DSC within HSM Model 102 ..... T.10.22
Table T.10-15 MCNP Back Detector Dose Rates for the Two 1x10 Arrays, 61BTH DSC within HSM Model 102 ..... T.10.23

Table T.10-16 MCNP Side Detector Dose Rates, 61BTH DSC within HSM Model 102 ..... T.10.24
Table T.10-17 MCNP Front Detector Dose Rates for 2x10 Array, 61BTH DSC within HSM Model 80 ..... T.10.25
Table T.10-18 MCNP Back Detector Dose Rates for the Two 1x10 Arrays, 61BTH DSC within HSM Model 80 ..... T.10.26
Table T.10-19 MCNP Side Detector Dose Rates, 61BTH DSC within HSM Model 80.... T.10.27
Table T.11-1 Comparison of Total Dose Rates for HSM with and without Adjacent HSM Shielding Effects T.11-13
Table T.11-2 Calculated Accident Dose Rates on the Side of the OS197FC-B TC T.11-14

LIST OF FIGURES

		Page
Figure T.1-1	NUHOMS®-61BTH DSC (Shown With Hold Down Ring Option)	T.1-14
Figure T.1-2	NUHOMS® 61BTH Top Grid Assembly	T.1-15
Figure T.1-3	Cross-Sectional View of the NUHOMS® 61BTH Type 2 DSC Basket	T.1-16
Figure T.1-4	NUHOMS® OS197FC-B TC Top Lid (Bottom View)	T.1-17
Figure T.2-1	Heat Load Zoning Configuration No. 1 for Type 1 or Type 2 61BTH DSCs	T.2-34
Figure T.2-2	Heat Load Zoning Configuration No. 2 for Type 1 or Type 2 61BTH DSCs	T.2-35
Figure T.2-3	Heat Load Zoning Configuration No. 3 for Type 1 or Type 2 61BTH DSCs	T.2-36
Figure T.2-4	Heat Load Zoning Configuration No. 4 for Type 1 or Type 2 61BTH DSCs	T.2-37
Figure T.2-5	Heat Load Zoning Configuration No. 5 for Type 2 61BTH DSC	T.2-38
Figure T.2-6	Heat Load Zoning Configuration No. 6 for Type 2 61BTH DSC	T.2-39
Figure T.2-7	Heat Load Zoning Configuration No. 7 for Type 2 61BTH DSC	T.2-40
Figure T.2-8	Heat Load Zoning Configuration No. 8 for Type 2 61BTH DSC	T.2-41
Figure T.2-9	Location of Damaged Fuel Assemblies Inside 61BTH DSC	T.2-42
Figure T.3.1-1	61BTH DSC Confinement Boundary	T.3.1-10
Figure T.3.4-1	Potential Versus pH Diagram for Aluminum-Water System	T.3.4-24
Figure T.3.4-2	Thermal Stress Analysis Geometry	T.3.4-25
Figure T.3.4-3	Bounding Basket Radial Temperature Polynomial Curve	T.3.4-26
Figure T.3.4-4	Type 1 Basket Radial Temperature Polynomial Curves – Vacuum Drying Conditions	T.3.4-27
Figure T.3.4-5	Type 2 Basket Radial Temperature Polynomial Curves – Vacuum Drying Conditions	T.3.4-28
Figure T.3.5-1	Variation of Modulus of Elasticity and Yield Stress with Temperature	T.3.5-16
Figure T.3.5-2	Location of Fuel Assemblies vs. Basket during 75g Side Drop	T.3.5-17
Figure T.3.5-3	Finite Element Model for Side Drop Analysis	T.3.5-18
Figure T.3.5-4	BWR 9x9 (Siemens, QFA) Fuel Assembly - Bending Stress at 75g (Side Drop) (Bottom-most Rod)	T.3.5-19
Figure T.3.5-5	Finite Element Model for Bottom End Drop Analysis	T.3.5-20
Figure T.3.5-6	Bottom End Drop Model Shown with Initial Bowing of 0.015 in., – BWR 9x9 Siemens, QFA	T.3.5-21
Figure T.3.5-7	BWR 9x9 (Siemens, QFA) - 0.015 Inch Bowing - Lateral Displacements at Midspans of Bottom Three Spans (Bottom End Drop Model)	T.3.5-22
Figure T.3.5-8	BWR 9x9 (Siemens, QFA - 0.015 Inch Bowing - Axial Stress at 0° (Span 1) (Bottom End Drop Model)	T.3.5-23
Figure T.3.5-9	BWR 9x9 (Siemens, QFA) - 0.039 Inch Bowing - Boundary Conditions (Bottom End Drop Model)	T.3.5-24
Figure T.3.5-10	BWR 9x9 (Siemens, QFA) - 0.039 Inch Bowing – Lateral Displacement at the Midspans of the Bottom Three Spans (Bottom End Drop Model)	T.3.5-25

Figure T.3.5-11 BWR 9x9 (Siemens, QFA) - 0.039 Inch Bowing - Axial Stress at 0° (Span 1) (Bottom End Drop Model) T.3.5-26
Figure T.3.5-12 BWR 9x9 (Siemens, QFA) -0.039 Inch Bowing - Axial Plastic Strain at 0° (Span 1) (Bottom End Drop Model) T.3.5-27
Figure T.3.6-1 Type 1 Finite Element Model – Full Basket Section T.3.6-42
Figure T.3.6-2 Type 2 Finite Element Model – Full Basket Section T.3.6-43
Figure T.3.6-3 Finite Element Model – Inner Boxes T.3.6-44
Figure T.3.6-4 Finite Element Model – Outer Boxes T.3.6-45
Figure T.3.6-5 Finite Element Model – Rails (Type 1 Basket) T.3.6-46
Figure T.3.6-6 Finite Element Model – Rails (Type 2 Basket) T.3.6-47
Figure T.3.6-7 NUHOMS®-61BTH Basket Drop Orientations 45°, 60°, 90°, 161.5°, 180° T.3.6-48
Figure T.3.6-8 Gap Sizes between Basket Rails and Canister Inner Surfaces T.3.6-49
Figure T.3.6-9 Gap Sizes Between Canister Outer Surface and Cask Inner Surfaces T.3.6-50
Figure T.3.6-10 Finite Element Model – Canister & Gaps T.3.6-51
Figure T.3.6-11 Finite Element Model – Canister & Gaps, Enlarged View T.3.6-52
Figure T.3.6-12 Type 1 Basket, Membrane Stress Intensity (psi) (Handling / Transfer Load - 2g axial + 2g transverse + 2g vertical) T.3.6-53
Figure T.3.6-13 Type 1 Basket, Membrane + Bending Stress Intensity (psi) (Handling / Transfer Load - 2g axial + 2g transverse + 2g vertical) T.3.6-54
Figure T.3.6-14 Type 1 Rail, Membrane Stress Intensity (psi) (Handling / Transfer Load - 2g axial + 2g transverse + 2g vertical) T.3.6-55
Figure T.3.6-15 Type 1 Rail, Membrane + Bending Stress Intensity (psi) (Handling / Transfer Load - 2g axial + 2g transverse + 2g vertical) T.3.6-56
Figure T.3.6-16 Type 1 Canister Shell, Membrane Stress Intensity (psi) (Handling / Transfer Load - 2g axial + 2g transverse + 2g vertical) T.3.6-57
Figure T.3.6-17 Type 1 Canister Shell, Membrane + Bending Stress Intensity (psi) (Handling / Transfer Load - 2g axial + 2g transverse + 2g vertical) T.3.6-58
Figure T.3.6-18 Type 2 Basket Membrane Stress Intensity (psi) (Handling/Transfer Load – 2g axial + 2g transverse + 2g vertical) T.3.6-59
Figure T.3.6-19 Type 2 Basket Membrane + Bending Stress Intensity (psi) (Handling/Transfer Load – 2g axial + 2g transverse + 2g vertical) T.3.6-60
Figure T.3.6-20 Type 2 SST Rail Membrane Stress Intensity (psi) (Handling/Transfer Load – 2g axial + 2g transverse + 2g vertical) T.3.6-61
Figure T.3.6-21 Type 2 SST Rail Membrane + Bending Stress Intensity (psi) (Handling/Transfer Load – 2g axial + 2g transverse + 2g vertical) T.3.6-62
Figure T.3.6-22 Type 2 Canister Shell, Membrane Stress Intensity (psi) (Handling /Transfer Load – 2g axial + 2g transverse + 2g vertical) T.3.6-63
Figure T.3.6-23 Type 2 Canister Shell, Membrane + Bending Stress Intensity (psi) (Handling /Transfer Load – 2g axial + 2g transverse + 2g vertical) T.3.6-64
Figure T.3.6-24 Type 1 Basket, Membrane Stress Intensity (psi) (Orientation / Storage Load – 2g axial + 2g transverse + 2g vertical) T.3.6-65
Figure T.3.6-25 Type 1 Basket, Membrane + Bending Stress Intensity (psi) (Orientation / Storage Load – 2g axial + 2g transverse + 2g vertical) T.3.6-66
Figure T.3.6-26 Type 1 Rail, Membrane Stress Intensity (psi) (Orientation / Storage Load – 2g axial + 2g transverse + 2g vertical) T.3.6-67

Figure T.3.6-27 Type 1 Rail, Membrane + Bending Stress Intensity (psi) (Orientation / Storage Load – 2g axial + 2g transverse + 2g vertical) T.3.6-68
Figure T.3.6-28 Type 1 Canister Shell, Membrane Stress Intensity (psi) (Orientation / Storage Load – 2g axial + 2g transverse + 2g vertical) T.3.6-69
Figure T.3.6-29 Type 1 Canister Shell, Membrane +Bending Stress Intensity (psi) (Orientation / Storage Load – 2g axial + 2g transverse + 2g vertical) T.3.6-70
Figure T.3.6-30 Type 2 Basket, Membrane Stress Intensity (psi) (Orientation / Storage Load – 2g axial + 2g transverse + 2g vertical) T.3.6-71
Figure T.3.6-31 Type 2 Basket, Membrane + Bending Stress Intensity (psi) (Orientation / Storage Load – 2g axial + 2g transverse + 2g vertical) T.3.6-72
Figure T.3.6-32 Type 2 SST Rail, Membrane Stress Intensity (psi) (Orientation / Storage Load – 2g axial + 2g transverse + 2g vertical) T.3.6-73
Figure T.3.6-33 Type 2 SST Rail, Membrane + Bending Stress Intensity (psi) (Orientation / Storage Load – 2g axial + 2g transverse + 2g vertical) T.3.6-74
Figure T.3.6-34 Type 2 Canister Shell, Membrane Stress Intensity (psi) (Orientation / Storage Load – 2g axial + 2g transverse + 2g vertical) T.3.6-75
Figure T.3.6-35 Type 2 Canister Shell, Membrane + Bending Stress Intensity (psi) (Orientation / Storage Load – 2g axial + 2g transverse + 2g vertical) T.3.6-76
Figure T.3.6-36 Post Test Appearance of the Test Fuel Rods in Tests HBO-1, JM-4 and JM-14 ..... T.3.6-77
Figure T.3.6-37 Morphologies of Cracks at 325 °C T.3.6-78
Figure T.3.6-38 Schematic Illustration of Microstructure, Sequence of Failure and Key Material Parameters Modeled for HBO-1 ..... T.3.6-79
Figure T.3.6-39 SEM Micrograph of a Crack Tip in the C6 Rod T.3.6-80
Figure T.3.6-40 Overlapping Cracks in A2 Rod T.3.6-81
Figure T.3.6-41 Burst Opening Region of Specimen from Rod KJE051 ..... T.3.6-82
Figure T.3.6-42 Fracture Behavior of Claddings by the High Pressurization-Rate Burst Test T.3.6-83
Figure T.3.6-43 Fracture Geometry #1 - Through-Wall Circumferential Crack in Cylinder under Bending T.3.6-84
Figure T.3.6-44 Fracture Geometry #2 - Ruptured Section Configurations T.3.6-85
Figure T.3.6-45 Stress Intensity Factor Solutions for Several Specimen Configurations T.3.6-86
Figure T.3.7-1 90° and 180° Orientation Side Drop – Pressure Distribution T.3.7-38
Figure T.3.7-2 45° Orientation Side Drop – Pressure Distribution T.3.7-39
Figure T.3.7-3 60° Orientation Side Drop – Pressure Distribution T.3.7-40
Figure T.3.7-4 161.5° Orientation Side Drop – Pressure Distribution T.3.7-41
Figure T.3.7-5 45° Orientation Side Drop – Type 1 Basket, P_m (76.25g) T.3.7-42
Figure T.3.7-6 45° Orientation Side Drop – Type 1 Basket, $P_m + P_b$ (76.25g) T.3.7-43
Figure T.3.7-7 45° Orientation Side Drop – Type 1 Rails, P_m (76.2g) T.3.7-44
Figure T.3.7-8 45° Orientation Side Drop – Type 1 Rails, $P_m + P_b$ (75.5g) T.3.7-45
Figure T.3.7-9 45° Orientation Side Drop – Type 1 Canister, P_m (76.25g) T.3.7-46
Figure T.3.7-10 45° Orientation Side Drop – Type 1 Canister, $P_m + P_b$ (76.25g) T.3.7-47
Figure T.3.7-11 60° Orientation Side Drop – Type 1 Basket, P_m (75.5g) T.3.7-48
Figure T.3.7-12 60° Orientation Side Drop – Type 1 Basket, $P_m + P_b$ (75.5g) T.3.7-49
Figure T.3.7-13 60° Orientation Side Drop – Type 1 Rails, P_m (75.5g) T.3.7-50

Figure T.3.7-14 60° Orientation Side Drop – Type 1 Rails, $P_m + P_b$ (75.5g) T.3.7-51
Figure T.3.7-15 60° Orientation Side Drop – Type 1 Canister, P_m (75.5g) T.3.7-52
Figure T.3.7-16 60° Orientation Side Drop – Type 1 Canister, $P_m + P_b$ (75.5g) T.3.7-53
Figure T.3.7-17 90° Orientation Side Drop – Type 1 Basket, P_m (75.5g) T.3.7-54
Figure T.3.7-18 90° Orientation Side Drop – Type 1 Basket, $P_m + P_b$ (75.5g) T.3.7-55
Figure T.3.7-19 90° Orientation Side Drop – Type 1 Rails, P_m (75.5g) T.3.7-56
Figure T.3.7-20 90° Orientation Side Drop – Type 1 Rails, $P_m + P_b$ (75.5g) T.3.7-57
Figure T.3.7-21 90° Orientation Drop – Type 1 Canister, P_m (75.5g) T.3.7-58
Figure T.3.7-22 90° Orientation Side Drop– Type 1 Canister, $P_m + P_b$ (75.5g) T.3.7-59
Figure T.3.7-23 161.5° Orientation Side Drop – Type 1 Basket, P_m (76.0g) T.3.7-60
Figure T.3.7-24 161.5° Orientation Side Drop – Type 1 Basket, $P_m + P_b$ (76.0g) T.3.7-61
Figure T.3.7-25 161.5° Orientation Side Drop – Type 1 Rails, P_m (76.0g) T.3.7-62
Figure T.3.7-26 161.5° Orientation Side Drop – Type 1 Rails, $P_m + P_b$ (76.0g) T.3.7-63
Figure T.3.7-27 161.5° Orientation Side Drop – Type 1 Canister, P_m (76.0g) T.3.7-64
Figure T.3.7-28 161.5° Orientation Side Drop – Type 1 Canister, $P_m + P_b$ (76.0g) T.3.7-65
Figure T.3.7-29 180° Orientation Side Drop – Type 1 Basket, P_m (75.5g) T.3.7-66
Figure T.3.7-30 180° Orientation Side Drop – Type 1 Basket, $P_m + P_b$ (75.5g) T.3.7-67
Figure T.3.7-31 180° Orientation Side Drop – Type 1 Rails, P_m (75.5g) T.3.7-68
Figure T.3.7-32 180° Orientation Side Drop – Type 1 Rails, $P_m + P_b$ (75.5g) T.3.7-69
Figure T.3.7-33 180° Orientation side Drop – Type 1 Canister, P_m (75.5g) T.3.7-70
Figure T.3.7-34 180° Orientation Side Drop – Type 1 Canister, $P_m + P_b$ (75.5g) T.3.7-71
Figure T.3.7-35 45° Orientation – Type 2 Basket, P_m (76.25G) T.3.7-72
Figure T.3.7-36 45° Orientation – Type 2 Basket, $P_m + P_b$, Top (76.25G) T.3.7-73
Figure T.3.7-37 45° Orientation – Type 2 Rails, P_m (76.25G) T.3.7-74
Figure T.3.7-38 45° Orientation – Type 2 Rails, $P_m + P_b$, Top (76.25G) T.3.7-75
Figure T.3.7-39 45° Orientation – Type 2 Canister, P_m (76.25G) T.3.7-76
Figure T.3.7-40 45° Orientation – Type 2 Canister, $P_m + P_b$, Bottom (76.25G) T.3.7-77
Figure T.3.7-41 60° Orientation – Type 2 Basket, P_m (75.5G) T.3.7-78
Figure T.3.7-42 60° Orientation – Type 2 Basket, $P_m + P_b$, Top (75.5G) T.3.7-79
Figure T.3.7-43 60° Orientation – Type 2 Rails, P_m (75.5G) T.3.7-80
Figure T.3.7-44 60° Orientation – Type 2 Rails, $P_m + P_b$, Top (75.5G) T.3.7-81
Figure T.3.7-45 60° Orientation – Type 2 Canister, P_m (75.5G) T.3.7-82
Figure T.3.7-46 60° Orientation – Type 2 Canister, $P_m + P_b$, Top (75.5G) T.3.7-83
Figure T.3.7-47 90° Orientation – Type 2 Basket, P_m (75.5G) T.3.7-84
Figure T.3.7-48 90° Orientation – Type 2 Basket, $P_m + P_b$, Top (75.5G) T.3.7-85
Figure T.3.7-49 90° Orientation – Type 2 Rails, P_m (75.5G) T.3.7-86
Figure T.3.7-50 90° Orientation – Type 2 Rails, $P_m + P_b$, Top (75.5G) T.3.7-87
Figure T.3.7-51 90° Orientation – Type 2 Canister, P_m (75.5G) T.3.7-88
Figure T.3.7-52 90° Orientation – Type 2 Canister, $P_m + P_b$, Bottom (75.5G) T.3.7-89
Figure T.3.7-53 161.5° Orientation – Type 2 Basket, P_m (76.0G) T.3.7-90
Figure T.3.7-54 161.5° Orientation – Type 2 Basket, $P_m + P_b$, Top (76.0G) T.3.7-91
Figure T.3.7-55 161.5° Orientation – Type 2 Rails, P_m (76.0G) T.3.7-92
Figure T.3.7-56 161.5° Orientation – Type 2 Rails, $P_m + P_b$, Top (76.0G) T.3.7-93
Figure T.3.7-57 161.5° Orientation – Type 2 Canister, P_m (76.0G) T.3.7-94
Figure T.3.7-58 161.5° Orientation – Type 2 Canister, $P_m + P_b$, Top (76.0G) T.3.7-95

Figure T.3.7-59 180° Orientation – Type 2 Basket, P_m (75.5G) T.3.7-96
Figure T.3.7-60 180° Orientation – Type 2 Basket, $P_m + P_b$, Top (75.5G) T.3.7-97
Figure T.3.7-61 180° Orientation – Type 2 Rails, P_m (75.5G) T.3.7-98
Figure T.3.7-62 180° Orientation – Type 2 Rails, $P_m + P_b$, Top (75.5G) T.3.7-99
Figure T.3.7-63 180° Orientation – Type 2 Canister, P_m (75.5G) T.3.7-100
Figure T.3.7-64 180° Orientation – Type 2 Canister, $P_m + P_b$, Top (75.5G) T.3.7-101
Figure T.3.7-65 NUHOMS®-61BTH Basket Drop Orientations T.3.7-102
Figure T.3.7-66 Finite Element Model – Full (Type 1 Basket) T.3.7-103
Figure T.3.7-67 Finite Element Model – Full (Type 2 Basket) T.3.7-104
Figure T.3.7-68 Finite Element Model - Inner Boxes T.3.7-105
Figure T.3.7-69 Finite Element Model - Outer Boxes T.3.7-106
Figure T.3.7-70 Finite Element Model – Rails (Type 1 Basket) T.3.7-107
Figure T.3.7-71 Finite Element Model – Rails (Type 2 Basket) T.3.7-108
Figure T.3.7-72 Finite Element Model - Canister & Gaps T.3.7-109
Figure T.3.7-73 Finite Element Model - Canister & Gaps (Enlarged View) T.3.7-110
Figure T.3.7-74 Finite Element Model – Fuel Assembly Channel Plates T.3.7-111
Figure T.3.7-75 0° Orientation - Couplings T.3.7-112
Figure T.3.7-76 30° Orientation - Couplings T.3.7-113
Figure T.3.7-77 45° Orientation - Couplings T.3.7-114
Figure T.3.7-78 0° Orientation – Loading Condition T.3.7-115
Figure T.3.7-79 30° Orientation – Loading Condition T.3.7-116
Figure T.3.7-80 45° Orientation – Loading Condition T.3.7-117
Figure T.3.7-81 Type 1 Basket 0° Side Drop – Last Converged Deformed Shape (79.27g) T.3.7-118
Figure T.3.7-82 Type 1 Basket 30° Side Drop – Last Converged Deformed Shape (80.85g) T.3.7-119
Figure T.3.7-83 Type 1 Basket 45° Side Drop – Last Converged Deformed Shape (80.36g) T.3.7-120
Figure T.3.7-84 Type 2 Basket 0° Side Drop – Last Converged Deformed Shape (90.05g) T.3.7-121
Figure T.3.7-85 Type 2 Basket 30° Side Drop – Last Converged Deformed Shape (87.60g) T.3.7-122
Figure T.3.7-86 Type 2 Basket 45° Side Drop – Last Converged Deformed Shape (81.04g) T.3.7-123
Figure T.3.7-87 NUHOMS®-61BTH, LS-DYNA Finite Element Model T.3.7-124
Figure T.3.7-88 Input Acceleration Time History T.3.7-125
Figure T.3.7-89 Von-Mises Stress Distribution, 75g Peak Acceleration T.3.7-126
Figure T.3.7-90 Von-Mises Stress Distribution, 85g Peak Acceleration T.3.7-127
Figure T.3.7-91 Von-Mises Stress Distribution, 95g Peak Acceleration T.3.7-128
Figure T.4-1 HSM-H Air Flow Diagram T.4-79
Figure T.4-2 Convection Regions around 61BTH DSC in the HSM-H T.4-80
Figure T.4-3 61BTH DSC Shell Assembly in HSM-H Finite Element Model T.4-81
Figure T.4-4 HSM-H Component Temperature Distributions for 61BTH Type 2 DSC, 31.2 kW, 100°F Ambient T.4-82
Figure T.4-5 HSM-H Component Temperature Distributions for 61BTH Type 2 DSC, 31.2 kW, 117°F Ambient T.4-83

Figure T.4-6 HSM-H Component Temperature Distributions for 61BTH Type 2 DSC, 31.2 kW, @ 40 hours of Blocked Vents, 117°F Ambient T.4-84
Figure T.4-7 HSM-H Component Temperature Time Histories for 61BTH Type 2 DSC, 31.2 kW, Blocked Vents Accident Condition, 117°F Ambient T.4-85
Figure T.4-8 Cone Adapter for Air Entrance at Ram Access Cover T.4-86
Figure T.4-9 Illustration of Wedge Segments at Bottom of OS197FC-B T.4-87
Figure T.4-10 OS197FC-B TC Lid with Slots for Air Exhaust Plan, and Isometric Views T.4-88
Figure T.4-11 Perspective View of OS197FC-B TC / 61BTH DSC Shell Thermal Model T.4-89
Figure T.4-12 Perspective View of 61BTH DSC Shell, Ends, and Fuel Basket Thermal Model T.4-90
Figure T.4-13 Perspective View of Thermal Model for OS197FC-B Closure Lid & NS-3 ..... T.4-91
Figure T.4-14 OS197FC-B TC Steady State Temperature Distribution, Vertical Transfer of Type 1 DSC with 22.0 kW Heat Load, No Insolation at 120°F Ambient T.4-92
Figure T.4-15 OS197FC-B TC Temperature Distribution @ 28 hours Vertical Transfer of Type 2 DSC with 31.2 kW Heat Load, No Insolation at 120°F Ambient T.4-93
Figure T.4-16 Horizontal Transfer Transient Temperature Response of Type 1 DSC with 22.0 kW Heat Load, Loss of Neutron Shield and Air Circulation Accident at 100°F Ambient T.4-94
Figure T.4-17 Vertical Transfer Transient Temperature Response of 61BTH Type 2 DSC with 31.2 kW Heat Load, No Insolation at 120°F Ambient T.4-95
Figure T.4-18 Horizontal Transfer Transient Temperature Response of Type 2 DSC with 31.2 kW Heat Load, Insolation at 100°F Ambient T.4-96
Figure T.4-19 Horizontal Transfer Transient Temperature Response of Type 2 DSC with 31.2 kW Heat Load, Loss of Air Circulation Accident, Insolation at 100°F Ambient T.4-97
Figure T.4-20 Horizontal Transfer Transient Temperature Response of Type 2 DSC with 31.2 kW Heat Load, Loss of Neutron Shield and Air Circulation Accident at 100°F Ambient T.4-98
Figure T.4-21 Horizontal Transfer Transient Temperature Response of Type 2 DSC with 31.2 kW Heat Load, 15-minute Fire Accident at 117°F Ambient T.4-99
Figure T.4-22 61BTH Type 1 DSC Thermal ANSYS Model T.4-100
Figure T.4-23 61BTH DSC Thermal ANSYS Model Shell and End Assemblies T.4-101
Figure T.4-24 61BTH DSC Thermal ANSYS Model Basket Components, Fuel Assemblies, and Neutron Absorbers T.4-102
Figure T.4-25 61BTH DSC Thermal ANSYS Model Fuel Compartments, R45 and R90 Rails T.4-103
Figure T.4-26 61BTH Type 1 DSC Thermal ANSYS Model Typical Radial and Transverse Gaps T.4-104
Figure T.4-27 61BTH Type 2 DSC Thermal ANSYS Model Typical Radial and Transverse Gaps T.4-105

Figure T.4-28 61BTH Type 1 and Type 2 DSC Thermal ANSYS Models Typical Axial Gaps at Both Ends T.4-106
Figure T.4-29 61BTH Type 1 DSC (22 kW) Temperature Distribution for Normal and Off-Normal Storage Conditions T.4-107
Figure T.4-30 61BTH Type 1 DSC (22 kW) Temperature Distribution for Normal and Off-Normal Transfer Conditions T.4-108
Figure T.4-31 61BTH Type 1 DSC (22 kW) Temperature Distribution for Accident Storage and Transfer Conditions T.4-109
Figure T.4-32 61BTH Type 1 DSC (22 kW) Temperature Distribution for Vacuum Drying Steady State Conditions T.4-110
Figure T.4-33 61BTH Type 2 DSC (31.2 kW) Temperature Distribution for Normal and Off-Normal Storage Conditions T.4-111
Figure T.4-34 61BTH Type 2 DSC (31.2 kW) Temperature Distribution for Normal and Off-Normal Transfer Conditions T.4-112
Figure T.4-35 FANP9 9x9-2 Fuel Assembly Finite Element Model T.4-113
Figure T.4-36 Transverse Fuel Effective Thermal Conductivity for FANP9 9x9-2 and GE4 Fuel Assemblies in Helium T.4-114
Figure T.4-37 Applied Axial Heat Flux Profile T.4-115
Figure T.5-1 Heat Zone Configuration Utilized for Model 102 Evaluation T.5-130
Figure T.5-2 ANISN OS197 TC Model T.5-131
Figure T.5-3 61BTH DSC Within HSM-H, Side View at Centerline of DSC T.5-132
Figure T.5-4 61BTH DSC Within HSM-H, Head-on View at Z=0 ..... T.5-133
Figure T.5-5 61BTH DSC Within HSM-H, Head-on View Showing Top Vents T.5-134
Figure T.5-6 61BTH DSC Within HSM-H, Head-on View at Lid End of DSC (Z=225 cm) T.5-135
Figure T.5-7 61BTH DSC Within HSM-H, Head-on View at Bottom End of DSC (Z=-225 cm) T.5-136
Figure T.5-8 61BTH DSC within HSM Model 102, Side View at Centerline of DSC T.5-137
Figure T.5-9 61BTH DSC within HSM Model 102, Head-on View at Z=-60 ..... T.5-138
Figure T.5-10 61BTH DSC within HSM Model 102, Horizontal Cut through Top Vents View at 1 Meter above DSC Axis T.5-139
Figure T.5-11 61BTH Type 1 DSC Within OS197FC-B TC, Axial View of Transfer Model T.5-140
Figure T.5-12 61BTH Type 1 DSC Within OS197FC-B TC, Top View of Transfer Model Showing Cask Lid with Gap, Top Nozzle, and Plenum T.5-141
Figure T.5-13 61BTH Type 1 DSC Within OS197FC-B TC, Bottom View of Transfer Model Showing Cask Bottom and Bottom Nozzle T.5-142
Figure T.5-14 61BTH DSC within OS197FC-B TC, Radial Cut View of Transfer Models Showing Fuel Locations T.5-143
Figure T.5-15 61BTH DSC within OS197FC-B TC, Longitudinal Cut View of Transfer Model Showing Undamaged and Normal Fuel Locations and Damaged Fuel Height T.5-144
Figure T.5-16 61BTH DSC within OS197FC-B TC, Radial Cut View of Transfer Models Showing Undamaged and Normal Fuel Locations T.5-145
Figure T.5-17 HSM-H with 61BTH DSC, Gamma Radiation Dose Rate along HSM-H Front Centerline in Vertical Elevation T.5-146

Figure T.5-18 HSM-H with 61BTH DSC, Neutron Radiation Dose Rate along HSM-H Front Centerline in Vertical Elevation T.5-147
Figure T.5-19 HSM-H with 61BTH DSC, Gamma Radiation Dose Rate at Roof Centerline T.5-148
Figure T.5-20 HSM-H with 61BTH DSC, Neutron Dose Rate at Roof Centerline T.5-149
Figure T.5-21 HSM-H with 61BTH DSC, Side Shield Wall Surface at DSC Centerline Gamma Radiation Dose Rate T.5-150
Figure T.5-22 HSM-H with 61BTH DSC, Side Shield Wall Surface at DSC Centerline Neutron Radiation Dose Rate T.5-151
Figure T.5-23 OS197FC-B TC with 61BTH DSC, Side Surface Dose Rate, Normal Conditions T.5-152
Figure T.5-24 OS197FC-B TC with 61BTH DSC, Top Surface Dose Rate, Normal Conditions T.5-153
Figure T.5-25 OS197FC-B TC with 61BTH DSC, Bottom Surface Dose Rate, Normal Conditions T.5-154
Figure T.6-1 NUHOMS®-61BTH Type 1 DSC Radial Cross Section T.6-94
Figure T.6-2 NUHOMS®-61BTH Type 2 DSC Radial Cross Section T.6-95
Figure T.6-3 Criticality Calculational KENO Model for Intact Fuel T.6-96
Figure T.6-4 Double Break – Beyond Poison Plates, Aluminum in DSC T.6-97
Figure T.6-5 Design Basis Damaged Assembly Loading – 4 Assemblies T.6-98
Figure T.6-6 Design Basis Damaged Assembly Loading – 16 Assemblies T.6-99
Figure T.8.1-1 NUHOMS® System Loading Operations Flow Chart T.8-13
Figure T.8.2-1 NUHOMS® System Retrieval Operations Flow Chart T.8-21
Figure T.10-1 Annual Exposure from the ISFSI as a Function of Distance, 61BTH DSC within HSM-H T.10-28
Figure T.10-2 Annual Exposure from the ISFSI as a Function of Distance, 61BTH DSC within HSM-Model 102 ..... T.10-29
Figure T.10-3 Annual Exposure from the ISFSI as a Function of Distance, 61BTH DSC within HSM-Model 80 ..... T.10-30
Figure T.11-1 HSM-H Dimensions for Missile Impact Stability Analysis T.11-15

T.4 Thermal Evaluation

T.4.1 Discussion

This chapter presents the thermal evaluations which demonstrate that the NUHOMS®-61BTH system meets the thermal requirements of 10CFR72 for the dry storage of spent fuel. The NUHOMS®-61BTH system is designed to passively reject decay heat during storage and transfer for normal, off-normal and accident conditions while maintaining temperatures and pressures within specified regulatory limits.

Several thermal design criteria are established for the thermal analysis of the 61BTH DSC basket as discussed below.

- Maximum temperatures of the confinement structural components must not adversely affect the confinement function,
- Maximum fuel cladding temperature limit of 400°C (752°F) is applicable to normal conditions of storage and all short term fuel loading and transfer operations including vacuum drying and helium backfilling of the 61BTH DSC per Interim Staff Guidance (ISG) No. 11, Revision 3 [4.15]. In addition, ISG-11 does not permit thermal cycling of the fuel cladding with temperature differences greater than 65°C (117°F) during drying and backfilling operations,
- Maximum fuel cladding temperature limit of 570°C (1058°F) is applicable to accidents or off-normal thermal transients [4.15],
- The maximum DSC cavity internal design pressures are as follows:
  - For 61BTH Type 1 DSC, the maximum design pressures for normal, off-normal and accident conditions are 10 psig, 20 psig, and 65 psig, respectively,
  - For 61BTH Type 2 DSC, the maximum design pressures for normal, off-normal and accident conditions are 15 psig, 20 psig, and 120 psig, respectively,
- A total of eight (8) Heat Load Zoning Configurations (HLZCs) are allowed for the 61BTH DSCs as shown in Figure T.2-1 through Figure T.2-8.

A summary of the two 61BTH DSC configurations analyzed in this chapter is shown below:

DSC Type	61BTH Type 1 DSC		61BTH Type 2 DSC	
Maximum Heat Load (kW)	19.4	22.0	27.4	31.2
Heat Load Zoning Configuration (1)	#3, #4	#1, #2	#8	#5, #6, #7
Neutron Absorber Material	Borated Aluminum or BORAL® or MMC	Borated Aluminum	Borated Aluminum or BORAL® or MMC	Borated Aluminum
Top Grid / Holddown Ring	Original 61BT or Alternate Designs		Alternate Designs	
R45 Rail Design	Steel Rail and Aluminum Shim		Steel Rail and 5/8" Aluminum Plates (on 3 sides)	
R90 Rail Design	Steel Rail and Aluminum Shim		Solid Aluminum Rail and 1/4" Steel Plate	
Transfer Cask	OS197, OS197H or OS197FC-B		OS197FC-B	
Storage Module	HSM(2) or HSM-H		HSM-H	

Notes:

(1) Refer to Section T.4.6.1 for a discussion on the applicability of Heat Load Zoning Configuration (HLZC) for each DSC type.

(2) Models 80, 102, 152, and 202

For the 61BTH Type 1 and Type 2 DSCs, sensitivity thermal analyses for the cask in vertical orientation when inside the fuel building at 120°F without insolation are performed to determine bounding configuration for thermal analyses.

The comparison of the sensitivity analysis results shows that for both the 61BTH Type 1 and Type 2 DSCs, the fuel cladding and component temperatures for the borated aluminum neutron absorber configurations with higher heat loads bound the corresponding temperatures for the BORAL® and MMC neutron absorber configurations with lower heat loads. Therefore, to bound the analysis results, a complete set of thermal analyses are required only for the borated aluminum neutron absorber option with higher heat loads for both 61BTH Type 1 and Type 2 DSCs.

The thermal evaluations presented herein include steady state and transient analyses of the thermal response of the NUHOMS®-61BTH system components to a defined set of thermal loading conditions. These loading conditions envelope the thermal conditions expected during all normal, off-normal, and postulated accident loading, transfer and dry storage operations for the design basis thermal conditions as defined in Section T.2. The applicable allowable temperatures are presented and comparisons are made with calculated temperatures as the basis for acceptance.

A description of the detailed analyses performed for the storage of 61BTH DSC under normal, off-normal, and accident conditions is provided in Section T.4.4 and for transfer is provided in Section T.4.5. Section T.4.6 describes the 61BTH DSC basket and fuel cladding analysis for storage and transfer conditions. The DSC cavity internal pressures are also discussed in Section T.4.6 for all conditions of storage and transfer. Section T.4.7 describes the evaluation performed for loading/unloading conditions. The thermal evaluation concludes that each of the two 61BTH Type 1 and Type 2 DSC configurations listed above meets all the design criteria.

The effective thermal conductivity of the fuel assemblies used in the 61BTH DSC thermal analysis is based on the conservative assumption of radiation and conduction heat transfer only, where any convection heat transfer is neglected. In addition, the lowest effective thermal conductivity among the fuel assemblies to be stored using 61BTH DSCs is selected as the basis for the thermal analysis. Section T.4.8 presents the calculations that determined the fuel assembly effective thermal conductivity in a helium or vacuum environment. The thermal analysis model conservatively neglects convection heat transfer in the basket region.

Although the NUHOMS® HSM is a proven design with extensive operational experience, the HSM-H incorporates several design variations to the basic HSM design to increase the module's thermal rating. The effectiveness of these design modifications was evaluated using a combination of computer (i.e., ANSYS finite element) modeling, and hand calculations.

The methodology used to evaluate the thermal performance of the HSM-H was validated by thermal tests performed on a 1:1 scale of an HSM-H mockup structure for heat loads varying from 32 to 44 kW [4.30].

The thermal tests showed that the HSM-H thermal analysis methodology described in Sections T.4.4.2 and T.4.4.3 conservatively predict the DSC shell and HSM-H component temperatures. Bounding values are used in Chapter T.3 for the thermal stress evaluation for these components.

T.4.2 Summary of Thermal Properties of Materials

The analyses performed herein use interpolated values where appropriate for intermediate temperatures. The interpolation assumes a linear relationship between the reported values. The use of linear interpolation between temperature values in the tables for determining intermediate value of property is justified by the near-linear behavior as a function of temperature for the range of interest.

The emissivities of the different materials used in the analyses are provided in the following table.

Component	Material	Fuel Assembly Effective Properties	TC and DSC Thermal Analysis	HSM-H Thermal Analysis
Fuel cladding	Zircaloy	0.74	-	-
Fuel compartment wall	Stainless steel	0.2	-	-
HSM roof and walls	Concrete	-	-	0.9
Heat Shield	Stainless steel	-	-	0.46(1)
Support structure	Carbon steel	-	-	0.55
DSC shell	Stainless steel	-	0.6	0.6
TC inner shell		-	0.6	-
Structural shell inner surface		-	0.6	-
TC exterior		-	0.6, 0.8(2)	-
TC top and bottom forgings		-	0.46(3)	-

Notes:
1. Used for surfaces of the side and top heat shields based on test report,
2. Used for all exterior surfaces of the cask during and after the 15-minute fire accident to account for the potential oxidation and sooting of the surfaces,
3. Used for the machined surfaces of the top and bottom forgings of the cask.

The tables below provide the thermal properties of materials used in the analysis of the NUHOMS®-61BTH DSC.

The effective thermal properties are the lowest calculated values among the various BWR fuel assembly types that may be stored in 61BTH DSC as described in Section T.4.8.

1. **Bounding BWR Fuel with Helium Backfill (from Section T.4.8)**

Temperature (°F)	Transverse Conductivity (Btu/min-in-°F)	Axial Conductivity (Btu/min-in-°F)	Density (lb_m/in^3)	Specific Heat (Btu/lb_m-°F)
200	2.618E-04	6.700E-04	0.103	0.0575
300	3.021E-04			
400	3.520E-04			
500	4.104E-04			
600	4.756E-04			
700	5.468E-04			
800	6.250E-04			

2. **Bounding BWR Fuel in Vacuum (from Section T.4.8)**

Temperature (°F)	Transverse Conductivity (Btu/min-in-°F)	Axial Conductivity (Btu/min-in-°F)	Density (lb_m/in^3)	Specific Heat (Btu/lb_m-°F)
200	8.693E-05	6.700E-04	0.103	0.0575
300	1.137E-04			
400	1.460E-04			
500	1.842E-04			
600	2.257E-04			
700	2.736E-04			
800	3.295E-04			

3. **Zircaloy [4.8]**

Temperature (°F)	Conductivity (Btu/min-in-°F)	Density (lb_m/in^3)	Specific Heat (Btu/lb_m-°F)
All	0.0100	0.237	0.0657

4. **UO_2 Fuel Pellet [4.8]**

Temperature (°F)	Conductivity (Btu/min-in-°F	Density (lb_m/in^3)	Specific Heat (Btu/lb_m-°F)
All	2.210E-3	0.396	0.05

5. Type 304 Stainless Steel [4.2]

Temperature (°F)	Conductivity (Btu/min-in-°F)	Density (lb_m/in^3)	Specific Heat (Btu/lb_m-°F)
70	0.0119	0.284	0.116
100	0.0121		0.117
150	0.0125		0.119
200	0.0129		0.122
250	0.0133		0.124
300	0.0136		0.125
350	0.0140		0.127
400	0.0144		0.129
450	0.0147		0.130
500	0.0151		0.131
550	0.0154		0.132
600	0.0157		0.133
650	0.0161		0.134
700	0.0164		0.135
750	0.0167		0.135
800	0.0169		0.135
850	0.0174		0.137
900	0.0176		0.137

6. Carbon Steel [4.2]

Temperature (°F)	Conductivity (Btu/min-in-°F)	Density (lb_m/in^3)	Specific Heat (Btu/lb_m-°F)
70	0.0488	0.284	0.103
100	0.0482		0.105
150	0.0474		0.108
200	0.0467		0.112
250	0.0457		0.115
300	0.0449		0.118
350	0.0439		0.121
400	0.0429		0.123
450	0.0421		0.125
500	0.0410		0.128
550	0.0400		0.130
600	0.0389		0.132
650	0.0379		0.135
700	0.0369		0.138
750	0.0360		0.141
800	0.0350		0.145
850	0.0340		0.149
900	0.0331		0.153

7. Aluminum, Type 1100 [4.2]

Temperature (°F)	Conductivity (Btu/min-in-°F)	Density (lb_m/in^3)	Specific Heat (Btu/lb_m-°F)
70	0.185	0.098	0.214
100	0.183		0.216
150	0.181		0.219
200	0.178		0.222
250	0.177		0.224
300	0.175		0.227
350	0.174		0.229
400	0.173		0.232
880	0.173 (*)		0.232 (*)

(*) For aluminum Type 1100 the calculated maximum temperatures do not exceed 880°F during transfer accident conditions. The assumption of constant conductivity value at 400°F for temperatures up to 880°F is justified since, for pure aluminum, the conductivity change is approximately 2.5% for range of 400°F – 880°F [4.11]. Therefore, this small change would have a negligible impact on thermal results.

8. Aluminum, Type 6061 [4.2]

Temperature (°F)	Conductivity (Btu/min-in-°F)	Density (lb_m/in^3)	Specific Heat (Btu/lb_m-°F)
70	0.133	0.098	0.213
100	0.135		0.215
150	0.136		0.218
200	0.138		0.221
250	0.139		0.223
300	0.140		0.226
350	0.141		0.228
400	0.142		0.230
880	0.142 (*)		0.230 (*)

(*) For aluminum Type 6061 the calculated maximum temperatures do not exceed 880°F during transfer accident conditions. The assumption of constant conductivity value at 400°F for temperatures up to 880°F is justified since, for pure aluminum, the conductivity change is approximately 2.5% for range of 400°F–880°F [4.11]. Therefore, this small change would have a negligible impact on thermal results.

9. ASTM B29 Lead [4.3, 4.16]

Temperature (°F)	Conductivity (Btu/min-in-°F)	Density (lb_m/in^3)	Specific Heat (Btu/lb_m-°F)
32	0.0279	0.41	0.03
212	0.0264		
572	0.0250		

10. NS-3 [4.12]

Temperature (°F)	Conductivity (Btu/min-in-°F)	Density (lb_m/in^3)	Specific Heat (Btu/lb_m-°F)
All	0.000678	0.0637	0.145

11. Air [4.4]

Temperature (°F)	Conductivity (Btu/min-in-°F)	Density (lb_m/in^3)	Specific Heat (Btu/lb_m-°F)	Dynamic Viscosity (lb_m/in-s)
-46	1.655E-05	5.551E-05	0.2402	8.366E-7
0	1.824E-05	4.995E-05	0.2401	9.115E-7
71	2.074E-05	4.323E-05	0.2403	1.020E-6
107	2.199E-05	4.049E-05	0.2405	1.072E-6
206	2.528E-05	3.445E-05	0.2415	1.210E-6
314	2.869E-05	2.964E-05	0.2432	1.347E-6
404	3.139E-05	2.655E-05	0.2451	1.454E-6
512	3.446E-05	2.360E-05	0.2479	1.576E-6
602	3.692E-05	2.160E-05	0.2506	1.671E-6
692	3.929E-05	1.992E-05	0.2533	1.762E-6
764	4.113E-05	1.874E-05	0.2556	1.832E-6
800	4.202E-05	1.820E-05	0.2568	1.866E-6
908	4.463E-05	1.677E-05	0.2602	1.966E-6

12. Nitrogen [4.3]

Temperature (°F)	Conductivity (Btu/min-in-°F)	Density (lb_m/in^3)	Specific Heat (Btu/lb_m-F)
200	3.364E-05	2.442E-05	0.249
300	2.922E-05	2.726E-05	0.250
400	2.582E-05	2.994E-05	0.252
500	2.313E-05	3.248E-05	0.254
600	2.094E-05	3.492E-05	0.256
700	1.914E-05	3.726E-05	0.259
800	1.762E-05	3.952E-05	0.262
900	1.632E-05	4.171E-05	0.265
1000	1.521E-05	4.383E-05	0.269
1100	1.470E-05	4.588E-05	0.272

13. Helium [4.3]

Temperature (°F)	Conductivity (Btu/min-in-°F)	Density (lb_m/in^3)	Specific Heat (Btu/lb_m-°F)
200	1.361E-04	4.808E-06	1.241
300	1.492E-04	4.175E-06	
400	1.634E-04	3.689E-06	
500	1.793E-04	3.305E-06	
600	1.948E-04	2.993E-06	
700	2.094E-04	2.735E-06	
800	2.231E-04	2.518E-06	
900	2.363E-04	2.333E-06	

(1) Thermal properties as listed are for atmospheric pressure; however, thermal conductivities for air and helium are assumed to be constant between atmospheric pressure and 0.1 Torr, absolute [4.14].

14. Water [4.18]

Temp. (°F)	Thermal Conductivity (Btu/min-in-°F)	Specific Heat (Btu/lb_m -°F)	Coef. Of Exp., 1/°R	Density (lb_m/ft^3)	Dynamic Viscosity (lb_m/hr-ft)
44	4.671E-04	1.003	2.56E-05	62.428	3.440
62	4.799E-04	0.999	9.67E-05	62.366	2.613
80	4.919E-04	0.998	1.534E-04	62.241	2.068
98	5.040E-04	0.998	2.01E-04	61.994	1.681
116	5.136E-04	0.998	2.43E-04	61.749	1.396
134	5.216E-04	0.999	2.80E-04	61.445	1.183
152	5.296E-04	1.000	3.14E-04	61.144	1.016
170	5.361E-04	1.002	3.468E-04	60.787	0.883
188	5.409E-04	1.004	3.88E-04	60.375	0.784
206	5.449E-04	1.006	4.05E-04	59.969	0.699
224	5.481E-04	1.009	4.38E-04	59.512	0.629
242	5.505E-04	1.012	4.67E-04	59.006	0.573
260	5.521E-04	1.017	4.978E-04	58.508	0.525
296	5.521E-04	1.028	5.61E-04	57.379	0.448

15. **Soil [4.19]**

Conductivity (Btu/min-in-°F)	Density (lb_m/in^3)	Specific Heat (Btu/lb_m-°F)
0.00024	0.0578	0.191

16. **Concrete(1)**

Temperature (°F)	Conductivity (Btu/min-in-°F) [4.20]	Density (lb_m/in^3)	Specific Heat (Btu/lb_m-°F) [4.28]
70	1.597E-3	0.084	0.22
1382	7.983E-4		

(1) Conservatively, the properties used herein for the HSM walls, and roof do not include the effects of rebar. Additionally, the ISFSI pad is conservatively modeled as concrete and does not include the effects of rebar. Including the effects of rebar would otherwise increase the effective conductivity of the HSM concrete walls, roofs, and ISFSI pad.

17. **Effective Neutron Shield Thermal Conductivity vs. Circumferential Cask Position (see Section T.4.8.5)**

Angle on Cask Body	Conductivity, Btu/min-in-°F [Error! Reference source not found.]	
	Water-Filled	Air-Filled
0°	0.011520	0.000385
30°	0.010848	0.000393
60°	0.010933	0.000408
90°	0.010708	0.000417
120°	0.008868	0.000391
150°	0.008695	0.000322
180°	0.007403	0.000227

18. **Neutron Absorber Thermal Conductivity (See Section T.4.3)**

19. **61BTH DSC Basket Effective Thermal Properties (See Section T.4.8)**

T.4.3 Specifications for Neutron Absorber Thermal Conductivity

The 61BTH DSC design allows for the use of various neutron absorber materials which include borated aluminum, BORAL® Composite Panel, and MMC. The neutron absorber material can be made from a single piece, or can be paired with aluminum sheet with a thickness not less than nominal 0.063". The neutron absorber materials are subjected to the following minimum thermal conductivity, which are used in the DSC thermal analyses.

Borated Aluminum

Temperature (°F)	Conductivity (Btu/min-in-°F)
68	0.123
212	0.132
392	0.141
482	0.145

MMC (Single Piece)

Temperature (°F)	Conductivity (Btu/min-in-°F)
All	0.0964

MMC (Paired with Aluminum sheet)

Temperature (°F)	Conductivity (Btu/min-in-°F)
All	0.0781

BORAL® Composite Panel (Single Piece)

Temperature (°F)	Transverse Conductivity (Btu/min-in-°F)	Axial Conductivity (Btu/min-in-°F)
100	0.0820	0.0905
500	0.0797	0.0964

BORAL® Composite Panel (Paired with Aluminum sheet)

Temperature (°F)	Transverse Conductivity (Btu/min-in-°F)	Axial Conductivity (Btu/min-in-°F)
100	0.0717	0.0778
500	0.0667	0.0781

T.4.4 Thermal Analysis of HSM and HSM-H with 61BTH DSC

The maximum decay heat loads that are considered for the NUHOMS®-61BTH DSCs as described in Section T.4.1 are 19.4 kW, 22.0 kW, 27.4 kW, and 31.2 kW.

61BTH Type 1 and Type 2 DSCs with up to a maximum decay heat load of 22 kW can be stored in HSM (either Model 80 or Model 102 or Model 152 or Model 202) or HSM-H, and 61BTH Type 2 DSC with maximum decay heat load exceeding 22 kW (up to a maximum heat load of 31.2 kW) can only be stored in HSM-H.

Since HSM-H is thermally more efficient than HSM with enhanced heat rejection capability (as described in Section T.4.4.2), the 61BTH DSC thermal analysis for the storage condition is performed using the bounding shell temperature from the HSM.

HSM is designed for a maximum heat load of 24 kW from a NUHOMS®-24P DSC as described in Section 8.1.3. The 61BTH and 24P DSCs have outside diameters of 67.25" and 67.19", respectively. The small difference of 0.06" in diameter has a negligible effect on the overall thermal analysis results. Therefore the shell temperatures calculated in Section 8.1.3.1 for 24P DSC in HSM with a 24 kW heat load are conservatively applied to 61BTH DSC with a 22 kW heat load. There is no change in the HSM thermal analysis due to the storage of 61BTH DSC inside HSM.

The DSC shell temperatures are summarized in Table T.4-28, and they are used in the 61BTH DSC model in Section T.4.6 to calculate the basket and fuel temperatures.

T.4.4.1 Ambient Temperature Specification

Ambient temperatures in the range of 0-100°F are considered as normal storage conditions. A maximum day temperature of 117°F is considered as off-normal, hot storage condition. A 24-hour average ambient temperature of 105°F is conservatively used for the off-normal steady state analysis, based on the 102°F calculated in Appendix M, Section M.4.5 [**Error! Reference source not found.**]. The lowest off-normal ambient temperature is considered to be -40°F.

T.4.4.2 Thermal Analysis of HSM-H with 61BTH DSC

The HSM-H is designed to provide an independent, passive system with substantial structural capacity to ensure safe storage of spent fuel assemblies in NUHOMS®-61BTH DSCs. The HSM-H (described in Appendix P, Section P.4.4.2) is an improved version of the HSM (described in Section 8.1.3) with superior design features to enhance its heat rejection and shielding capabilities.

This analysis determines the temperature distribution on the DSC shell, which is used to calculate the basket and fuel peak cladding temperature in a detailed model of the DSC basket (see Section T.4.6). The HSM-H wall temperatures are also determined in this analysis.

The HSM-H roof and front wall are the primary concrete surfaces conducting heat to the outside environment. For the analytical purpose of calculating maximum temperatures, an HSM-H centered in a group of HSM-Hs, each loaded with a 61BTH DSC, is assumed. Rows of modules are assumed to exist back-to-back for this model.

The HSM-H has been designed to accommodate the DSCs with a maximum decay heat load of 40.8 kW (see Appendix P, Section P.4.4). The maximum decay heat load that can be stored in the 61BTH DSCs is 31.2 kW, which is significantly less than the design heat load of the HSM-H.

The temperature distribution in the HSM-H is calculated at -40°F, 0°F, 100°F and 117°F ambient temperatures with a maximum decay heat load of 31.2 kW. The temperature distributions for these normal and off-normal conditions are determined using steady-state models.

Since the HSM-H is located outdoors, there is a remote probability that the air inlet or outlet openings become blocked by debris from events such as flooding, high wind, and tornados. The perimeter security fence around ISFSI and the location of the air inlet and outlet openings reduces the probability of such an accident. A complete blockage of all air inlets and outlets simultaneously is not a credible event. However, to bound this scenario, analysis is carried out assuming complete blockage of the inlet and outlet vents as an accident case.

T.4.4.3 HSM-H Air flow Analysis (Stack Effect Calculations)

The methodology used in the HSM-H airflow analysis (stack effect calculations) is presented in Appendix P, Section P.4.4.3. Different equations for computing the total pressure loss due to flow losses, air mass flow rate, temperature rise from air inlet to outlet, and the stack average temperature are also provided in Appendix P, Section P.4.4.3.

A summary of the HSM-H analyses with corresponding loss coefficients is listed below:

Summary of HSM-H Thermal Analyses with Loss Coefficients

Decay Heat Load (kW)	Operating Condition	Ambient Temperature (°F)	Total Equivalent Loss Coefficient (ft^{-4})
31.2	Off-Normal	-40	0.103
	Normal	0	0.104
	Normal	100	0.106
	Off-Normal	117	0.106

Using these loss coefficients in equation for $\Delta T_{HSM\text{-}H}$, the exit and stack air temperature for the normal and off-normal cases are calculated.

The DSC outer surface is divided into three regions along the DSC circumference as shown in Figure T.4-2. The bulk air temperatures at each of these specified regions on the DSC are shown in Table T.4-1 for the range of ambient conditions. These bulk air temperatures are used in the subsequent HSM-H analyses to calculate the temperatures throughout the HSM-H and the 61BTH DSC shell.

The accident blocked vents condition conservatively assumes no closed cavity convection.

T.4.4.4 Description of the Thermal Model of HSM-H with 61BTH DSC

A half symmetric, three dimensional, ANSYS [4.22] finite element model of the HSM-H loaded with a 61BTH DSC is shown in Figure T.4-3.

The thermal model consists of SOLID70 conduction elements that simulate concrete and steel support structures of the HSM-H, and SHELL57 elements superimposed on SOLID70 elements, as required, to model radiating surfaces using MATRIX50 super elements. As such, radiation between the DSC shell, heat shields, and HSM-H walls is modeled using the ANSYS /AUX12 methodology. For elements wherein radiation is not applicable, the SHELL57 elements are unselected prior to solving the model. Additionally, to reduce the number of nodes associated with the model's super-elements, the web of the supporting beam is modeled using only SHELL57 elements. As such, conservatively, radiation is not applied on the web of the supporting beam. This methodology is valid since the supporting beam's web greatly shields the support steel from the DSC radiation via its own flanges. The properties and dimensions of the support beam, such as the thickness of the web, are given as real constants to the appropriate SHELL57 elements.

Convection is included for the air within the space between the outer surface of the bottom cover plate and the inner surface of the HSM-H door. For this region the outer surface of the cover plate and the inner surface of the HSM-H door are connected to a space node through convection link elements (LINK34). To activate a LINK34 element, a convection surface area and a convection coefficient are required. The convection surface area is calculated for each LINK34 element separately and defined as a real constant for the corresponding element. The following approach is taken to calculate the convection surface area. Two-dimensional SHELL57 elements are overlaid on the outermost nodes of the DSC bottom plate and on the innermost nodes of the HSM-H door. Each node of the selected groups is attached to four SHELL57 elements. The radiating area of each LINK34 element is considered to be the average surface area of the SHELL57 elements attached to that LINK34 element. The surface areas of the SHELL57 elements are retrieved directly from the model and their average is applied as a real constant to the corresponding convection LINK34 element. SHELL57 elements are unselected prior to solving the model.

The side heat shields are modeled as flat stainless steel plates. The top heat shield is also a flat stainless steel plate design that is supported from the ceiling of the HSM-H.

The lower part of the HSM-H sidewall is offset by 6" toward the HSM-H cavity. The thickness of the offset wall is 18". To simplify the analysis, the HSM-H sidewall is modeled as a straight, 12" thick wall without the 6-inch offset. The modeling simplification has an insignificant effect on resultant temperature distribution output. This modeling simplification is justified since the majority of the heat removal is via convection, and only a small portion of the heat removal is via conduction through the walls. Modeling of this short segment of the HSM-H wall thinner than it is in actuality does not impact the overall results.

Boundary Conditions

The maximum off-normal ambient temperature of 117°F is considered. In the thermal analysis, a 24-hour average ambient temperature of 105°F (based on 102°F calculated in Appendix M, Section

M.4.5) is conservatively used as the ambient air temperature for the off-normal steady-state analyses.

Convection Coefficients

The correlation for heat transfer convection coefficients over the HSM-H surfaces, including the HSM-H vertical flat surfaces, horizontal surfaces, the side heat shield, the top heat shield and the horizontal DSC cylinder surface are determined in Section P.4.9.

For the space between the HSM-H sidewall and the HSM-H side shield, free convection correlation for a narrow channel is also presented in Appendix P, Section P.4.9.

Convection and radiation from the HSM-H roof and the front wall to the ambient are combined as a total effective coefficient as discussed in Appendix P, Section P.4.9.3.

Solar Heat Load

The modeling of insolation on the surfaces of the HSM-H roof and front wall that are exposed to the ambient is identical to one described in Appendix P, Section P.4.4.4.

Heat Load

The heat flux used in the HSM-H thermal model is determined using the same method as Appendix P, Chapter P.4 for a DSC heat load of 31.2 kW. The decay heat load is considered to be distributed evenly on the radial inner surface of the DSC with a length equivalent to the basket length (164"). This assumption is valid since the high conductivity of the basket plates and rails flattens the axial decay heat profile. The applied decay heat flux is calculated as follows:

$$\text{Decay heat flux} = \frac{Q}{\pi D_i L} \qquad \text{Btu/hr-in}^2$$

where,

Q = decay heat load = 31.2 kW
D_i = inner DSC diameter = 66.25"
L = DSC basket length = 164"

The thermal analysis of a typical HSM-H is performed for a loaded 61BTH DSC located in the interior of a multiple module array with a 61BTH DSC present in the two adjacent HSM-Hs. The HSM-H top and front surfaces are modeled as exposed to the prevailing ambient conditions in this model. The side and back surfaces are modeled as being adiabatic in order to simulate the adjacent modules.

T.4.4.5 Description of the HSM-H Blocked Vent Model

To determine the maximum temperatures of the HSM-H and the DSC shell for the blocked vent accident case, the finite element model of the HSM-H is modified to a transient model. The modeling approach is similar to one described in Appendix P, Section P.4.4.5.

During the blockage of the air inlet and outlet vents in the HSM-H, there will be convection within the closed HSM-H cavity. Conservatively, no convection is considered within the HSM-H cavity during the blocked vent condition. The analysis considers only the thermal conductivity of air within the HSM-H cavity.

The DSC basket including fuel assemblies and the top grid are modeled as two homogenized materials with effective properties for the transient case. Heat generating boundary conditions are applied uniformly on all of the elements representing the DSC basket. The amount of generated heat per unit volume of the DSC contents is calculated as follows:

$$\text{Heat generation rate} = \frac{Q}{(\pi/4\ D_i^2\ L)} \quad \text{Btu/hr-in}^3$$

where:

Q = decay heat load (31.2 kW)
D_i = inner DSC diameter = 66.25"
L = DSC basket length = 164"

The initial conditions for the blocked vent accident case are identical to the boundary conditions applied for the off-normal case with a 105°F daily average temperature (117°F maximum daylight temperature) and maximum solar heat flux. The emissivity of the support structure is assumed to be 0.55. The concrete and DSC shell temperatures are not sensitive to the emissivity of the support structure. The finite element model utilized for the transient runs is depicted in Figure T.4-3.

T.4.4.6 Description of Cases Evaluated for the HSM-H

The HSM-H thermal analyses are performed for the design basis ambient air temperatures defined in Section T.4.4.1.

A summary of the cases considered for HSM-H thermal analysis is presented in Section T.4.4.3.

T.4.4.7 HSM-H Thermal Model Results

T.4.4.7.1 Normal and Off-normal Operating Condition Results

Temperature distributions for the hot normal and off-normal cases are shown in Figure T.4-4 and Figure T.4-5. The maximum component temperatures for the normal and off-normal cases are listed in Table T.4-2.

T.4.4.7.2 Accident Condition Results

Temperature distributions for the blocked vent accident case with 31.2 kW decay heat load at 40 hours after blockage of the vents are shown in Figure T.4-6. The maximum component temperatures for the blocked vent accident case are listed in Table T.4-3.

Figure T.4-7 shows the time-temperature history of HSM-H components for this transient.

T.4.4.8 Evaluation of HSM-H Performance

The thermal performance of the HSM-H is evaluated under normal, off-normal, and accident conditions of operation as described above and is shown to satisfy all the temperature limits and criteria. The DSC shell temperatures calculated here are used in the DSC basket and fuel cladding models as a boundary condition in Section T.4.6. The results show that all the basket and fuel cladding material temperature limits are satisfied.

The results of the 117°F ambient blocked vent condition show that the maximum concrete temperature at the end of 40 hours in the blocked vent accident is 426°F. This is above the 350°F limit given in NUREG 1536 [4.5] for accident conditions. The CoC 1004 Condition 7 requires HSM-H concrete testing for evaluated temperatures to verify that there are no significant signs of spalling or cracking and that the concrete compressive strength is greater than that assumed in the structural analysis. The same condition will also be applicable to HSM-H when used with 61BTH DSCs. To account for the effect of higher concrete temperature on the concrete compressive strengths, the structural analysis of HSM-H concrete components in Section T.3 is based on 10% reduction in concrete material properties. Testing will be performed to document that concrete compressive strength will be greater than that used in the structural analysis documented in Section T.3.

T.4.5 Thermal Analysis of Transfer Casks with 61BTH DSC

The NUHOMS® OS197FC-B Transfer Cask (TC) or OS197/OS197H TC are used to transfer loaded 61BTH DSCs between the fuel building and the ISFSI. The design of the OS197FC-B TC is identical to the design of the OS197, OS197H or OS197FC TCs with the modification to the cask top lid and the addition of wedge shaped spacers at the bottom of the TC cavity, as described in Section T.1. Therefore, the OS197FC-B TC thermal model described in Section T.4.5.2 and T.4.5.3 is applicable to OS197 and OS197H TCs if operations are to occur without use of the air circulation feature. Thermal analyses methodology is the same as was used for OS197/OS197H/OS197FC located with 24PTH DSCs described in Appendix P, Section P.4.5.2. The analyses results for OS197FC-B TC in Section T.4.5.3, (excluding T.4.5.3.2), and the first accident case described in Section T.4.5.3.3 are also applicable to OS197 and OS197H TCs. Note that the OS197 and OS197H TCs are only allowed to transfer a 61BTH DSC with 22.0 kW or less heat load.

The following cask/DSC decay heat loads are analyzed herein:

1. The NUHOMS® OS197FC-B TC is designed and analyzed for transferring 61BTH DSCs with a maximum decay heat load of 31.2 kW,

2. The NUHOMS® OS197/OS197H TCs are designed and analyzed for transferring 61BTH DSCs with a maximum decay heat load of 22.0 kW.

T.4.5.1 Thermal Model of 61BTH DSC in the OS197FC-B

The NUHOMS® OS197FC-B TC is used to transfer the 61BTH DSCs between the fuel building and the HSM or HSM-H at the ISFSI site. The thermal performance of these TCs is evaluated under normal, off-normal, and accident conditions of operation. The thermal evaluation is conducted for a range of decay heat load, ambient conditions, and cask configurations.

The SINDA/FLUINT™ [4.26] and Thermal Desktop® [4.27] computer codes are used to model the OS197FC-B TC (or OS197/OS197H TC) and the 61BTH DSCs to determine the temperature distribution in the TC and the DSC shell. These DSC shell temperatures are then used in the model of the 61BTH DSCs to determine the basket and fuel cladding temperatures. A brief description of the computer code is provided below.

T.4.5.1.1 SINDA/FLUINT™ Thermal Desktop® General Code Description

The Thermal Desktop® and SINDA/FLUINT™ computer programs are designed to work together to provide the functions needed to build, exercise, and post-process a thermal model. The Thermal Desktop® computer program is used to provide graphical input and output display functions, as well as computing the radiation exchange conductors for the defined geometry and optical properties. Thermal Desktop® is designed as a module to the AutoCAD™ application. As such, all of the CAD tools available for generating geometry within AutoCAD™ can be used for generating a thermal model. In addition, the use of the AutoCAD™ layers tool presents a convenient means of segregating the thermal model into its various elements.

The SINDA/FLUINT™ computer program is a general-purpose code suitable for either finite difference or finite-element models. SINDA/FLUINT™ has been validated for simulating the thermal response of spent fuel packages.

The Thermal Desktop® and SINDA/FLUINT™ codes provide the capability to simulate steady state and transient temperatures using temperature dependent material properties and heat transfer via conduction, convection, and radiation. Complex algorithms may be programmed into the solution process for the purposes of computing heat transfer coefficients as a function of the local geometry, gas thermal properties as a function of species content, temperature, and pressure, or, for example, to estimate the effects of air circulation as a function of the flow geometry.

T.4.5.1.2 OS197FC-B TC SINDA/FLUINT™ Thermal Model

The thermal model used to simulate the thermal response of the OS197FC-B represents a 180° segment of the cask. The use of a 180° model permits the accurate simulation of the temperature distribution within the cask when the cask is in the horizontal orientation and the axis of the DSC is eccentric to that of the cask. Figure T.4-11 presents a perspective view of the thermal model of the cask and the DSC assembly (i.e., the cask body, closure lid, and DSC without fuel basket). The model uses approximately 5,800 nodes, 5,000 solids, and 3,900 planar elements to define the cask body geometry and to provide thermal resolution. The modeling divides the cask circumference into 15° segments with axial lengths of 8 inches or less. As seen in Figure T.4-11 the thermal model captures the fact that the structural shell increases from 1.5-inches thick to 2-inches thick at the upper portion of the cask.

Heat transfer across the water filled neutron shield is computed using the effective thermal properties from Appendix M, Section M.4.9. Under accident conditions where the neutron shield is assumed to be filled with air, radiation exchange is added to the appropriate effective thermal conductivity values from Appendix M, Section M.4.9. Heat transfer from the outer skin of the neutron shield is computed using the free convection correlation and thermal radiation exchange.

Figure T.4-13 illustrates the thermal modeling used for the cask closure lid. The cask closure lid model utilizes approximately 1,500 thermal nodes, 900 solids, and 1,000 planar surfaces. For the spacer, the model uses 130 planar surfaces and 130 nodes and 40 solids to represent the stainless steel plates that make up the spacer.

T.4.5.1.3 DSC Steady State and Transient Conditions Thermal Models

The 61BTH DSCs have a nominal length of 196 inches, an outside diameter (OD) of 67.25 inches, and a shell thickness of 0.5 inches. The bottom shield plug is 7.5 inches thick, while the DSC closure plug is nominally 9 inches thick.

Approximately 1,200 nodes and 1,000 solids are used to model the shell and ends of the DSC (see Figure T.4-11). The fuel basket and hold down ring are modeled as homogeneous solids with different effective thermal properties using approximately 1,700 nodes and 1,800 solids. The fuel basket is 164 inches long, while the hold down ring assembly is 14.5 inches long. A 0.40 inch helium filled gap is assumed between the bottom of the fuel basket region and the bottom of the DSC and between the top of the hold down ring assembly and the inside of the DSC's closure lid.

The decay heat loading is applied as a uniform volumetric heat load over the 164-inch length of the fuel basket. The upper 14.5 inch section of the basket representing the hold down ring assembly is assigned a zero decay heat loading. Figure T.4-12 illustrates the thermal model of the DSC and fuel basket. The fuel basket is simulated as a solid cylinder with an isotropic thermal conductivity and specific heat values, and the hold down ring assembly uses a different set of effective thermal properties.

T.4.5.1.4 Natural Convection Heat Transfer Coefficients

Heat transfer coefficients for natural convection on surfaces are computed using equations used for TC with 24PTH DSC described in Appendix P, Section P.4.5.2.4.

T.4.5.1.5 Neutron Shield Effective Thermal Conductivity

Effective thermal conductivity of water within the neutron shield of the OS197/OS197H/OS197FC TC was evaluated for water and air filled cases, respectively. These values are also applicable to OS197FC-B TC. The table values from Appendix M, Section M.4.9 are interpolated to yield values at the intermediate angles.

T.4.5.2 Analysis Cases for OS197FC-B TC with 61BTH DSC

The thermal performance of the NUHOMS® OS197FC-B TC was evaluated under normal, off-normal, and accident conditions of operation. The maximum heat load permitted when there is no time limit on DSC transfer operations was determined by using steady state conditions. If the results of steady state analysis were not acceptable relative to the fuel cladding or material temperature limits, then a transient analysis was performed to determine the time limit on DSC transfer operations for these heat load conditions. The time limit for transfer of the DSC is defined as the time after the annulus is completely drained of water and initiation of bolting of transfer cask top cover plate to the cask with a loaded DSC in the TC cavity until the time the bolted cask top cover is removed to expose the top of loaded DSC and the cask/DSC annulus to ambient conditions.

The geometry of OS197FC-B TC is similar to OS197FC TC. See Chapter T.1 for an OS197FC-B TC description.

The thermal performance of the OS197FC-B TC was evaluated for normal (i.e., 100°F and 0°F) and off-normal (i.e., 117°F) ambient temperatures, with and without insolation, and for various heat loads in the horizontal transfer condition. The TC was also evaluated for normal 120°F ambient temperature, without insolation, for various heat loads in the vertical transfer condition in the fuel loading building. Three accident scenarios are also evaluated for the OS197FC-B TC as described in Section T.4.5.3.3. Likewise, the available time to initiate air circulation via external fan or to restore the air circulation in case of system failure was determined. Table T.4-4 and Table T.4-5 provide an overview of each load case analyzed for 61BTH Type 1 and Type 2 DSCs, respectively.

The temperature profiles of the TCs and the 61BTH DSC shell and top and bottom cover plates and shield plugs obtained from the results of the OS197FC-B TC analysis with 19.4 kW, 22.0 kW, 27.4 kW, and 31.2 kW heat loads are used in thermal stress calculations.

T.4.5.3 OS197FC-B TC Thermal Model Results

The maximum temperature results for the 61BTH DSC shell assemblies and TC components during transfer are presented in Table T.4-7 through Table T.4-9. These results are for 31.2 kW and 22.0 kW heat loads. The DSC shell temperatures are then used as boundary conditions in the 61BTH DSC basket analysis presented in Section T.4.6.

T.4.5.3.1 Normal and Off-Normal Conditions Results

Table T.4-7 presents the maximum steady state component temperatures for the configuration of the TC with a 61BTH Type 1 DSC with 22.0 kW and 19.4 kW of decay heat. All component temperatures are well below their associated maximum allowable limits. Figure T.4-14 illustrates the temperature distribution within the TC at steady-state conditions during vertical transfer operations with no insolation and 120°F ambient.

Transient analyses are performed to determine the time limit for DSC transfer operations for 61BTH Type 2 DSC with a decay heat load higher than 22.0 kW up to 31.2 kW. The analyses assume that the transient analysis begins with water in the TC/DSC annulus and that with the TC in a vertical orientation (i.e., no credit is taken for heat transferred through the canister rails). At time = 0, the annulus water is assumed to be drained and the bolting of the TC top cover is initiated. This causes the system to heat up. Figure T.4-17 illustrates the predicted thermal response of the DSC and TC for this transient, assuming a decay heat load of 31.2 kW in a 61BTH Type 2 DSC. Figure T.4-17 also shows the steady state results of the same case. Based on targeted DSC shell temperatures of approximately 405°F (for HLZC 7) and 445°F (for HLZCs 5, 6 and 8) to avoid excessive fuel cladding temperatures, the transient analysis indicates that approximately 15 and 28 hours, respectively, are available to transfer the DSC into the HSM-H or take some other corrective actions. The anticipated corrective actions are:

- Complete the transfer of the DSC from the TC to the HSM-H, or
- Unbolt the TC top cover plate and flood the TC/DSC annulus with water if the TC is vertical, or
- Use of an external fan to circulate the air in the TC/DSC annulus if the TC is horizontal, or
- Initiate appropriate external cooling of the TC outer surface by other means, or
- Return the TC to the TC handling area, unbolt the TC top cover plate and reflood the TC/DSC annulus with clean water.

These DSC shell temperatures are then used in the DSC basket model described in Section T.4.6 to calculate the basket and fuel cladding temperatures. The results from Section T.4.6 documented in Table T.4-12 show that even with these shell temperatures, there is considerable margin in the calculated cladding temperatures (734°F and 728°F calculated for 22.0 kW and 31.2 kW total decay heat cases, respectively vs. a 752°F limit).

To verify that the TC in the vertical mode is the controlling configuration, the canister loading transient with 31.2 kW heat load was repeated, but with the exception that at time = 0, the annulus water is assumed to be drained, the TC top cover is bolted and TC is rotated to the horizontal

position and moved outdoors with exposure to 100°F ambient air and insolation. Figure T.4-18 illustrates the predicted thermal response of the DSC and TC for this transient. Comparing the transient results with those presented in Figure T.4-17 for the TC in the vertical mode shows that the heat up rate for the DSC shell and basket are essentially the same. In contrast, the TC liner, lead, and outer shell exhibit the expected faster heat up due to a combination of the additional heating from insolation and the direct contact heating through the canister support rails. Therefore, approximately 15 (for HLZC 7) and 28 (for HLZCs 5, 6 & 8) hours are available to transfer the DSC to the HSM-H after draining of the TC/DSC annulus with the TC top cover bolted on regardless of whether the TC is left in its vertical orientation inside the fuel storage building or rotated to its horizontal orientation and moved outdoors. Table T.4-8 presents the maximum component temperatures achieved under bounding normal and off-normal ambient operating conditions for the OS197FC-B TC with a 61BTH DSC with 31.2 kW of decay heat, no air circulation, and 28 hours after the annulus water is drained and the cask closure operations are initiated. Table T.4-8 also presents similar results for the 61BTH DSC with 27.4 kW of decay heat for the bounding case of vertical loading within the fuel handling facility. Figure T.4-15 illustrates the temperature distribution within the TC at the 28 hour point in the vertical transfer operation with no insolation and 120°F ambient.

T.4.5.3.2 Normal and Off-Normal Operations with Air Circulation Results

For a specific heat load limit and loading and/or transfer time periods exceeding the values determined in Section T.4.5.3.1, one of the corrective actions available to limit the temperature increase is to initiate air circulation in the TC/DSC annulus with the use of an external fan. The NUHOMS® OS197FC-B TC contains design provisions for the use of an external fan for air circulation in the TC DSC annulus if the time to transfer the 61BTH Type 2 DSC with decay heat load above 22.0 kW from the TC handling area in the TC to the HSM-H exceeds the specified time limits, depending upon the specific HLZCs employed.

The NUHOMS® cask support skid is modified by the addition of redundant, industrial grade pressure blowers and power systems, ducting, etc. as described in Section T.1.2.1.3 similar to OS197FC cask described in Appendix P, Section P.4.5. When operating, the fan system will generate a minimum flow rate of 400 cfm which will be ducted from an external fan system to the ram access cover location at the bottom of the cask via the use of an adaptor cone, illustrated in Figure T.4-8, which is used to mate the hose to the ram access opening. The inner cone of the adaptor aids in expanding the airflow and limiting the pressure loss in the airflow at this location. After entering the ram access opening, the airflow turns and enters ten (10) flow paths formed by 0.5-inch thick wedge segments arranged around the circumference of the TC's bottom. The layout of the wedge segments at the bottom of the TC is illustrated in Figure T.4-9.

The determination of the gap as a function of circumferential position was made assuming the DSC is resting on the support rails.

After exiting from the flow paths formed by the wedge segments, the airflow turns and flows in the annulus between the DSC and the cask's inner liner. The air flow exits the TC through sixteen (16) slots provided around the circumference of a specially modified lid. Figure T.4-10 illustrates the layout and dimensions of these slots.

Since the DSC will be eccentric to the TC axis for all horizontal operations and possibly for vertical operations, the gap between the DSC and the TC's inner liner will vary with circumferential position. Driven by the variation in the gap between the DSC and liner as a function of the circumferential position, plus variances in the density of the air due to the different heating rates depending on both axial and circumferential position, the airflow will distribute itself around the circumference of the DSC/cask liner until an equal pressure drop is achieved for all flow paths. For the purposes of this calculation, each half of the annulus is divided into 7 circumferential segments: 0 to 30°, 30 to 60°, 60 to 90°, 90 to 120°, 120 to 135°, 135 to 150°, and 150 to 180°. The 0° position is at the top of the horizontal TC and the 180° position is at the bottom.

Implementation of the air circulation option consisted of the determination of the mass flow rates and the pressure drops through the cask as a function of angular position, the convective heat transfer coefficients, and the thermal conductance between the various gas nodes until both mass and thermal balances are achieved. The methodology used is identical to that used in Appendix P, Section P.4.5.5.2. The following sections describe the methodology used for these calculations.

T.4.5.3.2.1.1 Pressure Drop Calculation

The pressure drop experienced by the circulating air from the fan discharge, through the DSC and TC annulus, and its subsequent exhausting back into the ambient is computed assuming 1-D flow pipe flow relationships. Table T.4-6 presents the calculations performed to determine the TC/DSC gap hydraulic characteristics as a function of circumferential position along the DSC shell. These gap hydraulic characteristics and loss coefficients along the flow path for the fittings and hoses from the blower to the TC top lid outlets are used to calculate the resultant total pressure drop. The loss coefficients for the fittings, hoses, entrance, exit, sudden expansion, contraction turns, bends and plenums along the flow path are taken from References [4.24] and [4.13]. A pressure drop of approximately 6 inches water gauge is calculated.

T.4.5.3.2.1.2 Convection Heat Transfer Coefficient for Circulating Air within the DSC Cask Annulus

The convection heat transfer within the DSC cask annulus is computed using the relationships for flow within ducts and pipes listed in Appendix P, Section P.4.5.5.2 (B).

T.4.5.3.2.1.3 Results

Table T.4-9 presents the maximum component temperatures achieved under bounding normal and off-normal ambient operating conditions for the OS197FC-B TC with a 61BTH DSC with 31.2 kW of decay heat and a flow rate of 400 cfm of air circulation. As seen, all component temperature are within their associated maximum allowable temperature limit.

Examination of the model output shows that nearly 85% of the total airflow in the TC DSC annulus occurs in the upper half of the annulus. This result is expected given the combination of flow area and hydraulic diameter (see Table T.4-6) for the various angular segments. The remaining 15% of the total fan airflow occurs in the lower half of the annulus, with 2/3 of that occurring within the 60° to 90° segment of the annulus.

T.4.5.3.3 Accident Conditions

Three accident scenarios are examined for the OS197FC-B TC. The first case considers an evaluation of system performance for the case wherein steady-state conditions are established with the fan in operation, and, subsequently the fan airflow is lost. To minimize the occurrence of this accident condition, the OS197FC-B TC skid is equipped with redundant industrial grade blowers, each one of these blowers capable of supplying the required minimum air flow rate. These blowers are also powered with a redundant power supply.

The analyses assume that the transient begins with DSC/TC at steady-state conditions with the cask horizontal, 100°F ambient, with insolation, and 31.2 kW decay heat. At time = 0, the fan airflow is lost and the system starts to heat up. Figure T.4-19 illustrates the calculated thermal response of the DSC and TC for this transient. Assuming an upper limit DSC shell temperature of 435°F, approximately 18 hours are available to complete the transfer to the HSM-H or re-establish the fan airflow. The 435°F shell temperature limit is selected because it will result in fuel cladding temperatures close to the 752°F limit but will not exceed it.

The second accident case involves the loss of both the fan air circulation system and the water in the neutron shield (TC drop accident). The resulting transient behavior of the TC and DSC is illustrated in Figure T.4-16 for the case with 22.0 kW and in Figure T.4-20 for the case with 31.2 kW. Table T.4-10 presents the peak component temperatures achieved under this accident at steady-state conditions. As seen, with the exception of the NS-3, all component temperatures remain under their allowable long-term limits. The temperature of the NS-3 for the 31.2 kW decay heat loading is within the allowable short-term limit of 300°F and slightly above the long-term limit of 250°F. As such, the results indicate that the shielding effectiveness of the NS-3 would not be impaired.

The third accident scenario involves a 15-minute hypothetical fire. The maximum duration of the fire event will be controlled by limiting the available fuel sources within the vicinity of the TC. To bound the heat input into the TC, the neutron shield is assumed to be filled with water during the fire duration and then the neutron shield water is assumed to be lost at the end of the 15-minute fire. The evaluation of TC thermal performance under the hypothetical fire accident scenario is illustrated in Figure T.4-21. As expected, with the exception of the exterior surfaces of the cask, the thermal mass of the DSC and cask components is sufficient to absorb the heat flux from the fire with an approximate 110°F increase in the peak structural shell temperature and only an 80 °F increase in the peak liner temperature. The rise in the structural shell temperature is not reflected by the lead gamma shield and inner liner temperatures because the assumed gap between the structural shell and the lead effectively limits the transient heat flow into these components. However, even if a perfect contact was assumed at the lead and the structural shell interface, a potential 110°F increase in the liner and lead temperatures would be modest for this type of accident event.

The cask components continue to heat up after the end of 15 minute fire because of the assumed loss of the fan air circulation system and the failure and draining of the neutron shield. As seen from Figure T.4-21, the maximum cask temperatures achieved under the fire accident scenario, with the exception of the exterior surfaces of the cask, will occur at the post-fire steady-state condition.

Table T.4-11 presents the peak component temperatures achieved at the end of the fire (i.e., 15 minutes into the transient) and for the post-fire steady-state condition. Comparison of the post-fire

steady-state temperatures from Table T.4-11 with the temperatures in Table T.4-10 shows that the loss of neutron shield accident scenario temperatures bound those for the post-fire steady-state temperatures. This occurs because the assumed sooting and oxidation of the exterior surfaces that is assumed for the fire event raises the surface emissivity, thus improving the heat transfer between the cask and the ambient.

T.4.5.4 Evaluation of OS197FC-B TC Performance

The thermal performance of the OS197FC-B TC is evaluated under normal, off-normal, and accident conditions of operation as described above and is shown to satisfy all the temperature limits and criteria. The results of the DSC shell temperatures are used in the DSC basket and fuel cladding temperature models and the results documented in Section T.4.6 show that all the basket and fuel cladding material temperature limits are satisfied. The results of the TC temperatures are used in Section T.3 to show that thermal stresses in the TC are also within these allowables.

T.4.6 NUHOMS®-61BTH DSC Thermal Analysis

The thermal analysis of the NUHOMS® 61BTH DSC is based on finite element models developed using the ANSYS computer code [4.22]. The methodology used is identical to that used for 24PTH DSC modeling described in Appendix P, Section P.4.6. ANSYS is a comprehensive thermal, structural and fluid flow analysis package. It is a finite element analysis code capable of solving steady state and transient thermal analysis problems in one, two or three dimensions. Heat transfer via a combination of conduction, radiation and convection can be modeled by ANSYS.

T.4.6.1 Heat Load Zoning Configurations

A total of eight (8) HLZCs are allowed for the 61BTH DSCs as shown in Figure T.2-1 through Figure T.2-8. The following table summarizes the different types of DSCs, the maximum total heat loads, and the different HLZCs that can be used for each DSC type.

61BTH DSC Type	Neutron Absorber Type	Max Heat Load (kW)	HLZC 3 (19.4 kW)	HLZC 4 (19.4 kW)	HLZC 1 (22.0 kW)	HLZC 2 (22.0 kW)	HLZC 8 (27.4 kW)	HLZC 5 (31.2 kW)	HLZC 6 (31.2 kW)	HLZC 7 (31.2 kW)
Type 1	Borated Aluminum/BORAL®/ MMC	19.4	√	√						
	Borated Aluminum	22.0	√	√	√	√				
Type 2	Borated Aluminum/BORAL®/ MMC	27.4	√	√	√	√	√			
	Borated Aluminum	31.2	√	√	√	√	√	√	√	√

The above table shows that the maximum decay heat loads for the Type 1 and the Type 2 DSCs are 22.0 kW, and 31.2 kW, respectively. The checked (√) box indicates the HLZC that is allowed for use in each DSC configuration.

Consider the following example: In a 61BTH Type 2 DSC with BORAL® neutron absorber, the maximum decay heat load is 27.4 kW. The HLZCs that can be used with this DSC are 3, 4, 1, 2, and 8. Since HLZCs 3, 4, 1, and 2 are bounded by HLZC 8, only HLZC 8 needs to be considered for bounding fuel loading analysis.

For the 61BTH Type 1 DSC with borated aluminum as neutron absorber, a complete set of DSC thermal analyses are carried out for HLZCs 1 and 2, with a decay heat load of 22.0 kW. Sensitivity analyses are performed to show that these analyses bound the DSC thermal analysis for 61BTH Type 1 DSC with BORAL®, MMC, for HLZCs 3 and 4, with a lower heat load of 19.4 kW.

Similarly for the 61BTH Type 2 DSC with borated aluminum as neutron absorber, a complete set of DSC thermal analyses are carried out for HLZCs 5, 6 and 7, with a decay heat load of 31.2 kW. Sensitivity analyses are also performed to show that these analyses bound the DSC thermal analysis for 61BTH Type 2 DSC with BORAL® / MMC, for HLZC 8, with a lower heat load of 27.4 kW.

T.4.6.2 NUHOMS® 61BTH DSC Thermal Analysis Model

The three-dimensional models representing the NUHOMS®-61BTH Type 1 and Type 2 DSCs are provided in Figure T.4-22 through Figure T.4-25. The 3D models are longitudinally full-length, one-half (180°) cross section models of the 61BTH DSC. The ANSYS models comprise the shell assembly (including the shell, and top and bottom end assemblies) and the basket assembly (including fuel compartment tubes, aluminum and neutron absorber plates, and the R45 and the R90 transition rails). All of these DSC components are modeled using SOLID70 elements. The total numbers of nodes and elements in the ANSYS model are approximately 833,000 and 820,000, respectively.

The DSC shell is modeled as being 0.5" thick with outer radius of 67.25". A hot annulus gap of 0.125" between the basket rails and the DSC shell is modeled. Sufficient mesh refinement has been built into the model. A fuel mesh size of 10x10 elements is modeled making the nominal dimension of the fuel element 0.6", which is more refined than 0.64" (i.e., 8.9 / 14 = 0.64) modeled in the 24PTH DSC (see Appendix P, Section P.4.6.1). Additional mesh sensitivity analyses are performed to show that the 10x10 fuel mesh used in the model is reasonable and acceptable (see Section T.4.6.3). The fuel in the model is shifted to the top end of the DSC cavity to the hotter airflow area when the 61BTH DSC is in the OS197FC-B TC with the air circulation option in use.

The gaps between adjacent basket components are also represented with SOLID70 elements with helium or vacuum (air) conductivity as appropriate. The material properties from Section T.4.2 are used for the fuel region. Within the model, heat is transferred via conduction through fuel regions, fuel compartments, aluminum and neutron absorber plates, and the gas gaps between all members. Generally, good surface contact is expected between adjacent components within the basket structure. However, to bound the heat conductance uncertainty between adjacent components due to imperfect contact between the neutron absorber material, aluminum and steel basket components, uniform gaps along the entire surfaces are assumed. This is a conservative assumption, because although there will be imperfect contact between the adjacent plates, they will be in contact with each other at most of the locations. Therefore, thermal resistance to heat flow from the fuel assembly out to the DSC surface is lower with the actual imperfect contact as compared with the modeled uniform gaps along the entire surfaces. The gaps used in the thermal analysis of the 61BTH DSC are shown in Figure T.4-26 through Figure T.4-28.

T.4.6.3 Mesh Sensitivity Study

The 61BTH DSC model described above is based on a 10x10 mesh for the cross section of each fuel assembly. A sensitivity study was performed with fuel mesh sizes of 8x8 and 12x12. The results show that convergence is achieved with a 10x10 mesh and the maximum fuel cladding temperature change is less than 2°F in comparison with 12x12 mesh. Hence the 10x10 mesh size model is reasonable and acceptable.

T.4.6.4 Axial Heat Flux Profile

In-core data from an operating BWR facility forms the basis for the evaluation. The data provides the burnup and moderator density for 25 axial locations along the length of a fuel assembly. Five

fuel assemblies at in different locations in the reactor core are utilized to generate a burnup (peaking factor) distribution for the assembly. The resulting axial heat flux profile is shown in Figure T.4-37.

The heat flux profile of Figure T.4-37 is used in the thermal model of the Transnuclear, Inc. TN-68 dry transport/storage cask, which can accommodate BWR spent fuel with a maximum bundle-average burnup of 40,000 MWd/MTU. The maximum bundle-average burnup allowed in 61BTH DSCs is 62,000 MWd/MTU, which is considerably higher than 40,000 MWd/MTU for TN-68. Reference [4.1] shows that at a higher burnup, the heat flux shape tends to flatten with a reduction in the maximum axial peaking factor in the middle region, and the flux shape becomes more pronounced in the fuel end regions. The reduction of the maximum axial peaking factor in a more flattened heat flux shape will result in lower fuel cladding temperatures. Therefore, the application of a heat flux shape for a lower burnup spent fuel (40,000 MWd/MTU) on a higher burnup spent fuel (62,000 MWd/MTD) is conservative.

T.4.6.5 Heat Generation for the DSC Basket Model

Heat generation is calculated based on the dimensions of the fuel and basket. The heat is assumed to be radially distributed evenly through the 6-inch square nominal fuel cell opening. Axial variations in decay heat flux (see Figure T.4-37) are applied along the active length of the BWR fuel assembly. Heat generation rates are applied along all of the active fuel length according to the decay HLZCs.

The equation below shows a typical calculation of a peak heat generation rate for 0.35 kW per fuel assembly with an active fuel length of 144 inches.

$$\dot{q} = \frac{1.20 \cdot 0.35\,kW \cdot 3414 \frac{Btu/hr}{kW} \cdot \frac{1\,hr}{60\,\min}}{(6.0\,in)^2 \cdot 144.0\,in} = 4.610e-3 \frac{Btu}{\min \cdot in^3}$$

T.4.6.6 DSC Thermal Evaluation for Normal Conditions of Storage and Transfer

The NUHOMS® System components are evaluated herein for normal conditions of storage and transfer over a range of design basis ambient temperatures. Ambient temperatures for these cases are assumed to occur for a sufficient duration such that a steady-state temperature distribution exists within the NUHOMS® System components.

T.4.6.6.1 Boundary Conditions, Storage

The NUHOMS®-61BTH DSC is evaluated for normal conditions of storage with maximum heat loads of 22.0 kW and 31.2 kW within the HSM and HSM-H, respectively. Each of these normal conditions of storage analysis cases are performed for the following ambient conditions:

- Maximum normal ambient temperature of 100°F with insolation, and
- Minimum normal ambient temperature of 0°F without insolation.

The NUHOMS®-61BTH Type 1 DSC is evaluated for normal conditions of storage with a maximum heat load of 22.0 kW in the HSM. The HSM thermal model as described in Section 8.1.3 provides the DSC shell surface temperatures with 24 kW total heat load, which is conservative for the 22 kW total heat load of 61BTH Type 1 DSC, which are summarized in Table T.4-28.

The NUHOMS®-61BTH Type 2 DSC is evaluated for normal conditions of storage with a maximum heat load of 31.2 kW in the HSM-H. The HSM-H thermal model as described in Section T.4.4 provides the surface temperatures of the DSC shell.

These normal conditions of storage DSC shell temperatures are then applied as boundary conditions to the DSC shell in the basket and fuel models, as presented. These models are used to calculate the temperature distributions in the basket components and fuel.

T.4.6.6.2 Boundary Conditions, Transfer

The normal conditions of transfer analyses are performed for the following ambient conditions:

- Maximum normal ambient temperature of 100°F with insolation, and
- Minimum normal ambient temperature of 0°F without insolation.

The 61BTH DSC temperature profiles calculated using the OS197FC-B thermal model as described in Section T.4.5 are applied to the corresponding surfaces of the DSC thermal analysis finite element model described in Section T.4.6.2.

T.4.6.6.3 Maximum Temperatures

T.4.6.6.3.1 Fuel Cladding

The maximum fuel cladding temperatures during normal conditions of storage and transfer are evaluated for all decay HLZCs and compared with the corresponding fuel cladding temperature limit for normal conditions of storage and transfer as listed in Table T.4-12. Figure T.4-29 and Figure T.4-30 show the DSC temperature distributions for 22.0 kW heat load and Figure T.4-33 and Figure T.4-34 show the DSC temperature distributions for 31.2 kW heat load.

The conservatisms in the basket model and in the cladding temperature limit methodology are described below:

1. No credit is taken for any convection in the DSC basket cavity and fuel regions.
2. Conservative gaps are assumed between the basket component plates even though adjacent basket components are connected to each other.
3. No credit is taken for any radiation in the gaps between the adjacent basket components.

Based on these conservatisms, there is a higher margin in the calculated maximum cladding temperatures than those shown in Table T.4-12. Thus, there is reasonable assurance that the cladding will maintain its integrity during storage conditions.

T.4.6.6.3.2 DSC Basket Component Temperatures

The maximum temperatures of the basket assembly components for normal conditions of storage and transfer for the bounding HLZCs are listed in Table T.4-13 and Table T.4-14.

T.4.6.6.4 Maximum Internal Pressures

Pressure Calculation

This section describes the internal pressure calculations for the NUHOMS®-61BTH DSC as loaded with fuel with a maximum burnup of 62 GWd/MTU for all storage and transfer operations. The limiting fuel assembly type considered in this evaluation is the FANP9 9x9-2 fuel assembly (refer to Section T.2.1).

The calculations account for the DSC free volume, the quantities of DSC backfill gas, fuel rod fill gas, and fission products and the average DSC cavity gas temperature. The internal pressures are then calculated using the ideal gas law, as follows:

$$P = \frac{nRT}{V}$$

where:

n	=	Total number of moles of gases,
R	=	Universal gas constant,
T	=	Gas temperature (°R),
V	=	Gas volume, and
P	=	Internal pressure.

DSC Free Volume

The 61BTH DSC cavity free volume is calculated as DSC cavity volume minus DSC basket and fuel assemblies' volume. The DSC cavity volume is calculated as

$$V_{DSC\ cavity} = \frac{\pi \cdot ID^2_{DSC\ shell}}{4 \cdot L_{DSC\ cavity}}$$

where

$ID_{DSC\ shell}$ - DSC shell inside diameter,

$L_{DSC\ cavity}$ - DSC cavity length.

The calculated 61BTH DSC cavity free volumes are shown in Table T.4-29.

Quantity of Helium Fill Gas in DSC

The DSC free volume is filled with a maximum 3.5 psig (2.5 psig +1) of helium after vacuum drying operation. The average steady state helium backfill temperature is used for the calculation of the helium fill gas quantity. Using the ideal gas law, the quantity of helium in each type of DSC is calculated and the results are presented in Table T.4-15.

Quantity of Helium Fill Gas in Fuel Rods per DSC

The volume of the helium fill gas in a GE12/GE14 10x10 fuel assembly, at cold unirradiated conditions is 2.066 in^3, and there are a maximum of 92 fuel pins in a fuel assembly. The GE12/GE14 10x10 fuel assembly has bounding (highest) number of fuel rods per assembly, which results in the highest quantity of helium fill gas in fuel rods per DSC. The maximum fill pressure is 140 psig (155 psia) and the fill temperature is assumed to be room temperature (70°F or 530°R). The mole quantity of fuel rod fill gas is given by:

$$n_{he} = \frac{(155\,psia)(6894.8\,Pa/psi)(61 \cdot 92 \cdot 2.066\,in^3)(1.6387 \cdot 10^{-5}\,m^3/in^3)}{(8.314\,J/(mol \cdot K))(530°R)(5/9\,K/°R)}$$

$$n_{he} = 83.0\,g-moles$$

Based on NUREG 1536 [4.5], the maximum fraction of the fuel pins that are assumed to rupture and release their fill and fission gas for normal, off-normal and accident events is 1, 10 and 100%, respectively. The amount of helium fill gas released per DSC for each of these conditions is summarized in Table T.4-30. For all of these events, 100% of the fill gas in each ruptured rod is assumed to be released.

Quantity of Fission Gas released as a Result of Irradiation in Fuel Rods per DSC

The GE12/GE14 10x10 fuel assembly used in the pressure calculations is assumed to have a maximum burnup of up to 62 GWd/MTU, which is the highest burnup proposed for the NUHOMS®-61BTH system configuration. The maximum burnup creates a bounding case for the amount of fission gas produced in a fuel rod during reactor operation. The amount of gas produced because of irradiation at STP for each fuel assembly is 20.2g-moles.

The number of moles of gas released into the DSC cavity from one fuel assembly because of irradiation is given by:

$$n_{ig\,1\,FA} = 20.2 \text{ g-moles} * 0.3 = 6.06 \text{ g-moles}$$

The amount of fission gas released into the DSC cavity for normal, off-normal and accident cases assuming a 30% gas release from the fuel pellets [4.5] and a 1%, 10%, and 100% rod rupture, respectively, is summarized in Table T.4-31.

The maximum average helium backfill gas temperature for normal conditions of storage and transfer occurs when the 61BTH DSC is in the fuel building during vertical transfer with an ambient temperature of 120°F. In addition, the maximum pressure will occur with the 62 GWd/MTU burnup fuel so that lesser burnups will be enveloped by this calculation. The average helium backfill gas

temperature based on the results in Section T.4.6.6.3, is 382°F (842°R) and 377°F (837°R) for Type 1 DSC and Type 2 DSC, respectively. The maximum normal operating condition pressures are summarized in Table T.4-16.

T.4.6.6.5 Evaluation of 61BTH DSC Performance for Normal Conditions

The NUHOMS®-61BTH DSC shell and basket are evaluated for the calculated temperatures and pressures as presented in Section T.3. The maximum fuel cladding temperatures are well below the allowable fuel temperature limit of 752°F (400°C) [4.15] as documented in Table T.4-12. The maximum DSC internal pressure remains below 10.0 psig for Type 1 DSC and 15.0 psig for Type 2 DSC used in Section T.3 during normal conditions of storage and transfer operations. Hence, it is concluded that the NUHOMS®-61BTH DSC design meets all applicable normal condition thermal requirements.

T.4.6.7 DSC Thermal Evaluation for Off-Normal Conditions

The NUHOMS®-61BTH system components are evaluated for the extreme ambient temperatures of -40°F (winter) and 117°F (summer). Should these extreme temperatures ever occur, they would be expected to last for a short duration. Nevertheless, these ambient temperatures are conservatively assumed to occur for a significant duration to result in a steady-state temperature distribution in the NUHOMS®-61BTH system components.

T.4.6.7.1 Off-Normal Ambient Temperatures during Storage

The thermal performance of the NUHOMS®-61BTH DSC within the HSM-H and within the HSM under the extreme minimum ambient temperatures of -40°F with no insolation and extreme maximum ambient temperature of 117°F with maximum insolation are evaluated for both Type 1 and Type 2 DSCs.

T.4.6.7.2 Bounding Conditions, Off-Normal Storage

Off-normal conditions of storage analyses of the NUHOMS®-61BTH DSC within the HSM-H and within the HSM include:

- Maximum off-normal ambient temperature of 117°F with insolation, and
- Minimum off-normal ambient temperature of -40°F without insolation.

The HSM-H thermal model described in Section T.4.4.4 above provides the surface temperatures that are applied to the DSC shell, basket and payload model. The results are presented in Table T.4-28.

T.4.6.7.3 Off-Normal Ambient Temperatures during Transfer

The thermal performance of the NUHOMS®-61BTH DSC during transfer under the minimum ambient temperature of 0°F with no insolation and 117°F with maximum insolation, for Type 1 and Type 2 DSCs are examined.

Note that a solar shield is used for transfer operations when the ambient temperature exceeds 100°F up to 117°F. This is done according to the NUHOMS® CoC 1004, Technical Specification 1.2.4, "TC/DSC Transfer Operations at High Ambient Temperatures" for transfer operations, when ambient temperatures exceed 100°F, which requires that a solar shield shall be used to provide protection against direct solar radiation.

T.4.6.7.4 Boundary Conditions, Off-Normal Transfer

The off-normal conditions of transfer analyses are performed for the following ambient conditions:

- Maximum off-normal ambient temperature of 117°F without insolation.

The 61BTH DSC temperature profiles calculated using the OS197FC-B thermal model as described in Section T.4.5 are applied to the corresponding surfaces of the DSC thermal analysis finite element model described in Section T.4.6.2.

T.4.6.7.5 61BTH DSC Thermal Analyses Results for Off-Normal Conditions of Storage and Transfer

Fuel Cladding Temperatures

The maximum fuel cladding temperatures during off-normal conditions of storage and transfer are evaluated for both Type 1 and Type 2 DSCs and compared with the corresponding fuel cladding temperature limits. The results are reported in Table T.4-17.

DSC Basket Component Temperatures

The maximum temperatures of the DSC components for off-normal conditions of storage and transfer are listed in Table T.4-18 and Table T.4-19 for Type 1 and Type 2 DSCs, respectively.

T.4.6.7.6 Off-Normal 61BTH DSC Maximum Internal Pressure during Storage/Transfer

The maximum average helium backfill gas temperature for off-normal conditions of storage and transfer occurs when the 61BTH DSC is in OS197FC-B TC with an ambient temperature of 117°F and sunshade. The average helium temperatures are 504°F (964°R) and 516°F (976°R) for Type 1 DSC and Type 2 DSC, respectively. Per NUREG 1536 [4.5], the percentage of fuel rods ruptured for off-normal cases is 10%.

A summary of the maximum off-normal operating pressures for the 61BTH Type 1 and Type 2 DSCs are presented in Table T.4-20.

T.4.6.7.7 Evaluation of 61BTH DSC Performance for Off-Normal Conditions

The NUHOMS®-61BTH DSC shell and basket are evaluated for calculated temperatures and pressures in Section T.3. The maximum fuel cladding temperatures are well below the allowable fuel temperature limit of 752°F (400°C) for transfer and 1058°F (570°C) for storage conditions. The maximum DSC internal pressures remain below 20.0 psig during off-normal conditions of storage

and transfer used in Section T.3. The pressures and temperatures associated with off-normal conditions in the NUHOMS®-61BTH DSC design meet all applicable off-normal thermal requirements.

T.4.6.8 DSC Thermal Evaluation for Accident Conditions

The NUHOMS®-61BTH DSC is evaluated for accident conditions of storage and transfer over a range of design basis off-normal ambient temperatures. A transient analyses of the NUHOMS® system components is performed at these ambient temperatures.

Since the NUHOMS® HSMs are located outdoors, there is a remote possibility that the ventilation air inlet and outlet openings could become blocked by debris from such unlikely events as floods and tornadoes. The NUHOMS® HSM system design features, such as the perimeter security fence and redundant protected location of the air inlet and outlet openings, reduce the probability of occurrence of such an accident. A complete blockage of all air inlets and outlet vents simultaneously is not a credible event. However, to bound the blockage of all inlets or outlets for this generic analysis, a complete blockage of all inlets and outlet vents accident is conservatively postulated to occur and is analyzed in Section T.4.4.5.

The controlling transfer accident considered involves a drop of the TC under maximum off-normal ambient temperature and insolation, the loss of the sun shield and the loss of the liquid neutron shield and loss of air circulation (if in use) in the TC as described in Section T.4.6.8.2.

The HSM, HSM-H and DSC contain no flammable material and the concrete and steel used for their fabrication can withstand any credible fire accident condition. Fire parameters are dependent on the amount and type of diesel and/or gasoline and/or other flammable liquids within the transporter and the fire accident conditions shall be addressed within site-specific applications. Licensees are required to verify that loadings resulting from potential fires and explosions are acceptable in accordance with 10CFR72.212(b)(2). The hypothetical fire evaluation for the NUHOMS®-61BTH system is presented in Section T.4.6.8.3.

T.4.6.8.1 Blocked Vent Accident Evaluation

For the postulated blocked vent accident condition, the HSM or HSM-H ventilation inlet and outlet openings are assumed to be completely blocked for a 40-hour period concurrent with the extreme off-normal ambient condition of 117°F with insolation.

When the inlet and outlet vents are blocked, the air surrounding the DSC in the HSM or HSM-H cavity is contained (trapped) in the HSM or HSM-H cavity. The temperature difference between the hot DSC surface and the surrounding HSM or HSM-H (cooler) heat shield and concrete surfaces results in closed cavity convection. However, closed cavity convection has been conservatively ignored. The analysis considers only the thermal conductivity of air.

Summaries of the calculated fuel cladding and DSC component temperatures are listed in Table T.4-21 through Table T.4-23.

T.4.6.8.2 Transfer Accident Evaluation

The postulated transfer accident event consists of 61BTH DSC transfer in the OS197/OS197H/OS197FC-B TC in a 117°F ambient environment with loss of the solar shield and the loss of liquid neutron shielding. Thermal model described in Section T.4.5.1.2 is used for this analysis. The results are shown in Table T.4-21 through Table T.4-23.

T.4.6.8.3 Hypothetical Fire Accident Evaluation

For the postulated worst-case fire accident, a 300 gallon diesel fire is simulated for a NUHOMS®-61BTH DSC with a decay heat load of 31.2 kW during transfer in the TC. This accident event bounds other fire scenarios associated with loading operations and storage within the HSM or HSM-H due to the large thermal mass of the HSM or HSM-H and its vent configuration which provides protection for the DSC and its payload.

Steady state, off-normal conditions are assumed prior to the fire, and consist of a 117°F ambient temperature without a solar shield in place on the TC but with water filled neutron shield. The fire has a temperature of 1,475°F, and an emittance of 0.9 and a duration of 15 minutes based on the 300-gallon diesel fuel source and complete engulfment of the TC for the duration of the fire. This is conservative because it allows the maximum amount of heat input into the NUHOMS® system components. Subsequent to the fire, the TC is subjected to 117°F ambient conditions with maximum insolation. Note that these hypothetical fire parameters and assumptions are very conservative.

It is assumed that liquid neutron shield (water) is present throughout the 15-minute fire transient even though it is expected to be lost and replaced with air very early in the fire transient. This assumption maximizes the heat input from the fire to the canister because of the high conductivity of water compared to air. To maximize the canister temperature during the post-fire transient, it is assumed that water in the neutron shield cavity is lost at the beginning of the post-fire transient and replaced by air as the heat flow is now from the canister to the ambient.

The gaps included in the thermal model of the 61BTH DSC basket are summarized in Figure T.4-26 through Figure T.4-28. These gaps are not removed for calculating the cladding temperatures during accident conditions. The canister shell temperatures change by a small amount during the accident fire transient. This change is small during the fire transient due to the large thermal mass of the transfer cask. This shows that heat input from the fire to the canister is not significant. Since the canister shell temperature is almost unchanged, the cladding temperatures during the 15-minute fire transient also are almost unchanged. Therefore, the assumption of not removing the gaps during the fire transient has a negligible impact on cladding temperatures.

The calculated temperature response of selected components in the TC and DSC during the first 360 minutes of the fire accident is shown in Figure T.4-21. A summary of the calculated maximum fire transient temperatures for components is listed in Table T.4-11. Comparison shows that the loss of neutron shield accident scenario temperatures bound those of the post-fire steady state temperatures. This occurs because sooting and oxidation of the exterior surfaces raise the surface emissivity, thus increasing the heat transfer between the cask and the ambient. Therefore, the NUHOMS®-61BTH DSC temperatures and pressures calculated for the transfer accident case bound the hypothetical fire accident case.

T.4.6.8.4 Fuel Cladding and Basket Materials

The maximum fuel cladding temperatures for the blocked vent transients are reported as a 40 hour transient in Table T.4-21. The maximum temperatures of the basket components are listed in Table T.4-22 and Table T.4-23.

T.4.6.8.5 Maximum Internal Pressures

The following conditions are considered in evaluating the maximum accident pressure for the 61BTH DSC:

The blocked vent case (61BTH DSCs in HSM-H or HSM) with maximum off-normal ambient temperature, and 10% fuel pin rupture. Note: 100% rupture is not assumed because a blocked vent cannot occur concurrently with a drop load. During the blocked vent case, the average helium gas temperature is 654°F (1114°R) (61BTH DSC in HSM).

The OS197/OS197H/OS197FC-B transfer cask accident case with maximum off-normal ambient temperature, loss of sun shield, liquid neutron shield, and air circulation (if used), and 100% fuel pin rupture.

The maximum accident case pressure occurs during 61BTH DSC (31.2 kW) transfer in the OS197FC-B cask under maximum off-normal ambient conditions, concurrent with loss of the solar shield, loss of liquid neutron shield, and loss of air circulation (if used). For this condition the average helium gas temperature is 615°F (1075°R) based on the results from Section T.4.6.8.2. In accordance with NUREG 1536, 100% of the fuel pins are assumed to rupture during this event.

A summary of the maximum accident operating pressures for the various 61BTH DSC configurations is presented in Table T.4-24.

T.4.6.8.6 Evaluation of the 61BTH DSC Performance during Accident Conditions

The NUHOMS®-61BTH DSC shell and basket are evaluated for the accident conditions pressures and temperatures as described in Section T.3.

The maximum fuel cladding temperature of 861°F is below the short-term limit of 1058°F (570°C). The accident pressures in the NUHOMS®-61BTH Type 1 and Type 2 DSCs are 56.1 psig and 68.7 psig, respectively. These pressures remain below the accident design pressures of 65.0 psig and 120 psig, respectively. It is concluded that the NUHOMS®-61BTH system maintains confinement during the postulated accident condition.

T.4.7 Thermal Evaluation for Loading/Unloading Conditions

All fuel transfer operations occur when the NUHOMS®-61BTH DSC and TC are in the spent fuel pool. The fuel is always submerged in free-flowing pool water permitting heat dissipation. After fuel loading is complete, the TC cask and DSC are removed from the pool and the DSC is drained, dried, sealed and backfilled with helium.

The bounding unloading operation considered is the reflood of the 61BTH DSC with water.

T.4.7.1 Maximum Fuel Cladding Temperatures during Vacuum Drying

The loading condition evaluated for the NUHOMS®-61BTH DSC is the heatup of the DSC before its cavity is backfilled with helium. This typically occurs during the performance of the vacuum drying operation of the DSC cavity with the TC in the vertical configuration inside the fuel handling building, and the annulus between the TC and the DSC is full of water.

Analyses were performed for the vacuum drying condition in order to ensure that the fuel cladding and 61BTH DSC structural component temperatures remain below the maximum allowable material limits. In addition, analysis was performed to ensure that the requirements defined by ISG-11 [4.15] for short-term operations (including vacuum during and helium backfilling operating conditions) are satisfied.

During vacuum drying operation, water in the DSC cavity is forced out of the cavity (blowdown operation) before the start of vacuum drying. Helium is used as the medium to remove water and subsequent vacuum drying occurs with a helium environment in the DSC cavity.

The vacuum drying of the DSC is assumed not to reduce the pressure sufficiently to reduce the thermal conductivity of the water vapor or helium in the DSC cavity [4.13], [4.14], and [4.25]. Therefore, with helium being used for blowdown operation, its presence is credited in the vacuum drying operations also. Radiation in the gaps within the basket and rail components is conservatively neglected.

Thermal analysis is performed using the three-dimensional model developed in Section T.4.6, with decay heat load of 22.0 kW for Type 1 DSC and 31.2 kW for Type 2 DSC at an initial DSC shell surface temperature of 225°F. The initial temperature of the DSC, basket and fuel is assumed to be 225°F, based on the saturation boiling temperature of the fill water. Table T.4-25 provides the maximum calculated temperatures for the fuel cladding and Table T.4-26 and Table T.4-27 provide the maximum calculated basket component temperatures for both the Type 1 and Type 2 DSCs, respectively.

The maximum cladding temperatures for vacuum drying using helium are 584°F for the Type 1 DSC and 592°F for the Type 2 DSC. These maximum cladding temperatures are well below the limit of 752°F [4.15].

T.4.7.2 Evaluation of Thermal Cycling of Fuel Cladding during Vacuum Drying, Helium Backfilling and Transfer Operations

ISG-11 [4.15] also states that thermal cycling is to be minimized and imposes a limit of 65°C (117°F) on thermal cycling (reduction in fuel clad temperature from previous peak temperature). The basis for the limit is that as the cladding temperature is reduced more than 65°C the concentration of hydrogen available for hydride reorientation becomes significant.

The thermal analysis of the 61BTH DSC during blowdown operation assumes helium is used to drain the water from the 61BTH DSC cavity and subsequent vacuum drying occurs with a helium environment. This configuration eliminates the thermal cycling of fuel cladding during helium backfilling of the 61BTH DSC subsequent to vacuum drying and it eliminates the need for a time limit on the vacuum drying operation, since the thermal conductivity of helium does not change with pressure during vacuum drying operations.

As shown in Table T.4-25 the maximum fuel cladding temperature limit of 400°C (752°F) in ISG-11 [4.15] is satisfied for the 61BTH DSC.

T.4.7.3 Reflooding Evaluation

For unloading operations, the DSC is filled with the spent fuel pool water through its siphon port. During this filling operation, the DSC vent port is maintained open with effluents routed to the plant's off-gas monitoring system. The NUHOMS®-61BTH DSC operating procedures recommend that the DSC cavity atmosphere be sampled prior to introducing any reflood water in the DSC cavity.

Initially, the pool water is added to the DSC cavity containing hot fuel and basket components, some of the water will flash to steam causing internal cavity pressure to rise. This steam pressure is released through the vent port. The procedures specify that the flow rate of the reflood water be controlled such that the internal pressure in the DSC cavity does not exceed 20 psig. This is assured by monitoring the maximum internal pressure in the DSC cavity during the reflood event. The reflood for the DSC is considered as a Service Level D event and the design pressure of the DSC is 120 psig for 61BTH Type 2 DSC and 65 psig for 61BTH Type 1 DSC. Therefore, there is sufficient margin in the DSC internal pressure during the reflooding event to assure that the DSC will not be over pressurized.

The maximum fuel cladding temperature during reflooding event is significantly less than the vacuum drying condition owing to the presence of water/steam in the DSC cavity. The analysis results presented in Table T.4-25 show that the maximum cladding temperature during vacuum drying is 592°F. Hence, the peak cladding temperature during the reflooding operation will be less than 592°F.

To evaluate the effects of the thermal loads on the fuel cladding during reflooding operations, a conservative assumption of high maximum fuel rod temperature of 750°F and a low quench water temperature of 50°F are used.

The material properties, corresponding to a temperature of 750°F, are used in the evaluation:

Modulus of Elasticity, E (psi) = 11.1 x10^6 [from Figure 4 of Reference [4.7]]
Coefficient of thermal expansion, α, (in/in/°F) = 3.73 x 10-6 [4.8]
Poisson's Ratio, ν, = 0.38 [4.9]
Yield Stress (irradiated), Sy, = 50,500 psi [4.10] [4.7]

The fuel cladding is evaluated as a hollow cylinder with an outer surface temperature of T (50°F), and the inner surface temperature of T+ΔT (750°F) using Reference [4.10] equations. The maximum thermal stress in the fuel cladding due to the temperature gradient during reflooding is calculated as follows:

The maximum circumferential stress at the outer surface is given by:

$$\sigma_t = \frac{\Delta T * \alpha \cdot E}{2(1-\nu)\log_e(c/b)} * (1 - \frac{2 * b^2}{(c^2 - b^2)} * \log_e c/b)$$

The maximum circumferential stress at the inner surface is given by:

$$\sigma_t = \frac{\Delta T * \alpha \cdot E}{2(1-\nu)\log_e(c/b)} * (1 - \frac{2 * c^2}{(c^2 - b^2)} * \log_e c/b)$$

The maximum stresses are calculated as 22,420 psi (outer surface) and 24,325 psi (inner surface). Based on the results of the thermal stress analysis, these stresses in the cladding during reflood are much less than the yield stress of 50,500 psi [4.7]. Therefore, cladding integrity is maintained during reflood operations.

Therefore, no cladding damage is expected due to the reflood event. This is also substantiated by the operating experience gained with the loading and unloading of transportation packages like IF-300 [4.6] which show that fuel cladding integrity is maintained during these operations and fuel handling and retrieval is not impacted.

T.4.8 Determination of Effective Thermal Properties of the Fuel, Basket and Air Within the HSM-H Closed Cavity

This section presents the methodology and determines the effective thermal conductivity, specific heat and density for the fuels to be stored within NUHOMS®-61BTH DSC with helium backfill and vacuum for use in the analysis of the thermal performance of the NUHOMS®-61BTH DSC.

This section also determines the effective thermal conductivity, density and specific heat load of the 61BTH DSC basket for use in the transient thermal analysis in Sections T.4.4 and T.4.5.

T.4.8.1 Determination of Bounding Effective Fuel Thermal Conductivity

T.4.8.1.1 Fuel Assemblies Evaluated

The fuel assemblies that are considered for storage in the NUHOMS® 61BTH DSC, including the design data for each fuel assemblies, are listed in Section T.2. This section includes calculation of the bounding properties among fuels to store in the 61BTH DSC with maximum total decay heat per DSC up to 31.2 kW.

T.4.8.1.2 Summary of Thermal Properties of Materials

The thermal conductivity and specific heat values of Zircaloy, UO_2 pellets, and Helium are presented in Section T.4.2. The emissivity of Zircaloy is also presented in Section T.4.2.

T.4.8.1.3 Calculation of Fuel Axial Effective Thermal Conductivity

The axial fuel conductivity is assumed to be limited to the cladding conductivity weighted by its fractional area as required in NUREG 1536 [4.5].

$$K_{axl} = (K_{zirc})(A_{zirc}/A_{eff}) \qquad (1)$$

K_{zirc} = Conductivity of Zircaloy
A_{eff} = (6") x (6") = 36 in^2
A_{zirc} = Cross section area of Zircaloy cladding in the fuel assembly

Equation (1) is used to calculate axial effective conductivity for the fuel assembly types listed in Section T.2.

T.4.8.1.4 Calculation of Fuel Transverse Effective Thermal Conductivity

The transverse fuel effective conductivity is determined by creating a two-dimensional finite element model of the fuel assembly centered within a fuel compartment. The outer surfaces, representing the fuel compartment tube walls, are held at a constant temperature and heat generating boundary condition is applied to the fuel pellets within the model. A maximum fuel assembly temperature is

then determined. The isotropic effective thermal conductivity of a heat generating square, such as the fuel assembly, can be calculated as described in Reference [4.16].

$$K_{eff} = 0.29468 \times \frac{Q'''a^2}{T_c - T_o} \qquad (2)$$

where:

Q''' = heat load per unit volume of fuel assembly (Btu/hr-in^3),
a = half width of fuel compartment opening = 6 / 2 = 3",
T_c = maximum temperature of fuel assembly (°F),
T_o = compartment wall temperature (°F).

with:

$$Q''' = \frac{Q}{4a^2 L_a} \qquad (3)$$

where:

Q = decay heat load per fuel assembly,
L_a = active fuel length

In determining the temperature dependent effective fuel conductivities, an average temperature, equal to $(T_c + T_o)/2$, is used for the fuel temperature.

2-D finite element models of each fuel assembly representing a quarter of the fuel assembly were modeled within ANSYS [4.22]. Plane 55 elements were used to model components such as the fuel pellets, fuel cladding, and the helium back fill gas. The gap between the fuel cladding and the fuel pellets is also included in the model.

Heat generated in the fuel pellets dissipates by conduction and radiation to the fuel compartment walls. Convection is not considered in the model. Radiation between the fuel rods, guide tubes, and basket walls was simulated using the radiation super-element processor (/AUX12). LINK32 elements were used for modeling of radiating surfaces in creating the radiation super-element and were unselected prior to the solution of the model. The compartment walls are not modeled as a solid entity. Only the LINK32 elements aligned with the outermost nodes of the model (not on symmetry lines) are given the emissivity of the compartment walls.

The emissivity of stainless steel (0.46) was applied to the LINK elements on fuel compartment tube walls. To eliminate the radiation heat transfer across the symmetry lines, the link elements on symmetry lines were given a very low emissivity (0.001).

The FANP9 9x9-2 fuel assembly finite element model is shown in Figure T.4-35 as a typical model for all the fuel types considered.

Since a quarter of fuel assembly is modeled in each case, the reaction solution after solving the 2D model is equal to the heat generated per unit length of the active fuel divided by four.

$$Q_{react} = \frac{Q}{4L_a} \qquad (4)$$

Substitution of equations (3) and (4) in equation (2) gives:

$$K_{eff} = 0.29468 \times \frac{Q_{react}}{(T_c - T_o)} \qquad (5)$$

Equation (5) is used to calculate the transverse effective fuel conductivity for each fuel assembly model.

The heat generating boundary conditions for each fuel assembly is calculated as shown in equation 6.

$$dhl = \frac{Q/N}{n\left(\frac{\pi}{4} d_p^{\,2}\right) L_a} \qquad (6)$$

dhl = Heat generating boundary condition, Btu/min-in-°F
Q = Total decay heat load, Btu/min
N = Number of assemblies, 61
n = Number of fuel rods
d_p = Pellet outer diameter, in
L_a = Active fuel length, in

The models were run with a series of isothermal boundary conditions applied to the nodes representing the fuel compartment walls. The symmetry lines going through the center of the fuel assembly are kept at the adiabatic boundary conditions.

T.4.8.1.5 Results

The Siemens QFA 9x9 assembly has the minimum (bounding) axial conductivity. Backfill gas property does not have any effect on the axial effective fuel conductivity. Therefore, identical axial effective fuel conductivity values can be used for helium and vacuum conditions.

The calculated transverse conductivities for fuels to store in the 61BTH DSC are presented in Figure T.4-36 for a helium environment. As shown herein, the FANP9 9 x 9-2 assembly has the (bounding) minimum transverse conductivity. The bounding transverse effective conductivity values for fuels to store in the 61BTH DSC are listed in Section T.4.2.

T.4.8.2 Calculation of Fuel Effective Specific Heat and Density

This section presents the calculation of the fuel effective specific heat and density used in the transient thermal analyses.

Volume average density and weight average specific heat are calculated to determine the effective density and specific heat for the fuel assembly.

The equations to determine the fuel effective density ρ_{eff} and specific heat $C_{p\,eff}$ are shown below.

$$\rho_{eff} = \frac{\sum \rho_i V_i}{V_{assembly}} = \frac{\rho_{UO_2}\ V_{UO_2} + \rho_{Zr}\ V_{Zr}}{4a^2 L_a}$$

$$C_{p,eff} = \frac{\sum \rho_i\ V_i\ C_{Pi}}{\sum \rho_i\ V_i} = \frac{\rho_{UO_2}\ V_{UO_2}\ C_{P,UO_2} + \rho_{Zr}\ V_{Zr}\ C_{P,Zr}}{\rho_{UO_2}\ V_{UO_2} + \rho_{Zr}\ V_{Zr}}$$

where:

ρ_i, $C_{p,i}$, V_i = density, specific heat, and volume of component,
L_a = active fuel length, and
a = half of compartment width.

The properties of Zircaloy and UO_2 are provided in Section T.4.2.

The calculated minimum (bounding) values of fuel effective specific heat and fuel effective density for fuel to store in the 61BTH DSC are summarized in Section T.4.2.

T.4.8.3 61BTH DSC Basket Effective Thermal Properties

The 61BTH DSC basket effective density, thermal conductivity and specific heat are calculated for use in the transient analyses of the 61BTH DSC in the OS197/OS197H/OS197FC-B transfer cask and in the HSM or HSM-H. The calculation of these thermal effective properties is based on the DSC component weights.

The 61BTH DSC effective density $\rho_{eff\,DSC\,basket}$, and specific heat $c_{p\,eff\,DSC\,basket}$ are calculated as volumetric and weight average values, respectively.

The effective transverse thermal conductivity is determined by theoretical solution for conduction in an infinite cylinder with uniform heat generation [4.28]:

$$k_{eff-basket} = \frac{Q}{4\pi \cdot L \cdot (T_c - T_s)}$$

where
- Q is total heat load, W
- L is cylinder (DSC cavity) length, m
- T_C is temperature at the cylinder center, °C
- T_S is temperature at the cylinder surface, °C

The effective transverse thermal conductivities of the 61BTH DSC basket $k_{eff\text{-}basket}$ are calculated for the Type 1 and Type 2 DSCs, using the corresponding ANSYS models.

The heat generation is applied to the fuel assemblies uniformly without a peaking factor. The temperatures from 100°F to 800°F are applied uniformly to the DSC shell.

An average, $(T_s+T_c)/2$, is used as the reference temperature, for which $k_{eff\text{-}basket}$ is reported.

The bounding radial and axial thermal conductivity values for 61BTH DSCs are shown in Section T.4.2.

T.4.8.4 Effective Air Conductivity in the HSM-H Closed Cavity

During blockage of the inlet and outlet vents, the air within the HSM-H is trapped. The convection heat transfer under these circumstances reduces to free convection in closed cavities. For conservatism, no convection is considered within the HSM-H cavity during blockage of the vents.

T.4.8.5 Effective Thermal Conductivity within Neutron Shield

The effective thermal conductivity within the neutron shield is directly proportional to the thermal conductivity of water or air and exponentially proportional to the associated Rayleigh number existing in the neutron shield cavity.

The thermal conductivity and the coefficient of thermal expansion increase with increasing temperature, while the density and viscosity decrease with increasing temperature (Table A.3 from Reference [4.16]). Therefore, the net effect of an increased heat load will be both a higher thermal conductivity and Rayleigh number. As such, the effective thermal conductivity computed for the 22 kW heat load in Appendix M, Chapter M.4, is conservatively less than the actual effective thermal conductivity for 31.2 kW heat load.

For the case of an air filled neutron shield, the thermal conductivity and viscosity of air increase with increasing temperature, while the density and the coefficient of thermal expansion decrease with increasing temperature. The net effect of operation at a higher temperature level will be a higher thermal conductivity, but a lower Rayleigh number for a given ΔT. Since increasing the heat load within the transfer cask will tend to increase both the operating temperature and the ΔT required to remove the heat from the cask, the lower ΔT associated with the 22 kW heat load used to compute the Appendix M, Chapter M.4, effective thermal properties effectively under-estimates the Rayleigh number for the 31.2 kW heat load.

The combined effect on the computed effective thermal conductivity due to operations at the proposed higher temperature level and a higher ΔT than assumed in Appendix M, Chapter M.4, results in effective thermal conductivity higher than the 22 kW from Chapter M.4. Therefore, use of Appendix M, Chapter M.4, values for the air filled neutron shield case is conservative for the 31.2 kW heat load case.

T.4.9 References

4.1 Report, "Topical Report on Actinide-Only Burnup Credit for PWR Spent Nuclear Fuel Packages," Office of Civilian Radioactive Waste Management, DOE/RW-0472, Revision 2, September 1998.

4.2 ASME Boiler and Pressure Vessel Code, Section II, Part D, Properties, 1998, including 2000 addenda.

4.3 Roshenow, W. M., J. P. Hartnett, and Y. I. Cho, "Handbook of Heat Transfer," 3rd Edition, 1998.

4.4 Bolz, R. E., G. L. Tuve, "CRC Handbook of Tables for Applied Engineering Science," 2nd Edition, 1973. Transfer, McGraw Hill, 1989.

4.5 NUREG-1536, "Standard Review Plan for Dry Cask Storage Systems," January 1997.

4.6 Consolidated Safety Analysis Report for IF-300 Shipping Cask, CoC 9001.

4.7 Chun, Ramsey; Witte, Monika; Schwartz, Martin, "Dynamic Impact Effects on Spent Fuel Assemblies," Lawrence Livermore National Laboratory, Report UCID-21246, October, 1987.

4.8 NUREG/CR-0497, "MATPRO-Version 11: "A Handbook of Materials Properties for Use in the Analysis of Light Water Reactor, Fuel Rod Behavior," EG&G, Inc. February, 1979.

4.9 Glasstone, S., Seasonske, A., "Nuclear Reactor Engineering," Third Edition, 1981.

4.10 Young, W.C., "Roark's Formulas for Stress and Strain," Sixth Edition, McGraw Hill.

4.11 Kreith, "The CRC Handbook of Thermal Engineering," 2000.

4.12 GESC NS-3, NAC International, Atlanta Corporate Headquarters (Test Report NS-3-001, while BISCO Products, Inc.).

4.13 Rohsenow, Hartnett, "Handbook of Heat Transfer Fundamentals," 2nd Edition, 1985.

4.14 Roth, A., "Vacuum Technology," 2nd Edition, 1982.

4.15 Interim Staff Guidance No. 11, Revision 3, "Cladding Considerations for the Transportation and Storage of Spent Fuel," November 17, 2003.

4.16 SAND90 2806, Sanders, T. L., et al., "A Method for Determining the Spent Fuel Contribution to Transport Cask Containment Requirements," TTC1019, UC 820, November 1992.

4.17 Not used.

4.18 Incropera and DeWitt, Handbook of Heat And Mass Transfer Fundamentals, 5th edition, Wiley Publishers, 2002, Table A.6, pp 924.

4.19 Bentz, "A Computer Model to Predict the Surface Temperature and Time-of-wetness of Concrete Pavements and Bridge Decks," Report # NISTIR 6551, National Institute of Standards and Technology, 2000.

4.20 Zoldners, "Thermal Properties of Concrete under Sustained Elevated Temperatures," ACI Publications, Paper SP 25-1, American Concrete Institute, Detroit, MI, 1970, Cavanaugh, Guide to Thermal Properties of Concrete and Masonry Systems, Reported by ACI Committee 122, Report #ACI 122R-02, American Concrete Institute, Detroit, MI, 2002.

4.21 Siegel, Howell, "Thermal Radiation Heat Transfer," 4th Edition, 2002.

4.22 ANSYS 8.1 Computer Code and Online User's Manuals.

4.23 NRC, Code of Federal Regulations, Part 71, "Packaging and Transportation of Radioactive Material," 2003.

4.24 I.E. Idelchik, "Handbook of Hydraulic Resistance," 3rd Edition, 1994.

4.25 David R. Lide, "CRC Handbook of Chemistry and Physics," 83rd edition, 2002-2003, CRC Press.

4.26 SINDA/FLUINT™, "Systems Improved Numerical Differencing Analyzer and Fluid Integrator," Version 4.7, Cullimore & Ring Technologies, Inc., Littleton, CO, 2004.

4.27 Thermal Desktop™, Version 4.7, Cullimore & Ring Technologies, Inc., Littleton, CO, 2004.

4.28 Incropera, F. P. M. D P. DeWitt, "Fundamentals of Heat and Mass Transfer," 3rd Edition, Wiley, 1990.

4.29 Not used.

4.30 "Thermal Testing of the NUHOMS® Horizontal Storage Module, Model HSM-H," Transnuclear Report No. E-21625, Revision 1.

4.31 Misumi, Toshiyuki, & Suzuki, Koji, & Kitamura, Kenzo, "Fluid Flow and Heat Transfer of Natural Convection Around Large Horizontal Cylinders: Experiments with Air, Heat Transfer – Asian Research," Volume 32, 2003.

Table T.4-1
Bulk Air Temperatures at Specified HSM-H Regions for the Various Cases(1)

Bulk Air Temperature	Case 1	Case 2	Case 3	Case 4
$T_{ambient}$ (°F)	-40	0	100	117
T_{exit} (°F)	18	64	179	185
$T_{average}$ (°F)	-11	32	139.5	151

(1) Cases are as listed in Section T.4.4.3.

Table T.4-2
HSM-H Components Normal and Off-Normal Maximum Temperatures, 31.2 kW Heat Load

Component	Maximum Temperature (°F)			
	Ambient -40°F	Ambient 0°F	Ambient 100°F	Ambient 117°F
	Case 1	Case 2	Case 3	Case 4
DSC Shell	337	365	436	439
Concrete	79	128	236	241
Top Heat Shield	38	95	218	225
Side Heat Shield	42	97	221	228
DSC Support Rail	134	176	280	285

Table T.4-3
HSM-H Components Maximum Temperatures (°F), 31.2 kW Decay Heat Load, 117°F Ambient, Blocked Vent Accident (Case 5)

Component	40 hr Blockage
DSC Shell	596
Concrete (1)	426
Top Heat Shield	386
Side Heat Shield	443
DSC Support Rail	516

(1) The calculated temperature is above the 350°F limit given in Reference [4.5]. Testing will be performed to document that concrete compressive strength will be greater than that assumed in the structural analyses.

Table T.4-4
Summary of OS197/OS197H/OS197FC-B Load Cases for 61BTH Type 1 DSC

Description	Applicable Conditions				
	Ambient Temperature (°F)	Insolation		Decay Heat kW[2]	Airflow, cfm
		Max.[1]	Zero		
Normal Hot	100	x		22	0
Normal Cold	0		x	22	0
Off-Normal Hot	117		x[3]	22	0
Vertical Loading Steady-State, Boral Option[5]	120		x	19.4[4]	0
Vertical Loading Steady-State[5]	120		x	22	0
Loss of Neutron Shield Transient[6]	100	x		22	0
Fire Accident[7]	117/1475/117	x		31.2[8]	0

(1) Insolation in accordance with 10 CFR §71.71(c)(1).

(2) Decay heat load applied as volumetric heat source over the 164" length of the solid cylindrical representation of the fuel basket. Unless noted otherwise, the neutron absorber material is borated aluminum.

(3) Sunshade assumed.

(4) Lower heat load limit applicable to Type 1 fuel basket with BORAL® or MMC as neutron absorber material.

(5) Assumes that TC is in the fuel handling facility, in the vertical orientation with the water in the DSC-cask annulus drained, and the air circulation option is not in use.

(6) Assumes initial steady-state conditions. At time = 0, the water in the neutron shield is drained, and the air circulation is not in use. Transient concludes with a steady-state analysis for horizontal operation, maximum insolation, a drained neutron shield, and no air circulation.

(7) 15 minute fire transient with 10 CFR §71.73 criteria used for fire properties. Sunshade assumed prior to fire, but lost for fire and post-fire analysis.

(8) Decay heat load for Type 2 fuel basket conservatively used for bounding analysis of the Type 1 fuel basket.

Table T.4-5
Summary of OS197FC-B Load Cases for 61BTH Type 2 DSC

Description	Applicable Conditions				
	Ambient Temperature (°F)	Insolation		Decay Heat kW[2]	Airflow, cfm
		Max.[1]	Zero		
Normal Hot	100	x		31.2	0
Normal Cold	0		x	31.2	0
Off-Normal Hot	117		x[3]	31.2	0
Normal Hot, FC	100	x		31.2	400
Normal Cold, FC	0		x	31.2	400
Off-Normal Hot, FC	117		x[3]	31.2	400
Vertical Load Transient[4]	120		x	31.2	0
Horizontal Load Transient[4]	100	x		31.2	0
Horizontal Load Transient[4]	117		x[3]	31.2	0
Horizontal Load Transient[4]	0		x	31.2	0
Vertical Load Transient[4]	120		x	27.4[5]	0
Loss of Air Circulation Transient[6]	100	x		31.2	0
Loss of Neutron Shield Transient[7]	100	x		31.2	0
Fire Accident[8]	117/1475/117	x		31.2	0

(1) Insolation in accordance with 10 CFR §71.71(c)(1).

(2) Decay heat load applied as volumetric heat source over the 164" length of the solid cylindrical representation of the fuel basket. Unless noted otherwise, the neutron absorber material is borated aluminum.

(3) Sunshade assumed.

(4) Assumes initial steady-state conditions with 215°F water in the cask-DSC annulus. At time = 0, the water is drained, the air circulation option is not used, and the system begins to heat up. Transient concludes with a steady-state analysis with no insolation, and no air circulation.

(5) Lower heat load limit applicable to Type 2 fuel basket with BORAL® or MMC as neutron absorber material.

(6) Assumes initial steady-state conditions. At time = 0, the air circulation is assumed lost. Transient concludes with a steady-state analysis for horizontal operation, maximum insolation, and no air circulation option used.

(7) Initial conditions taken from 28 hour point in 'Horizontal Load Transient' case with ambient temperature = 100°F. At time = 0, the water in the neutron shield is drained, and the air circulation is assumed to be unavailable. Transient concludes with a steady-state analysis for horizontal operation, maximum insolation, a drained neutron shield, and no air circulation.

(8) 15 minute fire transient. 10 CFR §71.73 criteria used for fire properties. Sunshade assumed prior to fire, but lost for fire and post-fire analysis.

Table T.4-6
Cask DSC Gap Hydraulic Characteristics as a Function of Circumferential Position

Angle (1)	DSC 'X' loc, Inches	DSC 'Y' loc, Inches	Cask 'X' loc, Inches	Cask 'Y' loc, Inches	Gap Width, Inches	Angle Segment	Flow Area, Sq. Inches	Hydraulic Dia., Inches
0°	0.0000	33.3659	0.0000	34.0000	0.6341	0 to 15	5.553	1.175
15°	-8.6380	32.2375	-8.7998	32.8415	0.6253	15 to 30	5.401	1.145
30°	-16.7003	28.9258	-17.0000	29.4449	0.5994	30 to 45	5.108	1.086
45°	-23.6469	23.6469	-24.0416	24.0416	0.5582	45 to 60	4.693	1.002
60°	-29.0079	16.7477	-29.4449	17.0000	0.5045	60 to 75	4.184	0.898
75°	-32.4145	8.6854	-32.8415	8.7998	0.4421	75 to 90	3.615	0.781
90°	-33.6250	0.0000	-34.0000	0.0000	0.3750	90 to 105	3.024	0.658
105°	-32.5440	-8.7201	-32.8415	-8.7998	0.3079	105 to 120	2.453	0.537
120°	-29.2323	-16.8773	-29.4449	-17.0000	0.2455	120 to 135	1.940	0.427
135°	-23.9060	-23.9060	-24.0416	-24.0416	0.1918	135 to 150	1.520	0.336
150°	-16.9247	-29.3144	-17.0000	-29.4449	0.1506	150 to 165	1.043	0.231
165°	-8.7676	-32.7210	-8.7998	-32.8415	0.1247	165 to 180	0.889	0.197
180°	0.0000	-33.8841	0.0000	-34.0000	0.1159			

Notes:
(1) 0° is at top of horizontal cask, 180° is at bottom of horizontal cask.
(2) DSC and cask 'X' and 'Y' positions measured with X= 0 and Y= 0 at the cask centerline.

Table T.4-7
OS197/OS197H/OS197FC-B TC Components and DSC Shell Steady State Temperatures for 61BTH Type 1 DSC under Normal and Off-Normal Conditions

Component	Temperature (°F)[1]					
	22 kW[1]				19.4 kW[2]	Max. Allowable
	100°F[3] Ambient	0°F[4] Ambient	117°F[5] Ambient	120°F[6] Ambient	120°F[6] Ambient	
Max. DSC Shell	418	358	413	446 / 429[7]	419/ 405[8]	800
Inner Liner	284	206	290	279	264	800
Gamma Shield	281	202	286	277	263	620
Structural Shell	248	155	250	248	236	800
Neutron Shield, Max. / Ave.	245 / 222	152 / 120	247 / 219	245 / 227	233 / 216	274 / -
Bulk Average NS-3, Bottom	209	106	207	279	263	300 / 250[9]
Closure Lid	196	91	192	191	185	800
Top Forging	209	107	204	201	193	800
Bottom Forging	243	151	246	323	303	800
Neutron Shield Outer Skin	239	140	235	237	226	-

Notes:

(1) 61BTH Type 1 DSC, with borated aluminum neutron absorber, and no air circulation.

(2) 61BTH Type 1 DSC, with BORAL® or MMC neutron absorber, and no air circulation.

(3) Normal hot condition with insolation for the horizontal transfer condition.

(4) Normal cold condition with no insolation for the horizontal transfer condition.

(5) Off-Normal hot condition with no insolation for the horizontal transfer condition.

(6) Normal hot condition with no insolation for the vertical loading/transfer condition in the fuel building.

(7) Peak temperature of 446°F occurs on the bottom shield plug for this condition, while the peak temperature noted on the sidewall is 429°F.

(8) Peak temperature of 419°F occurs on the bottom shield plug for this condition, while the peak temperature noted on the sidewall is 405°F.

(9) 300°F bulk average temperature limit used for short term, normal events like vertical loading. 250°F bulk average temperature limit used for long term, normal events.

Table T.4-8
OS197/OS197H/OS197FC-B TC Components and DSC Shell Temperatures for 61BTH Type 2 DSC under Normal and Off-Normal Conditions @ 28 Hr

Component	Temperature (°F)[1]					
	31.2 kW[1]				27.4 kW[2]	Max. Allowable
	100°F[3] Ambient	0°F[4] Ambient	117°F[5] Ambient	120°F[6] Ambient	120°F[6] Ambient	
Max. DSC Shell	441	408	437	445	417	800
Inner Liner	298	246	304	277	290	800
Gamma Shield	294	242	300	276	286	620
Structural Shell	249	186	257	241	247	800
Neutron Shield, Max. / Ave.	246 / 223	181 / 142	253 / 221	240 / 220	244 / 217	- / 274
Bulk Average NS-3, Bottom	203	119	201	245	241	300 / 250[7]
Closure Lid	193	115	191	182	183	800
Top Forging	209	134	206	197	199	800
Bottom Forging	237	173	241	280	272	800
Neutron Shield Outer Skin	239	167	241	232	233	-

Notes:

(1) 61BTH Type 2 DSC, with borated aluminum neutron absorber, and air circulation @ 28 hr.

(2) 61BTH Type 2 DSC, with BORAL® or MMC neutron absorber, and air circulation @ 28 hr.

(3) Normal hot condition with insolation for the horizontal transfer condition.

(4) Normal cold condition with no insolation for the horizontal transfer condition.

(5) Off-Normal hot condition with no insolation for the horizontal transfer condition.

(6) Normal hot condition with no insolation for the vertical loading/transfer condition in the fuel building.

(7) 300°F bulk average temperature limit used for short term, normal events like vertical loading. 250°F bulk average temperature limit used for long term, normal events.

Table T.4-9
OS197FC-B TC Components and DSC Shell Steady State Temperatures for 61BTH Type 2 DSC under Normal and Off-Normal Conditions and Air Circulation

Component	Temperature (°F)			
	31.2 kW[1]			Max. Allowable
	100°F[2] Ambient	0°F[3] Ambient	117°F[4] Ambient	
Max. DSC Shell	376	287	384	800
Inner Liner	288	195	298	800
Gamma Shield	283	191	294	620
Structural Shell	241	143	253	800
Neutron Shield, Max. / Ave.	238 / 194	140 / 79	250 / 198	- / 274
Bulk Average NS-3, Top	173	58	173	250
Closure Lid	217	112	219	800
Top Forging	222	124	227	800
Bottom Forging	195	87	207	800
Air Temperature, Inlet / Exit	100 / 240	0 / 126	117 / 246	n/a
Neutron Shield Outer Skin	226	130	238	-

Notes:

(1) 61BTH Type 2 DSC, with borated aluminum neutron absorber, and air circulation.
(2) Normal hot condition with insolation for the horizontal transfer condition.
(3) Normal cold condition with no insolation for the horizontal transfer condition.
(4) Off-Normal hot condition with no insolation for the horizontal transfer condition.

Table T.4-10
TC Components and DSC Shell Steady-State Temperatures for a Loss of Neutron Shield

Component	Temperature (°F)[1]		
	22 kW[2]	31.2 kW[3]	Max. Allowable
Max. DSC Shell	484	544	800
Inner Liner	375	428	800
Gamma Shield	372	424	620
Structural Shell	343	392	800
Neutron Shield, Max. / Ave.	n/a	n/a	- / 274
Bulk Average NS-3, Top	246	274	300
Closure Lid	230	252	800
Top Forging	266	300	800
Bottom Forging	294	334	800
Neutron Shield Outer Skin	243	267	-

Notes:

(1) Assume simultaneous loss of air circulation with fan (if used) and loss of water from neutron shield, with 100°F ambient with insolation.

(2) 61BTH Type 1 DSC with a heat load of 22.0 kW.

(3) 61BTH Type 2 DSC with a heat load of 31.2 kW.

Table T.4-11
TC Components and DSC Shell Temperatures for Fire Accident Temperatures with 31.2 kW Decay Heat Load

Component	Temperature (°F)[1]		
	End of Fire[2]	Post-Fire Steady-State[3]	Max. Allowable Short Term / Long Term
Max. DSC Shell	437	544	1000 / 800
Inner Liner	306	426	1000 / 800
Gamma Shield	303	422	620
Structural Shell	335	389	1000 / 800
Neutron Shield, Max. / Ave.	n/a	n/a	-
Bulk Average NS-3	707	220	1300 /250
Closure Lid	731	252	1000 / 800
Top Forging	996	299	1000 / 800
Bottom Forging	1182	330	1000 / 800
Neutron Shield Outer Skin	972	266	-

Notes:

(1) Assumes initial conditions with 61BTH Type 2 DSC with borated aluminum neutron absorber, 117°F ambient with sunshade @ 28 hours after drain down of cask-DSC annulus and no air circulation.

(2) Component temperatures at end of 15-minute fire transient.

(3) Assumes no air circulation and also loss of water in the neutron shield, 117°F ambient with insolation.

Table T.4-12
Fuel Cladding Normal Condition Maximum Temperatures

Operating Condition	61BTH Type 1 (1) (°F)	61BTH Type 2 (2) (°F)	Limit (3) (°F)
DSC in HSM, 0°F ambient	598	641	752
DSC in HSM, 100°F ambient	672	713	
DSC in TC, 0°F ambient, (Horizontal Transfer)	653	690	
DSC in TC, 100°F ambient, (Horizontal Transfer)	706	715	
DSC in TC, 120°F ambient, (Vertical Transfer)	734	728	

Notes:

(1) The maximum decay heat load for 61BTH Type 1 DSC is 22.0 kW.

(2) The maximum decay heat load for 61BTH Type 2 DSC is 31.2 kW.

(3) The fuel cladding limit is provided in ISG-11, Revision 3 [4.15].

Table T.4-13
61BTH Type 1 DSC Basket Assembly Maximum Normal Operating Component Temperatures

Operating Condition	Fuel Compart. (°F)	Neutron Absorber (°F)	R45 & R90 Rails (°F)	Top Grid (°F)	DSC Shell (°F)
DSC in HSM, 0°F ambient	570	570	438	411	278
DSC in HSM, 100°F ambient	647	646	523	492	374
DSC in TC, 0°F ambient, (Horizontal Transfer)	658	627	509	429	381
DSC in TC, 100°F ambient, (Horizontal Transfer)	683	682	565	490	439
DSC in TC, 120°F ambient, (Vertical Transfer)	711	710	579	510	430

Table T.4-14
61BTH Type 2 DSC Basket Assembly Maximum Normal Operating Component Temperatures

Operating Condition	Fuel Compart. (°F)	Neutron Absorber (°F)	R45 & R90 Rails (°F)	Top Grid (°F)	DSC Shell (°F)
DSC in HSM, 0°F ambient	590	589	420	405	364
DSC in HSM, 100°F ambient	666	665	504	486	434
DSC in TC, 0°F ambient, (1) (Horizontal Transfer, No Air)	660	659	511	462	410
DSC in TC, 100°F ambient, (1) (Horizontal Transfer, No Air)	686	686	539	493	438
DSC in TC, 0°F ambient, (2) (Horizontal Transfer, Air)	539	539	368	366	287
DSC in TC, 100°F ambient, (2) (Horizontal Transfer, Air)	629	628	461	457	376
DSC in TC, 120°F ambient, (1) (Vertical Transfer)	708	707	545	507	446

Notes:

(1) The analysis is performed for DSC shell temperatures at prescribed time limits; 15 hours for HLZC 7, and 28 hours for HLZCs 5 and 6, prior to air circulation being switched on.

(2) The analysis is performed for shell temperatures at steady state condition when the air circulation is switched on.

Table T.4-15
Initial Helium Fill Gas Molar Quantities

61BTH DSC Type	Helium Fill, g-moles
Type 1	192.9
Type 2	167.5

Table T.4-16
Maximum Normal Operating DSC Cavity Condition Pressures

61BTH DSC Type	DSC Cavity Volume	DSC Cavity Helium Fill Gas	Fuel Rod Volume	Fuel Rod Helium Fill Gas	Fission Product Gases	Total Gas	DSC Cavity Pressure	DSC Design Pressure	Bounding Case
	(in^3)	(g-mole)	(in^3)	(g-mole)	(g-mole)	(g-mole)	(psig)	(psig)	
Type 1	365,000	192.9	115.9	0.8	3.7	197.4	**7.3**	10	Vertical Transfer, 120°F Ambient
Type 2	315,000	167.5	115.9	0.8	3.7	172.0	**7.6**	15	Vertical Transfer, 120°F Ambient

Table T.4-17
Fuel Cladding Off-Normal Condition Maximum Temperatures

Operating Condition	61BTH Type 1 (1) (°F)	61BTH Type 2 (2) (°F)	Limit (3) (°F)
DSC in HSM, -40°F ambient	569	611	1,058
DSC in HSM, 117°F ambient	691	716	
DSC in TC, 117°F ambient, (No Insolation)	706	716(4)	752

Notes:

(1) The maximum decay heat load for 61BTH Type 1 DSC is 22.0 kW.

(2) The maximum decay heat load for 61BTH Type 2 DSC is 31.2 kW.

(3) The fuel cladding limit is provided in ISG-11, Revision 3 [4.15].

(4) The analysis is performed for shell temperatures at prescribed time limits; 15 hours for HLZC 7, and 28 hours for HLZCs 5 and 6, prior to air circulation being switched on.

Table T.4-18
61BTH Type 1 DSC Basket Assembly Maximum Off-Normal Operating Component Temperatures

Operating Condition	Fuel Compart. (°F)	Neutron Absorber (°F)	R45 & R90 Rails (°F)	Top Grid (°F)	DSC Shell (°F)
DSC in HSM, -40°F ambient	540	539	403	378	238
DSC in HSM, 117°F ambient	667	666	545	520	399
DSC in TC, 117°F ambient, (No Insolation)	682	682	562	489	416

Table T.4-19
61BTH Type 2 DSC Basket Assembly Maximum Off-Normal Operating Component Temperatures

Operating Condition	Fuel Compart. (°F)	Neutron Absorber (°F)	R45 & R90 Rails (°F)	Top Grid (°F)	DSC Shell (°F)
DSC in HSM, -40°F ambient	577	576	388	375	335
DSC in HSM, 117°F ambient	688	687	508	496	438
DSC in TC, 117°F ambient, (1) (No Insolation)	687	687	542	496	442

Note:

(1) The analysis is performed for shell temperatures at prescribed time limits; 15 hours for HLZC 7, and 28 hours for HLZCs 5 and 6, prior to air circulation being switched on.

Table T.4-20
Maximum Off-Normal Operating Condition DSC Cavity Pressures

61BTH DSC Type	DSC Cavity Volume	DSC Cavity Helium Fill Gas	Fuel Rod Volume	Fuel Rod Helium Fill Gas	Fission Product Gases	Total Gas	DSC Cavity Pressure	DSC Design Pressure	Bounding Case
	(in^3)	(g-mole)	(in^3)	(g-mole)	(g-mole)	(g-mole)	(psig)	(psig)	
Type 1	365,000	192.9	1159.4	8.3	37	238.1	**10.9**	20	Transfer, 117°F Ambient
Type 2	315,000	167.5	1159.4	8.3	37	212.8	**12.1**	20	Transfer, 117°F Ambient

Table T.4-21
Fuel Cladding Accident Condition Maximum Temperatures

Operating Condition	61BTH Type 1 (1) (°F)	61BTH Type 2 (2) (°F)	Limit (3) (°F)
DSC in HSM, Blocked Vents, (4) 117°F ambient	858	861	1,058
DSC in TC, loss of sun shade, neutron shield water, and air circulation with fan (if needed), 117°F ambient	749	824	

Notes:

(1) The maximum decay heat load for the 61BTH Type 1 DSC is 22.0 kW.

(2) The maximum decay heat load for the 61BTH Type 2 DSC is 31.2 kW.

(3) The fuel cladding limit is provided in ISG-11, Revision 3 [4.15].

(4) Temperature at 40 hours of blocked vents.

Table T.4-22
61BTH Type 1 DSC Basket Assembly Accident Maximum Component Temperatures

Operating Condition	Fuel Compart. (°F)	Neutron Absorber (°F)	R45 & R90 Rails (°F)	Top Grid (°F)	DSC Shell (°F)
DSC in HSM, Blocked Vents, (1) 117°F ambient	839	838	735	695	611
DSC in TC, loss of sun shade, neutron shield water, and air circulation with fan (if needed), 117°F ambient	727	727	609	531	467

Note:

(1) Temperature at 40 hours of blocked vents.

Table T.4-23
61BTH Type 2 DSC Basket Assembly Accident Maximum Component Temperatures

Operating Condition	Fuel Compart. (°F)	Neutron Absorber (°F)	R45 & R90 Rails (°F)	Top Grid (°F)	DSC Shell (°F)
DSC in HSM, Blocked Vents, (1) 117°F ambient	836	836	675	654	596
DSC in TC, loss of sun shade, neutron shield water, and air circulation with fan (if needed), 117°F ambient	799	798	640	587	546

Note:

(1) Temperature at 40 hours of blocked vents.

Table T.4-24
Maximum Accident Condition DSC Cavity Pressures

61BTH DSC Type	DSC Cavity Volume	DSC Cavity Helium Fill Gas	Fuel Rod Volume	Fuel Rod Helium Fill Gas	Fission Product Gases	Total Gas	DSC Cavity Pressure	DSC Design Pressure	Bounding Case
	(in^3)	(g-mole)	(in^3)	(g-mole)	(g-mole)	(g-mole)	(psig)	(psig)	
Type 1	365,000	192.9	11594.4	83	369.7	645.5	**56.1**	65	Transfer, 117°F Ambient
Type 2	315,000	167.5	11594.4	83	369.7	620.2	**68.7**	120	Transfer, 117°F Ambient

Table T.4-25
Vacuum Drying Fuel Cladding Maximum Temperatures

Operating Condition	61BTH Type 1 (1) (°F)	61BTH Type 2 (2) (°F)	Limit (3) (°F)
Vacuum Drying using Helium (or Helium backfilling) Steady State	584 (4)	592 (5)	752

Notes:

(1) The maximum decay heat load for 61BTH Type 1 DSC is 22.0 kW.
(2) The maximum decay heat load for 61BTH Type 2 DSC is 31.2 kW.
(3) The fuel cladding limit is provided in ISG-11, Revision 3 [4.15].
(4) Temperature is bounded by HLZC #1.
(5) Temperature is bounded by HLZC #7.

Table T.4-26
61BTH Type 1 DSC Basket Assembly Maximum Component Temperatures during Vacuum Drying

Operating Condition	Fuel Compart. (°F)	Neutron Absorber (°F)	R45 & R90 Rails (°F)	Top Grid (°F)	DSC Shell (°F)
Vacuum Drying using Helium (or Helium backfilling) Steady State	555	555	409	394	228

Table T.4-27
61BTH Type 2 DSC Basket Assembly Maximum Component Temperatures during Vacuum Drying

Operating Condition	Fuel Compart. (°F)	Neutron Absorber (°F)	R45 & R90 Rails (°F)	Top Grid (°F)	DSC Shell (°F)
Vacuum Drying using Helium (or Helium backfilling) Steady State	558	557	355	384	227

Table T.4-28
61BTH Type 1 DSC Shell Temperatures for Storage in HSM

Ambient Temperature (°F)	Top (°F)	Side (°F)	Bottom (°F)
-40	237	210	158
0	277	247	191
100	374	339	273
117	399	362	295
Blocked Vent	611	568	452

Note: The above temperatures correspond to a total decay heat load of 24.0 kW.

Table T.4-29
DSC Cavity Free Volumes

DSC Type	61BTH Type 1 DSC	61BTH Type 2 DSC
Cavity Volume, (in^3)	618,766	618,766
Basket Volume, (in^3)	108,888	160,372
No. of Fuel Assemblies	61	61
Fuel Volume, (in^3)	141,947	141,947
Free DSC Volume (in^3)	367,931	316,447
Bounding Free DSC Volume used in calculation (in^3)	365,000	315,000

Table T.4-30
Fuel Rod Helium Fill Gas Released per DSC

Operating Conditions	% of Ruptured Fuel Rods	Helium Fill Gas Release (g-moles)
Normal	1	0.83
Off-Normal	10	8.3
Accident	100	83.0

Table T.4-31
Fission Gas Released per DSC

Operating Conditions	% of Ruptured Fuel Rods	Fission Gas Release (g-moles)
Normal	1	3.7
Off-Normal	10	37.0
Accident	100	369.7

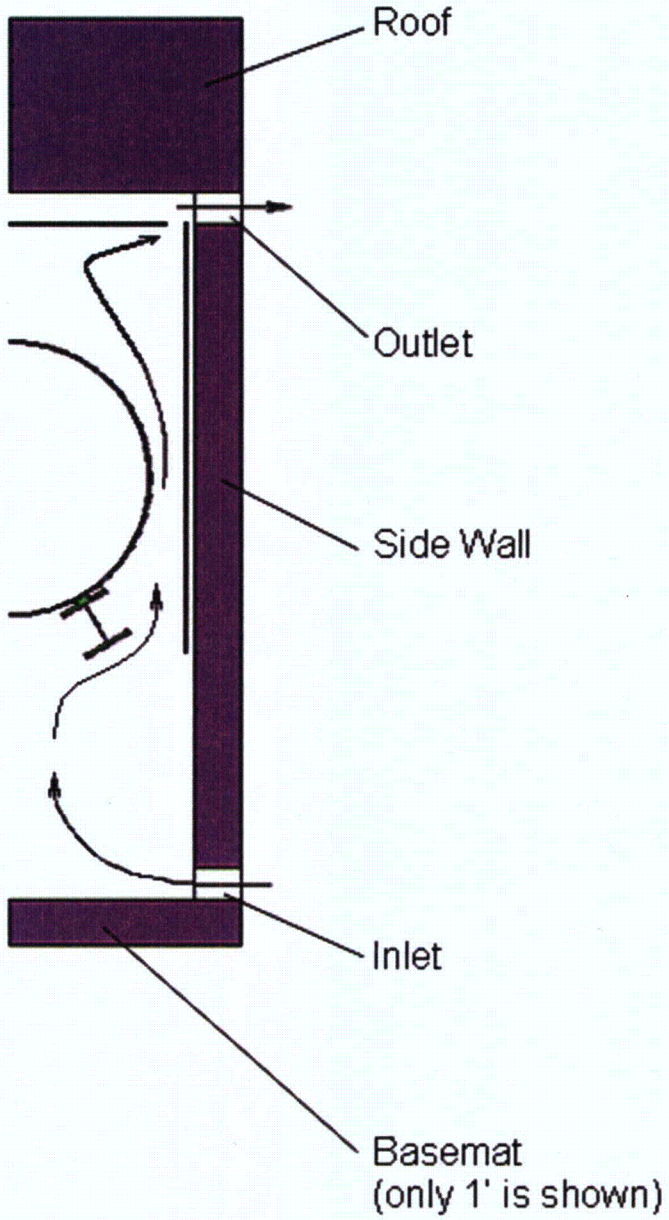

Figure T.4-1
HSM-H Air Flow Diagram

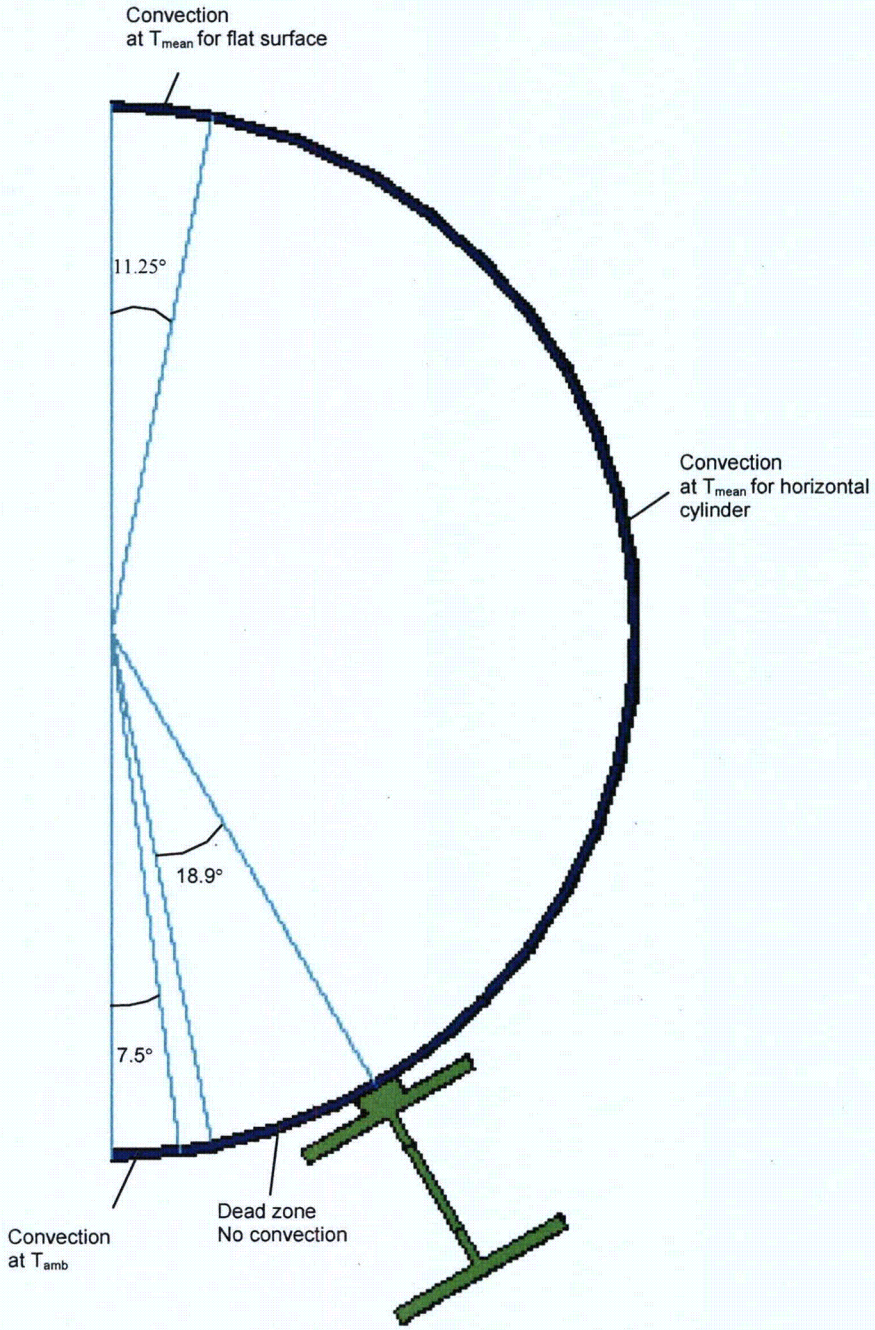

Figure T.4-2
Convection Regions around 61BTH DSC in the HSM-H

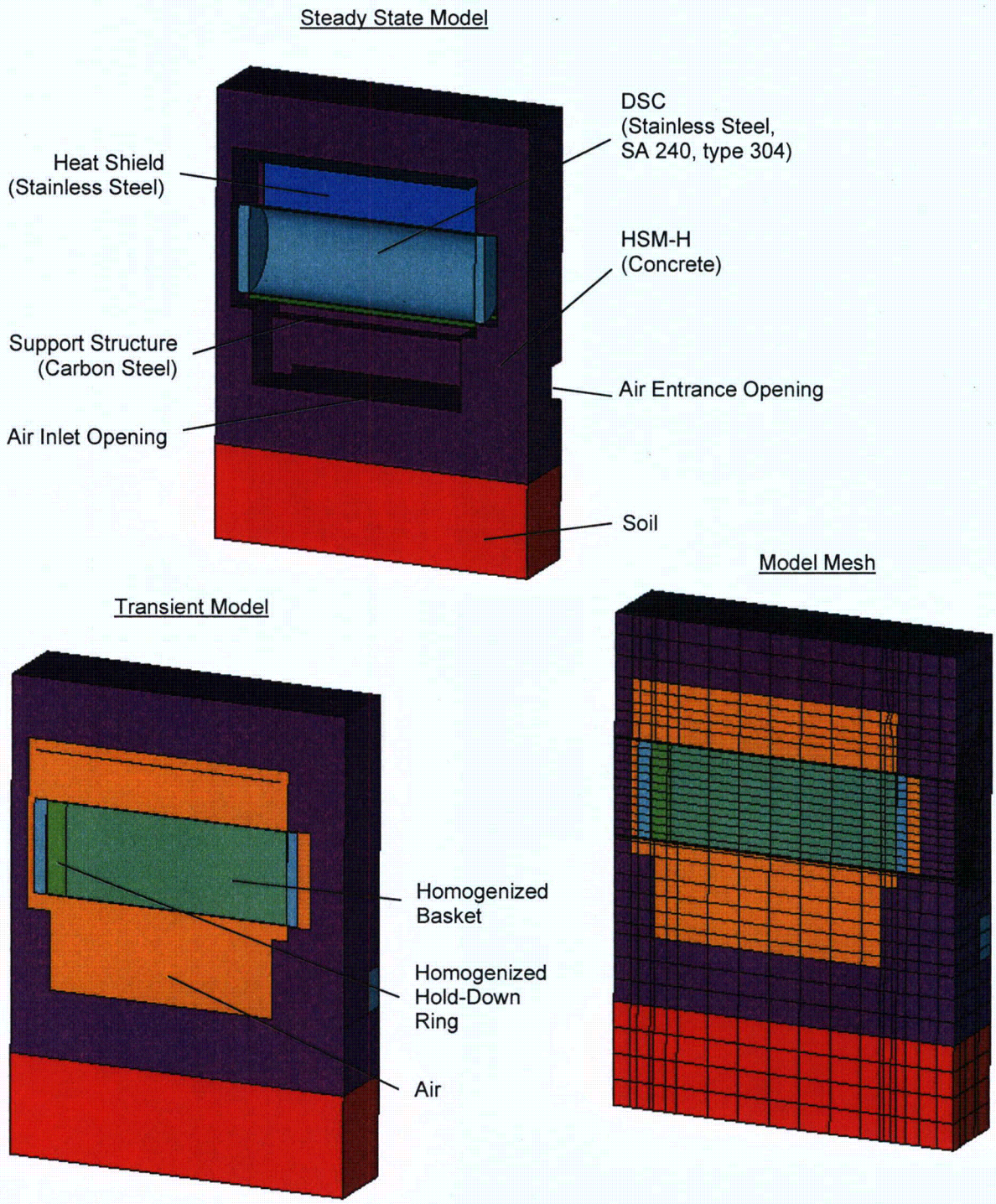

Figure T.4-3
61BTH DSC Shell Assembly in HSM-H Finite Element Model

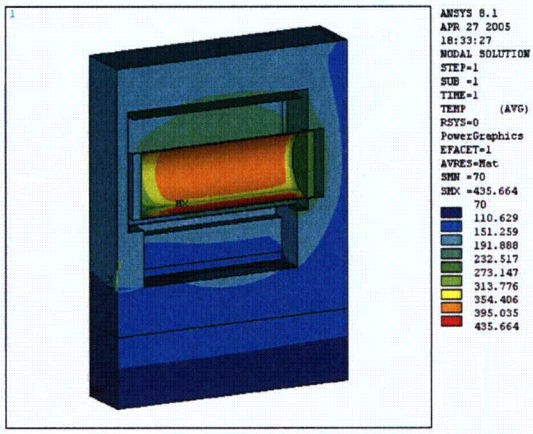

HSM-H

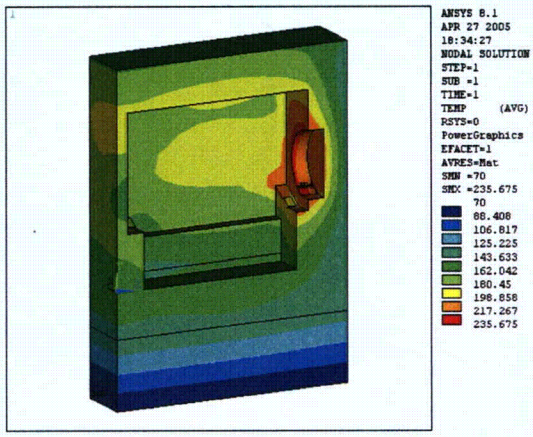

Concrete

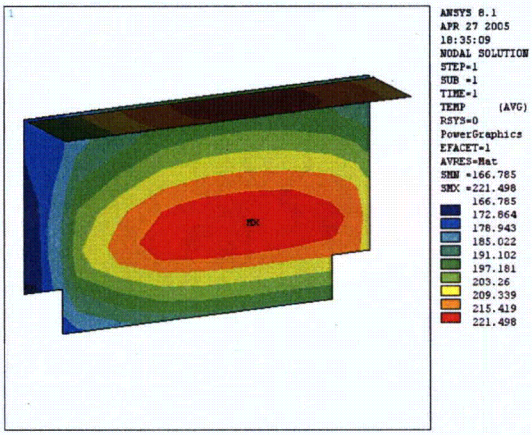

Heat Shields

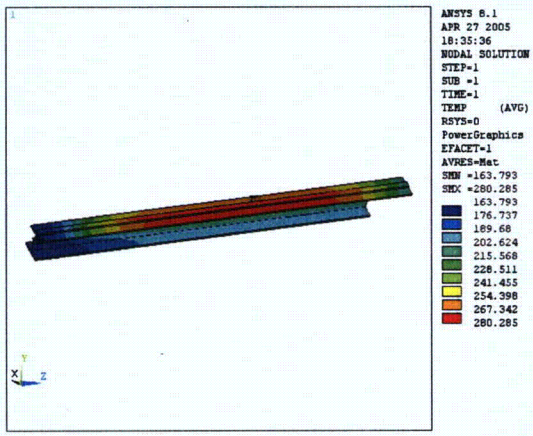

Support Rail

Figure T.4-4
HSM-H Component Temperature Distributions for 61BTH Type 2 DSC, 31.2 kW, 100°F Ambient

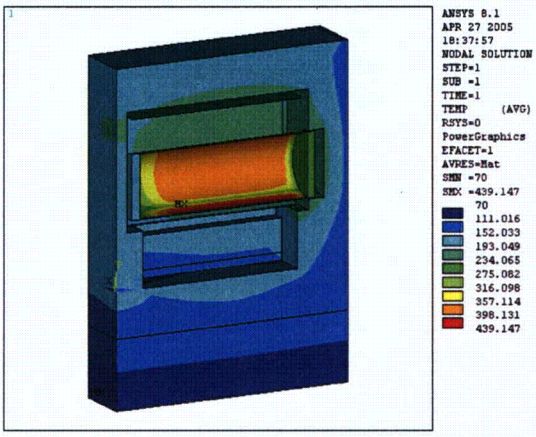

HSM-H

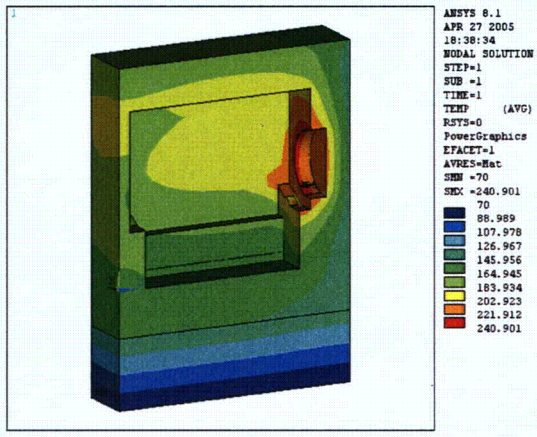

Concrete

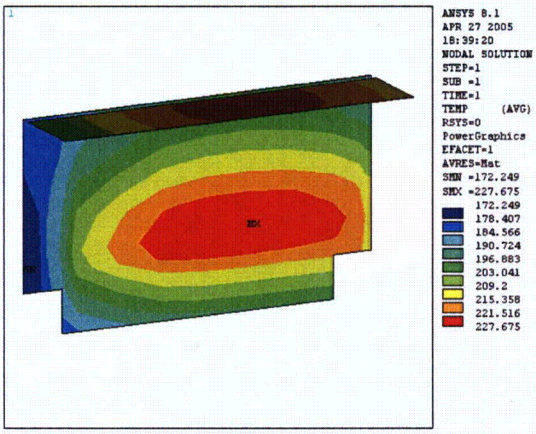

Heat Shields

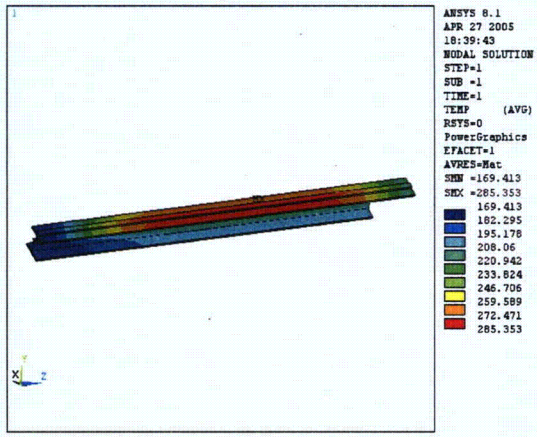

Support Rail

Figure T.4-5
HSM-H Component Temperature Distributions for 61BTH Type 2 DSC, 31.2 kW, 117°F Ambient

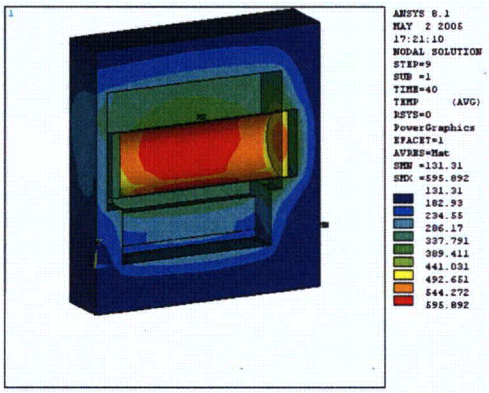

HSM-H

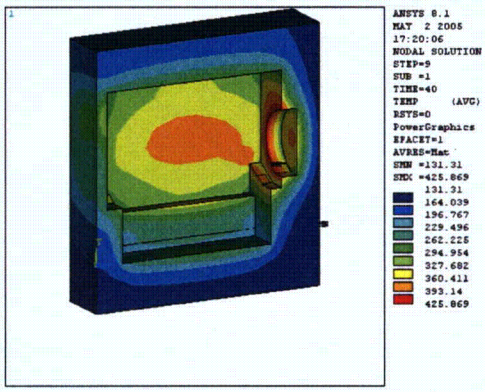

Concrete

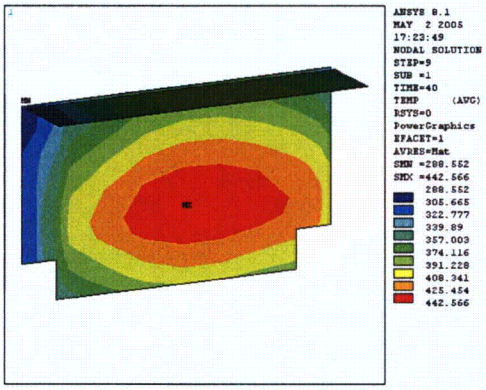

Heat Shields

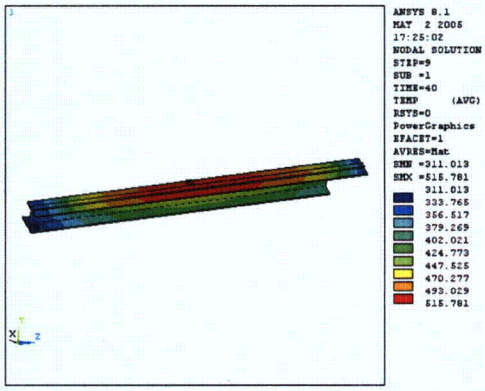

Support Rail

Figure T.4-6
HSM-H Component Temperature Distributions for 61BTH Type 2 DSC, 31.2 kW, @ 40 hours of Blocked Vents, 117°F Ambient

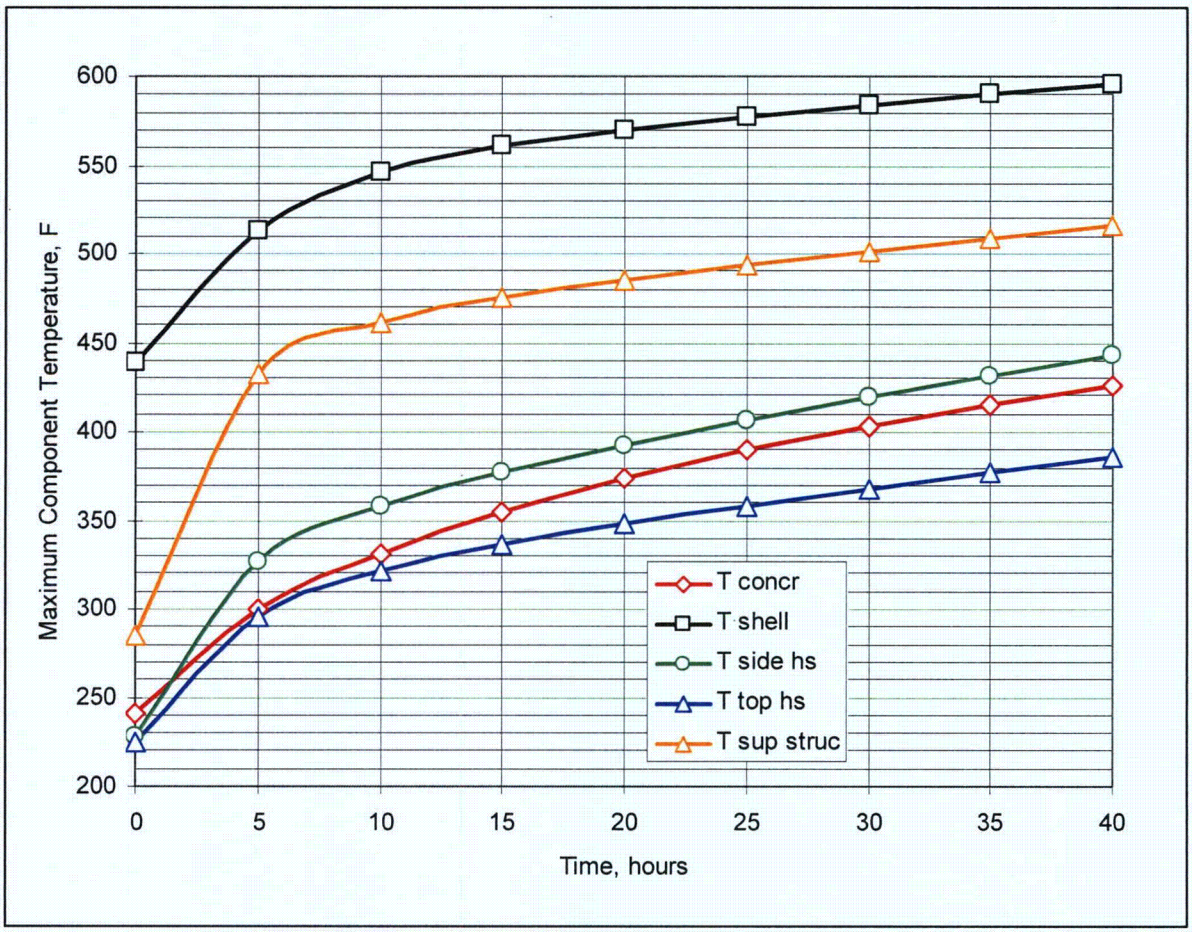

Figure T.4-7
HSM-H Component Temperature Time Histories for
61BTH Type 2 DSC, 31.2 kW, Blocked Vents Accident Condition, 117°F Ambient

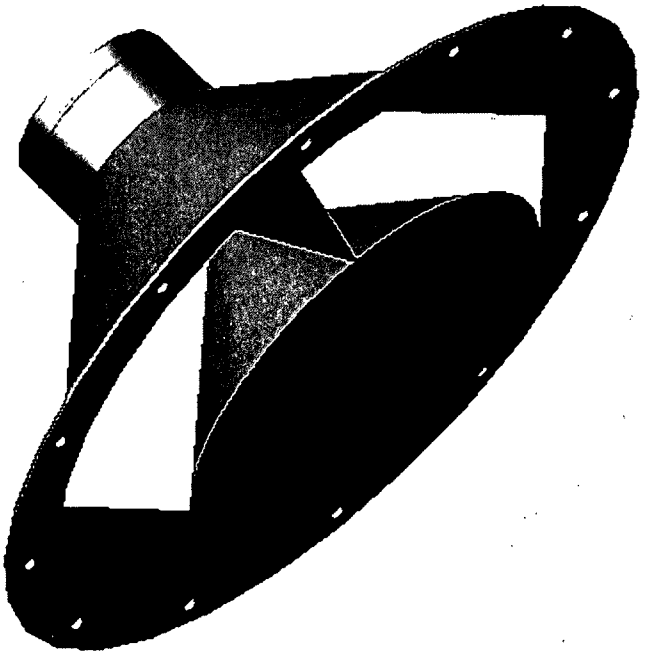

Figure T.4-8
Cone Adapter for Air Entrance at Ram Access Cover

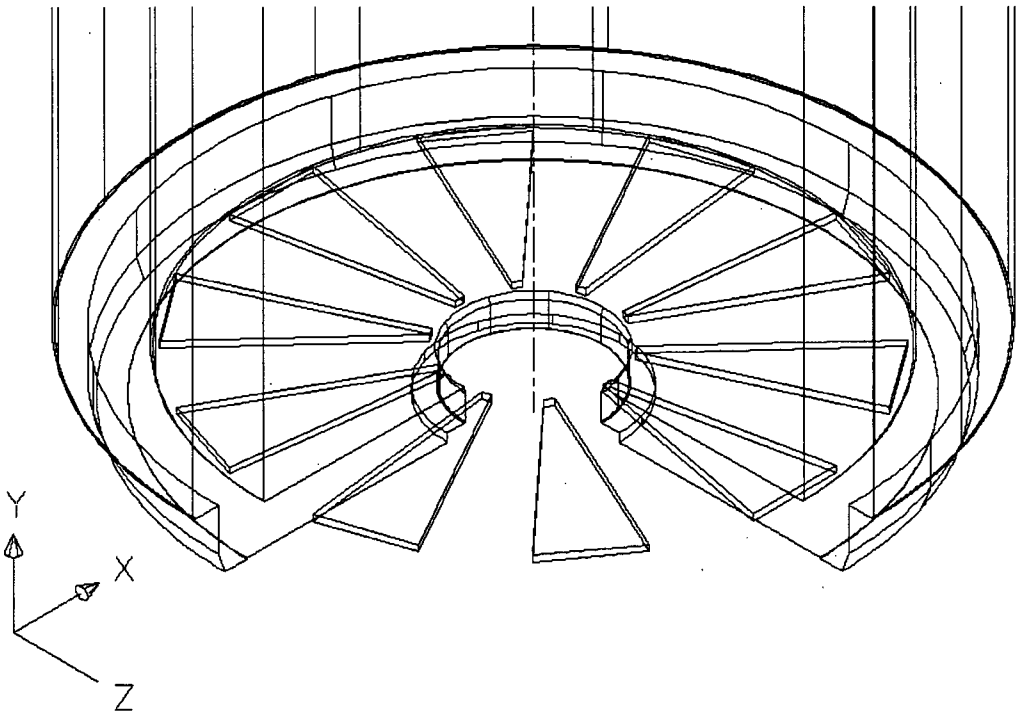

Figure T.4-9
Illustration of Wedge Segments at Bottom of OS197FC-B

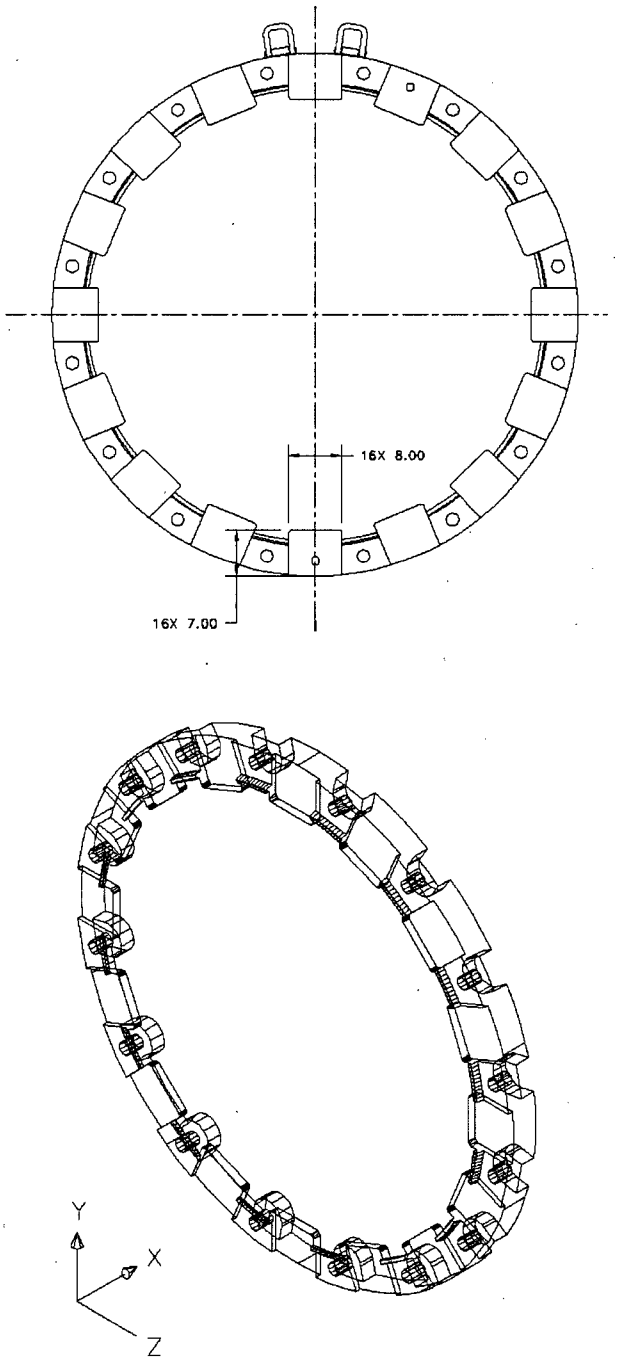

Figure T.4-10
OS197FC-B TC Lid with Slots for Air Exhaust
Plan, and Isometric Views

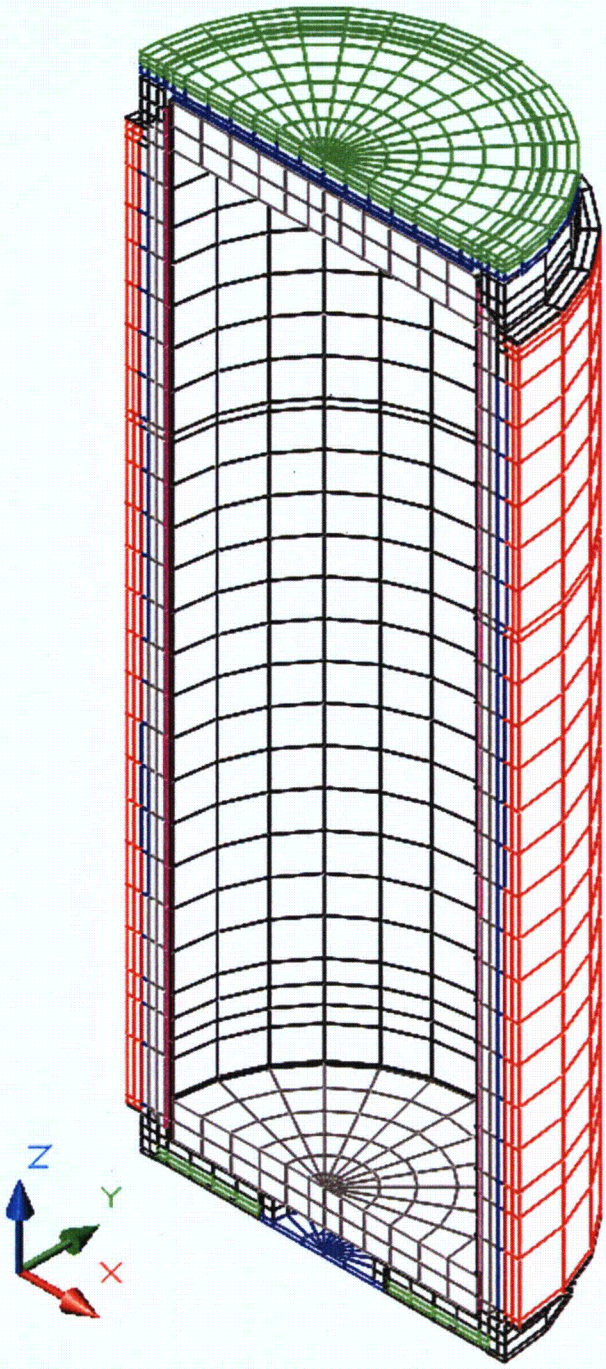

(Note: The positive z-axis is oriented along the cask length and the positive x-axis towards the bottom of the normally horizontal package.)

Figure T.4-11
Perspective View of OS197FC-B TC / 61BTH DSC Shell Thermal Model

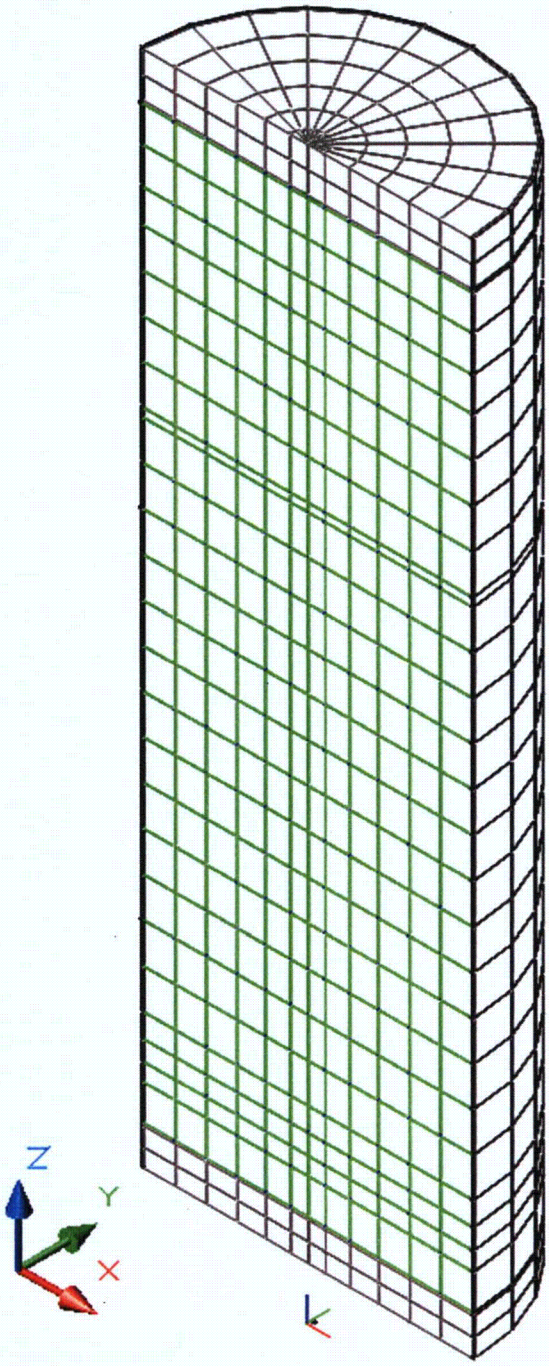

(Note: the positive z-axis is oriented along the cask length and the positive x-axis towards the bottom of the normally horizontal package)

Figure T.4-12
Perspective View of 61BTH DSC Shell, Ends, and Fuel Basket Thermal Model

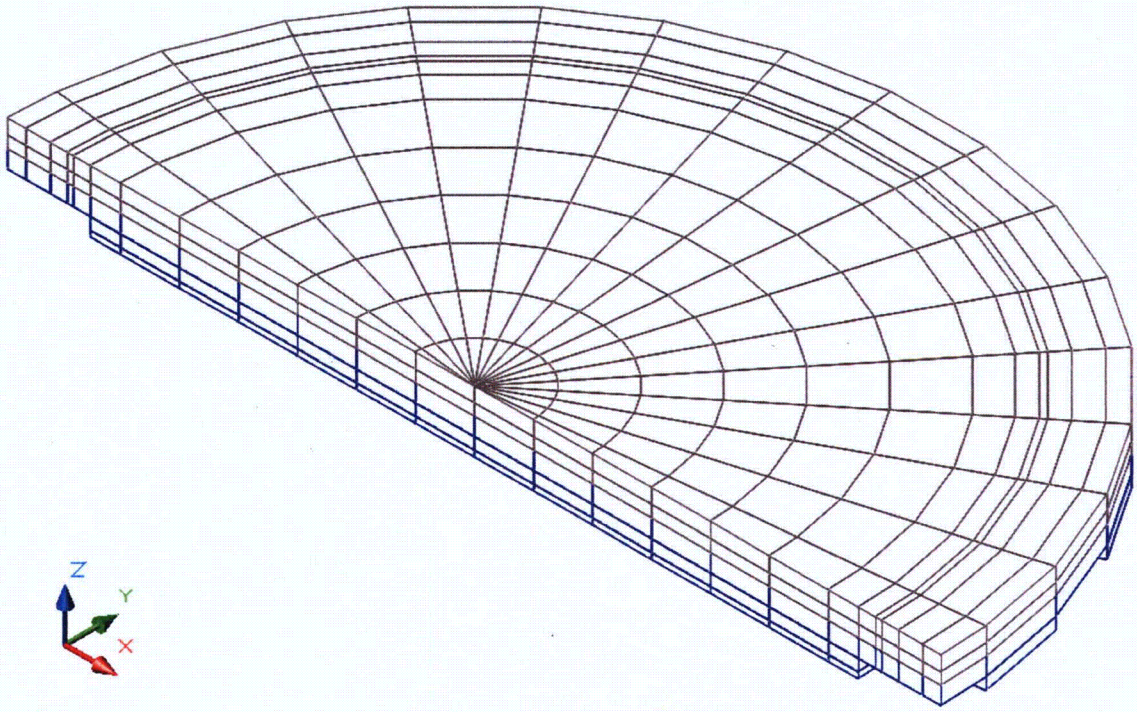

(Note: the positive z-axis is oriented along the cask length and the positive x-axis towards the bottom of the normally horizontal package)

Figure T.4-13
Perspective View of Thermal Model for OS197FC-B Closure Lid & NS-3

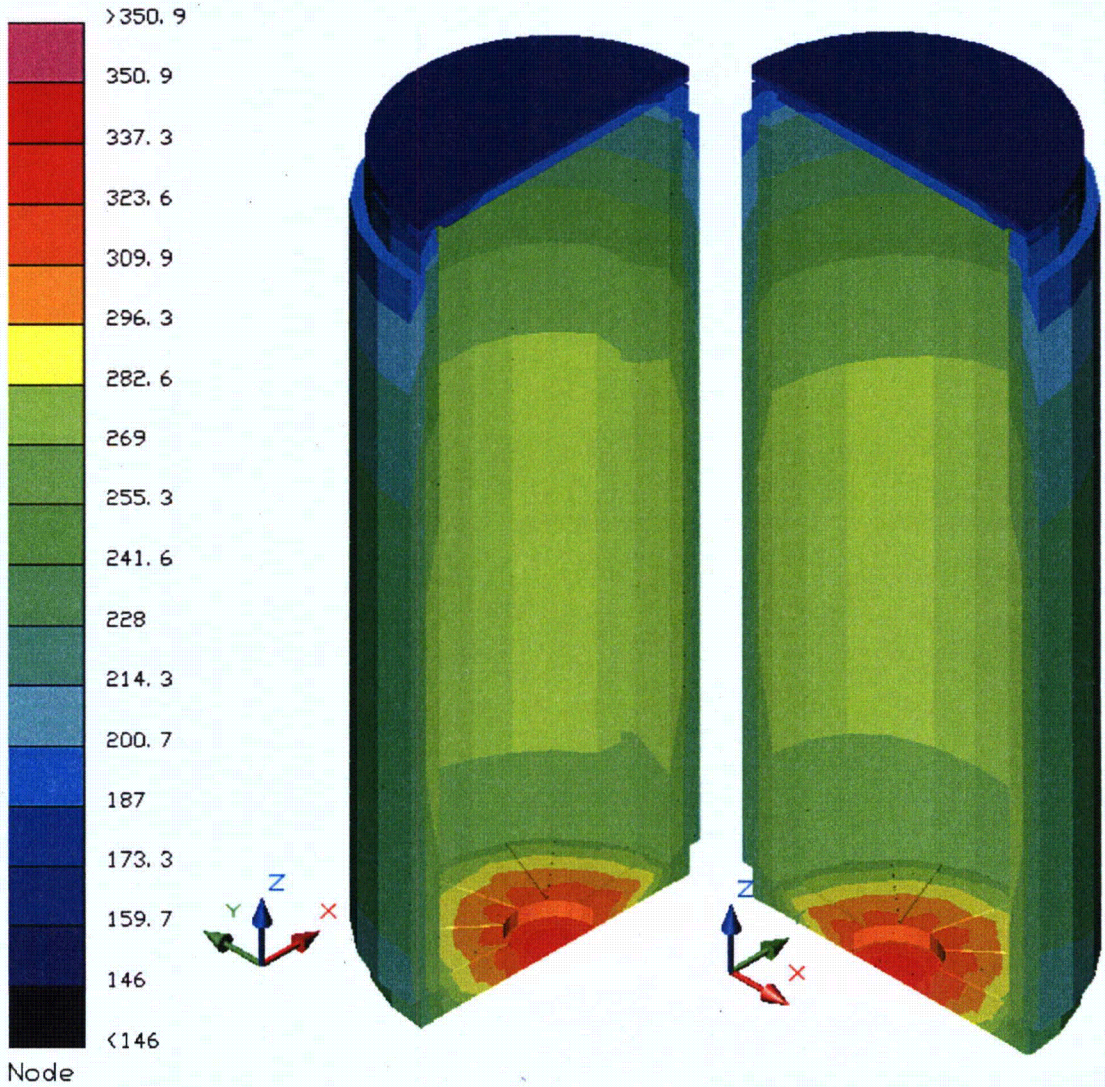

(Note: the positive z-axis is oriented along the cask length and the positive x-axis towards the bottom of the normally horizontal package)

Figure T.4-14
OS197FC-B TC Steady State Temperature Distribution,
Vertical Transfer of Type 1 DSC with 22.0 kW Heat Load,
No Insolation at 120°F Ambient

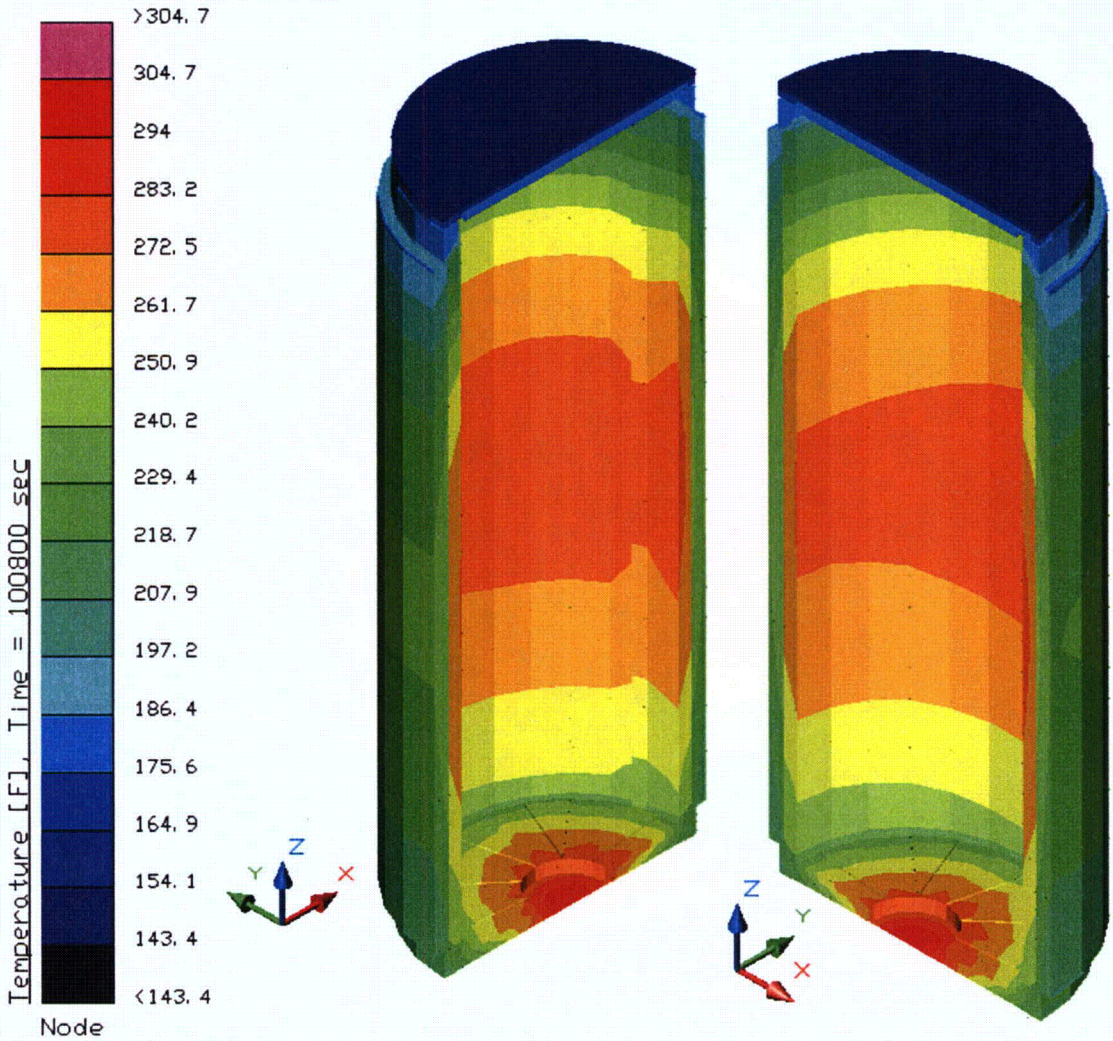

(Note: the positive z-axis is oriented along the cask length and the positive x-axis towards the bottom of the normally horizontal package)

Figure T.4-15
OS197FC-B TC Temperature Distribution @ 28 hours
Vertical Transfer of Type 2 DSC with 31.2 kW Heat Load,
No Insolation at 120°F Ambient

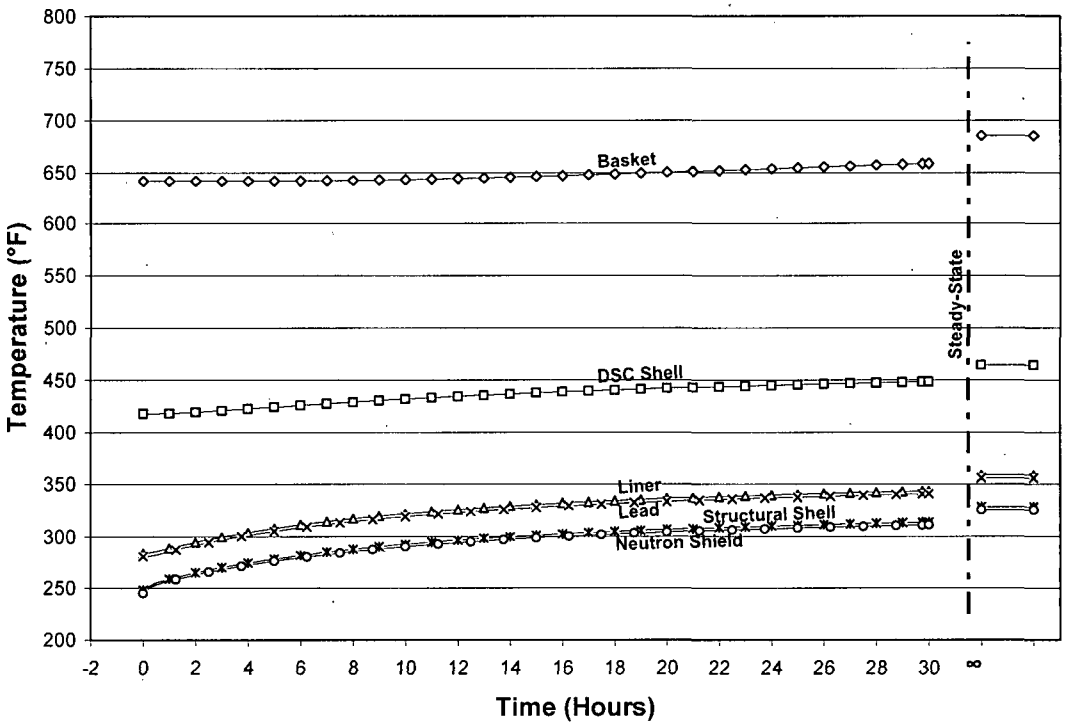

Figure T.4-16
Horizontal Transfer Transient Temperature Response of Type 1 DSC with 22.0 kW Heat Load, Loss of Neutron Shield and Air Circulation Accident at 100°F Ambient

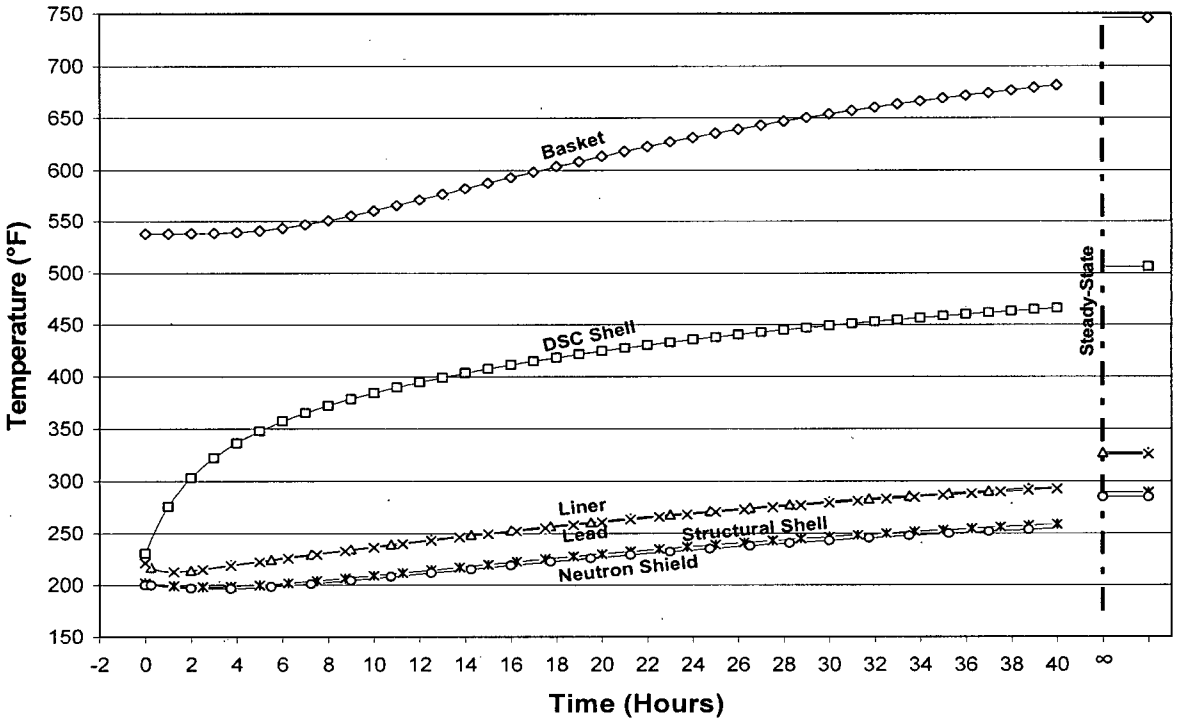

Figure T.4-17
Vertical Transfer Transient Temperature Response of 61BTH Type 2 DSC with 31.2 kW Heat Load, No Insolation at 120°F Ambient

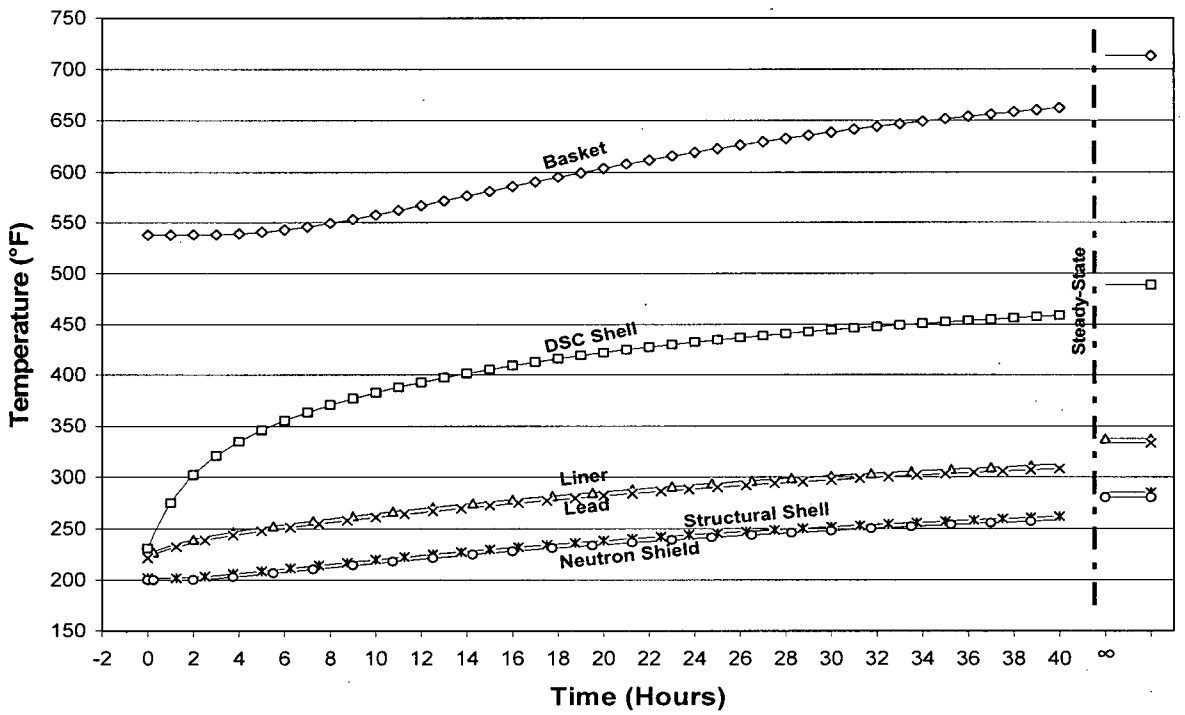

Figure T.4-18
Horizontal Transfer Transient Temperature Response of Type 2 DSC with 31.2 kW Heat Load, Insolation at 100°F Ambient

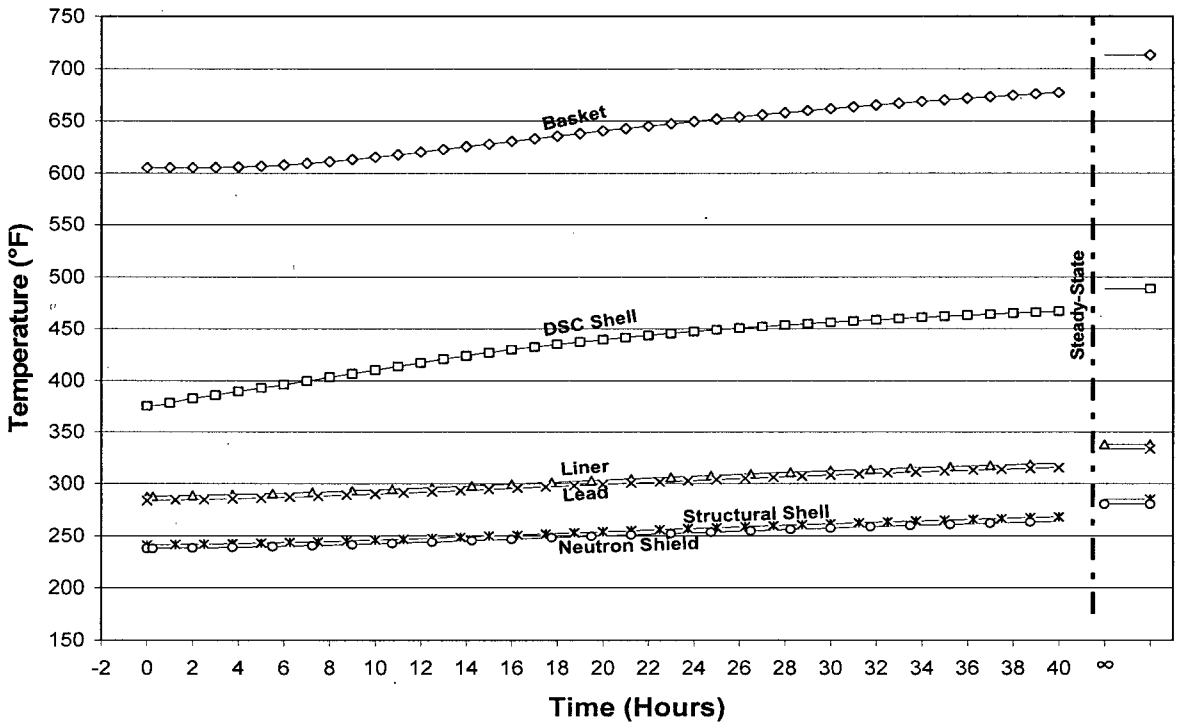

Figure T.4-19
Horizontal Transfer Transient Temperature Response of Type 2 DSC with 31.2 kW Heat Load, Loss of Air Circulation Accident, Insolation at 100°F Ambient

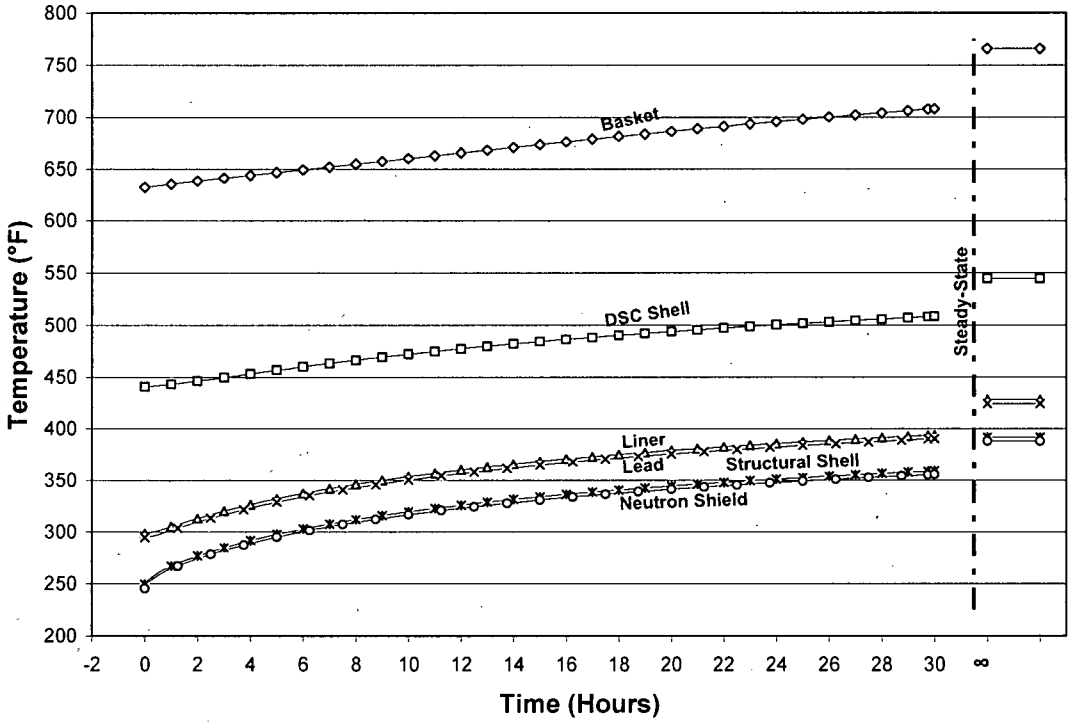

Figure T.4-20
Horizontal Transfer Transient Temperature Response of Type 2 DSC with 31.2 kW Heat Load, Loss of Neutron Shield and Air Circulation Accident at 100°F Ambient

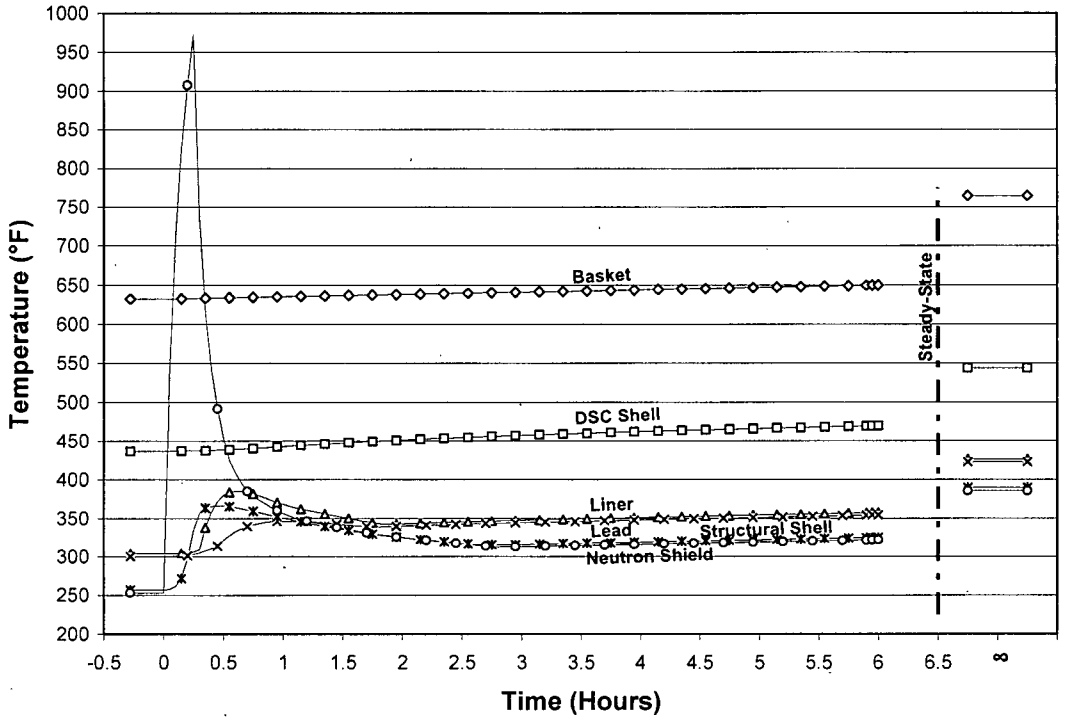

Figure T.4-21
Horizontal Transfer Transient Temperature Response of Type 2 DSC with 31.2 kW Heat Load, 15-minute Fire Accident at 117°F Ambient

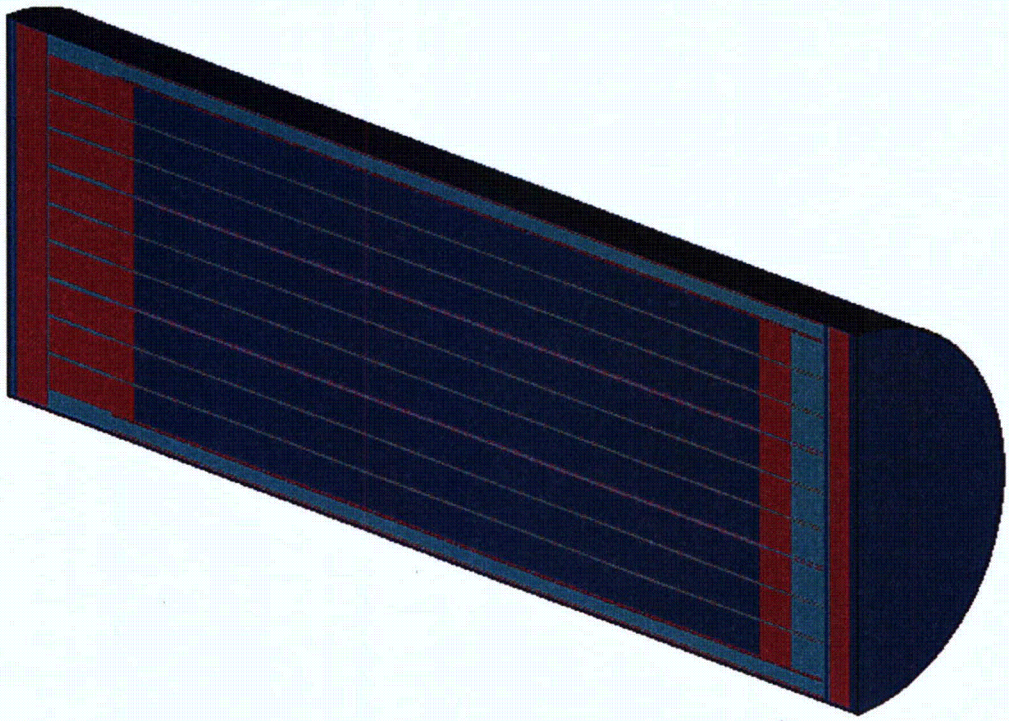

Figure T.4-22
61BTH Type 1 DSC Thermal ANSYS Model

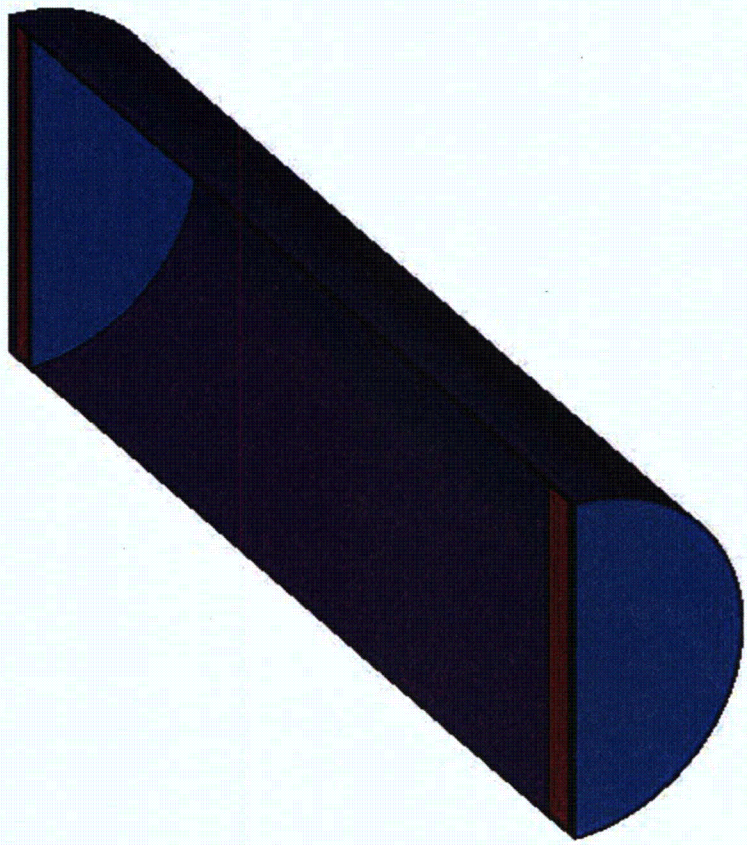

Figure T.4-23
61BTH DSC Thermal ANSYS Model Shell and End Assemblies

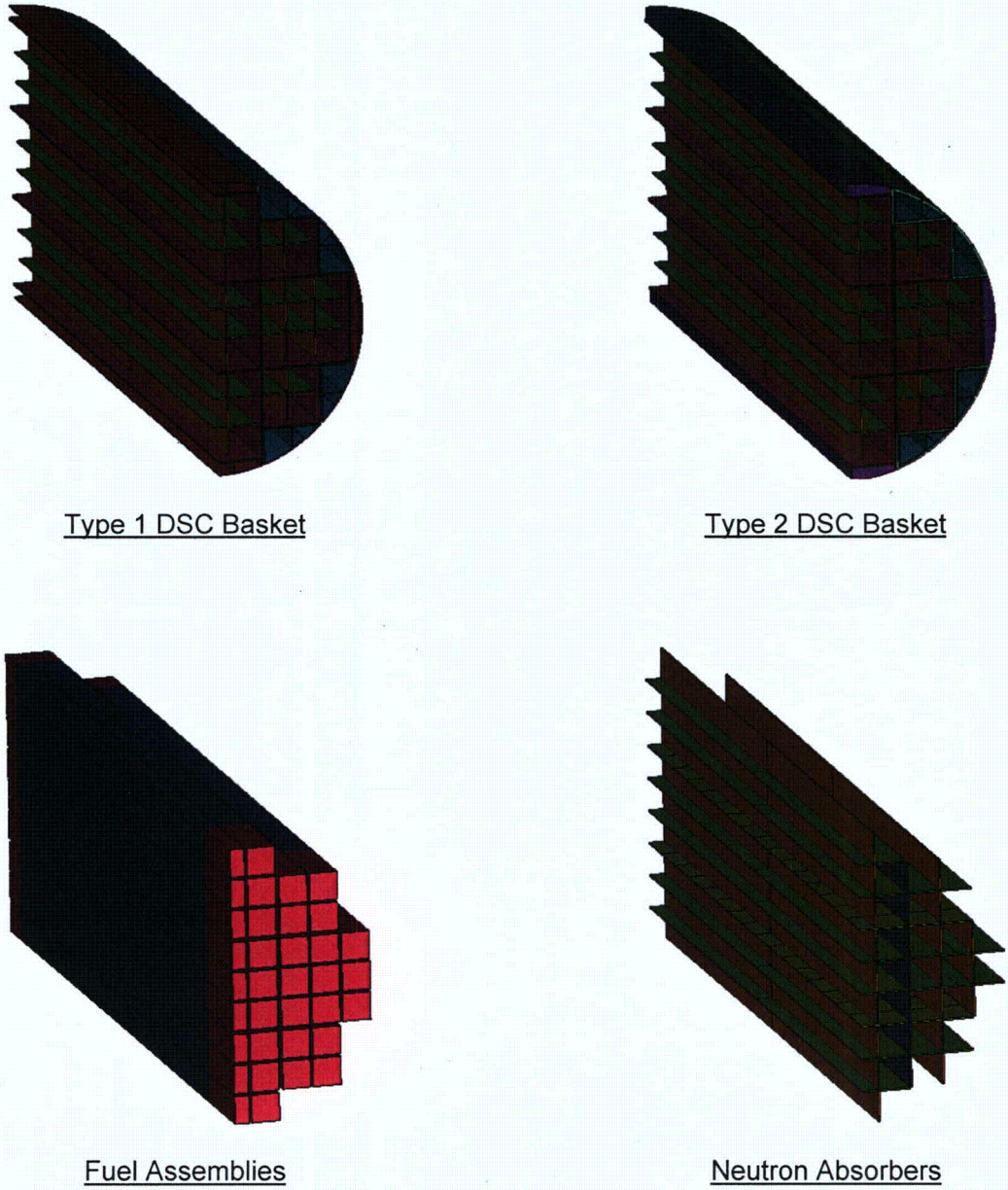

Figure T.4-24
61BTH DSC Thermal ANSYS Model
Basket Components, Fuel Assemblies, and Neutron Absorbers

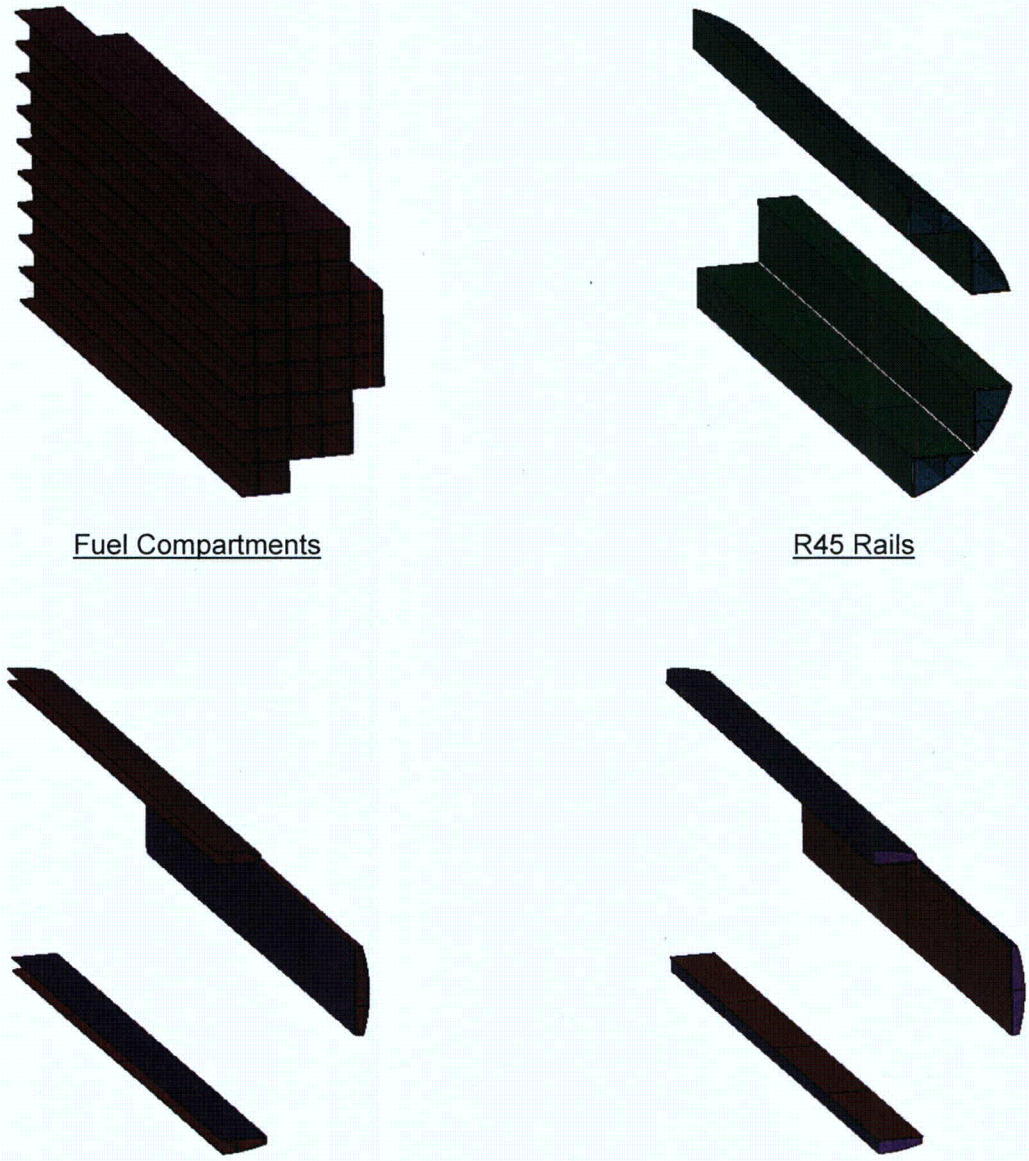

Figure T.4-25
61BTH DSC Thermal ANSYS Model
Fuel Compartments, R45 and R90 Rails

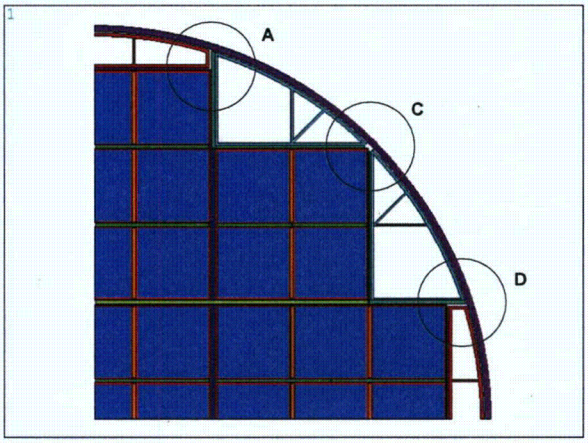

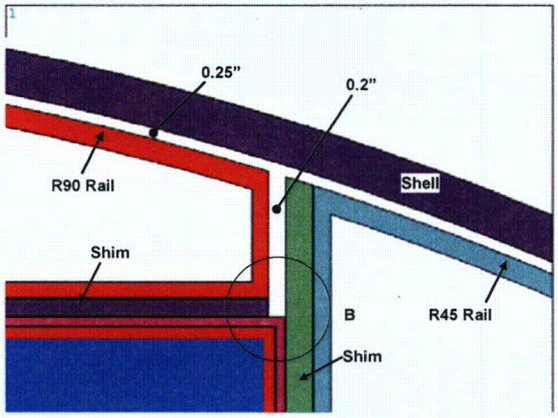

Detail A

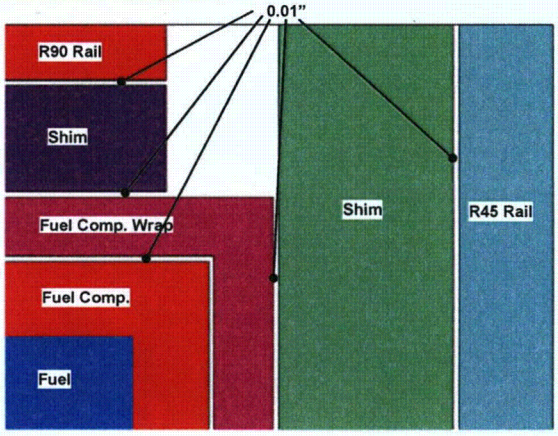

Detail B

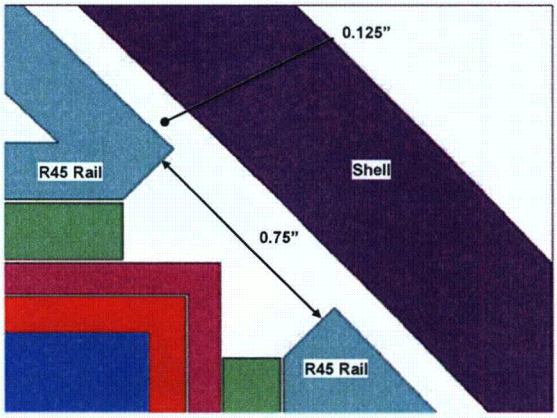

Detail C

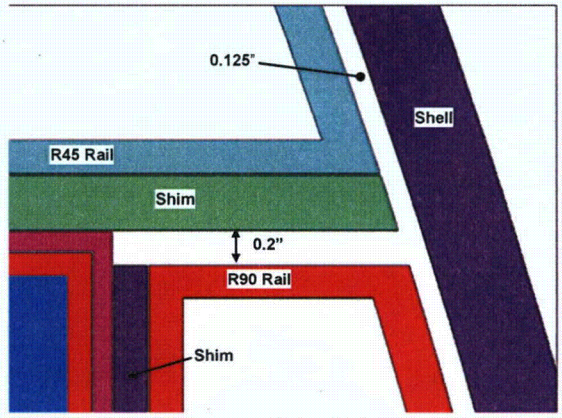

Detail D

Figure T.4-26
61BTH Type 1 DSC Thermal ANSYS Model
Typical Radial and Transverse Gaps

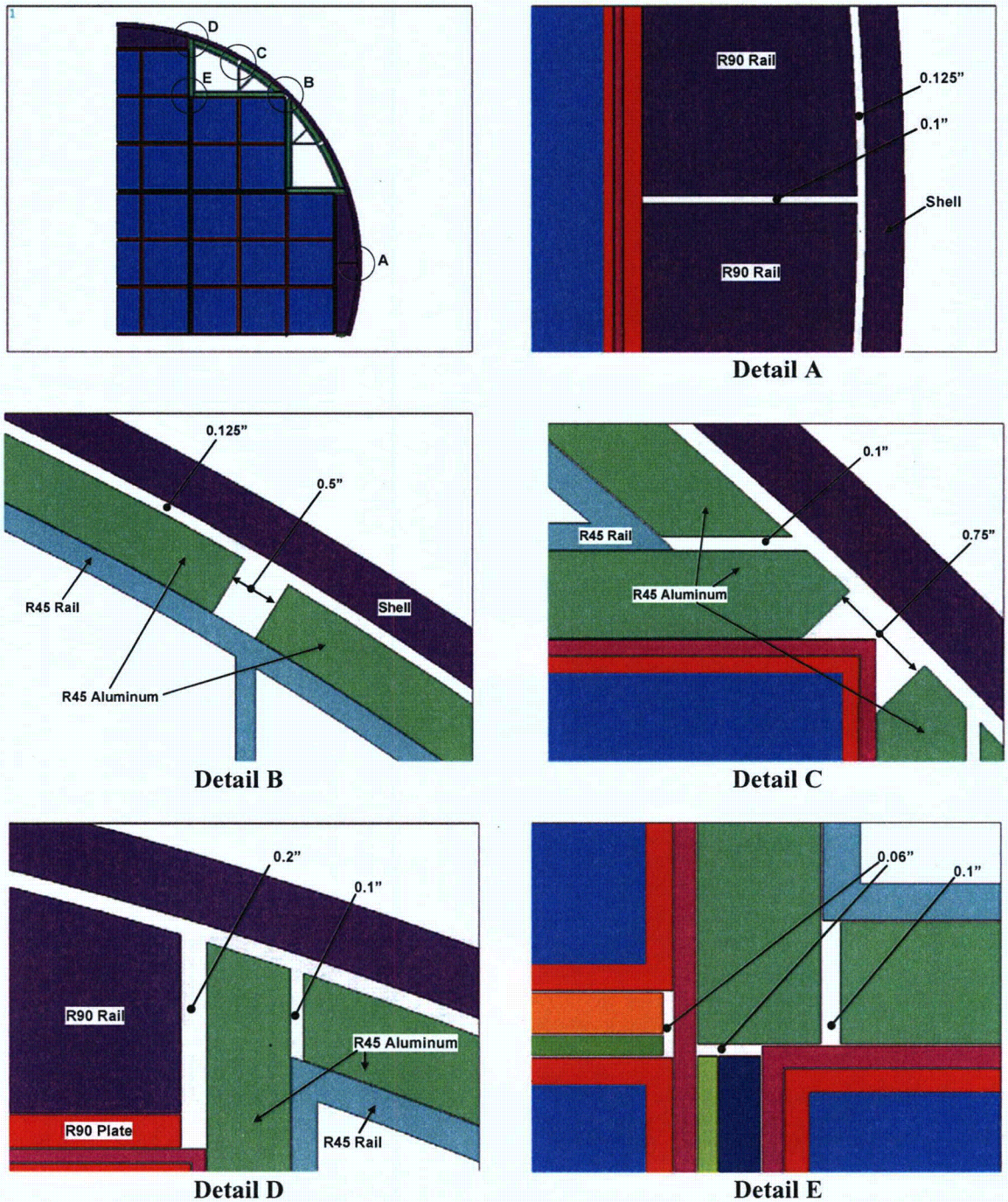

Figure T.4-27
61BTH Type 2 DSC Thermal ANSYS Model
Typical Radial and Transverse Gaps

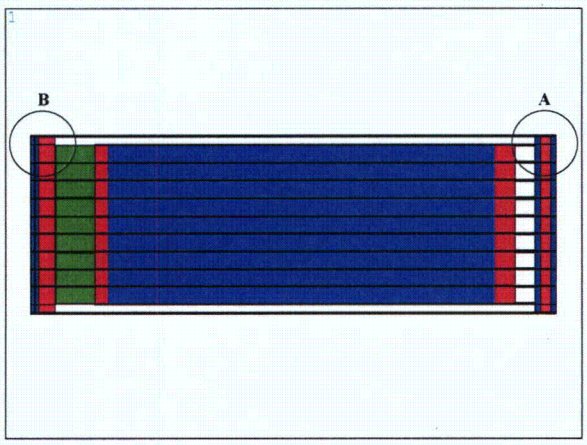

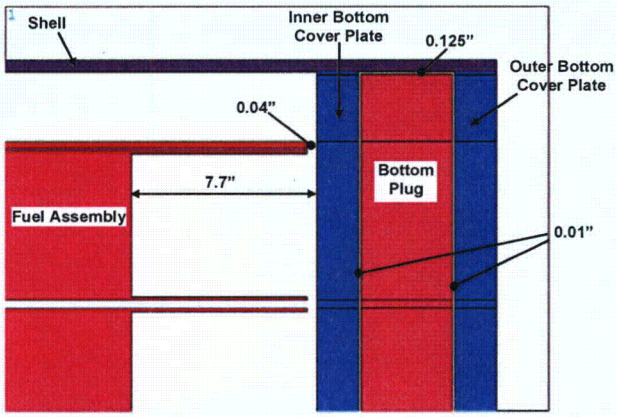

Detail A (Bottom End Assembly)

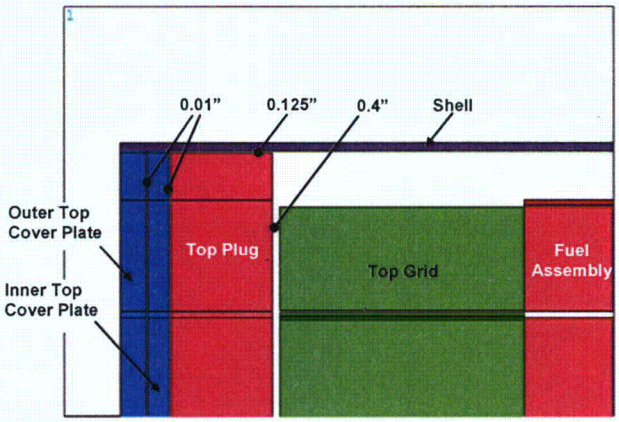

Detail B (Top End Assembly)

Figure T.4-28
61BTH Type 1 and Type 2 DSC Thermal ANSYS Models
Typical Axial Gaps at Both Ends

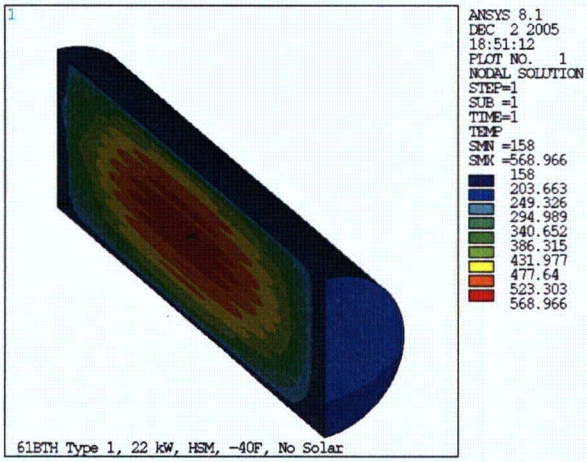

Off-Normal Storage, -40°F, No Insolation

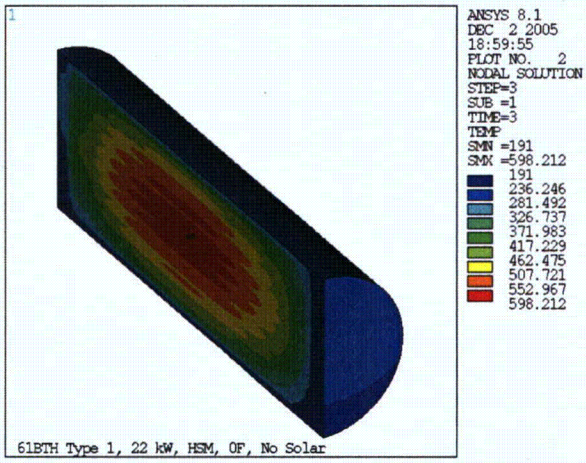

Normal Storage, 0°F, No Insolation

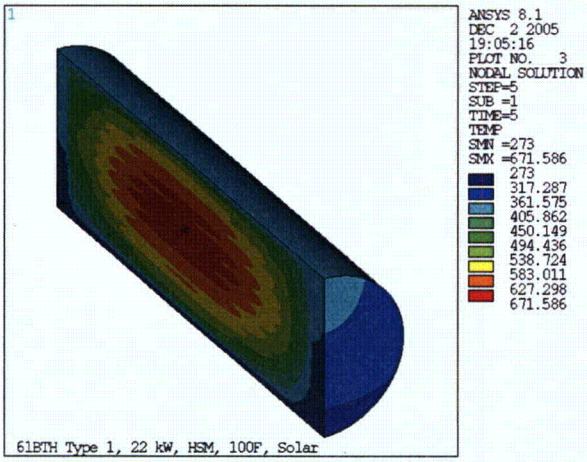

Normal Storage, 100°F, Insolation

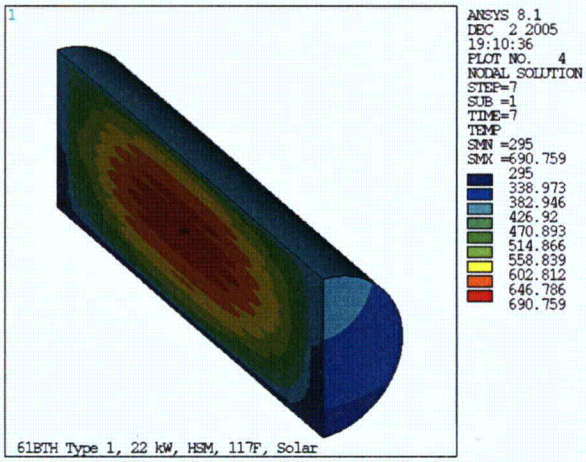

Off-Normal Storage, 117°F, Insolation

Figure T.4-29
61BTH Type 1 DSC (22 kW) Temperature Distribution for Normal and Off-Normal Storage Conditions

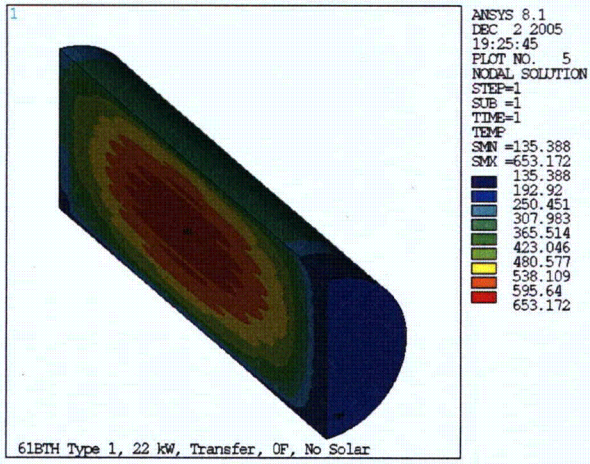

Normal Transfer, 0°F, No Insolation

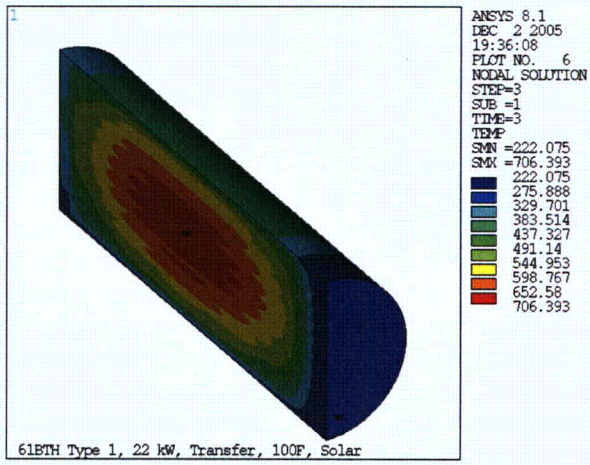

Normal Transfer, 100°F, Insolation

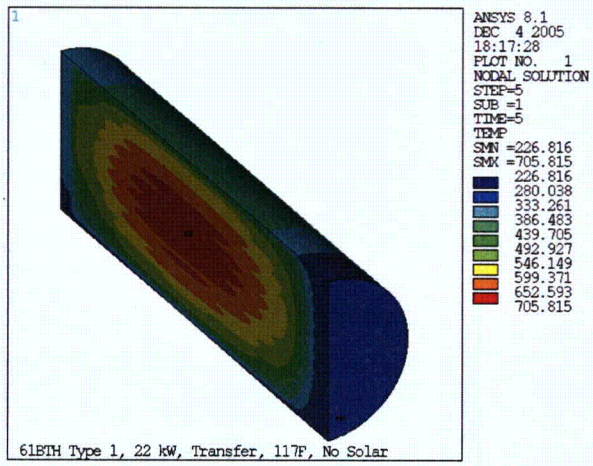

Off-Normal Transfer, 117°F, No Insolation

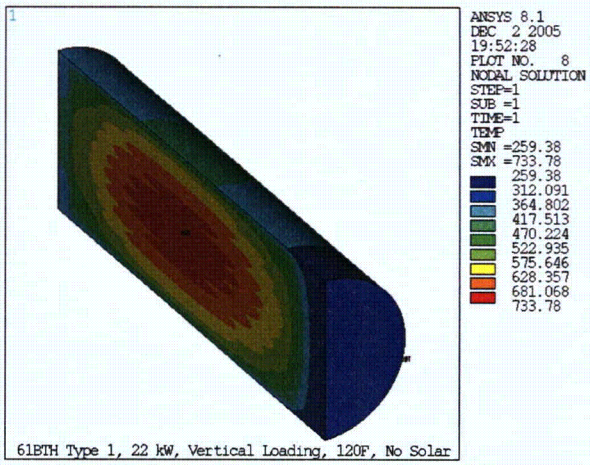

Vertical Loading, Steady State

Figure T.4-30
61BTH Type 1 DSC (22 kW) Temperature Distribution for Normal and Off-Normal Transfer Conditions

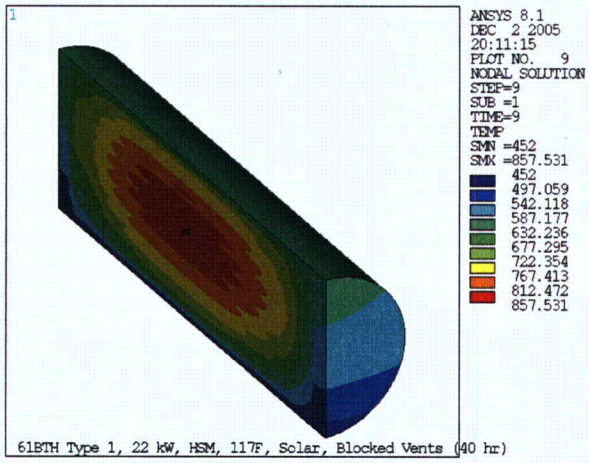

Accident Storage, Block Vents (@ 40 Hr)

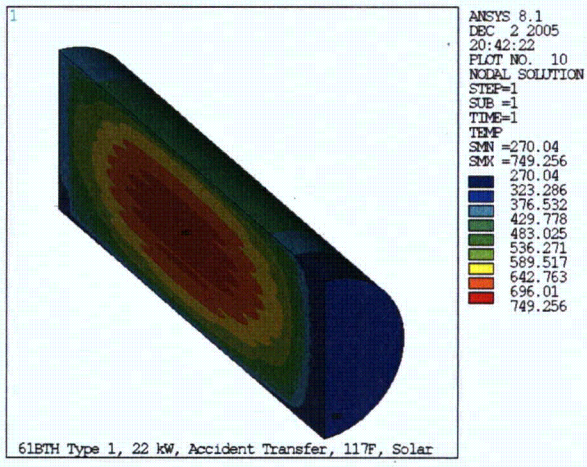

Accident Transfer, Steady State

Figure T.4-31
61BTH Type 1 DSC (22 kW) Temperature Distribution for Accident Storage and Transfer Conditions

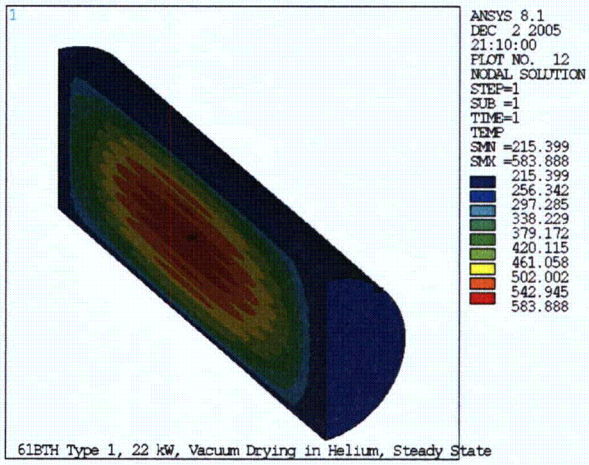

Figure T.4-32
61BTH Type 1 DSC (22 kW) Temperature Distribution for Vacuum Drying Steady State Conditions

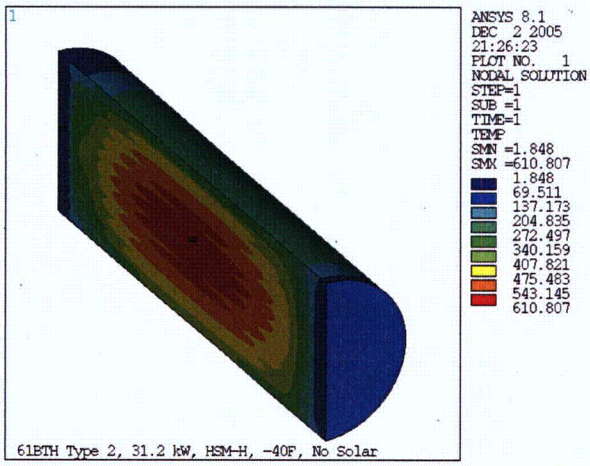

Off-Normal Storage, -40°F, No Insolation

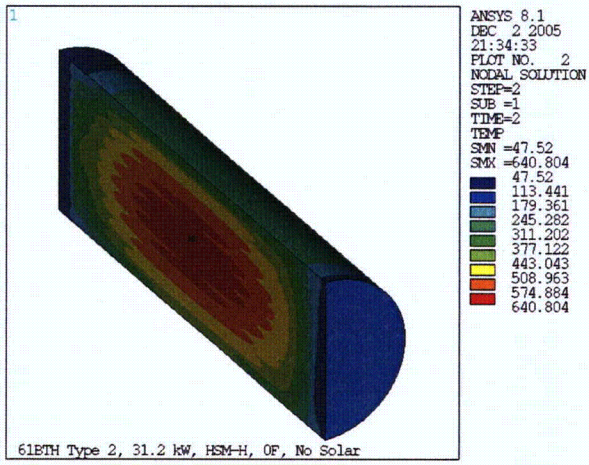

Normal Storage, 0°F, No Insolation

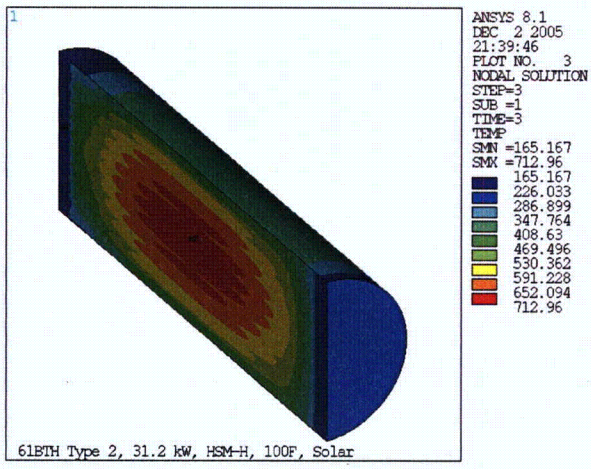

Normal Storage, 100°F, Insolation

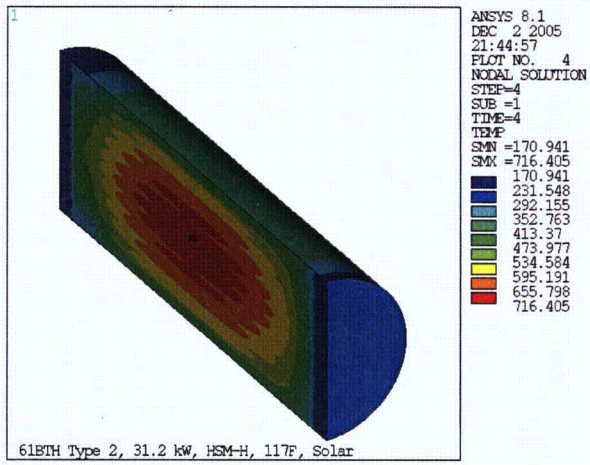

Off-Normal Storage, 117°F, Insolation

Figure T.4-33
61BTH Type 2 DSC (31.2 kW) Temperature Distribution for Normal and Off-Normal Storage Conditions

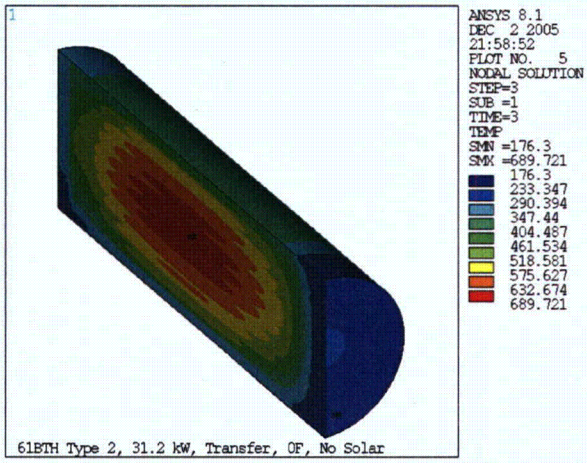

Normal Transfer, 0°F, No Insolation

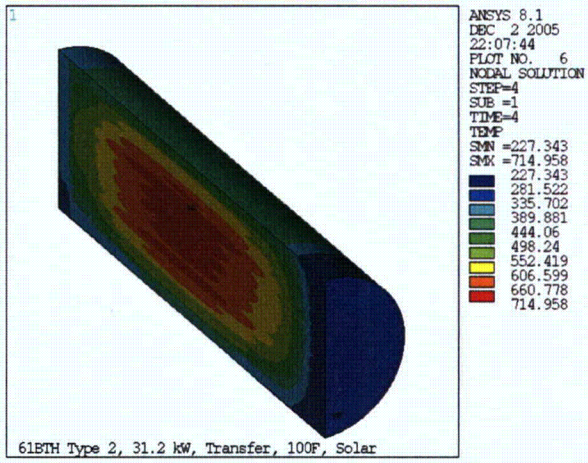

Normal Transfer, 100°F, Insolation

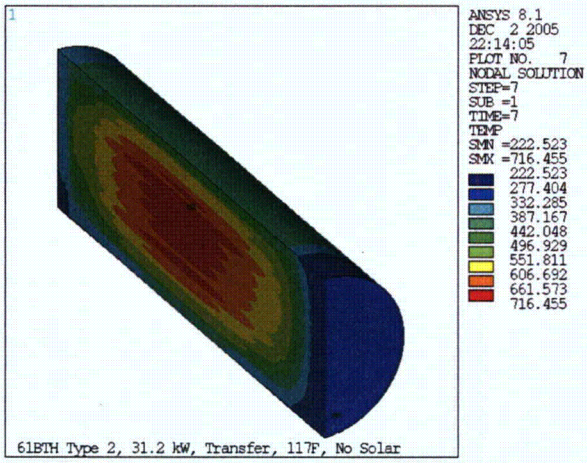

Off-Normal Transfer, 117°F, No Insolation

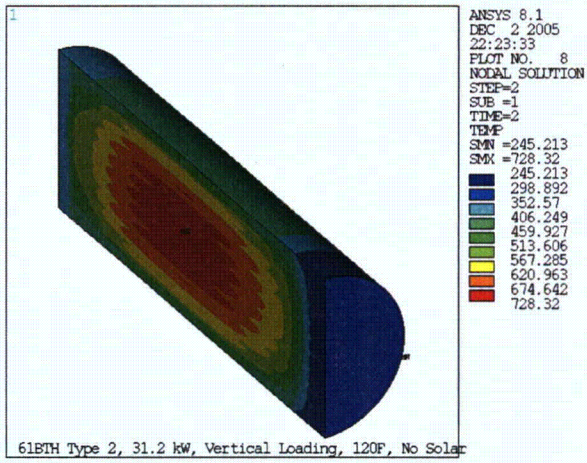

Vertical Loading, @ 28 Hr.

Figure T.4-34
61BTH Type 2 DSC (31.2 kW) Temperature Distribution for Normal and Off-Normal Transfer Conditions

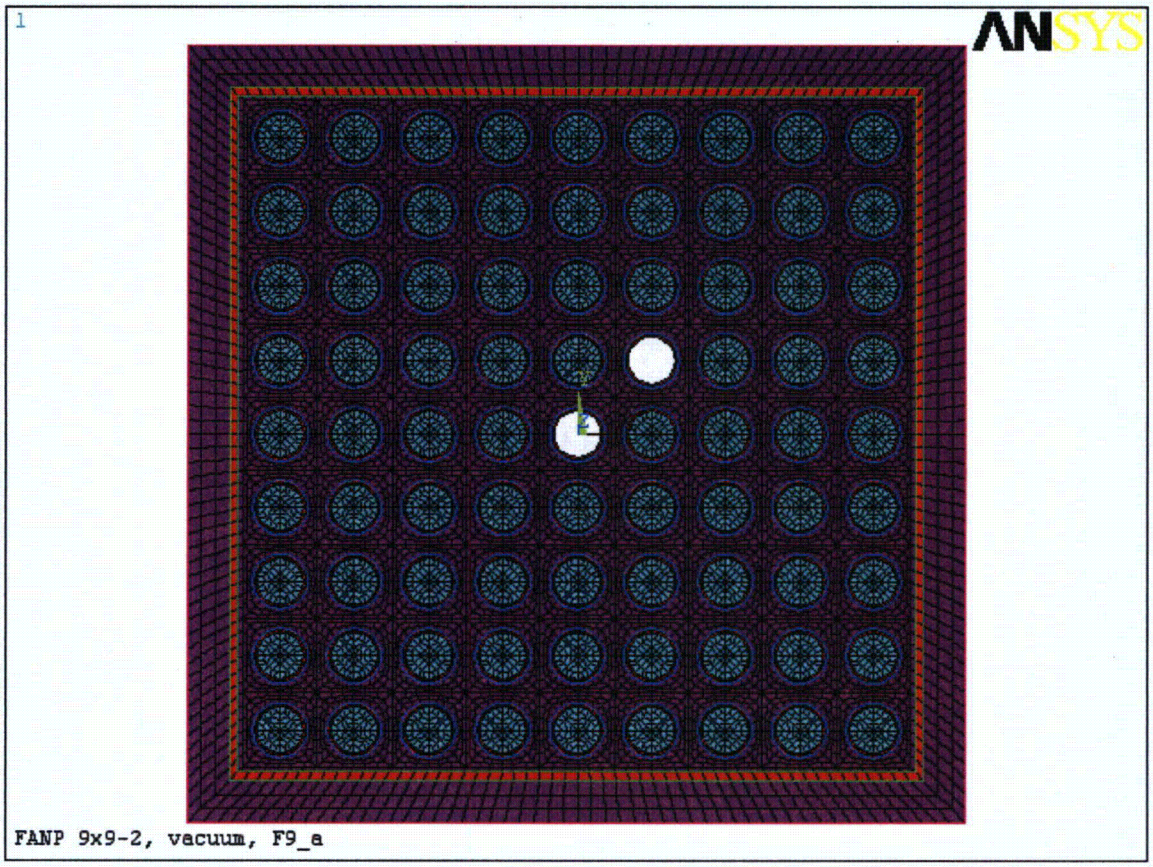

Figure T.4-35
FANP9 9x9-2 Fuel Assembly Finite Element Model

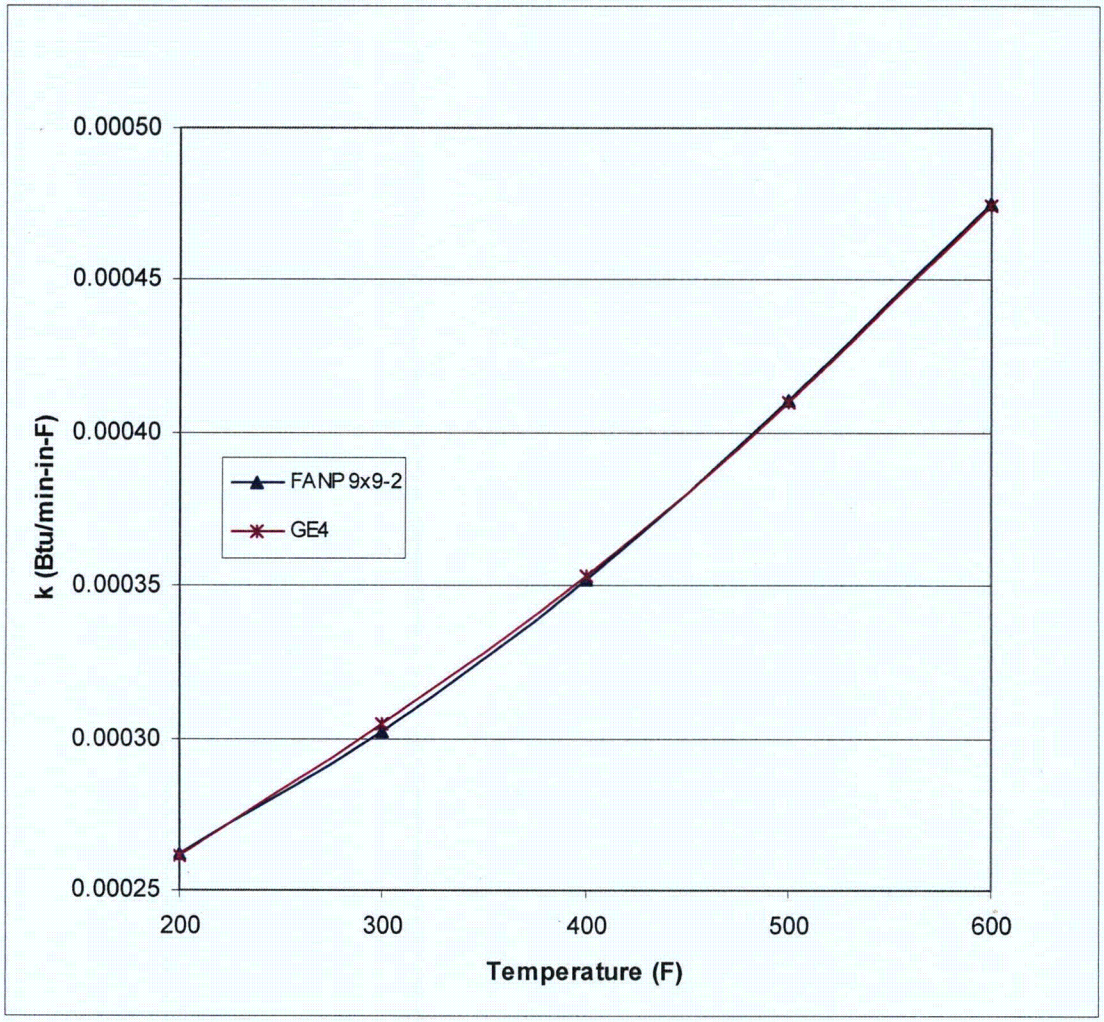

Figure T.4-36
Transverse Fuel Effective Thermal Conductivity
for FANP9 9x9-2 and GE4 Fuel Assemblies in Helium

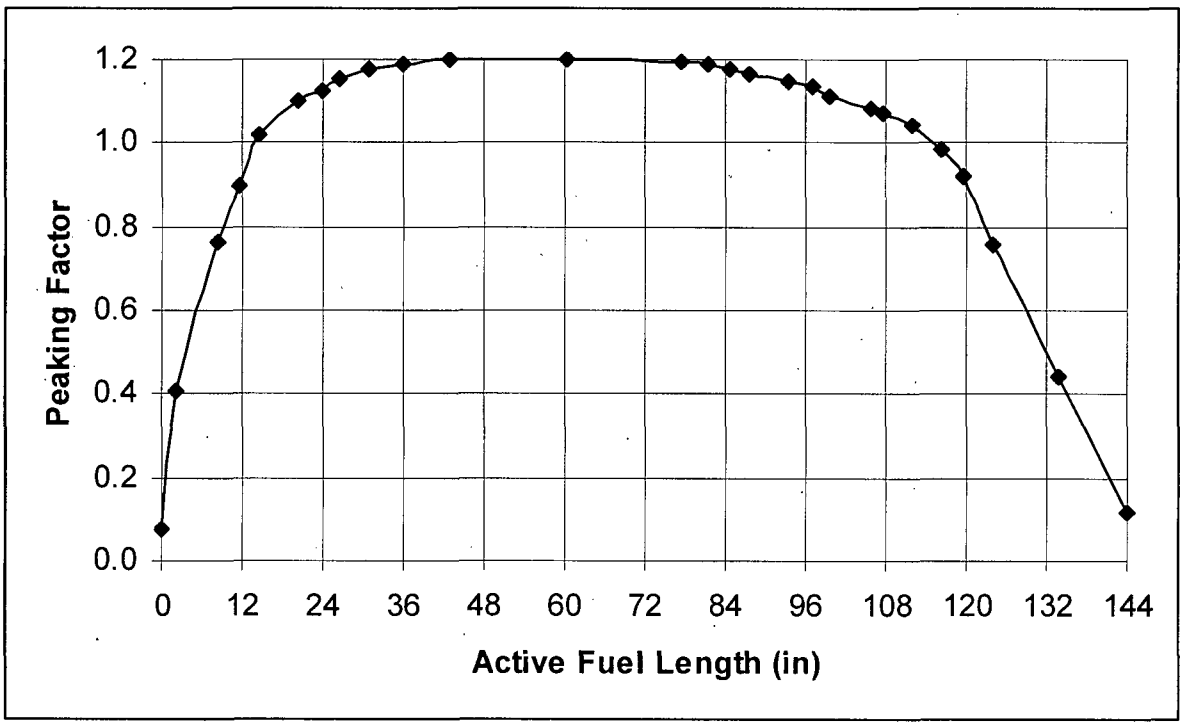

Figure T.4-37
Applied Axial Heat Flux Profile

T.5 Shielding Evaluation

This chapter specifically addresses the shielding evaluation of the NUHOMS® 61BTH system with design basis BWR fuel loaded in a NUHOMS®-61BTH DSC. The radiation shielding evaluation for the Standardized NUHOMS® System (during loading, transfer, and storage) for the other NUHOMS® canisters is discussed in other sections and appendices of the UFSAR. The NUHOMS®-61BTH system consists of the NUHOMS® HSM and HSM-H, the OS197 Transfer Cask (TC), and the 61BTH Type 1 and the Type 2 DSCs.

The 61BTH DSC will be transferred using either the OS197/OS197H or a modified version of the OS197FC transfer cask (OS197FC-B) if air circulation is required. The NUHOMS® 61BTH system will use either the HSM Model 80, Model 102, or the HSM-H module (up to 31.2 kW/DSC) for storage.

The radiation shielding evaluation described below is for the NUHOMS® 61BTH Type 1 and Type 2 DSCs loaded in a NUHOMS® System TC. For heat levels below 22 kW both DSC types can be transferred in any of the 3 transfer casks: 1) OS197, 2) OS197H, and 3) OS197FC-B, and stored in any of these Horizontal Storage Modules (HSMs): 1) HSM Model 80, 2) HSM Model 102, 3) HSM Model 152, 4) HSM Model 202, and 5) HSM-H. For heat loads exceeding 22 kW, the 61BTH Type 2 DSC must be used and can only be stored in HSM-H and transferred in the OS197FC-B TC. HSM Model 80 offers the least amount of shielding and therefore, bounds all other HSMs. With respect to shielding performance, seven possible loading combinations are considered as listed below:

(1) 61BTH Type 1/2 DSC → OS197 (bounded by #3)

(2) 61BTH Type 1/2 DSC → OS197H (bounded by #3)

(3) 61BTH Type 1 DSC → OS197FC-B (bounds OS197/OS197H and Type 2 DSC)

(4) 61BTH Type 2 DSC → OS197FC-B (bounded by #3)

(5) 61BTH Type 1/2 DSC → HSM Model 80 (bounding)

(6) 61BTH Type 1/2 DSC → HSM Model 102 (bounded by #5)

(7) 61BTH Type 1/2 DSC → HSM Model HSM-H (bounded by #5)

These design features of the HSM result in the occupational and site dose rates being ALARA.

The basket layout for Type 1 and Type 2 DSC configurations is identical except for the basket transition rails. Each DSC configuration is designed to store up to 61 intact BWR fuel assemblies or up to 16 damaged fuel assemblies combined with remaining intact fuel assemblies. For shielding purposes radiological sources related to the 61BTH Type 2 bound the 61BTH Type 1 because assemblies with higher neutron and gamma sources are loaded in the outer zones. When such bounding neutron and gamma sources are placed in a Type 1 DSC the resulting shielding configuration, HSM and TC dose rates are bounding for all the shielding configurations. Therefore, the shielding evaluation presented herein is performed for the hypothetical shielding configuration where radiological source terms bounding for Type 2 DSC are analyzed with the Type 1 DSC.

The NUHOMS® 61BTH Type 1 DSC is identical to the NUHOMS® 61BT DSC analyzed in UFSAR Appendix K, except for an optional redesigned basket hold-down ring. Relative to the existing 61BT DSC, the 61BTH Type 1 DSC allows for an increase in heat load from 18.3 kW to 22 kW, increase in maximum burnup from 40,000 MWd/MTU to 62,000 MWd/MTU, and an increase in maximum initial fuel enrichment from 4.4 wt. % U-235 to 5 wt. % U-235.

The 61BTH Type 2 DSC is also based on the basket design for the 61BT DSC with modifications to the shell assembly (cover plate thicknesses are increased to handle higher internal pressures) and to the basket transition rails to allow storage of fuel assemblies with a total heat load of up to 31.2 kW, with burnup of up to 62,000 MWd/MTU and with maximum initial fuel enrichments of up to 5 wt. % U-235. The Type 2 basket also incorporates the redesigned hold down ring.

The OS197FC-B is essentially the same as the OS197FC except that the lid and bottom have been modified to introduce air cooling design features to accommodate a higher decay heat load (>22 kW). The design of the OS197FC TC is identical to the design of OS197/OS197H TC except that the OS197FC TC has a modified top lid. For the shielding analysis OS197FC-B TC is used to bound the OS197/OS197H TC also because the design features in the TC radial direction are identical for all three TCs; and OS197FC top axial geometry bounds other TCs.

There are a total of eight possible Heat Load Zoning Configurations (HLZC) for the 61BTH Type 1 and Type 2 DSCs. Four out of eight total DSC HLZCs are for Type 2 DSC only. The remaining four can be used with either DSC type; however certain restrictions apply for Type 1 DSC in some cases. DSC HLZCs are depicted in Figures T.2-1 through Figure T.2-8 of Chapter T.2.

The NUHOMS®-61BTH DSCs are designed to store BWR fuel assemblies with the characteristics described in Table T.2-1 and Table T.2-2, and associated tables and figures of Chapter T.2.

Radiological sources related to Type 2 DSC HLZCs #5, #6, and #7 result in nearly the same maximum HSM dose rates and maximum dose rates at the "middle of transfer cask side." Bounding dose rates for the HSM and "middle of transfer cask side" are due to HLZC #6 radiological source terms. However HLZC #7 source terms are important when calculating dose rates on and around the ends of the transfer cask. Dose rates are also estimated for the HSM Model 80 and 102. The hypothetical DSC shielding configuration where bounding radiological HLZC #6 or #7 source terms are loaded into 61BTH Type 1 DSC is referred to as the "design basis DSC shielding configuration" or simply "design basis DSC" in the discussion that follows.

The design basis BWR fuel source terms are derived from a bounding "generic" fuel assembly. The parameters of the bounding "generic" fuel assembly are selected in such a way that the resulting radiological and decay heat source terms bound those from all other fuel assembly types that are authorized for loading into the NUHOMS® 61BTH DSC. This "generic" fuel assembly shares many common features with the GE-2,3 7x7 Type G2A assembly. It is bounding because it has the highest initial heavy metal loading as compared to the 8x8, 9x9 and 10x10 fuel assemblies which are also authorized for loading into the NUHOMS®-61BT DSC. Its parameters are described in Section T.5.2. In addition, the maximum Co-59 content of each

hardware region for the bounding fuel assembly type is used to determine the activation source for each fuel assembly region.

Maximum decay heat allowed for the 61BTH Type 1 DSC is 22 kW and a maximum heat load of 31.2 kW is allowed for the Type 2 DSC. The HLZCs to be used for the 61BTH Type 1 DSC are shown in Figure T.2-1 through Figure T.2-4 of Chapter T.2. Fuel assemblies loaded in 61BTH Type 2 DSC can have a maximum decay heat of 0.70 kW per assembly. The design basis fuel source terms for this evaluation are defined as the source terms from fuel with the burnup/initial enrichment/cooling time combination that results in a maximum calculated dose rate on the surface of the HSM and/or TC side because the highest source fuel assemblies are on the outer periphery of the basket region where self-shielding due to adjacent assemblies is limited.

The dose rates at the side of the TC are bounded by 61BTH DSC HLZC #6 and in specific areas the dose rates at the top/bottom of the TC are bounded by 61BTH Type 2 DSC HLZC #7. The bounding burnup, minimum initial enrichment, and cooling time combinations for the fuel assemblies used in the shielding analysis of the 61BTH design basis DSC in the OS197FC-B are as follows:

- Spent fuel parameters for HLZC #6, in OS197FC-B:
    - Central zone (0.22 kW per assembly): 31 GWd/MTU, 0.9 wt. % U-235, 11.7-year cooled fuel
    - Inner intermediate zone (0.7 kW per assembly): 62 GWd/MTU, 2.6 wt. % U-235, 7.1-year cooled fuel
    - Outer intermediate zone (0.48 kW per assembly): 25 GWd/MTU, 1.0 wt. % U-235, 3.2-year cooled fuel
    - Peripheral zone (0.54 kW per assembly): 25 GWd/MTU, 0.9 wt. % U-235, 3.0-year cooled fuel
- Spent fuel parameters for HLZC #7 in OS197FC-B:
    - Central two zones (0.48 kW per assembly): 62 GWd/MTU, 2.6 wt. % U-235, 14-year cooled fuel
    - Outer two zones (0.54 kW per assembly): 25 GWd/MTU, 0.9 wt. % U-235, 3.0-year cooled fuel

The bounding burnup, minimum initial enrichment, and cooling time combinations for the fuel assemblies used in the shielding analyses of the 61BTH design basis DSC, HLZC #6, in the HSM-H are as follows:

- Central zone (0.22 kW per assembly): 13 GWd/MTU, 1.8 wt. % U-235, 3.0-year cooled fuel

- Inner intermediate zone (0.7 kW per assembly): 34 GWd/MTU, 2.0 wt. % U-235, 3.1-year cooled fuel

- Outer intermediate zone (0.48 kW per assembly): 24 GWd/MTU, 1.3 wt. % U-235, 3.0-year cooled fuel

- Peripheral zone (0.54 kW per assembly) : 25 GWd/MTU, 0.9 wt. % U-235, 3.0-year cooled fuel

The bounding burnup, minimum initial enrichment, and cooling time combinations for the fuel assemblies used in the shielding analyses of the 61BTH Type 1 DSC in the HSM 80 or HSM-102 are as follows:

- Central and inner intermediate zones (0.393 kW per assembly): 62 GWd/MTU, 2.6 wt.% U-235, 21.4-year cooled fuel

- Outer intermediate zone (0.480 kW per assembly): 25 GWd/MTU, 1.0 wt.% U-235, 3.2-year cooled fuel

- Peripheral zone (0.540 kW per assembly): 25 GWd/MTU, 0.9 wt.% U-235, 3.0-year cooled fuel

Note that the source terms are different when calculating dose rates for the HSM and TC. The method of selecting the bounding source terms is explained in detail in Section T.5.2.

Reconstituted and/or damaged fuel is also acceptable for the DSC payload. Reconstituted fuel may contain up to 10 solid stainless steel rods. The reconstituted rods can be at any location in the fuel assemblies and the reconstituted assemblies can be placed anywhere in the basket. Reconstituted fuel has a pronounced effect on the dose rates that are due to assemblies with cooling times less than 10 years. An additional 5 years of cooling time is required if reconstituted fuel with steel rods that are irradiated are present. Under normal conditions damaged fuel has essentially no impact on the dose rate as the source term would not be impacted and gross axial source redistribution is not likely. Therefore, shielding analysis results with intact fuel are also applicable to the damaged fuel.

The methodology, assumptions, and criteria used in this evaluation are summarized in the following subsections.

T.5.1 Discussion and Results

All 61BTH DSC shielding analysis using MCNP Code are performed for a hypothetical shielding configuration in which bounding HLZC #6 or HLZC #7 radiological source terms are utilized in a 61BTH Type 1 DSC.

Table T.5-1 summarizes the maximum and average dose rates for the NUHOMS®-61BTH design basis DSC loaded into the NUHOMS® HSM-H.

Table T.5-2 summarizes the maximum and average dose rates for the NUHOMS®-61BTH design basis DSC loaded into the NUHOMS® HSM Model 102. Note that the HSM-H is more heavily shielded than the HSM Model 102 (thicker roof, shield walls, front and back wall including HSM door); therefore, HSM Model 102 is conservatively modeled to bound HSM-H.

Table T.5-3 provides a summary of the dose rates for the NUHOMS®-61BTH design basis DSC loaded into the NUHOMS® Model 80 HSM.

Table T.5-4 provides a summary of the dose rates on and around the OS197FC-B TC for transfer of the 61BTH design basis DSC under normal, off-normal and accident conditions.

Table T.5-5 provides a summary of the dose rates on and around the OS197FC-B TC for decontamination and welding operations for the 61BTH design basis DSC.

A discussion of the method used to determine the design basis fuel source terms is included in Section T.5.2. The shielding material densities are given in Section T.5.3. Thermal and radiological source terms are calculated with the SAS2H/ORIGEN-S modules of SCALE 4.4 [5.1] for the fuel. The shielding evaluation is performed with the MCNP Computer Code Version 5 [5.2, 5.3] and Version 4C2 [5.4] with the ENDF/B-VI cross section library. Sample input files used for calculating neutron and gamma source terms and dose rates are included in Section T.5.5.

T.5.2 Source Specification

Thermal and radiological source terms are calculated with the SAS2H/ORIGEN-S modules of SCALE 4.4 [5.1] for the fuel. The SAS2H/ORIGEN-S results are used to develop the fuel qualification tables listed in Table T.2-5 through Table T.2-10 of chapter T.2 and the design basis fuel source terms suitable for use in the shielding calculations.

The GE-2,3 7x7 Type G2A assembly is the bounding fuel assembly design for shielding purposes because it has the highest initial heavy metal loading in the fuel and Co-59 content in the hardware regions as compared to the 8x8, other 9x9, and 10x10 fuel assemblies which are also authorized contents of the NUHOMS®-61BTH DSC. The neutron flux during reactor operation is peaked in the active fuel region of the fuel assembly and drops off rapidly outside the active fuel region. Much of the fuel assembly hardware is outside of the in-core region of the fuel assembly. To account for this reduction in neutron flux, the fuel assembly is divided into four exposure "regions." The four axial regions used in the source term calculation are: the bottom (nozzle) region, the in-core region, the (gas) plenum region, and the top (nozzle) region. The GE 7x7 fuel assembly masses for each irradiation region are listed in Table T.5-6. The light elements that make up the various materials for the various fuel assembly materials are taken from Reference [5.6] and are listed in Table T.5-7. The design basis heavy metal loading is 0.198 MTU. These masses are irradiated in the appropriate fuel assembly region in the SAS2H/ORIGEN-S models. To account for the reduction in neutron flux outside the in-core regions, neutron flux (fluence) correction factors are applied to the light element composition for each region. The neutron flux correction factors which are from Reference [5.19] are given in Table T.5-8.

Evaluations of the existing Light Water Reactor (LWR) fuel data with SAS2H and the 44-group ENDF/B-V library used in the calculation of the design basis source terms are documented in References [5.17] and [5.18]. These comparisons all show generally good agreement between the calculations and measurements, and show no trend as a function of burnup in the data that would suggest that the isotopic predictions, and therefore neutron and gamma source terms, would not be in good agreement. A similar conclusion is also reached by the results documented in JAERI report [5.14]. In fact, for the case with 46,460 MWd/MTU burnup, the isotopic predictions are all within 2% of those measured. There are ongoing efforts, some of which are documented in Reference [5.12], to obtain more data for burnups above 45 GWd/MTU.

There are cross-section data on about 1600 isotopes in the cross section libraries available for SAS2H. Only about 20 isotopes are primary concern when dealing with high burnup spent fuel [5.13, 5.15]. According to Reference [5.15] 95 % of the decay heat is dominated by fewer than 10 nuclides for LWR assemblies at 5 years of cooling. Eight-five percent of the decay heat would be contributed by only 4 isotopes after 100 years.

Applicability of SAS2H for prediction of isotopic content in BWR assemblies was analyzed in [5.13]. A UO_2 sample was burned to 57 GWd/MTU in a BWR reactor. The sample U-235 enrichment was 4.97 wt. %. Also, the isotopic content of the discharged sample was measured experimentally. Measured content was reported for actinides and fission products. Among concentrations of 16 nuclides investigated, 5 agreed with the measured values to within ±5%.

Nine predictions were within ±10%. Also sensitivity to burnup for isotope concentrations was investigated as burnup varied between 90 and 110%.

The results suggest that there is no reason to expect that the ongoing evaluations of the higher burnup fuel will result in less favorable comparisons. Therefore, the uncertainty in the gamma source term, and associated dose rates, is estimated to be within ±10%.

As noted in References [5.15] and [5.12], there is no public data for the neutron component currently available that bounds a fuel burnup of up to 62 GWd/MTU. However, as documented in Reference [5.15] and confirmed in the SAS2H analysis, the total neutron source with increasing burnup is more and more dominated by spontaneous fission neutrons. Reviewing the output from the SAS2H runs, the neutron source term is due almost entirely to the spontaneous fission of ^{244}Cm (more than 90% of all neutrons both spontaneous fission and (α,n)) with (α, O–18) of lesser importance. It is claimed in Reference [5.13] that SAS2H tends slightly to over predict the concentration of ^{244}Cm when burnup is varied during the sensitivity study. Therefore, as the ^{244}Cm isotope accounts for more than 90% of the total neutron source term, the uncertainty in the neutron source and associated neutron dose rates is expected to be less than ±11%.

As documented in Reference [5.15] and as observed in preparing the fuel qualification tables, the gamma dose rate increases nearly linearly with burnup relative to the direct gamma component and the neutron dose rate increases with burnup to the fourth power. Therefore, as burnups go beyond 45 GWd/MTU, the contribution from neutron (and associated n,γ) components to the total dose rates measured on the surfaces of the DSC, TC and HSM increases in relative importance to that of the gamma component. However, this increase in the importance of the neutron source term has a relatively minor effect on the area dose rates on and around the HSM as these are dominated by the gamma component as shown in Table T.5-1 through Table T.5-3. The surface dose rates on the HSM are dominated by the gamma component because the HSM is constructed of thick reinforced concrete, which is an excellent neutron shield. Therefore, even a postulated substantial increase in the neutron source term would have a relatively minor effect on the site dose rate evaluation presented in Section T.10.

For the TC, the neutron source term has a relatively minor effect on the area dose rates during most of the cask handling operations, when the DSC cavity and the annulus between the TC and DSC is filled with water and most of the work is done around the top of the cask. The neutron component is of more importance on and around the TC during transfer operations but, in general, only represents a small portion of the total dose rate on the sides and top of the TC. The dose rates for the design basis fuel on the surfaces of HSM and TC are shown in Table T.5-1 through Table T.5-5. These tables show that gamma dose rates are substantially higher than neutron dose rates. Therefore, the neutron component of the dose is a relatively minor fraction of the total for HSM and site boundary dose.

As discussed above, any impact of uncertainties in source terms is expected to be negligible for the 61BTH system. Therefore, isotopic depletion calculations with SAS2H for fuel burned above 45 GWd/MTU are appropriate.

The fuel qualification tables are generated based on the decay heat limits for the various heat load zoning configurations shown in Figure T.2-1 through Figure T.2-8 of Chapter T.2. SAS2H is used to calculate the minimum required cooling time to the nearest 0.1 year (0.3 years at burnups greater than ~50 GWd/MTU when considering low, less than 0.35 kW/FA, decay heat powers) as a function of fuel assembly initial enrichment and burnup for each decay heat limit. These cooling times are rounded up to the nearest 0.5 year increment in the final fuel qualification tables. Because the decay heat generally increases slightly with decreasing enrichment for a given burnup, it is conservative to assume that the required cooling time for a higher enrichment assembly is the same as that for a lower enrichment assembly with the same burnup. The required cooling time for initial enrichments that fall between any two SAS2H runs are assumed to be that of the lower enrichment case results.

The design basis source terms are defined as the burnup/initial enrichment/cooling time combination given in the fuel qualification tables that result in the maximum dose rate on the surface of the HSM or TC. Note that for a given DSC design, the design basis HSM source will not necessarily be the same as the corresponding design basis TC source. The 1-D discrete ordinates code ANISN [5.7] and the CASK-81 22 neutron, 18 gamma-ray energy group, coupled cross-section library [5.5] is used to determine the relative HSM and TC dose rate for each entry in the fuel qualification tables and thereby determine the design basis source. As ANISN is a 1-D code, a single dose location must be selected for both the HSM and TC for analysis purposes. For the HSM, the roof can be selected as the dose location, and for the TC the cask side is selected as the dose location. This approach, described in detail in Section T.5.2.4, is consistent with the method used to determine the fuel qualification tables for the Standardized NUHOMS® 24PTH described in Appendix P, Chapter P.5. The radiological source terms generated in the SAS2H/ORIGEN-S runs are used in the ANISN evaluations to calculate the surface dose rates. The ANISN models are similar to the appropriate MCNP models for the locations of interest. Note that ANISN code is not used to calculate any design basis dose rates. MCNP code models are used for calculating design basis dose rates.

A sample SAS2H/ORIGEN-S input file for the In-Core Region of 0.70 kW/FA assembly is listed in Section **Error! Reference source not found.**. This case corresponds to 62 GWd/MTU, 2.6 wt. % U-235 and 7.1-years cooling case.

T.5.2.1 Gamma Source Term for MCNP Models

T.5.2.1.1 Design Basis Gamma Fuel Assembly Source Terms

Once the design basis burnup/enrichment/cooling time combinations have been determined for each shielding configuration of interest, four SAS2H/ORIGEN-S runs are required for each combination to determine gamma source terms for the four fuel assembly regions (i.e., bottom, in-core, plenum and top). The only difference between the runs is in Block #10 "Light Elements" of the SAS2H input and the 82$$ card in the ORIGEN-S input. Each run includes the appropriate Light Elements for the region being evaluated and the 82$$ card is adjusted to have ORIGEN-S output the total gamma source for the in-core region and only the light element source for the plenum, bottom, and top regions. Gamma source terms for the in-core region include contributions from actinides, fission products, and activation products. The bottom, plenum and top nozzle regions include the contribution from the activation products in the

specified region only. The SAS2H/ORIGEN-S gamma ray source is output in the CASK-81 energy group structure.

A design basis source is developed for each decay heat zone (0.22, 0.48, 0.54, and 0.70 kW for HLZC #6 of Type 2 DSC and 0.48 kW/FA for HLZC #7 of Type 2 DSC) and shielding structure combination used in the shielding analysis. Note that for a given decay heat, the design basis TC and HSM source may or may not be the same. Furthermore, the use of multiple heat zone loading patterns could also result in the design basis source for the TC side and ends being different because multiple heat zone loading patterns are used. Therefore, eight design basis sources are required: four for the TC loaded with a 61BTH Design Basis DSC and four for the HSM loaded with a 61BTH Design Basis DSC. Two more radiological source terms are required for a special consideration of dose rate around the TC from HLZC #7. This is related to 0.48 kW/FA assemblies being present in the central zone.

Design basis source terms used for the shielding analysis of the 61BTH design basis DSC are shown in Table T.5-9 through Table T.5-18. Bounding radiological sources for the shielding analysis of the 61BTH design basis DSC in a transfer cask are also shown in Table T.5-9 through Table T.5-13. Design basis source terms used for the shielding analysis of the 61BTH design basis DSC in HSM-H are shown in Table T.5-14 through Table T.5-17. Design basis source terms used for the shielding analysis of the 61BTH DSC in HSM-102 are shown in Table T.5-10, Table T.5-16 and Table T.5-18.

T.5.2.1.2 Uncertainty in Gamma Source Terms

Almost 100% of the gamma spectrum from light elements is in the range of 0.70 to 1.33 MeV which corresponds exactly to the two most prominent lines of ^{60}Co. As for fission products, the main contributors after six years with a fraction greater then 5% in the range of 0.01 to 0.90 MeV are: ^{90}Sr, ^{90}Y, ^{106}Rh, ^{137}Cs, ^{144}Pr, ^{154}Eu, and ^{155}Eu. Contributions from ^{90}Y, ^{106}Rh, ^{137}Cs, ^{144}Pr, and ^{154}Eu are dominant in the range of 0.90 to 1.50 MeV. ^{106}Rh, ^{147}Sm, and ^{142}Ce are the strongest emitters at energies greater then 2.0 MeV. The accuracy of the gamma spectrum is dependent upon the energy. Photon rates computed for fission products tend to be more accurate than those for actinides because the calculation of their inventory has less uncertainty [5.1].

Shortly after discharge the emission at higher energies is dominated by actinides. This is true for energies >4 MeV at all cooling times and energy above 3.5 MeV for cooling times greater than 10 years [5.1]. The major part of this emission comes from ^{244}Cm. Thus the uncertainty for energy groups of order 3.0 MeV and greater is bounded with the precision with which the inventory of ^{244}Cm is calculated. Per SCALE 4.4 [5.1], reported experimental ^{244}Cm densities are accurate within ± 20%. The gamma emission intensity from ^{244}Cm, which is proportional to the quantity of ^{244}Cm in the actinide inventory, is bounded by this value. Uncertainty in the source strength in the gamma energy range 0.5 to 2.5 MeV is in the vicinity of 10 to 15% [5.1].

T.5.2.2 Neutron Source Term for MCNP Models

One SAS2H/ORIGEN-S run is required for each burnup/initial enrichment/cooling time combination to determine the total neutron source term for the in-core regions. At discharge the neutron source is almost equally produced from ^{242}Cm and ^{244}Cm. The other strong contributor

is ^{252}Cf, which is approximately 1/10 of the Cm intensity, but its share vanishes after 6 years of cooling time because the half-life of ^{252}Cf is 2.65 years. The half-lives of ^{242}Cm and ^{244}Cm are 163 days and 18 years, respectively. Contributions from the next strongest emitters, ^{238}Pu and ^{240}Pu, are lower by a factor of 1000 and 100, respectively, relative to ^{244}Cm. For the ranges of exposures, enrichments, and cooling times in the fuel qualification tables, ^{244}Cm represents more than 90% of the total neutron source. The neutron spectrum is, therefore, relatively constant for the fuel parameters addressed herein.

The magnitude of the neutron source is provided as the final row in the gamma source term tables; see Table T.5-9 through Table T.5-18. Neutron source terms for use in the MCNP shielding models are calculated by multiplying the fuel assembly source by the number of assemblies in the in-core region and summing the terms from all the radial regions. The magnitude of the neutron source is also increased to account for the axial distribution in the fuel, as explained in Appendix P, Section P.5.2.3.

The fixed source spectrum in MCNP is assumed to follow a ^{244}Cm spontaneous fission spectrum for all of the calculations in Appendix T.5. It is based on the following relationship:

$$p(E) = C \exp(-E/a)\sinh(bE)^{1/2}$$

with input parameters a=0.906 MeV and b=3.848 $(MeV)^{-1}$, as given in the MCNP manual [5.4].

T.5.2.3 Axial Peaking

The axial peaking factors for both neutron and gamma sources in BWR fuel are provided in Appendix K Section K.5.2.3. The same peaking factors are used in the MCNP analysis presented herein. The peaking factors for both neutron and gamma sources as a function of active fuel height are listed in Appendix K, Table K.5.2-3. These factors are directly applied to MCNP source input for the fuel region.

These factors in Appendix K, Table K.5.2-3 are determined based on typical axial burnup distributions for BWR assemblies and based on typical axial water density distribution that occurs during core operation. Using the base SAS2H/ORIGEN-S input for the 7x7 BWR, selected as the design basis assembly for this application, neutron and gamma source terms are generated for axial zones as a function of burnup and moderator density. This estimates both the non-linear behavior of the neutron source with burnup and the core operating moderator density effects on the actinide isotopics (neutron source). This axial distribution is conservative at high burnup because the burnup distribution will flatten out with increased burnup resulting in a reduction in the overall peaking factor.

The average values of the axial peaking distributions are also provided in Appendix K, Table K.5.2-3. For the gamma distribution, the average value is 1.0. However, for the neutron distribution, the average value of the distribution is 1.33. The average value of the axial neutron distribution may be interpreted as the ratio of the true total neutron source in an assembly to the neutron source calculated by SAS2H/ORIGEN-S for an average assembly burnup. Therefore, to properly correct the magnitude of the neutron source, the neutron source per fuel assembly as reported in Table T.5-9 through Table T.5-18 is multiplied by 1.33.

T.5.2.4 ANISN Evaluation of Bounding Source Terms

As discussed above, the fuel qualification tables are generated based on the decay heat limits for the various heat load zoning configurations shown in Figure T.2-1 through Figure T.2-8 of Chapter T.2. SAS2H is used to calculate the minimum required cooling time as a function of fuel assembly initial enrichment and burnup for each decay heat limit. To determine which combination of burnup, wt. % initial enrichment and cooling time result in the bounding dose rates on the surface of the HSM-H and OS197FC TC, the total source term, which includes the contribution from the fuel as well as the hardware in the entire fuel assembly (including end fittings) is used to calculate its total dose rate on the HSM roof and TC radial model using the ANISN code. The methodology employed in the current analysis is similar to that used in Appendix P, Chapter P.5 for 24PTH DSCs. The notion behind using the response function for determination of the bounding combination is that if one burnup/enrichment/cooling time combination results in the highest dose rate at a selected location near or on the TC or HSM surface it will result in the highest dose rate at any location near or on the TC or HSM surface.

An ANISN model is developed only for the OS197 TC. The side shielding through the OS197FC TC is identical to the side shielding through the Standardized TC except that the Standardized TC has NS-3 rather than water as the neutron shield. Because the thickness of NS-3 and water are identical between the two casks, and the shielding properties of NS-3 and water are also similar, water was used instead of NS-3 in ANISN models. Therefore, the resulting ANISN model is consistent with the OS197FC-B design at the side of the cask.

ANISN [5.7] determines the fluence of particles through one-dimensional geometric systems by solving the Boltzmann transport equation using the method of discrete ordinates. Particles can be generated by either particle interaction with the transport medium or extraneous sources incident upon the system. Anisotropic cross-sections are expressed in a Legendre expansion of arbitrary order.

The ANISN code implements the discrete ordinates method as its primary mode of operation. Balance equations are solved for the flow of particles moving in a set of discrete directions in each cell of a spacial mesh and in each group of a multigroup energy structure. Iterations are performed until all implicitness in the coupling of cells, directions, groups, and source regeneration is resolved.

ANISN coupled with the CASK-81 (22 neutron, 18 gamma-ray) energy group, coupled cross-section library [5.5] and the ANSI/ANS-6.1.1-1977 flux-to-dose conversion factors [5.10] is chosen to generate the ANISN dose rates used to determine the relative strength of the various source terms from fuel assemblies and determine the design basis source terms for the HSM and TC. These design basis source terms are used with MCNP models of the 61BTH system to calculate the bounding system dose rates. ANISN provides an efficient method to select the design basis source terms.

The surface dose rates are calculated using ANISN models to perform the evaluation for the fuel assembly parameters in the fuel qualification table. The ANISN model used to generate the relative dose rates on the TC is similar to a cut through the center of the MCNP4C2 OS197FC-B TC side model used for the shielding evaluation. Figure T.5-2 provides a sketch for the ANISN

model of the OS197FC TC centerline. A sample ANISN input file is included in Section **Error! Reference source not found.**.

With the exception of the fuel region, the material densities used in the ANISN models are the same as those used in the MCNP models as provided in Table T.5-19. The ANISN and MCNP number densities in the fuel region differ because in the MCNP models, the basket is modeled explicitly, while in the ANISN models the basket is homogenized with the fuel. The ANISN number densities for the fuel/basket region are provided in Table T.5-20.

To reduce the number of ANISN calculations required, a "response function" is developed using ANISN. Separate response functions are developed for all the radial heat zones shown on Figure T.5-2. It allows estimation of the relative contribution to the dose rate due to individual decay HLZC used.

To generate a neutron response function, the neutron radiation source for the ANISN model corresponds to a single particle emitted per second for each fuel assembly. The radius of the entire homogenized source region in the ANISN model is 71.58 cm. The axial extent of the gamma source region includes the bottom nozzle, in-core, plenum and top nozzle zones. The total length of these zones is 447.55 cm. For the neutron ANISN models, the axial zone of the source corresponds to the in-core region only, which has a length of 365.76 cm.

For the gamma response function, a separate ANISN model is executed with a single gamma emitted per second in each of the 18 CASK-81 gamma energy groups. The ANISN source volume and number of assemblies are used to calculate the ANISN source strength in units of particles per sec per unit volume. The neutron response function is generated in a similar fashion to the gamma response function, although only one ANISN input file is required because the neutron spectrum is adequately represented by the ^{244}Cm spectrum provided in Table T.5-21. The dose rate from secondary capture gammas is calculated in addition to the neutron dose rate. This method allows for the calculation of the neutron and capture gamma dose rate due to individual radial zones on the surface of the TC or HSM knowing only the magnitude of the neutron source.

Response functions are generated for each radial fuel zone shown on Figure T.5-2. An effective compartment unit cell is derived by preserving the total fuel compartment area in the cask. This effective unit cell dimension is 6.26 inches. The one dimensional methodology employed in ANISN is not capable of accurately modeling the two dimensional nature of the radial zone distribution of the fuel compartments. To alleviate this issue, modified zone radii are employed so that the two dimensional shielding features of the radial zones are accounted for. Effective zone radii are assumed that represent the cylindrical regions such that the thickness of the shielding material the particle radiation traverses is preserved and hence would adequately simulate penetration of radiation to the surface of the HSM or transfer cask through each radial zone. The effective zone radii used in the ANISN models are shown on Figure T.5-2.

In order to preserve the volumetric source strength throughout the source regions, adjustment factors are applied to the calculated ANISN response functions. These adjustment factors are equal to the actual total compartment area divided by the ANISN zone area that represents such compartment in ANISN models.

As shown in Figure T.5-2, radial zone 4 contains 12 assemblies that shield the inner zones only at the 0, 90, 180 and 270 degree corners of the cask. However at the 45, 135, 225 and 315 degree corners radial zone 4 does not shield the inner zones. Therefore, radial zone 4 is treated as void in the calculation of zones 1 through 3 response functions.

Response functions as well as MCNP calculations performed demonstrate that dose rates on or near HSM surfaces are dominated by gamma radiation. The gamma component is larger than the neutron component by a factor of 10 to 100. That implies the burnup, enrichment and cooling time combination resulting in the highest gamma radiation only dose rate when using HSM response functions will be bounding for HSM dose rates.

Therefore, it is appropriate to use transfer cask gamma response functions when determining burnup/enrichment/cooling time combinations related to HSM dose rates.

The response functions for the OS197FC TC are provided in Table T.5-22 through Table T.5-25. These response functions are used to compute the dose rate for each entry in the fuel qualification tables. For each qualification table, the burnup/enrichment/cooling time combination that results in the highest dose rate is selected as the design basis source.

An example of an ANISN response function evaluation is given in Table T.5-29 for radial source zone 2. Note the example is applicable for definition of bounding burnup/enrichment/cooling time combinations related to the transfer cask dose rates. The maximum dose rate for each table corresponds to the design basis source for that decay heat and shielding configuration.

Further, note that the values presented in Table T.5-29 are based on decay heat values rounded to the nearest 0.1 year and not the final decay heat values as presented in the fuel qualification tables, which have been conservatively rounded up to the nearest 0.5 year, as the design basis sources were selected prior to the rounding process.

T.5.2.5 Reconstituted Fuel

As explained in Section T.5.2, each fuel assembly may have up to 10 solid stainless steel rods that replace fuel rods. Reconstituted fuel assemblies typically generate lower decay heat than a standard assembly because fuel is replaced with steel. However, the reconstituted fuel produces higher dose rates due to the irradiated stainless steel that contains a strong ^{60}Co source. As the half-life of ^{60}Co is 5.27 years, after 10 years the ^{60}Co activity in the stainless steel rods is reduced to approximately a factor of four and the reconstituted assembly no longer generates higher dose rates than an equivalent standard fuel assembly. To bound this effect, the fuel qualification tables require an additional 5 years of cooling time for reconstituted fuel assemblies.

To validate this approach SAS2H runs are generated for reconstituted fuel assemblies. Dose rates are estimated using the response functions for radial zone number 4 (see Figure T.5-2) shown in Table T.5-25. This zone is analyzed because it contributes the largest to the total dose rate at the side of the transfer cask when the 61BTH DSC is loaded according to HLZC #6.

The SAS2H model for reconstituted fuel is very similar to the model for standard fuel assemblies. The following changes are implemented to generate the SAS2H model for

reconstituted fuel. First, the number of fuel rods is decreased from 49 to 39. Second, the power is adjusted to maintain the desired burnup corresponding to the initial heavy metal loading of 0.198 MTU*39/49, or 0.158 MTU. Lastly, using the material masses shown in Table T.5-6 the SAS2H light elements are modified to account for the 10 fuel rods that have been replaced with stainless steel rods.

It is assumed that reconstituted fuel is irradiated during the second and third cycles because the first cycle will always correspond to fresh fuel that cannot be loaded with reconstituted rods. To accurately model this behavior, two SAS2H models are generated for a subset of burnup and enrichment combinations used to generate the fuel qualification table for the 0.54 kW/assembly fuel assemblies in HLZC #6 (radial zone 4). The first SAS2H model is for only one cycle of irradiation of 10 reconstituted rods, while the second model is for three cycles of irradiation of 10 reconstituted rods. By subtracting the single cycle source term of the reconstituted rods from the total source term (fuel and reconstituted rods) corresponding to three cycles, the effective source term of the reconstituted fuel assembly is generated (three irradiation cycles of fuel and two irradiation cycles of reconstituted fuel).

This source term is used with the response function shown in Table T.5-25 to calculate dose rates due to the reconstituted fuel assembly. If the dose rate of the reconstituted fuel assembly exceeds the dose rates due to the design basis source term of the standard fuel assembly, the cooling time of the reconstituted fuel assembly is increased until the design basis source term is bounding. The reconstituted fuel assembly was analyzed for all burnups at the lowest and highest enrichment to evaluate the cooling time increase as a function of enrichment. When the reconstituted fuel is examined in this fashion, no more than 5 additional years of cooling time is required for reconstituted fuel to be bounded by the design basis source. In most cases, the increase in cooling time is from 1 to 3 years.

Reconstituted fuel may contain up to 10 stainless steel rods that have been irradiated or an unlimited number of lower enriched UO_2 rods or Zircaloy rods or unirradiated stainless steel rods that replace fuel rods. All replacement rods shall be of similar OD and length such that the equivalent amount of water is displaced as the original fuel rod in the fuel assembly matrix. The lower enriched UO_2 rods are of similar design and behavior as the standard rods aside from the uranium enrichment. The reconstituted rods can be at any location in the fuel assemblies and the reconstituted assemblies can be placed anywhere in the basket.

Fuel assemblies reconstituted with Zircaloy replacement rods are bounded by the design basis source terms because Zircaloy has a low ^{59}Co content and therefore results in a much lower source term that the rod it replaces. Lower enriched UO_2 rods reduce the fuel assembly average initial enrichment. Using this reduced assembly average enrichment with the fuel qualification tables accurately addresses the actual source term for the reconstituted assembly. Finally, unirradiated stainless steel replacement rods contribute no source term and are therefore bounded by the intact fuel assembly source term on which the shielding analysis is based.

T.5.3 Material Densities

The material weights given in Table T.5-6 for the fuel are used to calculate material densities for in-core, plenum, top, and bottom regions of the fuel assembly.

In order to account for sub-critical multiplication, an initial enrichment of 4.0 wt. % U-235 is used to calculate the amount of U-235 in the shielding models.

Material densities used in the various MCNP models are summarized in Table T.5-19. Material densities for the homogenized fuel/basket region used only in the ANISN models are summarized in the last column of Table T.5-20.

T.5.4 Shielding Evaluation

Dose rate contributions from the bottom, in core, plenum and top regions, as appropriate, from 61 BWR fuel assemblies loaded into NUHOMS® -61BTH Type 1 DSC and Type 2 DSC are calculated with the MCNP4C2 Code [5.4] and MCNP 5 v 1.20 [5.2,5.3] at various locations on and around the Transfer Casks (TC) and Horizontal Storage Modules (HSM), respectively. The following evaluation specifically addresses the NUHOMS®-61BTH Type 1 DSC in HSM Model 80, 102 or HSM-H or OS197/OS197H/OS197FC-B TC using the design basis source terms determined in Section T.5.2.

T.5.4.1 Computer Program

MCNP4C2 [5.4] and MCNP 5 [5.2, 5.3] are general-purpose Monte Carlo N-Particle codes that can be used for neutron, photon, electron, or coupled neutron/photon/electron transport. The code treats an arbitrary three-dimensional configuration of materials in geometric cells bounded by first- and second-degree surfaces and some special fourth-degree surfaces. Pointwise (continuous energy) cross-section data are used. For neutrons, all reactions given in a particular cross-section evaluation are accounted for in the cross section set. For photons, the code takes account of incoherent and coherent scattering, the possibility of fluorescent emission after photoelectric absorption, absorption in pair production with local emission of annihilation radiation, and bremsstrahlung. Important standard features that make MCNP4C2 very versatile and easy to use include a powerful general source; an extensive collection of cross-section data; and an extensive collection of variance reduction techniques that can be employed to track particles through very complex deep penetration problems. MCNP 5 was employed to take advantage of its mesh tallies capabilities in calculating dose rates distributed over the surface of the HSM. It also allows more point detectors to be used in a single run that substantially reduces the number of input/out decks needed to perform ISFSI site dose rate calculations described in Section T.10. MCNP 5 is a more advanced version and it has all the capabilities included in MCNP4C2. Therefore, these codes will be referred to simply as MCNP unless a text implies usage of features pertinent to only MCNP 5.

T.5.4.2 Spatial Source Distribution

The source components are:

- The neutron sources due to the active fuel region,
- The gamma source due to the active fuel region,
- The gamma source due to the plenum,
- The gamma source due to the top region,
- The gamma source due to the bottom region,

Axial peaking is accounted for in the active fuel region by inputting an axial shape, as discussed in Section T.5.2.3.

T.5.4.3 Cross Section Data

The cross-section data used is the continuous energy ENDF/B-VI provided with the MCNP code. The cross-section data allows coupled neutron/gamma-ray dose rate evaluation to be made to account for the contributions from secondary gamma radiation (n,γ), if desired. All of the transfer cask dose rate calculations account for the dose rate due to secondary gamma radiation. For the HSM-H dose rate calculation, the dose rate contribution from the secondary gamma radiation is ignored because it is insignificant. On the other hand, neutron multiplication was accounted for twice: during MCNP runs by allowing the code to account for neutron subcritical multiplication and after post run processing of results when the neutron dose rates were multiplied by $1/(1-k_{eff})$ where $k_{eff}=0.40$, which is bounded by the criticality results shown in Table T.6-8. Such a treatment of neutron radiation dose rates overwhelms slight non-conservatism resulting from ignoring secondary gamma radiation.

T.5.4.4 Flux-to-Dose-Rate Conversion

The flux distribution calculated by the MCNP code is converted to dose rates using flux-to-dose rate conversion factors from ANSI/ANS-6.1.1-1977 [5.10] given in Table T.5-26.

T.5.4.5 Methodology

The methodology used in the shielding analysis of the 61BTH system has been updated compared to the DORT methodology previously used to support NUHOMS® storage and transportation applications for 61BT. In the current analysis, the 2-D DORT code has been replaced with the 3-D MCNP code. MCNP allows for explicit 3-D modeling of any shielding configuration and reduces the number of approximations needed in comparison to the 2-D DORT methodology. The methodology used herein is summarized below.

1. Sources are developed for all fuel regions using the source term data developed in Section T.5.2. Source regions include the active fuel region, bottom end fitting (including all materials below the active fuel region), plenum, and top end fitting (including all materials above the active fuel region).

2. Suitable shielding material densities are calculated for all regions modeled.

3. The 3-D Monte Carlo code MCNP is used to calculate dose rates on and around the HSM Model 102 and OS197/OS197H/OS197FC-B loaded with Type 1 DSC as well as the HSM-H and OS197FC-B loaded with a Type 2 DSC. The MCNP code is selected because of its ability to handle thick, multi-layered shields and account for streaming through both the HSM-H air vents and cask/DSC annulus using 3-D geometry. HSM Model 80 results are determined by applying scaling factors to the HSM Model 102 results.

4. MCNP results are used to calculate offsite exposures (see Section T.10).

5. MCNP models are also generated to determine the effects of accident scenarios, such as loss of cask neutron shield, for the OS197FC-B TC model (Section T.11).

T.5.4.6 Assumptions

The following general assumptions are used in the analyses.

T.5.4.6.1 Source Term Assumptions

- The primary neutron source in LWR spent fuel is the spontaneous fission of ^{244}Cm. For the ranges of exposures, enrichments, and cooling times in the fuel qualification tables, ^{244}Cm represents more than 90% of the total neutron source. The neutron spectrum is, therefore, relatively constant for the fuel parameters addressed herein and is assumed to follow the ^{244}Cm fission spectrum provided in Section T.5.2.2.

- The BWR heavy metal weight is assumed to be 0.198 MTU per fuel assembly to bound existing BWR fuel designs.

T.5.4.6.2 HSM-H Dose Rate Analysis Assumptions

- The 61BTH DSC and fuel assemblies are positioned as close to the HSM-H front door as possible to maximize the HSM-H front wall dose rates.

- Planes of reflection are used to simulate adjacent HSM-Hs.

- Embedment and rebar in the HSM-H concrete are conservatively neglected.

- Penetrations on the exterior of the HSM-H modules for instrumentation and ease of installation are not modeled since they do not result in any significant change in the dose rate distribution and are covered by other modeling conservatisms.

- The borated neutron absorber sheets in the 61BTH DSC are modeled as aluminum.

- An axial source distribution is discussed in Section T.5.2.3 is utilized.

- Fuel is homogenized within the fuel compartment, although the 61BTH DSC basket is modeled explicitly.

T.5.4.6.3 HSM Model 102 Dose Rate Analysis Assumptions

The dose rates for HSM Model 102 were also calculated using MCNP. Those dose rates are due to bounding 61BTH DSC Type 1 loading configuration sources. This configuration includes 0.393 kWt/FA assemblies in the central 25 fuel compartments. The next layer of 24 fuel compartments holds 0.54 kWt/FA assemblies, the outer compartments admit assemblies generating 0.54 kWt/FA. Note that this is also a fictitious loading configuration because more than 22.0 kWt/DSC heat load is not allowed for 61BTH DSC Type 1 and HSM Model 102 configuration. This "ficticious" configuration is depicted in Figure T.5-1. The same set of assumptions listed in Section T.5.4.6.2 applies to MCNP model of HSM Model 102.

T.5.4.6.4 OS197FC-B TC Dose Rate Analysis Assumptions

- The 61BTH Type 1 DSC is modeled within the OS197FC-B TC. It is assumed that fuel is placed inside of the Type 1 DSC in accordance with the Type 2 DSC decay HLZC #6 when calculating dose rates on and around the top and side of the transfer cask. Note that this is a hypothetical DSC loading combination. However, such an assumption results in the transfer cask dose rates that are bounding for all possible decay heat loading configurations. At the ends of the transfer cask Type 2 DSC HLZC #7 is also evaluated. Only the OS197FC-B is modeled as it bounds the Type 1 OS197 and OS197H TCs.

- Three inches of supplemental temporary neutron shielding and one inch of steel are assumed to be placed on top of the 61BTH Type 1 DSC cover plates during welding operations.

- During the accident case, the cask neutron shield (either water or NS-3) and the neutron shield jacket (outer steel skin) are assumed to be lost.

- The borated neutron absorber sheets in the 61BTH Type 1 and Type 2 DSC are modeled as aluminum.

- An axial source distribution discussed in Section T.5.2.3 is utilized. An additional factor of 1.326 was conservatively applied to the neutron source terms.

- Fuel is homogenized within the fuel assembly cross section, although the 61BTH Type 1 DSC basket is modeled explicitly.

- The OS197FC-B is equipped with channels to allow air flow through the bottom and the lid at the top. The air gaps formed by these channels are assumed to extend around the entire circumference of the cask.

T.5.4.7 Normal Condition Models

As stated above, only one MCNP shielding configuration is considered for the transfer cask and HSM shielding analyses: 61BTH Type 1 DSC. Such a shielding configuration is conservative and bounds other loading configurations. Unless otherwise indicated, the following discussion is related to the bounding 61BTH Type 1 DSC.

T.5.4.7.1 61BTH DSC in HSM-H

Two three-dimensional DSC models are developed for the 61BT Type 1 DSC within an HSM-H, one model for calculating neutron dose rates and the other for gamma dose rates. Note that the Type 1 DSC is loaded in accordance with the HLZC #6 pertinent to Type 2 DSC. This is a hypothetical combination, but it results in HSM dose rates that are bounding for all possible DSC/HSM shielding and source term combinations. These models are presented in Figure T.5-3 through Figure T.5-7. The HSM-H length is designated as the z axis, the width as the x axis, and the height as the y axis. The HSM-H door is designated as the south side and the –z direction,

with the east wall as the –x direction. The roof is the +y direction. The east wall is designated as a reflective boundary and an end shield wall (3 ft thick) is attached to the west wall.

The bottom (bottom of bottom fitting) of the fuel assembly is assigned to a z plane at -224.06 cm. The center of the HSM-H is at (x,y,z)=(0,0,0). The 61BTH Type 1 DSC lid is located 5" from the HSM-H rear wall (z=254.84 cm) which places the bottom of the DSC at z=-238.67 cm, about 28.78 cm from the door interior. The 61BTH DSC support rails are not included in the model. The heat shields are modeled as flat plates and horizontal vent "liner" plates (2 cm thick) are modeled in the top side vents.

The dose rates for the HSM-H are calculated based on a door design with 22.5" thick concrete and 3.875" thick steel. Dose rates are calculated on thin cells surrounding the HSM-H and are segmented into 30 cm increments to capture the peak dose rates. Dose rates are also calculated at the inlet and outlet vents. Bounding dose rates are provided in Table T.5-1. Gamma and neutron dose rates for the front, side shield wall and roof surface at the DSC centerline of the HSM-H are also plotted as a function of distance in Figure T.5-17 through Figure T.5-22, respectively.

An evaluation of an alternate door configuration is performed on a door design with 25" thick concrete and 3" thick steel. This evaluation results in small increases in the dose rates in and around the door region and has no impact on the average dose rates on the HSM-H front surface. Consequently, the effect on the ISFSI site dose rates, calculated in Chapter T.10, is negligible. Small changes to the steel (±1") or concrete (±6") thicknesses in the door region are not expected to have any significant effect on the front surface dose rates since the surface dose rates in the door region are lower than the HSM front average dose rates by more than a factor of 20.

A sample MCNP 5 model input file of HSM-H with 61BTH DSC is included in Section **Error! Reference source not found.**.

T.5.4.7.2 61BTH DSC in HSM Model 102

Two three-dimensional MCNP models are developed for the 61BTH DSC Type 1 within a HSM-Model 102, one model is for neutrons and the other for gammas. Note that DSC Type 1 is loaded in accordance with the bounding for 61BTH DSC Type 1 heat loading configuration. This is a fictitious combination but it results in HSM dose rates that are bounding for all possible DSC/HSM shielding and source terms combinations pertinent to the Type 1 DSC. These models are presented in Figure T.5-8 through Figure T.5-10. The HSM length is designated as the z axis, the width as the x axis, and the height as the y axis. The HSM door is designated as the south side and the –z direction, with the west wall as the –x direction. The roof is the +y direction. The west wall is designated as a reflective boundary and an end shield wall (2 ft thick) is attached to the east wall.

The bottom (bottom of bottom fitting) of the fuel assembly is assigned to a z plane at -224.06 cm. The center of the HSM-H is at (x,y,z)=(0,0,0). The 61BTH DSC Type 1 lid is located 2.31" from the HSM Model 102 rear wall (z=252.30 cm) which places the bottom of the DSC at z=-242.92 cm, about 5.07" from the door interior. The 61BTH DSC support rails are not

included in the model. Steel embodiments are modeled along vent perimeters as 1.5" thick plates.

Dose rates are calculated on thin cells surrounding the HSM Model 102 and are segmented into about 30 cm increments to capture the peak dose rates. Dose rates are also calculated at the inlet and outlet vents (in front and above frontal and top bird screens, respectively).

A sample MCNP 5 model input file of HSM Model 102 with 61BTH Type 1 DSC is included in Section T.5.5.3.

T.5.4.7.3 61BTH DSC in HSM Model 80

The dose rates for the 61BTH DSC in the HSM Model 80 were calculated utilizing ratios of gamma and neutron dose rates for the 61BT DSC in the Model 102 and Model 80 HSMs. The dose rates calculated for the 61BT DSC in the HSM Model 102 and Model 80 are taken from Appendix K, Chapter K.5. These dose rates are used to determine neutron and gamma dose rate ratios for the front, top, side and rear as shown in Table T.5-27 and Table T.5-28. (The surface averaged and maximum dose rates calculated for the 61BTH / Model 80 configuration are presented in Table T.5-3.) These ratios were then applied to the 61BTH DSC HSM Model 102 dose rates calculated in Section T.5.4.7.2. This method is reasonable, as the design basis source spectra for the 61BT canister is essentially equivalent to the 61BTH.

T.5.4.7.4 61BTH DSC in OS197FC-B TC

Two three-dimensional MCNP models are employed for shielding analyses of the 61BTH DSC within an OS197FC-B TC, one model calculating for neutron dose rates and the other for gamma dose rates. These models are presented in Figure T.5-11 through Figure T.5-16. The z-axis in the MCNP models coincides with the axis of rotation of the cask and the 61BTH DSC. Select features within the cask and on its surface are neglected because they produce only localized effects and have minimal impact on operational dose rates. Examples of neglected features include the 61 neutron shield panel support angles, the 4 trunnions, relief valves, clevises, and eyebolts. With the exception of the 61 neutron shield support angles and the trunnions, the balance of these items are local features that increase the shielding in a small area without replacing any of the shielding material which is included in the model. The additional shielding material that these features provide is not smeared into the bulk shielding, nor is any credit taken for it in the occupational exposure calculation. The 61 neutron shield support angles provide support for the neutron shield skin, which contains water for the neutron shield. The steel that forms these angles is not smeared with the water in the neutron shield; rather it is modeled as water. This is conservative for gamma radiation because water is less than one seventh the density of steel. The density of the neutron shield water used in the cask MCNP models is 1.0 g/cm^3. Therefore, replacing the steel with the full density water results in slightly nonconservative neutron dose rates outside the cask, but this is compensated for by increasing the neutron source by a factor of 1.326.

The trunnions penetrate the neutron shield, which locally changes the shielding configuration of the neutron shield. The trunnions are thick steel structures filled with an optional NS-3 neutron shielding material. These structures protrude well past the neutron shield and are made of

materials which provide more gamma shielding and comparable neutron shielding as compared to the 1.0 g/cm3 water that these replace. In addition, with the exception of the neutron shield support angles, none of these features is located near the axial center of the cask where the surface dose rate is the largest due to the axial peaking of the fuel.

Design features relevant to the shielding analysis of the OS197FC-B TC and 61BTH DSC are modeled in MCNP. The overall length of the OS197FC-B TC is 202.97". The outer diameter of the OS197FC-B TC is 85.50" (neutron shield included). The outer diameter excluding the neutron shield is 79.12". The bottom of the OS197FC-B TC is designed to mate with a 61BTH DSC. The overall length of the 61BTH DSC is 196.04" (excluding the grapple) and its outer diameter is 67.25". The bottom end of the 61BTH DSC is in contact with the structural shell assembly of the transfer cask.

The OS197FC-B TC has a ventilated top lid to facilitate air circulation. In MCNP, the ventilation cutouts in the top cover assembly are modeled as complete annular gaps. The supporting steel around the bolts is not included for modeling convenience and conservatism in the results. Likewise, the neutron shielding in the top lid is also reduced to the inner radial dimension to conservatively account for the bolt cutouts. Use of cone adapters and cask spacers during air circulation will offset shielding lost by the removal of the ram access cover.

Dose rates are provided in Table T.5-4. Dose rates at the sides, top, and bottom of this cask are presented graphically in Figure T.5-23 through Figure T.5-25.

A sample MCNP model input file for OS197FC-B TC with 61BTH DSC is included in Section 5.5.3.

T.5.4.8 Accident Condition Models

No accident condition models were developed for the HSM-H because no accident scenario in Chapter T.11 has been identified that would alter the dose rates provided in Table T.5-1. The HSM Model 102 in an array, in an accident condition, is assumed to slide next to an adjacent HSM and therefore double the gap on one side as described in Chapter T.11. It is further conservatively assumed the dose rates from the array double as a result of this accident. The HSM Model 102 accident analysis and results are provided in Chapter T.11.

For the OS197FC-B TC, an accident case is performed which assumes that the neutron shield and steel neutron shield jacket (outer skin of each) has been torn off. A second case is considered to analyze the effect of damaged fuel turning to rubble in the bottom of the cask following an accident. Figure T.5-15 and Figure T.5-16 show the MCNP fuel rubble accident model. The dose rates from fuel rubble exhibit local peaking however at far distances the accident dose rates without fuel rubble are conservative. Accident dose rates at 1m, 100m, and 500m from the side of the cask are presented in Table T.5-4.

T.5.4.9 OS197FC-B TC Models During Fuel Loading Operations

MCNP models are developed for the cask decontamination and welding operations during fuel loading using the 61BTH DSC. The dose rates calculated for these operations are utilized to estimate the occupational exposure which is documented in Chapter T.10.

Cask Decontamination. The 61BTH DSC and the OS197FC-B TC are assumed to be completely filled with water, including the region between 61BTH DSC and cask, which is referred to as the "TC/61BTH DSC annulus." The 61BTH DSC top shield plug and inner cover plate are assumed to be in place and the temporary shielding has not yet been installed (configuration prior to placement of the Automated Welding System (AWS)). Results for this case are provided in Table T.5-5.

Welding and 61BTH DSC Draining. Before the start of welding operation, approximately 60% of the water in the DSC cavity is removed due to hydrogen generation considerations. A dry DSC cavity is assumed in all welding models to be conservative. Temporary shielding consisting of three inches of NS-3 and one inch of steel is assumed to cover the 61BTH DSC top shield plug. In addition, the DSC outer top cover plate is not present. The cask/61BTH DSC annulus is assumed to remain completely filled with water. Results for this case are provided in Table T.5-5.

T.5.5 Appendix

Proprietary Information withheld under 10CFR2.390

Proprietary Information withheld under 10CFR2.390

Proprietary Information withheld under 10CFR2.390

Proprietary Information withheld under 10CFR2.390

Proprietary Information withheld under 10CFR2.390

Proprietary Information withheld under 10CFR2.390

Proprietary Information withheld under 10CFR2.390

Proprietary Information withheld under 10CFR2.390

Proprietary Information withheld under 10CFR2.390

Proprietary Information withheld under 10CFR2.390

Proprietary Information withheld under 10CFR2.390

Proprietary Information withheld under 10CFR2.390

Proprietary Information withheld under 10CFR2.390

Proprietary Information withheld under 10CFR2.390

Proprietary Information withheld under 10CFR2.390

Proprietary Information withheld under 10CFR2.390

Proprietary Information withheld under 10CFR2.390

Proprietary Information withheld under 10CFR2.390

Proprietary Information withheld under 10CFR2.390

Proprietary Information withheld under 10CFR2.390

Proprietary Information withheld under 10CFR2.390

Proprietary Information withheld under 10CFR2.390

Proprietary Information withheld under 10CFR2.390

Proprietary Information withheld under 10CFR2.390

Proprietary Information withheld under 10CFR2.390

Proprietary Information withheld under 10CFR2.390

Proprietary Information withheld under 10CFR2.390

Proprietary Information withheld under 10CFR2.390

Proprietary Information withheld under 10CFR2.390

Proprietary Information withheld under 10CFR2.390

Proprietary Information withheld under 10CFR2.390

Proprietary Information withheld under 10CFR2.390

Proprietary Information withheld under 10CFR2.390

Proprietary Information withheld under 10CFR2.390

Proprietary Information withheld under 10CFR2.390

Proprietary Information withheld under 10CFR2.390

Proprietary Information withheld under 10CFR2.390

Proprietary Information withheld under 10CFR2.390

Proprietary Information withheld under 10CFR2.390

Proprietary Information withheld under 10CFR2.390

Proprietary Information withheld under 10CFR2.390

Proprietary Information withheld under 10CFR2.390

Proprietary Information withheld under 10CFR2.390

Proprietary Information withheld under 10CFR2.390

Proprietary Information withheld under 10CFR2.390

Proprietary Information withheld under 10CFR2.390

Proprietary Information withheld under 10CFR2.390

Proprietary Information withheld under 10CFR2.390

Proprietary Information withheld under 10CFR2.390

Proprietary Information withheld under 10CFR2.390

Proprietary Information withheld under 10CFR2.390

Proprietary Information withheld under 10CFR2.390

Proprietary Information withheld under 10CFR2.390

Proprietary Information withheld under 10CFR2.390

Proprietary Information withheld under 10CFR2.390

Proprietary Information withheld under 10CFR2.390

Proprietary Information withheld under 10CFR2.390

Proprietary Information withheld under 10CFR2.390

Proprietary Information withheld under 10CFR2.390

Proprietary Information withheld under 10CFR2.390

Proprietary Information withheld under 10CFR2.390

Proprietary Information withheld under 10CFR2.390

Proprietary Information withheld under 10CFR2.390

Proprietary Information withheld under 10CFR2.390

Proprietary Information withheld under 10CFR2.390

Proprietary Information withheld under 10CFR2.390

Proprietary Information withheld under 10CFR2.390

Proprietary Information withheld under 10CFR2.390

Proprietary Information withheld under 10CFR2.390

Proprietary Information withheld under 10CFR2.390

Proprietary Information withheld under 10CFR2.390

Proprietary Information withheld under 10CFR2.390

T.5.6 References

5.1 Oak Ridge National Laboratory, RSICC Computer Code Collection, "SCALE: A Modular Code System for Performing Standardized Computer Analysis for Licensing Evaluations for Workstations and Personal Computers," NUREG/CR-0200, Revision 6, ORNL/NUREG/CSD-2/V2/R6.

5.2 MCNP – A General Monte Carlo N-Particle Transport Code, Version 5, Volume I: Overview and Theory, LA-UR-03-0245, 2003.

5.3 MCNP – A General Monte Carlo N-Particle Transport Code, Version 5, Volume II: User's Guide, LA-CP-03-0245, 2003.

5.4 "Monte Carlo N-Particle Transport Code System," CCC-701, Oak Ridge National Laboratory, RSICC Computer Code Collection, August 2001.

5.5 CASK-81 - 22 Neutron, 18 Gamma-Ray Group, P3, Cross Sections for Shipping Cask Analysis," DLC-23, Oak Ridge National Laboratory, RSIC Data Library Collection, August 1987.

5.6 S. B. Ludwig and J. P. Renier, "Standard- and Extended-Burnup BWR and PWR Reactor Models for the ORIGEN2 Computer Code," ORNL/TM-11018 Oak Ridge National Laboratory, December 1989.

5.7 "ANISN-ORNL - One-Dimensional Discrete Ordinates Transport Code System with Anisotropic Scattering," CCC-254, Oak Ridge National Laboratory, RSIC Computer Code Collection, April 1991.

5.8 Not used.

5.9 Not used.

5.10 "American National Standard Neutron and Gamma-Ray Flux-to-Dose Rate Factors," ANSI/ANS-6.1.1-1977, American Nuclear Society, LaGrange Park, Illinois, March 1977.

5.11 Not used.

5.12 U. S. Nuclear Regulatory Commission, "Review of Technical Issues Related to Predicting Isotopic Compositions and Source Terms for High Burnup LWR Fuel," NUREG/CR-6701, Published January 2001, ORNL/TM-2000/277.

5.13 B. D Murphy, "Prediction of Isotopic Composition of UO2 Fuel from a BWR: Analysis of the DU1 Sample from the Dodewaard Reactor," ORNL/TM-13687, October 1998.

5.14 Japan Atomic Energy Research Institute, "Technical Development on Burnup Credit for Spent LWR Fuels," JAERI-Tech 2000-071, September 21, 2000.

5.15 U. S. Nuclear Regulatory Commission, "Nuclide Importance to Criticality Safety, Decay Heating, and Source Terms Related to Transport and Interim Storage of High Burnup LWR Fuel," NUREG/CR-6700, Published January 2001, ORNL/TM-2000/284.

5.16 Not used.

5.17 O. W. Hermann, S. M. Bowman, M. C. Brady, C. V. Parks, "Validation of the SCALE System for PWR Spent Fuel Isotopic Composition Analyses," ORNL/TM-12667, March 1995.

5.18 M. D. DeHart and O. W. Hermann, "An Extension of the Validation of SCALE (SAS2H) Isotopic Predictions for PWR Spent Fuel," ORNL/TM-13317, September 1996.

5.19 Luksic, "Spent Fuel Assembly Hardware: Characterization and 10CFR61 Classification for Waste Disposal," PNL-6906, UC-85, August 1989.

Table T.5-1
Summary of NUHOMS®-61BTH DSC in HSM-H, Bounding Maximum and Average Dose Rates, HLZC #6(2)

Dose Rate Location	Maximum Gamma (mrem/hr)	Gamma MCNP 1σ Error	Maximum Neutron (mrem/hr)	Neutron MCNP 1σ Error	Maximum Total(1) (mrem/hr)	Total MCNP 1σ Error
HSM Roof (centerline)	24.91	0.15	0.76	0.04	25.67	0.14
HSM Roof Birdscreen	206.70	0.04	6.59	0.01	213.29	0.03
HSM End (Side) Shield Wall Surface	3.04	0.05	0.16	0.09	3.19	0.04
HSM Door Exterior Surface (centerline)	0.30	0.02	0.06	0.002	0.35	0.02
HSM Front Birdscreen	590.85	0.05	6.87	0.04	597.72	0.05

Dose Rate Location	Gamma Average (mrem/hr)	Gamma MCNP 1σ Error	Average Neutron (mrem/hr)	Neutron MCNP 1σ Error	Average Total (mrem/hr)	Total MCNP 1σ Error
HSM Roof	18.78	0.01	0.71	0.004	19.49	0.01
HSM End (Side) Shield Wall Surface	0.84	0.01	0.07	0.03	0.91	0.01
HSM Front	9.19	0.03	0.43	0.02	9.61	0.03
HSM Back Shield Wall	0.34	0.07	0.01	0.02	0.35	0.07

Notes:

(1) Gamma and neutron dose rate peaks do not always occur at the same location; therefore, the total dose rate is not always the sum of the gamma plus neutron dose rate.

(2) Dose calculated using a 61BTH Type 2 DSC configuration 6 source loaded into a Type 1 DSC bounds dose rates from all specified DSC configurations.

Table T.5-2
Summary of NUHOMS®-61BTH DSC in HSM Model 102, Bounding Maximum and Average Dose Rates

Dose Rate Location	Maximum Gamma (mrem/hr)	Gamma MCNP 1σ Error	Maximum Neutron (mrem/hr)	Neutron MCNP 1σ Error	Maximum Total (mrem/hr)	Total MCNP 1σ Error
HSM Roof (centerline)	53.82	0.05	1.43	0.02	55.21	0.05
HSM Roof Birdscreen	317.86	0.03	13.40	0.02	331.04	0.03
HSM End (Side) Shield Wall Surface	10.21	0.04	0.35	0.02	10.56	0.04
HSM Door Exterior Surface (centerline)	2.36	0.04	0.48	0.01	2.84	0.04
HSM Front Birdscreen	185.25	0.04	4.38	0.04	189.40	0.04
HSM Back Shield Wall	1.52	0.05	0.12	0.04	1.64	0.05

Dose Rate Location	Average Gamma (mrem/hr)	Gamma MCNP 1σ Error	Average Neutron (mrem/hr)	Neutron MCNP 1σ Error	Average Total (mrem/hr)	Total MCNP 1σ Error
HSM Roof	22.78	<0.01	0.71	0.01	23.49	<0.01
HSM End (Side) Shield Wall Surface	2.29	0.01	0.09	0.01	2.38	0.01
HSM Front	14.57	0.01	0.59	0.01	15.16	0.01
HSM Back Shield Wall	0.48	0.01	0.03	0.02	0.51	0.01

Table T.5-3
Summary of NUHOMS®-61BTH DSC in HSM Model 80 Maximum and Average Dose Rates

Dose Rate Location	Maximum Gamma (mrem/hr)	Maximum Neutron (mrem/hr)	Maximum Total (mrem/hr)
Roof Centerline	54.90	1.43	56.33
End Shield Wall	12.97	0.35	13.32
Door Exterior	34.93	53.44	88.37
Back Shield Wall	1.29	0.078	1.37
Front Birdscreen	172.28	4.12	176.40
Roof Birdscreen	1513.01	13.27	1526.30

Dose Rate Location	Average Gamma (mrem/hr)	Average Neutron (mrem/hr)	Average Total (mrem/hr)
Front	19.82	5.72	25.54
Top	57.63	0.72	58.35
Side	2.91	0.10	3.01
Rear	0.40	0.03	0.43

Table T.5-4
Summary of NUHOMS®-61BTH DSC, OS197FC-B TC Maximum Dose Rates During Transfer Operations

Dose Rate Location	Maximum Gamma (mrem/hr)	Gamma MCNP 1σ Error	Maximum Neutron (mrem/hr)	Neutron MCNP 1σ Error	Maximum Total(1) (mrem/hr)	Total MCNP 1σ Error
Cask Side Surface (Radial)	7.57E+02	0.0043	5.65E+02	0.0032	1.32E+03	0.0028
Cask Top Axial Surface	2.42E+02	0.0502	2.87E+01	0.0203	2.57E+02	0.0473
Cask Bottom Axial Surface(2)	5.01E+03	0.0468	8.96E+02	0.0087	5.91E+03	0.0397
1 ft from Cask Side (Radial)	4.91E+02	0.0043	3.53E+02	0.0026	8.44E+02	0.0027
1 ft from Cask Top Axial Surface	6.61E+01	0.0544	1.84E+01	0.0175	7.58E+01	0.0476
1 ft from Cask Bottom Axial Surface	2.66E+03	0.0519	3.19E+02	0.0104	2.98E+03	0.0463
3 ft from Cask Side (Radial)	2.95E+02	0.0040	2.00E+02	0.0028	4.95E+02	0.0027
3 ft from Cask Top Axial Surface	3.14E+01	0.0659	9.62E+00	0.0172	3.81E+01	0.0548
3 ft from Cask Bottom Axial Surface	8.67E+02	0.0669	9.21E+01	0.0165	9.60E+02	0.0605
Cask 1 m (Radial) Accident Condition	3.86E+02	0.0094	2.57E+03	0.0018	2.96E+03	0.0020
Cask 100 m (Radial) Accident Condition	1.65E-01	0.0065	3.52E-01	0.0045	5.16E-01	0.0037
Cask 500 m (Radial) Accident Condition	4.69E-04	0.0106	1.87E-04	0.0317	6.56E-04	0.0118

Notes:

(1) Gamma and neutron dose rate peaks do not always occur at the same location; therefore, the total dose rate is not always the sum of the gamma plus neutron dose rate.

(2) The peak bottom surface dose rate is directly below the grapple ring cut out in the bottom of the cask. The bottom average dose rates, including the grapple area, are 693 mrem/hr gamma, 164 mrem/hr neutron for a total average dose rate of 857 mrem/hr.

Table T.5-5
Summary of NUHOMS®-61BTH DSC, OS197FC-B TC Maximum Dose Rates During Decontamination and Welding Operations

Dose Rate Location	Maximum Gamma (mrem/hr)	Gamma MCNP 1σ Error	Maximum Neutron (mrem/hr)	Neutron MCNP 1σ Error	Maximum Total(1) (mrem/hr)	Total MCNP 1σ Error
Decontamination						
Cask Side Surface (Radial)	3.05E+02	0.0089	2.57E+02	0.0096	5.63E+02	0.0065
Top Axial Surface	1.98E+03	0.0190	6.18E+00	0.0333	1.98E+03	0.0190
Cask Bottom Axial Surface(2)	3.88E+03	0.0113	1.34E+02	0.0364	4.01E+03	0.0110
1 ft from Cask Side (Radial)	2.08E+02	0.0085	1.61E+02	0.0077	3.69E+02	0.0058
1 ft from Top Axial Surface	1.55E+03	0.0182	2.52E+00	0.0938	1.55E+03	0.0182
1 ft from Cask Bottom Axial Surface	2.03E+03	0.0132	5.08E+01	0.0438	2.08E+03	0.0129
3 ft from Cask Side (Radial)	1.29E+02	0.0079	9.07E+01	0.0080	2.20E+02	0.0057
3 ft from Top Axial Surface	8.70E+02	0.0217	2.53E+00	0.0450	8.70E+02	0.0217
3 ft from Cask Bottom Axial Surface	6.99E+02	0.0186	1.29E+01	0.0775	7.12E+02	0.0183
Welding						
Cask Side Surface (Radial)	6.57E+02	0.0128	4.00E+02	0.0032	1.06E+03	0.0081
Top Axial Surface	2.16E+03	0.1296	2.67E+01	0.0555	2.19E+03	0.1281
Cask Bottom Axial Surface(3)	5.09E+03	0.0129	8.13E+02	0.0080	5.90E+03	0.0112
1 ft from Cask Side (Radial)	4.38E+02	0.0125	2.52E+02	0.0030	6.89E+02	0.0080
1 ft from Top Axial Surface	1.02E+03	0.0773	1.21E+01	0.0769	1.03E+03	0.0767
1 ft from Cask Bottom Axial Surface(3)	2.62E+03	0.0153	2.90E+02	0.0100	2.91E+03	0.0138
3 ft from Cask Side (Radial)	2.67E+02	0.0116	1.42E+02	0.0041	4.08E+02	0.0077
3 ft from Top Axial Surface	5.69E+02	0.0069	7.11E+00	0.1031	5.74E+02	0.0068
3 ft from Cask Bottom Axial Surface(3)	9.25E+02	0.0223	8.02E+01	0.0163	1.01E+03	0.0205

Notes:

(1) Gamma and neutron dose rate peaks do not always occur at the same location; therefore, the total dose rate is not always the sum of the gamma plus neutron dose rate.

(2) The peak bottom surface dose rate is directly below the grapple ring cut out in the bottom of the cask. The bottom average dose rates, including the grapple area, are 517 mrem/hr gamma, 24 mrem/hr neutron for a total average dose rate of 541 mrem/hr.

(3) The peak bottom surface dose rate is directly below the grapple ring cut out in the bottom of the cask. The bottom average dose rates, including the grapple area, are 690 mrem/hr gamma, 143 mrem/hr neutron for a total average dose rate of 833mrem/hr. Note that this bottom axial dose rate has no impact on the occupational exposure because no operations are performed near the bottom axial location.

Table T.5-6
BWR Fuel Assembly Material Mass

Hardware Item	Material	Average Mass, (kg/FA)	Comments
In-core Zone, (**144.00** inch long, **4.73** g/FA total cobalt content)			
Cladding	Zircaloy-2	49.2	
Fuel Channel Sleeve	Zircaloy-4	37.1	
Grid Spacers	Zircaloy-4	1.95	7 spacers*~0.28 kg/spacer
Spacer Springs	Inconel X-750	0.36	7 springs*0.051 kg/spring
Channel Spring & Bolt	Inconel X-750	0.13	
Channel Fastener Guard	Stainless Steel	0.46	
Channel Spacer & Rivet	Stainless Steel	0.13	
Fuel	Uranium	198	wt. of UO_2=224.643 kg.=0.198 mtu/0.8814
Gas Plenum Zone, (**12.93** inch long, **0.89** g/FA total cobalt content)			
Cladding	Zircaloy-2	4.89	
Fuel Channel	Zircaloy-4	0.00	
Plenum Springs	Stainless Steel	1.05	
Top End Fitting Zone, (**12.62** inch long, **4.51** g/FA total cobalt content)			
Upper Tie Plate	Stainless Steel	2.08	
Lock Tab Washers & Nuts	Stainless Steel	0.05	
Expansion Springs	Inconel X-750	0.43	
End Plugs	Zircaloy	1.26	
Bottom End Fitting Zone, (**6.65** inch long, **4.10** g/FA total cobalt content)			
Finger Springs	Inconel	0.05	
End Plugs	Zircaloy	1.26	
Lower Tie Plate	Stainless Steel	4.7	
Total, kgs.(1)		329.7	
Total, lbs.(1)		726.3	

Note 1: This mass is very conservative for the source term calculation because the maximum weight of fuel assembly with or without channel is limited to 705 lbs per Chapter T.2.

Table T.5-7
Elemental Composition of LWR Fuel-Assembly Structural Materials

Element	Atomic Number	Material Composition, grams per kg of material				UO_2 Fuel, Grams/1.345 kgs
		Zircaloy-4	Inconel-718	Inconel X-750	Stainless Steel 304	
H	1	1.30E-02	-	-	-	-
Li	3	-	-	-	-	1.00E-03
B	5	3.30E-04	-	-	-	1.00E-03
C	6	1.20E-01	4.00E-01	3.99E-01	8.00E-01	8.94E-02
N	7	8.00E-02	1.30E+00	1.30E+00	1.30E+00	2.50E-02
O	8	9.50E-01	-	-	-	1.34E+02
F	9	-	-	-	-	1.07E-02
Na	11	-	-	-	-	1.50E-02
Mg	12	-	-	-	-	2.00E-03
Al	13	2.40E-02	5.99E+00	7.98E+00	-	1.67E-02
Si	14	-	2.00E+00	2.99E+00	1.00E+01	1.21E-02
P	15	-	-	-	4.50E-01	3.50E-02
S	16	3.50E-02	7.00E-02	7.00E-02	3.00E-01	-
Cl	17	-	-	-	-	5.30E-03
Ca	20	-	-	-	-	2.00E-03
Ti	22	2.00E-02	7.99E+00	2.49E+01	-	1.00E-03
V	23	2.00E-02	-	-	-	3.00E-03
Cr	24	1.25E+00	1.90E+02	1.50E+02	1.90E+02	4.00E-03
Mn	25	2.00E-02	2.00E+00	6.98E+00	2.00E+01	1.70E-03
Fe	26	2.25E+00	1.80E+02	6.78E+01	6.88E+02	1.80E-02
Co	27	1.00E-02	4.69E+00	6.49E+00	8.00E-01	1.00E-03
Ni	28	2.00E-02	5.20E+02	7.22E+02	8.92E+01	2.40E-02
Cu	29	2.00E-02	9.99E-01	4.99E-01	-	1.00E-03
Zn	30	-	-	-	-	4.03E-02
Zr	40	9.79E+02	-	-	-	-
Nb	41	-	5.55E+01	8.98E+00	-	-
Mo	42	-	3.00E+01	-	-	1.00E-02
Ag	47	-	-	-	-	1.00E-04
Cd	48	2.50E-04	-	-	-	2.50E-02
In	49	-	-	-	-	2.00E-03
Sn	50	1.60E+01	-	-	-	4.00E-03
Gd	64	-	-	-	-	2.50E-03
Hf	72	7.80E-02	-	-	-	-
W	74	2.00E-02	-	-	-	2.00E-03
Pb	82	-	-	-	-	1.00E-03
U	92	2.00E-04	-	-	-	1.00E-03

Table T.5-8
Flux Scaling Factors By Fuel Assembly Region

Fuel Assembly Region	Flux Factor
Bottom	0.15
In-Core	1.00
Plenum	0.20
Top	0.10

Table T.5-9
Gamma and Neutron Source Term for 0.22 kW Fuel in TC for HLZC 6
(31 GWd/MTU, 0.9 wt. % U-235 and 11.7-Year Cooled Fuel)

E_{lower} (MeV)		E_{upper} (MeV)	Bottom Region (γ/s/assembly)	Fuel Region (γ/s/assembly)	Plenum Region (γ/s/assembly)	Top Region (γ/s/assembly)
0	to	0.05	5.6674e+10	3.0110e+14	2.8977e+10	4.2312e+10
0.05	to	0.1	6.9435e+09	5.7063e+13	2.1327e+09	5.1521e+09
0.1	to	0.2	1.8231e+09	4.0413e+13	1.6301e+09	1.3859e+09
0.2	to	0.3	9.2049e+07	1.1633e+13	9.2404e+07	7.0301e+07
0.3	to	0.4	1.4456e+08	7.3679e+12	3.0027e+08	1.1516e+08
0.4	to	0.6	7.9956e+08	3.0315e+13	5.9661e+09	7.6953e+08
0.6	to	0.8	4.2198e+08	4.8684e+14	3.0886e+09	4.4250e+08
0.8	to	1.0	2.3387e+08	1.6376e+13	8.4074e+07	1.6865e+08
1.0	to	1.33	2.0241e+12	2.5198e+13	6.0185e+11	1.5014e+12
1.33	to	1.66	5.7161e+11	5.3578e+12	1.6996e+11	4.2399e+11
1.66	to	2.0	3.4974e+00	2.3432e+10	2.6792e+01	3.4519e+00
2.0	to	2.5	1.3565e+07	6.1091e+09	4.0335e+06	1.0062e+07
2.5	to	3.0	2.1034e+04	4.9729e+08	6.2543e+03	1.5602e+04
3.0	to	4.0	2.5349e-12	7.5232e+07	9.3744e-16	1.7213e-11
4.0	to	5.0	0	6.2013e+06	0	0
5.0	to	6.5	0	2.4889e+06	0	0
6.5	to	8.0	0	4.8826e+05	0	0
8.0	to	10.0	0	1.0367e+05	0	0
Total Gamma			2.6629e+12	9.8169e+14	8.1409e+11	1.9758e+12
Total Neutron			1.80e+8 n/s/assembly			

Table T.5-10
Gamma and Neutron Source Term for 0.48 kW Fuel in TC for HLZC 6, HSM Model 80 and 102 for HLZC 1
(25 GWd/MTU, 1.0 wt. % U-235 and 3.2-Year Cooled Fuel)

E_{lower} (MeV)		E_{upper} (MeV)	Bottom Region (γ/s/assembly)	Fuel Region (γ/s/assembly)	Plenum Region (γ/s/assembly)	Top Region (γ/s/assembly)
0	to	0.05	1.5767e+11	1.0846e+15	1.9068e+11	1.2116e+11
0.05	to	0.1	1.6981e+10	2.4167e+14	5.6723e+09	1.2771e+10
0.1	to	0.2	5.1010e+09	2.1043e+14	9.0221e+09	4.0617e+09
0.2	to	0.3	2.6492e+08	5.9161e+13	5.3713e+08	2.1288e+08
0.3	to	0.4	5.0740e+08	4.5265e+13	1.9215e+09	4.3552e+08
0.4	to	0.6	5.3991e+09	4.1178e+14	4.0981e+10	5.2686e+09
0.6	to	0.8	2.8120e+09	8.1035e+14	2.1314e+10	2.7711e+09
0.8	to	1.0	1.0518e+11	1.4113e+14	4.5006e+10	4.6043e+10
1.0	to	1.33	4.9362e+12	7.2668e+13	1.4864e+12	3.7075e+12
1.33	to	1.66	1.3940e+12	2.3412e+13	4.1975e+11	1.0470e+12
1.66	to	2.0	1.0611e+05	1.3819e+12	4.3329e+04	1.0363e+05
2.0	to	2.5	3.3081e+07	3.3957e+12	9.9618e+06	2.4847e+07
2.5	to	3.0	5.1296e+04	1.1210e+11	1.5446e+04	3.8527e+04
3.0	to	4.0	1.4138e-12	1.3964e+10	4.5348e-16	1.0104e-11
4.0	to	5.0	0	3.7908e+06	0	0
5.0	to	6.5	0	1.5214e+06	0	0
6.5	to	8.0	0	2.9846e+05	0	0
8.0	to	10.0	0	6.3370e+04	0	0
Total Gamma			6.6241e+12	3.1054e+15	2.2213e+12	4.9472e+12
Total Neutron			1.10e+8 n/s/assembly			

Table T.5-11
Gamma and Neutron Source Term for 0.54 kW Fuel in TC for HLZCs 6 and 7 (25 GWd/MTU, 0.9 wt. % U-235 and 3.0-Year Cooled Fuel)

E_{lower} (MeV)		E_{upper} (MeV)	Bottom Region (γ/s/assembly)	Fuel Region (γ/s/assembly)	Plenum Region (γ/s/assembly)	Top Region (γ/s/assembly)
0	to	0.05	1.6854e+11	1.2121e+15	2.1150e+11	1.2917e+11
0.05	to	0.1	1.7923e+10	2.7252e+14	5.9980e+09	1.3438e+10
0.1	to	0.2	5.4001e+09	2.3891e+14	9.6161e+09	4.2887e+09
0.2	to	0.3	2.8126e+08	6.7134e+13	5.7783e+08	2.2547e+08
0.3	to	0.4	5.3945e+08	5.1646e+13	2.0501e+09	4.6187e+08
0.4	to	0.6	5.7905e+09	4.5751e+14	4.3741e+10	5.6293e+09
0.6	to	0.8	3.0305e+09	8.4881e+14	2.2863e+10	2.9703e+09
0.8	to	1.0	1.2519e+11	1.5349e+14	5.3430e+10	5.4651e+10
1.0	to	1.33	5.2090e+12	7.8190e+13	1.5639e+12	3.9003e+12
1.33	to	1.66	1.4710e+12	2.5486e+13	4.4164e+11	1.1014e+12
1.66	to	2.0	2.1625e+05	1.6212e+12	8.9896e+04	2.1135e+05
2.0	to	2.5	3.4909e+07	4.0106e+12	1.0482e+07	2.6139e+07
2.5	to	3.0	5.4130e+04	1.3173e+11	1.6252e+04	4.0531e+04
3.0	to	4.0	1.5207e-12	1.6406e+10	4.9680e-16	1.0817e-11
4.0	to	5.0	0	4.1984e+06	0	0
5.0	to	6.5	0	1.6850e+06	0	0
6.5	to	8.0	0	3.3055e+05	0	0
8.0	to	10.0	0	7.0184e+04	0	0
Total Gamma			7.0067e+12	3.4116e+15	2.3553e+12	5.2126e+12
Total Neutron			1.22e+8 n/s/assembly			

Table T.5-12
Gamma and Neutron Source Term for 0.7 kW Fuel in TC for HLZC 6
(62 GWd/MTU, 2.6 wt. % U-235 and 7.1-Year Cooled Fuel)

E_{lower} (MeV)		E_{upper} (MeV)	Bottom Region (γ/s/assembly)	Fuel Region (γ/s/assembly)	Plenum Region (γ/s/assembly)	Top Region (γ/s/assembly)
0	to	0.05	1.6049e+11	8.7307e+14	1.2219e+11	1.1977e+11
0.05	to	0.1	1.9063e+10	1.6524e+14	6.0001e+09	1.3995e+10
0.1	to	0.2	5.4625e+09	1.2858e+14	7.8870e+09	4.2016e+09
0.2	to	0.3	2.8011e+08	3.6606e+13	4.5777e+08	2.1712e+08
0.3	to	0.4	5.0614e+08	2.4052e+13	1.6342e+09	4.1729e+08
0.4	to	0.6	4.6371e+09	3.3200e+14	3.4436e+10	4.4263e+09
0.6	to	0.8	2.4119e+09	1.3532e+15	1.7829e+10	2.3601e+09
0.8	to	1.0	1.1119e+10	1.5373e+14	4.6735e+09	4.9432e+09
1.0	to	1.33	5.5493e+12	8.1128e+13	1.6305e+12	4.0703e+12
1.33	to	1.66	1.5671e+12	2.2226e+13	4.6046e+11	1.1495e+12
1.66	to	2.0	1.0637e+01	2.6740e+11	8.3311e+01	1.0853e+01
2.0	to	2.5	3.7190e+07	3.4795e+11	1.0927e+07	2.7278e+07
2.5	to	3.0	5.7667e+04	1.9576e+10	1.6944e+04	4.2298e+04
3.0	to	4.0	1.5605e-11	2.5255e+09	1.2045e-14	8.7714e-11
4.0	to	5.0	0	2.9245e+07	1.4013e-45	0
5.0	to	6.5	0	1.1738e+07	0	0
6.5	to	8.0	0	2.3028e+06	0	0
8.0	to	10.0	0	4.8896e+05	0	0
Total Gamma			7.3204e+12	3.1705e+15	2.2861e+12	5.3702e+12
Total Neutron			8.58e+8 n/s/assembly			

Table T.5-13
Gamma and Neutron Source Term for 0.48 kW Fuel in TC for HLZC 7
(62 GWd/MTU, 2.6 wt. % U-235 and 14.0-Year Cooled Fuel)

E_{lower} (MeV)		E_{upper} (MeV)	Bottom Region (γ/s/assembly)	Fuel Region (γ/s/assembly)	Plenum Region (γ/s/assembly)	Top Region (γ/s/assembly)
0	to	0.05	6.2705E+10	6.0443E+14	3.0490E+10	4.6250E+10
0.05	to	0.1	7.6758E+09	1.1423E+14	2.3239E+09	5.6341E+09
0.1	to	0.2	2.0011E+09	8.1546E+13	1.6771E+09	1.5023E+09
0.2	to	0.3	1.0090E+08	2.3973E+13	9.4763E+07	7.6093E+07
0.3	to	0.4	1.5641E+08	1.5345E+13	3.0348E+08	1.2276E+08
0.4	to	0.6	8.0801E+08	4.2635E+13	5.9705E+09	7.7062E+08
0.6	to	0.8	4.3131E+08	9.0441E+14	3.0909E+09	4.6880E+08
0.8	to	1.0	1.5371E+08	2.4473E+13	4.6363E+07	1.5879E+08
1.0	to	1.33	2.2377E+12	3.4749E+13	6.5760E+11	1.6420E+12
1.33	to	1.66	6.3193E+11	6.3797E+12	1.8571E+11	4.6369E+11
1.66	to	2.0	8.8611E+00	4.1313E+10	7.0222E+01	9.0483E+00
2.0	to	2.5	1.4997E+07	3.9388E+09	4.4071E+06	1.1004E+07
2.5	to	3.0	2.3254E+04	3.8898E+08	6.8336E+03	1.7063E+04
3.0	to	4.0	1.3486E-11	8.7109E+07	7.7693E-15	7.5829E-11
4.0	to	5.0	0	2.1926E+07	1.4013E-45	0
5.0	to	6.5	0	8.8000E+06	0	0
6.5	to	8.0	0	1.7264E+06	0	0
8.0	to	10.0	0	3.6657E+05	0	0
Total Gamma			2.9437E+12	1.8522E+15	8.8731E+11	2.1607E+12
Total Neutron			6.37e+8 n/s/assembly			

Table T.5-14
Gamma and Neutron Source Term for 0.22 kW Fuel in HSM-H for HLZC 6
(13 GWd/MTU, 1.8 wt. % U-235 and 3.0-Year Cooled Fuel)

E_{lower} (MeV)		E_{upper} (MeV)	Bottom Region (γ/s/assembly)	Fuel Region (γ/s/assembly)	Plenum Region (γ/s/assembly)	Top Region (γ/s/assembly)
0	to	0.05	6.5305e+10	5.8578e+14	9.2883e+10	5.5595e+10
0.05	to	0.1	6.8749e+09	1.2988e+14	2.5686e+09	5.7480e+09
0.1	to	0.2	2.0940e+09	1.1486e+14	4.2165e+09	1.8477e+09
0.2	to	0.3	1.0931e+08	3.0690e+13	2.5332e+08	9.7300e+07
0.3	to	0.4	2.1236e+08	2.3573e+13	9.0173e+08	2.0076e+08
0.4	to	0.6	2.3467e+09	1.3188e+14	1.9265e+10	2.4828e+09
0.6	to	0.8	1.2253e+09	3.4362e+14	1.0068e+10	1.3082e+09
0.8	to	1.0	5.1873e+10	4.0576e+13	2.3964e+10	2.4518e+10
1.0	to	1.33	1.9975e+12	2.7871e+13	6.6806e+11	1.6679e+12
1.33	to	1.66	5.6409e+11	8.8709e+12	1.8866e+11	4.7102e+11
1.66	to	2.0	1.4732e+05	5.6907e+11	5.8013e+04	1.4896e+05
2.0	to	2.5	1.3387e+07	2.1325e+12	4.4774e+06	1.1178e+07
2.5	to	3.0	2.0758e+04	4.0975e+10	6.9424e+03	1.7333e+04
3.0	to	4.0	7.9717e-14	4.9998e+09	1.5076e-17	7.6784e-13
4.0	to	5.0	0	1.0901e+05	0	0
5.0	to	6.5	0	4.3703e+04	0	0
6.5	to	8.0	0	8.5655e+03	0	0
8.0	to	10.0	0	1.8175e+03	0	0
Total Gamma			2.6916e+12	1.4403e+15	1.0108e+12	2.2307e+12
Total Neutron			3.25e+6 n/s/assembly			

Table T.5-15
Gamma and Neutron Source Term for 0.48 kW Fuel in HSM-H for HLZC 6 (24 GWd/MTU, 1.3 wt. % U-235 and 3.0-Year Cooled Fuel)

E_{lower} (MeV)		E_{upper} (MeV)	Bottom Region (γ/s/assembly)	Fuel Region (γ/s/assembly)	Plenum Region (γ/s/assembly)	Top Region (γ/s/assembly)
0	to	0.05	1.4580e+11	1.1458e+15	1.9131e+11	1.1396e+11
0.05	to	0.1	1.5391e+10	2.5679e+14	5.2683e+09	1.1764e+10
0.1	to	0.2	4.6693e+09	2.2580e+14	8.6764e+09	3.7869e+09
0.2	to	0.3	2.4356e+08	6.2648e+13	5.2196e+08	1.9942e+08
0.3	to	0.4	4.7095e+08	4.8081e+13	1.8559e+09	4.1215e+08
0.4	to	0.6	5.1466e+09	4.0226e+14	3.9656e+10	5.1043e+09
0.6	to	0.8	2.6931e+09	7.8358e+14	2.0730e+10	2.6926e+09
0.8	to	1.0	1.1358e+11	1.3567e+14	4.9239e+10	5.0361e+10
1.0	to	1.33	4.4722e+12	6.8605e+13	1.3682e+12	3.4134e+12
1.33	to	1.66	1.2629e+12	2.2410e+13	3.8636e+11	9.6395e+11
1.66	to	2.0	2.1488e+05	1.4221e+12	8.7150e+04	2.0936e+05
2.0	to	2.5	2.9972e+07	3.8703e+12	9.1699e+06	2.2876e+07
2.5	to	3.0	4.6474e+04	1.1295e+11	1.4218e+04	3.5472e+04
3.0	to	4.0	9.9700e-13	1.4016e+10	3.0347e-16	7.3979e-12
4.0	to	5.0	0	2.4822e+06	0	0
5.0	to	6.5	0	9.9615e+05	0	0
6.5	to	8.0	0	1.9541e+05	0	0
8.0	to	10.0	0	4.1489e+04	0	0
Total Gamma			6.0231e+12	3.1571e+15	2.0718e+12	4.5657e+12
Total Neutron			7.20e+7 n/s/assembly			

Table T.5-16
Gamma and Neutron Source Term for 0.54 kW Fuel in HSM-H for HLZC 6, HSM Model 80 and 102 for HLZC 2
(25 GWd/MTU, 0.9 wt. % U-235 and 3.0-Year Cooled Fuel)

E_{lower} (MeV)		E_{upper} (MeV)	Bottom Region (γ/s/assembly)	Fuel Region (γ/s/assembly)	Plenum Region (γ/s/assembly)	Top Region (γ/s/assembly)
0	to	0.05	1.6853e+11	1.2121e+15	2.1150e+11	1.2917e+11
0.05	to	0.1	1.7923e+10	2.7252e+14	5.9980e+09	1.3438e+10
0.1	to	0.2	5.3997e+09	2.3891e+14	9.6161e+09	4.2887e+09
0.2	to	0.3	2.8124e+08	6.7134e+13	5.7783e+08	2.2547e+08
0.3	to	0.4	5.3938e+08	5.1646e+13	2.0501e+09	4.6187e+08
0.4	to	0.6	5.7892e+09	4.5751e+14	4.3741e+10	5.6293e+09
0.6	to	0.8	3.0299e+09	8.4881e+14	2.2863e+10	2.9703e+09
0.8	to	1.0	1.2517e+11	1.5349e+14	5.3430e+10	5.4651e+10
1.0	to	1.33	5.2088e+12	7.8190e+13	1.5639e+12	3.9003e+12
1.33	to	1.66	1.4710e+12	2.5486e+13	4.4164e+11	1.1014e+12
1.66	to	2.0	2.1615e+05	1.6212e+12	8.9902e+04	2.1136e+05
2.0	to	2.5	3.49098+07	4.0106e+12	1.0482e+07	2.6139e+07
2.5	to	3.0	5.4129e+04	1.3173e+11	1.6252e+04	4.0531e+04
3.0	to	4.0	1.5221e-12	1.6406e+10	4.9681e-16	1.0817e-11
4.0	to	5.0	0	4.1984e+06	0	0
5.0	to	6.5	0	1.6850e+06	0	0
6.5	to	8.0	0	3.3055e+05	0	0
8.0	to	10.0	0	7.0184e+04	0	0
Total Gamma			7.0065e+12	3.4116e+15	2.3553e+12	5.2126e+12
Total Neutron			1.22e+8 n/s/assembly			

Table T.5-17
Gamma and Neutron Source Term for 0.7 kW Fuel in HSM-H for HLZC 6
(34 GWd/MTU, 2.0 wt. % U-235 and 3.1-Year Cooled Fuel)

E_{lower} (MeV)		E_{upper} (MeV)	Bottom Region (γ/s/assembly)	Fuel Region (γ/s/assembly)	Plenum Region (γ/s/assembly)	Top Region (γ/s/assembly)
0	to	0.05	1.7677e+11	1.5462e+15	2.4216e+11	1.3845e+11
0.05	to	0.1	1.8456e+10	3.4424e+14	6.3684e+09	1.4113e+10
0.1	to	0.2	5.6953e+09	3.0279e+14	1.1181e+10	4.6405e+09
0.2	to	0.3	2.9761e+08	8.3737e+13	6.7100e+08	2.4487e+08
0.3	to	0.4	5.8772e+08	6.3725e+13	2.4089e+09	5.1772e+08
0.4	to	0.6	6.6813e+09	6.1096e+14	5.1639e+10	6.6397e+09
0.6	to	0.8	3.4875e+09	1.1671e+15	2.6917e+10	3.4950e+09
0.8	to	1.0	1.4378e+11	2.2115e+14	6.2426e+10	6.3835e+10
1.0	to	1.33	5.3611e+12	9.1910e+13	1.6403e+12	4.0933e+12
1.33	to	1.66	1.5140e+12	3.1246e+13	4.6321e+11	1.1559e+12
1.66	to	2.0	1.7722e+05	1.8288e+12	7.3743e+04	1.7110e+05
2.0	to	2.5	3.5929e+07	5.0595e+12	1.0994e+07	2.7432e+07
2.5	to	3.0	5.5711e+04	1.4432e+11	1.7046e+04	4.2537e+04
3.0	to	4.0	2.2013e-12	1.7900e+10	9.4751e-16	1.5321e-11
4.0	to	5.0	0	5.4023e+06	0	0
5.0	to	6.5	0	2.1682e+06	0.	0
6.5	to	8.0	0	4.2533e+05	0	0
8.0	to	10.0	0	9.0309e+04	0	0
Total Gamma			7.2309e+12	4.4701e+15	2.5073e+12	5.4812e+12
Total Neutron			1.57e+8 n/s/assembly			

Table T.5-18
Gamma and Neutron Source Term for 0.393 kW Fuel in HSM Model 80 and Model 102 for HLZC 2
(62 GWd/MTU, 2.6 wt. % U-235 and 21.4-Year Cooled Fuel)

E_{lower} (MeV)		E_{upper} (MeV)	Bottom Region (γ/s/assembly)	Fuel Region (γ/s/assembly)	Plenum Region (γ/s/assembly)	Top Region (γ/s/assembly)
0.00e+00	to	5.00e-02	2.4047e+10	4.9243e+14	8.8167e+09	1.7549e+10
5.00e-02	to	1.00e-01	2.8985e+09	9.5577e+13	8.6231e+08	2.1273e+09
1.00e-01	to	2.00e-01	7.2167e+08	6.3759e+13	3.7845e+08	5.3503e+08
2.00e-01	to	3.00e-01	3.6074e+07	1.9274e+13	2.0567e+07	2.6817e+07
3.00e-01	to	4.00e-01	5.0988e+07	1.2624e+13	5.4327e+07	3.8645e+07
4.00e-01	to	6.00e-01	1.2510e+08	1.2432e+13	9.1227e+08	1.1895e+08
6.00e-01	to	8.00e-01	7.8537e+07	7.3583e+14	4.7218e+08	1.3197e+08
8.00e-01	to	1.00e+00	5.1503e+07	7.8680e+12	1.1111e+07	9.5887e+07
1.00e+00	to	1.33e+00	8.4517e+11	1.6306e+13	2.4839e+11	6.2027e+11
1.33e+00	to	1.66e+00	2.3868e+11	2.3903e+12	7.0145e+10	1.7516e+11
1.66e+00	to	2.00e+00	7.3831e+00	3.2435e+10	5.8513e+01	7.5403e+00
2.00e+00	to	2.50e+00	5.6641e+06	1.7533e+09	1.6646e+06	4.1569e+06
2.50e+00	to	3.00e+00	8.7828e+03	1.9620e+08	2.5812e+03	6.4457e+03
3.00e+00	to	4.00e+00	1.1536e-11	4.9170e+07	6.6224e-15	6.4875e-11
4.00e+00	to	5.00e+00	0	1.6551e+07	1.4013e-45	0
5.00e+00	to	6.50e+00	0	6.6430e+06	0	0
6.50e+00	to	8.00e+00	0	1.3032e+06	0	0
8.00e+00	to	1.00e+01	0	2.7671e+05	0	0
Total Gamma:			1.1119e+12	1.4585e+15	3.3006e+11	8.1606e+11
Total Neutrons, n/(sec*FA)			4.80e+8			

Table T.5-19
Shielding Material Densities

Assembly Region Material Densities

Element/ Isotope	Atomic Number	Number Density (atom/b-cm)			
		Bottom Fitting	Fuel	Plenum	Top Fitting
C	6	5.846E-5	3.389E-7	6.717E-6	1.396E-5
O	8	-	1.433E-2	-	-
Si	14	3.208E-4	5.573E-6	3.591E-5	1.123E-4
P	15	1.275E-5	7.392E-8	1.465E-6	3.045E-6
Ti	22	4.876E-6	2.207E-6	-	2.210E-5
Cr	24	3.239E-3	3.927E-5	3.775E-4	8.903E-4
Mn	25	3.195E-4	1.852E-6	3.671E-5	7.630E-5
Fe	26	1.077E-2	8.418E-5	1.252E-3	2.624E-3
Ni	28	1.537E-3	6.079E-5	1.632E-4	8.655E-4
Zr	40	2.534E-3	4.750E-3	5.057E-3	1.335E-3
Sn	50	2.874E-5	5.388E-5	5.736E-5	1.514E-5
Hf	72	1.318E-7	2.471E-7	2.631E-7	6.946E-8
U-234	92	-	2.593E-6	-	-
U-235	92	-	2.901E-4	-	-
U-236	92	-	1.329E-6	-	-
U-238	92	-	6.872E-3	-	-
Total		1.882E-2	2.649E-2	6.989E-3	5.958E-3

Table T.5-19
Shielding Material Densities
(Continued)
HSM Shielding Materials

Element/ Isotope	Atomic Number	Number Density (atom/b-cm)				
		Concrete	Air	Carbon Steel	Stainless Steel	Aluminum/ BORAL
H	1	7.758E-3				
C	6		8.423E-9	3.907E-3		
N	7		3.897E-5			
O	8	4.312E-2	1.047E-5			
Na	11	1.021E-3				
Al	13	2.340E-3				6.031E-2
Si	14	1.557E-2				
Ar	18		2.330E-7			
K	19	6.768E-4				
Ca	20	2.852E-3				
Cr	24				1.743E-2	
Mn	25				1.736E-3	
Fe	26	3.015E-4		8.348E-2	5.935E-2	
Ni	28				7.720E-3	
Total		7.364E-2	4.969E-5	8.739E-2	8.624E-2	6.031E-2

Table T.5-19
Shielding Material Densities
(Concluded)
TC Shielding Materials

Element/ Isotope	Atomic Number	Number Density (atom/b-cm)						
		NS-3	Water	Air	Lead	Carbon Steel	Stainless Steel	Aluminum/ BORAL
H	1	4.498E-2	6.687E-2					
B-10	5	6.077E-5						
B-11	5	2.446E-4						
C	6	9.595E-3		8.642E-9		3.939E-3	3.188E-4	
N	7			3.995E-5				
O	8	3.704E-2	3.344E-2	1.073E-5				
Al	13	6.887E-3						6.031E-2
Si	14	1.243E-3					1.702E-3	
P	15						6.947E-5	
Ar	18			2.388E-7				
Ca	20	1.454E-3						
Cr	24						1.747E-2	
Mn	25						1.741E-3	
Fe	26	1.042E-4				8.380E-2	5.854E-2	
Ni	28						7.739E-3	
Pb	82				3.296E-2			
Total		1.016E-1	1.003E-1	5.093E-5	3.296E-2	8.774E-2	8.758E-2	6.031E-2

Table T.5-20
Material Densities Used in ANISN Models

Material Name	Composition	Densities of Components Atoms/barn-cm
Stainless Steel SS304	Cr	1.743E-2
	Fe	6.128E-2
	Ni	7.511E-3
Air	N	3.587E-5
	O	9.534E-6
Lead	Pb	3.296E-2
Water	H	6.393E-2
	O	3.203E-2
Concrete	H	7.767E-3
	O	4.317E-2
	Na	1.022E-3
	Al	2.343E-3
	Si	1.559E-2
	K	6.776E-4
	Ca	2.855E-3
	Fe	3.019E-4
In-Core (Fuel with Basket Material)	O	7.539E-3
	Fe	6.372E-3
	Zr	2.544E-3
	U235	1.526E-4
	U238	3.617E-3

Table T.5-21
Neutron Source for ANISN Calculation

CASK-81 Energy Group	Energy Group Upper Limit E_{upper} (eV)	Normalized Fission Source
1	1.49E+07	1.26E-04
2	1.22E+07	1.07E-03
3	1.00E+07	2.94E-03
4	8.18E+06	1.46E-02
5	6.36E+06	3.71E-02
6	4.96E+06	4.90E-02
7	4.06E+06	1.23E-01
8	3.01E+06	1.01E-01
9	2.46E+06	2.46E-02
10	2.35E+06	1.27E-01
11	1.83E+06	2.27E-01
12	1.11E+06	2.01E-01
13	5.50E+05	9.25E-02
14	1.11E+05	3.99E-06
15	3.35E+03	0
16	5.83E+02	0
17	1.01E+02	0
18	2.90E+01	0
19	1.01E+01	0
20	3.06E+00	0
21	1.12E+00	0
22	4.14E-01	0
Total		1.00E+00

Table T.5-22
ANISN Response Function for the OS197FC-B TC Due to Radial Zone 1

Response Function Parameter for	Lower Boundary of Energy Group, MeV	Upper Boundary of Energy Group, MeV	Middle of OS197 Side Surface		
			Neutron (mrem/hr)	Gamma (mrem/hr)	Total (mrem/hr)
Neutrons	0.00E+00	2.0E+01	8.17594E-08	2.69109E-08	1.08670E-07
Group 40	0.00E+00	5.00E-02	0.00E+00	0.00E+00	0.00E+00
Group 39	5.00E-02	1.00E-01	0.00E+00	0.00E+00	0.00E+00
Group 38	1.00E-01	2.00E-01	0.00E+00	0.00E+00	0.00E+00
Group 37	2.00E-01	3.00E-01	0.00E+00	1.87235E-38	1.87235E-38
Group 36	3.00E-01	4.00E-01	0.00E+00	6.33108E-29	6.33108E-29
Group 35	4.00E-01	6.00E-01	0.00E+00	5.10220E-24	5.10220E-24
Group 34	6.00E-01	8.00E-01	0.00E+00	2.57731E-19	2.57731E-19
Group 33	8.00E-01	1.00E+00	0.00E+00	6.09621E-17	6.09621E-17
Group 32	1.00E+00	1.33E+00	0.00E+00	3.76892E-15	3.76892E-15
Group 31	1.33E+00	1.66E+00	0.00E+00	4.61125E-14	4.61125E-14
Group 30	1.66E+00	2.00E+00	0.00E+00	1.95920E-13	1.95920E-13
Group 29	2.00E+00	2.50E+00	0.00E+00	6.01033E-13	6.01033E-13
Group 28	2.50E+00	3.00E+00	0.00E+00	1.23504E-12	1.23504E-12
Group 27	3.00E+00	4.00E+00	0.00E+00	2.10110E-12	2.10110E-12
Group 26	4.00E+00	5.00E+00	0.00E+00	2.72885E-12	2.72885E-12
Group 25	5.00E+00	6.50E+00	0.00E+00	2.94688E-12	2.94688E-12
Group 24	6.50E+00	8.00E+00	0.00E+00	2.72036E-12	2.72036E-12
Group 23	8.00E+00	1.00E+01	0.00E+00	2.07508E-12	2.07508E-12

Table T.5-23
ANISN Response Function for the OS197FC-B TC Due to Radial Zone 2

Response Function Parameter for	Lower Boundary of Energy Group, MeV	Upper Boundary of Energy Group, MeV	Middle of OS197 Side Surface		
			Neutron (mrem/hr)	Gamma (mrem/hr)	Total (mrem/hr)
Neutrons	0.00E+00	2.0E+01	2.75268E-07	7.47833E-08	3.50051E-07
Group 40	0.00E+00	5.00E-02	0.00E+00	0.00E+00	0.00E+00
Group 39	5.00E-02	1.00E-01	0.00E+00	0.00E+00	0.00E+00
Group 38	1.00E-01	2.00E-01	0.00E+00	8.71170E-38	8.71170E-38
Group 37	2.00E-01	3.00E-01	0.00E+00	8.82801E-27	8.82801E-27
Group 36	3.00E-01	4.00E-01	0.00E+00	2.15249E-22	2.15249E-22
Group 35	4.00E-01	6.00E-01	0.00E+00	3.54612E-20	3.54612E-20
Group 34	6.00E-01	8.00E-01	0.00E+00	8.26522E-17	8.26522E-17
Group 33	8.00E-01	1.00E+00	0.00E+00	6.73629E-15	6.73629E-15
Group 32	1.00E+00	1.33E+00	0.00E+00	1.78286E-13	1.78286E-13
Group 31	1.33E+00	1.66E+00	0.00E+00	1.34677E-12	1.34677E-12
Group 30	1.66E+00	2.00E+00	0.00E+00	4.31749E-12	4.31749E-12
Group 29	2.00E+00	2.50E+00	0.00E+00	1.05815E-11	1.05815E-11
Group 28	2.50E+00	3.00E+00	0.00E+00	1.89215E-11	1.89215E-11
Group 27	3.00E+00	4.00E+00	0.00E+00	2.88576E-11	2.88576E-11
Group 26	4.00E+00	5.00E+00	0.00E+00	3.54800E-11	3.54800E-11
Group 25	5.00E+00	6.50E+00	0.00E+00	3.75783E-11	3.75783E-11
Group 24	6.50E+00	8.00E+00	0.00E+00	3.49085E-11	3.49085E-11
Group 23	8.00E+00	1.00E+01	0.00E+00	2.74442E-11	2.74442E-11

Table T.5-24
ANISN Response Function for the OS197FC-B TC Due to Radial Zone 3

Response Function Parameter for	Lower Boundary of Energy Group, MeV	Upper Boundary of Energy Group, MeV	Middle of OS197 Side Surface		
			Neutron (mrem/hr)	Gamma (mrem/hr)	Total (mrem/hr)
Neutrons	0.00E+00	2.0E+01	4.21627E-07	8.96257E-08	5.11252E-07
Group 40	0.00E+00	5.00E-02	0.00E+00	0.00E+00	0.00E+00
Group 39	5.00E-02	1.00E-01	0.00E+00	3.06524E-40	3.06524E-40
Group 38	1.00E-01	2.00E-01	0.00E+00	2.65752E-29	2.65752E-29
Group 37	2.00E-01	3.00E-01	0.00E+00	2.95054E-21	2.95054E-21
Group 36	3.00E-01	4.00E-01	0.00E+00	1.06062E-17	1.06062E-17
Group 35	4.00E-01	6.00E-01	0.00E+00	3.88226E-17	3.88226E-17
Group 34	6.00E-01	8.00E-01	0.00E+00	4.17244E-15	4.17244E-15
Group 33	8.00E-01	1.00E+00	0.00E+00	1.58084E-13	1.58084E-13
Group 32	1.00E+00	1.33E+00	0.00E+00	2.26923E-12	2.26923E-12
Group 31	1.33E+00	1.66E+00	0.00E+00	1.19527E-11	1.19527E-11
Group 30	1.66E+00	2.00E+00	0.00E+00	3.09995E-11	3.09995E-11
Group 29	2.00E+00	2.50E+00	0.00E+00	6.43181E-11	6.43181E-11
Group 28	2.50E+00	3.00E+00	0.00E+00	1.03536E-10	1.03536E-10
Group 27	3.00E+00	4.00E+00	0.00E+00	1.45717E-10	1.45717E-10
Group 26	4.00E+00	5.00E+00	0.00E+00	1.72080E-10	1.72080E-10
Group 25	5.00E+00	6.50E+00	0.00E+00	1.80114E-10	1.80114E-10
Group 24	6.50E+00	8.00E+00	0.00E+00	1.68841E-10	1.68841E-10
Group 23	8.00E+00	1.00E+01	0.00E+00	1.36728E-10	1.36728E-10

Table T.5-25
ANISN Response Function for the OS197FC-B TC Due to Radial Zone 4

Response Function Parameter for	Lower Boundary of Energy Group, MeV	Upper Boundary of Energy Group, MeV	Middle of OS197 Side Surface		
			Neutron (mrem/hr)	Gamma (mrem/hr)	Total (mrem/hr)
Neutrons	0.00E+00	2.0E+01	3.83466E-07	8.07827E-08	4.64249E-07
Group 40	0.00E+00	5.00E-02	0.00E+00	0.00E+00	0.00E+00
Group 39	5.00E-02	1.00E-01	0.00E+00	2.68668E-40	2.68668E-40
Group 38	1.00E-01	2.00E-01	0.00E+00	2.84255E-29	2.84255E-29
Group 37	2.00E-01	3.00E-01	0.00E+00	9.24759E-29	9.24759E-29
Group 36	3.00E-01	4.00E-01	0.00E+00	1.07514E-17	1.07514E-17
Group 35	4.00E-01	6.00E-01	0.00E+00	4.76562E-17	4.76562E-17
Group 34	6.00E-01	8.00E-01	0.00E+00	4.03504E-15	4.03504E-15
Group 33	8.00E-01	1.00E+00	0.00E+00	1.49689E-13	1.49689E-13
Group 32	1.00E+00	1.33E+00	0.00E+00	2.12203E-12	2.12203E-12
Group 31	1.33E+00	1.66E+00	0.00E+00	1.10401E-11	1.10401E-11
Group 30	1.66E+00	2.00E+00	0.00E+00	2.84520E-11	2.84520E-11
Group 29	2.00E+00	2.50E+00	0.00E+00	5.87376E-11	5.87376E-11
Group 28	2.50E+00	3.00E+00	0.00E+00	9.42423E-11	9.42423E-11
Group 27	3.00E+00	4.00E+00	0.00E+00	1.32234E-10	1.32234E-10
Group 26	4.00E+00	5.00E+00	0.00E+00	1.55995E-10	1.55995E-10
Group 25	5.00E+00	6.50E+00	0.00E+00	1.63180E-10	1.63180E-10
Group 24	6.50E+00	8.00E+00	0.00E+00	1.52890E-10	1.52890E-10
Group 23	8.00E+00	1.00E+01	0.00E+00	1.24032E-10	1.24032E-10

Table T.5-26
Flux to Dose Rate Conversion Factors

Neutron		Gamma	
E (MeV)	(mrem/hr)/(n/cm^2/s)	E (MeV)	(mrem/hr)/(γ/cm^2/s)
2.50E-08	3.67E-03	0.01	3.96E-03
1.00E-07	3.67E-03	0.03	5.82E-04
1.00E-06	4.46E-03	0.05	2.90E-04
1.00E-05	4.54E-03	0.07	2.58E-04
1.00E-04	4.18E-03	0.1	2.83E-04
0.001	3.76E-03	0.15	3.79E-04
0.01	3.56E-03	0.2	5.01E-04
0.1	2.17E-02	0.25	6.31E-04
0.5	9.26E-02	0.3	7.59E-04
1	1.32E-01	0.35	8.78E-04
2.5	1.25E-01	0.4	9.85E-04
5	1.56E-01	0.45	1.08E-03
7	1.47E-01	0.5	1.17E-03
10	1.47E-01	0.55	1.27E-03
14	2.08E-01	0.6	1.36E-03
20	2.27E-01	0.65	1.44E-03
		0.7	1.52E-03
		0.8	1.68E-03
		1	1.98E-03
		1.4	2.51E-03
		1.8	2.99E-03
		2.2	3.42E-03
		2.6	3.82E-03
		2.8	4.01E-03
		3.25	4.41E-03
		3.75	4.83E-03
		4.25	5.23E-03
		4.75	5.60E-03
		5	5.80E-03
		5.25	6.01E-03
		5.75	6.37E-03
		6.25	6.74E-03
		6.75	7.11E-03
		7.5	7.66E-03
		9	8.77E-03
		11	1.03E-02
		13	1.18E-02
		15	1.33E-02

Table T.5-27
Surface Average Dose Rates (mrem/hr) on HSM Model 80 and 102 with 61BT DSC

Location	Neutron			Gamma		
	Model 80	Model 102	Ratio	Model 80	Model 102	Ratio
Front	8.54	0.88	9.70	109	79.9	1.36
Top	0.6	0.59	1.02	109	43	2.53
Side	0.042	0.037	1.14	3.57	2.81	1.27
Rear	0.025	0.025	1.00	1.04	1.25	0.83

Table T.5-28
Maximum Surface Dose Rates (mrem/hr) on HSM Model 80 and 102 with 61BT DSC

Location	Neutron			Gamma		
	Model 80	Model 102	Ratio	Model 80	Model 102	Ratio
Roof Centerline	0.6	0.6	1.00	66.6	65.1	1.02
End Shield Wall	0.2	0.2	1.00	13.5	10.6	1.27
Door Exterior	33.4	0.3	111.33	159.8	10.8	14.80
Back Shield Wall	0.065	0.1	0.65	3.16	3.7	0.85
Front Birdscreen	10.3	10.9	0.94	1229	1319.8	0.93
Roof Birdscreen	15.6	15.7	0.99	2773.2	582	4.76

Table T.5-29
Total Dose Rates (mrem/hr) at the Center of Transfer Cask Side Surface for 0.70 kW/FA HLZC #6

Burn-Up, GWD/MTU	*Maximum Lattice Average Initial U-235 Enrichment, wt %*																																											
	0.9	1.0	1.1	1.2	1.3	1.4	1.5	1.6	1.7	1.8	1.9	2.0	2.1	2.2	2.3	2.4	2.5	2.6	2.7	2.8	2.9	3.0	3.1	3.2	3.3	3.4	3.5	3.6	3.7	3.8	3.9	4.0	4.1	4.2	4.3	4.4	4.5	4.6	4.7	4.8	4.9	5.0
6	21	21	20	20	20	19	19	19	19	19	18	18	18	18	18	18	18	17	17	17	17	17	17	17	17	17	17	17	17	17	17	16	16	16	16	16	16	16	16	16	16	16
7	25	25	24	24	23	23	23	22	22	22	22	22	21	21	21	21	21	21	21	20	20	20	20	20	20	20	20	20	20	20	19	19	19	19	19	19	19	19	19	19	19	19
8	29	29	28	28	27	27	26	26	26	25	25	25	25	25	24	24	24	24	24	24	23	23	23	23	23	23	23	23	23	23	22	22	22	22	22	22	22	22	22	22	22	22
9	33	33	32	31	31	30	30	30	29	29	29	28	28	28	28	28	27	27	27	27	27	27	26	26	26	26	26	26	26	26	26	25	25	25	25	25	25	25	25	25	25	25
10	38	37	36	36	35	34	34	33	33	33	32	32	32	31	31	31	31	31	30	30	30	30	30	30	29	29	29	29	29	29	29	29	28	28	28	28	28	28	28	28	28	28
11	42	41	41	40	39	38	38	37	37	37	36	36	35	35	35	35	34	34	34	34	33	33	33	33	33	33	32	32	32	32	32	32	32	32	31	31	31	31	31	31	31	31
12	47	46	45	44	43	43	42	41	41	40	40	40	39	39	38	38	38	38	37	37	37	37	36	36	36	36	36	36	35	35	35	35	35	35	35	35	34	34	34	34	34	34
13	52	51	50	49	48	47	46	46	45	45	44	44	43	43	42	42	42	41	41	41	40	40	40	40	39	39	39	39	39	39	38	38	38	38	38	38	38	38	37	37	37	37
14	57	56	55	54	53	52	51	50	49	49	48	48	47	47	46	46	45	45	45	44	44	44	44	43	43	43	43	42	42	42	42	42	41	41	41	41	41	41	41	41	40	40
15	63	62	60	59	58	57	56	55	54	53	52	52	51	51	50	50	49	49	48	48	48	47	47	47	47	46	46	46	46	45	45	45	45	45	45	44	44	44	44	44	44	44
16	69	67	66	64	63	62	61	60	59	58	57	56	56	55	54	54	53	53	52	52	52	51	51	51	50	50	50	49	49	49	49	49	48	48	48	48	48	47	47	47	47	47
17	75	73	72	70	68	67	66	65	64	63	62	61	60	59	59	58	58	57	57	56	56	55	55	54	54	54	53	53	53	53	52	52	52	52	52	51	51	51	51	51	50	50
18	82	80	78	76	74	73	71	70	69	68	67	66	65	64	63	63	62	61	61	60	60	59	59	58	58	58	57	57	57	56	56	56	56	55	55	55	55	54	54	54	54	54
19	89	87	84	82	80	79	77	75	74	73	72	71	70	69	68	67	66	66	65	64	64	63	63	62	62	62	61	61	61	60	60	60	59	59	59	59	58	58	58	58	57	57
20	97	94	91	89	87	85	83	81	80	78	77	76	75	74	73	72	71	70	70	69	68	68	67	67	66	66	65	65	64	64	64	63	63	63	63	62	62	62	61	61	61	61
21	105	102	99	96	94	91	89	87	86	84	83	81	80	79	78	77	76	75	74	74	73	72	72	71	70	70	69	69	69	68	68	67	67	67	66	66	66	65	65	65	65	64
22	113	110	106	104	101	98	96	94	92	90	89	87	86	84	83	82	81	80	79	78	78	77	76	75	75	74	74	73	73	72	72	71	71	71	70	70	70	69	69	69	68	68
23	122	118	115	111	108	106	103	101	99	97	95	93	91	90	89	87	86	85	84	83	82	82	81	80	79	79	78	78	77	77	76	76	75	75	74	74	74	73	73	73	72	72
24	131	127	123	120	116	113	111	108	106	103	101	99	98	96	94	93	92	91	89	88	87	87	86	85	84	83	83	82	82	81	80	80	79	79	79	78	78	77	77	77	76	76
25	141	137	132	129	125	122	118	116	113	110	108	106	104	102	101	99	98	96	95	94	93	92	91	90	89	88	87	87	86	85	85	84	84	83	83	82	82	81	81	81	80	80
26	152	147	142	138	134	130	127	124	121	118	115	113	111	109	107	105	104	102	101	99	98	97	96	95	94	93	92	92	91	90	89	89	88	88	87	87	86	86	85	85	84	84
27	163	157	152	147	143	139	135	132	129	126	123	120	118	116	114	112	110	108	107	105	104	103	101	100	99	98	97	97	96	95	94	94	93	92	92	91	91	90	90	89	89	88
28	174	168	163	158	153	149	145	141	137	134	131	128	125	123	121	119	117	115	113	111	110	109	107	106	105	104	103	102	101	100	99	98	98	97	96	96	95	95	94	93	93	93
29	186	180	174	168	163	159	154	150	146	143	139	136	133	131	128	126	124	121	120	118	116	115	113	112	110	109	108	107	106	105	104	103	103	102	101	100	100	99	99	98	97	97
30	191	192	185	179	174	169	164	160	156	152	148	145	141	139	136	133	131	129	126	124	123	121	119	118	116	115	114	113	112	111	110	109	108	107	106	105	105	104	103	103	102	101
31	204	197	190	184	178	173	175	170	166	161	157	154	150	147	144	141	138	136	134	131	129	128	126	124	123	121	120	118	117	116	115	114	113	112	111	110	110	109	108	107	107	106

-- Bounding Neutron Source -- Bounding Gamma Source --TC Bounding FA

Table T.5-29 **(Concluded)**

Burnup, GWd/MTU	Maximum Lattice Average Initial U-235 Enrichment, wt. %																																													
	0.9	1.0	1.1	1.2	1.3	1.4	1.5	1.6	1.7	1.8	1.9	2.0	2.1	2.2	2.3	2.4	2.5	2.6	2.7	2.8	2.9	3.0	3.1	3.2	3.3	3.4	3.5	3.6	3.7	3.8	3.9	4.0	4.1	4.2	4.3	4.4	4.5	4.6	4.7	4.8	4.9	5.0
32									168	164	160	163	159	156	152	149	146	144	141	139	137	134	133	131	129	127	126	124	123	122	121	120	118	117	116	116	115	114	113	112	112	111
33									179	174	170	165	161	157	154	150	155	152	149	146	144	142	140	138	136	134	132	131	129	128	127	125	124	123	122	121	120	119	118	117	117	116
34									176	171	166	175	171	167	163	159	156	153	150	147	144	142	147	145	143	141	139	137	136	134	133	131	130	129	128	126	125	124	124	123	122	121
35									187	181	176	171	167	162	158	154	165	161	158	155	152	149	147	145	142	140	138	136	135	140	139	137	136	135	133	132	131	130	129	128	127	126
36											174	181	177	172	167	163	159	156	152	149	146	143	155	152	150	147	145	143	141	140	138	136	135	133	132	131	129	136	135	134	133	132
37											184	179	174	169	164	160	169	165	161	157	154	151	148	145	143	140	138	136	148	146	144	143	141	139	138	137	135	134	133	132	131	129
38											183	190	184	179	174	169	165	161	157	153	149	159	156	153	150	148	145	143	141	139	137	135	133	131	130	128	141	140	139	137	136	135
39											195	189	183	177	172	167	174	170	165	161	158	154	151	148	145	142	139	150	148	145	143	141	139	138	136	134	133	131	130	128	127	126
40																		167	163	159	154	151	159	156	152	150	147	144	142	139	137	135	133	131	142	140	139	137	136	134	133	131
41																		177	172	168	163	159	155	152	148	145	142	151	149	146	144	141	139	137	135	133	131	130	128	127	125	124
42																		181	176	171	167	162	158	155	151	148	144	153	150	147	144	142	140	137	135	133	131	130	128	126	125	123
43																		181	175	170	165	161	167	163	159	156	152	149	146	143	140	137	135	132	142	140	138	136	134	132	130	129
44																		181	185	180	175	170	165	161	157	153	149	146	153	150	147	144	142	139	137	134	132	130	128	126	125	134
45																		192	186	180	175	169	165	170	166	161	158	154	150	147	144	141	138	135	143	141	138	136	134	132	130	128
46																		193	187	181	185	179	174	169	165	160	156	152	149	155	151	148	145	142	139	137	134	132	130	128	126	134
47																		205	198	192	186	180	175	170	165	169	165	161	157	153	149	146	143	140	146	144	141	138	136	134	132	130
48																		204	205	198	192	186	180	175	170	174	169	165	160	156	152	149	145	142	139	146	143	140	137	135	133	130
49																		216	208	201	195	189	191	185	180	174	169	165	160	156	152	157	153	150	146	143	140	137	135	132	130	127
50																		220	212	205	206	199	193	187	181	176	171	174	169	165	160	156	153	149	145	142	147	144	141	139	136	134
51																		225	225	217	210	203	196	190	184	186	180	175	170	165	161	157	160	157	153	149	146	143	140	137	134	131
52																		238	230	222	214	207	208	201	195	189	183	177	172	175	170	165	161	157	153	149	145	142	147	144	141	138
53																		244	236	228	220	219	212	205	198	192	186	187	182	176	171	167	162	158	154	157	153	149	146	143	140	137
54																		255	246	237	229	221	220	213	206	199	193	187	188	182	177	172	167	163	158	154	157	153	150	146	143	140
55																		262	253	244	235	234	226	218	211	204	197	197	191	185	180	175	170	171	167	162	158	154	150	147	143	140
56																		271	261	251	249	240	232	224	216	216	208	202	195	189	183	184	179	174	169	164	160	155	151	154	151	147
57																		279	269	265	256	247	239	230	229	221	214	207	200	194	193	188	182	177	172	167	169	164	160	156	152	148
58																		288	278	274	264	255	246	243	235	227	219	212	205	204	198	192	186	180	175	176	171	166	162	158	153	150
59																		301	290	280	270	266	257	248	239	237	229	221	214	207	206	199	193	188	182	177	177	172	168	163	159	154
60																		311	300	289	279	275	265	256	247	244	236	228	220	213	211	205	198	192	186	186	180	176	171	166	161	163
61																		321	310	299	288	284	274	264	255	252	243	235	227	225	217	210	204	197	197	191	185	179	174	169	170	165
62																		327	321	309	298	293	283	273	264	260	251	242	234	231	224	217	210	203	202	196	190	184	179	178	173	169
Enr. wt. %	0.9	1.0	1.1	1.2	1.3	1.4	1.5	1.6	1.7	1.8	1.9	2.0	2.1	2.2	2.3	2.4	2.5	2.6	2.7	2.8	2.9	3.0	3.1	3.2	3.3	3.4	3.5	3.6	3.7	3.8	3.9	4.0	4.1	4.2	4.3	4.4	4.5	4.6	4.7	4.8	4.9	5.0

Not Analyzed

Notes: Cells highlighted with yellow correspond to burnup/enrichment combinations with a cooling time of less than 3 years while meeting the 0.70 kW/FA decay heat power limit.

Cells not highlighted in the table above correspond to burnup/enrichment combinations cooled more than 3 years while meeting the 0.70 kW/FA limit.

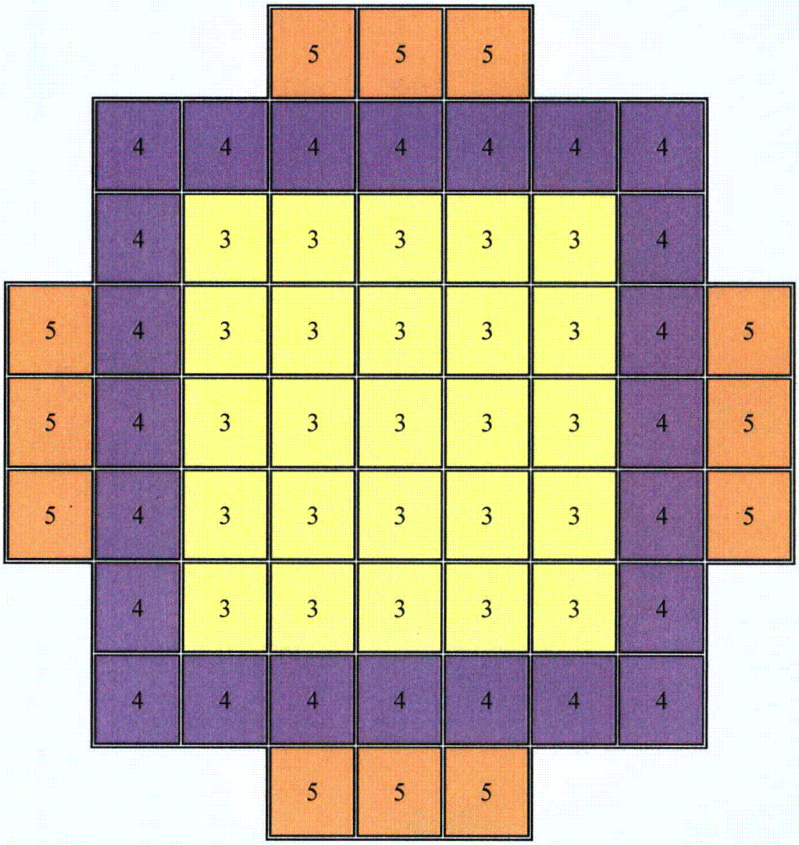

	Zone 1	Zone 2	Zone 3	Zone 4	Zone 5	Zone 6
Maximum Decay Heat (kW/FA)	NA	NA	0.393	0.48	0.54	NA
Maximum Decay Heat per Zone (kW)	NA	NA	9.825	11.52	6.48	NA
Maximum Decay Heat per DSC (kW)	27.825					

Figure T.5-1
Heat Zone Configuration Utilized for Model 102 Evaluation

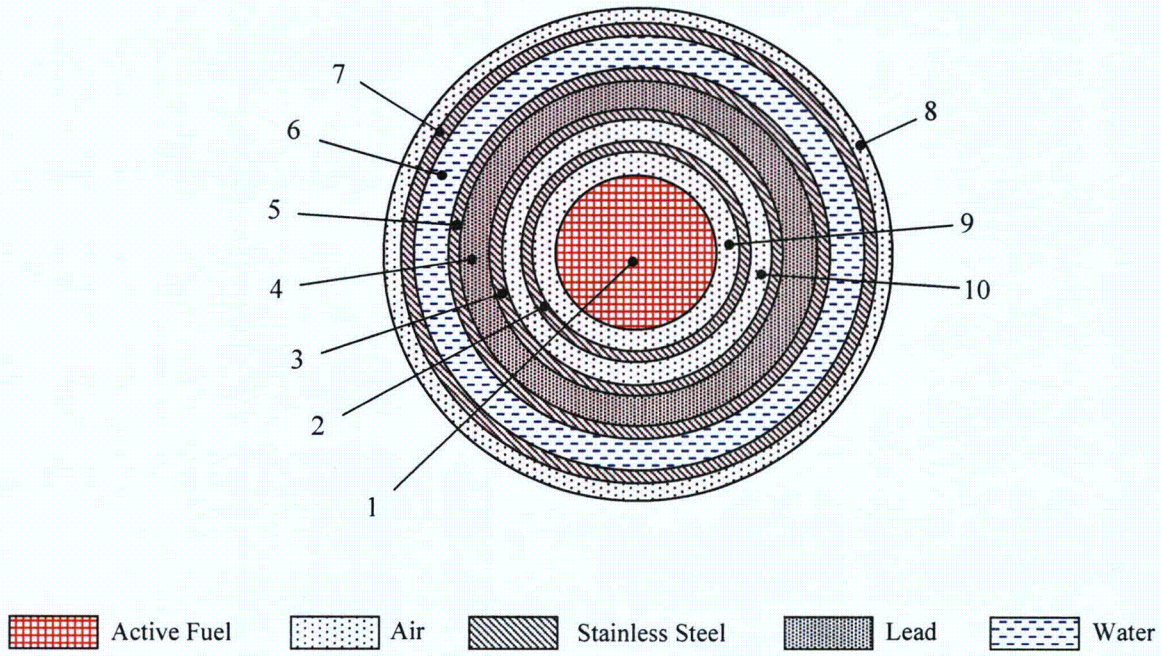

Item No.	Nomenclature or Description	Material	Inner Radius (cm)	Outer Radius (cm)
1	Active Fuel (In-core Region)	In-Core	0	71.58
2	DSC Cylindrical Shell, 0.49" thk.	SS 304	84.15	85.42
3	TC Inner Liner Plate, 1/2" thk.	SS 304	86.36	87.63
4	TC Lead Gamma Shield	Lead	87.63	96.67
5	TC Structural Shell	SS 304	96.67	100.48
6	Neutron Shielding Material	Water	100.48	108.11
7	Neutron Shield Panel, 3/16" thk.	SS 304	108.11	108.59
8	Air Outside of TC	Air	108.59	Any
9	Air Cavity Between Active Fuel and DSC Structural Shell	Air	72.10	84.09
10	Air Cavity Between DSC and TC	Air	85.33	86.36

Figure T.5-2
ANISN OS197 TC Model

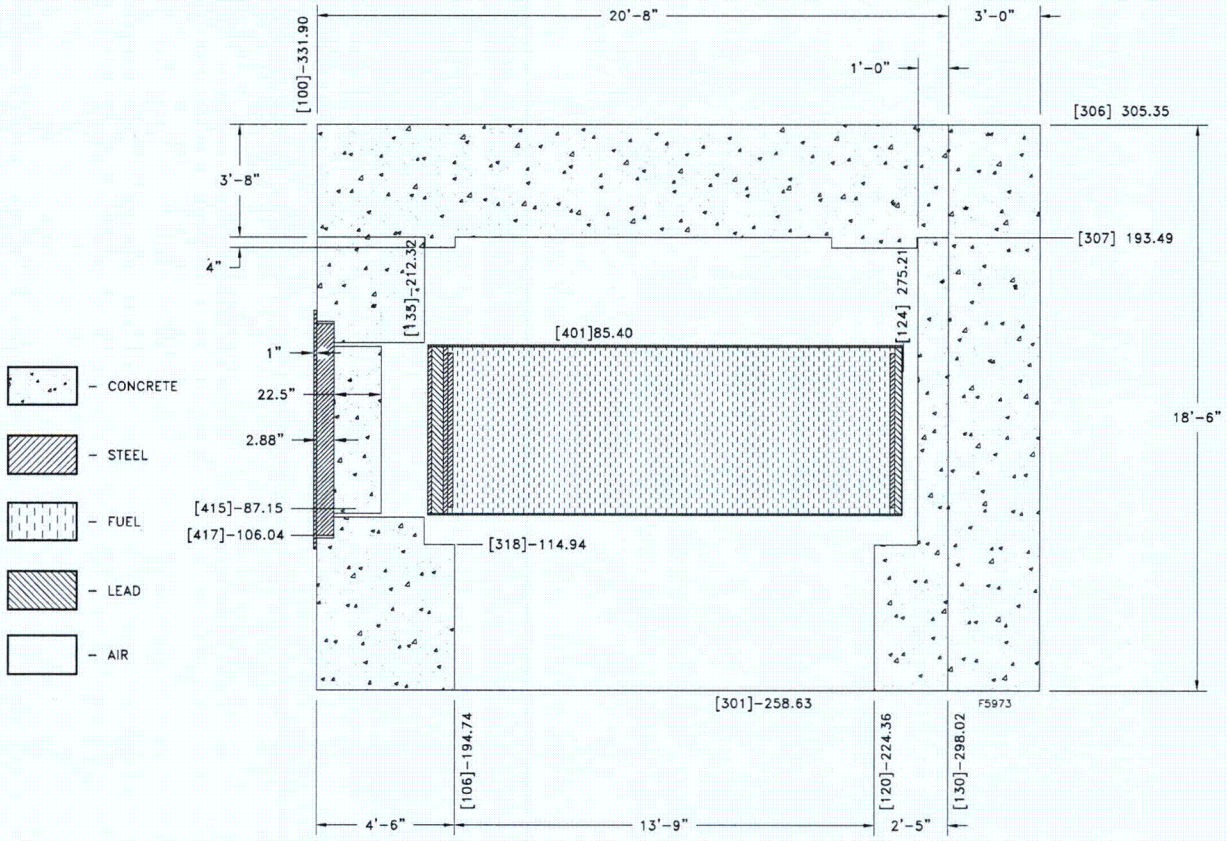

Figure T.5-3
61BTH DSC Within HSM-H, Side View at Centerline of DSC

[xxx] = MCNP surface numbers, all dimensions without units are in cm

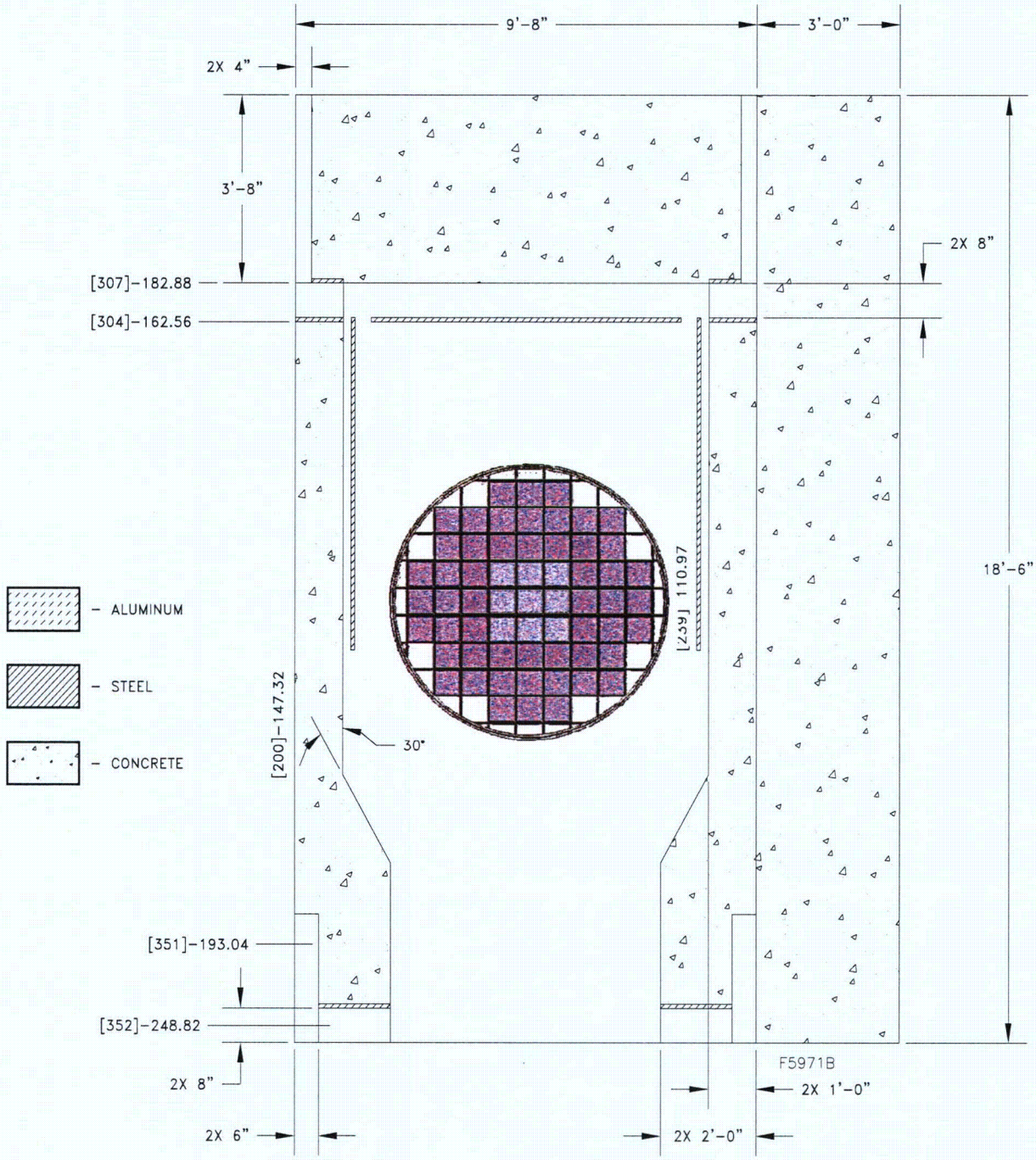

Figure T.5-4
61BTH DSC Within HSM-H, Head-on View at Z=0

[xxx] = MCNP surface numbers, all dimensions without units are in cm

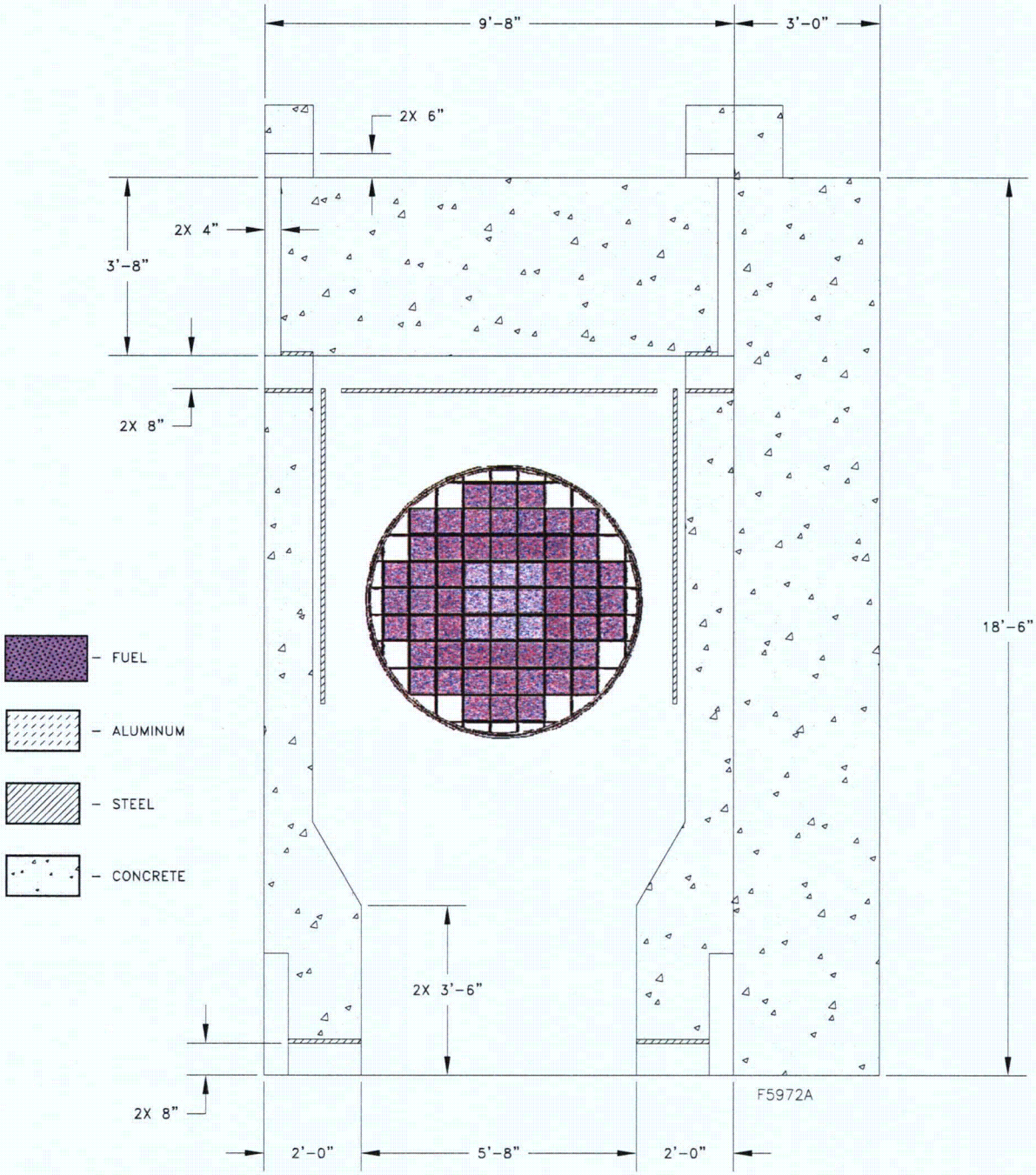

Figure T.5-5
61BTH DSC Within HSM-H, Head-on View Showing Top Vents

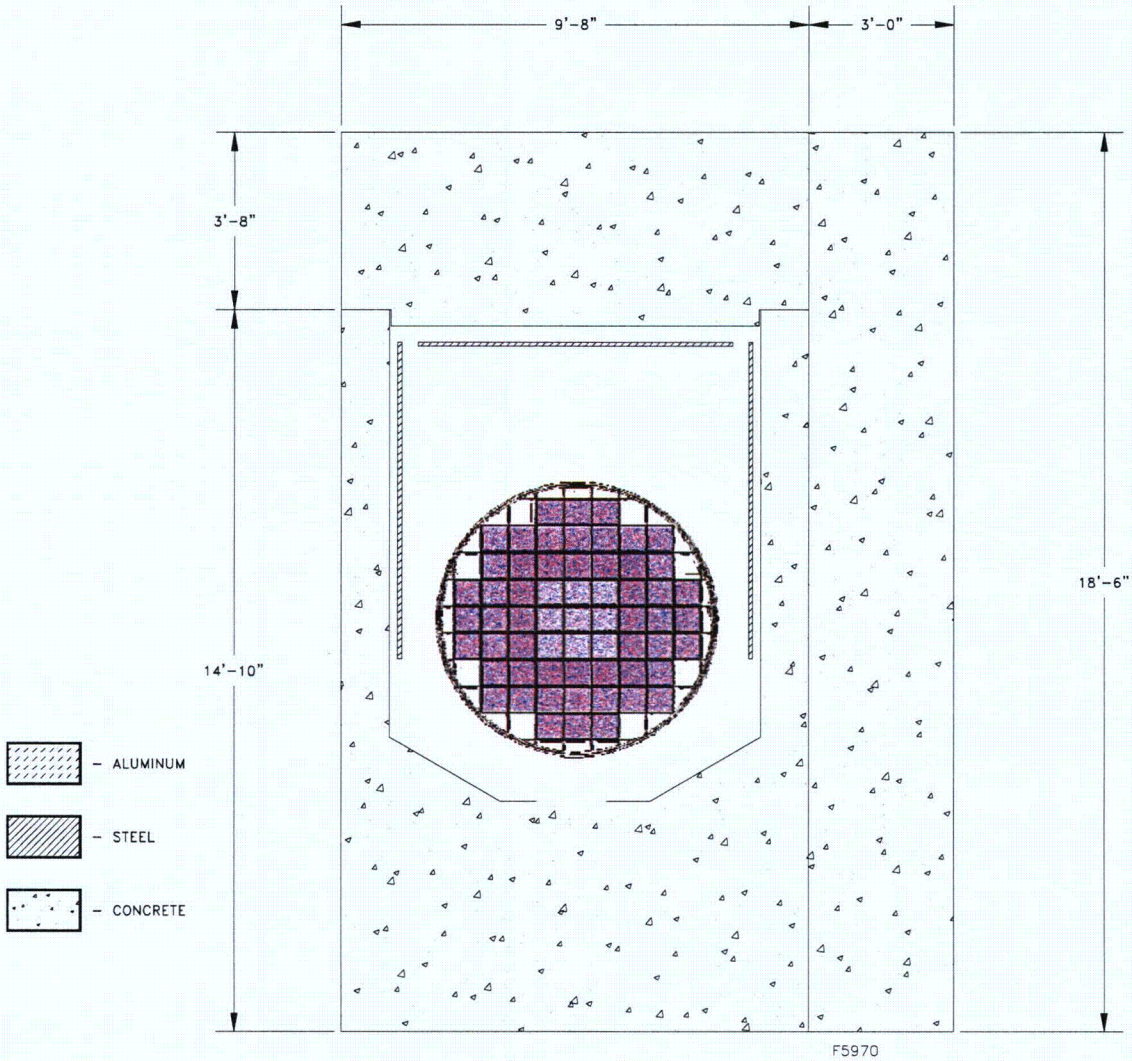

Figure T.5-6
61BTH DSC Within HSM-H, Head-on View at Lid End of DSC (Z=225 cm)

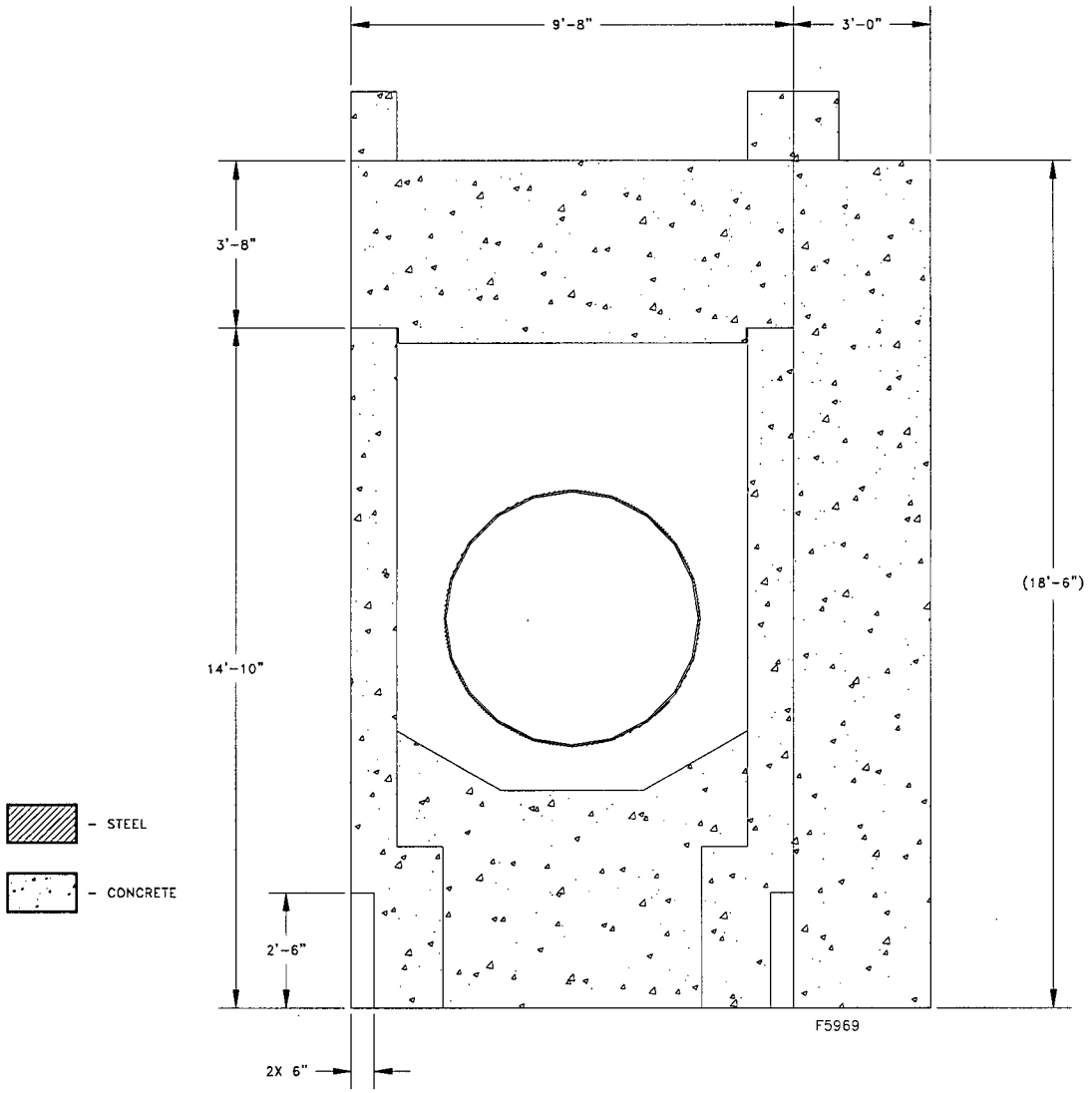

Figure T.5-7
61BTH DSC Within HSM-H, Head-on View at Bottom End of DSC (Z=-225 cm)

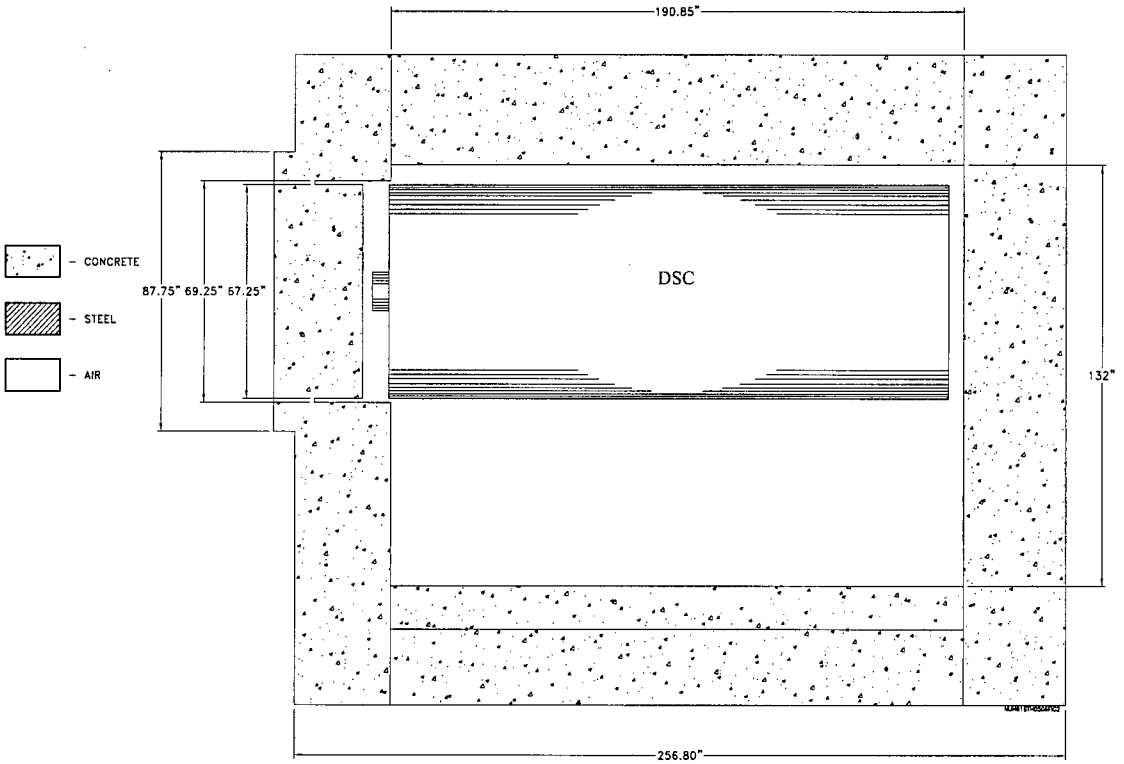

Figure T.5-8
61BTH DSC within HSM Model 102, Side View at Centerline of DSC

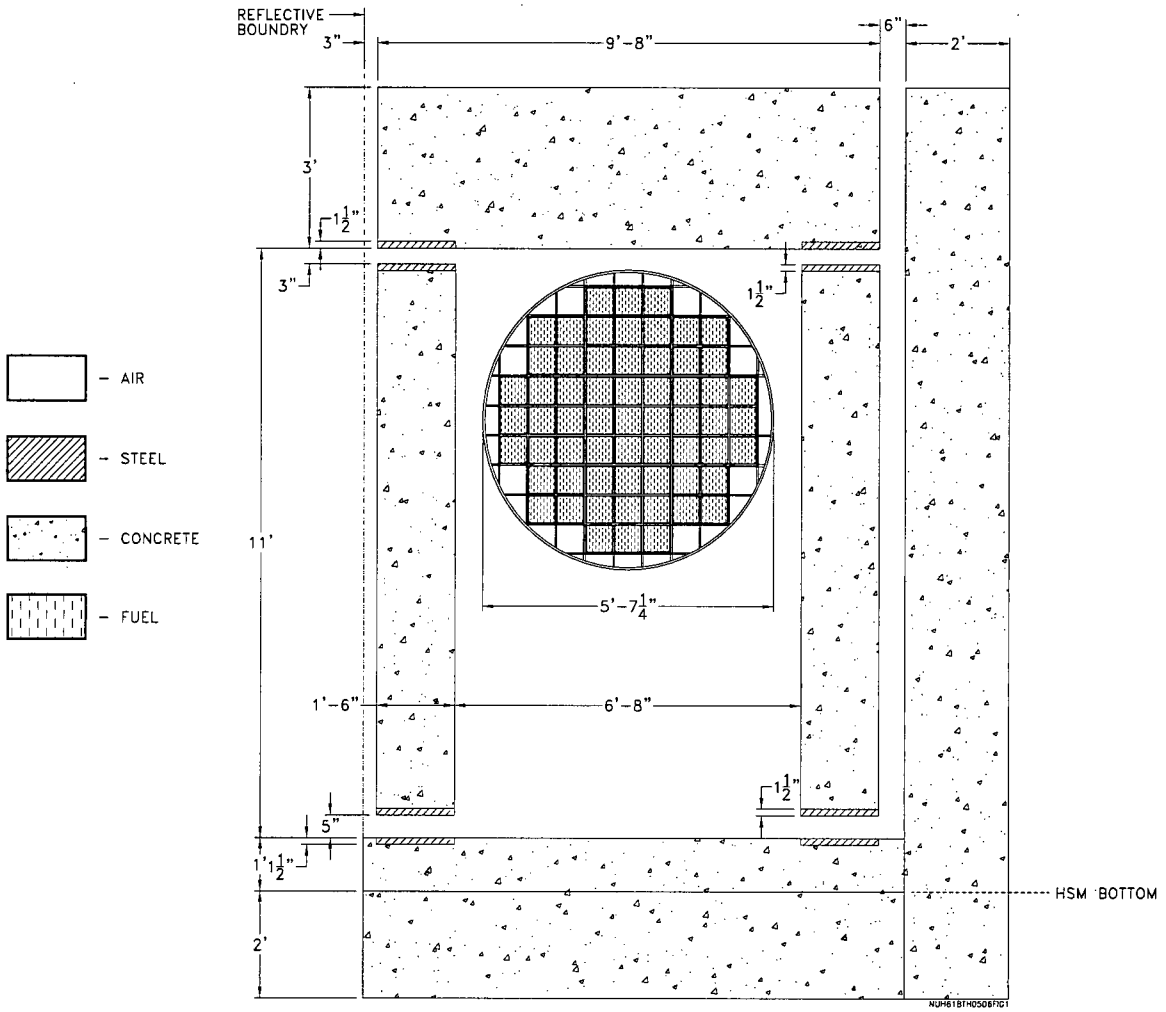

Figure T.5-9
61BTH DSC within HSM Model 102, Head-on View at Z=-60

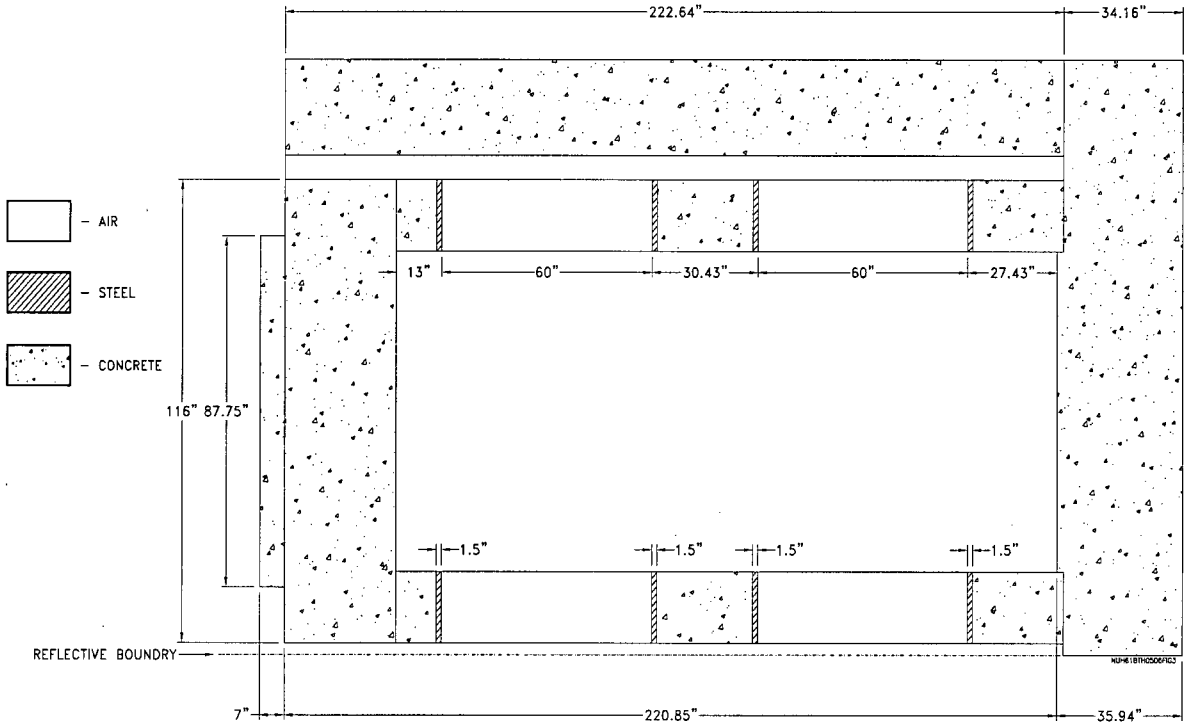

Figure T.5-10
61BTH DSC within HSM Model 102, Horizontal Cut through Top Vents View at 1 Meter above DSC Axis

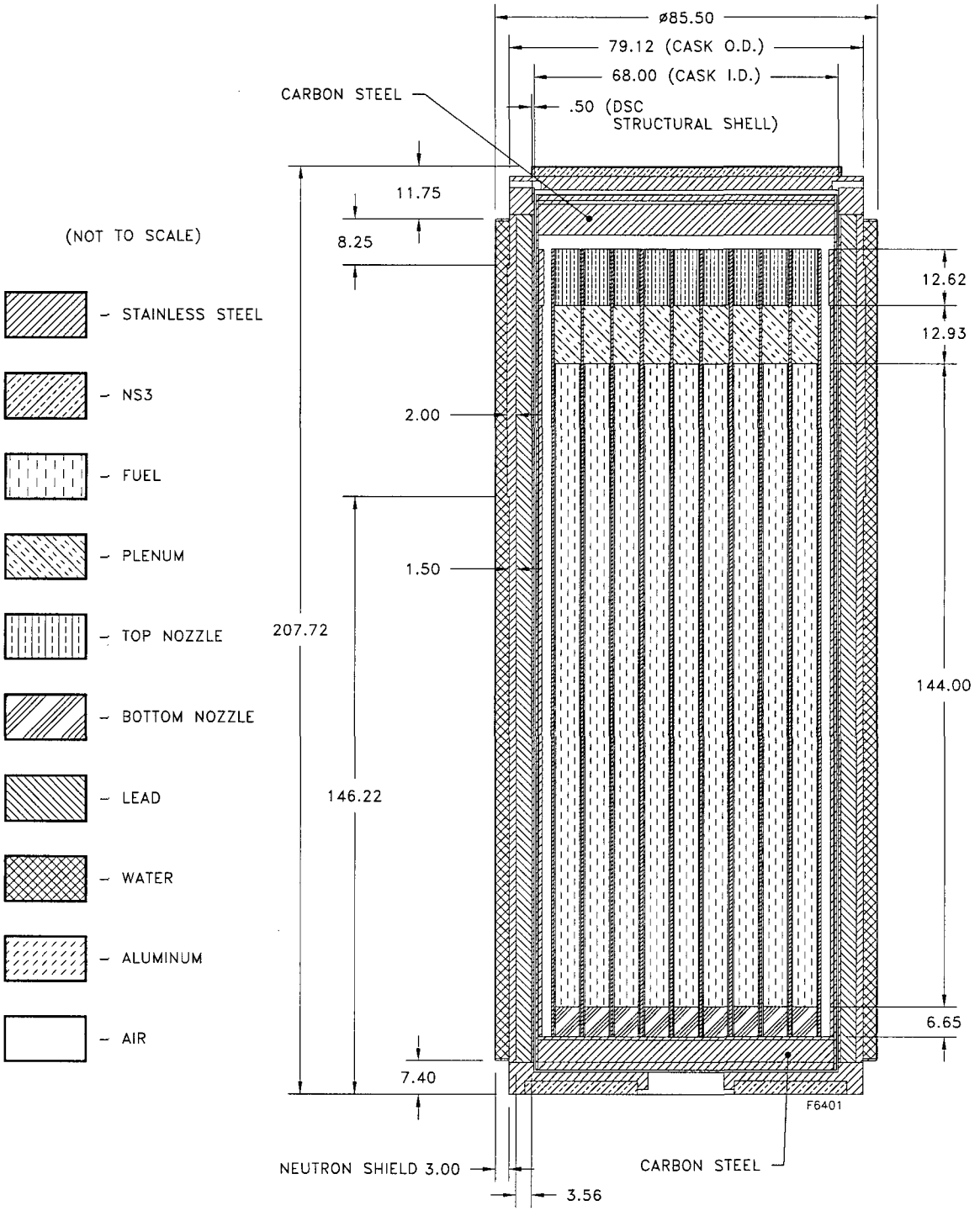

Note: All dimensions are in inches.

Figure T.5-11
61BTH Type 1 DSC Within OS197FC-B TC, Axial View of Transfer Model

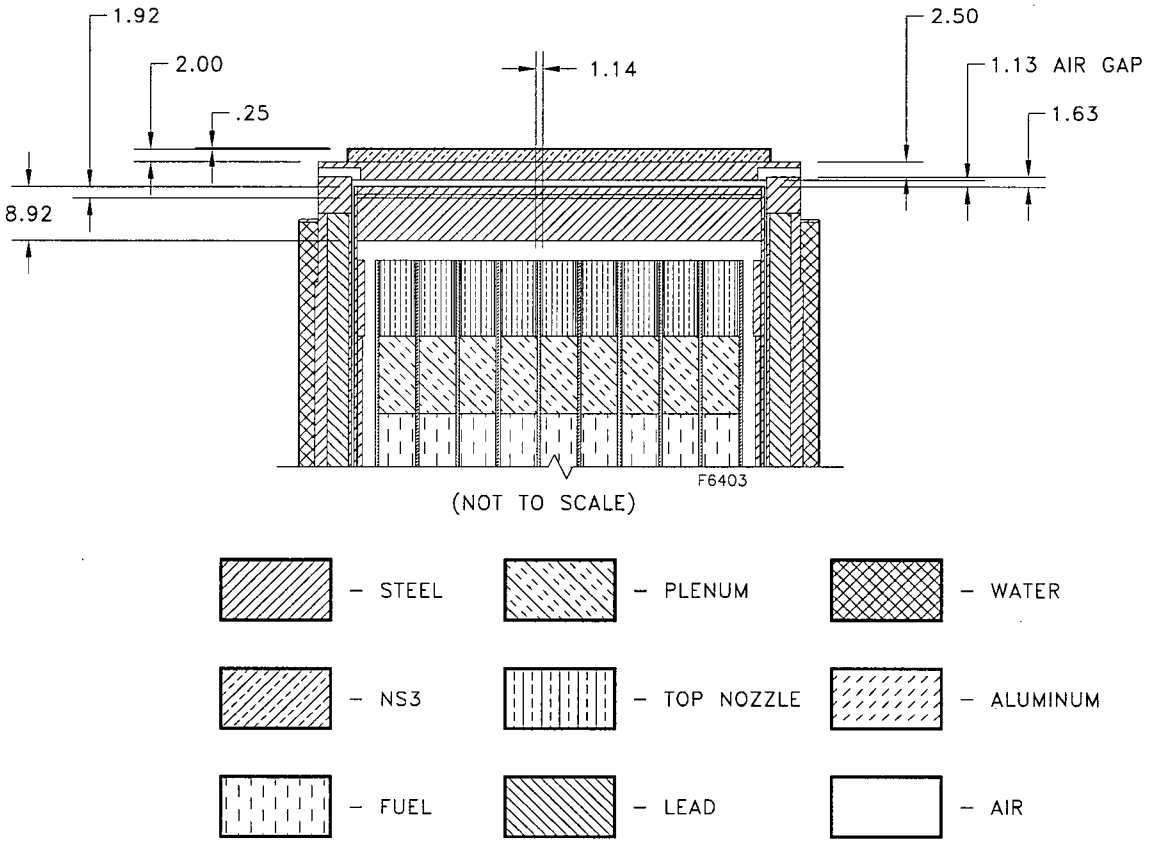

Note: All dimensions are in inches.

Figure T.5-12
61BTH Type 1 DSC Within OS197FC-B TC, Top View of Transfer Model Showing Cask Lid with Gap, Top Nozzle, and Plenum

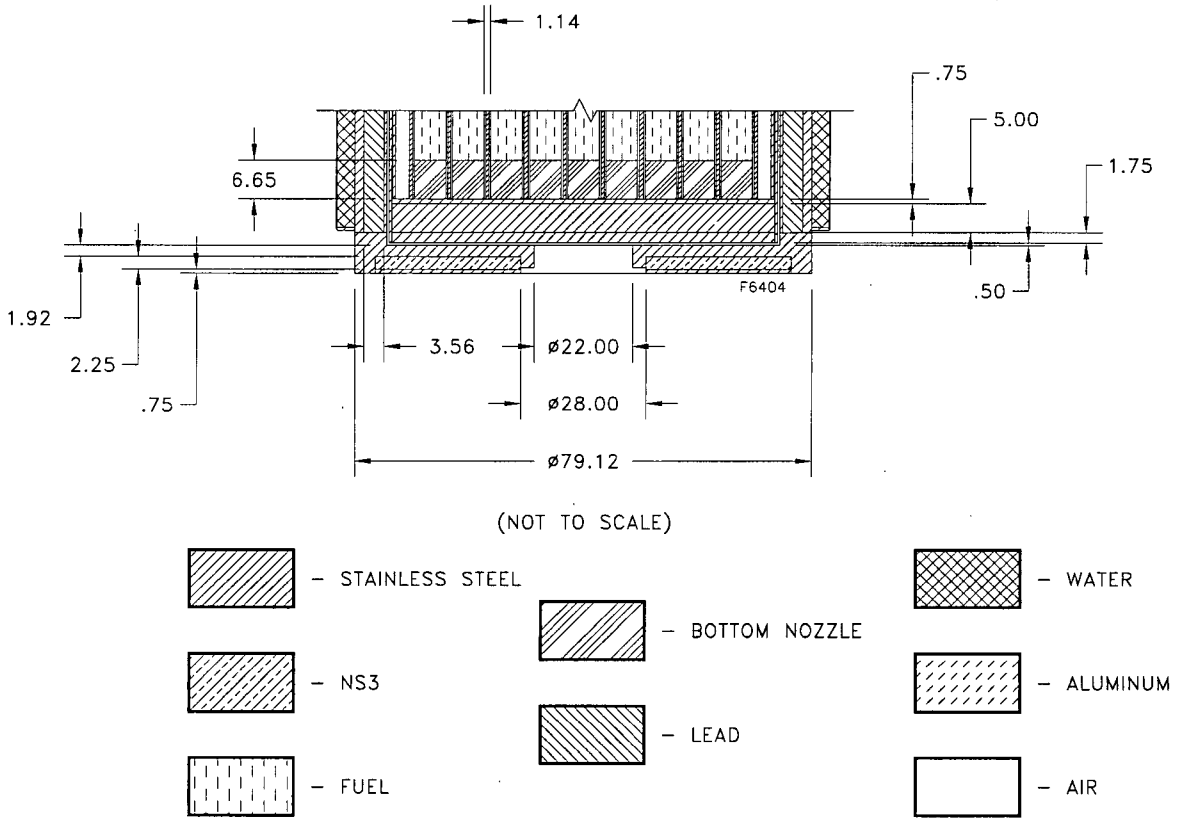

Note: All dimensions are in inches.

Figure T.5-13
61BTH Type 1 DSC Within OS197FC-B TC, Bottom View of Transfer Model Showing Cask Bottom and Bottom Nozzle

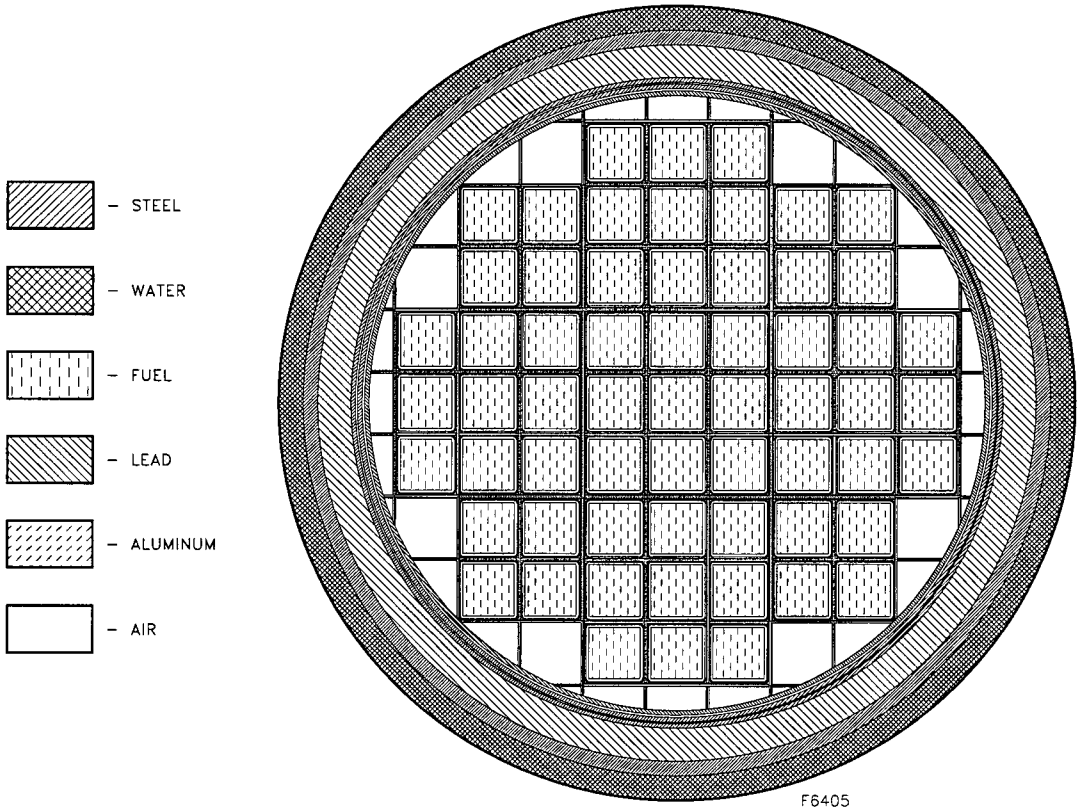

Figure T.5-14
61BTH DSC within OS197FC-B TC, Radial Cut View of Transfer Models Showing Fuel Locations

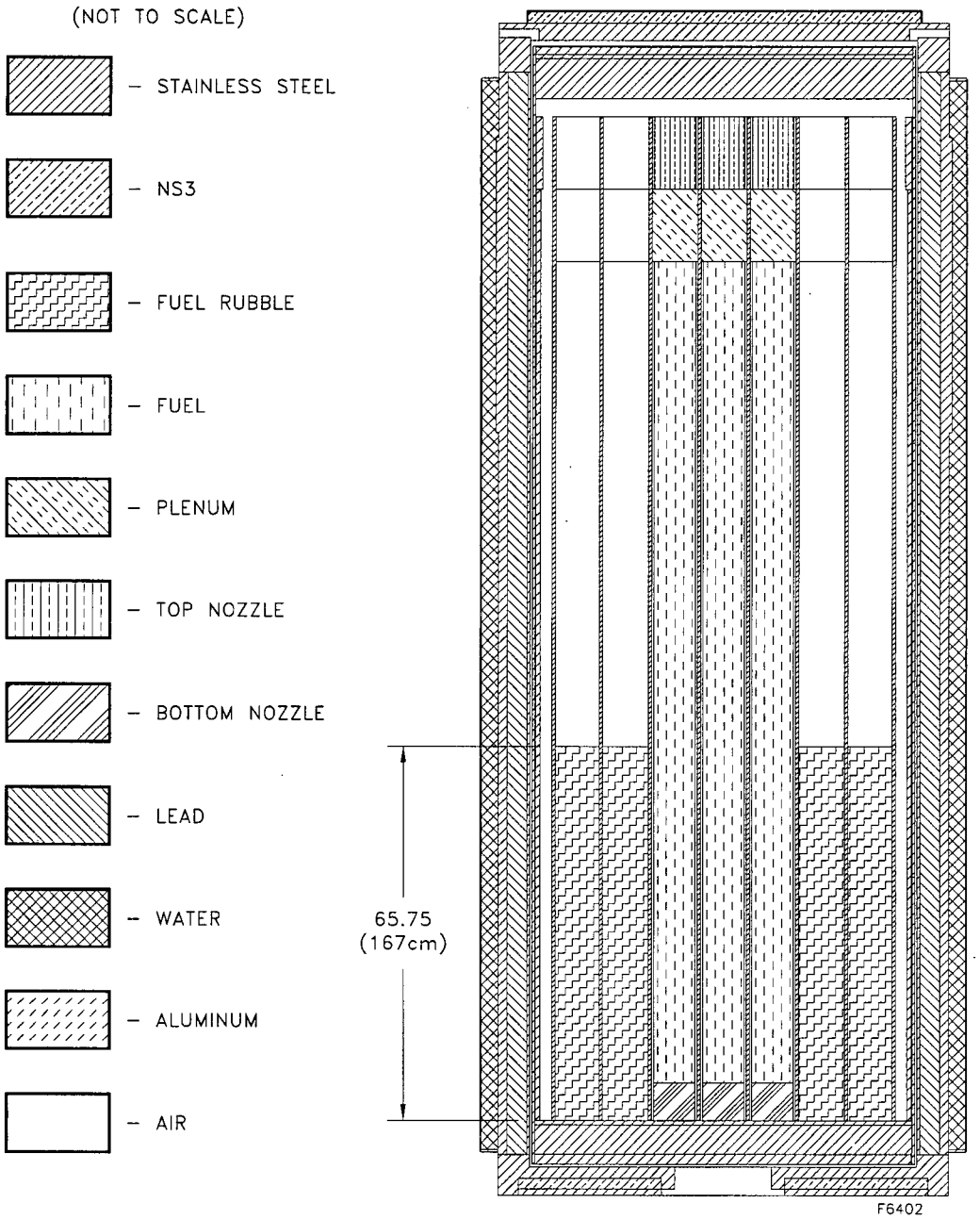

Figure T.5-15
61BTH DSC within OS197FC-B TC, Longitudinal Cut View of Transfer Model Showing Undamaged and Normal Fuel Locations and Damaged Fuel Height

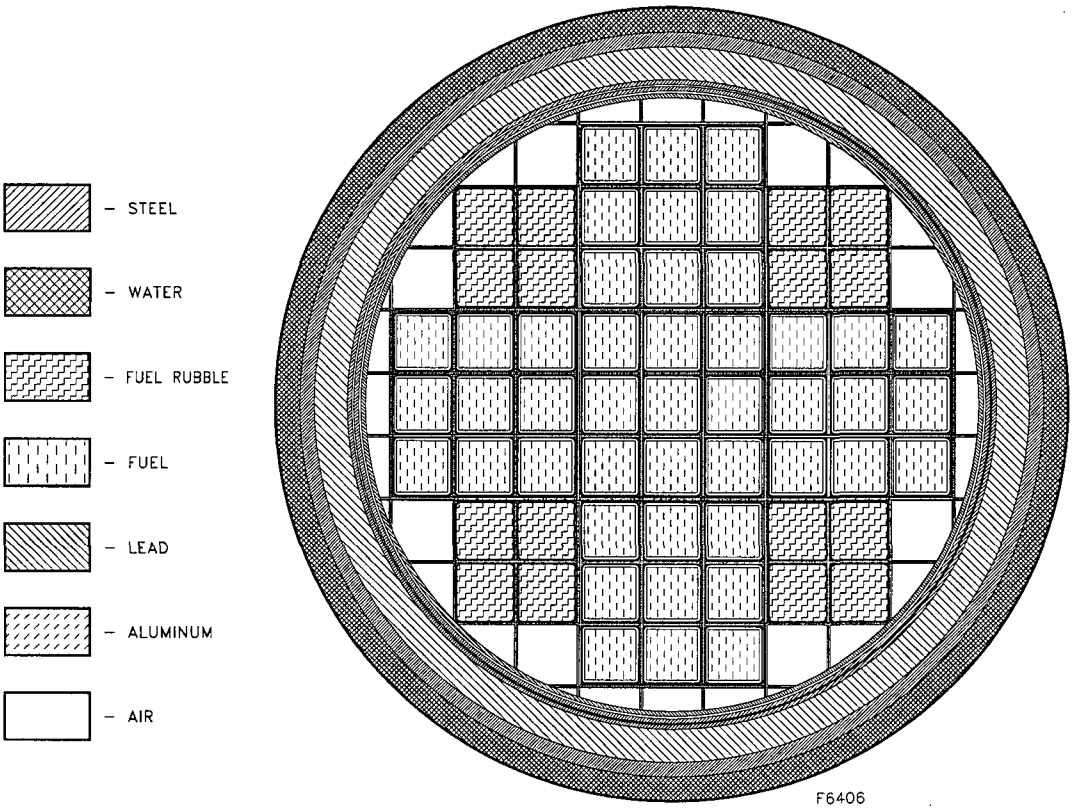

Figure T.5-16
61BTH DSC within OS197FC-B TC, Radial Cut View of Transfer Models Showing Undamaged and Normal Fuel Locations

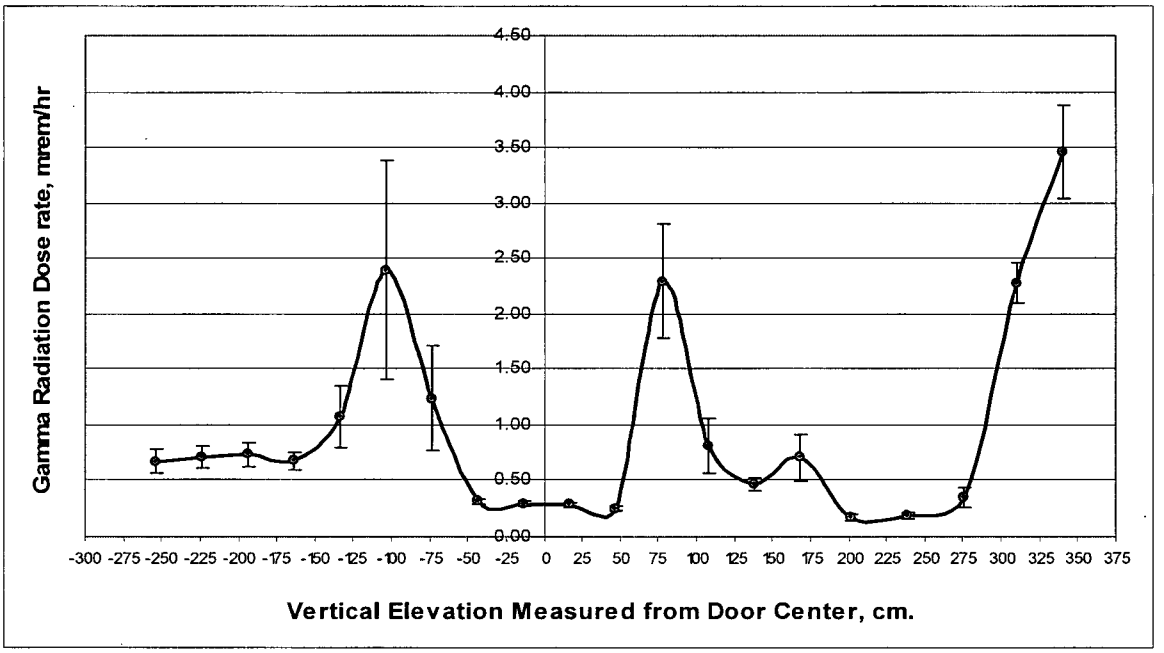

Figure T.5-17
HSM-H with 61BTH DSC, Gamma Radiation Dose Rate along HSM-H Front Centerline in Vertical Elevation

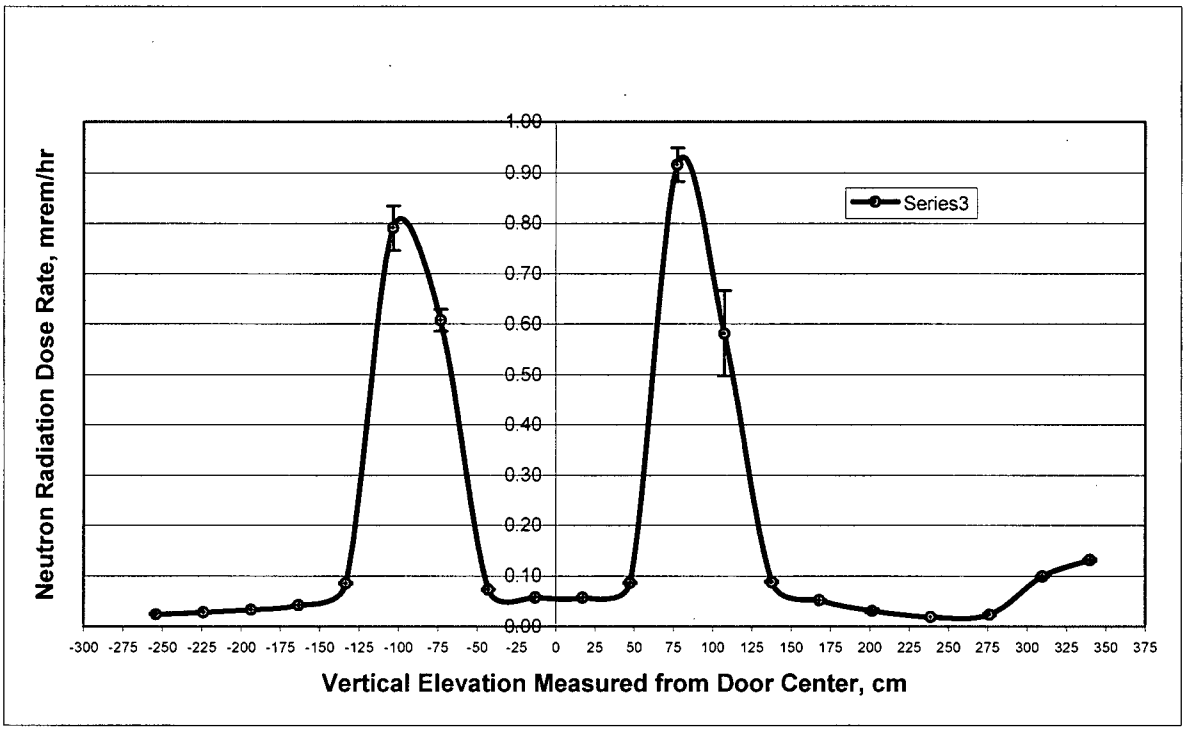

Figure T.5-18
HSM-H with 61BTH DSC, Neutron Radiation Dose Rate along HSM-H Front Centerline in Vertical Elevation

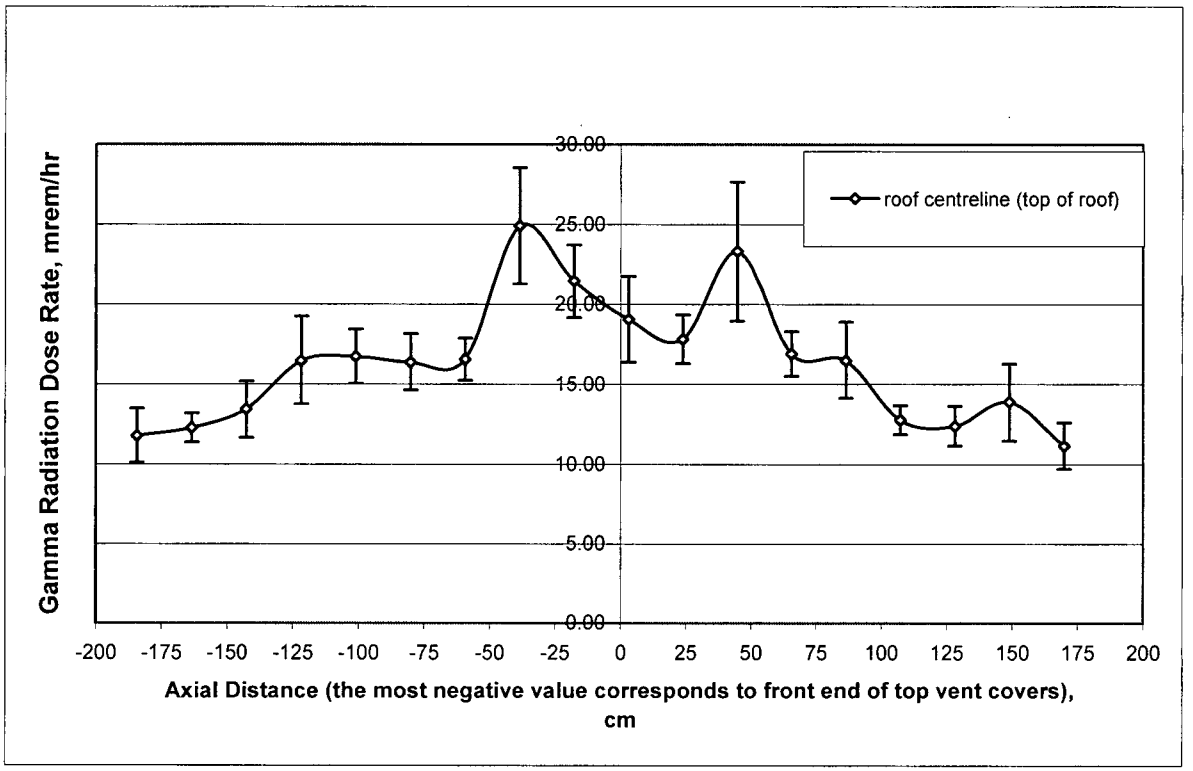

Figure T.5-19
HSM-H with 61BTH DSC, Gamma Radiation Dose Rate at Roof Centerline

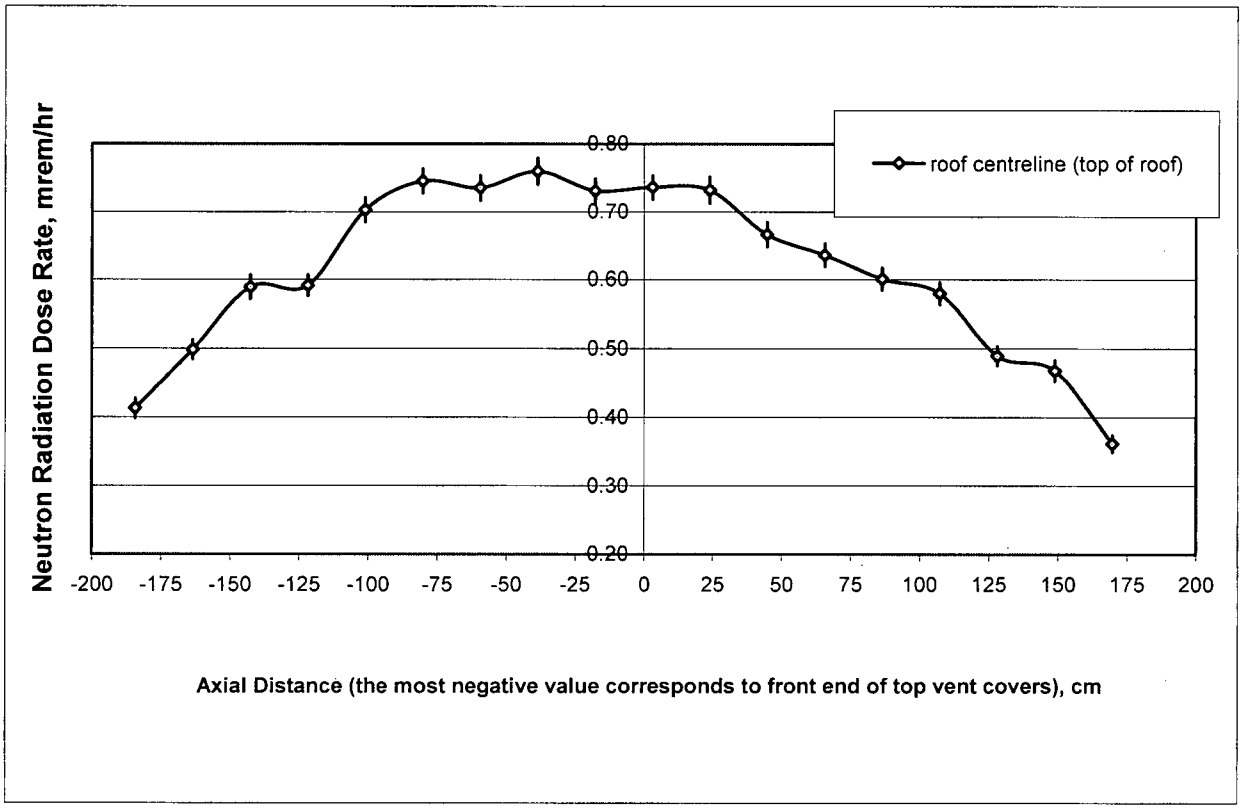

Figure T.5-20
HSM-H with 61BTH DSC, Neutron Dose Rate at Roof Centerline

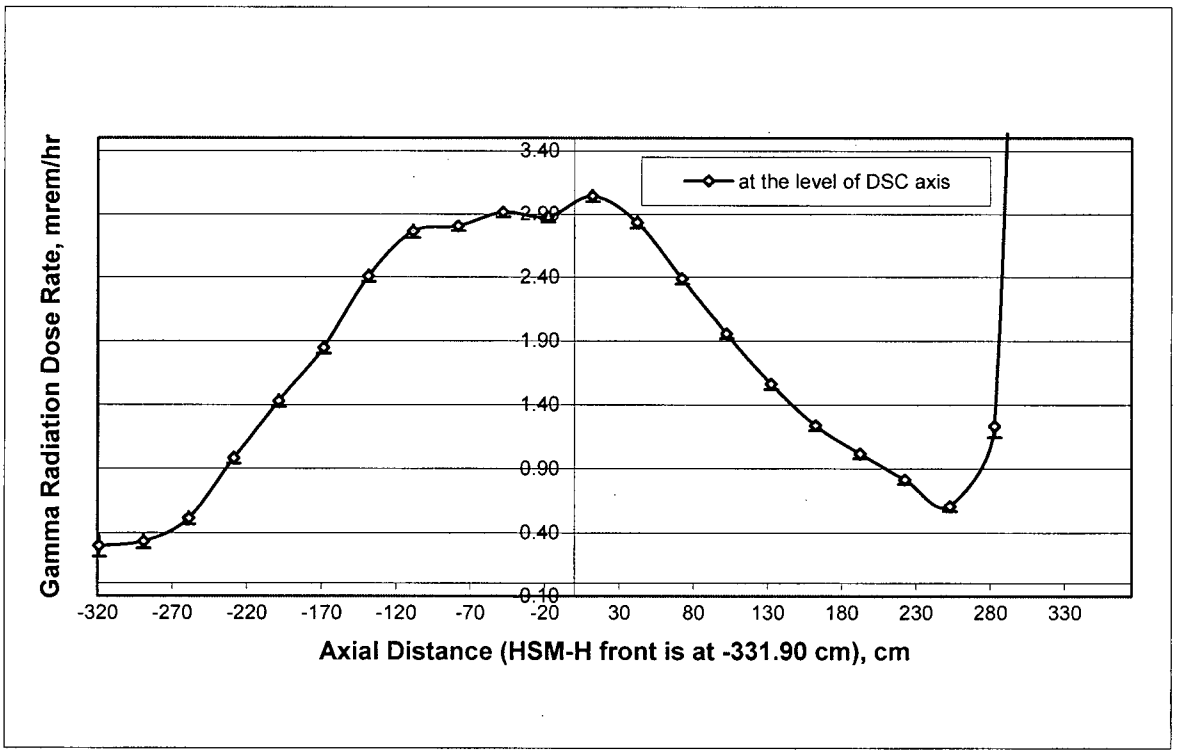

Figure T.5-21
HSM-H with 61BTH DSC, Side Shield Wall Surface at DSC Centerline Gamma Radiation Dose Rate

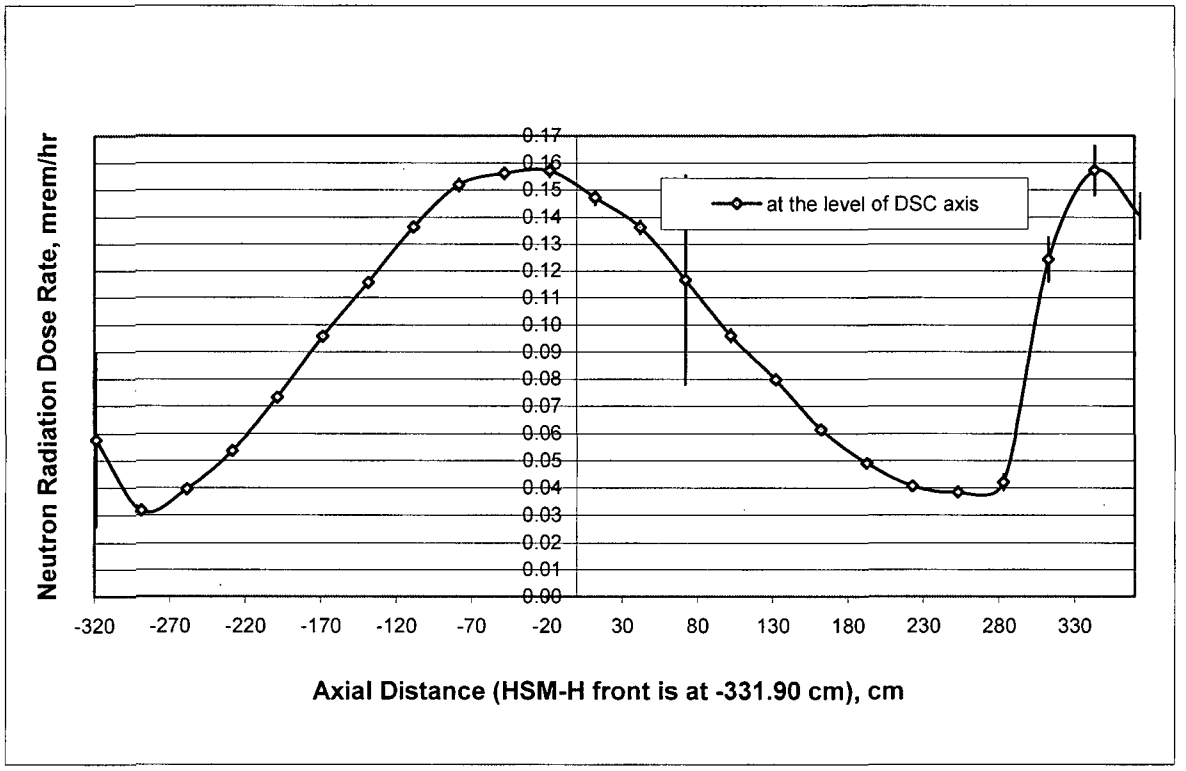

Figure T.5-22
HSM-H with 61BTH DSC, Side Shield Wall Surface at DSC Centerline Neutron Radiation Dose Rate

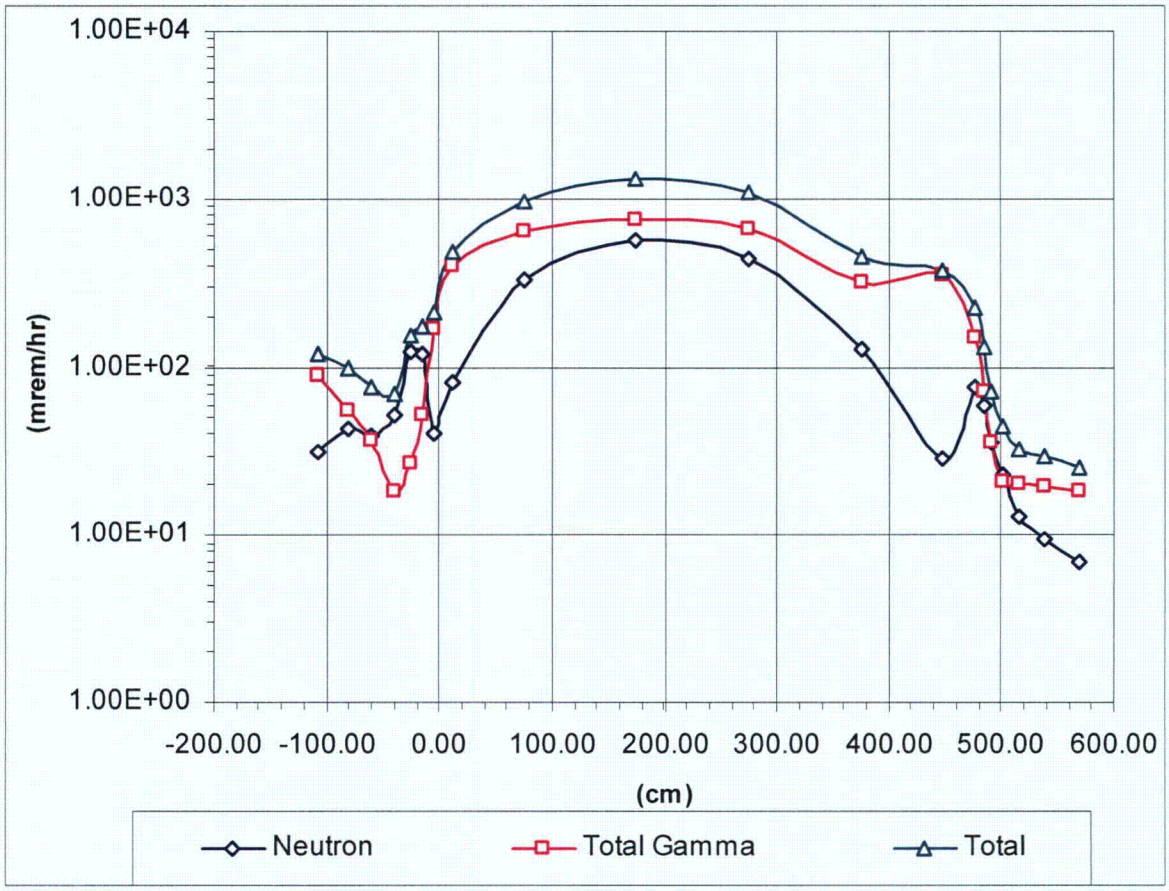

Figure T.5-23
OS197FC-B TC with 61BTH DSC, Side Surface Dose Rate, Normal Conditions

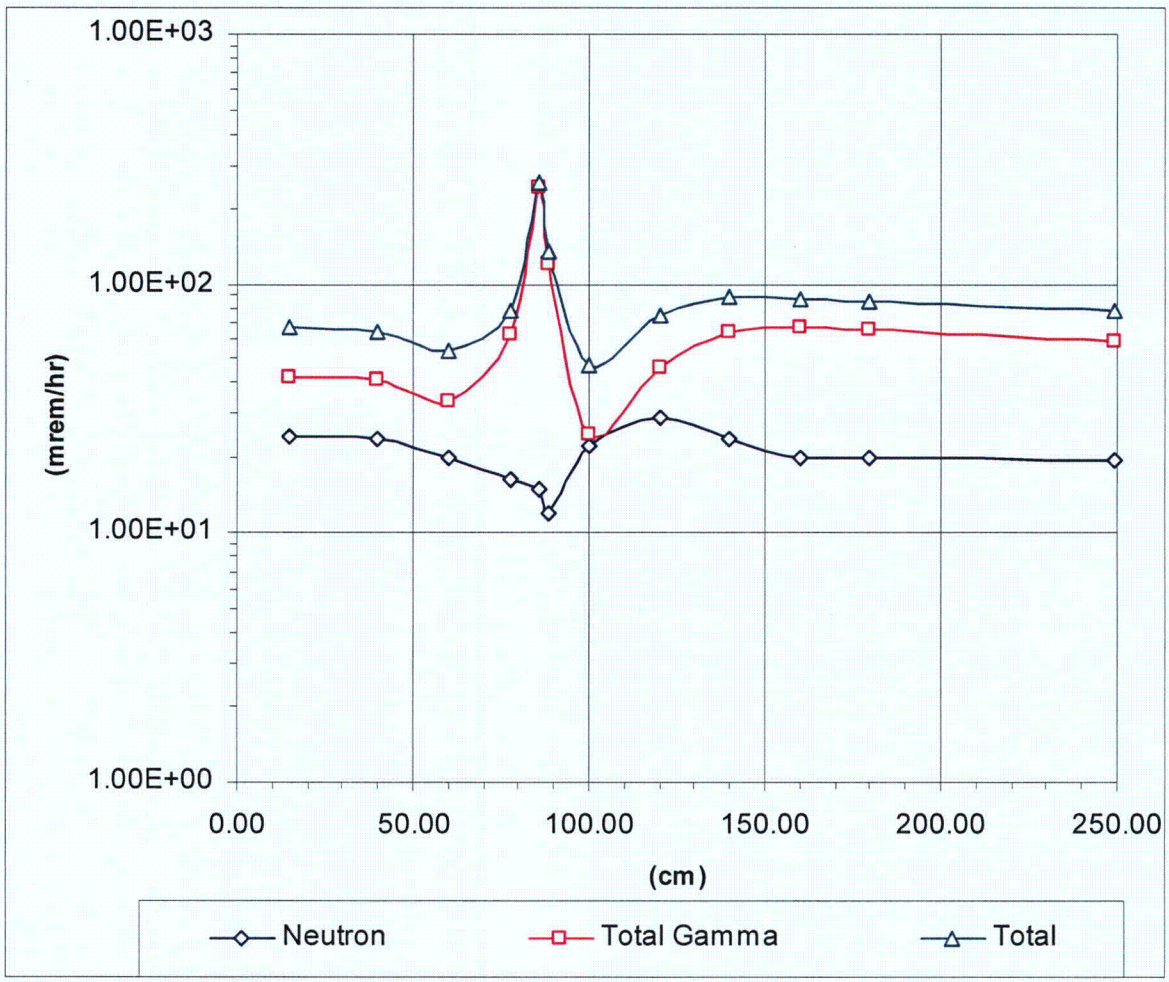

Figure T.5-24
OS197FC-B TC with 61BTH DSC, Top Surface Dose Rate, Normal Conditions

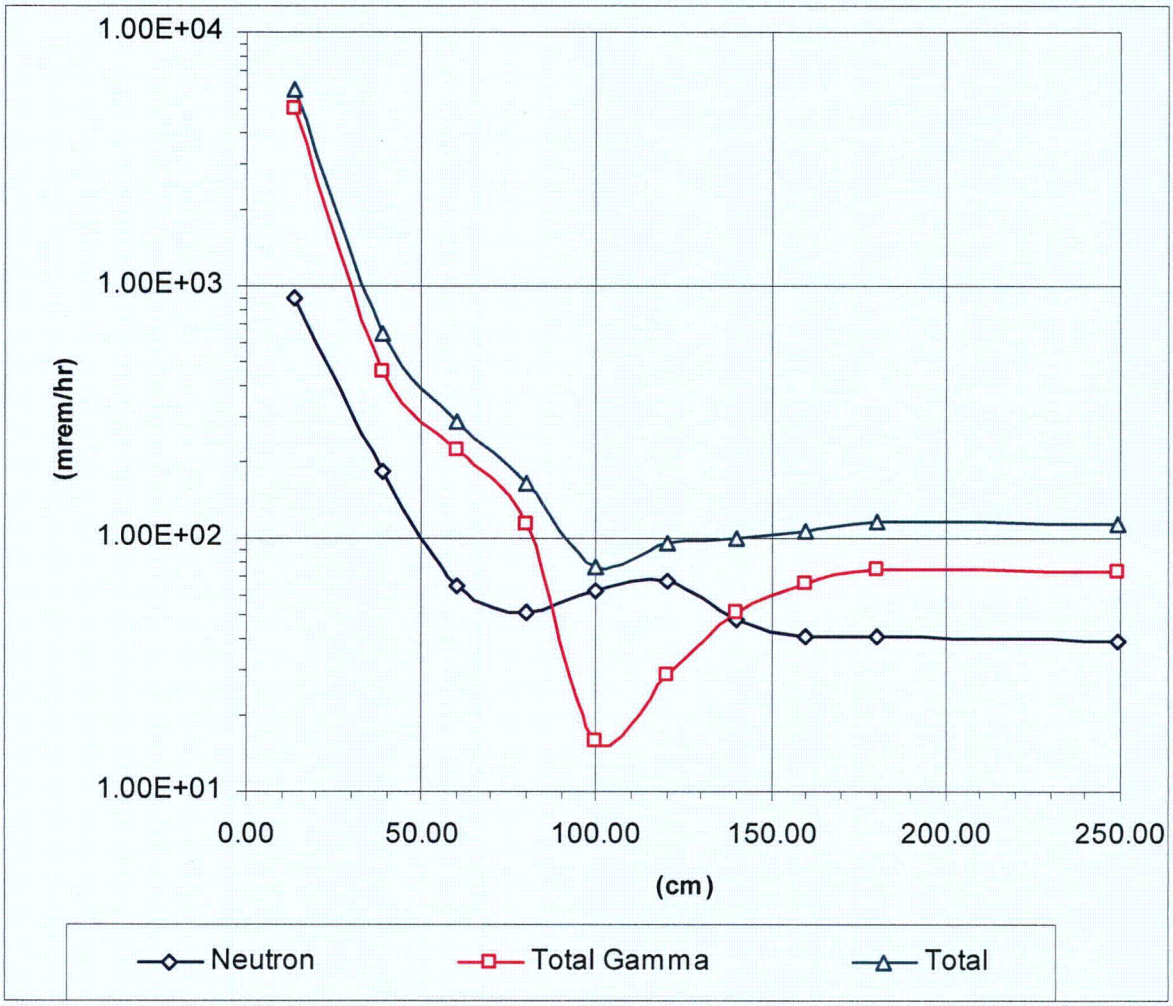

Figure T.5-25
OS197FC-B TC with 61BTH DSC, Bottom Surface Dose Rate, Normal Conditions

T.6 Criticality Evaluation

The design criteria for the NUHOMS®-61BTH Dry Shielded Canister (DSC) to be stored as part of the standardized NUHOMS®-61BTH system requires that the NUHOMS®-61BTH DSC be designed to remain subcritical under normal, off-normal, and accident conditions as defined in both 10CFR Part 72 and 10CFR Part 71.

The NUHOMS®-61BTH system consists of the NUHOMS® HSM and HSM-H, the OS197 Transfer Cask (TC), and the 61BTH Type 1 and Type 2 DSCs.

The NUHOMS®-61BTH system's criticality safety is ensured by both fixed neutron absorbers and favorable geometry. Burnup credit is not taken in this criticality evaluation. The fixed neutron absorber is present in the form of metallic aluminum plates that include boron-containing particles. This material is ideal for long-term use in radiation and thermal environments of a DSC. Table T.6-1 lists the minimum B10 poison loading required as a function of assembly initial lattice average enrichment.

T.6.1 Discussion and Results

Figure T.6-1 and Figure T.6-2 show the radial cross section of the NUHOMS®-61BTH Type 1 and Type 2 DSCs. The generic cask consists of an inner stainless steel shell, and lead gamma shield, a stainless steel structural shell and a hydrogenous neutron shield. This analysis is applicable to any licensed cask of similar construction. The NUHOMS®-61BTH DSC/Cask configuration is shown to be subcritical under both normal, off-normal and accident conditions.

The criticality calculations assume the General Electric (GE) 10x10-fuel assembly because it is the most reactive fuel assembly allowed by the authorized contents. The calculations determine k_{eff} with the CSAS25 control module of SCALE-4.4 [6.1] for various configurations and initial enrichments, including all uncertainties to assure criticality safety under all credible conditions.

The results of the evaluation demonstrate that the maximum k_{eff}–including statistical uncertainty–is less than the Upper Subcritical Limit (USL) determined from a statistical analysis of benchmark criticality experiments. The statistical analysis procedure includes a confidence band with an administrative safety margin of 0.05.

T.6.2 Package Fuel Loading

The NUHOMS®-61BTH DSC is capable of transporting BWR fuel assemblies with or without fuel channels and as intact or damaged fuel assemblies. The fuel assemblies considered as authorized contents are listed in Table T.6-2.

Table T.6-3 lists the fuel parameters for the BWR fuel assemblies. Reload fuel from other manufacturers, for the same fuel assembly class, with the same parameters are also allowed. The design basis fuel chosen for the NUHOMS®-61BTH system is the GE 10x10 fuel assembly. The GE 10x10 assembly is used because, as demonstrated in Section T.6.4, it is the most reactive assembly of those authorized to be shipped in the NUHOMS®-61BTH DSC system.

T.6.3 Model Specification

The following subsections describe the physical models and materials of the NUHOMS®-61BTH DSC system used for input to the CSAS25 module of SCALE-4.4 [6.1] to perform the criticality evaluation.

T.6.3.1 Description of Calculational Model

Due to the similarity of the designs of the NUHOMS®-61BT and the 61BTH DSCs, the results of several sensitivity calculations are directly utlilized from Appendix K, Chapter K.6, whenever applicable.

The cask and canister were explicitly modeled using the appropriate geometry options in KENO V.a of the CSAS25 module in SCALE-4.4.

Several models were developed. The first model is a full-active fuel height model and full-radial cross section of the canister alone with water boundary conditions on the ends and reflective boundary conditions on the sides. This model is identical to the one utilized for the 61BT DSC described in Appendix K, Chapter K6. This model does not include the gaps between the poison plates and is more fully described in Appendix K, Section K.6.6.2. This model is only used to determine the most reactive fuel assembly/channel combination and to justify use of the lattice average enrichment for the intact fuel analysis.

The second model is a full-active fuel height model and full radial cross section of the cask and canister with reflective boundary conditions on all sides. This model includes the worst case gaps between the poison plates and the basket internals modeled at minimum material conditions. This model includes the GE12 10x10-fuel assembly only because this assembly type is determined to be the most reactive fuel assembly type of the authorized contents. The GE12 10x10 fuel assembly is modeled as a 10x10 array comprising 92 fuel rods, including fuel, gap and cladding and two large water holes. The fuel cladding OD is also conservatively reduced by 0.010 inches in the final models to conservatively bound fuel manufacturing tolerances. The cask neutron shield and outer steel skin are modeled as water.

Parametric calculations are done to make minor modifications to the previous model such that the resulting model (third model) is applicable and conservative to represent both the Type 1 and Type 2 DSC basket designs. This model is the design basis model for intact assembly calculation and is flexible enough such that the fixed neutron poison in the basket can be modeled as a single sheet or can be paired with aluminum. This model is shown in Figure T.6-3.

The following description is for the damaged fuel assembly evaluation. The methodology for single shear and double shear is identical to the one utilized for the 61BT DSC described in Appendix K, Chapter K.6.

The fourth model conservatively models 45 intact fuel assemblies and 16 "damaged" fuel assemblies in the four 2x2 compartments in the corners of the basket. This model is very similar to the second model with the following changes:

- Initial sensitivity models are based on 7x7 (GE2) and the 8x8 (GE9) fuel assemblies and are utilized to determine the most reactive damaged fuel assembly configuration.
- The axial boundary conditions are water rather than reflective.
- One row of fuel rods is assumed to shear off from the rest of the fuel assembly.
- The single row of "damaged" rods is assumed to slide 12.5 inches above the bottom of the poison plates (Single-Break).
- For the case of a double ended shear, an extra row of fuel is assumed to be present in each damaged fuel cell (compartment) to simulate a portion of the severed rods breaking off and moving adjacent to the rest of the assembly in the fuel cell. This is a very conservative assumption because the total fuel loading in the fuel assembly (kg U) is increased.
- The damaged fuel reactivity comparisons are then carried out for the other classes of fuel assemblies to determine the most reactive fuel assembly for the double ended shear damaged configuration.
- A lattice average enrichment of 4.0 wt. % U-235 is used for all of the initial sensitivity calculations with damaged assemblies. For these sensitivity calculations, the "damaged" row of fuel is modeled with a peak enrichment of 4.4 wt. % U-235.
- The fuel assembly pitch is varied from a minimum to a maximum constrained only by the size of the fuel compartment to determine the optimum rod pitch for each fuel assembly class. Subsequently, fuel rods are removed to determine the optimum number of fuel rods for any given lattice design and the most reactive damaged rod configuration is determined.
- As with the case with intact fuel, the GE 10x10 fuel assembly is once again determined to be the most reactive damaged fuel assembly. The damaged assembly is modeled with an optimum rod pitch configuration containing 95 fuel rods and 5 water pin locations.
- The design basis damaged assembly model is then synthesized from the design basis intact assembly model.

Figure K.6-2 of Appendix K is a sketch of each KENO V.a unit showing all materials and dimensions for each unit and an annotated cross section map showing the assembled geometry units in the radial direction of the model. The fuel assembly-to-fuel assembly pitch is a variable in the model, with the fuel assemblies modeled in the center of the fuel cells (compartments) and pushed towards the center of the compartments and away from the center of the canister. The poison plates are modeled with minimum plate thickness, width and length. The maximum axial gap between the plates is modeled in the worst case orientation to maximize the amount of "uncovered" fuel. The axial gaps between the poison plates are due to the need to provide space for thermal expansion of the poison plates relative to the stainless steel parts of the basket and to allow for fabrication tolerances in the basket. In addition, the design allows the poison plates to be fabricated in sections, rather than one continuous piece. In the axial direction, all gaps are

modeled at the maximum width. Table K.6-4 of Appendix K shows the axial position of the assembled KENO V.a geometry units.

The criticality calculational models are similar to the model described in Table K.6-4. The only differences in the basket geometry is the modeling of the fixed poison as a paired combination of poison/aluminum and modeling the basket periphery (rails and water holes) to include conservative considerations for 61BTH Type 1 and Type 2 DSC designs.

Table T.6-4 is a comprehensive summary of the various criticality analyses carried out for the NUHOMS®-61BTH DSC. It includes a brief description of the analyses carried out for this evaluation. Since some of the evaluations utilized are obtained for the 61BT DSC from Appendix K, Chapter K.6, such a summary is useful to maintain continuity.

T.6.3.2 Package Regional Densities

The Oak Ridge National Laboratory (ORNL) SCALE code package [6.1] contains a standard material data library for common elements, compounds, and mixtures. All the materials used for the cask and canister analysis are available in this data library. The neutron shield material in the cask is modeled as water and the cask skin is not modeled.

Table T.6-5 provides a complete list of all the relevant material property data used for the criticality evaluation. The cask neutron shield material is conservatively modeled as water. The hydrogen atom density of the solid neutron shield (for the transportation cask) is lower than that of water; therefore, replacing the neutron shield with water is slightly conservative.

T.6.4 Criticality Calculation

This section describes the models used for the criticality analysis. The analyses were performed with the CSAS25 module of the SCALE system. A series of calculations were performed to determine the most reactive fuel and configuration. The most reactive fuel, as demonstrated by the analyses, is the GE 10x10 assembly for both the intact and damaged lattices. The most reactive credible configuration is an infinite array of flooded casks with minimum assembly-to-assembly pitch and the poison plate gaps located near the center of the basket and at the centerline of the active fuel region.

The NUHOMS®-61BTH DSC is analyzed for additional considerations arising from mechanical uncertainties of damaged fuel assemblies after a hypothetical accident. In case of a severe transportation accident, rod breakage may be postulated to occur in rods with known pre-existing gross cladding failure. These models were constructed to evaluate the effects of radial movement of fuel rod pieces (the result of "single-ended" breaks), and axial movement (the result of "double-ended" breaks). Loose fuel pellets or shards may become dislodged if a rod becomes severed, but this will not result in a more reactive state than the cases described below because the fuel assembly is under-moderated by design. The models used to study these limiting breaks are described below.

Single breaks- "Free ends" caused by a break are assumed to move away from the rest of the fuel assembly. Increasing the rod spacing of the broken rods is found to increase k_{eff}. Conversely, k_{eff} is expected to decrease for local decreases in rod pitch. Rods on the exterior of the fuel assembly are displaced in the models and the fuel assembly is assumed to be pressed in the corner of the fuel cell, thus maximizing the potential rod displacement. Since internal rods cannot move as far as rods on the outside of the assembly, they are not limiting. For modeling simplicity, an entire face of 7 rods for the 7x7 array and 8 rods for the 8x8 array are assumed to evenly move away from the remainder of an assembly, as shown in Figure K.6-6 of Appendix K. This overpredicts the effect of single rod breaks since the grid spacers of the fuel will limit radial rod displacement over most of the length of the rod.

Double breaks- The affect of pieces of fuel rod migrating axially was investigated by conservatively adding an entire row of fuel rods in the models. Again, the fuel assembly was assumed to be in the worst case position: pressed in the corner of the fuel compartment as shown in Figure K.6-7 of Appendix K. In addition, total cladding loss was assumed for the damaged rows of rods to simulate the bare fuel rod case. The limiting case was the double-ended break with the damaged rods being modeled without the cladding. This is expected to be the limiting case because the extra row of rods added to the model represents an increase in the fuel loading of the canister.

Rod Pitch Variation- The effect of bending and bowing of rods together with the total loss of grid spacers was investigated by varying the fuel rod pitch for all the fuel assembly classes from a minimum (where the rods are close to each other) to a maximum (bounded by the internal dimension of the rod compartment). This was done to determine the optimum rod pitch where the reactivity of the fuel lattice is maximized. In addition, rods were removed (non mechanistically) from within the lattice to determine the optimum rod positions (and the number of rods) to bound the expected lattice configurations. This hypothetical accident case is modeled

to maximize the reactivity of the damaged fuel assembly and also to qualify fuel assemblies with damaged grids and missing rods to be loaded in the damaged fuel assembly locations.

The most reactive damaged fuel assembly configuration is based on a 10x10 lattice with optimum pitch and 95 fueled rods.

T.6.4.1 Calculational Method

T.6.4.1.1 Computer Codes

The CSAS25 control module of SCALE-4.4 [6.1] was used to calculate the effective multiplication factor (k_{eff}) of the fuel in the cask. The CSAS25 control module allows simplified data input to the functional modules BONAMI-S, NITAWL-S, and KENO V.a. These modules process the required cross sections and calculate the k_{eff} of the system. BONAMI-S performs resonance self-shielding calculations for nuclides that have Bondarenko data associated with their cross sections. NITAWL-S applies a Nordheim resonance self-shielding correction to nuclides having resonance parameters. Finally, KENO V.a calculates the k_{eff} of a three-dimensional system. A sufficiently large number of neutron histories are run so that the standard deviation is below 0.0016 for all calculations.

Validation and verification of the SCALE 4.4 computer system were performed. Criticality benchmarking calculations were performed.

T.6.4.1.2 Physical and Nuclear Data

The physical and nuclear data required for the criticality analysis include the fuel assembly data and cross-section data as described below.

Table T.6-3 lists the pertinent data for criticality analysis with the GE12 10x10 fuel assembly in the NUHOMS®-61BTH DSC as loaded in a generic cask described in Section T.6.1.

The criticality analysis used the 44-group cross-section library built into the SCALE system. ORNL used ENDF/B-V data to develop this broad-group library specifically for criticality analysis of a wide variety of thermal systems.

T.6.4.1.3 Bases and Assumptions

The analytical results reported in Section T.3 demonstrate that the cask containment boundary and canister basket structure do not experience any significant distortion under hypothetical accident conditions. The fuel assembly drop analyses documented in Section T.3-5 also demonstrate that the fuel rods do not experience any deformation significant to cause a change in the fuel geometry. Therefore, for both normal and hypothetical accident conditions the cask geometry is identical except for the neutron shield and skin. As discussed above, the neutron shield and skin are conservatively modeled as water.

The cask was modeled with KENO V.a using the permissible geometry options. These options allow a model to be constructed with regular geometric shapes and define the material

boundaries. No cases have been made to model the fuel assemblies with fission products, burnable absorbers, or radial and axial variations in the initial fuel enrichment. Instead, fuel assemblies have been modeled as unirradiated fuel with a uniform enrichment. This results in a very large margin of conservatism in the calculated k_{eff}.

The following conservative assumptions were also incorporated into the criticality calculations:

1. Omission of grid plates, spacers, and hardware in the fuel assembly.

2. Unirradiated fuel - no credit taken for fissile depletion, fission product poisoning or burnable absorbers.

3. For intact fuel, the pins are modeled assuming a lattice average uniform enrichment everywhere in the lattice. Natural Uranium blankets, Gadolinia, Integral Fuel Burnable Absorber (IFBA), Erbia or any other burnable absorber rods and axial or radial enrichment zones are modeled as enriched Uranium, uniform everywhere.

4. All fuel rods are assumed to be filled with 100% pure water in the fuel/cladding gap to account for the possibility of water being entrained in the fuel pin and because it has a slight positive effect on reactivity.

5. The fuel pellet stack was conservatively modeled at 96.5% of theoretical density with no allowance for dishing or chamfer.

6. Water density at optimum internal and external moderator density.

7. Only the active fuel length of each assembly type is explicitly modeled. The presence of the plenum, end fittings, and channels above and below the active fuel reduce the k_{eff} of the system; therefore, these regions are modeled as water or the reflective boundary conditions. For the cases with reflective boundary condition, the model is effectively infinitely long. For intact fuel the active fuel region is conservatively assumed to start level with the bottom of the poison plates even though the fixed poison spans the entire length of the basket.

8. For all of the transportation Hypothetical Accident Conditions (HAC) cases the neutron shield and stainless steel skin of the cask assumed to be replaced with external moderator.

9. The least material condition (LMC) is assumed for the fuel compartment, poison plates and wrappers. This minimizes neutron absorption in the steel sheets and poison plates.

10. The maximum allowed gap between the poison plates in the worst case position is explicitly modeled to maximize k_{eff}.

11. Impact limiters on the cask ends are not included because they have negligible effect on the k_{eff} of the system.

12. Temperature at 20°C (293K).

13. All zirconium based materials in the fuel are modeled as Zircalloy-2. The small differences in the composition of the various clad / tube / channel materials have no effect on the results of the calculation.

14. In calculating the equivalent diameter of the water holes at the basket periphery, it is assumed that the volume of the aluminum and stainless steel in the R45 rails is not greater than 56,000 in^3 against the current value of 46,608 in^3.

15. For damaged fuel, the lattice average enrichment is modeled as uniform throughout the entire fuel assembly except for the "damaged" face rods (for the single and double shear cases) which are modeled with the maximum peak pellet enrichment.

16. The cask containment boundary does not experience any significant distortion under hypothetical accident conditions.

17. The worst case gross damage resulting from a cask-drop accident is assumed to be either a single-ended or double-ended rod shear with flooding in pure water. A maximum of 12.5 inches of fuel may be uncovered by the poison plates due to shifting of the sheared rods.

18. The single-ended fuel rod shear cases assume that fuel rods that form one fuel assembly face shear in one place and are displaced to new locations. The fuel pellets are conservatively assumed to remain in the fuel rods.

19. The double-ended fuel rod shear cases assume that the fuel rods that form one fuel assembly face shear in two places and the intact fuel rod pieces are separated from the parent fuel rods.

20. For damaged fuel that contains bent or bowed fuel rods assume that the fuel is intact but that the rod pitch is allowed to vary from its nominal fuel rod pitch.

T.6.4.1.4 Determination of k_{eff}

The criticality calculations were performed with the CSAS25 control module in SCALE-4.4. The Monte Carlo calculations performed with CSAS25 (KENO V.a) used a flat neutron starting distribution. The total number of histories traced for each calculation was approximately 500,000. This number of histories was sufficient for the source to converge and produce standard deviations of around 0.0016 or less in Δk_{eff} units. The maximum k_{eff} for the calculation was determined with the following formula:

$$k_{eff} = k_{KENO} + 2\sigma_{KENO.}$$

T.6.4.2 Fuel Loading Optimization

All fuel lattices with and without channels, listed in Table T.6-3 are qualified to be stored in the 61BTH DSC as intact fuel if they are not damaged. In addition, lattices containing reconstituted rods (lower enriched fuel rods, stainless steel / zircalloy / aluminum rods) or non-fuel rods that displace the same amount of water are conservatively considered intact assemblies. Short loading of the DSC is permitted (empty locations or locations containing dummy fuel assemblies) and is not analyzed here since that configuration will result in a reduction in the system k_{eff}.

A. Determination of the Most Reactive Fuel Lattice

All fuel lattices, with and without channels, listed in Table T.6-3 are evaluated to determine the most reactive fuel assembly type. The lattices are analyzed with water in the fuel pellet cladding annulus and are centered in the fuel compartments. Each lattice is also analyzed with a 0.065, 0.080 and 0.120 inch thick channel to determine the most reactive configuration. The presence of fuel channels in general should reduce reactivity because the un-channeled fuel/canister combination is under-moderated. The results show that the reactivity change due to the fuel channels is within the statistical uncertainty of the KENO V.a calculations. Finally, this model is used to demonstrate that the use of lattice average enrichment is conservative. Several cases are run to demonstrate that the use of the lattice average enrichment is conservative for intact fuel. Appendix K, Section K.6.6.2 includes a more detailed description of these models.

For this analysis, only the canister is modeled. The canister is modeled over the active fuel height of the fuel with water reflectors at the ends (z) and reflective boundary conditions outside the canister (infinite array in the x-y directions). The canister model for this evaluation differs from the actual design in the following ways:

- Type 1 DSC basket design is utilized since these are relative reactivity calculations and basket design has no impact.
- No gaps between poison plates are modeled.
- Stainless steel basket rails, which hold the basket together, are modeled as water

In all other respects, the model is the same as the first model described in Section T.6.3.1. The sole purpose of this model is to determine the relative reactivity of different fuel lattices in a configuration similar to the actual canister. The model is more fully discussed in Appendix K, Section K.6.6.2.

These calculations are carried out with an enrichment of 4.4 wt. % U-235, a fixed poison loading of 36.0 mg B-10/cm^2 and a poison plate (poison is modeled as a single plate) thickness of 0.310".

Calculations were also carried out for the GE 8x8 fuel assembly design to qualify fuel with non-standard (lesser) number of fuel rods, particularly the GE 4 lattice with 59 fueled rods. The normal GE 4 fuel assembly has 63 fueled rods. These results are included in Table T.6-6 and show that the GE 4 fuel assembly can be loaded with a minimum of 58 fueled rods. The arrangement of the fuel rods within the lattice in these evaluations is based on expected maximum reactivity. Representative, reactive variations are analyzed in order to verify

conclusions about relative reactivity. Above all, the limit of 58 fueled rods (and 6 water rods) was arrived at so that the k_{eff} of this analyzed configuration is at least 3σ below the most reactive GE 10x10 fuel lattice.

A typical input file is included in Appendix K, Section K.6.6.2. The results of these calculations are listed in Table T.6-6. The most reactive fuel lattice evaluated for the canister design is the GE 10x10, without a fuel channel.

B. Determination of the Most Reactive Configuration – Intact Fuel

The fuel-loading configuration of the canister/cask affects the reactivity of the package. Several series of analyses determined the most reactive configuration for the canister/cask.

For this analysis, the canister/cask is modeled over the active fuel height of the fuel assembly with reflective boundary conditions on all sides of the model. This represents an infinite array in the x-y direction of canister/casks that are infinite in length. The canister/cask model for this evaluation differs from the actual design in the following ways:

- the B-10 absorber loading in the poison plates is lower than specified,
- maximum gaps between poison plates are modeled in their worst case configuration,
- the stainless steel rails which hold the Type 1 DSC basket together are modeled as water,
- the rail structure for the Type 2 DSC basket are modeled using solid aluminum with water holes at the eight corner locations, and
- the neutron shield and the skin of the cask are conservatively modeled as water.

The models are fully described in Section T.6.3.1 except for the additional considerations for paired aluminum/poison plates and the representation of the Type 2 DSC basket. These additional modeling considerations are described in this section. The purpose of these models is to determine the most reactive configuration for intact fuel assemblies.

The first series of analyses determined the most reactive fuel assembly-to-assembly pitch. The GE 10x10 fuel assembly (determined in the previous section as the most reactive fuel assembly) with a lattice average fuel enrichment of 4.4 wt. % U-235 and a poison plate boron-10 loading of 36.0 mg/cm^2 are used in the model. The results in Table T.6-7 show the most reactive configuration occurs with minimum fuel assembly-to-assembly pitch. The model is similar to the model shown in Table K.6-4 and Figure K.6-2 of Appendix K, except that the nominal fuel cell size, nominal poison sheet thickness fuel clad OD are used, and the assemblies are moved within the fuel compartment to vary the fuel assembly-to-assembly pitch.

The second set of analyses evaluates the effect of canister shell thickness on the system reactivity. The model starts with the most reactive fuel assembly-to-assembly pitch (minimum pitch) case above and the canister shell thickness is varied from 0.49 to 0.55 inches. As demonstrated by the results the variation of shell thickness within the tolerance range is statistically insignificant. The nominal shell thickness is used throughout the rest of the analysis except that one additional case is added for the most reactive canister configuration (minimum poison plate thickness and minimum fuel cell size) to demonstrate that the slightly higher result for the maximum shell thickness is indeed a result of the statistics of the calculation.

The third set of analyses evaluates the effect of poison plate thickness on the system reactivity. The model starts with the most reactive fuel assembly-to-assembly pitch (minimum pitch) case above and the poison plate thickness is modeled at 0.3 inches (minimum). The poison plate B-10 loading (volume density) is increased to account for the reduction in plate thickness to maintain the same areal density. Based on the results of this evaluation the balance of the calculations will use the minimum poison plate thickness because it represents a more reactive condition.

The fourth set of analyses evaluates the sensitivity of the system reactivity on fuel cladding OD. The model starts with the minimum poison plate case above and the assembly cladding thickness is varied from 0.404 to 0.394 inches. Based on the results of this analysis, the GE 10x10 assembly cladding is conservatively modeled as 0.010 inches less than that reported in Table T.6-3 for the balance of this evaluation because it represents a more reactive condition.

The fifth set of analyses evaluates the effect of fuel compartment internal dimension (cell width) on the system reactivity. The model starts with the most reactive fuel clad OD thickness case above and the canister fuel cell width is varied from 5.8 to 6.1 inches. The results show that the most reactive configuration is with the minimum fuel compartment width. One additional run is made to verify that the canister maximum shell thickness does not increase reactivity. The balance of this evaluation will use the minimum cell size because it represents the most reactive configuration.

The sixth set of analyses evaluates the effect of internal moderator density on reactivity. The model starts with the most reactive fuel cell width (minimum fuel cell width) case above and the internal moderator is varied from 100 to 0 percent full density. The results in Table T.6-7 show that the most reactive condition occurs at full internal moderator density.

The seventh set of analyses evaluates the effect of external moderator density on reactivity. The model uses the most reactive fuel cell width case and the most reactive internal moderator (full density) density and the external internal moderator is varied from 100 to 0 percent full density. The results in Table T.6-7 show that the system reactivity is not affected by external moderator density. The variation in the results is due entirely to the statistical uncertainties in Keno V.a. However, the optimum external moderator density will be utilized to determine the maximum k_{eff}.

All the sensitivity calculations described so far are directly obtained from Appendix K, Chapter K.6. These results are directly obtained from Appendix K, Table K.6-7.

The following additional analyses are performed to obtain the most reactive criticality configurations that include the effect of Type 2 DSC basket and paired aluminum / poison plates.

The eighth set of analyses determines the effect of poison plate modeling using paired plates of poison and aluminum on the reactivity of the system. The most reactive model from the previous calculations without the effect of external moderator density is used as a model for these calculations. This model is modified as model "V8", the only difference being the material input for the borated aluminum poison. The borated aluminum poison input to KENO is based on the specification shown in Table T.6-1 and the required loading (36 mg B-10/cm^2) is achieved by adjusting the weight fractions of the constituent elements. Paired plate modeling is effected

by changing the Units 15, 17, 18, 19, 21, 22, 24, 25, 27, 29, 31, 50, 53, 55 and 57 such that the 0.300″ poison material is modeled as 0.125″ borated aluminum poison and the remaining as aluminum. The KENO Unit 25 is split into Units 125 and 225 so that the poison and aluminum are modeled separately. Similar treatment is accorded to Units 27, 29 and 31. This parametric evaluation scoping is also extended to include Boral® material as the poison. The Boral® material is modeled based on the specification shown in Table T.6-1 for a B-10 loading of 36 mg/cm^2 and a thickness of 0.064″. The results of this evaluation demonstrate that the effect of modeling the paired plates is statistically insignificant. The results also show that the effect of the various poison plate material specifications is also statistically insignificant as long as the amount of absorber material present in the model does not change. The statistically insignificant results arising due to the variation in the thickness of the poison plates (0.300″, 0.125″ and 0.064″) and hence, the thickness of the aluminum plates indicates that there is no reactivity effect due to the modeling of cladding materials for the poison (like for Boral®). These results are shown in Table T.6-7.

The KENO model implementation of the paired plates has been effected in three ways in the same input model. For Units 15, 17, 18, 19, 21, 22 and 24 the poison in the paired plates is surrounded by aluminum. For Units 25, 27, 29 and 31 the poison and the aluminum are modeled as two distinct plates. For Units 50, 53, 55 and 57 the aluminum in the paired plates is surrounded by poison. Though the geometry in the actual basket for the paired plates is expected to be similar to what is modeled in Unit 25, this representation provides further insight to the results shown in Table T.6-7 and the conclusions herein with regard to variation in the poison plate and aluminum plate thicknesses. Therefore, treatment of paired plates does not result in any significant change in the system reactivity.

The ninth set of calculations determines the effect of basket rail modeling on the system reactivity. In order to obtain an acceptable, yet conservative model for both Type 1 and Type 2 DSC basket designs, the peripheral rails were modeled with solid aluminum and 7.5 cm (approximately 5.9″ diameter, about 15% less than the actual water volume fraction at those locations) water holes in the eight corner positions. The configuration is similar to that shown in Appendix K, Table K.6-4. The water holes (circular cross section) were also modeled using water squares to determine the effect due to the "hole" geometry. The results of this evaluation indicate that the assumption of solid aluminum rails with water holes conservatively bounds the internal moderator rails for the Type 1 DSC basket. It is also clear from the results that the use of solid aluminum as a rail material alone results in an overly conservative model. These results are shown in Table T.6-7. The water area calculations are shown in Section T.6.6.2.

Finally, minimum boron loading in the poison plate as a function of lattice average initial enrichment is evaluated. These models represent the most reactive intact fuel assembly (GE12, 10x10) with a minimum assembly-to-assembly pitch, nominal shell thickness, minimum paired plate thickness, minimum fuel clad OD, minimum fuel cell width with full internal and optimum external moderator density. Moreover, the calculational criticality analysis KENO model is also based on internal moderator gaps, paired plates with minimum poison thickness, solid aluminum rails with water holes that bounds both the Type 1 and Type 2 DSC basket designs.

The boron-10 areal density in the poison plate (and hence thickness of the poison plate) is varied to determine the maximum lattice average fuel assembly enrichment. Thus, these cases can be

used to specify the minimum boron-10 poison plate loading (and the appropriate thickness) as a function of maximum lattice average assembly enrichment. The results are reported in Table T.6-8. For selected poison plate loadings, the criticality analyses results are reported for Type 1 and Type 2 DSC baskets separately because it was necessary to maintain the same boron-10 loading and maximum lattice enrichment as determined in Appendix K. In order to ensure that there is no significant change in the results due to poison type (as discussed in earlier evaluations), some of the most reactive cases are re-run with Boral® as the poison material. These cases are modeled with slightly lower poison loading so that appropriate conclusions can be drawn for the applicability of these results for all cases. One case with MMC is also analyzed. It may be noted that since the MMC poison material composition is similar to that of Boral® poison, additional runs with this poison for other thicknesses are not necessary.

The most reactive case is modified to model the paired plates "correctly" to determine if there is any significant variation due to poison material distribution within the basket. A comparison of the results indicates that the paired plate geometry as implemented in the design basis KENO model is adequate.

The Type 1 DSC basket is modeled similarly to the bounding model described above except that the rail material is based on internal moderator and not aluminum with water holes.

The dry case k_{eff} results for intact fuel are shown in Table T.6-8. The dry k_{eff} calculations were not performed for all the enrichment types but only for the most reactive fuel enrichment. This is done due to the assertion that the most reactive optimum moderator density configuration is most likely to yield the most reactive dry configuration and that the differences in reactivity at dry conditions are insignificant. The dry case k_{eff} result for shielding analysis to determine the sub-critical multiplication factor at an enrichment of 2.6 wt. % U-235 is also shown in Table T.6-8.

The KENO input file for the most reactive intact assembly case is listed in Section T.6.6.4.

C. Determination of the Most Reactive Configuration – Damaged Fuel

This section determines the most reactive configuration for the damaged fuel. This evaluation includes sensitivity calculations to determine the most reactive damaged fuel model with 7x7 and 8x8 lattices and then, subsequently, to determine the most reactive fuel assembly design. All the discussion and results for the 7x7 and 8x8 models (Case 1 through Case 17) are directly from Appendix K, Section K.6.6.3.

Five damaged fuel configurations are evaluated using two assembly arrays, 7x7 and 8x8, to demonstrate that a fuel assembly with up to seven fuel rods with gross cladding damage and a peak pellet enrichment of 4.4 wt. % U-235 and a lattice average of 4.0 wt. % U-235 will remain subcritical under all conditions of transfer and storage. These models evaluate the effects of radial movement of fuel rod pieces (the result of "single-ended" breaks), and axial movement (the result of "double-ended" breaks). The models all include water in the fuel pellet cladding annulus. Section T.6.6.3 (almost identical to Appendix K, Section K.6.6.3) includes a more detailed description of these models.

<u>GE 7x7 Array</u>: The first two models, Case 1 and Case 2, are used to demonstrate that the difference between reflective and water boundary conditions on the ends has a minimal effect on

the system reactivity. The first model, Case 1, is identical to the model used to determine the most reactive configuration for intact fuel, except that 1) the GE12 10x10 assembly is replaced with the GE 7x7 assembly, and 2) the fuel material is changed from 4.4 wt. % U-235 to 4.0 wt. % U-235 except for the "failed" face row, which is still modeled as 4.4 wt. % U-235. The second model, Case 2, is identical to Case 1 except that the axial boundary conditions are changed from reflective to water. This demonstrates that changing the axial boundary conditions has little, if any effect on the calculated k_{eff}. Cases 4 and 6 determine the effect of moving a single row of seven fuel rods away from the remaining portion of the fuel assembly. As expected, reactivity increases slightly (<1% in k_{eff}) by moving the fuel rods away. Case 8 demonstrates that the most reactive configuration is when the seven fuel rods break in two and move next to the balance of the assembly. Case 8 is extremely conservative in that an entire extra row of fuel is added to the model. Therefore, this case more than bounds the reactivity increase that can possibly occur due to seven fuel rods breaking in two during the postulated accident. Also, note that this "extra" row of fuel rods completely fills the fuel compartment, thereby limiting the number of rods that can move within the fuel compartment.

Another set of runs was performed to determine the effect of sliding the "failed" row of fuel up 12.5 inches above the top of the poison plates. These models are identical to the other models except the model is 12.5 in. longer with the "failed" fuel extended above the poison.

GE 8x8 Array: The GE 8x8 array utilized herein is expected to bound all 8x8 arrays for these evaluations. Case 10 is identical to Case 2 except that the GE 8x8 replaces the GE 7x7 assembly. Cases 12 and 14 determine the effect of moving a single row of eight fuel rods away from the remaining portion of the fuel assembly. As expected the reactivity of the GE 8x8 is unaffected by moving the fuel rods away because the water holes in the center of the assembly control the reactivity of the assembly. Case 16 demonstrates that the most reactive configuration is when the eight fuel rods break in two and move next to the balance of the assembly. Case 16 is extremely conservative in that an entire extra row of fuel is added to the model. Therefore, this case more than bounds the reactivity increase that can possibly occur due to eight fuel rods breaking in two during the postulated accident. Also, note that this "extra" row of fuel rods completely fills the fuel compartment, thereby limiting the number of rods that can move within the fuel compartment.

Finally, as with the 7x7 array, a set of runs was performed to determine the effect of sliding the "failed" row of fuel up 12.5 inches above the top of the poison plates. These models are identical to the other models except the model is 12.5 in. longer with the "failed" fuel extended above the poison.

For all of the cases above, both the cask and DSC are modeled in the radial direction. The cask and DSC are modeled over the active fuel height of the fuel with water reflectors at the ends (z) and reflective boundary conditions outside the DSC (infinite array in the x-y directions). The DSC model for this evaluation differs from the actual design additionally in the following ways:

- Only 90% credit for poison plates made of a Boron-Aluminum alloy or MMC and 75% credit for poison plates made with Boral® is taken for the B10 content in the poison plates.

- Maximum gaps between poison plates are modeled in their worst case configuration.
- The stainless steel basket rails which hold the Type 1 DSC basket together are modeled as water.
- The rail structures for the Type 2 DSC basket are modeled using solid aluminum with water holes at the eight corner locations.
- Unit 84, and associated arrays and units, are added to model the "uncovered" row of fuel above the poison plates.

In all other respects, the model is the same as that described in Sections T.6.3.1 and T.6.3.2. The model is more fully discussed in Section T.6.6.3.

A typical input file is included in Appendix K, Section K.6.6.3.

The results of the sensitivity calculations shown in Appendix K, Chapter K.6, Table K.6-8 and Table K.6-9 for 7x7 and 8x8 fuel designs indicate that the most reactive configuration is based on the double-ended shear with a conservative addition of an extra row or rods for the entire fuel length. This configuration, together with the "UP" model that includes a 12.5″ un-covering of the poison for this extra row of rods, forms the most reactive configuration. Note that the implementation of the "UP" configuration in the KENO model is done by adding the 12.5″ row of rods at the bottom of the fuel. There is no difference between adding the 12.5″ of fuel above or below the remainder of the fuel.

An additional modeling consideration in the damaged assembly KENO model is the treatment of the additional lattice. The "Dancoff" factor, an input parameter, is required to describe all additional fuel lattices in the input model. In the intact assembly calculations, only one fuel lattice is described in the model and therefore, KENO calculates all the required parameters for this lattice. In the damaged assembly model, two lattices are described, the intact fuel lattice and the damaged fuel lattice. The "Dancoff" factor for the damaged fuel lattice is a required input to the KENO model. This factor is a strong function of the internal moderator density. Since, most of the calculations are performed with full internal moderator density, only one value of the "Dancoff" factor is used for most of the damaged assembly calculations. This value, 2.6461172E-01, is obtained from the output files of the intact calculations.

The next set of calculations determine the most reactive damaged fuel assembly design and the most reactive damaged configuration for both the Type 1 and Type 2 DSC basket designs. The starting models for this set of calculations are based on Cases 16 and 17 listed in Appendix K, Table K.6-9. The most case reactive intact 9x9 assembly design is the Siemens QFA fuel assembly. The relevant KENO case ID numbers are 18, 19. The most reactive intact 10x10 assembly design is the GE12 (GE14) 10x10 assembly; the relevant KENO case ID numbers for these calculations are 20, 21. The results of these calculations are shown in Table T.6-9. The results indicate that the most reactive damaged assembly is the GE 10x10 fuel assembly (also the most reactive intact fuel assembly) and the most reactive damaged rod configuration is the double-shear with 12.5″-rod movement ("UP" model) above the poison.

The next series of damaged fuel analyses involves a study on the effect of the fuel rod pitch on the system reactivity. The rod pitch study is carried out for the four lattice designs - 7x7, 8x8, 9x9 and 10x10. KENO models with rod pitches ranging from a minimum (based on the rod OD) and a maximum bounded by the fuel compartment ID are created and analyzed. All models assume 100% internal and external moderator density, 100% moderator flooded fuel-cladding gap and specular radial and water axial boundary conditions. All these calculations for each lattice were carried out assuming that all of the lattice positions were occupied by fuel rods.

Once the most reactive pitch was determined, a series of calculations were performed that subtracted fuel rods from the base assembly to ensure that the limiting fuel assembly geometry was determined. The removal of fuel rods was restricted to those in the interior locations of the four lattice designs. The selection of the rod loading patterns is aimed at maximizing the reactivity and those that are investigated are representative. It is concluded that the reactivities of other cases (not investigated) with the same number of rods but with different loading patterns are within statistical uncertainty. Sufficient rods were removed from these lattices to ensure that the optimum rod configuration is determined and also to ensure that further removal of rods would only result in a lower k_{eff}.

All the fuel rod pitch and rod removal cases are analyzed utilizing the base models shown in Appendix K, Table K.6-4. The rod pitch variation is carried out for all the bound lattices for the 61BTH DSC. A lattice average enrichment of 4.4 wt. % was utilized in these models. The results of these evaluations are used to determine the most reactive damaged rod configuration with optimum pitch and are not to be compared to USL since such a configuration (61 damaged assemblies) will not be authorized. Moreover, most of these results show a k_{eff} value that is much greater than the USL indicating that these results shall only be utilized to perform a *relative reactivity* comparison. The results of these calculations are shown in Table T.6-10 and demonstrate that the most reactive configuration is based on the GE 12 10x10 lattice at maximum pitch (0.600") containing 95 fueled rods. These calculations are done to qualify fuel assemblies with missing rods as damaged without any limits on the number of missing rods.

The next series of calculations determine the effect of the material composition within the DSC, excluding the damaged assembly locations, for Unit 84 in the model (the shifted zone). These calculations also determine the most reactive damaged assembly configuration to be utilized in the design basis criticality calculations. The most reactive damaged configurations determined from the previous set of calculations are utilized as the starting models for this evaluation. Both the double shear with the "UP" model and the optimum pitch (10x10, 95 rod) models are modified so that reactivity comparisons of these two limiting damaged assembly mechanisms can be made directly. The fuel assemblies were modeled with a uniform lattice average enrichment of 4.4 wt. % U-235 while the damaged rods (for the double ended shear case) were modeled with a peak pellet enrichment of 4.6 wt. % U-235. For the optimum pitch cases, the damaged assemblies were modeled with a uniform lattice average enrichment of 4.4 wt. % U-235. The cases for this evaluation are Case 22 (for Type 1 DSC) and Case 23 (for Type 2 DSC) and are identical to Case 21 except the change in the fuel enrichment and density. The evaluation is performed with both water and aluminum (Cases 24, 25 for Type 2) as the material surrounding the damaged assemblies in the shifted region. The results of the evaluation, shown in Table T.6-11, indicate that there is statistically insignificant effect due to material composition. Further discussion of the KENO models is provided in Section T.6.6.3.

One important difference between the design basis intact assembly models and the damaged assembly models is in the treatment of axial boundary conditions. In the intact assembly models, the axial boundary conditions are reflective and therefore, the fuel assembly length was essentially infinite axially (conservative modeling). In the case of the damaged assembly models, a fuel assembly active length of 144″ was utilized with an additional 12.5″ of shifted damaged row of rods and water boundary conditions axially. The active fuel length of the GE 10x10 assembly is 150″ and even though it is expected to contain at least 6″ length of blankets, it is necessary to evaluate the effect of an increase in the active fuel length, if any, on the system reactivity.

Case ID 25 was modified to create the Case ID 26 where the active fuel length was increased to 150″. These results are also shown in Table T.6-11 and indicate that there is no significant change in the system reactivity due to the modeling of shorter active fuel length.

Case ID 23 was modified to create Case ID 27 where the outermost damaged rows of rods was modeled without cladding (clad replaced with internal moderator). This configuration is expected to result in an increase in k_{eff} because of the fact that fuel assemblies, in general, are undermoderated. Therefore, increasing the moderation by replacing the clad with moderator will result in an increase in k_{eff}. Variations to the above case included modeling the two outermost rows of rods with bare fuel, Case ID 28. The results of these cases are also shown in Table T.6-11. The most reactive configuration for the double shear cases is based on the Case ID 28, as expected, since it contains more bare rods.

The optimum rod pitch case, Case ID 29, was based on a modification to Case ID 23 except that there was no "UP" modeling included in the model. The "Dancoff" factor to be used to describe the damaged lattice is obtained from the rod array cases documented in Table T.6-10. A comparison of the k_{eff} obtained from this case, also shown in Table T.6-11, with the design basis double shear case from the previous evaluation (Case ID 28) clearly shows that the worst case damaged assembly configuration is based on the optimum rod pitch model.

Finally, minimum boron loading in the poison plate as a function of lattice average initial enrichment is evaluated. These models represent the DSC with the most reactive damaged fuel assemblies (GE12, 10x10, optimum pitch, 95 rods) for both the 4 and 16 assembly loading configurations with the most reactive configuration determined in the previous analyses. The remaining locations are loaded with the most reactive intact fuel assembly (GE12, 10x10) with the most reactive configuration determined in Section T.6.4.2B. The calculational criticality analysis KENO model is also based on internal moderator gaps, paired plates with minimum poison thickness, solid aluminum rails with water holes that bounds both the Type 1 and Type 2 DSC basket designs. Above all, all the damaged assembly criticality models for the paired plates are based on the "correct" arrangement (as described at the end of Section T.6.4.2B) of these plates. All the damaged assembly calculations are carried out with the borated aluminum poison.

A sensitivity calculation was performed to determine the effect of the specification of the second lattice or the "Dancoff" factor in the criticality analyses. This is due to the fact that both the intact and damaged fuel assemblies can be specified as the second lattice. The "Dancoff" factor for the intact fuel assemblies is 2.6461172E-01 while that for the damaged fuel assemblies is 1.4377643E-01.

In addition, sensitivity calculations are performed to determine the most reactive position for the twelve intact assemblies that are adjacent to the damaged assemblies for the 4-damaged assembly configuration in the DSC. There are three different positions involved– intact fuel centered in their respective compartment, intact fuel in an inward arrangement with respect to the center of the DSC, and intact fuel in an outward arrangement such that they are closest to each other within the 2x2 array of fuel compartments. All three arrangements are also evaluated for the effect of the second lattice specification as described above. These calculations are carried out with both the intact and damaged assemblies at an initial enrichment of 5.00 wt. % U-235 with the poison plate modeled with a thickness of 0.199″ and a B-10 loading of 56.2 mg/cm^2.

The results of these calculations are also shown in Table T.6-11 and indicate that the centered arrangement of the 12 intact fuel assemblies together with the intact fuel being specified as the second lattice results in the most reactive configuration for the 4-damaged assembly configuration. For the configuration with 16 damaged assemblies, the damaged lattice is specified as the second lattice since this configuration is more close to the "inward" configuration which does not show any variation with the second lattice specification.

The fuel initial lattice average enrichment is varied as well as the boron-10 density and thickness in the poison plates. The results are reported in Table T.6-12 for the 4-damaged assembly loading configuration and Table T.6-13 for the 16-damaged assembly loading configuration. For certain poison plate loadings, the criticality analyses results are reported for Type 1 and Type 2 DSC baskets separately to determine the required boron loadings. An active fuel length of 154″ was utilized in the damaged assembly calculations.

The dry case calculations are performed for the most reactive initial enrichment / poison plate loading combination. The case selected for performing the dry calculations is based on the most reactive fully flooded case (100% internal and external moderator density). For the dry cases, which include evaluation at different moderator densities, the "Dancoff" factors are obtained from the corresponding intact assembly KENO calculations.

The Type 1 DSC basket is modeled similar to the bounding model described above except that the rail material is based on internal moderator and not aluminum with water holes. The dry case k_{eff} results for damaged fuel are also shown in Table T.6-12. The KENO input files for the most reactive damaged assembly case are listed in Section **Error! Reference source not found.**.

T.6.4.3 Criticality Results

Table T.6-14 lists the results as applicable to the various storage conditions.

The criterion for subcriticality is that

$$k_{KENO} + 2\sigma_{KENO} < USL,$$

where USL is the upper subcritical limit established by an analysis of benchmark criticality experiments. From Section T.6.5, the minimum USL over the parameter range (in this case, pitch) is 0.9415. From Table T.6-14, for the most reactive case,

$$k_{KENO} + 2\sigma_{KENO} = 0.9376 + 2\ (0.0012) = 0.9400 < 0.9415.$$

T.6.5 Critical Benchmark Experiments

The criticality safety analysis of the NUHOMS®-61BTH system used the CSAS25 module of the SCALE system of codes. The CSAS25 control module allows simplified data input to the functional modules BONAMI-S, NITAWL-S, and KENO V.a. These modules process the required cross-section data and calculate the k_{eff} of the system. BONAMI-S performs resonance self-shielding calculations for nuclides that have Bondarenko data associated with their cross sections. NITAWL-S applies a Nordheim resonance self-shielding correction to nuclides having resonance parameters. Finally, KENO V.a calculates the effective neutron multiplication (k_{eff}) of a 3-D system.

The analysis presented herein uses the fresh fuel assumption for criticality analysis. The analysis employed the 44-group ENDF/B-V cross-section library because it has a small bias, as determined by 125 benchmark calculations. The upper safety limit (USL-1) was determined using the results of these 125 benchmark calculations. All the calculations are based on the Windows NT system. The verification and validation performed on the SCALE code system in Windows XP environment is documented. A similar criticality benchmark analysis for BWR fuel is documented and is performed in the Windows XP system. The results demonstrate that CSAS25 produces essentially identical results and exhibits no significant bias due to operating system. Therefore, the benchmark results can be utilized in this calculation although all the design basis calculations are performed in the Windows XP system.

The benchmark problems used to perform this verification are representative of benchmark arrays of commercial light water reactor (LWR) fuels with the following characteristics:

(1) water moderation

(2) boron neutron absorbers

(3) unirradiated light water reactor type fuel (no fission products or "burnup credit") near room temperature (vs. reactor operating temperature)

(4) close reflection

(5) Uranium Oxide.

The 125 uranium oxide experiments were chosen to model a wide range of uranium enrichments, fuel pin pitches, assembly separation, fixed neutron absorbers in order to test the ability of the code to accurately calculate k_{eff}.

T.6.5.1 Benchmark Experiments and Applicability

A summary of all of the pertinent parameters for each experiment is included in Table T.6-15 along with the results of each run. The best correlation is observed for fuel assembly separation distance with a correlation of 0.65. All other parameters show much lower correlation ratios indicating no real correlation. All parameters were evaluated for trends and to determine the most conservative USL.

The Upper Subcritical Limit (USL) is calculated in accordance with NUREG/CR-6361 [6.4]. USL Method 1 (USL-1) applies a statistical calculation of the bias and its uncertainty plus an administrative margin (0.05) to the linear fit of results of the experimental benchmark data. The basis for the administrative margin is from Reference [6.5]. Results from the USL evaluation are presented in Table T.6-16.

The criticality evaluation used the same cross section set, fuel materials and similar material/geometry options that were used in the 125 benchmark calculations as shown in Table T.6-15. The modeling techniques and the applicable parameters listed in Table T.6-17 for the actual criticality evaluations fall within the range of those addressed by the benchmarks in Table T.6-15.

T.6.5.2 Results of the Benchmark Calculations

The results from the comparisons of physical parameters of each of the fuel assembly types to the applicable USL value are presented in Table T.6-17. The minimum value of the USL was determined to be 0.9415 based on comparisons to the limiting assembly parameters as shown in Table T.6-17.

T.6.6 Appendix

T.6.6.1 References

6.1 Oak Ridge National Laboratory, RSIC Computer Code Collection, "SCALE: A Modular Code System for Performing Standardized Computer Analysis for Licensing Evaluations for Workstations and Personal Computers," NUREG/CR-0200, Revision 6, ORNL/NUREG/CSD-2/V2/R6.

6.2 Not used.

6.3 Not used.

6.4 U.S. Nuclear Regulatory Commission, "Criticality Benchmark Guide for Light-Water-Reactor fuel in Transportation and Storage Packages," NUREG/CR-6361, Published March 1997, ORNL/TM-13211.

6.5 U.S. Nuclear Regulatory Commission, "Recommendations for Preparing the Criticality Safety Evaluation of Transportation Packages," NUREG/CR-5661, Published April 1997, ORNL/TM-11936.

T.6.6.2 Calculation of Water Area at the Corner Rail Locations

The area of water at the corner rail locations (R45) is calculated in this section. This area is utilized to determine the diameter of the water holes that are used to approximate the presence of water at these locations.

Area of Stainless Steel 2 Aluminum Rails	=	32.8 in^2	
Area of Water	=	44.3 in2	
Equivalent Diameter	=	$[(44.3*4)/\pi]^{1/2}$	= 7.51″
	~	19.0 cm	

For the purpose of this analysis, a diameter of 15.0 cm is considered conservative and is utilized in the design basis criticality model. Note that it is conservative to increase the amount of aluminum and reduce the amount of water in the rails. This also implies that there is at least a 20% margin for the combined area of stainless steel and aluminum utilized in this evaluation.

T.6.6.3 Damaged Fuel Analysis

The models for the damaged fuel analysis are based on the intact fuel analysis models. Section T.6.3 provides a complete description of the intact fuel model. The following list identifies the major changes made to the intact fuel model as described in Appendix K, Figure K.6-2 and Table K.6-4.

The modeling descriptions for 7x7 and 8x8 single and double shear cases are identical to those described in Appendix K, Section K.6.6.3.

- Revised Material 1, UO_2 enrichment to 4.0 wt. % U-235.
- Added Material 10, UO_2 with an enrichment of 4.4 wt. % U-235.
- Revised the "squarepitch" card to reflect the 7x7 dimensions.
- Added "more data res=10 cylinder 0.61849 dan(10)=0.16513124 end more data" card to correctly account for resonance and rod shadow effects.
- Revised array 1 to model the 7x7 assembly rather than the 10x10.
- Revised Unit 1 to model the rod/pitch etc. for the 7x7.
- Replaced array 1 with array 42 in Units 11 and 14 to model the "damaged" fuel in the 2x2 compartments.
- Replaced array 1 with array 45 in Units 12 and 13 to model the "damaged" fuel in the 2x2 compartments.
- Revised Units 32, 33, 46 and 47 to model the rows of rods above the rest of the fuel assembly.

- Revised Units 58 and 59 to replace holes 46 and 47 with the revised 48 and 49.
- Replaced arrays 23 and 24 with arrays 2 and 3 in Units 61 and 62 to model the damaged fuel in the 2x2 compartments above the rest of the assemblies.
- Revised Unit 79 to replace holes 75 and 76 with the revised 77 and 78.
- Moved Unit 82 to Unit 83.
- Deleted the old Unit 81 (water space for the 10x10 assembly).
- Added Units 81 and 85 to model the row of displaced rods. This unit contains the same materials and geometry as Unit 1, except that the fuel uses material 10 (higher enrichment) and the water cuboid dimensions are adjusted to account for pin spacing.
- Added Unit 82 to model the water spaces next to the moved row of fuel in the array.
- Added Unit 84 to model the portion of the canister/cask with the moved rows of damaged fuel rods. (See Appendix K, Figure K.6-8 for cross section of this unit.)
- Arrays 2 through 5, 18, 19, 23, 24, 26, 26, 37, 38, 40 and 41 are revised to model to account for the displaced rods for the single break or to insert the extra row of fuel for the double break cases.
- Arrays 42 through 45 are added to model the "damaged" fuel assemblies for use in the units, which define the "damaged" fuel cells.
- Finally, array 21 is modified to add 50 Unit 79's to the front of the array, (12.5 inches uncovered fuel) to model the "damaged" rods which can move above the top of the poison plates for the "UP" cases.

Appendix K, Figure K.6-6 is a cross section of Single Break case. This case models the maximum separation between the sheared rods and remaining assembly. Figure K.6-7 is a cross section of Double Break case. Figure K.6-8 is a cross section of the Single Break case through Unit 79. Figure K.6-9 is a cross section of the Double Break case through Unit 79.

Finally, Figure T.6-4 is a cross section of the Double Break case through Unit 84 with aluminum surrounding the damaged fuel.

Modifications to the KENO models to produce the optimum rod pitch models were minor. Most of the changes to the models were confined to describe the damaged assembly (Units 100 through 108, array 42) and the location (Unit 111, Units 132 – 135, Units 161 – 164, and the associated arrays). The location modifications were done only for the 4 damaged-assembly configuration. Figure T.6-5 is a cross section plot of the design basis KENO criticality model with 4 damaged assemblies. Figure T.6-6 is a cross section plot of the design basis KENO criticality model with 16 damaged assemblies.

T.6.6.4 CSAS25 Input Deck for Design Basis Intact Fuel Assembly Case

Priority Information withheld under 10CFR2.390

Priority Information withheld under 10CFR2.390

Priority Information withheld under 10CFR2.390

Priority Information withheld under 10CFR2.390

Priority Information withheld under 10CFR2.390

Priority Information withheld under 10CFR2.390

Priority Information withheld under 10CFR2.390

Priority Information withheld under 10CFR2.390

Priority Information withheld under 10CFR2.390

Priority Information withheld under 10CFR2.390

Priority Information withheld under 10CFR2.390

Priority Information withheld under 10CFR2.390

Priority Information withheld under 10CFR2.390

Priority Information withheld under 10CFR2.390

Priority Information withheld under 10CFR2.390

Priority Information withheld under 10CFR2.390

Priority Information withheld under 10CFR2.390

Priority Information withheld under 10CFR2.390

Priority Information withheld under 10CFR2.390

Priority Information withheld under 10CFR2.390

Priority Information withheld under 10CFR2.390

Priority Information withheld under 10CFR2.390

Priority Information withheld under 10CFR2.390

Priority Information withheld under 10CFR2.390

Priority Information withheld under 10CFR2.390

Priority Information withheld under 10CFR2.390

Priority Information withheld under 10CFR2.390

Priority Information withheld under 10CFR2.390

Priority Information withheld under 10CFR2.390

Priority Information withheld under 10CFR2.390

Priority Information withheld under 10CFR2.390

Priority Information withheld under 10CFR2.390

Priority Information withheld under 10CFR2.390

Priority Information withheld under 10CFR2.390

Priority Information withheld under 10CFR2.390

Priority Information withheld under 10CFR2.390

Priority Information withheld under 10CFR2.390

Priority Information withheld under 10CFR2.390

Priority Information withheld under 10CFR2.390

Table T.6-1
Minimum B10 Content as a Function of Enrichment

Poison ID	Maximum Lattice Average Initial Enrichment (wt. % U-235)			Minimum B-10 Content (mg/cm^2)		
	Intact Assemblies	Up to 4 Damaged Assemblies (Corner Locations)(1)	5 or More Damaged Assemblies (Interior Locations)(1)	Utilized in this Analysis	Specified for 90% Credit	Specified for 75% Credit
Type 1 DSC						
A	3.70	3.70	2.80	18.9	21.0	25.2
B	4.10	4.10	3.10	28.8	32.0	38.4
C	4.40	4.40	3.20	36.0	40.0	48.0
D	4.60	4.60	3.40	43.2	48.0	57.6
E	4.80	4.80	3.50	49.5	55.0	66.0
F	5.00	5.00	3.60	56.2	62.4	74.9
Type 2 DSC						
A	3.70	3.70	2.80	20.1	22.3	26.8
B	4.10	4.10	3.10	28.8	32.0	38.4
C	4.40	4.40	3.20	37.5	41.7	50.0
D	4.60	4.60	3.40	43.2	48.0	57.6
E	4.80	4.80	3.50	49.5	55.0	66.0
F	5.00	5.00	3.60	56.2	62.4	74.9

(1) See Figure T.2-9 of Chapter T.2 for the locations of these assemblies in the DSC.

Table T.6-2
Authorized Contents for NUHOMS®-61BTH System

General Electric 7x7 /GE1	7x7
General Electric 7x7 /GE2	7x7
General Electric 7x7 /GE3	7x7
Exxon/ANF 7x7 /ENC III-A	7x7
Exxon/ANF 7x7 /ENC III	7x7
General Electric 8x8 /GE4	8x8
General Electric 8x8 /GE5	8x8
General Electric 8x8 /GE-Pres	8x8
General Electric 8x8 /GE-Barrier	8x8
General Electric 8x8 /GE8 Type I	8x8
General Electric 8x8 /GE8 Type II	8x8
General Electric 8x8 /GE9	8x8
General Electric 8x8 /GE10	8x8
Exxon/ANF 8x8 /ENC Va and Vb	8x8
Framatome ANP 8x8-62/2	8x8
General Electric 9x9 /GE11	9x9
General Electric 9x9 / GE13	9x9
Siemens QFA	9x9
Framatome ANP 9x9-79/2 [FANP9]	9x9
General Electric 10x10/GE12	10x10
General Electric 10x10/GE14	10x10
Framatome ANP ATRIUM-10	10x10

Table T.6-3
Parameters for BWR Assemblies for Shipment
(Part 1 of 2)

Manufacturer[1]	Array	Version	Active Fuel Length (in)	Number Fuel Rods per Assembly	Pitch (in)	Fuel Pellet OD (in)
GE	7x7	GE1	144	49	0.738	0.487
GE	7x7	GE2	144	49	0.738	0.487
GE	7x7	GE3	144	49	0.738	0.487
Exxon/ANF	7x7	ENC III-A	144	49	0.738	Note 2
Exxon/ANF	7x7	ENC III	144	48	0.738	Note 3
GE	8x8	GE4	146	63	0.640	0.416
GE	8x8	GE5	150	62	0.640	0.410
GE	8x8	GE-Pres	150	62	0.640	0.410
GE	8x8	GE-Barrier	150	62	0.640	0.410
GE	8x8	GE8 Type I	150	62	0.640	0.410
GE	8x8	GE8 Type II	150	60	0.640	0.411
GE	8x8	GE9	150	60	0.640	0.411
GE	8x8	GE10	150	60	0.640	0.411
Exxon/ANF	8x8	ENC Va and Vb	144	60	0.642	0.4195
Framatome ANP	8x8	8x8-62/2	150	62	0.641	Note 4
GE	9x9	GE11 GE13	146	14	0.566	0.376
Framatome ANP	9x9	9x9-79/2	150	79	0.572	0.3565
Siemens	9x9	QFA	145.24	72	0.569	0.3737
GE	10x10	GE12 GE14	150	92	0.510	0.345
Framatome-ANP	10x10	ATRIUM-10	150	91	0.510	0.3413

Table T.6-3
Parameters for BWR Assemblies for Shipment (Concluded)
(Part 2 of 2)

Manufacturer [1]	Array	Version	Clad Thickness (in)	Clad OD (in)	Water Rod OD[5] (in)	Water Rod ID (in)
GE	7x7	GE1	0.032	0.563	NA	NA
GE	7x7	GE2	0.032	0.563	NA	NA
GE	7x7	GE3	0.032	0.563	NA	NA
Exxon/ANF	7x7	ENC III-A	0.0355[5]	0.570	NA	NA
Exxon/ANF	7x7	ENC III	0.0355[5]	0.570	0.572[6]	NA
GE	8x8	GE4	0.034	0.493	0.493	0.425
GE	8x8	GE5	0.032	0.483	0.591	0.531
GE	8x8	GE-Pres	0.032	0.483	0.591	0.531
GE	8x8	GE-Barrier	0.032	0.483	0.591	0.531
GE	8x8	GE8 Type I	0.032	0.483	0.591	0.531
GE	8x8	GE8 Type II	0.032	0.483	2@0.591 2@0.483	2@0.531 2@0.419
GE	8x8	GE9	0.032	0.483	1.34	1.26
GE	8x8	GE10	0.032	0.483	1.34	1.26
Exxon/ANF	8x8	ENC Va and Vb	0.036	0.5015	0.5015[6]	NA
Framatome-ANP	8x8	8x8-62/2	0.035	0.484	0.484	0.414
GE	9x9	GE11	0.028	0.440	0.98	0.92
GE	9x9	GE13	0.028	0.440	0.98	0.92
Framatome-ANP	9x9	9x9-79/2	0.030	0.424	0.425	0.364
Siemens	9x9	QFA	0.0262	0.433	1.516[7]	1.458
GE	10x10	GE12	0.026	0.404	0.98	0.92
GE	10x10	GE14	0.026	0.404	0.98	0.92
Framatome-ANP	10x10	ATRIUM-10	0.0239	0.3957	1.378[7]	1.321

Notes:
(1) Reload fuel from other manufacturers with these parameters are also acceptable.
(2) Variable Fuel Pellet OD – evaluated from 0.468 to 0.488 in same assembly.
(3) Variable Fuel Pellet OD – evaluated from 0.468 to 0.491 in same assembly.
(4) Variable Fuel Pellet OD – evaluated from 0.4045 to 0.4055 in same assembly.
(5) Water rods for some fuel designs occupy more than one lattice position. Therefore, the number of water pin positions can be determined by subtracting the number of fuel rods from the total number of lattice positions for the array. As an example, the GE 10x10 fuel assembly has two water rods that occupy eight pin positions.
(6) Variable Fuel Clad Thickness – Thinnest clad thickness listed and conservatively used in the analysis.
(7) Solid Zirc rod(s)
(8) The water rod is more like a water box occupying 9 pin positions (3x3 pin array) and the ID and OD refer to Inside and Outside Dimensions of the box.

Table T.6-4
Summary of Criticality Analyses

Description of Evaluation	Summary of Analyses	Reference
Determine the most reactive intact fuel assembly design	Reactivity of various GE, and Exxon (7x7 and 8x8) fuel assemblies are compared.	Appendix K, Chapter K.6
	Reactivity of the Framatome-ANP 8x8, 9x9, Siemens QFA and Atrium 10x10 fuel assemblies are compared. In addition, the number of fuel rods for GE 8x8 assembly is varied from 63 to 54 to allow these fuel assemblies with missing rods to be treated as intact assemblies.	Chapter T.6
Determine the most reactive configuration with intact fuel assemblies	The reactivity effect of the various DSC and fuel assembly geometry and material design parameters like assembly pitch, DSC shell thickness, poison thickness, fuel cladding OD, fuel cell width, internal and external moderator density are evaluated. KENO model described in Figure K.6.2 is developed.	Appendix K, Chapter K.6
	The reactivity effects of additional parameters like paired poison / aluminum plate thicknesses and rail material modeling for Type 2 DSC basket design are evaluated. The design basis criticality analysis KENO model shown in Figure T.6-3 for intact assemblies is developed.	Chapter T.6
Intact assembly criticality analyses	Using the design basis KENO model the lattice average enrichment of intact fuel assemblies as a function of fixed poison loading is determined.	Chapter T.6
Determine the most reactive damaged assembly mechanism and configuration	Reactivity of various postulated damaged assembly mechanisms for 7x7 and 8x8 fuel assemblies are compared using a minor modification to the KENO model described in Appendix K, Section K.6.6.3.	Appendix K, Chapter K.6
	The reactivity of the double shear mechanism for Siemens 9x9 QFA and the GE 10x10 fuel assemblies are compared using the KENO model described in Section T.6.6.3.	Appendix T, Chapter T.6
	The fuel rod pitch is varied for all assembly classes to determine the optimum pitch for each design. Additionally, rods are removed to determine the most reactive rod loading pattern within a lattice. This will determine the most reactive fuel assembly configuration for the rod pitch mechanism.	Appendix T, Chapter T.6
	The reactivity effect due the presence of material surrounding the sheared row of rods is determined. The maximum reactivity using the 16 damaged assembly configurations with double shear and rod pitch mechanisms are compared. The design basis criticality analysis KENO model for damaged assemblies is developed by synthesizing the KENO model geometries developed for most reactive intact configuration (basket and intact fuel) and the most reactive damaged configuration (rod pitch).	Appendix T, Chapter T.6
Damaged assembly criticality analyses	Using the design basis KENO model the lattice average enrichment of damaged fuel assemblies as a function of fixed poison loading for the 4 and 16 damaged assembly configurations is determined.	Appendix T, Chapter T.6

Table T.6-5
Material Property Data

Material	Density g/cm^3	Element	Weight %	Atom Density (atom/b-cm)
UO_2 (Enrichment - 5.0 wt%)	10.576	U-235	4.408	1.1944E-03
		U-238	83.742	2.2406E-02
		O	11.850	4.7201E-02
UO_2 (Enrichment - 4.4 wt%)	10.576	U-235	3.879	1.0510E-03
		U-238	84.272	2.2548E-02
		O	11.849	4.7197E-02
Zircaloy-2	6.56	Zr	98.250	4.2550E-02
		Sn	1.450	4.8254E-04
		Fe	0.135	9.5501E-05
		Cr	0.100	7.5978E-05
		Ni	0.055	3.7023E-05
		Hf	0.010	2.2133E-06
Water	0.9982	H	11.1	6.6769E-02
		O	88.9	3.3385E-02
Carbon Steel	7.8212	Fe	99.0	8.3498E-02
		C	1.0	3.9250E-03
Stainless Steel (SS304)	7.94	C	0.080	3.1877E-04
		Si	1.000	1.7025E-03
		P	0.045	6.9468E-05
		Cr	19.000	1.7473E-02
		Mn	2.000	1.7407E-03
		Fe	68.375	5.8545E-02
		Ni	9.500	7.7402E-03
Lead	11.344	Pb	100	3.2969E-02
Borated Aluminum Poison (56.2 mg B-10/cm^2) (0.199″)	2.693	B-10	4.139	6.7040E-03
		B-11	0.460	6.7747E-04
		Al	95.401	5.7342E-02
Boral® Poison (37.3 mg B-10/cm^2) (0.099″)	2.450	B-10	6.060	8.9288E-03
		B-11	26.819	3.5940E-02
		C	9.123	1.1217E-02
		Al	57.999	3.1716E-02
BorTec® Poison (36.2 mg B-10/cm^2) (0.160″, MMC)	2.682	B-10	3.318	5.3526E-03
		B-11	14.686	2.1545E-02
		C	4.996	6.7244E-03
		Al	76.999	4.6092E-02

Table T.6-6
Most Reactive Fuel Type

Manufacturer	Array	Version	k_{KENO}	1σ	k_{eff}
The results shown in this part of the table are obtained directly from Appendix K, Table K.6-6.					
GE	7x7	GE2, GE3	0.9037	0.0012	0.9061
GE	7x7 0.120 channel	GE2, GE3	0.9033	0.0015	0.9063
GE	7x7 0.080 channel	GE2, GE3	0.9028	0.0012	0.9052
GE	7x7 0.065 channel	GE2, GE3	0.9043	0.0013	0.9069
Exxon/ANF	7x7	ENC III-A(1)	0.8983	0.0011	0.9005
Exxon/ANF	7x7 0.120 channel	ENC III-A(1)	0.8996	0.0013	0.9022
Exxon/ANF	7x7 0.080 channel	ENC III-A(1)	0.9007	0.0012	0.9031
Exxon/ANF	7x7 0.065 channel	ENC III-A(1)	0.8985	0.0011	0.9007
Exxon/ANF	7x7	ENC III(2)	0.8962	0.0013	0.8988
Exxon/ANF	7x7 0.120 channel	ENC III(2)	0.8971	0.0013	0.8997
Exxon/ANF	7x7 0.080 channel	ENC III(2)	0.8956	0.0012	0.8980
Exxon/ANF	7x7 0.065 channel	ENC III(2)	0.8967	0.0011	0.8989
Exxon/ANF	7x7	ENC III(3)	0.8976	0.0014	0.9004
Exxon/ANF	7x7 0.120 channel	ENC III(3)	0.8959	0.0011	0.8981
Exxon/ANF	7x7 0.080 channel	ENC III(3)	0.8925	0.0014	0.8953
Exxon/ANF	7x7 0.065 channel	ENC III(3)	0.8958	0.0013	0.8984
GE	7x7 w/ variable enrichment	GE2, GE3	0.8947	0.0012	0.8971
GE	8x8	GE4	0.8951	0.0013	0.8977
GE	8x8 0.120 channel	GE4	0.8927	0.0013	0.8953
GE	8x8 0.080 channel	GE4	0.8930	0.0013	0.8956
GE	8x8 0.065 channel	GE4	0.8940	0.0012	0.8964
GE	8x8	GE5	0.9009	0.0011	0.9031
		GE-Pres			
		GE-Barrier			
		GE8 Type I			
GE	8x8 0.120 channel	GE5	0.9015	0.0012	0.9039
GE	8x8 0.080 channel	GE5	0.9027	0.0013	0.9053
GE	8x8 0.065 channel	GE5	0.9012	0.0011	0.9034
GE	8x8	GE8 Type II	0.9020	0.0012	0.9044
GE	8x8 0.120 channel	GE8 Type II	0.9054	0.0014	0.9082
GE	8x8 0.080 channel	GE8 Type II	0.9043	0.0014	0.9071
GE	8x8 0.065 channel	GE8 Type II	0.9023	0.0013	0.9049

Table T.6-6
Most Reactive Fuel Type
(Continued)

Manufacturer	Array	Version	k_{KENO}	1σ	k_{eff}
GE	8x8	GE9, GE10	0.9043	0.0013	0.9069
GE	8x8 0.120 channel	GE9, GE10	0.9062	0.0013	0.9088
GE	8x8 0.080 channel	GE9, GE10	0.9054	0.0011	0.9076
GE	8x8 0.065 channel	GE9, GE10	0.9052	0.0014	0.9080
Exxon/ANF	8x8	ENC Va and Vb	0.8851	0.0011	0.8873
Exxon/ANF	8x8 0.120 channel	ENC Va and Vb	0.8827	0.0011	0.8849
Exxon/ANF	8x8 0.080 channel	ENC Va and Vb	0.8831	0.0012	0.8855
Exxon/ANF	8x8 0.065 channel	ENC Va and Vb	0.8821	0.0014	0.8849
GE	8x8 w/variable enrichment	GE5	0.8951	0.0011	0.8973
GE	8x8 w/variable enrichment	GE9	0.9008	0.0013	0.9034
GE	9x9	GE11, GE13	0.9042	0.0014	0.9070
GE	9x9 0.120 channel	GE11, GE13	0.9025	0.0014	0.9053
GE	9x9 0.080 channel	GE11, GE13	0.9066	0.0012	0.9090
GE	9x9 0.065 channel	GE11, GE13	0.9040	0.0013	0.9066
GE	**10x10**	**GE12, 14**	**0.9095**	**0.0013**	**0.9121**
GE	10x10 0.120 channel	GE12, 14	0.9094	0.0010	0.9114
GE	10x10 0.080 channel	GE12, 14	0.9092	0.0013	0.9118
GE	10x10 0.065 channel	GE12, 14	0.9076	0.0011	0.9098
The results shown in this part of the table are based on CSAS25 runs.					
Framatome-ANP	8x8[4]	8x8-62/2	0.8991	0.0013	0.9017
Framatome-ANP	8x8 0.120 channel	8x8-62/2	0.8966	0.0012	0.8990
Framatome-ANP	8x8 0.080 channel	8x8-62/2	0.9005	0.0014	0.9033
Framatome-ANP	8x8 0.065 channel	8x8-62/2	0.8973	0.0013	0.8999
Framatome-ANP	9x9	9x9-79/2	0.9072	0.0015	0.9102
Framatome-ANP	9x9 0.120 channel	9x9-79/2	0.9065	0.0013	0.9091
Framatome-ANP	9x9 0.080 channel	9x9-79/2	0.9075	0.0013	0.9101
Framatome-ANP	9x9 0.065 channel	9x9-79/2	0.9054	0.0012	0.9078
Siemens	9x9	QFA	0.9078	0.0013	0.9096
Siemens	9x9 0.120 channel	QFA	0.9084	0.0012	0.9098
Siemens	9x9 0.080 channel	QFA	0.9085	0.0012	0.9105
Siemens	9x9 0.065 channel	QFA	0.9077	0.0012	0.9096
Framatome-ANP	10x10	Atrium-10	0.9070	0.0013	0.9104
Framatome-ANP	10x10 0.120 channel	Atrium-10	0.9070	0.0014	0.9108
Framatome-ANP	10x10 0.080 channel	Atrium-10	0.9081	0.0012	0.9109
Framatome-ANP	10x10 0.065 channel	Atrium-10	0.9072	0.0012	0.9101

Table T.6-6
Most Reactive Fuel Type

(Concluded)

Description[5]	k_{KENO}	1σ	k_{eff}
GE 4 fuel from 1st page of this table	0.8951	0.0013	0.8977
GE 4, 62 fueled rods	0.8966	0.0012	0.8990
GE 4, 61 fueled rods	0.8973	0.0013	0.8999
GE 4, 60 fueled rods	0.8971	0.0012	0.8995
GE 4, 59 fueled rods, alternate	0.8964	0.0013	0.8990
GE 4, 59 fueled rods, alternate	0.8955	0.0013	0.8981
GE 4, 59 fueled rods, alternate	0.9043	0.0014	0.9071
GE 4, 59 fueled rods	0.9007	0.0011	0.9029
GE 4, 58 fueled rods, alternate	0.9048	0.0013	0.9074
GE 4, 58 fueled rods	0.8965	0.0013	0.8991
GE 12/14 fuel from 2nd page of this table	**0.9095**	**0.0013**	**0.9121**

(1) Small fuel pellet OD (Note large pellet OD identical to GE1 analysis)
(2) Small fuel pellet OD
(3) Large fuel pellet OD
(4) Used maximum pellet OD
(5) For certain fueled rod configurations, alternate arrangements have also been analyzed.

Table T.6-7
Most Reactive Configuration – Intact Fuel

Model Description	k_{KENO}	1σ	k_{eff}
Assembly-to-Assembly Pitch Evaluation			
Maximum Assembly-to-Assembly Pitch	0.8710	0.0013	0.8736
Assemblies Centered in Sleeves	0.9110	0.0012	0.9134
Minimum Assembly-to-Assembly Pitch	0.9110	0.0014	0.9138
Canister Shell Variation Evaluation			
Minimum Shell Thickness	0.9125	0.0012	0.9149
Nominal Shell Thickness	0.9110	0.0014	0.9138
Maximum Shell Thickness	0.9141	0.0011	0.9163
Poison Thickness Evaluation			
Nominal PoisonThickness (0.31 inches)	0.9110	0.0014	0.9138
Minimum Poison Thickness (0.3 inches)	0.9163	0.0012	0.9187
Fuel Cladding O.D. Evaluation			
Fuel Clad OD = 0.404 inches	0.9163	0.0012	0.9187
Fuel Clad OD = 0.402 inches	0.9157	0.0010	0.9177
Fuel Cald OD = 0.400 inches	0.9183	0.0011	0.9205
Fuel Clad OD = 0.398 inches	0.9201	0.0013	0.9227
Fuel Clad OD = 0.396 inches	0.9222	0.0012	0.9246
Fuel Clad OD = 0.394 inches	0.9229	0.0012	0.9253
Fuel Cell Width Evaluation			
Maximum Fuel Cell Width	0.9194	0.0011	0.9216
Nominal Fuel Cell Width	0.9229	0.0012	0.9253
Minimum Fuel Cell Width	0.9349	0.0011	0.9371
Minimum Fuel Cell Width with Maximum Shell Thickness	0.9326	0.0014	0.9354

Table T.6-7
Most Reactive Configuration – Intact Fuel
(Concluded)

Model Description	k_{KENO}	1σ	k_{eff}
Internal Moderator Density (IMD) Evaluation			
Internal Moderator at 100% TD	0.9349	0.0011	0.9371
Internal Moderator at 90% TD	0.9079	0.0013	0.9105
Internal Moderator at 80% TD	0.8772	0.0013	0.8798
Internal Moderator at 70% TD	0.8401	0.0012	0.8425
Internal Moderator at 60% TD	0.7980	0.0010	0.8000
Internal Moderator at 50% TD	0.7466	0.0010	0.7486
Internal Moderator at 40% TD	0.6862	0.0010	0.6882
Internal Moderator at 30% TD	0.6236	0.0008	0.6252
Internal Moderator at 20% TD	0.5628	0.0010	0.5648
Internal Moderator at 10% TD	0.5078	0.0006	0.5090
Internal Moderator at 0% TD	0.4364	0.0004	0.4372
External Moderator Density (EMD) Evaluation			
External Moderator at 100% TD	0.9349	0.0011	0.9371
External Moderator at 90% TD	0.9340	0.0011	0.9362
External Moderator at 80% TD	0.9324	0.0012	0.9348
External Moderator at 70% TD	0.9365	0.0011	0.9387
External Moderator at 60% TD	0.9363	0.0011	0.9385
External Moderator at 50% TD	0.9336	0.0011	0.9358
External Moderator at 40% TD	0.9345	0.0011	0.9367
External Moderator at 30% TD	0.9332	0.0013	0.9358
External Moderator at 20% TD	0.9332	0.0012	0.9356
External Moderator at 10% TD	0.9321	0.0013	0.9347
External Moderator at 0% TD	0.9321	0.0012	0.9345
Effect of Poison Plate Thickness Variation			
Reference KENO model, void gaps	0.9349	0.0011	0.9371
Reference model with 0.300″ poison (V8)	0.9348	0.0011	0.9370
V8 model with 0.125″ Borated Aluminum	0.9357	0.0014	0.9385
V8 model with 0.064″ Boral® poison	0.9344	0.0012	0.9368
Effect of Rail Material Modeling for Type 2			
Reference KENO model (R9), void gaps	0.9357	0.0014	0.9385
R9 with water gaps, solid alum rails (V9)	0.9393	0.0011	0.9415
V9 with 7.5 cm water holes	0.9365	0.0011	0.9387
V9 with 6.0 cm water squares	0.9359	0.0012	0.9383

Table T.6-8
Criticality Analysis Results for Intact Fuel

Model Description	k_{KENO}	1σ	k_{eff}
Type 1 DSC Basket only, 3.70 wt. % U-235, 18.9 mg B-10/cm^2, Borated Aluminum 0.102″			
EMD=100%	0.9349	0.0012	0.9373
EMD=001%	0.9362	0.0011	0.9384
EMD=010%	0.9363	0.0010	0.9383
EMD=030%	0.9362	0.0011	0.9384
EMD=050%	0.9372	0.0012	0.9396
EMD=050%, Boral® 0.050″, 18.8 mg B-10/cm^2	0.9361	0.0013	0.9387
EMD=070%	0.9358	0.0011	0.9380
EMD=090%	0.9359	0.0010	0.9379
Type 2 DSC Basket only, 3.70 wt. % U-235, 20.1 mg B-10/cm^2, Borated Aluminum 0.102″			
EMD=100% (1)	0.9360	0.0014	0.9388
EMD=100% (2)	0.9368	0.0010	0.9388
EMD=100%, Boral® 0.053″, 20.0 mg B-10/cm^2	0.9357	0.0011	0.9379
EMD=001%	0.9356	0.0012	0.9380
EMD=010%	0.9357	0.0013	0.9383
EMD=030%	0.9357	0.0013	0.9383
EMD=050%	0.9353	0.0012	0.9377
EMD=070%	0.9361	0.0012	0.9385
EMD=090%	0.9361	0.0011	0.9383
Both Baskets, 4.10 wt. % U-235, 28.8 mg B-10/cm^2, Borated Aluminum 0.102″			
EMD=100% (1)	0.9340	0.0011	0.9362
EMD=100% (2)	0.9358	0.0013	0.9384
EMD=001%	0.9361	0.0013	0.9387
EMD=010%	0.9359	0.0011	0.9381
EMD=030%	**0.9376**	**0.0012**	**0.9400**
Above case with actual paired plates configuration	0.9375	0.0012	0.9399
EMD=030%, Boral® 0.076″	0.9370	0.0013	0.9396
EMD=050%	0.9371	0.0011	0.9393
EMD=070%	0.9353	0.0011	0.9375
EMD=090%	0.9369	0.0011	0.9391

1) The basket is modeled with internal moderator rails and void gaps.

2) The basket is based on the design basis criticality configuration.

Table T.6-8
Criticality Analysis Results for Intact Fuel

(Continued)

Model Description	k_{KENO}	1σ	k_{eff}
Type 1 DSC Basket only, 4.40 wt. % U-235, 36.0 mg B-10/cm², Borated Aluminum 0.127″			
EMD=100%	0.9322	0.0012	0.9346
EMD=001%	0.9353	0.0013	0.9379
EMD=010%	0.9350	0.0012	0.9374
EMD=030%	0.9363	0.0015	0.9393
EMD=030%, Boral® 0.095″	0.9363	0.0012	0.9387
EMD=050%	0.9360	0.0013	0.9386
EMD=070%	0.9329	0.0012	0.9353
EMD=090%	0.9355	0.0012	0.9379
Type 2 DSC Basket only, 4.40 wt. % U-235, 37.5 mg B-10/cm², Borated Aluminum 0.132″			
EMD=100%	0.9342	0.0014	0.9370
EMD=001%	0.9356	0.0012	0.9380
EMD=010%	0.9350	0.0012	0.9374
EMD=030%	0.9355	0.0012	0.9379
EMD=050%,	0.9352	0.0014	0.9380
EMD=050%, Boral® 0.099″, 37.3 mg B-10/cm²	0.9331	0.0014	0.9359
EMD=050%, Bortec® 0.160″, 36.2 mg B-10/cm²	0.9338	0.0011	0.9360
EMD=070%	0.9341	0.0013	0.9367
EMD=090%	0.9346	0.0012	0.9370
Both Baskets, 4.60 wt. % U-235, 43.2 mg B-10/cm², Borated Aluminum 0.153″			
EMD=100%	0.9357	0.0011	0.9379
EMD=001%	0.9343	0.0013	0.9369
EMD=010%	0.9361	0.0013	0.9387
EMD=030%	0.9355	0.0011	0.9377
EMD=050%,	0.9375	0.0011	0.9397
EMD=050%, Boral® 0.114″, 43.1 mg B-10/cm²	0.9352	0.0012	0.9376
EMD=070%	0.9367	0.0011	0.9389
EMD=090%	0.9340	0.0012	0.9364

Table T.6-8
Criticality Analysis Results for Intact Fuel

(Concluded)

Model Description	k_{KENO}	1σ	k_{eff}
Both Baskets, 4.80 wt. % U-235, 49.5 mg B-10/cm^2, Borated Aluminum 0.175″			
EMD=100%	0.9338	0.0013	0.9364
EMD=001%	0.9359	0.0011	0.9381
EMD=010%	0.9367	0.0012	0.9391
EMD=030%	0.9343	0.0010	0.9363
EMD=050%,	0.9320	0.0010	0.9340
EMD=070%	0.9366	0.0013	0.9392
EMD=070%, Boral® 0.130″, 49.0 mg B-10/cm^2	0.9366	0.0012	0.9390
EMD=090%	0.9350	0.0012	0.9374
Both Baskets, 5.00 wt. % U-235, 56.2 mg B-10/cm^2, Borated Aluminum 0.199″			
EMD=100%	0.9364	0.0012	0.9388
EMD=001%	0.9367	0.0012	0.9391
EMD=001%, Boral® 0.149″, 56.1 mg B-10/cm^2	0.9331	0.0011	0.9353
EMD=010%	0.9353	0.0011	0.9375
EMD=030%	0.9362	0.0011	0.9384
EMD=050%,	0.9367	0.0012	0.9391
EMD=050%, Boral®	0.9338	0.0011	0.9360
EMD=070%	0.9342	0.0012	0.9366
EMD=090%	0.9352	0.0013	0.9378
Both Baskets, 4.10 wt. % U-235, 28.8 mg B-10/cm^2, Borated Aluminum 0.102″, IMD			
IMD=090%	0.9137	0.0012	0.9161
IMD=070%	0.8509	0.0014	0.8537
IMD=050%	0.7609	0.0009	0.7627
IMD=030%	0.6466	0.0009	0.6484
IMD=010%	0.5162	0.0006	0.5174
IMD=001%, Dry	0.4633	0.0004	0.4641
Type 1 DSC Basket, 2.60 wt. % U-235, 18.9 mg B-10/cm^2, Borated Aluminum 0.102″Dry Case for Shielding Analysis			
IMD=001%, Dry	0.3799	0.0004	0.3807

Table T.6-9
Most Reactive Configuration – Double Shear

Model Description	k_{KENO}	1σ	k_{eff}	Case ID
Most Reactive Damaged Assembly Evaluation				
8x8 Lattice with Double Shear	0.8979	0.0012	0.9003	Case 16
Same as above with 12.5″ rod shift	0.9011	0.0012	0.9035	Case 17
9x9 Lattice with Double Shear	0.8999	0.0011	0.9021	Case 18
Same as above with 12.5″ rod shift	0.8998	0.0013	0.9024	Case 19
10x10 Lattice with Double Shear	0.9098	0.0012	0.9122	Case 20
Same as above with 12.5″ rod shift	**0.9116**	**0.0012**	**0.9140**	Case 21

Table T.6-10
Most Reactive Configuration – Optimum Rod Pitch

Model Description	k_{KENO}	1σ	k_{eff}
Optimum Rod Pitch Calculations for the 7x7 Lattice : GE 2 Lattice			
7x7 Lattice, Pitch = 0.563″	0.6734	0.0013	0.6760
7x7 Lattice, Pitch = 0.600″	0.7267	0.0013	0.7293
7x7 Lattice, Pitch = 0.640″	0.7807	0.0014	0.7835
7x7 Lattice, Pitch = 0.680″	0.8349	0.0011	0.8371
7x7 Lattice, Pitch = 0.720″	0.8866	0.0013	0.8892
7x7 Lattice, Pitch = 0.738″	0.9037	0.0012	0.9061
7x7 Lattice, Pitch = 0.760″	0.9281	0.0013	0.9307
7x7 Lattice, Pitch = 0.800″	0.9639	0.0011	0.9661
7x7 Lattice, Pitch = 0.825″	0.9832	0.0012	0.9856
7x7 Lattice, Pitch = 0.850″	0.9960	0.0013	0.9986
Above Case, Optimum Pitch, 7x7 Base	0.9960	0.0013	0.9986
7x7 Base, 1 rod removed	0.9959	0.0013	0.9985
7x7 Base, 2 rods removed	**0.9970**	**0.0011**	**0.9992**
7x7 Base, 3 rods removed	0.9937	0.0011	0.9959
7x7 Base, 4 rods removed	0.9928	0.0011	0.9950
7x7 Base, 5 rods removed	0.9877	0.0013	0.9903
7x7 Base, 8 rods removed	0.9773	0.0012	0.9797
7x7 Base, 12 rods removed	0.9336	0.0011	0.9358
7x7 Base, 16 rods removed	0.9142	0.0013	0.9168
7x7 Base, 20 rods removed	0.8724	0.0011	0.8746
Optimum Rod Pitch Calculations for the 8x8 Lattice : GE 9 Lattice			
8x8 Lattice, Pitch = 0.483″	0.6615	0.0014	0.6643
8x8 Lattice, Pitch = 0.520″	0.7161	0.0012	0.7185
8x8 Lattice, Pitch = 0.560″	0.7839	0.0012	0.7863
8x8 Lattice, Pitch = 0.600″	0.8427	0.0011	0.8449
8x8 Lattice, Pitch = 0.640″	0.8974	0.0013	0.9000
8x8 Lattice, Pitch = 0.680″	0.9425	0.0012	0.9449
8x8 Lattice, Pitch = 0.700″	0.9599	0.0013	0.9625
8x8 Lattice, Pitch = 0.725″	0.9829	0.0014	0.9857
8x8 Lattice, Pitch = 0.750″	0.9992	0.0011	1.0014
Above Case, Optimum Pitch, 8x8 Base	0.9992	0.0011	1.0014

Table T.6-10
Most Reactive Configuration – Optimum Rod Pitch
(Continued)

Model Description	k_{KENO}	1σ	k_{eff}
8x8 Base, 1 rod removed	**0.9999**	**0.0013**	**1.0025**
8x8 Base, 2 rods removed	0.9967	0.0012	0.9991
8x8 Base, 3 rods removed	0.9969	0.0013	0.9995
8x8 Base, 4 rods removed	0.9963	0.0010	0.9983
8x8 Base, 5 rods removed	0.9921	0.0012	0.9945
8x8 Base, 6 rods removed	0.9919	0.0012	0.9943
8x8 Base, 7 rods removed	0.9861	0.0011	0.9883
8x8 Base, 10 rods removed	0.9727	0.0014	0.9755
8x8 Base, 12 rods removed	0.9659	0.0011	0.9681
Optimum Rod Pitch Calculations for the 9x9 Lattice : Siemens QFA Lattice			
9x9 Lattice, Pitch = 0.433″	0.6686	0.0013	0.6712
9x9 Lattice, Pitch = 0.470″	0.7359	0.0010	0.7379
9x9 Lattice, Pitch = 0.510″	0.8032	0.0012	0.8056
9x9 Lattice, Pitch = 0.540″	0.8563	0.0011	0.8585
9x9 Lattice, Pitch = 0.569″	0.9021	0.0013	0.9047
9x9 Lattice, Pitch = 0.580″	0.9169	0.0015	0.9199
9x9 Lattice, Pitch = 0.600″	0.9455	0.0013	0.9481
9x9 Lattice, Pitch = 0.620″	0.9679	0.0014	0.9707
9x9 Lattice, Pitch = 0.640″	0.9881	0.0013	0.9907
9x9 Lattice, Pitch = 0.660″	1.0038	0.0013	1.0064
Above Case, Optimum Pitch, 9x9 Base	1.0038	0.0013	1.0064
9x9 Base, 1 rod removed	**1.0060**	**0.0013**	**1.0086**
9x9 Base, 2 rods removed	1.0053	0.0013	1.0079
9x9 Base, 3 rods removed	1.0050	0.0013	1.0076
9x9 Base, 4 rods removed	1.0045	0.0010	1.0065
9x9 Base, 5 rods removed	1.0048	0.0012	1.0072
9x9 Base, 6 rods removed	1.0024	0.0013	1.0050
9x9 Base, 8 rods removed	1.0016	0.0012	1.0040
9x9 Base, 9 rods removed	0.9970	0.0012	0.9994
9x9 Base, 12 rods removed	0.9960	0.0013	0.9986

Table T.6-10
Most Reactive Configuration – Optimum Rod Pitch
(Concluded)

Model Description	k_{KENO}	1σ	k_{eff}
Optimum Rod Pitch Calculations for the 10x10 Lattice : GE 12/14 Lattice			
10x10 Lattice, Pitch = 0.404″	0.6817	0.0011	0.6839
10x10 Lattice, Pitch = 0.440″	0.7530	0.0013	0.7556
10x10 Lattice, Pitch = 0.480″	0.8329	0.0011	0.8351
10x10 Lattice, Pitch = 0.510″	0.8876	0.0013	0.8902
10x10 Lattice, Pitch = 0.520″	0.9059	0.0013	0.9085
10x10 Lattice, Pitch = 0.540″	0.9361	0.0011	0.9383
10x10 Lattice, Pitch = 0.560″	0.9637	0.0013	0.9663
10x10 Lattice, Pitch = 0.580″	0.9895	0.0012	0.9919
10x10 Lattice, Pitch = 0.600″	1.0074	0.0011	1.0096
Above Case, Optimum Pitch, 10x10 Base	1.0074	0.0011	1.0096
10x10 Base, 1 rod removed	1.0096	0.0013	1.0122
10x10 Base, 2 rods removed	1.0111	0.0012	1.0135
10x10 Base, 3 rods removed	1.0130	0.0011	1.0152
10x10 Base, 4 rods removed	1.0134	0.0011	1.0156
10x10 Base, 5 rods removed	1.0148	0.0012	1.0172
10x10 Base, 7 rods removed	1.0136	0.0013	1.0162
10x10 Base, 8 rods removed	1.0119	0.0012	1.0143
10x10 Base, 9 rods removed	1.0120	0.0012	1.0144
10x10 Base, 10 rods removed	1.0118	0.0014	1.0146
10x10 Base, 12 rods removed	1.0117	0.0013	1.0143
10x10 Base, 16 rods removed	1.0084	0.0011	1.0106

Table T.6-11
Most Reactive Configuration – Variations

Model Description	k_{KENO}	1σ	k_{eff}	Case ID
Same as Case 21 except for the change in fuel density (96.5% instead of 95.0%) and enrichment. **Reference Case**	0.9343	0.0011	0.9365	Case 22
Same as Case 22 except the rails were modified for Type 2 DSC basket in the active fuel region.	0.9375	0.0013	0.9401	Case 23
Same as Case 23 except the gaps were modeled with internal moderator.	0.9353	0.0012	0.9377	Case 24
Same as Case 24 except that UNIT 84 was modeled with the Type 2 DSC Rail configuration.	0.9354	0.0013	0.9380	Case 25
Same as Case 25 except that the active fuel was extended to 150″.	0.9320	0.0014	0.9348	Case 26
Same as Case 23 except that the outermost row of fuel rods are modeled bare (no cladding).	0.9382	0.0016	0.9414	Case 27
Same as Case 23 except that the two outermost rows of fuel rods are modeled bare (no cladding).	0.9406	0.0012	0.9430	Case 28
Design basis (10x10 array, 95 fuel rods) optimum pitch & rod array case with the geometry as in Case 23.	**0.9486**	**0.0012**	**0.9510**	**Case 29**

Dancoff Factor and Position Variation Evaluation

Model Description	k_{KENO}	1σ	k_{eff}
Second Lattice – Intact Fuel, Centered	**0.9371**	**0.0012**	**0.9395**
Second Lattice – Intact Fuel, Inward	0.9364	0.0013	0.9390
Second Lattice – Intact Fuel, Outward	0.9319	0.0013	0.9345
Second Lattice – Damaged Fuel, Centered	0.9356	0.0011	0.9378
Second Lattice – Damaged Fuel, Inward	0.9345	0.0011	0.9367
Second Lattice – Damaged Fuel, Outward	0.9340	0.0013	0.9366

Table T.6-12
Criticality Analysis Results for Damaged Fuel (4 Assemblies)

Model Description	k_{KENO}	1σ	k_{eff}
Type 1 DSC only, Intact 3.70 wt. % U-235, Damaged 3.90 wt. % U-235, 18.9 mg B-10/cm^2, B/Alum 0.102″			
EMD=100%	0.9358	0.0011	0.9380
EMD=001%	0.9345	0.0013	0.9371
EMD=010%	0.9345	0.0011	0.9367
EMD=030%	0.9358	0.0014	0.9386
EMD=050%	0.9353	0.0012	0.9377
EMD=070%	0.9333	0.0013	0.9359
EMD=090%	0.9364	0.0013	0.9390
Type 2 DSC only, Intact 3.70 wt. % U-235, Damaged 3.90 wt. % U-235, 20.1 mg B-10/cm^2, B/Alum 0.102″			
EMD=100%	0.9339	0.0012	0.9363
EMD=001%	0.9336	0.0012	0.9360
EMD=010%	0.9348	0.0011	0.9370
EMD=030%	0.9332	0.0012	0.9356
EMD=050%	0.9360	0.0012	0.9384
EMD=070%	0.9345	0.0014	0.9373
EMD=090%	0.9334	0.0013	0.9360
Both Baskets, Intact 4.10 wt. % U-235, Damaged 4.30 wt. % U-235, 28.8 mg B-10/cm^2, B/Alum 0.102″			
EMD=100%	0.9356	0.0013	0.9382
EMD=001%	0.9360	0.0012	0.9384
EMD=010%	0.9356	0.0012	0.9380
EMD=030%	0.9356	0.0014	0.9384
EMD=050%	0.9362	0.0012	0.9386
EMD=070%	0.9344	0.0011	0.9366
EMD=090%	0.9357	0.0012	0.9381
Type 1 DSC only, Intact 4.40 wt. % U-235, Damaged 5.00 wt. % U-235, 36.0 mg B-10/cm^2, B/Alum 0.127″			
EMD=100%	0.9335	0.0012	0.9359
EMD=001%	0.9348	0.0013	0.9374
EMD=010%	0.9349	0.0012	0.9373
EMD=030%	0.9310	0.0012	0.9334
EMD=050%	0.9322	0.0012	0.9346
EMD=070%	0.9336	0.0013	0.9362
EMD=090%	0.9319	0.0012	0.9343
Type 2 DSC only, Intact 4.40 wt. % U-235, Damaged 5.00 wt. % U-235, 37.5 mg B-10/cm^2, B/Alum 0.132″			
EMD=100%	0.9365	0.0012	0.9389
EMD=001%	0.9335	0.0012	0.9359
EMD=010%	0.9359	0.0011	0.9381

Table T.6-12
Criticality Analysis Results for Damaged Fuel (4 Assemblies)

(Concluded)

Model Description	k_{KENO}	1σ	k_{eff}
EMD=030%	0.9340	0.0012	0.9364
EMD=050%	0.9356	0.0011	0.9378
EMD=070%	0.9360	0.0012	0.9384
EMD=090%	0.9332	0.0013	0.9358
IMD=090%	0.9068	0.0013	0.9094
IMD=070%	0.8437	0.0011	0.8459
IMD=050%	0.7559	0.0011	0.7581
IMD=030%	0.6383	0.0009	0.6401
IMD=010%	0.5046	0.0007	0.5060
IMD=001%, Dry	0.4536	0.0005	0.4546
Both Baskets, Intact 4.60 wt. % U-235, Damaged 5.00 wt. % U-235, 43.2 mg B-10/cm^2, B/Alum 0.153″			
EMD=100%	0.9340	0.0012	0.9364
EMD=001%	0.9326	0.0013	0.9352
EMD=010%	0.9351	0.0011	0.9373
EMD=030%	0.9367	0.0012	0.9391
EMD=050%	0.9332	0.0012	0.9356
EMD=070%	0.9351	0.0012	0.9375
EMD=090%	0.9335	0.0013	0.9361
Both Baskets, Intact 4.80 wt. % U-235, Damaged 5.00 wt. % U-235, 49.5 mg B-10/cm^2, B/Alum 0.175″			
EMD=100%	0.9348	0.0011	0.9370
EMD=001%	0.9346	0.0012	0.9370
EMD=010%	0.9346	0.0011	0.9368
EMD=030%	0.9344	0.0014	0.9372
EMD=050%	0.9338	0.0012	0.9362
EMD=070%	0.9346	0.0012	0.9370
EMD=090%	0.9330	0.0012	0.9354
Both Baskets, Intact 5.00 wt. % U-235, Damaged 5.00 wt. % U-235, 56.2 mg B-10/cm^2, B/Alum 0.199″			
EMD=100%	0.9371	0.0012	0.9395
EMD=001%	0.9343	0.0012	0.9367
EMD=010%	0.9347	0.0012	0.9371
EMD=030%	0.9335	0.0012	0.9359
EMD=050%	0.9327	0.0012	0.9351
EMD=070%	0.9333	0.0012	0.9357
EMD=090%	0.9348	0.0012	0.9372

Table T.6-13
Criticality Analysis Results for Damaged Fuel (16 Assemblies)

Model Description	k_{KENO}	1σ	k_{eff}
Type 1 DSC only, Intact 3.70 wt. % U-235, Damaged 2.80 wt. % U-235, 18.9 mg B-10/cm^2, B/Alum 0.102″			
EMD=100%	0.9332	0.0013	0.9358
EMD=001%	0.9344	0.0013	0.9370
EMD=010%	0.9343	0.0015	0.9373
EMD=030%	0.9329	0.0012	0.9353
EMD=050%	0.9340	0.0012	0.9364
EMD=070%	0.9366	0.0011	0.9388
EMD=090%	0.9350	0.0011	0.9372
Type 2 DSC only, Intact 3.70 wt. % U-235, Damaged 2.80 wt. % U-235, 20.1 mg B-10/cm^2, B/Alum 0.102″			
EMD=100%	0.9338	0.0011	0.9360
EMD=001%	0.9352	0.0011	0.9374
EMD=010%	0.9327	0.0012	0.9351
EMD=030%	0.9328	0.0012	0.9352
EMD=050%	0.9323	0.0011	0.9345
EMD=070%	0.9328	0.0012	0.9352
EMD=090%	0.9346	0.0011	0.9368
Both Baskets, Intact 4.10 wt. % U-235, Damaged 3.10 wt. % U-235, 28.8 mg B-10/cm^2, B/Alum 0.102″			
EMD=100%	0.9337	0.0011	0.9359
EMD=001%	0.9345	0.0011	0.9367
EMD=010%	0.9357	0.0013	0.9383
EMD=030%	0.9375	0.0011	0.9397
EMD=050%	0.9353	0.0012	0.9377
EMD=070%	0.9367	0.0012	0.9391
EMD=090%	0.9367	0.0011	0.9389
Type 1 DSC only, Intact 4.40 wt. % U-235, Damaged 3.20 wt. % U-235, 36.0 mg B-10/cm^2, B/Alum 0.127″			
EMD=100%	0.9338	0.0013	0.9364
EMD=001%	0.9306	0.0011	0.9328
EMD=010%	0.9316	0.0014	0.9344
EMD=030%	0.9355	0.0012	0.9379
EMD=050%	0.9322	0.0014	0.9350
EMD=070%	0.9352	0.0013	0.9378
EMD=090%	0.9340	0.0011	0.9362

Table T.6-13
Criticality Analysis Results for Damaged Fuel (16 Assemblies)

(Concluded)

Model Description	k_{KENO}	1σ	k_{eff}
Type 2 DSC only, Intact 4.40 wt. % U-235, Damaged 3.20 wt. % U-235, 37.5 mg B-10/cm^2, B/Alum 0.132″			
EMD=100%	0.9330	0.0013	0.9356
EMD=001%	0.9334	0.0013	0.9360
EMD=010%	0.9340	0.0012	0.9364
EMD=030%	0.9354	0.0012	0.9378
EMD=050%	0.9332	0.0012	0.9356
EMD=070%	0.9346	0.0012	0.9370
EMD=090%	0.9323	0.0013	0.9349
Both Baskets, Intact 4.60 wt. % U-235, Damaged 3.40 wt. % U-235, 43.2 mg B-10/cm^2, B/Alum 0.153″			
EMD=100%	0.9338	0.0012	0.9362
EMD=001%	0.9329	0.0012	0.9353
EMD=010%	0.9342	0.0012	0.9366
EMD=030%	0.9348	0.0010	0.9368
EMD=050%	0.9360	0.0014	0.9388
EMD=070%	0.9347	0.0013	0.9373
EMD=090%	0.9359	0.0012	0.9383
Both Baskets, Intact 4.80 wt. % U-235, Damaged 3.50 wt. % U-235, 49.5 mg B-10/cm^2, B/Alum 0.175″			
EMD=100%	0.9361	0.0013	0.9387
EMD=001%	0.9348	0.0012	0.9372
EMD=010%	0.9351	0.0011	0.9373
EMD=030%	0.9356	0.0011	0.9378
EMD=050%	0.9333	0.0013	0.9359
EMD=070%	0.9355	0.0013	0.9381
EMD=090%	0.9361	0.0011	0.9383
Both Baskets, Intact 5.00 wt. % U-235, Damaged 3.60 wt. % U-235, 56.2 mg B-10/cm^2, B/Alum 0.199″			
EMD=100%	0.9337	0.0013	0.9363
EMD=001%	0.9368	0.0010	0.9388
EMD=010%	0.9365	0.0011	0.9387
EMD=030%	0.9354	0.0014	0.9382
EMD=050%	0.9359	0.0013	0.9385
EMD=070%	0.9346	0.0015	0.9376
EMD=090%	0.9349	0.0011	0.9371

Table T.6-14
Criticality Results

Model Description	k_{KENO}	1σ	k_{eff}
Regulatory Requirements for Storage			
Dry Storage (Bounded by infinite array of undamaged casks)	0.4633	0.0004	0.4641
Normal Conditions (Wet Loading)	0.9378	0.0011	0.9400
Off-Normal Conditions (damaged transfer cask while fuel still wet)	0.9378	0.0011	0.9400
Design Basis Cases for Intact Fuel			
3.7 wt% U-235; 20.1 mgB-10/cm^2 100 % IMD	0.9368	0.0010	0.9388
4.1 wt% U-235; 28.8 mgB-10/cm^2 100 % IMD, Optimum EMD	0.9376	0.0012	0.9400
Design Basis Cases for Damaged Fuel			
Intact @ 4.4 wt% U-235; 4 Damaged @ 5.0 wt% U-235 37.5 mgB-10/cm^2, Type 2 100 % IMD	0.9371	0.0012	0.9395
Intact @ 4.1 wt% U-235; 16 Damaged @ 3.1 wt% U-235 28.8 mgB-10/cm^2, 100 % IMD, Optimum EMD	0.9375	0.0011	0.9397

Table T.6-15
Benchmarking Results

Run ID	U Enrich. Wt%	Pu Enrich. Wt%	Pitch (cm)	H_2O/fuel volume	Separation of assemblies (cm)	AEG	k_{eff}	1σ
B1645SO1	2.46		1.41	1.015		32.8194	0.9967	0.0009
B1645SO2	2.46		1.41	1.015		32.7584	1.0002	0.0011
BW1231B1	4.02		1.511	1.139		31.1427	0.9966	0.0012
BW1231B2	4.02		1.511	1.139		29.8854	0.9972	0.0009
BW1273M	2.46		1.511	1.376		32.2106	0.9965	0.0009
BW1484A1	2.46		1.636	1.841	1.636	34.5304	0.9962	0.0010
BW1484A2	2.46		1.636	1.841	4.908	35.1629	0.9931	0.0010
BW1484B1	2.46		1.636	1.841		33.9421	0.9979	0.0010
BW1484B2	2.46		1.636	1.841	1.636	34.5820	0.9955	0.0012
BW1484B3	2.46		1.636	1.841	4.908	35.2609	0.9969	0.0011
BW1484C1	2.46		1.636	1.841	1.636	34.6463	0.9931	0.0011
BW1484C2	2.46		1.636	1.841	4.908	35.2422	0.9939	0.0012
BW1484S1	2.46		1.636	1.841	1.636	34.5105	1.0001	0.0010
BW1484S2	2.46		1.636	1.841	1.636	34.5569	0.9992	0.0010
BW1484SL	2.46		1.636	1.841	6.544	35.4151	0.9935	0.0011
BW1645S1	2.46		1.209	0.383	1.778	30.1040	0.9990	0.0010
BW1645S2	2.46		1.209	0.383	1.778	29.9961	1.0037	0.0011
BW1810A	2.46		1.636	1.841		33.9465	0.9984	0.0008
BW1810B	2.46		1.636	1.841		33.9631	0.9984	0.0009
BW1810C	2.46		1.636	1.841		33.1569	0.9992	0.0010
BW1810D	2.46		1.636	1.841		33.0821	0.9985	0.0013
BW1810E	2.46		1.636	1.841		33.1600	0.9988	0.0009
BW1810F	2.46		1.636	1.841		33.9556	1.0031	0.0011
BW1810G	2.46		1.636	1.841		32.9409	0.9973	0.0011
BW1810H	2.46		1.636	1.841		32.9420	0.9972	0.0011
BW1810I	2.46		1.636	1.841		33.9655	1.0037	0.0009
BW1810J	2.46		1.636	1.841		33.1403	0.9983	0.0011
DSN399-1	4.74		1.6	3.807	1.8	33.9520	1.0036	0.0015
DSN399-2	4.74		1.6	3.807	5.8	34.4207	0.9989	0.0016
DSN399-3	4.74		1.6	3.807		35.3140	1.0024	0.0015
DSN399-4	4.74		1.6	3.807		35.3784	0.9977	0.0013
EPRU65	2.35		1.562	1.196		33.9106	0.9960	0.0011
EPRU65B	2.35		1.562	1.196		33.4013	0.9993	0.0012
EPRU75	2.35		1.905	2.408		35.8671	0.9958	0.0010
EPRU75B	2.35		1.905	2.408		35.3043	0.9996	0.0010
EPRU87	2.35		2.21	3.687		36.6129	1.0007	0.0011
EPRU87B	2.35		2.21	3.687		36.3499	1.0007	0.0011
NSE71SQ	4.74		1.26	1.823		33.7610	0.9979	0.0012
NSE71W1	4.74		1.26	1.823		34.0129	0.9988	0.0013
NSE71W2	4.74		1.26	1.823		36.3037	0.9957	0.0010
P2438BA	2.35		2.032	2.918	5.05	36.2277	0.9979	0.0013
P2438SLG	2.35		2.032	2.918	8.39	36.2889	0.9986	0.0012
P2438SS	2.35		2.032	2.918	6.88	36.2705	0.9974	0.0011
P2438ZR	2.35		2.032	2.918	8.79	36.2840	0.9987	0.0010
P2615BA	4.31		2.54	3.883	6.72	35.7286	1.0019	0.0014
P2615SS	4.31		2.54	3.883	8.58	35.7495	0.9952	0.0015
P2615ZR	4.31		2.54	3.883	10.92	35.7700	0.9977	0.0014
P2827L1	2.35		2.032	2.918	13.27	36.2526	1.0057	0.0011
P2827L2	2.35		2.032	2.918	11.25	36.2908	0.9999	0.0012

Table T.6-15
Benchmarking Results
(Continued)

Run ID	U Enrich. Wt%	Pu Enrich. Wt%	Pitch (cm)	H_2O/fuel volume	Separation of assemblies (cm)	AEG	k_{eff}	1σ
P2827L3	4.31		2.54	3.883	20.78	35.6766	1.0092	0.0012
P2827L4	4.31		2.54	3.883	19.04	35.7131	1.0073	0.0012
P2827SLG	2.35		2.032	2.918	8.31	36.3037	0.9957	0.0010
P3314BA	4.31		1.892	1.6	2.83	33.1881	0.9988	0.0012
P3314BC	4.31		1.892	1.6	2.83	33.2284	0.9992	0.0012
P3314BF1	4.31		1.892	1.6	2.83	33.2505	1.0037	0.0013
P3314BF2	4.31		1.892	1.6	2.83	33.2184	1.0009	0.0013
P3314BS1	2.35		1.684	1.6	3.86	34.8594	0.9956	0.0013
P3314BS2	2.35		1.684	1.6	3.46	34.8356	0.9949	0.0010
P3314BS3	4.31		1.892	1.6	7.23	33.4247	0.9970	0.0013
P3314BS4	4.31		1.892	1.6	6.63	33.4162	0.9998	0.0012
P3314SLG	4.31		1.892	1.6	2.83	34.0198	0.9974	0.0012
P3314SS1	4.31		1.892	1.6	2.83	33.9601	0.9999	0.0012
P3314SS2	4.31		1.892	1.6	2.83	33.7755	1.0022	0.0012
P3314SS3	4.31		1.892	1.6	2.83	33.8904	0.9992	0.0013
P3314SS4	4.31		1.892	1.6	2.83	33.7625	0.9958	0.0011
P3314SS5	2.35		1.684	1.6	7.8	34.9531	0.9949	0.0013
P3314SS6	4.31		1.892	1.6	10.52	33.5333	1.0020	0.0011
P3314W1	4.31		1.892	1.6		34.3994	1.0024	0.0013
P3314W2	2.35		1.684	1.6		35.2167	0.9969	0.0011
P3314ZR	4.31		1.892	1.6	2.83	33.9954	0.9971	0.0013
P3602BB	4.31		1.892	1.6	8.3	33.3221	1.0029	0.0013
P3602BS1	2.35		1.684	1.6	4.8	34.7750	1.0027	0.0012
P3602BS2	4.31		1.892	1.6	9.83	33.3679	1.0039	0.0012
P3602N11	2.35		1.684	1.6	8.98	34.7438	1.0023	0.0012
P3602N12	2.35		1.684	1.6	9.58	34.8391	1.0030	0.0012
P3602N13	2.35		1.684	1.6	9.66	34.9337	1.0013	0.0012
P3602N14	2.35		1.684	1.6	8.54	35.0282	0.9974	0.0013
P3602N21	2.35		2.032	2.918	11.2	36.2821	0.9987	0.0011
P3602N22	2.35		2.032	2.918	10.36	36.1896	1.0025	0.0011
P3602N31	4.31		1.892	1.6	14.87	33.2094	1.0057	0.0013
P3602N32	4.31		1.892	1.6	15.74	33.3067	1.0093	0.0012
P3602N33	4.31		1.892	1.6	15.87	33.4174	1.0107	0.0012
P3602N34	4.31		1.892	1.6	15.84	33.4683	1.0045	0.0013
P3602N35	4.31		1.892	1.6	15.45	33.5185	1.0013	0.0012
P3602N36	4.31		1.892	1.6	13.82	33.5855	1.0004	0.0014
P3602N41	4.31		2.54	3.883	12.89	35.5276	1.0109	0.0013
P3602N42	4.31		2.54	3.883	14.12	35.6695	1.0071	0.0014
P3602N43	4.31		2.54	3.883	12.44	35.7542	1.0053	0.0015
P3602SS1	2.35		1.684	1.6	8.28	34.8701	1.0025	0.0013
P3602SS2	4.31		1.892	1.6	13.75	33.4202	1.0035	0.0012
P3926L1	2.35		1.684	1.6	10.06	34.8519	1.0000	0.0011
P3926L2	2.35		1.684	1.6	10.11	34.9324	1.0017	0.0011
P3926L3	2.35		1.684	1.6	8.5	35.0641	0.9949	0.0012
P3926L4	4.31		1.892	1.6	17.74	33.3243	1.0074	0.0014
P3926L5	4.31		1.892	1.6	18.18	33.4074	1.0057	0.0013
P3926L6	4.31		1.892	1.6	17.43	33.5246	1.0046	0.0013
P3926SL1	2.35		1.684	1.6	6.59	33.4737	0.9995	0.0012
P3926SL2	4.31		1.892	1.6	12.79	33.5776	1.0007	0.0012

Table T.6-15
Benchmarking Results
(Concluded)

Run ID	U Enrich. Wt%	Pu Enrich. Wt%	Pitch (cm)	H_2O/fuel volume	Separation of assemblies (cm)	AEG	k_{eff}	1σ
P4267B1	4.31		1.8901	1.59		31.8075	0.9990	0.0010
P4267B2	4.31		0.89	1.59		31.5323	1.0033	0.0010
P4267B3	4.31		1.715	1.09		30.9905	1.0050	0.0011
P4267B4	4.31		1.715	1.09		30.5061	0.9996	0.0011
P4267B5	4.31		1.715	1.09		30.1011	1.0004	0.0011
P4267SL1	4.31		1.89	1.59		33.4737	0.9995	0.0012
P4267SL2	4.31		1.715	1.09		31.9460	0.9988	0.0016
P62FT231	4.31		1.891	1.6	5.19	32.9196	1.0012	0.0013
P71F14F3	4.31		1.891	1.6	5.19	32.8237	1.0009	0.0014
P71F14V3	4.31		1.891	1.6	5.19	32.8597	0.9972	0.0014
P71F14V5	4.31		1.891	1.6	5.19	32.8609	0.9993	0.0013
P71F214R	4.31		1.891	1.6	5.19	32.8778	0.9969	0.0012
PAT80L1	4.74		1.6	3.807	4.9	35.0253	1.0012	0.0012
PAT80L2	4.74		1.6	3.807	4.9	35.1136	0.9993	0.0015
PAT80SS1	4.74		1.6	3.807	4.9	35.0045	0.9988	0.0013
PAT80SS2	4.74		1.6	3.807	4.9	35.1072	0.9960	0.0013
W3269A	5.7		1.422	1.93		33.1480	0.9988	0.0012
W3269B1	3.7		1.105	1.432		32.4055	0.9961	0.0011
W3269B2	3.7		1.105	1.432		32.3921	0.9963	0.0011
W3269B3	3.7		1.105	1.432		32.2363	0.9944	0.0011
W3269C	2.72		1.524	1.494		33.7727	0.9989	0.0012
W3269SL1	2.72		1.524	1.494		33.3850	0.9981	0.0014
W3269SL2	5.7		1.422	1.93		33.0910	1.0005	0.0013
W3269W1	2.72		1.524	1.494		33.5114	0.9966	0.0014
W3269W2	5.7		1.422	1.93		33.1680	1.0014	0.0014
W3385SL1	5.74		1.422	1.932		33.2387	1.0009	0.0012
W3385SL2	5.74		2.012	5.067		35.8818	0.9997	0.0013
EPRI70UN	0.71	2	1.778	1.2		31.6775	0.9983	0.0012
EPRI70B	0.71	2	1.778	1.2		30.9021	1.0009	0.0012
EPRI87UN	0.71	2	2.2098	2.53		33.3230	1.0096	0.0011
EPRI87B	0.71	2	2.2098	2.53		31.6775	0.9983	0.0012
EPRI99UN	0.71	2	2.5146	3.64		35.1817	1.0063	0.0011
EPRI99B	0.71	2	2.5146	3.64		34.4098	1.0095	0.0011
SAXTON52	0.71	6.6	1.3208	1.68		30.2980	1.0020	0.0014
SAXTON56	0.71	6.6	1.4224	2.16		31.4724	1.0010	0.0014
SAXTON56B	0.71	6.6	1.4224	2.16		31.0038	0.9994	0.0013
SAXTN735	0.71	6.6	1.8669	4.7		34.1848	1.0007	0.0016
SATN792	0.71	6.6	2.01168	5.67		34.6401	1.0026	0.0013
SAXTN104	0.71	6.6	2.6416	10.75		35.8333	1.0054	0.0014
Correlation	0.31	-0.26	0.43	0.25	0.65	-0.01	N/A	N/A

Table T.6-16
USL-1 Results

Parameter	Range of Applicability	USL-1
U Enrichment (wt. % U-235)	2.4 2.8 3.3 3.8 – 5.7	0.9424 0.9430 0.9435 0.9438
Pu Enrichment (wt. % Pu)	2.0 – 6.6	0.9417
Fuel Rod Pitch (cm)	0.89 1.1 1.4 1.6 1.9 – 2.6	0.9396 0.9408 0.9421 0.9433 0.9439
Water/Fuel Volume Ratio	0.38 1.9 3.3 – 11	0.9414 0.9425 0.9426
Assembly Separation (cm)	1.6 4.4 7.1 9.8 – 21	0.9410 0.9425 0.9440 0.9441
Average Energy Group Causing Fission (AEG)	30 – 37	0.9433

Table T.6-17
USL Determination for Criticality Analysis

Parameter	Value from Limiting GE 10x10 Analysis	Bounding USL
Pin Pitch (cm)	1.2954	0.9416
Water to Fuel Volume Ratio	1.411	0.9421
Average Energy Group Causing Fission (AEG)	< 34[1]	0.9433
Assembly Separation (cm)	2.58[2]	0.9415
Enrichment (wt. % U-235)	3.7 (minimum)	0.9438

1. Examination of the results shows that the value is between 32 and 34 and hence, a conservative value that produces the minimum USL was chosen.
2. Separation Distance ≥ (5.80"-5.278") + 0.09" + 0.105 + 0.30" = 1.02" = 2.58 cm, calculated with minimum dimensions for the basket, un-channeled fuel assembly width and centered fuel assembly positioning.

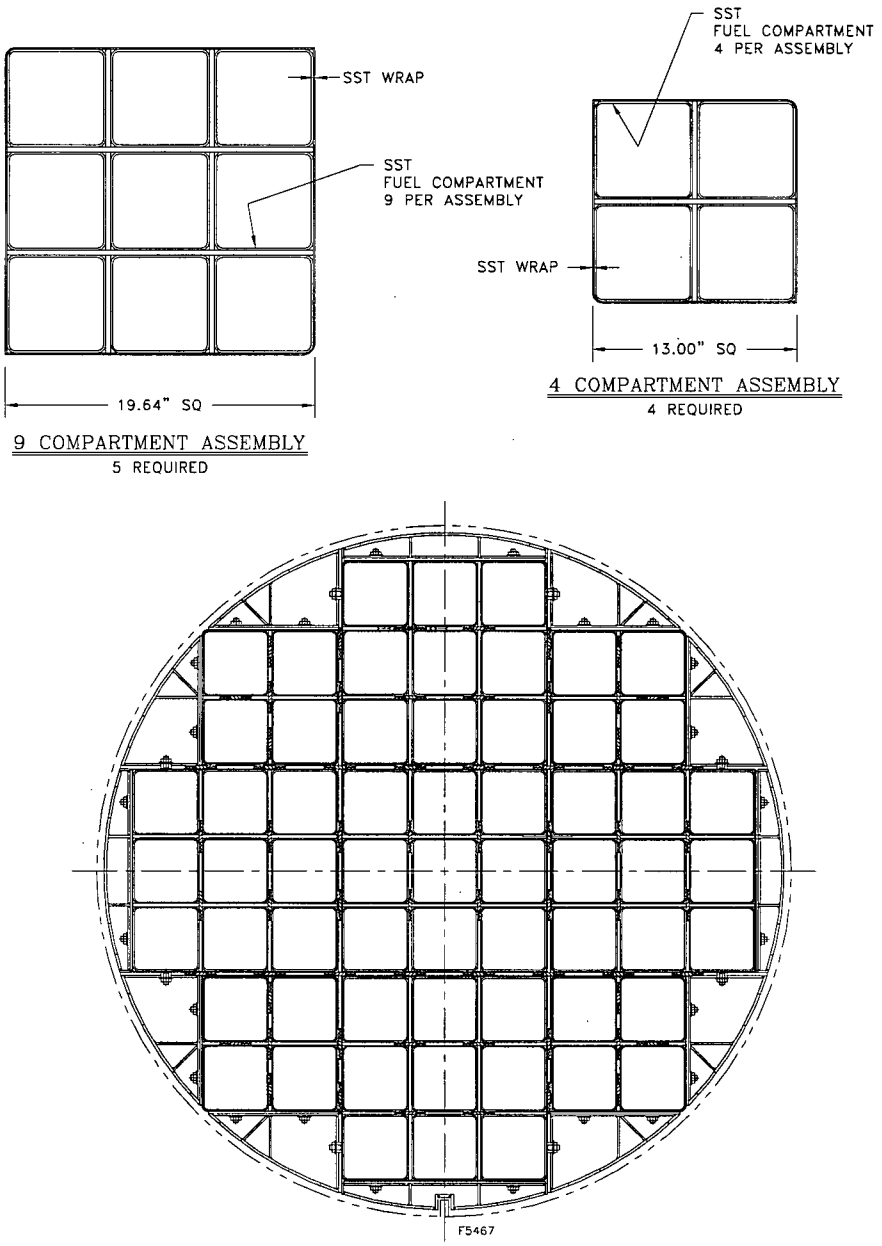

Figure T.6-1
NUHOMS®-61BTH Type 1 DSC Radial Cross Section

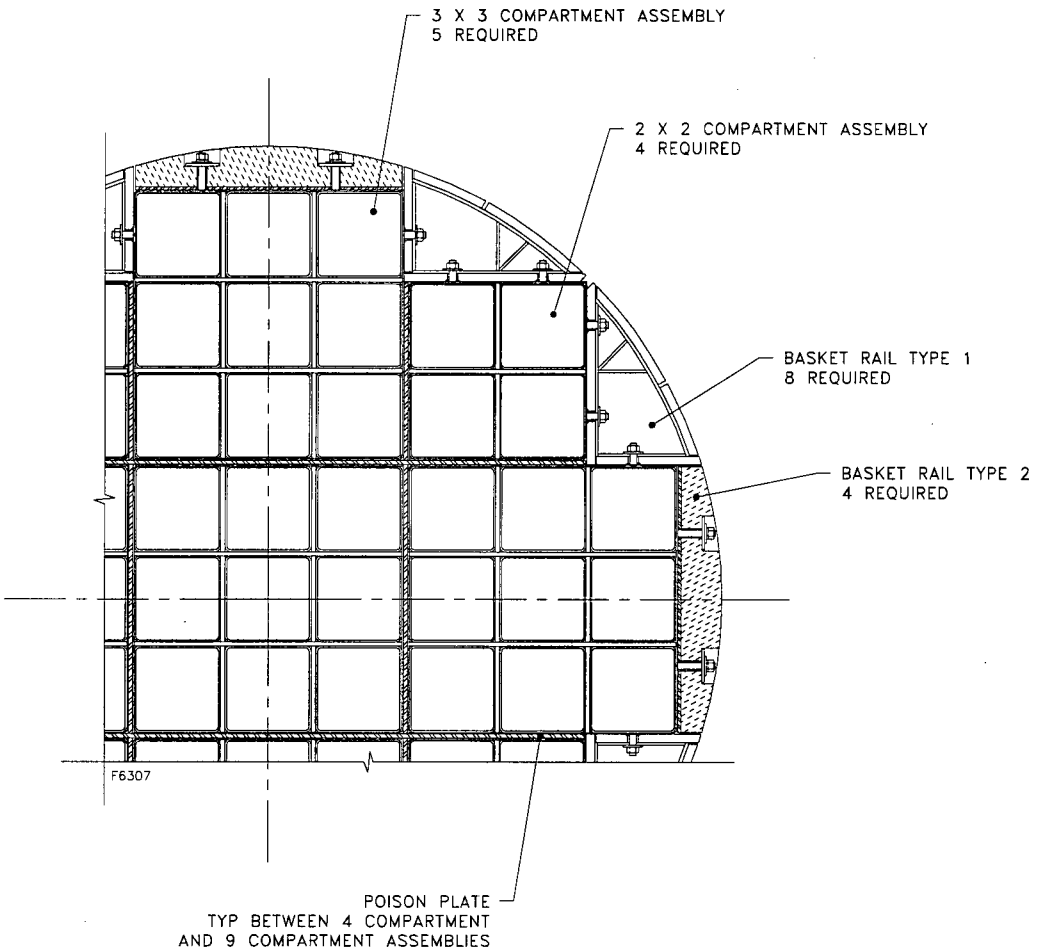

Figure T.6-2
NUHOMS®-61BTH Type 2 DSC Radial Cross Section

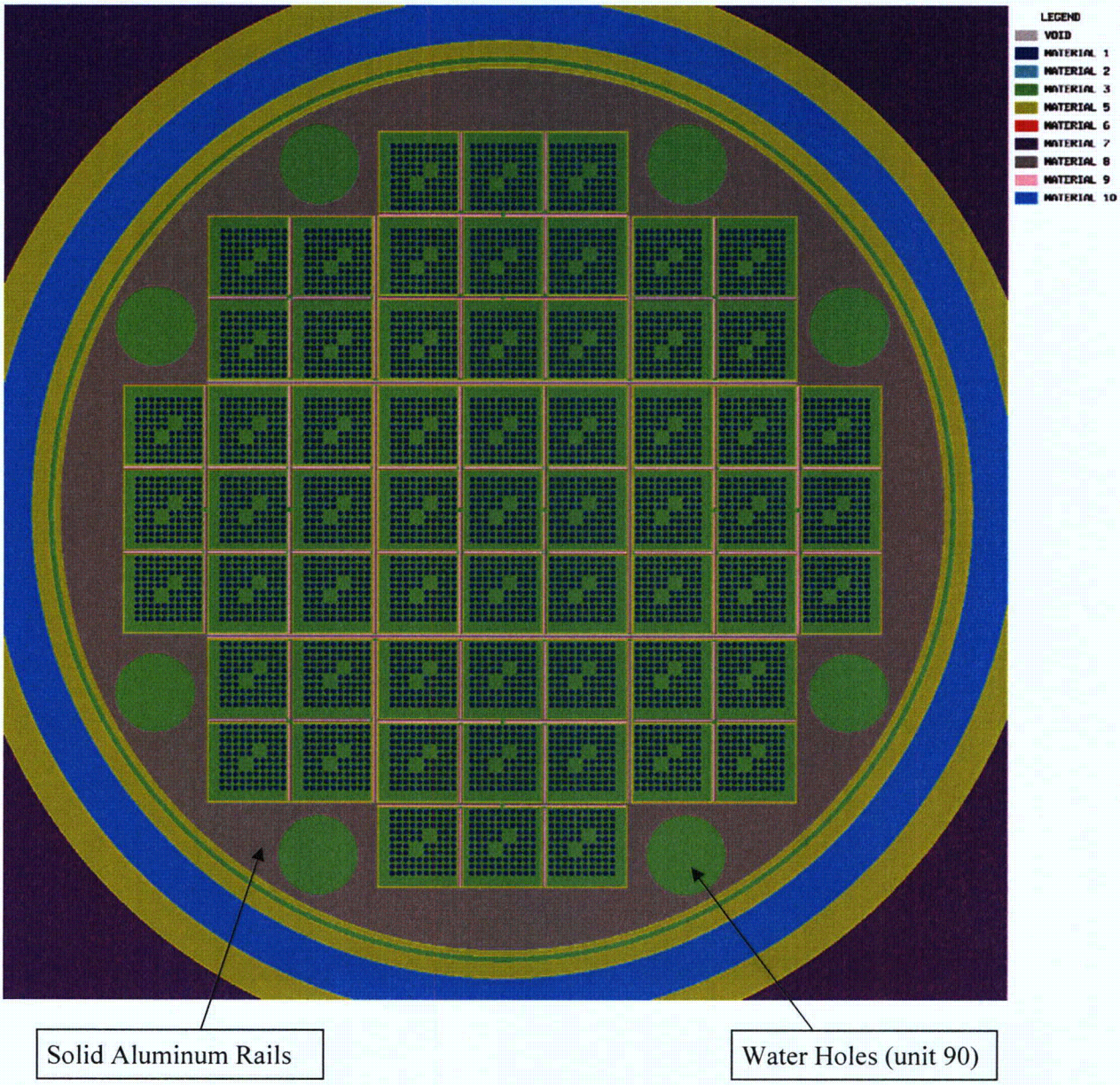

Figure T.6-3
Criticality Calculational KENO Model for Intact Fuel

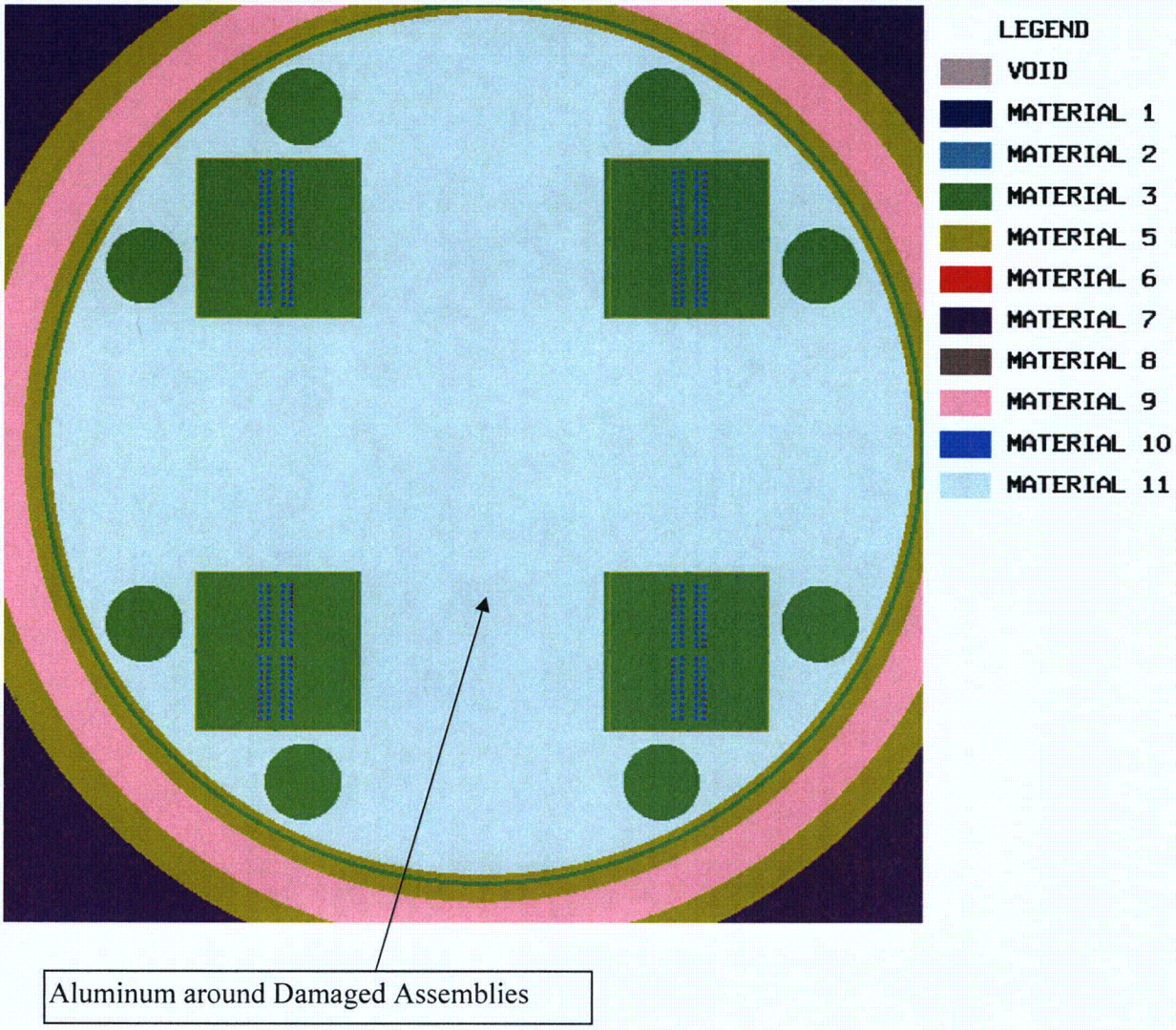

Figure T.6-4
Double Break – Beyond Poison Plates, Aluminum in DSC

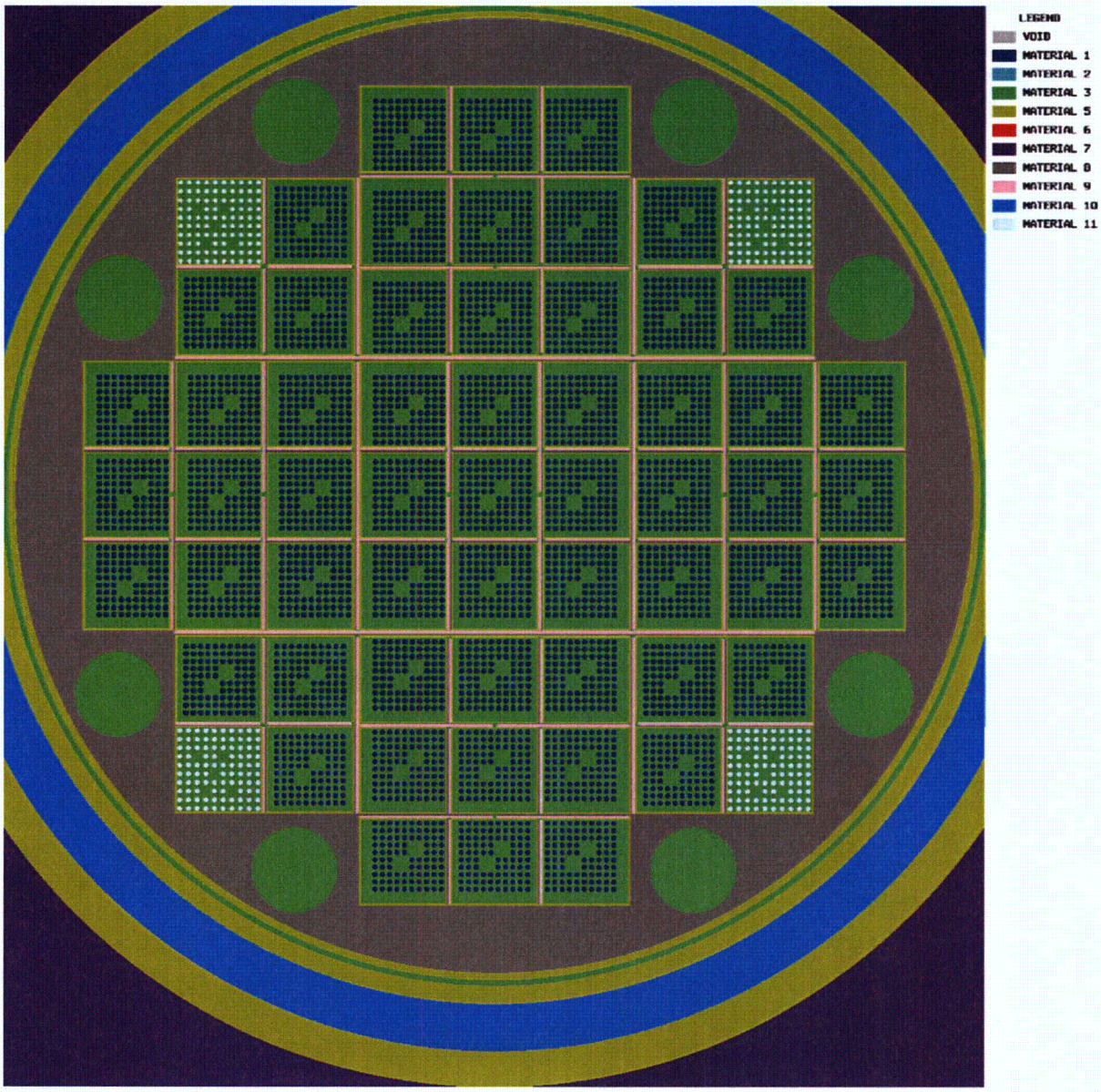

Figure T.6-5
Design Basis Damaged Assembly Loading – 4 Assemblies

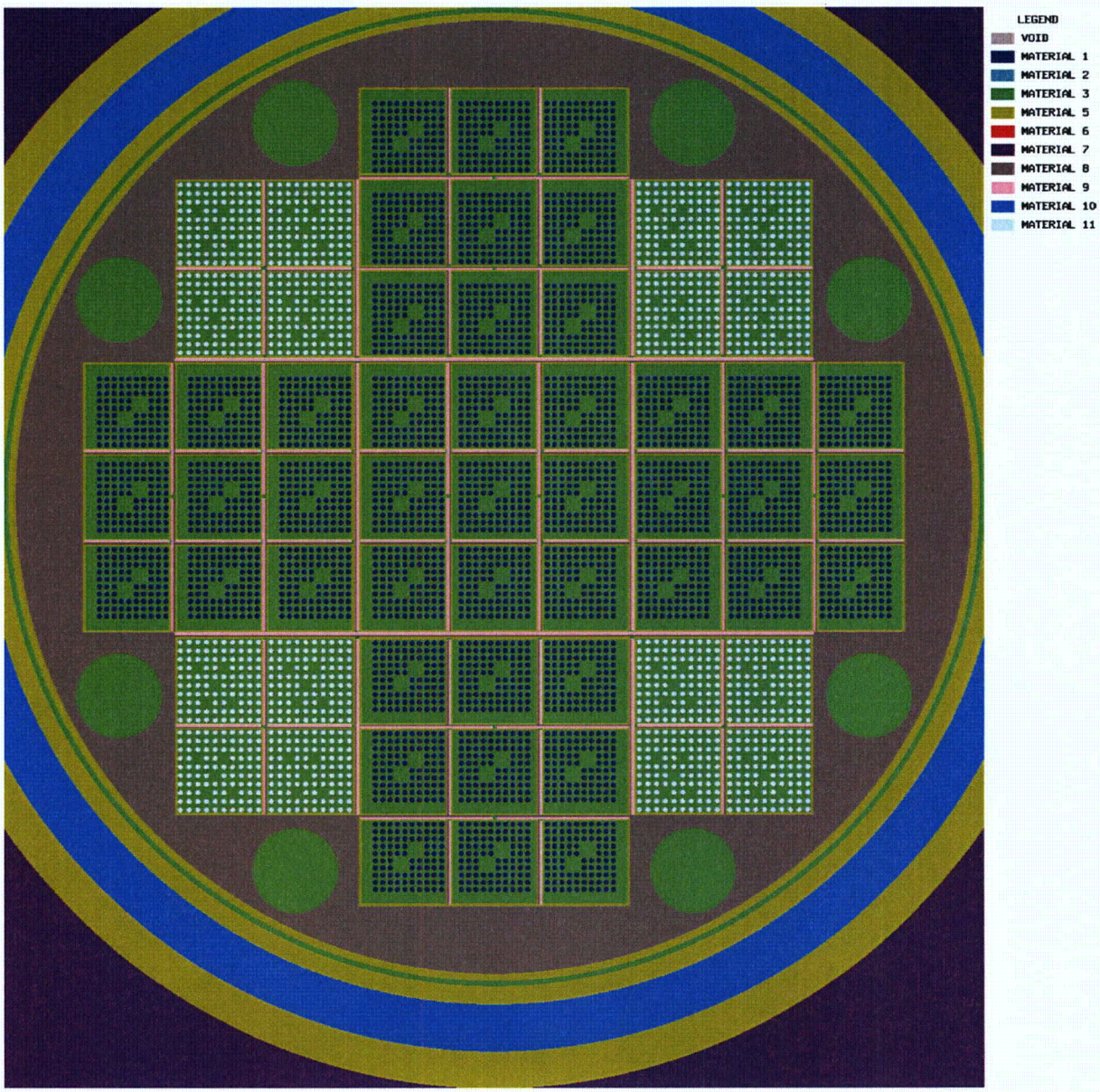

Figure T.6-6
Design Basis Damaged Assembly Loading – 16 Assemblies

T.7 Confinement

Confinement of all radioactive materials in the NUHOMS®-61BTH system is provided by the NUHOMS®-61BTH DSC which is designed and tested to meet the leak tight criteria of ANSI N14.5 1997 [7.1].

As discussed in Section 7.2.2 of the UFSAR, the release of airborne radioactive material is addressed for three phases of system operation: fuel handling in the spent fuel pool, drying and sealing of the DSC, and DSC transfer and storage. Potential airborne releases from irradiated fuel assemblies in the spent fuel pool are discussed in the plant's existing 10CFR50 license.

DSC drying and sealing operations are performed using procedures which prohibit airborne leakage. During these operations, all vent lines are routed to the existing radwaste systems of the plant. Once the DSC is dried and sealed, there are no design basis accidents which could result in a breach of the DSC and the airborne release of radioactivity. Design provisions to preclude the release of gaseous fission products as a result of accident conditions are discussed in Section 8.2.9.

During transfer of the sealed DSC and subsequent storage in the HSM, the only postulated mechanism for the release of airborne radioactive material is the dispersion of non-fixed surface contamination on the DSC exterior. By filling the TC/DSC annulus with demineralized water, placing an inflatable seal over the annulus, and utilizing procedures which require examination of the annulus surfaces for smearable contamination, the contamination limits on the DSC can be maintained below the permissible level for off-site shipments of fuel. Therefore, there is no possibility of significant radionuclide release from the DSC exterior surface during transfer or storage.

T.7.1 Confinement Boundary

Once inside the DSC, the SFAs are confined by the DSC shell and by multiple barriers at each end of the DSC. For intact fuel, the fuel cladding is the first barrier for confinement of radioactive materials. The fuel cladding is protected by maintaining the cladding temperatures during storage below those levels which may cause degradation of the cladding. In addition, the SFAs are stored in an inert atmosphere to prevent degradation of the fuel, specifically cladding rupture due to oxidation and its resulting volumetric expansion of the fuel. Thus, a helium atmosphere for the DSC is incorporated into the design to protect the fuel cladding integrity by inhibiting the ingress of oxygen into the DSC cavity.

Helium is known to leak through valves, mechanical seals, and escape through very small passages because of its small atomic diameter and because it is an inert element and exists in a monatomic species. Negligible leakage rates can be achieved with careful design of vessel closures. Helium will not, to any practical extent, diffuse through stainless steel. For this reason, the DSC has been designed as a redundant weld-sealed containment pressure vessel with no mechanical or electrical penetrations.

For damaged fuel assemblies, top and bottom end caps are provided to contain fuel debris such as broken rods, loose pellets and/or pieces of cladding in the fuel compartment. The end caps fit snugly into the top and bottom of the fuel compartment. They are held in place by the fuel compartments and the inner bottom cover plate and the top shield plug during transfer and storage. The end caps have multiple small through holes to permit unrestricted flooding and draining of the fuel cells.

T.7.1.1 Confinement Vessel

The confinement vessel is provided by the NUHOMS®-61BTH DSC. The DSC is designed to provide confinement of all radionuclides under normal and accident conditions. The DSC is designed, fabricated and tested in accordance with the applicable requirements of the ASME Boiler and Pressure Vessel Code, Division 1, Section III, Subsection NB [7.2] with alternatives to the code as discussed in Chapter T.3 Section T.3.1.2.3. The DSC shell and inner and outer bottom cover plates are delivered to the site as an assembly. The shell and the inner bottom cover plate, which provide the confinement boundary as shown in Figure T.3.1-1, are pressure tested in accordance with the ASME code, Section III, NB-6300 and leak tested to meet the ANSI N14.5 [7.1] leak-tight criteria. The pneumatic pressure test and leak test are performed on the finished shell and the inner bottom cover plate during fabrication. The outer bottom cover plate root and final layer closure welds are inspected using dye penetrant inspection methods in accordance with requirements of the ASME code [7.2].

Once the fuel assemblies are loaded into the DSC, the heavy shield plug is installed to provide radiation shielding to minimize radiation exposure to workers during DSC closure operations. The inner top cover plate is welded into place along with the vent and siphon port cover plates. These welds and associated components define the confinement boundary at the top end of the DSC as shown in Figure T.3.1-1. These welds are applied using a multiple layer technique with multi-level PT in accordance with the alternative to the ASME code as specified in Section T.3.1.2.3 and ISG-15 [7.4]. Finally, the outer top cover plate is welded into place to provide

redundant sealing. The outer top cover plate is a structural attachment to the DSC confinement boundary. The welds of the inner plate are tested using the test port in the outer top cover plate or other alternate means to meet the leak tight criteria of ANSI N14.5 [7.1]. A test port plug (if used) is then threaded into the outer top cover plate and seal welded in place. The root, mid and final layer closure welds are inspected using dye penetrant inspection methods in accordance with requirements of the ASME code [7.2].

T.7.1.2 Confinement Penetrations

The DSC confinement boundary contains two penetrations (vent and siphon ports) for draining, vacuum drying and backfilling the DSC cavity. The vent and siphon ports are closed with welded cover plates and the DSC outer top cover plate provides the redundant closure. The DSC outer top cover plate has an optional single penetration used for leak testing the closure welds. A test port plug (if used) is threaded into the outer top cover plate and seal welded in place after testing to complete the redundant closure. The DSC has no bolted closures or mechanical seals.

T.7.1.3 Seals and Welds

The welds made during fabrication of the 61BTH DSC that affect the confinement boundary include the weld applied to the shell bottom and the circumferential and longitudinal seam welds applied to the cylindrical shell. These welds are inspected (radiographic or ultrasonic inspection, and liquid penetrant inspection) according to the requirements of Subsection NB of the ASME code.

The welds applied to the vent and siphon port covers and the inner top cover plate during closure operations, define the confinement boundary at the top end of the 61BTH DSC. These welds are applied using a multiple-layer technique with multi-level PT in accordance with alternatives to the ASME code as specified in Chapter T.3 Section T.3.1.2.3 and ISG-15 [7.4]. This effectively eliminates any pinhole leak which might occur in a single-pass weld, since the chance of pinholes being in alignment on successive weld passes is negligibly small. Chapter T.3, Figure T.3.1-1 provides a graphic representation of the confinement boundaries and welds.

T.7.1.4 Closure

All top end closure welds are multiple-layer welds. This effectively eliminates a pinhole leak which might occur in a single pass weld, since the chance of pinholes being in alignment on successive weld passes is negligibly small. Furthermore, the DSC cover plates are sealed by separate, redundant closure welds. Finally, the inner closure welds are tested to the leak tight criteria of ANSI N14.5 [7.1]. There are no bolted closures or mechanical seals.

T.7.2 Requirements for Normal Conditions of Storage

T.7.2.1 Release of Radioactive Material

The NUHOMS®-61BTH DSC is designed, fabricated and tested to meet the leak tight criteria of ANSI N14.5 [7.1]. Therefore, there is no release of radioactive material under normal conditions of storage. As noted in acceptance criteria IV-4 of [7.3], a closure monitoring system is not required. The confinement boundary ensures that the inert fill gas does not leak or diffuse through the weld or parent material of the DSC. The continued effectiveness of the confinement boundary is demonstrated by (a) either a daily visual inspection of the HSM inlets and outlets or a daily monitoring of the HSM thermal performance, and (b) the use of radiation monitors (typically TLDs) on the ISFSI boundary fence. A breach of the confinement boundary would result in an increase in the measured dose at the ISFSI fence. If an increase were detected, steps would be initiated to enable the licensee to take corrective actions to maintain safe storage conditions.

T.7.2.2 Pressurization of Confinement Vessel

The maximum internal pressures in the NUHOMS®-61BTH DSC during normal operations are reported in Section T.4.6.6.4 to be 7.3 psig for the Type 1 DSC and 7.6 psig for the Type 2 DSC. The maximum internal pressures during off-normal conditions are 10.9 psig and 12.1 psig for the Type 1 and Type 2 DSCs, respectively. These pressures are below the design pressures of the DSC as shown in Section T.4.1.

T.7.3 Confinement Requirements for Hypothetical Accident Conditions

T.7.3.1 Fission Gas Products

The analysis presented in Section T.3 demonstrates that the confinement boundary (pressure boundary) is not compromised following hypothetical accident conditions. Therefore, there is no need to calculate the fission gas products available for release.

T.7.3.2 Release of Contents

The NUHOMS®-61BTH DSC is designed and tested to meet the leak tight criteria of ANSI N14.5 [7.1]. The analysis presented in Section T.3 demonstrates that the confinement boundary (pressure boundary) is not compromised following hypothetical accident conditions. Therefore, there is no release of radioactive material under hypothetical accident conditions of storage.

T.7.4 References

7.1 "American National Standard for Radioactive Materials – Leakage Tests on Packages for Shipment," ANSI N14.5-1997, American National Standards Institute, Inc., New York, New York, 1997.

7.2 ASME Boiler and Pressure Vessel Code, Section III, Division 1, Subsection NB, 1998, including 2000 addenda.

7.3 U.S. Nuclear Regulatory Commission, Interim Staff Guidance (ISG)-5, "Confinement Evaluation," Revision 1.

7.4 U.S. Nuclear Regulatory Commission, Interim Staff Guidance (ISG)-15, "Materials Evaluation."

T.8 Operating Systems

This Chapter presents the operating procedures for the standardized NUHOMS®-61BTH system described in previous chapters and shown on the drawings in Section T.1.5. The procedures include preparation of the DSC and fuel loading, closure of the DSC, transport to the ISFSI, DSC transfer into the HSM, monitoring operations, and DSC retrieval from the HSM. The standardized NUHOMS® transfer equipment, and the existing plant systems and equipment are used to accomplish these operations. Procedures are delineated here to describe how these operations are to be performed and are not intended to be limiting. Standard fuel and cask handling operations performed under the plant's 10CFR50 operating license are described in less detail. Existing operational procedures may be revised by the licensee and new ones may be developed according to the requirements of the plant, provided that the limiting conditions of operation specified in Technical Specifications, Functional and Operating Limits of the NUHOMS® CoC are not exceeded.

The following sections outline the typical operating procedures for the standardized NUHOMS® system. These generic NUHOMS® procedures have been developed to minimize the amount of time required to complete the subject operations, to minimize personnel exposure, and to assure that all operations required for DSC loading, closure, transfer, and storage are performed safely. Plant specific ISFSI procedures are to be developed by each licensee in accordance with the requirements of 10CFR72.24 (h) and the guidance of Regulatory Guide 3.61 [8.1]. The generic procedures presented here are provided as a guide for the preparation of plant specific procedures and serve to point out how the NUHOMS® system operations are to be accomplished. They are not intended to be limiting, in that the licensee may judge that alternate acceptable means are available to accomplish the same operational objective.

Process flow diagrams for the NUHOMS® system operation are presented Figure T.8.1-1 and Figure T.8.2-1. The location of the various operations may vary with individual plant requirements. The following steps describe the recommended generic operating procedures for the standardized NUHOMS® system.

Note: The generic terms used throughout this section are as follows, depending on the system configuration. See Chapter T.1 for a description of the components.

- Transfer Cask (TC) may be either a NUHOMS® OS197/OS197H or OS197FC-B,
- DSC may be a NUHOMS® 61BTH Type 1 or Type 2, and
- HSM may be a NUHOMS® HSM-H or a standardized NUHOMS® HSM (Model 80, Model 102, Model 152, or Model 202).

T.8.1 Procedures for Loading the Cask

T.8.1.1 Preparation of the Transfer Cask and DSC

1. Prior to placement in dry storage, the candidate intact and damaged fuel assemblies shall be evaluated (by plant records or other means) to verify that they meet the physical, thermal and radiological criteria specified in Technical Specification 1.2.1.

2. Prior to being placed in service, the transfer cask is to be cleaned or decontaminated as necessary to insure a surface contamination level of less than those specified in Technical Specification 1.2.12.

3. Place the transfer cask in the vertical position in the cask decon area using the cask handling crane and the transfer cask lifting yoke.

4. Place scaffolding around the cask so that the transfer cask top cover plate and surface of the cask are easily accessible to personnel.

5. Remove the transfer cask top cover plate and examine the cask cavity for any physical damage and ready the cask for service.

6. Examine the DSC for any physical damage which might have occurred since the receipt inspection was performed. The DSC is to be cleaned and any loose debris removed. Record the DSC serial number which is located on the grapple ring. Verify the correct DSC type, basket type, and poison material types against the DSC serial number. Verify that the DSC is appropriate for the specific fuel loading campaign per Technical Specification 1.2.1.

7. Using a crane, lower the DSC into the cask cavity by the internal lifting lugs and rotate the DSC to match the cask and DSC alignment marks.

8. If damaged fuel assemblies are to be included in a specific loading campaign, place the required number of bottom end caps provided (up to a maximum of 16) into the bottom of the appropriate 2x2 compartments of the basket, as shown in Figure 1-25 of Technical Specification 1.2.1.

9. Fill the TC/DSC annulus with clean, demineralized water. Place the inflatable seal into the upper cask liner recess and seal the TC/DSC annulus by pressurizing the seal with compressed air.

10. Fill the DSC cavity with water from the fuel pool or an equivalent source.

    Note: A TC/DSC annulus pressurization tank filled with water from the fuel pool as described above is connected to the top vent port of the TC via a hose to provide a positive head above the level of water in the TC/DSC annulus. This is an optional arrangement, which provides additional assurance that contaminated water from the fuel pool will not enter the TC/DSC annulus, provided a positive head is maintained at all times.

11. a. For DSCs with removable hold down rings, test fit the hold down ring into the canister. Examine the hold down ring to ensure a proper fit. Remove hold down ring. (Note this step may be completed earlier and hold down ring may be left in place while testing the top shield plug fit-up.)

    b. Place the top shield plug onto the DSC. Examine the top shield plug to ensure a proper fit. If using the rigging cables under the yoke to install the shield plug, attach the rigging cables to the shield plug and adjust the rigging cables as necessary to obtain even cable tension. Remove top shield plug and hold down ring, if present. (Note this step may be complete earlier.)

12. Position the cask lifting yoke above the transfer cask and engage the cask lifting trunnions.

13. Visually inspect the yoke lifting hooks to insure that they are properly positioned and engaged on the cask lifting trunnions.

14. Provide for later connection to a water draining/pumping device to the siphon port of the DSC and position any connecting hose such that the hose will not interfere with loading (yoke, fuel, shield plug, rigging, etc.). A flowmeter or other suitable means for measuring the amount of water removed must be provided for at a suitable location as part of this connection.

15. Move the scaffolding away from the cask as necessary.

16. Lift the cask just far enough to allow the weight of the cask to be distributed onto the yoke lifting hooks. Reinspect the lifting hooks to insure that they are properly positioned on the cask trunnions.

17. a. Optionally, secure a sheet of suitable material to the bottom of the transfer cask to minimize the potential for ground-in contamination. This may also be done prior to initial placement of the cask in the decon area.

    b. Fill the TC liquid neutron shield as required by licensee ALARA requirements and crane capacity limits. This step may be completed at any time prior to immersion of the TC/DSC into the pool.

18. Prior to the cask being lowered into the fuel pool, the water level in the pool should be adjusted as necessary to accommodate the TC/DSC volume. If the water placed in the DSC cavity was obtained from the fuel pool, a level adjustment may not be necessary.

T.8.1.2 <u>DSC Fuel Loading</u>

1. Lift the TC/DSC and position it over the cask loading area of the spent fuel pool in accordance with the plant's 10CFR50 cask handling procedures.

2. Lower the cask into the fuel pool until the bottom of the cask is at the height of the fuel pool surface. As the cask is lowered into the pool, spray the exterior surface of the cask with demineralized water.

3. Place the cask in the designated location of the fuel pool.

4. Disengage the lifting yoke from the cask lifting trunnions and move the yoke. Spray the lifting yoke with clean water if it is raised out of the fuel pool.

5. The potential for fuel misloading is essentially eliminated through the implementation of procedural and administrative controls. The controls instituted to ensure that damaged and/or intact fuel assemblies are placed into a known cell location within a DSC, will typically consist of the following:

   - A TC/DSC loading plan is developed to verify that the damaged and/or intact fuel assemblies meet the burnup, enrichment and cooling time parameters of Technical Specification 1.2.1.

   - The loading plan is independently verified and approved before the fuel load.

   - A fuel movement schedule is then written, verified and approved based upon the loading plan. All fuel movements from any rack location are performed under strict compliance with the fuel movement schedule.

   - If loading damaged fuel assemblies, verify that the required number of bottom end caps are installed in appropriate fuel compartment tube locations before fuel load.

6. Prior to insertion of a spent fuel assembly into the DSC, the identity of the assembly is to be verified by two individuals using an underwater video camera or other means. Read and record the fuel assembly identification number from the fuel assembly and check this identification number against the DSC loading plan which indicates which fuel assemblies are acceptable for dry storage.

7. Position the fuel assembly for insertion into the selected DSC storage cell and load the fuel assembly. Repeat Steps 5 through 7 for each SFA loaded into the DSC. If loading damaged fuel assemblies, place top end caps over each damaged fuel assembly placed into the basket. A maximum of 16 damaged fuel assemblies may be loaded into the appropriate 2x2 compartments of the 61BTH DSC basket per Technical Specification 1.2.1. After the DSC has been fully loaded, check and record the identity and location of each fuel assembly in the DSC.

8. a. After all the SFAs have been placed into the DSC and their identities verified, place the hold down ring or optional top grid assembly as applicable. Visually verify that the hold down ring is properly seated.

b. Position the lifting yoke and the top shield plug and lower the shield plug into the DSC. Note that separate rigging may be used to install the shield plug prior to engaging the trunnions with the lifting yoke.

CAUTION: Verify that all the lifting height restrictions as a function of temperature specified in Technical Specification 1.2.13 can be met in the following steps which involve lifting of the transfer cask.

9. Visually verify that the top shield plug is properly seated within the DSC.

10. Position the lifting yoke with the cask trunnions and verify that it is properly engaged.

11. Raise the transfer cask to the pool surface. Prior to raising the top of the cask above the water surface, stop vertical movement.

12. Inspect the top shield plug to verify that it is properly seated within the DSC. If not, lower the cask and reposition the top shield plug and or remove the shield plug and reposition the hold down ring. Repeat Steps 8 through 12 as necessary.

13. Continue to raise the cask from the pool and spray the exposed portion of the cask with water until the top region of the cask is accessible.

14. Drain any excess water from the top of the DSC shield plug back to the fuel pool. Check the radiation levels at the center of top shield plug and around the perimeter of the cask. Disconnect the top shield plug rigging.

15. Drain a minimum of 50 gallons of water. Optionally approximately 1100 gallons of water (as indicated on the flow meter) may be drained from the DSC back into the fuel pool or other suitable location to meet the weight limit on the crane. Use 1-3 psig of helium to backfill the DSC with an inert gas per ISG-22 [8.2] guidance as water is being removed from the DSC.

16. Lift the cask from the fuel pool. As the cask is raised from the pool, continue to spray the cask with water and decon as directed.

17. Move the cask with loaded DSC to the cask decon area.

18. Install cask seismic restraints if required by Technical Specification 1.2.16 (required only on plant specific basis).

T.8.1.3 <u>DSC Drying and Backfilling</u>

CAUTION: During performance of steps listed in Section T.8.1.3, monitor the TC/DSC annulus water level and replenish as necessary until drained.

1. Check the radiation levels along the perimeter of the cask. The cask exterior surface should be decontaminated as necessary in accordance with the limits specified in Technical

Specification 1.2.12. Temporary shielding may be installed as necessary to minimize personnel exposure.

2. Place scaffolding around the cask so that any point on the surface of the cask is easily accessible to personnel.

3. Disengage the rigging cables from the top shield plug and remove the eyebolts. Disengage the lifting yoke from the trunnions and position it clear of the cask.

4. Decontaminate the exposed surfaces of the DSC shell perimeter and remove the inflatable TC/DSC annulus seal.

5. Connect the cask drain line to the cask, open the cask cavity drain port and allow water from the annulus to drain out until the water level is approximately twelve inches below the top edge of the DSC shell. Take swipes around the outer surface of the DSC shell and check for smearable contamination in accordance with the Technical Specification 1.2.12 limits.

   CAUTION: Radiation dose rates are expected to be high at the vent and siphon port locations. Use proper ALARA practices (e.g., use of temporary shielding, appropriate positioning of personnel, etc.) to minimize personnel exposure.

6. Drain approximately 1100 gallons of water (as indicated on a flowmeter) from the DSC back into the fuel pool or other suitable location if not drained in Step 8.1.2.15. Consistent with ISG-22 [8.2] guidance, helium at 1-3 psig is used to backfill the DSC with an inert gas (helium) as water is being removed from the DSC.

7. Monitor TC/DSC annulus water level and replenish as necessary until drained.

8. Install the automatic welding machine onto the inner top cover plate and place the inner top cover plate with the automatic welding machine onto the DSC. Optionally, the inner top cover plate and the automatic welding machine can be placed separately. Verify proper fit-up of the inner top cover plate with the DSC shell.

9. Check radiation levels along the surface of the inner top cover plate. Temporary shielding may be installed as necessary to minimize personnel exposure. Verify that the TC dose rates are compliant with the limits specified in Technical Specification 1.2.11d.

10. Insert approximately ¼ inch tubing of sufficient length and adequate temperature resistance through the vent port such that it terminates just below the DSC top shield plug. Connect the tubing to a hydrogen monitor to allow continuous monitoring of the hydrogen atmosphere in the DSC cavity during welding of the inner top cover plate.

11. Cover the TC/DSC annulus to prevent debris and weld splatter from entering the annulus.

12. Ready the automatic welding machine and tack weld the inner top cover plate to the DSC shell. Install the inner top cover plate weldment and remove the automatic welding machine.

CAUTION: Continuously monitor the hydrogen concentration in the DSC cavity using the arrangement or other alternate methods described in step 10 during the inner top cover plate cutting/welding operations. Verify that the measured hydrogen concentration does not exceed a safety limit of 2.4% [8.3 and 8.4]. If this limit is exceeded, stop all welding operations and purge the DSC cavity with 2-3 psig helium via the tubing to reduce the hydrogen concentration safely below the 2.4% limit.

13. Perform dye penetrant weld examination of the inner top cover plate weld in accordance with the Technical Specification 1.2.5 requirements.

14. If loading a Type 2 61BTH DSC or if using a suction pump rather than blowdown to remove water, skip to step 16; otherwise, place the strongback so that it sits on the inner top cover plate and is oriented such that:

    - The DSC siphon and vent ports are accessible
    - The strongback stud holes line up with the TC lid bolt holes

15. Lubricate the studs and, using a crossing pattern, adjust the strongback studs to snug tight ensuring approximately even pressure on the cover plate.

16. Remove purge lines and connect the VDS to the DSC siphon and vent ports.

17. Install temporary shielding to minimize personnel exposure throughout the subsequent welding operations as required.

18. a. If using blowdown method to remove water, engage helium supply (up to 10 psig for Type 1 DSC or 15 psig for Type 2 DSC) and open the valve on the vent port and allow helium to force the water from the DSC cavity through the siphon port.

    b. If using water pump to remove water without blowdown pump water from DSC.

19. Once the water stops flowing from the DSC, close the DSC siphon port and disengage the gas source or turn off the suction pump, as applicable.

20. Connect the hose from the vent port and the siphon port to the intake of the vacuum pump. Connect a hose from the discharge side of the VDS to the plant's radioactive waste system or spent fuel pool. Connect the VDS to a helium source.

    NOTE: Proceed cautiously when evacuating the DSC to avoid freezing consequences.

21. Open the valve on the suction side of the pump, start the VDS and draw a vacuum on the DSC cavity. The cavity pressure should be reduced in steps of approximately 100 mm Hg, 50 mm Hg, 25 mm Hg, 15 mm Hg, 10 mm Hg, 5 mm Hg, and 3 mm Hg. After pumping down to each level (these levels are optional), the pump is valved off and the cavity pressure monitored. The cavity pressure will rise as water and other volatiles in the cavity evaporate. When the cavity pressure stabilizes, the pump is valved in to complete the vacuum drying process. It may be necessary to repeat some steps, depending on the rate and

extent of the pressure increase. Vacuum drying is complete when the pressure stabilizes for a minimum of 30 minutes at 3 mm Hg or less as specified in Technical Specification 1.2.2.

CAUTION: Radiation dose rates are expected to be high at the vent and siphon port locations. Use proper ALARA practices (e.g., use of temporary shielding, appropriate positioning of personnel, etc.) to minimize personnel exposure.

22. Open the valve to the vent port and allow the helium to flow into the DSC cavity.

23. Pressurize the DSC with helium (up to 10 psig for Type 1 DSC or 15 psig for Type 2 DSC).

24. Helium leak test the inner top cover plate weld for a leak rate of 1×10^{-4} atm cm^3/sec. This test is optional.

25. If a leak is found, repair the weld, repressurize the DSC and repeat the helium leak test.

26. Once no leaks are detected, depressurize the DSC cavity by releasing the helium through the VDS to the plant's spent fuel pool or radioactive waste system.

27. Re-evacuate the DSC cavity using the VDS. The cavity pressure should be reduced in steps of approximately 10 mm Hg, 5 mm Hg, and 3 mm Hg. After pumping down to each level, the pump is valved off and the cavity pressure is monitored (these levels are optional). When the cavity pressure stabilizes, the pump is valved in to continue the vacuum drying process. Vacuum drying is complete when the pressure stabilizes for a minimum of 30 minutes at 3 mm Hg or less in accordance with Technical Specification 1.2.2 limits.

28. Open the valve on the vent port and allow helium to flow into the DSC cavity to pressurize the DSC 22.5-23.5 psig and hold for 10 minutes. Depressurize the DSC cavity by releasing the helium through the VDS to the plant spent fuel pool or radioactive waste system to about 2.5 psig in accordance with Technical Specification 1.2.3a limits.

    CAUTION: Radiation dose rates are expected to be high at the vent and siphon port locations. Use proper ALARA practices (e.g., use of temporary shielding, appropriate positioning of personnel, etc.) to minimize personnel exposure.

29. Close the valves on the helium source.

30. Remove the strongback, if installed in step 14 above, decontaminate as necessary, and store.

T.8.1.4 DSC Sealing Operations

CAUTION: During performance of steps listed in Section T.8.1.4, monitor the cask/DSC annulus water level and replenish as necessary to maintain cooling.

1. Disconnect the VDS from the DSC. Seal weld the prefabricated plugs over the vent and siphon ports. Inject helium into blind space just prior to completing welding and perform a

dye penetrant weld examination in accordance with the Technical Specification 1.2.5 requirements.

2. Temporary shielding may be installed as necessary to minimize personnel exposure. Install the automatic welding machine onto the outer top cover plate and place the outer top cover plate with the automatic welding system onto the DSC. Optionally, outer top cover plate may be installed separately from the welding machine. Verify proper fit up of the outer top cover plate with the DSC shell.

3. Tack weld the outer top cover plate to the DSC shell. Place the outer top cover plate weld root pass.

4. Helium leak test the inner top cover plate and vent/siphon port plate welds using the leak test port in the outer top cover plate in accordance with Technical Specification 1.2.4a limits. Verify that the personnel performing the leak test are qualified in accordance with SNT-TC-1A [8.5]. Alternatively, this can be done with a test head in step 1 of Section T.8.1.4.

5. If a leak is found, remove the outer cover plate root pass (if not using test head), the vent and siphon port plugs and repair the inner cover plate welds. Then install the strongback (if used) and repeat procedure steps from T.8.1.3 step 21.

6. Perform dye penetrant examination of the root pass weld. Weld out the outer top cover plate to the DSC shell and perform dye penetrant examination on the weld surface in accordance with the Technical Specification 1.2.5 requirements.

7. Install and seal weld the prefabricated plug, if applicable, over the outer cover plate test port and perform dye penetrant weld examinations in accordance with Technical Specification 1.2.5 requirements.

8. Remove the automatic welding machine from the DSC.

9. Open the cask drain port valve and drain the water from the cask/DSC annulus.

10. Rig the cask top cover plate and lower the cover plate onto the transfer cask.

11. Bolt the cask cover plate into place, tightening the bolts to the required torque in a star pattern.

    CAUTION: Monitor the applicable time limits of Technical Specification 1.2.18a until the completion of DSC transfer step 6 of Section T.8.1.6, if loading Type 2 61BTH DSC.

12. Verify that the TC dose rates are compliant with limits specified in Technical Specification 1.2.11d.

T.8.1.5 <u>Transfer Cask Downending and Transport to ISFSI</u>

NOTE:

Alternate Procedure for Downending of Transfer Cask: Some plants have limited floor hatch openings above the cask/trailer/skid, which limit crane travel (within the hatch opening) that would be needed in order to downend the TC with the trailer/skid in a stationary position. For these situations, alternate procedures are to be developed on a plant-specific basis, with detailed steps for downending.

1. Re-attach the transfer cask lifting yoke to the crane hook, as necessary. Ready the transport trailer and cask support skid for service.

2. Move the scaffolding away from the cask as necessary. Engage the lifting yoke and lift the cask over the cask support skid on the transport trailer.

3. The transport trailer should be positioned so that the cask support skid is accessible to the crane with the trailer supported on the vertical jacks.

4. Position the cask lower trunnions onto the transfer trailer support skid pillow blocks.

5. Move the crane forward while simultaneously lowering the cask until the cask upper trunnions are just above the support skid upper trunnion pillow blocks.

6. Inspect the positioning of the cask to insure that the cask and trunnion pillow blocks are properly aligned.

7. Lower the cask onto the skid until the weight of the cask is distributed to the trunnion pillow blocks.

8. Inspect the trunnions to insure that they are properly seated onto the skid and install the trunnion tower closure plates if required.

9. Remove the bottom ram access cover plate from the cask if integral ram/trailer is not used. Install the two-piece temporary neutron/gamma shield plug to cover the bottom ram access. Install the ram trunnion support frame on the bottom of the transfer cask. (The temporary shield plug and ram trunnion support frame are not required with the integral ram/trailer.)

T.8.1.6 DSC Transfer to the HSM

1. Prior to transporting the cask to the ISFSI or prior to positioning the transfer cask at the HSM designated for storage, remove the HSM door using a porta-crane, inspect the cavity of the HSM, removing any debris and ready the HSM to receive a DSC. The doors on adjacent HSMs should remain in place.

   CAUTION: Very high dose rates in the empty HSM are expected if they are adjacent to a loaded HSM due to high heat loads in 61BTH DSC. Proper ALARA practices should be followed during these operations.

2. Inspect the HSM air inlet and outlets to ensure that they are clear of debris. Inspect the screens on the air inlet and outlets for damage.

CAUTION: Verify that the requirements of Technical Specification 1.2.14, "TC/DSC Transfer Operations at High Ambient Temperatures," are met prior to the next step.

3. Using a suitable vehicle, transport the cask from the plant's fuel/reactor building to the ISFSI along the designated transfer route.

4. Once at the ISFSI, position the transport trailer to within several inches of the HSM.

5. Check the position of the trailer to ensure the centerline of the HSM and cask approximately coincide. If the trailer is not properly oriented, reposition the trailer, as necessary.

6. Using a crane, unbolt and remove the cask top cover plate.

   CAUTION: Verify that the applicable time limits of Technical Specification 1.2.18a are met if loading Type 2 61BTH DSC.

7. Back the cask to within a few inches of the HSM, set the trailer brakes and disengage the tractor. Drive the tractor clear of the trailer. Extend the transfer trailer vertical jacks.

8. Remove the skid tie-down bolts and use the skid positioning system to bring the cask into approximate vertical and horizontal alignment with the HSM. Using optical survey equipment and the alignment marks on the cask and the HSM, adjust the position of the cask until it is properly aligned with the HSM.

9. Using the skid positioning system, fully insert the cask into the HSM access opening docking collar.

10. Secure the cask trunnions to the front wall embedments of the HSM using the cask restraints.

11. After the cask is docked with the HSM, verify the alignment of the transfer cask using the optical survey equipment.

12. Position the hydraulic ram behind the cask in approximate horizontal alignment with the cask and level the ram. Remove either the bottom ram access cover plate or the outer plug of the two-piece temporary shield plug if installed. Power up the ram hydraulic power supply and extend the ram through the bottom cask opening into the DSC grapple ring.

13. Activate the hydraulic cylinder on the ram grapple and engage the grapple arms with the DSC grapple ring.

14. Recheck all alignment marks in accordance with the Technical Specification 1.2.9 limits and ready all systems for DSC transfer.

15. Activate the hydraulic ram to initiate insertion of the DSC into the HSM. Stop the ram when the DSC reaches the support rail stops at the back of the module.

16. Disengage the ram grapple mechanism so that the grapple is retracted away from the DSC grapple ring.

17. Retract and disengage the hydraulic ram system from the cask and move it clear of the cask. Remove the cask restraints from the HSM.

18. Using the skid positioning system, disengage the cask from the HSM access opening. Insert the DSC axial retainer.

19. Install the HSM door using a portable crane and secure it in place. Door may be welded for security. Verify that the HSM dose rates are compliant with the limits specified in Technical Specification 1.2.7e or 1.2.7f as appropriate.

20. Replace the transfer cask top cover plate. Secure the skid to the trailer, retract the vertical jacks and disconnect the skid positioning system.

21. Tow the trailer and cask to the designated equipment storage area. Return the remaining transfer equipment to the storage area.

22. Close and lock the ISFSI access gate and activate the ISFSI security measures.

T.8.1.7 Monitoring Operations

1. Perform routine security surveillance in accordance with the licensee's ISFSI security plan.

2. Perform one of the two alternate daily surveillance activities listed below:

   a. A daily visual surveillance of the HSM air inlets and outlets to insure that no debris is obstructing the HSM vents in accordance with Technical Specification 1.3.1 requirements.

   b. A temperature measurement of the thermal performance, for each HSM, on a daily basis in accordance with Technical Specification 1.3.2 requirements.

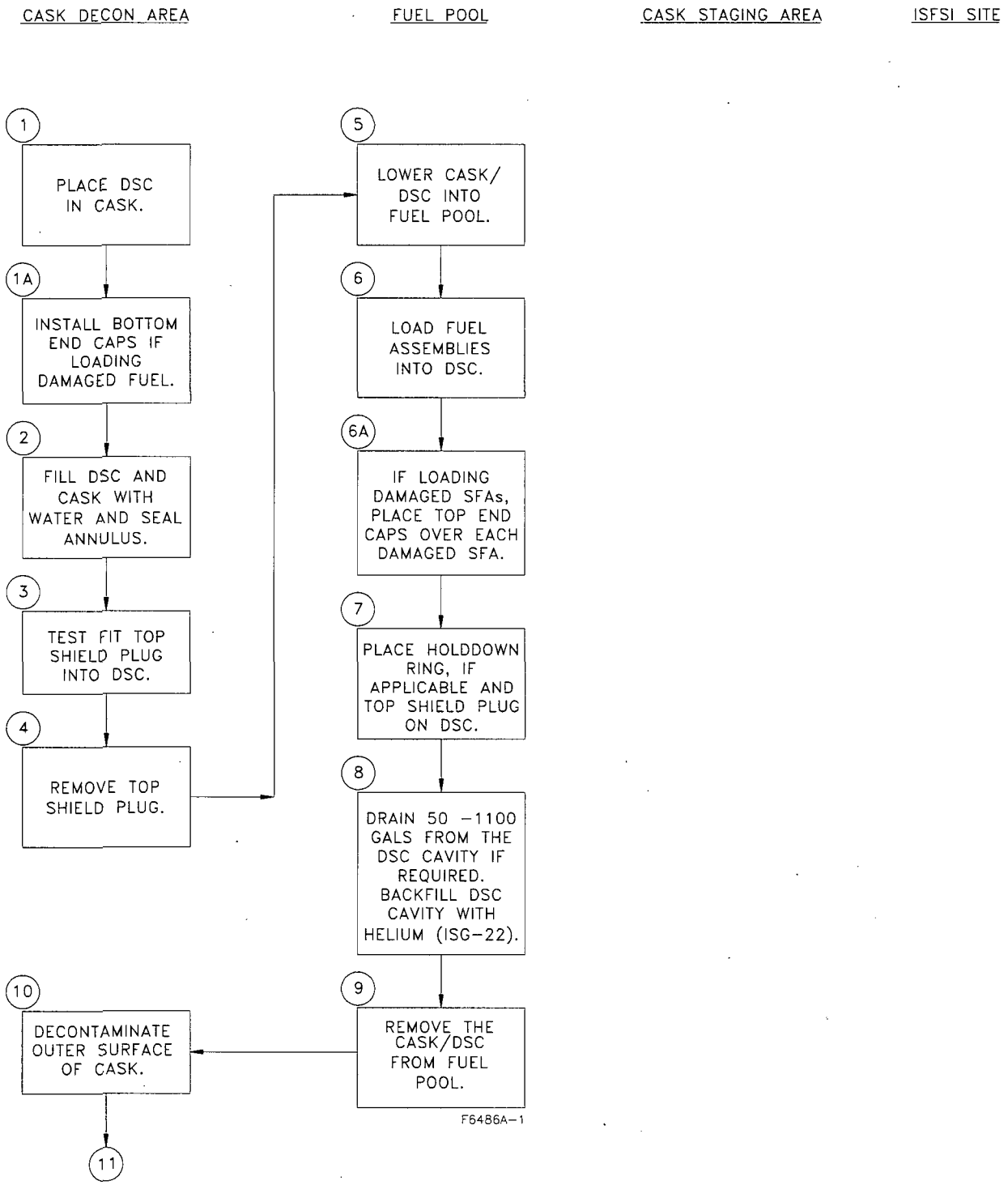

Figure T.8.1-1
NUHOMS® System Loading Operations Flow Chart

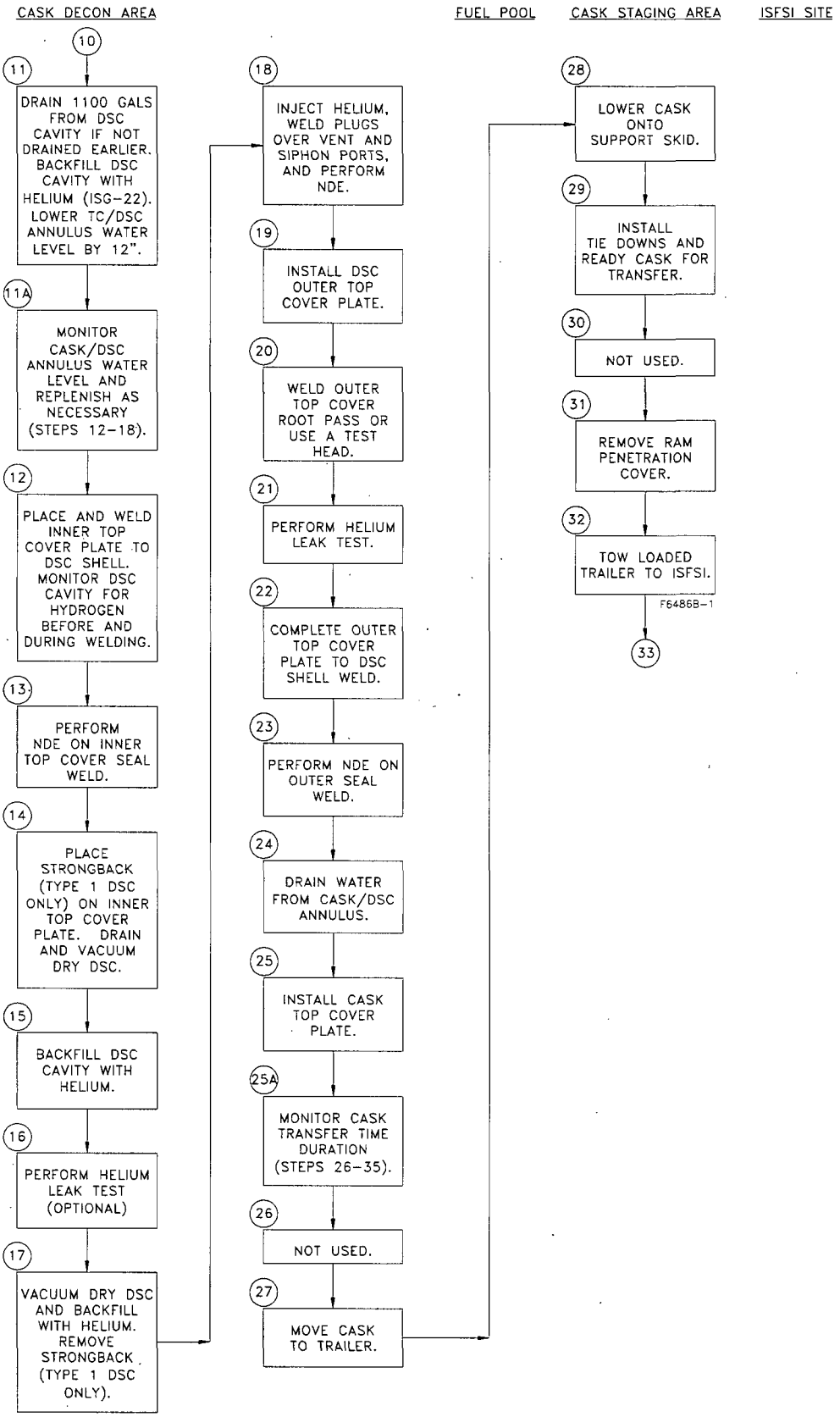

Figure T.8.1-1
NUHOMS® System Loading Operations Flow Chart

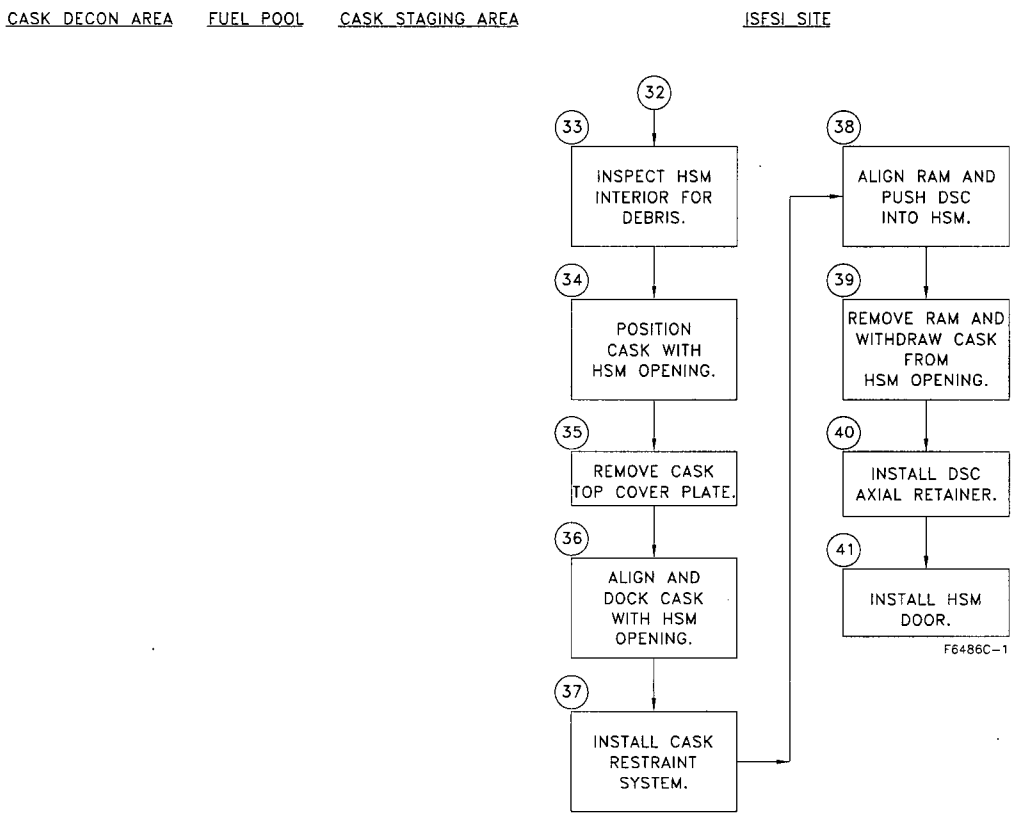

Figure T.8.1-1
NUHOMS® System Loading Operations Flow Chart

(Concluded)

T.8.2 Procedures for Unloading the Cask

T.8.2.1 DSC Retrieval from the HSM

1. Ready the transfer cask, transport trailer, and support skid for service and tow the trailer to the HSM.

2. Back the trailer to within a few inches of the HSM and remove the cask top cover plate.

   CAUTION: High dose rates are expected in the HSM cavity after removal of HSM door. Proper ALARA practices should be followed.

3. Remove the HSM door using a porta-crane. Remove the DSC axial retainer.

4. Using the skid positioning system, align the cask with the HSM and position the skid until the cask is docked with the HSM access opening.

5. Using optical survey equipment, verify alignment of the cask with respect to the HSM. Install the cask restraints.

6. Install (if required) and align the hydraulic ram with the cask.

7. Extend the ram through the cask into the HSM until it is inserted in the DSC grapple ring.

8. Activate the arms on the ram grapple mechanism with the DSC grapple ring.

9. Retract ram and pull the DSC into the cask.

10. Retract the ram grapple arms.

11. Disengage the ram from the cask. Install the ram access penetration cover plate.

12. Remove the cask restraints.

13. Using the skid positioning system, disengage the cask from the HSM.

14. Install the cask top cover plate and ready the trailer for transport.

15. Replace the door on the HSM.

T.8.2.2 Removal of Fuel from the DSC

When the DSC has been removed from the HSM, there are several potential options for off-site shipment of the fuel. It is preferred to ship the DSC intact to a reprocessing facility, monitored retrievable storage facility or permanent geologic repository in a compatible shipping cask licensed under 10CFR71.

If it becomes necessary to remove fuel from the DSC prior to off-site shipment, there are two basic options available at the ISFSI or reactor site. The fuel assemblies could be removed and reloaded into a shipping cask using dry transfer techniques, or if the applicant so desires, the initial fuel loading sequence could be reversed and the plant's spent fuel pool utilized. Procedures for unloading the DSC in a fuel pool are presented here. However, wet or dry unloading procedures are essentially identical to those of DSC loading through the DSC weld removal (beginning of preparation for placement of the cask in the fuel pool). Prior to opening the DSC, the following operations are to be performed.

1. The cask may now be transported to the cask handling area inside the plant's fuel/reactor building.

2. Position and ready the trailer for access by the crane.

3. Attach the lifting yoke to the crane hook.

4. Engage the lifting yoke with the trunnions of the cask.

5. Visually inspect the yoke lifting hooks to insure that they are properly aligned and engaged onto the cask trunnions.

6. Lift the cask approximately one inch off the trunnion supports.

7. Move the crane backward in a horizontal motion while simultaneously raising the crane hook vertically and lift the cask off the trailer. Move the cask to the cask decon area.

8. Lower the cask into the cask decon area in the vertical position.

9. Wash the cask to remove any dirt which may have accumulated on the cask during the DSC loading and transfer operations.

10. Place scaffolding around the cask so that any point on the surface of the cask is easily accessible to personnel.

11. Unbolt the cask top cover plate.

12. Connect the rigging cables to the cask top cover plate and lift the cover plate from the cask. Set the cask cover plate aside and disconnect the lid lifting cables.

13. Install temporary shielding to reduce personnel exposure as required. Fill the TC/DSC annulus with clean demineralized water and seal the annulus.

The process of DSC unloading is similar to that used for DSC loading. DSC opening operations described below are to be carefully controlled in accordance with plant procedures. This operation is to be performed under the site's standard health physics guidelines for welding, grinding, and handling of potentially highly contaminated equipment. These are to include the use of prudent housekeeping measures and monitoring of airborne particulates. Procedures may require personnel to perform the work using respirators or supplied air.

If fuel needs to be removed from the DSC, either at the end of service life or for inspection after an accident, precautions must be taken against the potential for the presence of damaged or oxidized fuel and to prevent radiological exposure to personnel during this operation. A sampling of the atmosphere within the DSC will be taken prior to inspection or removal of fuel.

If the work is performed outside the fuel/reactor building, a tent may be constructed over the work area, which may be kept under a negative pressure to control airborne particulates. Any radioactive gas release will be Kr-85, which is not readily captured. Whether the krypton is vented through the plant stack or allowed to be released directly depends on the plant operating requirements.

Following opening of the DSC, the cask and DSC are filled with water prior to lowering the top of the cask below the surface of the fuel pool to prevent a sudden inrush of pool water. Cask placement into the pool is performed in the usual manner. Fuel unloading procedures will be governed by the plant operating license under 10CFR50. The generic procedures for these operations are as follows:

14. Locate the DSC siphon and vent port using the indications on the outer top cover plate. Place a portable drill press on the top of the DSC. Position the drill with the siphon port.

15. Place an exhaust hood or tent over the DSC, if necessary. The exhaust should be filtered or routed to the site radwaste system.

    CAUTION: Radiation dose rates are expected to be high at the vent and siphon port locations. Use proper ALARA practices (e.g., use of temporary shielding, appropriate positioning of personnel, etc.) to minimize personnel exposure.

16. Drill a hole through the DSC top cover plates to expose the siphon port quick connect.

17. Drill a second hole through the top cover plates to expose the vent port quick connect.

18. Obtain a sample of the DSC atmosphere. Fill the DSC with water from the fuel pool through the siphon port with the vent port open and routed to the plant's off-gas system.

    CAUTION:

    (a) The water fill rate must be regulated during this reflooding operation to ensure that the DSC vent pressure does not exceed 20.0 psig.

    (b) Provide for continuous hydrogen monitoring of the DSC cavity atmosphere during all subsequent cutting operations to ensure that a safety limit of 2.4% is not exceeded [8.3]. Purge with 2-3 psig helium as necessary to maintain the hydrogen concentration safely below this limit.

19. Place welding blankets around the cask and scaffolding to keep dose rates ALARA.

20. Using plasma arc-gouging, a mechanical cutting system or other suitable means, remove the seal weld from the outer top cover plate and DSC shell. A fire watch should be placed on

the scaffolding with the welder, as appropriate. The exhaust system should be operating at all times.

21. The material or waste from the cutting or grinding process should be treated and handled in accordance with the plant's low level waste procedures unless determined otherwise.

22. Remove the top of the tent, if necessary.

23. Remove the exhaust hood, if necessary.

24. Remove the DSC outer top cover plate.

25. Reinstall tent and temporary shielding, as required. Remove the seal weld from the inner top cover plate to the DSC shell in the same manner as the top cover plate. Remove the inner top cover plate. Remove any remaining excess material on the inside shell surface by grinding.

26. Clean the cask surface of dirt and any debris which may be on the cask surface as a result of the weld removal operation. Any other procedures which are required for the operation of the cask should take place at this point as necessary.

27. Engage the yoke onto the trunnions, install eyebolts into the top shield plug and connect the rigging cables to the eyebolts.

28. Visually inspect the lifting hooks or the yoke to insure that they are properly positioned on the trunnions.

29. The cask should be lifted just far enough to allow the weight of the cask to be distributed onto the yoke lifting hooks. Inspect the lifting hooks to insure that they are properly positioned on the trunnions.

30. Install suitable protective material onto the bottom of the transfer cask to minimize cask contamination. Move the cask to the fuel pool.

31. Prior to lowering the cask into the pool, adjust the pool water level, if necessary, to accommodate the volume of water which will be displaced by the cask during the operation.

32. Lower the cask into the fuel pool leaving the top surface of the cask approximately one foot above the surface of the pool water.

33. Lower the cask into the pool. As the cask is being lowered, the exterior surface of the cask should be sprayed with clean demineralized water.

34. Not used.

35. Position the cask over the designated area in the fuel pool.

36. Disengage the lifting yoke from the cask and lift the top shield plug from the DSC.

37. Remove the holddown ring (if not integral to the basket). If the DSC contains damaged fuel assemblies, remove the top end caps. Remove the fuel from the DSC and place the fuel into the spent fuel racks.

38. Lower the top shield plug into the DSC.

39. Visually verify that the top shield plug is properly positioned within the DSC.

40. Engage the lifting yoke onto the cask trunnions.

41. Visually verify that the yoke lifting hooks are properly engaged with the cask trunnions.

42. Lift the cask by a small amount and verify that the lifting hooks are properly engaged with the trunnions.

43. Lift the cask to the pool surface. Prior to raising the top of the cask to the water surface, stop vertical movement and inspect the top shield plug to ensure that it is properly positioned.

44. Spray the exposed portion of the cask with demineralized water.

45. Visually inspect the top shield plug of the DSC to insure that it is properly seated within the cask. If the top shield plug is not properly seated, lower the cask back to the fuel pool and reposition the plug.

46. Drain any excess water from the top of the top shield plug into the fuel pool.

47. Lift the cask from the pool. As the cask is rising out of the pool, spray the cask with demineralized water.

48. Move the cask to the cask decon area.

49. Check radiation levels around the perimeter of the cask. The cask exterior surface should be decontaminated if necessary.

50. Place scaffolding around the cask so that any point along the surface of the cask is easily accessible to personnel.

51. Connect a water draining/pumping device to the siphon port of the DSC and remove water from DSC cavity.

52. The top cover plates may be welded into place as required.

53. Decontaminate the DSC, as necessary, and handle in accordance with low-level waste procedures. Alternatively, the DSC may be repaired for reuse.

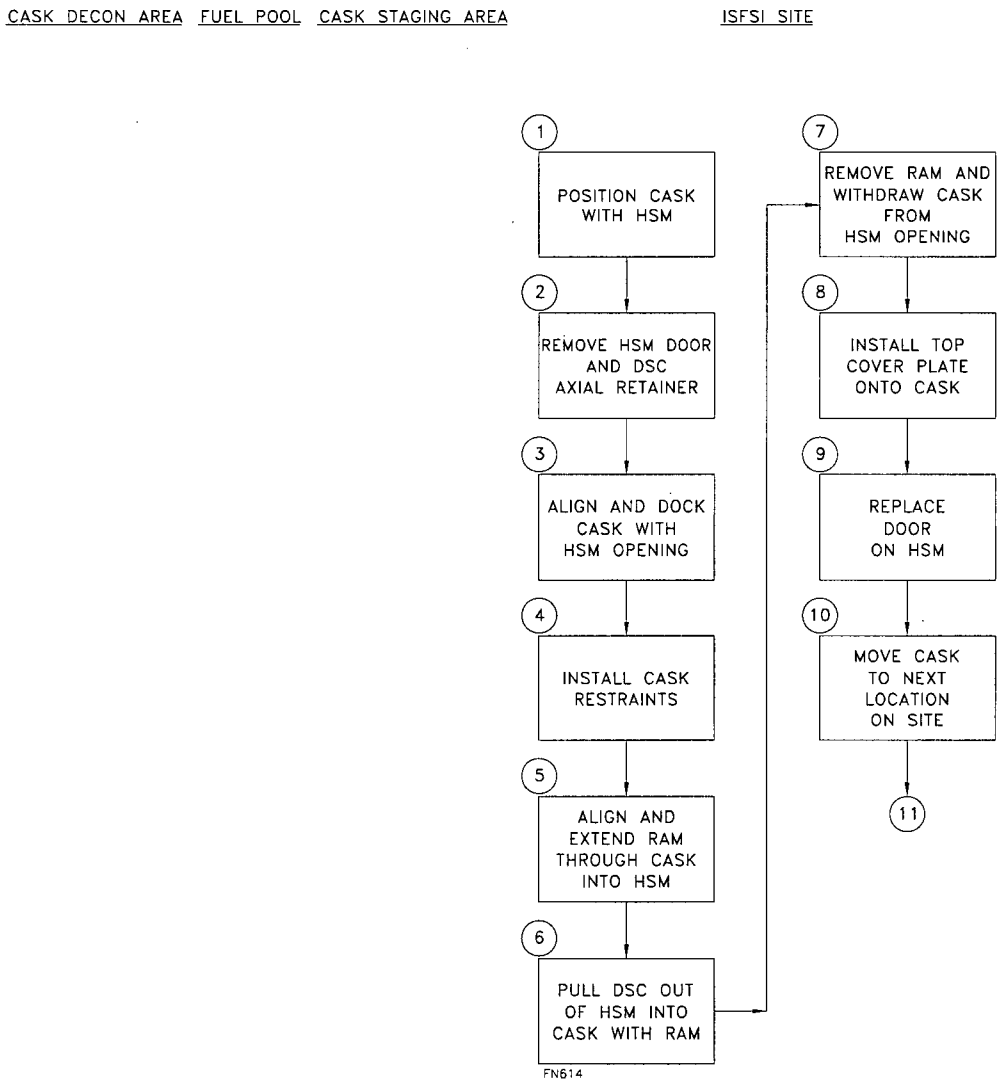

Figure T.8.2-1
NUHOMS® System Retrieval Operations Flow Chart

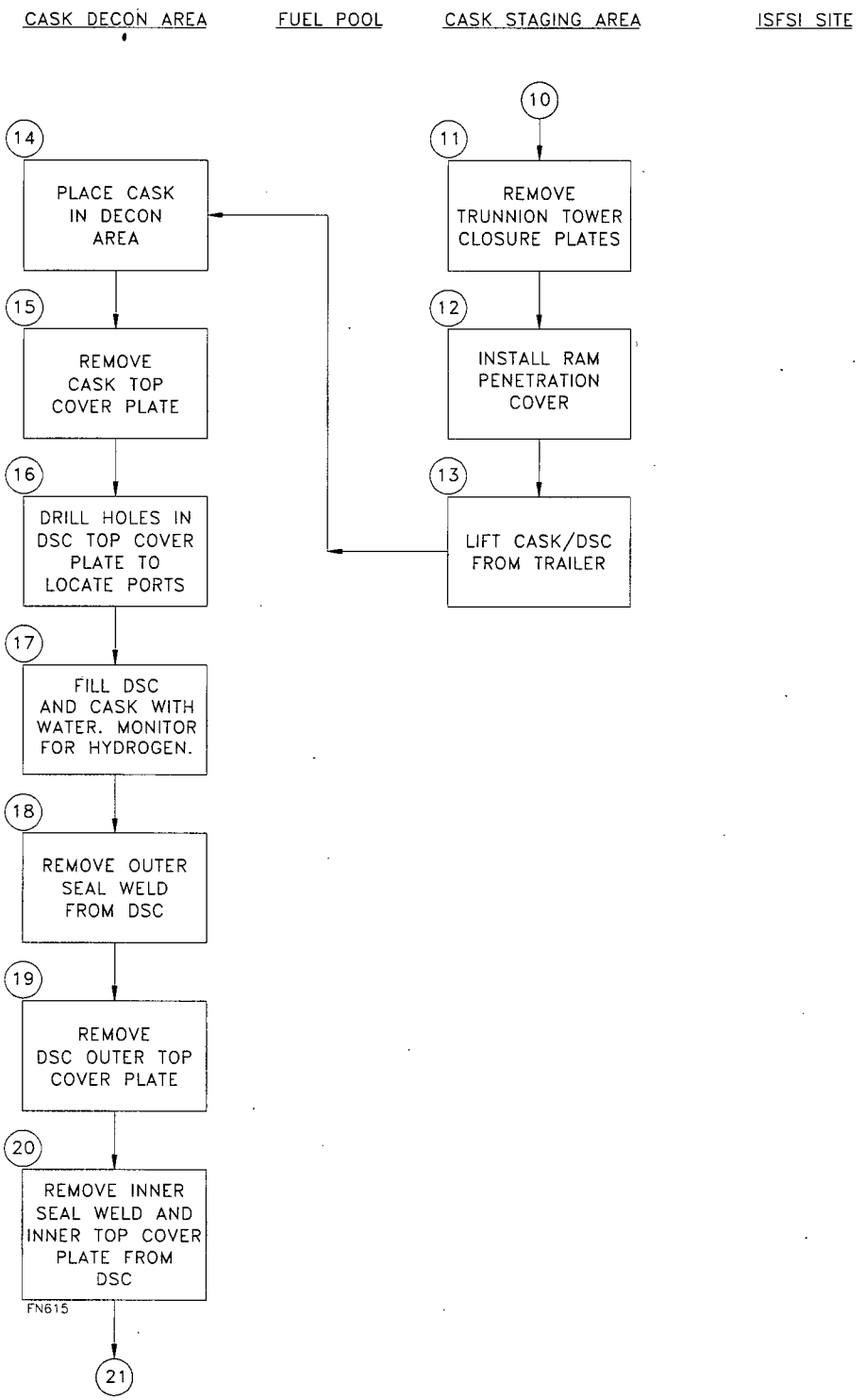

Figure T.8.2-1
NUHOMS® System Retrieval Operations Flow Chart

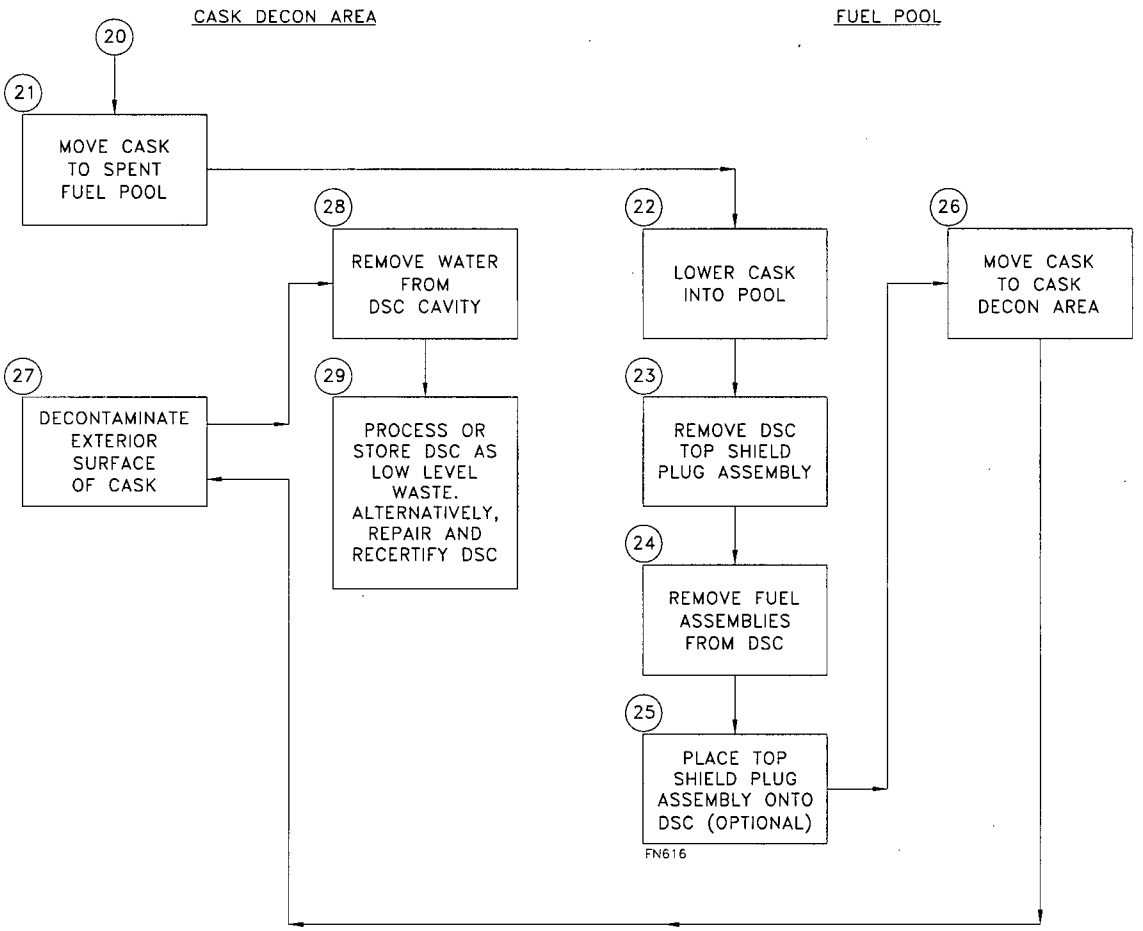

Figure T.8.2-1
NUHOMS® System Retrieval Operations Flow Chart

(Concluded)

T.8.3 Identification of Subjects for Safety Analysis

No change.

T.8.4 Fuel Handling Systems

No change.

T.8.5 Other Operating Systems

No change.

T.8.6 Operation Support System

No change.

T.8.7 Control Room and/or Control Areas

No change.

T.8.8 Analytical Sampling

No change.

T.8.9 References

8.1 U.S. Nuclear Regulatory Commission, "Standard Format and Content for a Topical Safety Analysis Report for a Spent Fuel Dry Storage Container," Regulatory Guide 3.61, February 1989.

8.2 U.S. Nuclear Regulatory Commission, Interim Staff Guidance (ISG)-22, "Potential Rod Splitting Due to Exposures to an Oxidizing Atmosphere during Short-term Cask Loading Operations in LWR or Other Uranium Oxide Based Fuel."

8.3 U.S. Nuclear Regulatory Commission, Office of the Nuclear Material Safety and Safeguards, "Safety Evaluation of VECTRA Technologies' Response to Nuclear Regulatory Commission Bulletin 96-04 for the NUHOMS®-24P and NUHOMS®-7P."

8.4 U.S. Nuclear Regulatory Commission Bulletin 96-04, "Chemical, Galvanic or Other Reactions in Spent Fuel Storage and Transportation Casks," July 5, 1996.

8.5 SNT-TC-1A, "American Society for Nondestructive Testing, Personnel Qualification and Certification in Nondestructive Testing," 1992.

T.9 Acceptance Tests and Maintenance Program

T.9.1 Acceptance Tests

The pre-operational testing requirements for the NUHOMS® system are given in Chapter 9.0, with the exceptions described in the following sections. The NUHOMS®-61BTH DSC has been enhanced to provide leaktight confinement and the basket includes an updated poison plate design. Additional acceptance testing of the NUHOMS®-61BTH DSC welds and of the poison plates are described.

T.9.1.1 Visual Inspection

Visual inspections are performed at the fabricator's facility to ensure that the DSC, the Transfer Cask and the HSM conform to the drawings and specifications. The visual inspections include weld, dimensional, surface finish, and cleanliness inspections. Visual inspections specified by codes applicable to a component are performed in accordance with the requirements and acceptance criteria of those codes.

All weld inspection is performed using qualified processes and qualified personnel according to the applicable code requirements, e.g., ASME or AWS. Non-destructive examination (NDE) requirements for welds are specified on the drawings provided in Chapter T.1; acceptance criteria are as specified by the governing code. NDE personnel are qualified in accordance with SNT-TC-1A [9.2].

The confinement welds on the DSC are inspected in accordance with ASME B&PV Code Subsection NB [9.1] including alternatives to ASME Code specified in Section T.3.1.2.3.

DSC non-confinement welds are inspected to the NDE acceptance criteria of ASME B&PV Code Subsection NG or NF, based on the applicable code for the components welded.

T.9.1.2 Structural

The DSC confinement boundary except the inner top cover/shield plug to the DSC shell weld is pressure tested at the fabricator's shop in accordance with ASME Article NB-6300. The test pressure is set between 16.5 to 18.0 psig for 61BTH DSC with Type 1 basket for future 10CFR71 application. This bounds the 1.1xDSC design pressure of 10 psig. The test pressure is set between 22.5 to 24.0 psig for 61BTH DSC with Type 2 basket for future 10CFR71 application. This bounds the 1.1xDSC design pressure of 15 psig.

The inner top cover/shield plug to the DSC shell weld is also pressure tested between 16.5 to 18.0 psig for 61BTH DSC with Type 1 basket and between 22.5 to 24.0 psig for 61BTH DSC with Type 2 basket. This pressure test is performed at the field after the fuel assemblies are loaded in the DSC. This test is in accordance with the alternatives to the ASME Code specified in Section T.3.1.2.3.

HSM-H reinforcement and concrete are tested as described in Section 3.4.2.

T.9.1.3 Leak Tests

DSC confinement welds in the DSC shell and bottom are leak tested at the fabricator's shop to an acceptance criterion of $1x10^{-7}$ ref cm^3/s, i.e., "leaktight" as defined in ANSI N14.5 [9.4]. Personnel performing the leak test are qualified in accordance with SNT-TC-1A [9.2].

The weld between the DSC shell and inner top cover/shield plug and siphon/vent cover welds are also leak tested to an acceptance criteria of 1×10^{-7} ref cm^3/s at the field after the fuel assemblies are loaded in the canister.

T.9.1.4 Components

The NUHOMS® system does not include any components such as valves, rupture discs, pumps, or blowers. The gaskets in the Transfer Cask do not require acceptance testing other than the leak testing cited above. No other components of the NUHOMS® system require testing, except as discussed in this chapter.

T.9.1.5 Shielding Integrity

The Transfer Cask poured lead shielding integrity will be confirmed via gamma scanning prior to first use. The detector and examination grid will be matched to provide coverage of the entire lead-shielded surface area. For example, for a 6" × 6" grid, the detector will encompass a 6" × 6" square. The acceptance criterion is attenuation greater than or equal to that of a test block matching the cask through-wall configuration with lead and steel thicknesses equal to the design minima less 5%.

The radial neutron shielding is provided by filling the neutron shield shell with water during operations. No testing is necessary. The neutron shield material in the lid and bottom end is a proprietary polymer resin. The shielding performance of the resin will be assured by written procedures controlling temperature, measuring, and mixing of the components, degassing of the resin, and verification of the mass or volume of resin installed.

The gamma and neutron shielding materials of the storage system itself are limited to concrete HSM components and steel shield plugs in the DSC. The integrity of these shielding materials is ensured by the control of their fabrication in accordance with the appropriate ASME, ASTM or ACI criteria. No additional acceptance testing is required.

T.9.1.6 Thermal Acceptance

No thermal acceptance testing is required to verify the performance of each storage unit other than that specified in the Technical Specifications for initial loading.

The heat transfer analysis for the basket includes credit for the thermal conductivity of neutron-absorbing materials, as specified in Section T.4.3. Because these materials (with the exception of Boral®) do not have publicly documented values for thermal conductivity, testing of such materials will be performed in accordance with Section T.9.1.7.4

T.9.1.7 Poison Acceptance

> ***CAUTION***
>
> *Sections T.9.1.7.1 through T.9.1.7.3 below are incorporated by reference into the NUHOMS® CoC 1004 Technical Specifications (paragraph 1.2.1) and shall not be deleted or altered in any way without a CoC amendment approval from the NRC. The text of these sections is shown in bold type to distinguish it from other sections.*

The neutron absorber used for criticality control in the DSC basket may consist any of the following types of material:

(a) Boron-aluminum alloy (borated aluminum)

(b) Boron carbide-aluminum metal matrix composite (MMC)

(c) Boral®

The 61BTH DSC safety analyses do not rely upon the tensile strength of these materials. The radiation and temperature environment in the cask is not sufficiently severe to damage these metallic/ceramic materials. To assure performance of the neutron absorber's design function only the presence of B10 and the uniformity of its distribution need to be verified, with testing requirements specific to each material. The boron content of these three types of materials is given in Table T.9-1, Table T.9-2 and Table T.9-3, respectively.

T.9.1.7.1 Boron Aluminum Alloy (Borated Aluminum)

See the Caution in Section T.9.1.7 before deletion or modification to this section.

The material is produced by direct chill (DC) or permanent mold casting with boron precipitating as a uniform fine dispersion of discrete AlB_2 or TiB_2 particles in the matrix of aluminum or aluminum alloy. For extruded products, the TiB_2 form of the alloy shall be used. For rolled products, either the AlB_2, the TiB_2, or a hybrid may be used.

Boron is added to the aluminum in the quantity necessary to provide the specified minimum B10 areal density in the final product, with sufficient margin to minimize rejection, typically 10 % excess. The amount required to achieve the specified minimum B10 areal density will depend on whether boron with the natural isotopic distribution of the isotopes B10 and B11, or boron enriched in B10 is used. In no case shall the boron content in the aluminum or aluminum alloy exceed 5% by weight.

The criticality calculations take credit for 90% of the minimum specified B10 areal density of borated aluminum. The basis for this credit is the B10 areal density acceptance testing, which shall be as specified in Section T.9.1.7.5. The specified acceptance testing assures that at any location in the material, the minimum specified areal density of B10 will be found with 95% probability and 95% confidence.

Visual inspections shall follow the recommendations in Aluminum Standards and Data, Chapter 4 "Quality Control, Visual Inspection of Aluminum Mill Products and Castings"[9.5]. Local or cosmetic conditions such as scratches, nicks, die lines, inclusions, abrasion, isolated pores, or discoloration are acceptable. Widespread blisters, rough surface, or cracking shall be evaluated for acceptance in accordance with the Certificate Holder's QA procedures.

T.9.1.7.2 **Boron Carbide / Aluminum Metal Matrix Composites (MMC)**

See the Caution in Section T.9.1.7 before deletion or modification to this section.

The material is a composite of fine boron carbide particles in an aluminum or aluminum alloy matrix. The material shall be produced by either direct chill casting, permanent mold casting, powder metallurgy, or thermal spray techniques. It is a low-porosity product, with a metallurgically bonded matrix. The boron carbide content shall not exceed 40% by volume. The boron carbide content for MMCs with an integral aluminum cladding shall not exceed 50% by volume.

Prior to use in the 61BTH DSC, MMCs shall pass the qualification testing specified in Section T.9.1.7.6, and shall subsequently be subject to the process controls specified in Section T.9.1.7.7.

The criticality calculations take credit for 90% of the minimum specified B10 areal density of MMCs. The basis for this credit is the B10 areal density acceptance testing, which is specified in Section T.9.1.7.5. The specified acceptance testing assures that at any location in the final product, the minimum specified areal density of B10 will be found with 95% probability and 95% confidence.

Visual inspections shall follow the recommendations in Aluminum Standards and Data, Chapter 4 "Quality Control, Visual Inspection of Aluminum Mill Products and Castings" [9.5]. Local or cosmetic conditions such as scratches, nicks, die lines, inclusions, abrasion, isolated pores, or discoloration are acceptable. Widespread blisters, rough surfaces, or cracking shall be evaluated for acceptance in accordance with the Certificate Holder's QA procedures.

References to metal matrix composites throughout this chapter are not intended to refer to Boral®, which is described in the following section.

T.9.1.7.3 **Boral®**

See the Caution in Section T.9.1.7 before deletion or modification to this section.

This material consists of a core of aluminum and boron carbide powders between two outer layers of aluminum, mechanically bonded by hot-rolling an "ingot" consisting of an aluminum box filled with blended boron carbide and aluminum powders. The core, which is exposed at the edges of the sheet, is slightly porous. The average size of the boron carbide particles in the finished product is approximately 85 microns after rolling. The nominal boron carbide content shall be limited to 65% (+ 2% tolerance limit) of the core by weight.

The criticality calculations take credit for 75% of the minimum specified B10 areal density of Boral®. B10 areal density will be verified by chemical analysis and by certification of the B10 isotopic fraction for the boron carbide powder, or by neutron transmission testing. Areal density testing is performed on an approximately 1 cm^2 area of a coupon taken near one of the corners of the sheet produced from each ingot. If the measured areal density is below that specified, all the material produced from that ingot will be either rejected, or accepted only on the basis of alternate verification of B10 areal density for each of the final pieces produced from that ingot.

Visual inspections shall verify that the Boral® core is not exposed through the face of the sheet at any location.

T.9.1.7.4 Thermal Conductivity Testing

All poison plate materials except Boral® will be qualification tested to verify that the thermal conductivity equals or exceeds the values listed in Section T.4.3. Testing of Boral® is not required since the thermal conductivity values utilized in Section T.4.3 were conservatively derived from References [9.7] and [9.8].

Testing shall conform to ASTM E1225 [9.9], ASTM E1461 [9.10], or equivalent method, performed at room temperature on coupons taken from the rolled or extruded production material. Previous testing of borated aluminum and metal matrix composite, shows that thermal conductivity increases slightly with temperature. Initial sampling shall be one test per lot, defined by the heat or ingot, and may be reduced if the first five tests meet the specified minimum thermal conductivity.

If a thermal conductivity test result is below the specified minimum, additional tests may be performed on the material from that lot. If the mean value of those tests falls below the specified minimum, the associated lot shall be rejected.

After twenty five tests of a single type of material, with the same aluminum alloy matrix, the same boron content, and the boron appearing in the same phase, e.g., B_4C, TiB_2, or AlB_2, if the mean value of all the test results less two standard deviations meets the specified thermal conductivity, no further testing of that material is required. This exemption may also be applied to the same type of material if the matrix of the material changes to a more thermally conductive alloy (e.g., from 6000 to 1000 series aluminum), or if the boron content is reduced without changing the boron phase.

The thermal analysis in Chapter T.4 assumes the neutron absorber can be made from a single piece or can be paired with aluminum 1100 plate. The minimum thermal conductivity of the neutron absorber plate shall be equal to or greater than that assumed in the analysis, as shown in Section T.4.3 for the borated aluminum and MMC poison materials.

The aluminum 1100 plate does not need to be tested for thermal conductivity; the material may be credited with the values published in the ASME Code Section II part D.

T.9.1.7.5 Specification for Acceptance Testing of Neutron Absorbers by Neutron Transmission

CAUTION

Section T.9.1.7.5 is incorporated by reference into the NUHOMS® CoC 1004 Technical Specifications (paragraph 1.2.1) and shall not be deleted or altered in any way without a CoC amendment approval from the NRC. The text of this section is shown in bold type to distinguish it from other sections.

Neutron Transmission acceptance testing procedures shall be subject to approval by the Certificate Holder. Test coupons shall be removed from the rolled or extruded production material at locations that are systematically or probabilistically distributed throughout the lot. Test coupons shall not exhibit physical defects that would not be acceptable in the finished product, or that would preclude an accurate measurement of the coupon's physical thickness.

A lot is defined as all the pieces produced from a single ingot or heat. If this definition results in lot size too small to provide a meaningful statistical analysis of results, an alternate larger lot definition may be used, so long as it results in accumulating material that is uniform for sampling purposes.

The sampling rate for neutron transmission measurements shall be such that there is at least one neutron transmission measurement for each 2000 square inches of final product in each lot.

The B10 areal density is measured using a collimated thermal neutron beam of up to 1.2 centimeter diameter. A beam size greater than 1.2 centimeter diameter but no larger than 1.7 centimeter diameter may be used if computations are performed to demonstrate that the calculated $k_{effective}$ of the system is still below the calculated Upper Subcritical Limit (USL) of the system assuming defect areas the same area as the beam. Alternatively, the confidence and probability levels can be increased such that it will result in equivalent acceptance rates for the material as the 1.2 centimeter diameter beam size.

The neutron transmission through the test coupons is converted to B10 areal density by comparison with transmission through calibrated standards. These standards are composed of a homogeneous boron compound without other significant neutron absorbers. For example, boron carbide, zirconium diboride or titanium diboride sheets are acceptable standards. These standards are paired with aluminum shims sized to match the effect of neutron scattering by aluminum in the test coupons. Uniform but non-homogeneous materials such as metal matrix composites may be used for standards, provided that testing shows them to provide neutron attenuation equivalent to a homogeneous standard.

Alternatively, digital image analysis may be used to compare neutron radioscopic images of the test coupon to images of the standards. The area of image analysis shall be up to 1.1 cm^2.

The minimum areal density specified shall be verified for each lot at the 95% probability, 95% confidence level or better. The following illustrates one acceptable method.

The acceptance criterion for individual plates is determined from a statistical analysis of the test results for their lot. The minimum B10 areal densities determined by neutron transmission are converted to volume density, i.e., the minimum B10 areal density is divided by the thickness at the location of the neutron transmission measurement or the maximum thickness of the coupon. The lower tolerance limit of B10 volume density is then determined, defined as the mean value of B10 volume density for the sample, less K times the standard deviation, where K is the one-sided tolerance limit factor for a normal distribution with 95% probability and 95% confidence [Error! Reference source not found.**].**

Finally, the minimum specified value of B10 areal density is divided by the lower tolerance limit of B10 volume density to arrive at the minimum plate thickness which provides the specified B10 areal density.

Any plate which is thinner than this minimum or the minimum design thickness, whichever is greater, shall be treated as non-conforming, with the following exception. Local depressions are acceptable, so long as they total no more than 0.5% of the area on any given plate, and the thickness at their location is not less than 90% of the minimum design thickness.

Non-conforming material shall be evaluated for acceptance in accordance with the Certificate Holder's QA procedures.

T.9.1.7.6 Specification for Qualification Testing of Metal Matrix Composites

T.9.1.7.6.1 Applicability and Scope

Metal matrix composites (MMCs) shall consist of fine boron carbide particles in an aluminum or aluminum alloy matrix. The ingot shall be produced by either powder metallurgy (PM), thermal spray techniques, or by direct chill (DC) or permanent mold casting. In any case, the final MMC product shall have density greater than 98% of theoretical, a metallurgically bonded matrix, and boron carbide content no greater than 40% by volume. (For MMCs with an integral aluminum cladding, the maximum boron carbide content shall be no greater than 50% by volume and the density shall be greater than 97% of theoretical density.) Boron carbide particles for the products considered here typically have an average size in the range 10-40 microns, although the actual specification may be by mesh size, rather than by average particle size. No more than 10% of the particles shall be over 60 microns. The material shall have negligible interconnected porosity exposed at the surface or edges.

Prior to initial use in a spent fuel dry storage or transport system, such MMCs shall be subjected to qualification testing that will verify that the product satisfies the design function. Key process controls shall be identified per Section T.9.1.7.7 so that the production material is equivalent to or better than the qualification test material. Changes to key processes shall be subject to qualification before use of such material in a spent fuel dry storage or transport system.

ASTM test methods and practices are referenced below for guidance. Alternative methods may be used with the approval of the certificate holder.

T.9.1.7.6.2 Design Requirements

In order to perform its design functions the product must have at a minimum sufficient strength and ductility for manufacturing and for the normal and accident conditions of the storage/ transport system. This is demonstrated by the tests in Section T.9.1.7.6.4. It must have a uniform distribution of boron carbide. This is demonstrated by the tests in Section T.9.1.7.6.5.

T.9.1.7.6.3 Durability

There is no need to include accelerated radiation damage testing in the qualification. Such testing has already been performed on MMCs, and the results confirm what would be expected of materials that fall within the limits of applicability cited above. Metals and ceramics do not experience measurable changes in mechanical properties due to fast neutron fluences typical over the lifetime of spent fuel storage, about 10^{15} neutrons/cm^2.

The need for thermal damage and corrosion (hydrogen generation) testing shall be evaluated case-by-case based on comparison of the material composition and environmental conditions with previous thermal or corrosion testing of MMCs.

Thermal damage testing is not required for MMCs consisting only of boron carbide in an aluminum 1100 matrix, because there is no reaction between aluminum and boron carbide below 842°F, well above the basket temperature under normal conditions of storage or transport[1].

Corrosion testing is not required for full density MMCs consisting only of boron carbide in an aluminum 1100 matrix, because testing on one such material has already been performed by Transnuclear[2].

T.9.1.7.6.4 Required Qualification Tests and Examinations to Demonstrate Mechanical Integrity

At least three samples, one each from the two ends and middle of the test material production run shall be subject to:

a) room temperature tensile testing (ASTM- B557[3]) demonstrating that the material has the following tensile properties:

- Minimum yield strength, 0.2% offset: 1.5 ksi
- Minimum ultimate strength: 5 ksi
- Minimum elongation in 2 inches: 0.5%

---

1 **Sung, C., "Microstructural Observation of Thermally Aged and Irradiated Aluminum/Boron Carbide (B_4C) Metal Matrix Composite by Transmission and Scanning Electron Microscope," 1998.**

2 **Boralyn testing submitted to the NRC under docket 71-1027, 1998.**

3 **ASTM B557 Standard Test Methods of Tension Testing Wrought and Cast Aluminum and Magnesium-Alloy Products.**

(Alternatively show that the material fails in a ductile manner, e.g., by scanning electron microscopy of the fracture surface or by bend testing.)

and

b) testing (ASTM-B311[4]) to verify more than 98% (or 97% for MMCs with integral aluminum cladding) of theoretical density. Testing or examination for exposed interconnected porosity shall be performed by a means to be approved by the Certificate Holder.

T.9.1.7.6.5 Required Tests and Examinations to Demonstrate B10 Uniformity

CAUTION

Section T.9.1.7.6.5 is incorporated by reference into the NUHOMS® CoC 1004 Technical Specifications (paragraph 1.2.1) and shall not be deleted or altered in any way without a CoC amendment approval from the NRC. The text of this section is shown in bold type to distinguish it from other sections.

Uniformity of the boron distribution shall be verified either by:

a) Neutron radioscopy or radiography (ASTM E94[5], E142[6], and E545[7]) of material from the ends and middle of the test material production run, verifying no more than 10% difference between the minimum and maximum B10 areal density, or

b) Quantitative testing for the B10 areal density, B10 density, or the boron carbide weight fraction, on locations distributed over the test material production run, verifying that one standard deviation in the sample is less than 10% of the sample mean. Testing may be performed by a neutron transmission method similar to that specified in Section 9.1.7.5, or by chemical analysis for boron carbide content in the composite.

T.9.1.7.6.6 Approval of Procedures

Qualification procedures shall be subject to approval by the Certificate Holder.

---

[4] **ASTM B311, Test Method for Density Determination for Powder Metallurgy (P/M) Materials Containing Less than Two Percent Porosity**

[5] **ASTM E94, Recommended Practice for Radiographic Testing**

[6] **ASTM E142, Controlling Quality of Radiographic Testing**

[7] **ASTM E545, Standard Method for Determining Image Quality in Thermal Neutron Radiographic Testing**

T.9.1.7.7 Specification for Process Controls for Metal Matrix Composites

T.9.1.7.7.1 Applicability and Scope

The applicability of this section is the same as that of Section T.9.1.7.6. It addresses the process controls to ensure that the material delivered for use is equivalent to the qualification test material.

Key processing changes shall be subject to qualification prior to use of the material produced by the revised process. The Certificate Holder shall determine whether a complete or partial re-qualification program per Section T.9.1.7.7 is required, depending on the characteristics of the material that could be affected by the process change.

T.9.1.7.7.2 Definition of Key Process Changes

Key process changes are those which could adversely affect the uniform distribution of the boron carbide in the aluminum, reduce density, or reduce the mechanical strength or ductility of the MMC.

T.9.1.7.7.3 Identification and Control of Key Process Changes

CAUTION

Section T.9.1.7.7.3 is incorporated by reference into the NUHOMS® CoC 1004 Technical Specifications (paragraph 1.2.1) and shall not be deleted or altered in any way without a CoC amendment approval from the NRC. The text of this section is shown in bold type to distinguish it from other sections.

The manufacturer shall provide the Certificate Holder with a description of materials and process controls used in producing the MMC. The Certificate Holder and manufacturer shall identify key process changes as defined in Section T.9.1.7.7.2.

An increase in nominal boron carbide content over that previously qualified shall always be regarded as a key process change. The following are examples of other changes that may be established as key process changes, as determined by the Certificate Holder's review of the specific applications and production processes:

a) Changes in the boron carbide particle size specification that increase the average particle size by more than 5 microns or that increase the amount of particles larger than 60 microns from the previously qualified material by more than 5% of the total distribution but less than the 10% limit,

b) Change of the billet production process, e.g., from vacuum hot pressing to cold isostatic pressing followed by vacuum sintering,

c) Change in the nominal matrix alloy,

d) **Changes in mechanical processing that could result in reduced density of the final product, e.g., for PM or thermal spray MMCs that were qualified with extruded material, a change to direct rolling from the billet,**

e) **For MMCs using a 6000 series aluminum matrix, changes in the billet formation process that could increase the likelihood of magnesium reaction with the boron carbide, such as an increase in the maximum temperature or time at maximum temperature, and**

f) **Changes in powder blending or melt stirring processes that could result in less uniform distribution of boron carbide, e.g., change in duration of powder blending.**

In no case shall process changes be accepted if they result in a product outside the limits in Sections T.9.1.7.6.1 and T.9.1.7.6.4.

T.9.2 Maintenance Program

The NUHOMS®-61BTH system is a totally passive system and therefore will require little, if any, maintenance over the lifetime of the ISFSI. Typical NUHOMS®-61BTH system maintenance tasks will be performed in accordance with the UFSAR.

T.9.3 References

9.1 ASME Boiler and Pressure Vessel Code, Section III, 1998 Edition with 2000 Addenda.

9.2 SNT-TC-1A, "American Society for Nondestructive Testing, Personnel Qualification and Certification in Nondestructive Testing," 1992.

9.3 ANSI N14.6, "American National Standard for Special Lifting Devices for Shipping Containers Weighing 10,000 Pounds or More for Nuclear Materials," New York, 1996.

9.4 ANSI N14.5-1997, "American National Standard for Leakage Tests on Packages for Shipment of Radioactive Materials", February 1998.

9.5 "Aluminum Standards and Data, 2003" The Aluminum Association.

9.6 Natrella, "Experimental Statistics," Dover, 2005.

9.7 AAR Advanced Structures, "Boral®, The Proven Neutron Absorber."

9.8 AAR Advanced Structures, Boral® Product Performance Report 624."

9.9 ASTM E1225, "Thermal Conductivity of Solids by Means of the Guarded-Comparative-Longitudinal Heat Flow Technique."

9.10 ASTM E1461, "Thermal Diffusivity of Solids by the Flash Method."

Table T.9-1
Boron Content Borated Aluminum (90% B10 Credit)

Basket Type	Reference	Section T.6 Analysis	Specified Minimum
	Nominal Boron Content (wt. % Boron)	B10 Areal Density (mg/cm^2)	B10 Areal Density (mg/cm^2)
Type 1 DSC			
A	1.1	18.9	21.0
B	1.6	28.8	32.0
C	2.1	36.0	40.0
D	2.5	43.2	48.0
E	2.8	49.5	55.0
F	3.2	56.2	62.4
Type 2 DSC			
A	1.2	20.1	22.3
B	1.7	28.8	32.0
C	2.2	37.5	41.7
D	2.5	43.2	48.0
E	2.8	49.5	55.0
F	3.2	56.2	62.4

Table T.9-2
Specified Boron Carbide Areal Density
Metal Matrix Composites (90% B10 Credit)

Basket Type	Reference	Section T.6 Analysis	Specified Minimum
	Nominal Boron Carbide Content (volume %)	B10 Areal Density (mg/cm^2)	B10 Areal Density (mg/cm^2)
Type 1 DSC			
A	8	18.9	21.0
B	12	28.8	32.0
C	15	36.0	40.0
D	17	43.2	48.0
E	20	49.5	55.0
F	23	56.2	62.4
Type 2 DSC			
A	8	20.1	22.3
B	12	28.8	32.0
C	15	37.5	41.7
D	17	43.2	48.0
E	20	49.5	55.0
F	23	56.2	62.4

Table T.9-3
Specified B10 Areal Density Boral® (75% B10 credit)

Basket Type	Section T.6 Analysis B10 Areal Density (mg/cm^2)	Specified Minimum B10 Areal Density (mg/cm^2)
Type 1 DSC		
A	18.9	25.2
B	28.8	38.4
C	36.0	48.0
D	43.2	57.6
E	49.5	66.0
F	56.2	74.9
Type 2 DSC		
A	20.1	26.8
B	28.8	38.4
C	37.5	50.0
D	43.2	57.6
E	49.5	66.0
F	56.2	74.9

T.10 Radiation Protection

Section 7.4.1 discusses the anticipated cumulative dose exposure to site personnel during the fuel handling and transfer activities associated with utilizing one NUHOMS® HSM for storage of one DSC. Chapter 5 describes in detail the NUHOMS® operational procedures, several of which involve potential exposure to personnel. This section of the Appendix provides occupational exposure and off-site dose rates from a NUHOMS®-61BTH Type 1 or 2 DSC stored in each of the following HSM types: NUHOMS® HSM-H, Model 80, Model 102, Model 152, or Model 202. The dose rates calculated with the HSM Model 80 are bounding because it is designed with the least amount of shielding among these various HSM models.

T.10.1 Occupational Exposure

The expected occupational dose for placing a canister of spent fuel into dry storage is based on the operational steps outlined in Table 7.4-1 of the UFSAR. The total exposure for the occupational dose due to placing a single NUHOMS®-61BTH DSC into storage is conservatively estimated to be 2.37 person-rem as described in Table T.10-1. This value bounds the exposure for loading either a 61BTH-Type 1 or 61BTH-Type 2 DSC into storage. This is a very conservative estimate because the dose rates on and around the 61BTH DSCs used in these calculations are based on very conservative assumptions for the design-basis source terms and analyses models. The calculated exposures are due mainly to the expected gamma dose rate during preparation for welding.

The NUHOMS®-61BTH System loading operations, the number of workers required for each operation, and the amount of time required for each operation are presented in Table T.10-1. This information is used as the basis for estimating the total occupational exposure associated with one fuel load. This evaluation is performed for the storage of either the design-basis NUHOMS®-61BTH Type 1 or 2 DSC in an HSM. The loading operations are identical for the 61BTH-Type 1 and 61BTH-Type 2 DSC. The dose rates applicable for each operation are based on the results presented in Section T.5.4 of the UFSAR for loading operations. Engineering judgment and operational experience are used to estimate dose rates that were not explicitly evaluated. This evaluation assumes that a transfer trailer/skid with an integral ram is used for the DSC transfer operations. Licensees may elect to use different equipment and/or different procedures. Each licensee must evaluate any such changes in accordance with its ALARA program.

Unique steps are sometimes necessary at the individual site to load the canister, complete closure operations and place the canister in the HSM. Specifically, the licensee may choose to modify the sequence of operations in order to achieve reduced dose rates for a larger number of steps, with the end result of reduced total exposure. The only requirement is that the licensee practice ALARA with respect to the total exposure received for a loading campaign. These estimated durations, manloading and dose rates are not limits.

The amount of time required to complete some operations as identified in Table T.10-1 may be greater than the actual amount of time spent in a radiation field. The process of vacuum drying the DSC includes setting up the vacuum drying system (VDS), verifying that the VDS is operating correctly, evacuating the DSC cavity, monitoring the DSC pressure, and disconnecting the VDS from the DSC. Of these tasks, only setup and removal of the VDS require a worker to spend time near the DSC. The most time consuming task, evacuating the DSC, does not require anyone to be present near the DSC at all. The total exposure calculated for each task is therefore not necessarily equal to the number of workers multiplied by the total time required, multiplied by a dose rate. The exposure estimation for each task correctly accounts for cases such as vacuum drying and assumes that good ALARA practices are followed.

The results of the evaluations of the 61BTH are presented in Table T.10-1.

T.10.2 Off-Site Dose Calculations

Calculated dose rates in the immediate vicinity of the NUHOMS®-61BTH System are presented in Chapter T.5, which provides a detailed description of source term configuration, analysis models and bounding dose rates. The bounding dose rates are based upon contributions from the design basis fuel. Off-site dose rates and annual doses are presented in this section. This evaluation determines the neutron and gamma-ray off-site dose rates (including skyshine) in the vicinity of two generic ISFSI layouts containing design-basis fuel in the NUHOMS®-61BTH DSCs.

The first generic ISFSI evaluated is a 2x10 back-to-back array of HSM-Hs loaded with design-basis fuel in NUHOMS®-61BTH DSCs (DSC Type 2 Heat Load Zoning Configuration 6 from Chapter T.2). The second generic layout evaluated is two 1x10 front-to-front arrays of HSM-Hs loaded with design-basis fuel in NUHOMS®-61BTH DSCs (DSC Type 2 Heat Load Zoning Configuration 6 from Chapter T.2). This evaluation provides results for distances ranging from 6.1 to 600 meters from each face of the two arrays of HSMs. Similar calculations are performed for the NUHOMS®-61BTH DSCs within HSM Model 102s, although the source term used is different because the HSM Model 102 is limited to 24.0 kW decay heat (see Figure T.5-1 of Chapter T.5). Dose rates for the NUHOMS®-61BTH Type 1 DSCs within HSM Model 80s filled with design basis fuel assemblies are generated by scaling the HSM Model 102 results. The dose rates that are obtained with the HSM Model 80 are conservatively applicable to HSM Model 152 and 202.

The total annual exposure for each ISFSI layout as a function of distance from each face is given in Table T.10-2, Table T.10-3, and Table T.10-4 for the HSM-H, HSM Model 102, and the HSM Model 80, respectively. These data are also plotted in Figure T.10-1, Figure T.10-2, and Figure T.10-3 for the HSM-H, HSM Model 102, and HSM Model 80, respectively. The total annual exposure estimates assume 100% occupancy for 365 days.

The Monte Carlo computer code MCNP [10.1] calculates the dose rates at the specified locations around the arrays of HSM-Hs and HSM Model 102s. The results of these calculations provide an example of how to demonstrate compliance with the relevant radiological requirements of 10CFR20 [10.2], 10CFR72 [10.3], and 40CFR190 [10.4] for a specific site. Each site must perform site specific calculations to account for the actual layout of the HSMs and fuel source.

The assumptions used to generate the geometry of the ISFSIs for the MCNP analyses are summarized below. The following discussion applies to both the HSM-H and HSM Model 102 analyses.

- The 20 HSMs in the 2x10 back-to-back array are modeled as a box enveloping the 2x10 array of HSMs including the shield walls on the two sides of the array. MCNP starts the source particles on the surfaces of the box. The interiors of the HSMs and shield walls are modeled as air. Most particles that enter the interiors of the HSMs and shield walls will therefore pass through unhindered.

- The 20 HSMs in the two 1x10 front-to-front arrays are modeled as two boxes which envelop each 1x10 array of HSMs including the shield walls on the two sides and back of each array.

The interiors of one array of HSMs and shield walls are modeled as air (the "source" array). Most particles that enter the interiors of these HSMs and shield walls will therefore pass through unhindered. The other 1x10 array (the "shield" array) is modeled as concrete to simulate the shielding provided by the second array of HSMs for the direct radiation from the front of the opposing 1x10 array. The dose rates around the ISFSI are then generated using superposition.

- The ISFSI approach slab is modeled as concrete. Because the ground composition has, at best, only a secondary impact on the dose rates at the detectors, any differences between this assumed layout and the actual layout would not have a significant effect on the site dose rates.

- The "universe" is a sphere surrounding the ISFSI. To account for skyshine, the radius of this sphere (r=500,000 cm) is more than 10 mean free paths for neutrons and 50 mean free paths for gammas greater than that of the outermost surface, thus ensuring that the model is of a sufficient size to include all interactions, including skyshine, affecting the dose rate at the detectors.

The assumptions used for the MCNP analyses are summarized below.

- The HSM-H surface sources are bootstrapped (input to provide an equivalent boundary condition) using modified values of the HSM-H surface average dose rates calculated in Section T.5.4. In an ISFSI, most HSMs have an adjacent HSM on each side. In the Section T.5.4 analysis, the dose rates are calculated assuming an adjacent HSM on only one side (on the other side is a shield wall). Therefore, the average front and roof dose rates as reported in Section T.5.4 are increased prior to input into the site dose analysis to estimate the effects of having an adjacent HSM on both sides. The front and roof HSM-H gamma dose rates used in the site dose analysis are 14.2 and 29.3 mrem/hr, respectively. The front and roof HSM-H neutron dose rates used in the site dose analysis are 0.54 and 1.08 mrem/hr, respectively.

- The HSM Model 102 front and roof average dose rates are also increased prior to input in the site dose calculation, consistent with the HSM-H approach described in the preceding paragraph. The front and roof HSM Model 102 gamma dose rates used in the site dose analysis are 17.34 and 27.14 mrem/hr, respectively. The front and roof HSM Model 102 neutron dose rates used in the site dose analysis are 0.72 and 0.86 mrem/hr, respectively.

- MCNP starts the source particles on the ISFSI array surface with initial directions following a cosine distribution. Radiation fluxes outside thick shields such as the HSM walls and roof tend to have forward peaked angular distributions; therefore, a cosine function is a reasonable approximation for the starting direction distribution. Vents through shielding regions such as the HSM vents tend to collimate particles such that a semi-isotropic assumption would not be appropriate.

- Point detectors determine the dose rates on the four sides of the ISFSI as a function of distance from the ISFSI. All detectors represent the dose rate at three feet above ground level.

- Source information required by MCNP includes gamma-ray and neutron spectra for the HSM array surfaces, total gamma-ray and neutron activities for each HSM array face and total gamma-ray and neutron activities for the entire ISFSI. The neutron and gamma-ray spectra are determined using MCNP tallies averaged over the HSM roof (including vents) using the design-basis in-core neutron and gamma fuel sources. Use of the roof gives an average spectrum for the vented surfaces at which the dose rates are the highest. For gammas that penetrate the roof block, the thicker shield increases the dose rate importance of the higher energy gamma-rays from the fuel because the thicker shield filters out the lower energy particles. This roof spectrum is also used for neutrons for convenience, as gammas dominate neutrons in the site dose analysis. The HSM spectra are normalized to a one mrem/hour source using the flux-to-dose-factors from Reference [10.5]. These normalized spectra are then input into the MCNP ERG source variable.

- The probability of a particle being born on a given surface is proportional to the total activity of that surface. The activity of each surface is determined by multiplying the sum of the normalized group fluxes, calculated above, by the average surface dose rate and by the area of the surface. This calculation is performed for the roof, sides, back and front of the HSM. The sum of the surface activities is then input as the tally multiplier for each of the MCNP tallies to convert the tally results to fluxes (particles per second per square centimeter).

- Gamma-ray spectrum calculations for the HSM-H are shown in Table T.10-5. The group-wise dose rates on the HSM-H roof are taken from the MCNP run. The flux contribution from each group is computed as the quotient of the dose rate and the flux-to-dose factor. The "Input Current" column in Table T.10-5 is simply half the roof flux in each group, divided by the total dose rate and represents the roof current normalized to one mrem per hour. Similar calculations for neutrons are shown in Table T.10-6.

- Gamma-ray spectrum calculations for the HSM Model 102 are shown in Table T.10-7. Both the group-wise dose rates and fluxes are taken directly from the MCNP runs. As both the fluxes and dose rates are taken from MCNP, flux-to-dose factors are not listed as in Table T.10-5. The "Input Current" column in Table T.10-7 is simply half the roof flux in each group, divided by the total dose rate and represents the roof current normalized to one mrem per hour. Similar calculations for neutrons are shown in Table T.10-8.

The assumptions used to generate the HSM Model 80 dose rates are summarized below.

- For the HSM Model 80 analysis, the dose rates calculated for the HSM Model 102 ISFSI are simply scaled. The HSM Model 80 and Model 102 are geometrically identical, the only differences being the steel vent liners and thicker door for the HSM Model 102. The MCNP site dose calculation output provides the contribution of each surface source to the total dose rate. Therefore, the HSM Model 80 dose rates may be computed by multiplying each dose rate component by the ratio of the HSM Model 80 to HSM Model 102 surface source and summing the results. These ratios are provided in Section T.5.4.7.3.

T.10.2.1 Activity Calculations

Activity calculations are performed for the HSM-H and HSM Model 102, as the activity is required in the MCNP input. Similar activity calculations are not performed for the Model 80 because the site dose rates for the Model 80 are generated by scaling rather than by MCNP.

2x10 Back-to-Back Array

A box that envelops the HSM array and shield walls, as modeled in MCNP, approximates the 2x10 back-to-back array of HSMs. The dimensions of the box also include the width of the HSM end shield walls. As discussed above, the total activity of each face of the box is calculated by multiplying the current mrem/hr by the average dose rate of the face and by the area of the face.

Two 1x10 Front-to-Front Arrays

A box that envelops the HSM array and shield walls, as modeled in MCNP, approximates the two 1x10 arrays of HSMs. The dimensions of the box also include the width of the HSM end and back shield walls. As discussed above, the total activity of each face of the box is calculated by multiplying the current mrem/hr by the average dose rate of the face and by the area of the face.

The surface activities are summarized in Table T.10-9 and Table T.10-10 for the HSM-H and HSM Model 102, respectively.

T.10.2.2 Dose Rates

Dose rates are calculated for distances of 6.1 meters (20 feet) to 600 meters from the edges of the two ISFSI designs. The HSM is modeled in MCNP as a box representing the HSM arrays.

Neutron and gamma-ray sources are placed on each HSM surface (including shield walls) using the spectra and activities determined above. The angular distribution of source particles is modeled as a cosine distribution. The contribution of capture gamma-rays has been neglected, as has the contribution of bremsstrahlung electrons. The inclusion of coherent scattering greatly increases the variance in a problem with point detector tallies without improving the accuracy of the calculation. Thus, coherent scattering of photons is ignored.

The MCNP models of the ISFSI layouts are described herein. For the 2x10 back-to-back array of HSM-Hs with end shield walls, the "box" dimensions are as follows. The total width is 1260 cm. The length of the "box" is 3129 cm and the height of the "box" is 564 cm. For the HSM Model 102, these dimensions are 1209 cm, 3221 cm, and 457 cm.

For the two 1x10 front-to-front arrays of HSM-Hs with end and back shield walls, the "box" dimensions for each array are as follows. The total width is 721 cm. The length of the "box" is 3129 cm and the height of the "box" is 564 cm. The two 1x10 arrays are 1067 cm (35 feet) apart. For the HSM Model 102, these dimensions are 665 cm, 3221 cm, and 457 cm.

Point detectors are placed at the following locations as measured from each face of the "box": 6.095 m (20 feet), 10 m, 20 m, 30 m, 40 m, 50 m, 60 m, 70 m, 80 m, 90 m, 100 m, 200 m, 300 m, 400 m, 500 m, and 600 m. Each point detector is placed 91.4 cm (3 feet) above the ground.

The HSM-H MCNP site dose rate results are summarized in Table T.10-11 through Table T.10-13. The front dose rates for the 2x10 configuration are provided in Table T.10-11, the back dose rates for the 2-1x10 configuration are provided in Table T.10-12, and the side dose rates for

both ISFSI configurations are provided in Table T.10-13. Similar results for the HSM Model 102 are provided in Table T.10-14 through Table T.10-16, and results for the HSM Model 80 are provided in Table T.10-17 through Table T.10-19.

The preceding analyses are intended to provide typical dose rates for the generic ISFSI layouts described in Section T.10.2. They may not be applicable to an actual ISFSI. The written evaluations performed by a licensee for an actual ISFSI must consider the type and number of storage units, layout, characteristics of the irradiated fuel to be stored, site characteristics (e.g., berms, distance to the controlled area boundary, etc.), and reactor operations at the site in order to demonstrate compliance with 10CFR72.104.

T.10.3 References

10.1 "MCNP – A General Monte Carlo N-Particle Transport Code, Version 5, Volume II: User's Guide, " LA-CP-03-0245, 2003.

10.2 Title 10, "Energy," Code of Federal Regulations, Part 20, "Standards for Protection Against Radiation."

10.3 Title 10, "Energy," Code of Federal Regulations, Part 72, "Licensing Requirements for the Independent Storage of Spent Nuclear Fuel and High-Level Radioactive Waste."

10.4 Title 40, "Protection of Environment," Code of Federal Regulations, Part 190, "Environmental Radiation Protection Standards for Nuclear Power Operations."

10.5 "American National Standard Neutron and Gamma-Ray Fluence-to-Dose Factors," ANSI/ANS-6.1.1-1977, American Nuclear Society, La Grange Park, Illinois, March 1977.

Table T.10-1
Occupational Exposure Summary, 61BTH System

Location	Task Description	# of workers	Duration (hr)	Area Dose Rate (mrem/hr)	Total Exposure (person-mrem)
Auxiliary Building and Fuel Pool	Place the DSC into the Transfer Cask	3	1	0	0
	Fill the Cask/DSC Annulus with Clean Water and Install the Inflatable Seal	2	2	0	0
	Fill the DSC Cavity with Water	1	6	0	0
	Place the Cask Containing the DSC in the Fuel Pool	5	0.5	0	0
	Verify and Load the Candidate Fuel Assemblies into the DSC	3	5	0	0
	Place the Top Shield Plug on the DSC	2	1	0	0
	Remove the Cask/DSC from the Fuel Pool and Place them in the Decon Area	5	0.5	0	0
		1	0.033	175	6
		1	0.667	110	73
Cask Decontamination Area	Decontaminate the Outer Surface of the Cask	1	1.75	110	192
		1	1	0	0
	Decontaminate the Top Region of the Cask and DSC	1	0.5	364	182
		1	0.5	43	22
	Drain Water from the DSC	1	0.083	175	15
	Remove Cask/DSC Annulus Seal and Set-Up Welding Machine	1	0.167	779	130
		1	0.75	192	144
		1	0.5	119	59
	Weld the Inner Top Cover to the DSC Shell and Perform NDE (PT)	2	6	0	0
		1	0.333	384	128
	Drain the DSC Cavity	1	0.25	192	48
		1	0.017	384	6
		1	0.5	0	0
	Vacuum Dry and Backfill the DSC with Helium	1	0.5	119	59
		2	30	0	0
	Helium Leak Test the Shield Plug Weld	2	1	0	0
	Seal Weld the Prefabricated Plugs to the Vent and Siphon Ports and Perform NDE (PT)	1	0.5	192	96
	Fit-Up the DSC Outer Top Cover Plate	1	0.25	384	96
		1	0.5	192	96
	Weld the Outer Top Cover Plate to DSC Shell and Perform NDE (PT)	1	1	119	119
		1	0.167	384	64
		2	14	0	0
		1	0.333	384	128
	Install The Cask Lid	2	0.667	141	188
Reactor/ Fuel Building Bay	Ready the Cask Support Skid and Transport Trailer for Service	2	2	0	0
	Place the Cask onto the Skid and Trailer	2	0.25	166	83
	Secure the Cask to the Skid	1	0.25	166	42
ISFSI Site	Ready The Cask Support Skid and Transport Trailer for Service	2	2	negligible	0
	Transport the Cask to ISFSI	6	1	negligible	0
	Position the Cask in Close Proximity with the HSM	3	1	negligible	0.00
	Remove the Cask Lid	2	0.667	58	78
	Align and Dock the Cask with the HSM	2	0.25	166	83
	Position and Align Ram with Cask	2	0.5	132	132
	Remove Ram Access Cover Plate	1	0.083	747	62
	Transfer the DSC from the Cask to the HSM	3	0.5	negligible	0.00
	Lift the Ram Back onto the Trailer and Un-Dock the Cask from the	2	0.083	78	13
	Install HSM Access Door	2	0.5	26	26
Totals		**N/A**	**66**	**N/A**	**2370**

Total estimated dose is 2.37 person-rem per 61BTH canister load.
This dose bounds the expected dose for the 61BTH Type 1 DSC and Type 2 DSC canister loads in the HSM-H, HSM Model 102 and HSM Model 80.

Table T.10-2
Total Annual Exposure, 61BTH within HSM-H

2x10 Back to Back Array

Distance (meters)	Front Total Dose (mrem)	1σ Uncertainty (mrem)	1σ Relative Uncertainty
6.1	41,291	37	0.001
10	25,850	28	0.001
20	10,656	20	0.002
30	5,684	13	0.002
40	3,514	11	0.003
50	2,377	10	0.004
60	1,695	8	0.005
70	1,259	7	0.005
80	958	6	0.006
90	754	6	0.009
100	590	5	0.008
200	91	2	0.020
300	18	0.4	0.024
400	5	0.2	0.038
500	1	0.06	0.044
600	0.4	0.01	0.029

Distance (meters)	Side Total Dose (mrem)	1σ Uncertainty (mrem)	1σ Relative Uncertainty
6.1	7,013	19	0.003
10	5,152	17	0.003
20	3,012	12	0.004
30	2,039	10	0.005
40	1,483	7	0.005
50	1,122	7	0.006
60	874	9	0.010
70	685	6	0.009
80	547	6	0.011
90	440	4	0.010
100	363	4	0.012
200	59	1	0.020
300	12	0.3	0.028
400	3	0.1	0.039
500	1	0.03	0.042
600	0.3	0.02	0.084

Two 1x10 Front to Front Arrays

Distance (meters)	Back Total Dose (mrem)	1σ Uncertainty (mrem)	1σ Relative Uncertainty
6.1	5,894	17	0.003
10	4,982	18	0.004
20	3,272	15	0.005
30	2,304	12	0.005
40	1,676	11	0.007
50	1,287	10	0.008
60	1,010	9	0.009
70	786	7	0.009
80	633	6	0.010
90	520	9	0.017
100	419	4	0.010
200	74	2	0.030
300	15	0.4	0.026
400	4	0.2	0.055
500	1	0.04	0.043
600	0.4	0.1	0.282

Distance (meters)	Side Total Dose (mrem)	1σ Uncertainty (mrem)	1σ Relative Uncertainty
6.1	16,536	34	0.002
10	9,881	31	0.003
20	4,351	23	0.005
30	2,618	19	0.007
40	1,802	15	0.008
50	1,316	13	0.010
60	1,001	12	0.012
70	779	9	0.012
80	617	9	0.015
90	487	6	0.012
100	413	14	0.034
200	64	1	0.022
300	13	0.3	0.025
400	3	0.2	0.059
500	1	0.1	0.108
600	0.3	0.02	0.057

Table T.10-3
Total Annual Exposure, 61BTH within HSM Model 102

2x10 Back to Back Array

Distance (meters)	Front Total Dose (mrem)	1σ Uncertainty (mrem)	1σ Relative Uncertainty
6.1	40,670	39	0.001
10	24,332	26	0.001
20	9,481	16	0.002
30	4,898	15	0.003
40	2,920	7	0.002
50	1,948	7	0.004
60	1,369	6	0.005
70	1,005	4	0.004
80	764	4	0.006
90	593	3	0.006
100	468	3	0.006
200	79	1	0.012
300	20	0.4	0.019
400	7	0.2	0.028
500	2	0.1	0.039
600	0.8	0.01	0.017

Distance (meters)	Side Total Dose (mrem)	1σ Uncertainty (mrem)	1σ Relative Uncertainty
6.1	6,792	14	0.002
10	4,234	10	0.002
20	2,080	9	0.004
30	1,343	10	0.007
40	956	10	0.010
50	703	5	0.008
60	539	4	0.007
70	439	5	0.011
80	335	2	0.007
90	284	4	0.015
100	228	2	0.008
200	45	1	0.014
300	14	1.1	0.084
400	4	0.1	0.027
500	1	0.1	0.063
600	0.6	0.1	0.170

Two 1x10 Front to Front Arrays

Distance (meters)	Back Total Dose (mrem)	1σ Uncertainty (mrem)	1σ Relative Uncertainty
6.1	4,316	12	0.003
10	3,373	13	0.004
20	2,078	11	0.005
30	1,407	8	0.005
40	1,028	5	0.005
50	786	6	0.007
60	607	4	0.007
70	481	4	0.008
80	392	4	0.009
90	321	4	0.012
100	262	3	0.010
200	53	1	0.021
300	14	0.3	0.023
400	5	0.2	0.036
500	2	0.1	0.039
600	0.6	0.05	0.074

Distance (meters)	Side Total Dose (mrem)	1σ Uncertainty (mrem)	1σ Relative Uncertainty
6.1	15,381	31	0.002
10	8,614	21	0.002
20	3,327	18	0.005
30	1,847	13	0.007
40	1,197	8	0.006
50	859	11	0.013
60	643	7	0.011
70	495	5	0.009
80	396	5	0.012
90	321	9	0.029
100	254	3	0.012
200	49	1	0.019
300	13	0.5	0.036
400	4	0.4	0.089
500	1	0.03	0.023
600	0.5	0.04	0.074

Table T.10-4
Total Annual Exposure, 61BTH within HSM Model 80

2x10 Back to Back Array

Distance (meters)	Back Total Dose (mrem)
6.1	74,425
10	44,676
20	17,604
30	9,218
40	5,590
50	3,731
60	2,663
70	1,970
80	1,492
90	1,166
100	926
200	161.3
300	40.9
400	13.7
500	4.6
600	1.7

Distance (meters)	Side Total Dose (mrem)
6.1	11,496
10	7,673
20	4,128
30	2,750
40	2,005
50	1,486
60	1,140
70	939
80	718
90	609
100	492
200	97.9
300	30.0
400	8.0
500	3.0
600	1.3

Two 1x10 Front to Front Arrays

Distance (meters)	Back Total Dose (mrem)
6.1	8,622
10	7,112
20	4,660
30	3,212
40	2,368
50	1,815
60	1,398
70	1,097
80	901
90	742
100	601
200	122
300	32
400	11
500	4
600	1.4

Distance (meters)	Side Total Dose (mrem)
6.1	28,765
10	16,436
20	6,776
30	3,898
40	2,606
50	1,907
60	1,439
70	1,113
80	895
90	726
100	578
200	113
300	31
400	10
500	3
600	1.4

Table T.10-5
HSM-H Gamma-Ray Spectrum Calculation Results

E_{upper} (MeV)	E_{mean} (MeV)	Flux-Dose ANSI/ANS-6.1.1-1977 (mR/hr)/(γ/cm²-sec)	Roof Flux (γ/cm²-sec)	Dose Rate (mR/hr)	Input Current (γ/cm²-sec per mrem/hr)
3.5	3	4.191E-03	8.12E+00	0.03	2.161E-01
2.5	2.25	3.469E-03	6.63E+01	0.23	1.764E+00
2	1.83	3.019E-03	5.87E+01	0.18	1.563E+00
1.66	1.495	2.628E-03	1.09E+02	0.29	2.889E+00
1.33	1.165	2.205E-03	1.85E+02	0.41	4.912E+00
1	0.9	1.833E-03	1.67E+02	0.31	4.454E+00
0.8	0.7	1.523E-03	2.87E+02	0.44	7.631E+00
0.6	0.5	1.173E-03	8.65E+02	1.01	2.302E+01
0.4	0.35	8.759E-04	1.69E+03	1.48	4.490E+01
0.3	0.25	6.306E-04	4.23E+03	2.67	1.125E+02
0.2	0.15	3.834E-04	1.50E+04	5.75	3.993E+02
0.1	0.08	2.669E-04	2.12E+04	5.65	5.632E+02
0.05	0.03	9.348E-04	3.76E+02	0.35	1.002E+01
		Totals	4.42E+04	18.78	1.1764E+03

Table T.10-6
HSM-H Neutron Spectrum Calculation Results

E_{upper} (MeV)	E_{mean} (MeV)	Flux-Dose ANSI/ANS-6.1.1-1977 (mR/hr)/(n/cm²-sec)	Roof Flux (n/cm²-sec)	Dose Rate (mR/hr)	Input Current (n/cm²-sec per mrem/hr)
20.0	17.5	2.200E-01	6.09E-06	1.34E-06	4.285E-06
15.0	12.5	1.853E-01	9.49E-05	1.76E-05	6.679E-05
10.0	8	1.471E-01	6.05E-03	8.90E-04	4.259E-03
6.0	5	1.562E-01	2.30E-02	3.59E-03	1.617E-02
4.0	3	1.326E-01	2.36E-01	3.13E-02	1.663E-01
2.0	1.75	1.275E-01	1.47E-01	1.87E-02	1.033E-01
1.5	1.25	1.299E-01	2.15E-01	2.79E-02	1.512E-01
1.0	0.75	1.137E-01	5.77E-01	6.56E-02	4.056E-01
0.5	0.375	7.146E-02	6.64E-01	4.74E-02	4.671E-01
0.25	0.175	3.598E-02	1.22E+00	4.37E-02	8.553E-01
0.1	0.055	1.360E-02	2.47E+00	3.35E-02	1.735E+00
0.01	0.005	3.575E-03	1.22E+02	4.38E-01	8.617E+01
		Totals	1.28E+02	7.1E-01	9.01E+01

Table T.10-7
HSM Model 102 Gamma-Ray Spectrum Calculation Results

E_{upper} (MeV)	E_{mean} (MeV)	Roof Flux (γ/cm^2-sec)	Dose Rate (mR/hr)	Input Current (γ/cm^2-sec per mrem/hr)
10	9	1.40E+00	1.21E-02	2.582E-02
8	7.25	9.88E+00	7.51E-02	1.820E-01
6.5	5.75	1.62E+01	1.05E-01	2.992E-01
5	4.5	1.82E+01	1.02E-01	3.352E-01
4	3.5	2.81E+01	1.29E-01	5.177E-01
3	2.75	3.68E+01	1.44E-01	6.775E-01
2.5	2.25	3.34E+02	1.14E+00	6.149E+00
2	1.83	3.09E+02	9.31E-01	5.696E+00
1.66	1.495	5.99E+02	1.55E+00	1.103E+01
1.33	1.165	1.07E+03	2.30E+00	1.973E+01
1	0.9	1.01E+03	1.82E+00	1.861E+01
0.8	0.7	1.57E+03	2.36E+00	2.886E+01
0.6	0.5	3.02E+03	3.47E+00	5.566E+01
0.4	0.35	2.85E+03	2.47E+00	5.258E+01
0.3	0.25	5.38E+03	3.31E+00	9.919E+01
0.2	0.15	1.31E+04	4.85E+00	2.423E+02
0.1	0.08	8.43E+03	2.28E+00	1.553E+02
0.05	0.03	2.87E+02	9.56E-02	5.289E+00
	Totals	3.81E+04	2.714E+01	7.024E+02

Table T.10-8
HSM Model 102 Neutron Spectrum Calculation Results

E_{upper} (MeV)	E_{mean} (MeV)	Roof Flux (n/cm^2-sec)	Dose Rate (mR/hr)	Input Current (n/cm^2-sec per mrem/hr)
1.49E+01	1.36E+01	1.04E-04	1.95E-05	6.079E-05
1.22E+01	1.11E+01	6.88E-04	1.06E-04	4.023E-04
1.00E+01	9.09E+00	1.98E-03	2.91E-04	1.156E-03
8.18E+00	7.27E+00	1.93E-02	2.85E-03	1.126E-02
6.36E+00	5.66E+00	4.93E-02	7.54E-03	2.881E-02
4.96E+00	4.51E+00	5.39E-02	8.12E-03	3.150E-02
4.06E+00	3.54E+00	7.36E-02	1.02E-02	4.303E-02
3.01E+00	2.74E+00	1.43E-01	1.83E-02	8.372E-02
2.46E+00	2.41E+00	1.25E-01	1.57E-02	7.315E-02
2.35E+00	2.09E+00	5.08E-01	6.41E-02	2.971E-01
1.83E+00	1.47E+00	5.88E-01	7.60E-02	3.437E-01
1.11E+00	8.30E-01	7.88E-01	8.91E-02	4.606E-01
5.50E-01	3.31E-01	2.10E+00	1.09E-01	1.227E+00
1.11E-01	5.72E-02	4.62E+00	3.89E-02	2.700E+00
3.35E-03	1.97E-03	2.50E+00	9.34E-03	1.460E+00
5.83E-04	3.42E-04	2.57E+00	1.03E-02	1.501E+00
1.01E-04	6.50E-05	2.08E+00	8.90E-03	1.217E+00
2.90E-05	1.96E-05	2.03E+00	9.03E-03	1.185E+00
1.01E-05	6.58E-06	2.24E+00	1.01E-02	1.312E+00
3.06E-06	2.09E-06	1.96E+00	8.79E-03	1.147E+00
1.12E-06	7.67E-07	2.10E+00	9.08E-03	1.230E+00
4.14E-07	2.12E-07	9.47E+01	3.49E-01	5.537E+01
	Totals	1.19E+02	8.55E-01	6.97E+01

Table T.10-9
Summary of ISFSI Surface Activities, 61BTH DSC within HSM-H

2x10 Back-to-Back Array

Source	Area (cm^2)	Neutron Activity (neutrons/sec)	Gamma-Ray Activity (γ/sec)
Roof	3,942,392.1	3.835E+08	1.357E+11
Front 1	1,764,538.4	8.583E+07	2.948E+10
Front 2	1,764,538.4	8.583E+07	2.948E+10
Side 1	710,398.6	4.479E+06	7.020E+08
Side 2	710,398.6	4.479E+06	7.020E+08
Total	8,892,266.1	5.641E+08	1.961E+11

Two 1x10 Front-to-Front Arrays

Source	Area (cm^2)	Neutron Activity (neutrons/sec)	Gamma-Ray Activity (γ/sec)
Roof	2,257,337.4	2.196E+08	7.770E+10
Front	1,764,538.4	8.583E+07	2.948E+10
Back	1,764,538.4	1.589E+06	7.058E+08
Side 1	406,760.5	2.565E+06	4.019E+08
Side 2	406,760.5	2.565E+06	4.019E+08
Total	6,599,935.2	3.121E+08	1.087E+11

Table T.10-10
Summary of ISFSI Surface Activities, 61BTH DSC within HSM Model 102

2x10 Back-to-Back Array

Source	Area (cm^2)	Neutron Activity (neutrons/sec)	Gamma-Ray Activity (γ/sec)
Roof	3,893,979.3	2.322E+08	7.422E+10
Front 1	1,472,513.2	7.426E+07	1.793E+10
Front 2	1,472,513.2	7.426E+07	1.793E+10
Side 1	552,773.1	3.553E+06	8.901E+08
Side 2	552,773.1	3.553E+06	8.901E+08
Total	7,944,551.9	3.878E+08	1.119E+11

Two 1x10 Front-to-Front Arrays

Source	Area (cm^2)	Neutron Activity (neutrons/sec)	Gamma-Ray Activity (γ/sec)
Roof	2,143,324.7	1.278E+08	4.085E+10
Front	1,472,513.2	7.426E+07	1.793E+10
Back	1,472,513.2	3.819E+06	5.961E+08
Side 1	304,257.5	1.955E+06	4.899E+08
Side 2	304,257.5	1.955E+06	4.899E+08
Total	5,696,866.0	2.098E+08	6.036E+10

Table T.10-11
MCNP Front Detector Dose Rates for 2x10 Array, 61BTH DSC within HSM-H

Distance (meters)	Gamma Dose Rate (mrem/hr)	Gamma MCNP 1σ Uncertainty	Neutron Dose Rate (mrem/hr)	Neutron MCNP 1σ Uncertainty	Total Dose Rate (mrem/hr)	Combined MCNP 1σ Uncertainty
6.1	4.42E+00	9.00E-04	2.90E-01	4.70E-03	4.71E+00	0.0009
10	2.76E+00	1.10E-03	1.93E-01	6.00E-03	2.95E+00	0.0011
20	1.12E+00	1.90E-03	9.34E-02	9.40E-03	1.22E+00	0.0019
30	5.93E-01	2.30E-03	5.60E-02	1.15E-02	6.49E-01	0.0023
40	3.64E-01	3.10E-03	3.74E-02	1.43E-02	4.01E-01	0.0031
50	2.44E-01	4.40E-03	2.71E-02	1.71E-02	2.71E-01	0.0043
60	1.74E-01	4.70E-03	1.99E-02	1.86E-02	1.93E-01	0.0046
70	1.28E-01	5.20E-03	1.60E-02	2.32E-02	1.44E-01	0.0053
80	9.70E-02	5.70E-03	1.24E-02	2.71E-02	1.09E-01	0.0059
90	7.64E-02	8.80E-03	9.64E-03	3.13E-02	8.61E-02	0.0086
100	5.98E-02	8.20E-03	7.46E-03	2.48E-02	6.73E-02	0.0078
200	9.06E-03	1.69E-02	1.32E-03	1.12E-01	1.04E-02	0.0204
300	1.86E-03	2.60E-02	2.23E-04	6.98E-02	2.08E-03	0.0244
400	4.61E-04	3.60E-02	6.69E-05	1.63E-01	5.28E-04	0.0376
500	1.29E-04	4.66E-02	1.45E-05	1.31E-01	1.44E-04	0.0439
600	3.81E-05	2.62E-02	5.36E-06	1.40E-01	4.35E-05	0.0287

Table T.10-12
MCNP Back Detector Dose Rates for the Two 1x10 Arrays, 61BTH DSC within HSM-H

Distance (meters)	Gamma Dose Rate (mrem/hr)	Gamma MCNP 1σ Uncertainty	Neutron Dose Rate (mrem/hr)	Neutron MCNP 1σ Uncertainty	Total Dose Rate (mrem/hr)	Combined MCNP 1σ Uncertainty
6.1	5.82E-01	0.0030	9.13E-02	0.0103	6.73E-01	0.0029
10	4.90E-01	0.0037	7.89E-02	0.0125	5.69E-01	0.0036
20	3.21E-01	0.0048	5.29E-02	0.0146	3.74E-01	0.0046
30	2.25E-01	0.0055	3.79E-02	0.0178	2.63E-01	0.0053
40	1.64E-01	0.0070	2.71E-02	0.0173	1.91E-01	0.0065
50	1.25E-01	0.0088	2.15E-02	0.0195	1.47E-01	0.0080
60	9.89E-02	0.0098	1.64E-02	0.0223	1.15E-01	0.0090
70	7.64E-02	0.0097	1.33E-02	0.0291	8.97E-02	0.0093
80	6.11E-02	0.0098	1.11E-02	0.0367	7.23E-02	0.0100
90	5.05E-02	0.0183	8.83E-03	0.0415	5.93E-02	0.0167
100	4.08E-02	0.0101	7.05E-03	0.0380	4.78E-02	0.0103
200	7.30E-03	0.0298	1.17E-03	0.1081	8.47E-03	0.0297
300	1.46E-03	0.0257	2.29E-04	0.0930	1.69E-03	0.0255
400	3.96E-04	0.0608	4.66E-05	0.0781	4.43E-04	0.0550
500	1.04E-04	0.0451	1.37E-05	0.1504	1.17E-04	0.0435
600	4.49E-05	0.3155	5.60E-06	0.2132	5.05E-05	0.2816

Table T.10-13
MCNP Side Detector Dose Rates, 61BTH DSC within HSM-H

2x10 Back-to-Back Array

Distance (meters)	Gamma Dose Rate (mrem/hr)	Gamma MCNP 1σ Uncertainty	Neutron Dose Rate (mrem/hr)	Neutron MCNP 1σ Uncertainty	Total Dose Rate (mrem/hr)	Combined MCNP 1σ Uncertainty
6.1	6.98E-01	2.60E-03	1.03E-01	1.11E-02	8.01E-01	0.0027
10	5.09E-01	3.30E-03	7.89E-02	1.10E-02	5.88E-01	0.0032
20	2.96E-01	4.30E-03	4.83E-02	1.31E-02	3.44E-01	0.0041
30	1.99E-01	4.90E-03	3.42E-02	1.96E-02	2.33E-01	0.0051
40	1.45E-01	5.00E-03	2.46E-02	1.86E-02	1.69E-01	0.0051
50	1.09E-01	5.50E-03	1.89E-02	2.34E-02	1.28E-01	0.0058
60	8.53E-02	1.11E-02	1.44E-02	2.96E-02	9.98E-02	0.0104
70	6.65E-02	9.40E-03	1.17E-02	3.30E-02	7.82E-02	0.0094
80	5.34E-02	1.06E-02	9.04E-03	3.75E-02	6.25E-02	0.0106
90	4.29E-02	1.00E-02	7.36E-03	3.58E-02	5.02E-02	0.0100
100	3.53E-02	1.14E-02	6.08E-03	4.81E-02	4.14E-02	0.0120
200	5.82E-03	2.21E-02	9.27E-04	5.40E-02	6.74E-03	0.0205
300	1.22E-03	2.82E-02	1.86E-04	1.03E-01	1.40E-03	0.0280
400	3.07E-04	4.22E-02	4.68E-05	1.04E-01	3.54E-04	0.0391
500	7.73E-05	3.87E-02	1.50E-05	1.62E-01	9.23E-05	0.0418
600	2.44E-05	9.60E-02	4.13E-06	1.08E-01	2.86E-05	0.0836

Two 1x10 Front-to-Front Arrays

Distance (meters)	Gamma Dose Rate (mrem/hr)	Gamma MCNP 1σ Uncertainty	Neutron Dose Rate (mrem/hr)	Neutron MCNP 1σ Uncertainty	Total Dose Rate (mrem/hr)	Combined MCNP 1σ Uncertainty
6.1	1.73E+00	2.00E-03	1.55E-01	1.05E-02	1.89E+00	0.0020
10	1.02E+00	3.20E-03	1.05E-01	1.16E-02	1.13E+00	0.0031
20	4.37E-01	5.30E-03	5.93E-02	1.95E-02	4.97E-01	0.0052
30	2.59E-01	7.50E-03	3.96E-02	2.39E-02	2.99E-01	0.0072
40	1.78E-01	8.30E-03	2.75E-02	2.75E-02	2.06E-01	0.0081
50	1.29E-01	9.10E-03	2.16E-02	4.47E-02	1.50E-01	0.0101
60	9.89E-02	1.26E-02	1.55E-02	3.34E-02	1.14E-01	0.0118
70	7.52E-02	8.70E-03	1.36E-02	6.16E-02	8.89E-02	0.0120
80	6.06E-02	1.55E-02	9.81E-03	4.40E-02	7.04E-02	0.0147
90	4.80E-02	1.16E-02	7.59E-03	4.21E-02	5.56E-02	0.0115
100	4.07E-02	3.81E-02	6.45E-03	5.36E-02	4.71E-02	0.0337
200	6.35E-03	2.24E-02	9.66E-04	7.07E-02	7.31E-03	0.0216
300	1.33E-03	2.72E-02	1.67E-04	6.65E-02	1.50E-03	0.0253
400	3.29E-04	6.14E-02	5.38E-05	1.81E-01	3.83E-04	0.0586
500	1.09E-04	1.20E-01	1.23E-05	1.42E-01	1.21E-04	0.1085
600	2.77E-05	6.04E-02	4.25E-06	1.62E-01	3.19E-05	0.0566

Table T.10-14
MCNP Front Detector Dose Rates for the 2x10 Array, 61BTH DSC within HSM Model 102

Distance (meters)	Gamma Dose Rate (mrem/hr)	Gamma MCNP 1σ Uncertainty	Neutron Dose Rate (mrem/hr)	Neutron MCNP 1σ Uncertainty	Total Dose Rate (mrem/hr)	Combined MCNP 1σ Uncertainty
6.1	4.36E+00	1.00E-03	2.83E-01	3.80E-03	4.64E+00	0.0010
10	2.60E+00	1.10E-03	1.74E-01	5.40E-03	2.78E+00	0.0011
20	1.01E+00	1.70E-03	7.13E-02	6.90E-03	1.08E+00	0.0017
30	5.21E-01	3.10E-03	3.84E-02	1.10E-02	5.59E-01	0.0030
40	3.10E-01	2.30E-03	2.38E-02	1.59E-02	3.33E-01	0.0024
50	2.06E-01	3.70E-03	1.61E-02	2.03E-02	2.22E-01	0.0037
60	1.45E-01	4.60E-03	1.08E-02	2.24E-02	1.56E-01	0.0046
70	1.07E-01	3.90E-03	7.40E-03	2.53E-02	1.15E-01	0.0040
80	8.15E-02	5.60E-03	5.67E-03	3.43E-02	8.72E-02	0.0057
90	6.36E-02	5.80E-03	4.16E-03	3.06E-02	6.77E-02	0.0058
100	5.03E-02	6.00E-03	3.17E-03	2.58E-02	5.34E-02	0.0058
200	8.58E-03	1.19E-02	4.63E-04	5.37E-02	9.04E-03	0.0116
300	2.18E-03	1.96E-02	1.28E-04	6.78E-02	2.31E-03	0.0189
400	7.09E-04	2.95E-02	4.30E-05	6.52E-02	7.52E-04	0.0281
500	2.34E-04	3.42E-02	2.29E-05	2.60E-01	2.57E-04	0.0388
600	8.62E-05	1.71E-02	7.18E-06	8.43E-02	9.34E-05	0.0171

Table T.10-15
MCNP Back Detector Dose Rates for the Two 1x10 Arrays, 61BTH DSC within HSM Model 102

Distance (meters)	Gamma Dose Rate (mrem/hr)	Gamma MCNP 1σ Uncertainty	Neutron Dose Rate (mrem/hr)	Neutron MCNP 1σ Uncertainty	Total Dose Rate (mrem/hr)	Combined MCNP 1σ Uncertainty
6.1	4.23E-01	0.0030	6.96E-02	0.0083	4.93E-01	0.0028
10	3.30E-01	0.0041	5.50E-02	0.0105	3.85E-01	0.0038
20	2.05E-01	0.0060	3.17E-02	0.0126	2.37E-01	0.0055
30	1.40E-01	0.0058	2.03E-02	0.0150	1.61E-01	0.0054
40	1.03E-01	0.0051	1.41E-02	0.0188	1.17E-01	0.0051
50	8.01E-02	0.0074	9.62E-03	0.0238	8.98E-02	0.0071
60	6.22E-02	0.0067	7.14E-03	0.0304	6.93E-02	0.0068
70	4.97E-02	0.0082	5.14E-03	0.0227	5.49E-02	0.0077
80	4.08E-02	0.0099	3.95E-03	0.0323	4.48E-02	0.0095
90	3.36E-02	0.0133	3.08E-03	0.0309	3.67E-02	0.0124
100	2.75E-02	0.0102	2.41E-03	0.0413	3.00E-02	0.0099
200	5.71E-03	0.0225	3.87E-04	0.0621	6.09E-03	0.0215
300	1.52E-03	0.0243	9.42E-05	0.0392	1.61E-03	0.0230
400	5.04E-04	0.0380	3.53E-05	0.0453	5.39E-04	0.0357
500	1.62E-04	0.0417	1.45E-05	0.0589	1.76E-04	0.0386
600	6.56E-05	0.0803	6.12E-06	0.0827	7.17E-05	0.0738

Table T.10-16
MCNP Side Detector Dose Rates, 61BTH DSC within HSM Model 102

2x10 Back-to-Back Array

Distance (meters)	Gamma Dose Rate (mrem/hr)	Gamma MCNP 1σ Uncertainty	Neutron Dose Rate (mrem/hr)	Neutron MCNP 1σ Uncertainty	Total Dose Rate (mrem/hr)	Combined MCNP 1σ Uncertainty
6.1	6.99E-01	2.10E-03	7.62E-02	7.40E-03	7.75E-01	0.0020
10	4.30E-01	2.50E-03	5.29E-02	9.30E-03	4.83E-01	0.0024
20	2.10E-01	4.40E-03	2.76E-02	1.30E-02	2.37E-01	0.0042
30	1.36E-01	8.00E-03	1.75E-02	1.65E-02	1.53E-01	0.0073
40	9.73E-02	1.12E-02	1.18E-02	1.87E-02	1.09E-01	0.0102
50	7.20E-02	8.00E-03	8.22E-03	2.34E-02	8.03E-02	0.0076
60	5.56E-02	6.70E-03	5.93E-03	2.85E-02	6.15E-02	0.0066
70	4.52E-02	1.11E-02	4.82E-03	4.37E-02	5.01E-02	0.0109
80	3.50E-02	7.10E-03	3.23E-03	3.34E-02	3.83E-02	0.0071
90	2.99E-02	1.62E-02	2.56E-03	3.64E-02	3.25E-02	0.0152
100	2.40E-02	8.60E-03	2.05E-03	3.22E-02	2.61E-02	0.0083
200	4.84E-03	1.33E-02	3.52E-04	7.92E-02	5.19E-03	0.0135
300	1.47E-03	8.87E-02	8.90E-05	7.49E-02	1.56E-03	0.0838
400	3.80E-04	2.75E-02	3.89E-05	1.19E-01	4.19E-04	0.0273
500	1.36E-04	4.50E-02	2.26E-05	3.52E-01	1.59E-04	0.0632
600	5.86E-05	1.88E-01	6.05E-06	9.53E-02	6.47E-05	0.1705

Two 1x10 Front-to-Front Arrays

Distance (meters)	Gamma Dose Rate (mrem/hr)	Gamma MCNP 1σ Uncertainty	Neutron Dose Rate (mrem/hr)	Neutron MCNP 1σ Uncertainty	Total Dose Rate (mrem/hr)	Combined MCNP 1σ Uncertainty
6.1	1.63E+00	2.10E-03	1.24E-01	7.90E-03	1.76E+00	0.0020
10	9.06E-01	2.40E-03	7.72E-02	1.24E-02	9.83E-01	0.0024
20	3.44E-01	5.80E-03	3.57E-02	1.70E-02	3.80E-01	0.0055
30	1.90E-01	7.40E-03	2.06E-02	2.29E-02	2.11E-01	0.0070
40	1.23E-01	6.40E-03	1.33E-02	2.76E-02	1.37E-01	0.0064
50	8.90E-02	1.41E-02	9.12E-03	2.96E-02	9.81E-02	0.0131
60	6.70E-02	1.23E-02	6.37E-03	2.60E-02	7.34E-02	0.0115
70	5.18E-02	9.60E-03	4.72E-03	3.31E-02	5.65E-02	0.0092
80	4.13E-02	1.20E-02	3.88E-03	5.94E-02	4.52E-02	0.0121
90	3.41E-02	3.09E-02	2.63E-03	3.54E-02	3.67E-02	0.0288
100	2.69E-02	1.23E-02	2.04E-03	3.13E-02	2.89E-02	0.0116
200	5.21E-03	1.91E-02	3.52E-04	9.67E-02	5.56E-03	0.0189
300	1.41E-03	3.78E-02	1.02E-04	8.07E-02	1.51E-03	0.0357
400	4.71E-04	9.47E-02	3.31E-05	5.56E-02	5.04E-04	0.0885
500	1.29E-04	2.37E-02	1.47E-05	7.88E-02	1.44E-04	0.0228
600	5.49E-05	7.49E-02	7.57E-06	2.78E-01	6.25E-05	0.0739

Table T.10-17
MCNP Front Detector Dose Rates for 2x10 Array, 61BTH DSC within HSM Model 80

Distance (meters)	Gamma Dose Rate (mrem/hr)	Gamma MCNP 1σ Error	Neutron Dose Rate (mrem/hr)	Neutron MCNP 1σ Error	Total Dose Rate (mrem/hr)	Combined MCNP 1σ Error
6.10E+00	6.25E+00	1.06E-03	2.25E+00	4.00E-03	8.50E+00	1.32E-03
1.00E+01	3.81E+00	1.23E-03	1.29E+00	5.31E-03	5.10E+00	1.63E-03
2.00E+01	1.55E+00	2.16E-03	4.64E-01	7.82E-03	2.01E+00	2.46E-03
3.00E+01	8.27E-01	4.11E-03	2.25E-01	1.16E-02	1.05E+00	4.07E-03
4.00E+01	5.08E-01	3.50E-03	1.31E-01	2.09E-02	6.38E-01	5.11E-03
5.00E+01	3.47E-01	5.54E-03	7.93E-02	1.97E-02	4.26E-01	5.82E-03
6.00E+01	2.50E-01	7.47E-03	5.35E-02	2.65E-02	3.04E-01	7.73E-03
7.00E+01	1.88E-01	6.36E-03	3.68E-02	3.87E-02	2.25E-01	8.27E-03
8.00E+01	1.45E-01	9.11E-03	2.56E-02	3.40E-02	1.70E-01	9.28E-03
9.00E+01	1.14E-01	9.50E-03	1.87E-02	2.85E-02	1.33E-01	9.09E-03
1.00E+02	9.11E-02	9.08E-03	1.46E-02	4.70E-02	1.06E-01	1.02E-02
2.00E+02	1.64E-02	1.83E-02	1.98E-03	8.88E-02	1.84E-02	1.89E-02
3.00E+02	4.16E-03	2.77E-02	5.12E-04	1.11E-01	4.67E-03	2.75E-02
4.00E+02	1.40E-03	4.75E-02	1.63E-04	5.44E-02	1.56E-03	4.29E-02
5.00E+02	4.46E-04	5.36E-02	7.88E-05	1.39E-01	5.25E-04	5.01E-02
6.00E+02	1.62E-04	2.60E-02	2.69E-05	1.00E-01	1.89E-04	2.65E-02

Table T.10-18
MCNP Back Detector Dose Rates for the Two 1x10 Arrays, 61BTH DSC within HSM Model 80

Distance (meters)	Gamma Dose Rate (mrem/hr)	Gamma MCNP 1σ Error	Neutron Dose Rate (mrem/hr)	Neutron MCNP 1σ Error	Total Dose Rate (mrem/hr)	Combined MCNP 1σ Error
6.10E+00	7.53E-01	5.37E-03	2.31E-01	1.55E-02	9.84E-01	5.49E-03
1.00E+01	6.27E-01	6.53E-03	1.85E-01	1.73E-02	8.12E-01	6.40E-03
2.00E+01	4.20E-01	8.57E-03	1.11E-01	2.23E-02	5.32E-01	8.23E-03
3.00E+01	2.96E-01	8.21E-03	7.10E-02	2.54E-02	3.67E-01	8.25E-03
4.00E+01	2.21E-01	6.91E-03	4.93E-02	3.23E-02	2.70E-01	8.16E-03
5.00E+01	1.73E-01	8.76E-03	3.42E-02	4.21E-02	2.07E-01	1.01E-02
6.00E+01	1.35E-01	8.74E-03	2.46E-02	4.24E-02	1.60E-01	9.86E-03
7.00E+01	1.08E-01	8.90E-03	1.70E-02	3.05E-02	1.25E-01	8.73E-03
8.00E+01	8.92E-02	1.32E-02	1.37E-02	3.87E-02	1.03E-01	1.25E-02
9.00E+01	7.38E-02	1.71E-02	1.09E-02	5.94E-02	8.47E-02	1.68E-02
1.00E+02	6.05E-02	1.28E-02	8.12E-03	5.15E-02	6.86E-02	1.28E-02
2.00E+02	1.27E-02	2.83E-02	1.26E-03	8.33E-02	1.39E-02	2.69E-02
3.00E+02	3.34E-03	2.73E-02	3.20E-04	7.39E-02	3.66E-03	2.58E-02
4.00E+02	1.10E-03	4.50E-02	1.17E-04	5.65E-02	1.22E-03	4.11E-02
5.00E+02	3.55E-04	5.01E-02	5.23E-05	1.48E-01	4.07E-04	4.77E-02
6.00E+02	1.45E-04	9.91E-02	1.85E-05	4.41E-02	1.64E-04	8.80E-02

Table T.10-19
MCNP Side Detector Dose Rates, 61BTH DSC within HSM Model 80

2x10 Back-to-Back Array

Distance (meters)	Gamma Dose Rate (mrem/hr)	Gamma MCNP 1σ Error	Neutron Dose Rate (mrem/hr)	Neutron MCNP 1σ Error	Total Dose Rate (mrem/hr)	Combined MCNP 1σ Error
6.10E+00	1.14E+00	3.72E-03	1.69E-01	2.61E-02	1.31E+00	4.67E-03
1.00E+01	7.55E-01	4.73E-03	1.21E-01	2.14E-02	8.76E-01	5.04E-03
2.00E+01	4.06E-01	7.45E-03	6.49E-02	2.42E-02	4.71E-01	7.24E-03
3.00E+01	2.73E-01	1.24E-02	4.06E-02	2.74E-02	3.14E-01	1.14E-02
4.00E+01	1.99E-01	1.58E-02	2.95E-02	5.39E-02	2.29E-01	1.54E-02
5.00E+01	1.50E-01	1.15E-02	1.97E-02	4.60E-02	1.70E-01	1.15E-02
6.00E+01	1.16E-01	9.07E-03	1.39E-02	4.46E-02	1.30E-01	9.41E-03
7.00E+01	9.52E-02	1.41E-02	1.19E-02	7.91E-02	1.07E-01	1.53E-02
8.00E+01	7.39E-02	9.39E-03	8.03E-03	5.97E-02	8.19E-02	1.03E-02
9.00E+01	6.34E-02	1.63E-02	6.08E-03	5.54E-02	6.95E-02	1.56E-02
1.00E+02	5.12E-02	1.13E-02	4.97E-03	5.30E-02	5.62E-02	1.13E-02
2.00E+02	1.04E-02	1.54E-02	8.16E-04	1.38E-01	1.12E-02	1.75E-02
3.00E+02	3.23E-03	1.15E-01	1.91E-04	9.07E-02	3.42E-03	1.09E-01
4.00E+02	8.34E-04	3.53E-02	7.99E-05	1.06E-01	9.14E-04	3.35E-02
5.00E+02	3.03E-04	5.72E-02	3.89E-05	2.96E-01	3.42E-04	6.08E-02
6.00E+02	1.32E-04	2.34E-01	1.36E-05	2.18E-01	1.45E-04	2.13E-01

Two 1x10 Front-to-Front Arrays

Distance (meters)	Gamma Dose Rate (mrem/hr)	Gamma MCNP 1σ Error	Neutron Dose Rate (mrem/hr)	Neutron MCNP 1σ Error	Total Dose Rate (mrem/hr)	Combined MCNP 1σ Error
6.10E+00	2.45E+00	2.67E-03	8.38E-01	9.42E-03	3.28E+00	3.12E-03
1.00E+01	1.43E+00	3.78E-03	4.47E-01	1.30E-02	1.88E+00	4.23E-03
2.00E+01	6.07E-01	1.05E-02	1.66E-01	2.28E-02	7.73E-01	9.60E-03
3.00E+01	3.61E-01	1.27E-02	8.41E-02	3.15E-02	4.45E-01	1.19E-02
4.00E+01	2.44E-01	1.03E-02	5.35E-02	4.76E-02	2.97E-01	1.20E-02
5.00E+01	1.82E-01	2.22E-02	3.55E-02	3.91E-02	2.18E-01	1.96E-02
6.00E+01	1.40E-01	1.84E-02	2.43E-02	3.79E-02	1.64E-01	1.67E-02
7.00E+01	1.09E-01	1.27E-02	1.80E-02	5.59E-02	1.27E-01	1.35E-02
8.00E+01	8.82E-02	1.69E-02	1.40E-02	6.55E-02	1.02E-01	1.71E-02
9.00E+01	7.36E-02	4.34E-02	9.30E-03	4.32E-02	8.29E-02	3.88E-02
1.00E+02	5.80E-02	1.65E-02	7.94E-03	6.74E-02	6.60E-02	1.66E-02
2.00E+02	1.15E-02	2.30E-02	1.31E-03	2.56E-01	1.28E-02	3.33E-02
3.00E+02	3.19E-03	4.81E-02	3.72E-04	1.80E-01	3.56E-03	4.70E-02
4.00E+02	1.09E-03	1.16E-01	1.06E-04	9.82E-02	1.19E-03	1.06E-01
5.00E+02	2.92E-04	2.95E-02	4.22E-05	1.50E-01	3.34E-04	3.20E-02
6.00E+02	1.25E-04	9.30E-02	3.75E-05	6.01E-01	1.63E-04	1.56E-01

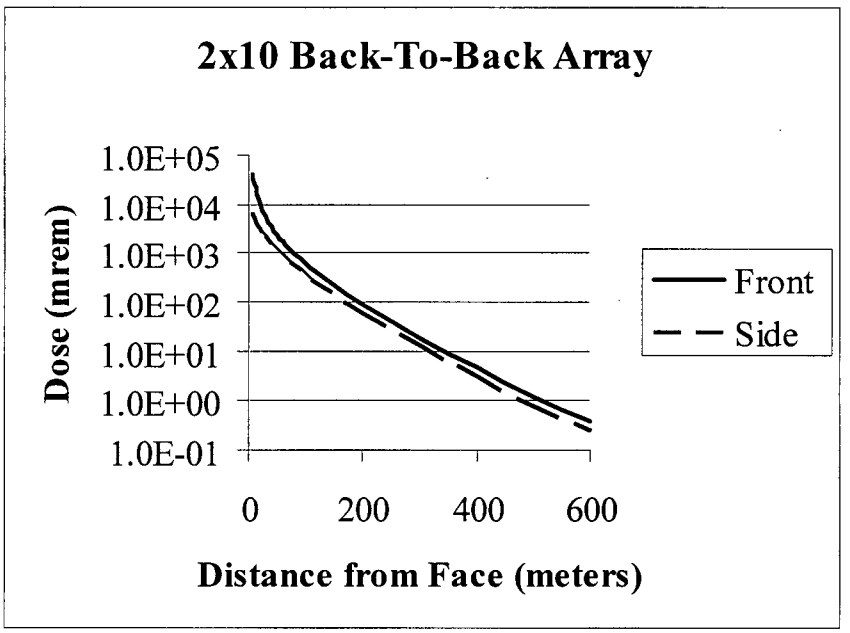

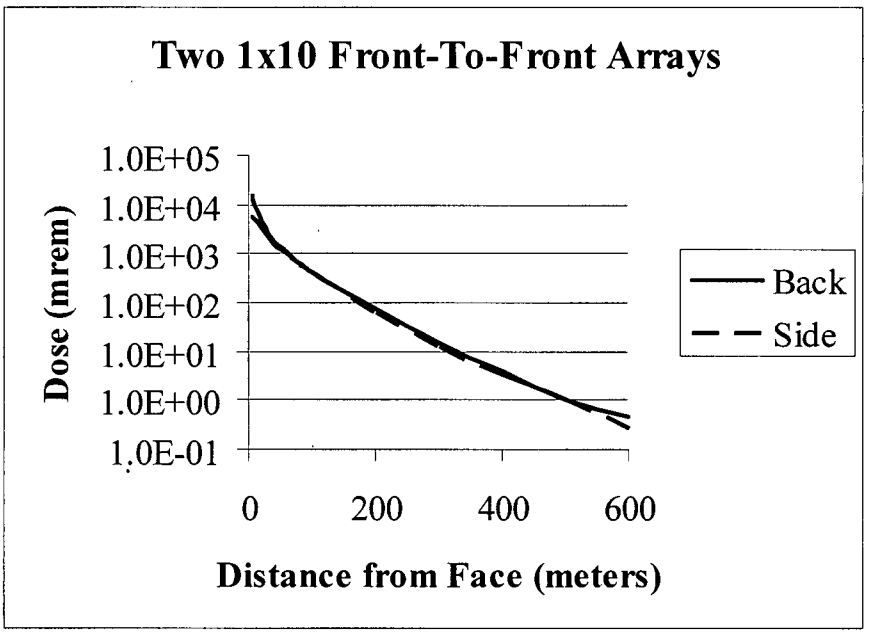

Figure T.10-1
Annual Exposure from the ISFSI as a Function of Distance, 61BTH DSC within HSM-H

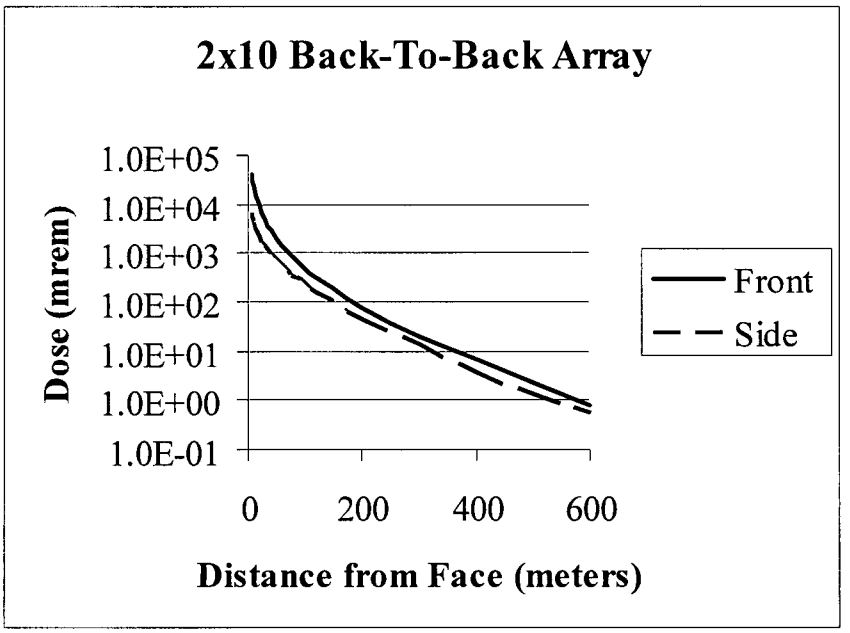

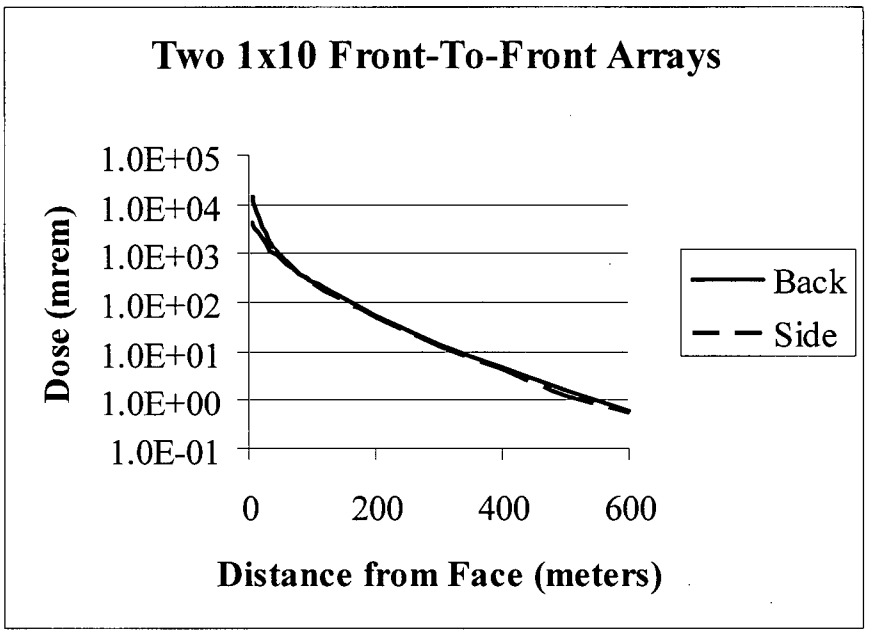

Figure T.10-2
Annual Exposure from the ISFSI as a Function of Distance, 61BTH DSC within HSM-Model 102

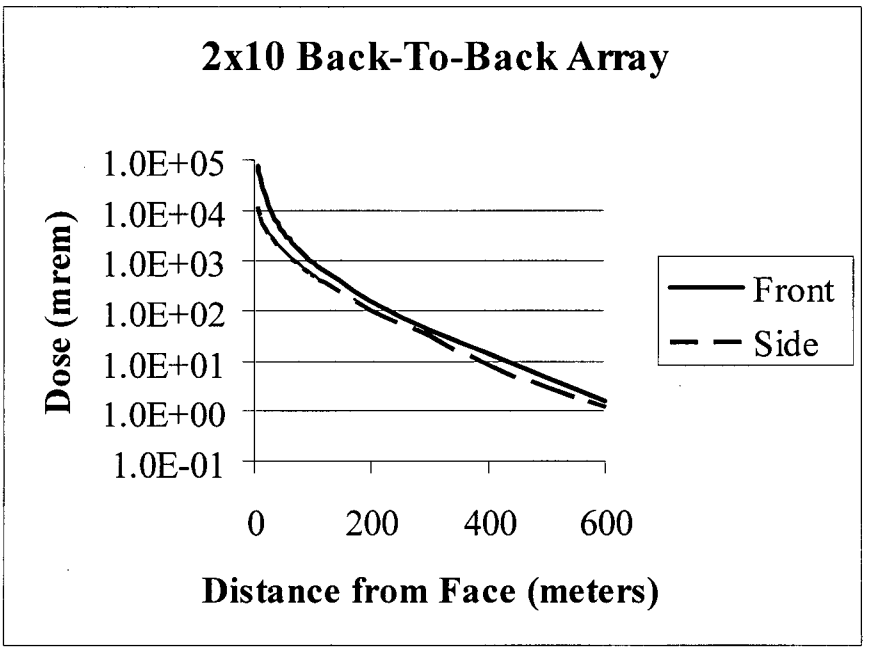

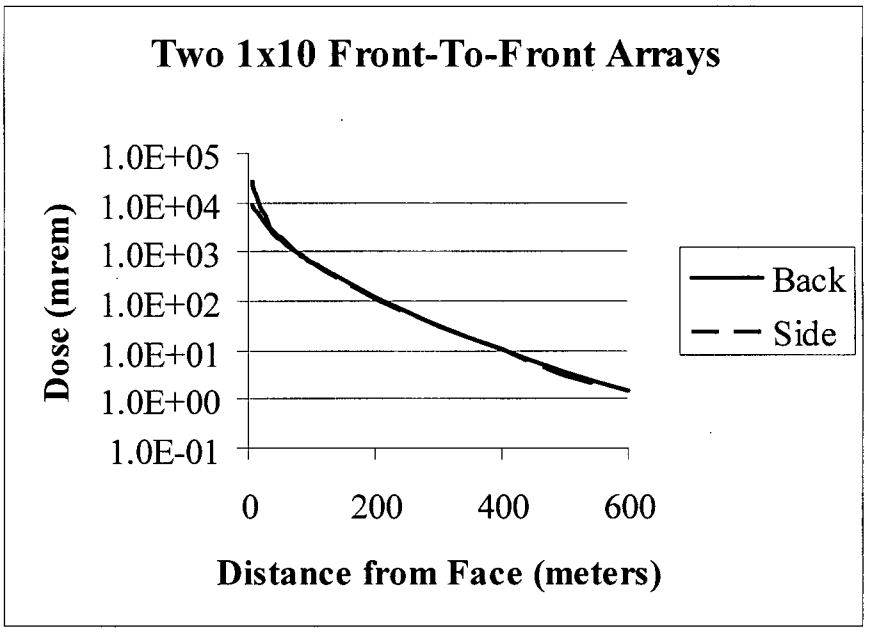

Figure T.10-3
Annual Exposure from the ISFSI as a Function of Distance, 61BTH DSC within HSM-Model 80

T.11 Accident Analyses

This section describes the postulated off-normal and accident events that could occur during transfer and storage of the NUHOMS®-61BTH DSC. Sections which do not affect the evaluation presented in Section 8.0 are identified as "No change." Detailed analysis of the events are provided in other sections and referenced herein.

T.11.1 Off-Normal Operations

Off-normal operations are design events of the second type (Design Event II) as defined in ANSI/ANS 57.9 [11.1]. Off-normal conditions consist of that set of events that, although not occurring regularly, can be expected to occur with moderate frequency or on the order of once during a calendar year of ISFSI operation.

The off-normal conditions considered for the NUHOMS®-61BTH DSC are off-normal transfer loads, extreme temperatures and a postulated release of radionuclides.

The term "Standardized HSM" used in this Chapter, is applicable to HSM Model 80, Model 102 and Model 152 or Model 202.

T.11.1.1 Off-Normal Transfer Loads

No change.

T.11.1.1.1 Postulated Cause of Event

Same as Section 8.1.2. The probability of a jammed DSC does not increase with the NUHOMS®-61BTH DSC, since the interfacing design features and dimensions of the transfer cask top end and HSM access opening are not changed. The 61BTH DSC is provided with similar beveled lead-ins as the 61BT/52B. The maximum allowed misalignment of the sliding surfaces has not changed nor have any of the HSM insertion/retrieval procedures.

T.11.1.1.2 Detection of Event

No change.

T.11.1.1.3 Analysis of Effects and Consequences

A detailed evaluation of this event is presented in Section T.3.6.2 and is summarized below. The NUHOMS®-61BTH DSC has a 0.5 inch shell wall thickness, while the NUHOMS®-24P and NUHOMS®-52B have a 0.62 inch shell. Therefore the stresses in the canister shell are increased. The DSC shell stress due to the 2,690 in-kip moment due to axial sticking of the DSC is S_{mx} = 1.55 ksi. This magnitude of stress is negligible when compared to the allowable membrane stress of 17.2 ksi.

The DSC shell stress due to the 1,400 pound axial load during the binding of the DSC is 15.7 ksi. This stress is well within the ASME Code Service Level C allowable of 21.7 ksi for an off-normal jammed DSC event.

The evaluation of the basket due to normal and off-normal handling and transfer loads is presented in Section T.3.6.1.3.3.

T.11.1.1.4 Corrective Actions

No change.

T.11.1.2 Extreme Temperatures

No change. The off-normal maximum ambient temperature of 125°F is used in Section 8.1.2.2. For the NUHOMS®-61BTH system, a maximum ambient temperature of 117°F is used. Therefore, the analyses in Section 8.1.2.2 bound TCs and Standardized HSM used in the NUHOMS®-61BTH system.

T.11.1.2.1 Postulated Cause of Event

No change.

T.11.1.2.2 Detection of Event

No change.

T.11.1.2.3 Analysis of Effects and Consequences

The thermal evaluation of the NUHOMS®-61BTH system for off-normal conditions is presented in Chapter T.4. The 100°F normal condition with insolation bounds the 117°F case without insolation for the DSC in the TC. Therefore the normal condition maximum temperatures are bounding. The 117°F case with the DSC in the HSM-H is not bounded by the normal conditions and therefore evaluated in Chapter T.4.

The NUHOMS® TC and the Standardized HSM were evaluated for a maximum heat load of 24 kW and maximum off-normal ambient temperature of 125°F. The maximum heat load of the 61BTH Type 1 DSC in the TC or the Standardized HSM is limited to 22 kW. Therefore the evaluations presented in Section 8.1.2.2 (for HSM Models 80/102) or in their respective appendices (for Models 152/202) are bounding for these components.

The structural evaluation of the 61BTH Type 2 DSC in HSM-H off-normal temperature conditions is presented in Section T.3.6.2.2. The structural evaluation of the basket due to off-normal thermal conditions is presented in Section T.3.6.1.3. The structural evaluation of HSM-H and OS197FC-B Transfer Cask for off-normal conditions with 61BTH DSC are presented in Section T.3.6.

T.11.1.2.4 Corrective Actions

Restrictions for onsite handling of the transfer cask with a loaded DSC under extreme temperature conditions are presented in Technical Specifications 1.2.13 and 1.2.14. There is no change to this requirement as a result of addition of the NUHOMS®-61BT DSC.

T.11.1.3 Off-Normal Releases of Radionuclides

The NUHOMS®-61BTH DSC is designed and tested to the leak tight criteria of ANSI N14.5 [11.2]. Therefore the estimated quantity of radionuclides expected to be released annually to the environment due to normal or off-normal events is zero.

T.11.1.3.1 Postulated Cause of Event

In accordance with the Standard Review Plan, NUREG-1536 [11.3] and Interim Staff Guidance ISG-5 Rev. 1 [11.4], for off-normal conditions, it is conservatively assumed that 10% of the fuel rods fail.

T.11.1.3.2 Detection of Event

Failed fuel rods would go undetected, but are not a safety concern since the canister is designed and tested to leak tight criteria of ANSI N14.5 [11.2].

T.11.1.3.3 Analysis of Effects and Consequences

The bounding off-normal pressure for the NUHOMS®-61BTH DSC is calculated with the DSC in either the HSM-H or Standardized HSM or in the TCs in Section T.4.6 as 12.1 psig. The NUHOMS®-61BTH DSC stresses were evaluated in Section T.3.6 assuming conservatively a 20 psig off-normal internal DSC pressure. The results show that the stresses due to these pressures are below the allowable stresses for off-normal conditions, as shown in T.3.6.

The NUHOMS®-61BTH DSC is designed and tested to the leak tight criteria of ANSI N14.5 [11.2]. Therefore the estimated quantity of radionuclides expected to be released annually to the environment due to normal or off-normal events is zero.

T.11.1.3.4 Corrective Actions

None required.

T.11.1.4 Radiological Impact from Off-Normal Operations

The NUHOMS®-61BTH DSC is designed and tested to the leak tight criteria of ANSI N14.5 [11.2]. The off-normal conditions have been evaluated in accordance with the ASME B&PV code. The resulting stresses are below the allowable stresses, and there will be no breach of the confinement boundary due to the off-normal conditions. Therefore the estimated quantity of radionuclides expected to be released annually to the environment due to off-normal events is zero.

T.11.2 Postulated Accidents

T.11.2.1 Reduced HSM Air Inlet and Outlet Shielding

This event is described in UFSAR Section 8.2.10 for Models 80/102 or in their respective appendices for Models 152/202.

T.11.2.1.1 Cause of Accident

No change to the cause of the accident for Standardized HSM as described in UFSAR Section 8.2.1.1 for Models 80/102 or in their respective appendices for Models 152/202.

For the HSM-H and HSM Models 152 and 202, this accident is not credible since the an array composed of these HSM types is designed with the elimination of 6-inch gaps between the adjacent HSMs. These HSM types are placed next to each other and even in the unlikely event of large settlement of the ISFSI foundation, shifting of adjacent HSMs occurring and causing these HSMs to separate is not credible.

T.11.2.1.2 Accident Analysis

There are no structural consequences that affect the safe operation of the NUHOMS®-61BTH system resulting from the separation of the Standardized HSM . The thermal effects of this accident result from the blockage of Standardized HSM air inlet and outlet openings. However, the effect on the NUHOMS®-61BTH Type 1 DSC, Standardized HSM and fuel temperatures is bounded by the complete blockage of air inlet and outlet openings described in Section T.11.2.7. The radiological consequences of this accident are described in the paragraph below.

T.11.2.1.3 Accident Dose Calculations

The off-site radiological effects that result from a partial loss of adjacent Standardized HSM shielding is an increase in the air scattered (skyshine) and direct doses from the 12 inch gap between the separated HSMs. The air scattered (skyshine) and direct doses are reduced from the gap between the HSMs that are in contact with each other. On-site radiological effects result from an increase in the direct radiation during recovery operations and increased skyshine radiation. Table 8.2-2 shows the comparisons of the increased dose rate as a function of distance due to the reduced shielding effects of the adjacent HSM for the 24P DSC with 5-year cooled design basis fuel. Table T.11-1 provides a similar table for the NUHOMS®-61BTH system. For the NUHOMS®-61BTH system the dose increase to a person located 100 meters away from the NUHOMS® installation for eight hours a day for five days (estimated recovery time) would be 8.8 mrem. The increased dose to an off-site person for 24 hours a day for five days located 600 m away would be about 0.05 mrem. Thus, the 10CFR72.106 requirements for this postulated event are met.

T.11.2.1.4 Corrective Actions

No change. See Section UFSAR 8.2.1.4 for Models 80/102 or in their respective appendices for Models 152/202.

T.11.2.2 Earthquake

This event is described in Section 8.2.3.1.

T.11.2.2.1 Cause of Accident

This accident is described in Section 8.2.3.1. No change.

T.11.2.2.2 Accident Analysis

Section 8.2.3.2 describes the analyses performed to demonstrate that the NUHOMS® system will withstand the design basis seismic event. Section T.3.7.2 presents the changes to this analysis resulting from the addition of NUHOMS®-61BTH DSC. The results of this analysis show that the leak-tight integrity of the canister is not compromised. No damage to the HSM is postulated. The basket stresses are also low and do not result in deformations that would prevent fuel from being unloaded from the canister.

T.11.2.2.3 Accident Dose Calculations

The NUHOMS® 61BTH system is designed and analyzed to withstand the design basis earthquake accident. Hence, no radioactivity is released and there is no associated dose increase due to this event.

T.11.2.2.4 Corrective Actions

After a seismic event, the NUHOMS® HSMs (HSM-H and Standardized HSM) and TC would be inspected for damage. Any debris would be removed. An evaluation would be performed to determine if the system components were still within the licensed design basis.

T.11.2.3 Extreme Wind and Tornado Missiles

This event is described in Section 8.2.2.

T.11.2.3.1 Cause of Accident

The determination of the tornado wind and tornado missile loads action on the HSM are detailed in UFSAR Section 3.2.1 and is supplemented by their respective appendices for the HSM-H and HSM Models 152/202.

No change to the determination of the tornado wind and tornado missile loads acting on the Standardized HSM or HSM-H as detailed in Section T.2.2.1.

T.11.2.3.2 Accident Analysis

An evaluation of the HSM and transfer cask with respect to tornado winds and tornado missiles is presented in Section 8.2.2. Changes to this analysis, as a result of the addition of the NUHOMS®-61BTH DSC, are presented in Section T.3.7.1. Evaluation of the Standardized

HSM and TC with respect to tornado missile is also presented in Section 8.2.2. The tornado missile impact evaluation of the HSM-H is presented in the following sections.

The evaluation of the HSM-H for the effect of DBT wind pressure loads is addressed in Section P.3.7.1.1.

The missile impact analysis presented in Section P.11.2.3.2.1 is applicable here. Therefore, a loaded HSM-H rotates a maximum of 0.60° from vertical. The loaded HSM-H is stable against overturning as tip-over does not occur until the CG rotates past the edge point (point B, Figure T.11-1) to an angle of more than 24.65° [= $\tan^{-1}(52.0/118.77)$].

T.11.2.3.3 Accident Dose Calculations

The NUHOMS®-61BTH DSC is designed and tested as a leak-tight containment boundary. As shown in Section T.11.2.3.2, tornado wind and tornado missiles do not breach the containment boundary. Therefore there is no increase in site boundary dose due to this accident event.

T.11.2.3.4 Corrective Actions

After excessive high winds or a tornado, the HSMs and TCs would be inspected for damage. Any debris would be removed. Any damage resulting from impact with a missile would be evaluated to determine if the system was still within the licensed design basis.

T.11.2.4 Flood

This event is described in Section 8.2.4.

T.11.2.4.1 Cause of Accident

No change.

T.11.2.4.2 Accident Analysis

No change to the Standardized HSM analysis presented in UFSAR Section 8.2.4.2 for Models 80/102 and in their respective appendices for Models 152/202. The HSM-H and DSCs are evaluated for flooding in Section T.3.7.3.

The DSC is designed and tested to be leak tight to the criteria of ANSI N14.5 [11.2]. The stresses in the DSC due to the design basis flood are well below the allowable stresses for Service Level C of the ASME Code Subsection NB [11.5]. Therefore, the NUHOMS®-61BTH DSC will withstand the design basis flood without breach of the confinement boundary.

T.11.2.4.3 Accident Dose Calculations

The radiation dose due to flooding of the HSMs (HSM-H, Standardized HSM) is negligible. The NUHOMS®-61BTH DSC is designed and tested as a leak-tight containment boundary. Flooding

does not breach the containment boundary. Therefore radioactive material inside the DSC will remain sealed in the DSC and, therefore, will not contaminate the encroaching flood water.

T.11.2.4.4 Corrective Actions

No change. See Section 8.2.4.4.

T.11.2.5 Accidental TC Drop

This event is described in Section 8.2.5.

T.11.2.5.1 Cause of Accident

See Section T.3.7.4.1.

T.11.2.5.2 Accident Analysis

The evaluation of the NUHOMS®-61BTH DSC shell and basket assemblies due to an accidental drop is presented in Section T.3.7.4. As documented in Chapter T.3.7, the TCs have been evaluated for a payload that bounds the 24PTH DSC payload, and therefore is not affected by the 61BTH DSC. As shown in Section T.3.7.4, the DSC shell and basket stress intensities are within the appropriate ASME Code Service Level D allowable limits and maintains their structural integrity.

For the case of a liquid neutron shield, a complete loss of neutron shield was evaluated at the 100°F ambient condition with full solar load in Chapter T.4. It is conservatively assumed that the neutron shield jacket is still present but all the liquid is lost. The maximum DSC shell temperature is 544°F. The maximum cask inner liner, cask outer shell, and cask neutron shield jacket temperatures are 428°F, 392°F and 267°F, respectively, for 61BTH Type 2 DSC with 31.2 kW decay heat load as shown in Table T.4-10. The fuel cladding temperatures are below their limit as shown in Table T.4-25. Accident thermal conditions, such as loss of the liquid neutron shield, need not be considered in the load combination evaluation. Rather the peak stresses resulting from the accident thermal conditions must be less than the allowable fatigue stress limit for 10 cycles from the appropriate fatigue design curves in Appendix I of the ASME Code. Similar analyses of other NUHOMS® TCs have shown that fatigue is not a concern. Therefore, these thermal stresses in a TC with a liquid neutron shield need not be evaluated for the accident condition.

T.11.2.5.3 Accident Dose Calculations for Loss of Neutron Shield

The postulated accident condition for the onsite TC assumes that after a drop event, the water in the neutron shield is lost. The loss of neutron shield is modeled using the normal operation models described in Section T.5.4 by replacing the neutron shield with air. Also, damaged fuel is modeled as fuel rubble that falls to the bottom of the cask. The dose rates due to the fuel rubble model are bounded by the results from assuming intact fuel in damaged fuel locations at far distances. The accident condition dose rates from Chapter T.5, are summarized in Table T.11-2 for the bounding 61BTH DSC Type 1 loaded with design basis fuel.

Table T.11-2 shows the accident condition dose rates at 1,100 and 500 meters from the TC (OS197 or OS197H or OS197FC-B). The dose received by a person located 100 meters away from the NUHOMS® 61BTH system installation for an assumed 8 hour duration would be less than 5 mrem with the OS197FC-B. The increased dose to an offsite person located 500 meters away for the assumed 8 hour duration would be less than 0.01 mrem with both the OS197FC-B TC with NUHOMS® 61BTH DSC. These exposures are well within the limits of 10CFR72.106 for an accident condition.

T.11.2.5.4 Corrective Action

No change. See Section 8.2.5.4.

T.11.2.6 Lightning

No change. The evaluation presented in Section 8.2.6 is not affected by the addition of the NUHOMS®-61BTH DSC to the NUHOMS® system.

T.11.2.7 Blockage of Air Inlet and Outlet Openings

This accident conservatively postulates the complete blockage of the ventilation air inlet and outlet openings of the Standardized HSM or HSM-H.

T.11.2.7.1 Cause of Accident

No change.

T.11.2.7.2 Accident Analysis

This event is evaluated in Section 8.2.7.2 for Standardized HSM with 24 kW heat load. The maximum heat load (22 kW) in the Type 1 61BTH DSC within a Standardized HSM is bounded by 24 kW. Therefore, the evaluation presented in Section 8.2.7.2 is also applicable to the Standardized HSM with the 61BTH DSC.

The thermal evaluation of this event is presented in Chapter T.4 for HSM-H and a 61BTH DSC. The temperatures determined in Chapter T.4 are used in the structural evaluation of this event, which is presented in Sections T.3.7.7 and T.3.4.4.3 for HSM-H and 61BTH DSC.

The section below describes the additional analyses performed to demonstrate the acceptability of the system with the NUHOMS®-61BTH DSC.

T.11.2.7.3 Accident Dose Calculations

There are no off-site dose consequences as a result of this accident. The only significant dose increase is that related to the recovery operation. Based on the results presented in Chapter T.5, Table T.5-1 and Table T.5-2, the bounding average dose on HSM front or roof is 19.5 mrem/hr and 58.4 mrem/hr for the HSM-H and Standardized HSM, respectively.

It is conservatively estimated that the on-site workers will receive an additional dose of no more than 467 mrem during an estimated eight hour period that may be required for removal of debris from the inlet and outlet vent openings. These exposures are well within the limits of 10CFR72.106 for an accident condition.

T.11.2.7.4 Corrective Action

No change.

T.11.2.8 DSC Leakage

The NUHOMS®-61BTH DSC is designed as a pressure retaining containment boundary to prevent leakage of contaminated materials. The analyses of normal, off-normal, and accident conditions have shown that no credible conditions can breach the DSC shell or fail the double seal welds at each end of the DSC. The NUHOMS®-61BTH DSC is designed and tested to be leak tight [11.2]. Therefore DSC leakage is not considered a credible accident scenario. See Chapter T.7 for additional details on the confinement evaluation.

T.11.2.9 Accident Pressurization of DSC

T.11.2.9.1 Cause of Accident

The bounding internal pressurization of the NUHOMS®-61BTH DSC is postulated to result from cladding failure of the spent fuel in combination with the transfer accident case with the loss of sunshield and liquid neutron shield in the transfer cask under extreme ambient temperature conditions of 117°F and maximum insolation and the consequent release of spent fuel rod fill gas and free fission gas. The evaluation conservatively assumes that 100% of the fuel rods have failed.

T.11.2.9.2 Accident Analysis

The pressure due to this case is evaluated in Section T.4.6. The maximum accident condition pressure calculated is 68.7 psig for the 61BTH Type 2 DSC and 56.1 psig for the 61BTH Type 1 DSC. The accident design pressure is conservatively assumed to be 120 psig and 65 psig in the structural load combinations presented in Table T.2-11 for 61BTH Type 2 DSC and 61BTH Type 1 DSC, respectively.

T.11.2.9.3 Accident Dose Calculations

There is no increase in dose rates as a result of this event.

T.11.2.9.4 Corrective Actions

This is a hypothetical event. Therefore no corrective actions are required. The canister is designed to withstand the pressure as a Level D condition. There will be no structural damage to the canister or leakage of radioactive material as a result of this event.

T.11.2.10 Fire and Explosion

T.11.2.10.1 Cause of the Accident

Combustible materials will not normally be stored at an ISFSI. Therefore, a credible fire would be very small and of short duration such as that due to a fire or explosion from a vehicle or portable crane.

However, a hypothetical fire accident is evaluated for the NUHOMS®-61BTH system based on a fuel fire. The source of fuel is postulated to be from a ruptured fuel tank of the transfer cask transporter tow vehicle. The bounding capacity of the fuel tank is 300 gallons and the bounding hypothetical fire is an engulfing fire around the transfer cask. Direct engulfment of the HSM is highly unlikely. Any fire within the ISFSI boundary while the DSC is in the HSM would be bounded by the fire during transfer cask movement. The HSM concrete acts as a significant insulating fire wall to protect the 61BTH DSC from the high temperatures of the fire.

T.11.2.10.2 Accident Analysis

The evaluation of the hypothetical fire event is presented in Section T.4.6.8.3. The fire thermal evaluation is performed primarily to demonstrate the confinement integrity and fuel retrievability of the 61BTH DSC. This is assured by demonstrating that the DSC temperatures and internal pressures will not exceed those of the blocked vent condition (see Section T.11.2.7) during the fire scenario. Peak temperatures for the NUHOMS®-61BTH system components are summarized in Table T.4-11.

T.11.2.10.3 Accident Dose Calculations

The 61BTH DSC confinement boundary will not be breached as a result of the postulated fire/explosion scenario. Accordingly, no 61BTH DSC damage or release of radioactivity is postulated. Because no radioactivity is released, no resultant dose increase is associated with this event.

The fire scenario may result in the loss of cask neutron shielding should the fire occur while the 61BTH DSC is in the cask. The effect of loss of the neutron shielding due to a fire is bounded by that resulting from a cask drop scenario. See Section T.11.2.5.3 for evaluation of the dose consequences of a cask drop.

T.11.2.10.4 Corrective Actions

Evaluation of HSM or cask neutron shield damage as a result of a fire is to be performed to assess the need for temporary shielding (for HSM or cask, if fire occurs during transfer operations) and repairs to restore the transfer cask and HSM to pre-fire design conditions.

T.11.3 References

11.1 American Nuclear Society, ANSI/ANS-57.9, Design Criteria for an Independent Spent Fuel Storage Installation (Dry Storage Type), 1992.

11.2 ANSI N14.5-1997, "Leakage Tests on Packages for Shipment," February 1998.

11.3 NUREG-1536, "Standard Review Plan for dry Storage Casks, Final Report," US Nuclear Regulatory Commission, January 1997.

11.4 U.S. Nuclear Regulatory Commission, Interim Staff Guidance (ISG)-5, Rev. 1, "Confinement Evaluation."

11.5 American Society of Mechanical Engineers, ASME Boiler and Pressure Vessel Code, Section III, 1998 including 2000 addenda.

Table T.11-1
Comparison of Total Dose Rates for HSM with and without Adjacent HSM Shielding Effects

Distance from Nearest HSM Wall, 2x10 Array (meters)	Normal Case Dose Rate(1) (mrem/hr)	Accident Case Dose Rate(1) (mrem/hr)
10	5.1	10.2
100	0.11	0.22
500	5.3×10^{-4}	1.1×10^{-3}
600	1.9×10^{-4}	3.8×10^{-4}

(1) Air scattered plus direct radiation

Table T.11-2
Calculated Accident Dose Rates on the Side of the OS197FC-B TC

Distance (meters)	Neutron		Total Gamma		Total	
	mRem/hr	1σ error	mRem/hr	1σ error	mRem/hr	1σ error
1	2.57E+03	0.0018	3.86E+02	0.0094	2.96E+03	0.0020
100	3.52E-01	0.0045	1.65E-01	0.0065	5.16E-01	0.0037
500	1.87E-04	0.0317	4.69E-04	0.0106	6.56E-04	0.0118

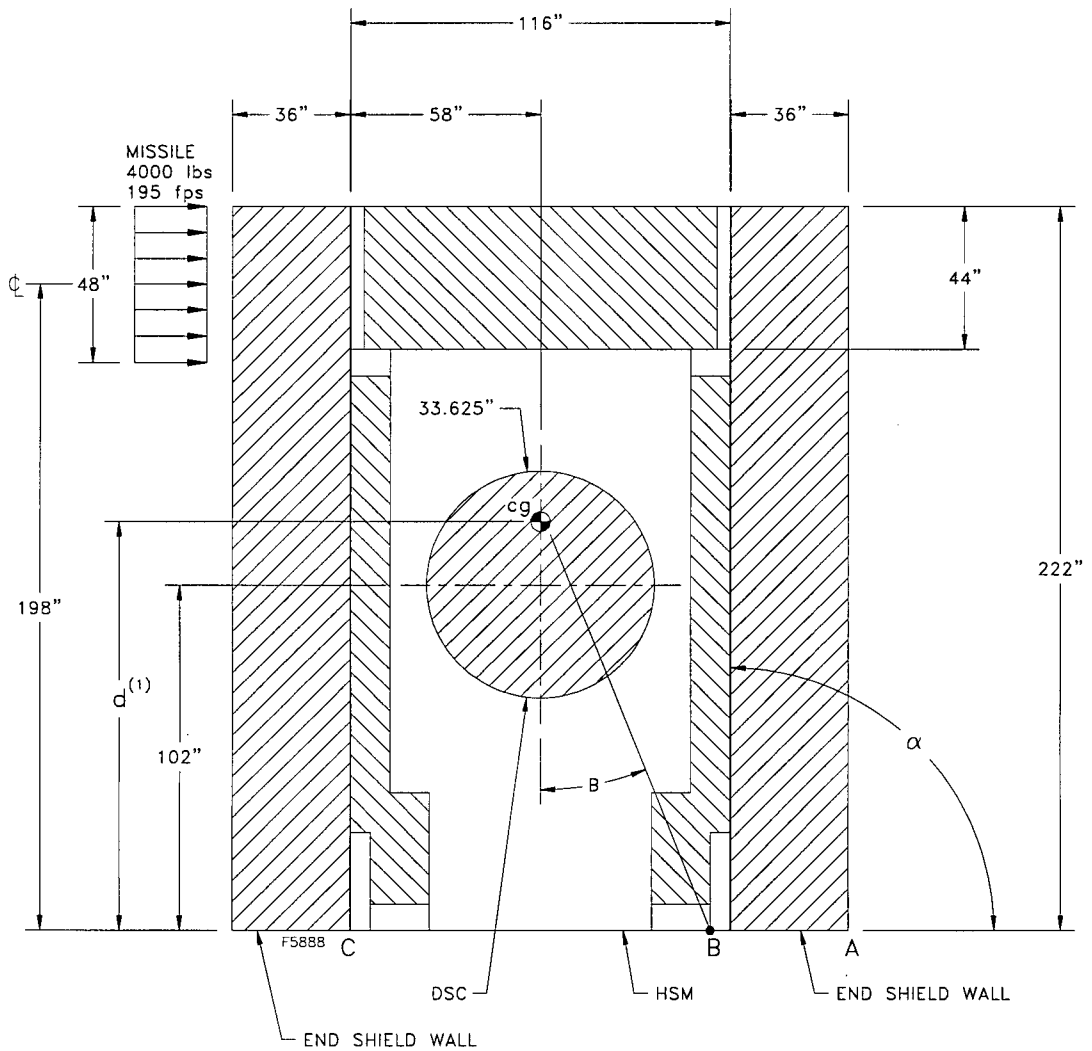

(α is the angle between the side of the rotated HSM-H and the horizontal)

(1) d =118.77" with DSC weight of 110 kips, loaded module.

d = 123.45" with out the DSC, empty module.

Figure T.11-1
HSM-H Dimensions for Missile Impact Stability Analysis

T.12 Conditions for Cask Use - Operating Controls and Limits or Technical Specifications

The Technical Specifications changes, due to the addition of the 61BTH DSC to the NUHOMS® system, are included in the NUHOMS® CoC 1004 Amendment Number 10 application.

T.13 Quality Assurance

Chapter 11.0 provides a description of the Quality Assurance Program to be applied to the safety related and important to safety activities associated with the standardized NUHOMS® system. The addition of the 61BTH DSC to the NUHOMS® system requires the following clarification to the contents of Section 11.2:

> "In lieu of the requirements listed in paragraph A through H, Category A items may also be procured as commercial grade items and dedicated in accordance with the guidelines of EPRI NP-5652."

T.14 Decommissioning

There is no change from the decommissioning evaluation presented in Section 9.6 due to the addition of the 61BTH DSC to the NUHOMS® system.